Ignition and Heat Release Behaviour of iso-Butanol and Gasoline Blended Fuels: An Experimental and Kinetic Modelling Study

Christian Alexander Michelbach

Submitted in accordance with the requirements for the degree of Doctor of Philosophy

The University of Leeds

The Centre for Doctoral Training in Bioenergy

September 2020

The candidate confirms that the work submitted is his own and that appropriate credit has been given where reference has been made to the work of others.

This thesis is dedicated to my grandad, Gary Neal.

Grandad, you were an inspiration to me, and I hope you are proud.

We miss you every day.

Acknowledgements

Firstly, I would like to acknowledge my family and friends for their encouragement and support throughout the course of my studies, of which I am extremely grateful. Specific thanks go to my parents, my nan, my brother Joel, my sisters Heidi and Athena, and my partner Sammi. Without their support the completion of my studies may not have been possible, and I am incredibly lucky to call them my family.

I would like to express my appreciation to my supervisor Prof. Alison S. Tomlin for her guidance and patience throughout the course of my research. The experience and knowledge you have shared throughout the project has been invaluable, and I would specifically like to thank you for your support during the completion of the thesis. I am also grateful for the assistance of Dr Malcolm Lawes during my research. Thank you for your valuable input and discussion during group meetings early in the project, as well as your assistance during the modification and repair of the RCM. I also want to give thanks to Prof. Derek Bradley, for his knowledgeable discussions during group meetings and his infectious passion for combustion science.

My sincere appreciation to the technical staff of the Thermofuids lab, Mark Batchelor, Samuel Flint and Peter Grieve, for their continuous assistance throughout the project, particularly during the many RCM equipment failures which seemed to plague my experiments.

I would like to thank members of the Combustion Group who have provided assistance during my PhD and made the experience memorable: Edirin Agbro, Inna Gorbatenko, Scott Wiseman, Moustafa Shehata, Pervez Ahmed, Wankang “Peter” Zhang, Prof. Junfeng Yang, Junior “James” Achumu and Jinzhou Li. I would also like to thank the members of the Bioenergy CDT cohort, with special thanks to Chris Holt, for being a good friend, and Ric Birley, for always being ready for a quick coffee break.

During my time on the Bioenergy CDT, I spent a small amount of time on placement at NUI Galway, where I learnt a great deal. I would like to sincerely thank Prof. Henry Curran for enabling my visit. I would also like to thank everyone at NUI Galway that made my time there memorable, enjoyable, and valuable: Kieran Somers, Nitin Lokachari and Ultan Burke.

Grateful acknowledgements are also offered to Scott Wagnon (LLNL) for his generous assistance in the development of the five component gasoline surrogate, Roger Cracknell and Shell Global Solutions for the provision of the gasoline fuel, and Mani Sarathy and the group at KAUST for providing the combined mechanism.

Abstract

The decarbonisation of transport and the introduction of further renewable energy sources are required to minimise the impacts of climate change, while meeting the energy needs of a developing global population. Introducing alternative fuels into existing and developing spark ignition (SI) engine technologies requires the thorough characterisation of the fuel's combustion behaviour. The propensity of fuel to autoignite is a key property which limits SI engine performance through the development of engine knock. Autoignitive behaviour can be characterised by ignition delay time (IDT) measurements in rapid compression machines (RCM) or by measuring knocking behaviour within practical engines. RCMs provide an opportunity to study a fuels ignition behaviour at the fundamental level, the measurements of which often serve as a prediction for behaviour in more complex systems, such as SI engines. Through the application of both techniques, this work investigates the influence of iso-butanol blending on the combustion behaviour of gasoline (with particular focus given to the anti-knock properties of fuel blends), as well as assessing the validity of applying fundamental studies to predict practical engine level combustion behaviour. Accurate computational modelling provides an opportunity for the prediction of combustion behaviour quickly and cheaply when compared to experiments, facilitating the rapid optimisation of engine and fuel blend designs.

To enable the computational modelling of gasoline, surrogate fuels are required which replicate the target behaviours of the reference fuel, while minimising molecular complexity. The ability of a newly developed five component surrogate (5-C) to reproduce the autoignition behaviour of a research grade gasoline (RON 95 MON 86.6) is investigated within an RCM, at temperatures of 675-870 K, a pressure of 20 bar and equivalence ratios of 0.5 and 1.0, producing an excellent representation at stoichiometric conditions but displaying much lower reactivity than gasoline at lean conditions. When blended with iso-butanol (at 10, 30, 50 and 70% iso-butanol by volume), the representation of gasoline by 5-C continues to be generally good but at low temperatures (<770 K) and high iso-butanol concentrations (iB50/70), 5-C blends are considerably less reactive than gasoline blends. Upon investigation within a motored, skip-firing SI research engine, the 5-C continued to provide an accurate representation of gasoline's normal and knocking combustion behaviour at spark advance timings of 2-10 CA° bTDC. Under blending with iso-butanol the surrogate continued to perform well but blends were observably less reactive at spark advance timings <8 CA° bTDC. Blends of 20-50% iso-butanol were found to be optimal for use in SI engines, providing considerable anti-knock benefits and comparable indicated power to gasoline. Correlations between RCM and engine measurements

display the proficiency of fundamental measurements in predicting combustion behaviour within an engine at similar thermodynamic conditions.

Changes in the autoignition behaviour of 5-C due to blending with iso-butanol (5-70% iso-butanol) were studied experimentally within the RCM and computationally via chemical kinetic modelling. At low temperatures, iso-butanol generally reduces reactivity, suppressing the intensity of LTHR. As temperatures are increased, iso-butanol appears to suppress NTC behaviour and a cross-over in IDT measurements is observed between blends of 5 and 10% iso-butanol, wherein the 10% blend becomes the most reactive at intermediate to high temperatures. Modelling results largely failed to replicate complex blending behaviour and largely underpredicted IDTs in the NTC region. It is proposed that the model's misrepresentation of LTHR behaviour is a cause for such global model failures, as evidenced by local OH, brute force enthalpy of formation and reaction A-factor sensitivity analyses which highlighted the importance of reactions and species of significance to first stage ignition and low temperature oxidation processes, in the determination of IDTs and characteristic LTHR properties. Minimising uncertainties in the thermodynamic properties of complex oxygenated species typical of low temperature oxidation would produce more accurate model predictions, as these uncertainties are currently large for many important species. The influence of these uncertainties on the parameters investigated in this study is substantial. Current computer models therefore cannot be effectively applied in the prediction of the combustion behaviour for gasoline/iso-butanol blends until these issues are resolved. Further studies of the species and key reactions identified in this research would help to improve current kinetic mechanisms.

Table of Contents

List of Figures

List of Tables

Nomenclature

Symbol	Units	Description
A	-	Pre-exponential A-factor
a	m	Crank Radius
B	m	Cylinder Bore
C_P	J/kg/K	Specific Heat Capacity at Constant Pressure
C_V	J/kg/K	Specific Heat Capacity at Constant Volume
E_a	J/mol	Activation Energy
$H°$	J/mol/K	Standard Molar Enthalpy
L	m	Stroke Length
l	m	Connecting Rod Length
k	-	Rate Constant
k_f	-	Rate Constant (Forward Reaction)
k_r	-	Rate Constant (Reverse Reaction)
k_{eq}	-	Equilibrium Rate Constant
K	-	K-value
M	kg/mol	Molecular Weight
m	kg	Mass
P	bar	Pressure
P_i	bar	Initial Pressure
P_{in}	bar	Intake Pressure
P_C	bar	Compressed Pressure
P_{CY}	bar	Cylinder Pressure
P_r	bar	Reduced Pressure

R	J/mol/K	Universal Gas Constant
$S°$	J/mol/K	Standard Molar Entropy
T	K	Temperature
T_i	K	Initial Temperature
T_{in}	K	Intake Pressure
T_C	K	Compressed Temperature
U	J	Internal Energy
V_c	m^3	Clearance Volume
V_d	m^3	Displacement Volume
w	mol/s	Molar Rate of Production
γ	-	Ratio of Specific Heats
θ	degrees	Crank Angle
ξ	moles	Extent of Reaction
τ_i	s	Ignition Delay Time
τ_1	s	First Stage Ignition Delay Time
τ_2	s	Second Stage Ignition Delay Time
ρ	kg/m^3	Density
Φ	-	Equivalence Ratio

Abbreviations

ABE	Acetone-Butanol-Ethanol
aHR	Accumulated Heat Release
AKI	Anti-Knock Index
aTDC	After Top Dead Centre
BDC	Bottom Dead Centre
BDE	Bond Dissociation Energy

bTDC	Before Top Dead Centre
CA	Crank Angle
CFD	Computational Fluid Dynamics
CFR	Comparative Fuel Research
CI	Compression Ignition
CoV	Coefficient of Variation
CR	Compression Ratio
DAQ	Data Acquisition
DDM	Decoupled Direct Method
DEE	Di-ethyl Ether
DME	Dimethyl Ether
DRGEP	Direct Relation Graph with Error Propagation
EGR	Exhaust Gas Recirculation
EOC	End of Compression
GA	Group Additivity
GFM	Green's Function Method
GHG	Greenhouse Gas
HCCI	Homogeneous Charge Compression Ignition
HRA	Heat Release Analysis
HRR	Heat Release Rate
HTHR	High Temperature Heat Release
HVO	Hydrogenated Vegetable Oil
IC	Internal Combustion
IDT	Ignition Delay Time
IMEP	Indicated Mean Effective Pressure
IPCC	Intergovernmental Panel on Climate Change
ITHR	Intermediate Temperature Heat Release
KN	Knock Onset
LHV	Lower Heating Value
LLNL	Lawrence Livermore National Laboratory
LPG	Liquified Petroleum Gas
LTHR	Low Temperature Heat Release
LUPOE	Leeds University Ported Optical Access Engine
MBMS	Molecular Beam Mass Spectrometry

MON	Motor Octane Number
Mt	Million Tonnes
NASA	National Aeronautics and Space Administration
NDC	Nationally Determined Contribution
NIST	National Institute of Standards and Technology
NOx	Nitrous Oxides
NTC	Negative Temperature Coefficient
ODE	Ordinary Differential Equation
OI	Octane Index
ON	Octane Number
PIHR	Pre-Ignition Heat Release
PLIF	Planar Laser Induced Fluorescence
PRF	Primary Reference Fuel
RCCI	Reactivity Controlled Compression Ignition
RCM	Rapid Compression Machine
RED	Renewable Energy Directive
RON	Research Octane Number
RPM	Revolutions per Minute
S	Sensitivity (Octane)
SI	Spark Ignition
SOC	Start of Compression
soHTHR	Start of High Temperature Heat Release
soITHR	Start of Intermediate Temperature Heat Release
TDC	Top Dead Centre
TRF	Toluene Reference Fuel
TST	Transition State Theory

1 Introduction and Thesis Scope

1.1 Background

In 2018 and 2019, global primary energy consumption grew by rates of 2.9% and 1.3%, respectively [1,2]. This corresponded with increases of 2.0% and 0.5% in carbon emissions from energy worldwide. Approximately 20% of global energy consumption is due to the transport sector, producing a resultant ~23% of global CO_2 emissions and 14% of total greenhouse gas (GHG) emissions [3–5]. Due to a growing global population and the increasing transport demands of large rapidly developing regions, such as Africa, China and India, global energy demand is predicted to increase significantly [5,6]. A combination of this increasing energy demand and the heavy reliance of the transport sector on oil for energy [7], highlights the need for the development of advanced engine technologies and alternative fuels to minimise the resultant GHG emissions. Developing engine technologies, such as homogeneous charge compression ignition (HCCI) engines, reactivity controlled compression ignition (RCCI) engines and various low temperature combustion engine technologies, have been shown to provide significant benefits in terms of improved thermal efficiency, reduced fuel consumption, fuel versatility and reductions in pollutant emissions [8,9]. However, while prototypes exist for these engine technologies, with multiple vehicle manufacturers taking particular interest in HCCI engine development [10,11], they are largely still undergoing research and development. A combination of such technologies and alternative fuels would contribute greatly towards the reduction of GHG while meeting the growing energy needs of developing populations. Currently, approximately 40% of all transport energy is used in passenger cars, of which about 95% is derived from fossil fuels produced by the refinement of liquid petroleum [3]. This translates to a global daily demand for gasoline in excess of 4.8 billion litres. The use of internal combustion (IC) engines is likely to remain as a cost-effective transportation propulsion system for the near future [12,13]. Therefore, it is crucial that research into the effective use of alternative fuels is pursued, in both conventional and advanced engine technologies. Potential alternative fuels for use in the transport sector include a wide range of biofuels [13], synthetic fuels/“e-fuels” [14,15], natural gas [16] and liquified petroleum gas (LPG) [17]. Biofuels can be produced from a range of biomass resources, including food crops such as corn, sugarcane, and sugar beet in the case of first generation biofuels. Advanced biofuels (second generation onwards) are produced from resources such as non-food crops (jatropha), waste (hydrogenated vegetable oil (HVO) and animal fat), agriculture and forestry residuals and algae [18,19]. These fuels typically provide net

carbon emission reductions and can be produced locally and sustainably, creating increased energy security and the potential to positively influence the economic development of rural regions.

To combat climate change and address global environmental concerns, multiple international policies and agreements have set in place legally binding emissions targets. One such piece of legislation was the Kyoto Convention. After meeting targets for the first period of commitment (2008-2012), the EU made a collective commitment to reduce its emissions of CO_2 by 20% from 1990 levels by the end of the second commitment period (2013-2020) [20]. The UK then committed to further reducing the emissions of all six Kyoto GHGs by 80% of 1990 levels by 2050, as set out by the UKs domestic emissions targets in the Climate Change Act 2008 [21]. Following the 2015 Paris Agreement [22], which requires that signatory nations (including the UK) hold global temperature rises this century to less than 2 °C higher than pre-industrial levels and make the best possible efforts (through nationally determined contributions (NDCs)) to limit this increase further to less than 1.5 °C, a 2018 report by the Intergovernmental Panel on Climate Change (IPCC) highlighted the pressing need to limit global temperature rises due to climate change to 1.5 °C above pre-industrial levels, in order to mitigate the impact of climate change [23]. In response to this report, the UK government amended the original 2008 Climate Change Act, signing into law a net zero target for UK GHG emissions by 2050 [24]. In the UK, 28% of all GHG emission originate from transport (not including international aviation and shipping), with approximately 90% of transport emissions associated with road transport. While emissions in other sectors of the UK energy economy are decreasing, transport emissions have remained relatively constant in recent years, decreasing by 1.4% (1.8 $MtCO_2e$) in 2018: the first decrease since 2013. This means that, in 2018, UK transport emissions were only 3.0% lower than values measured in 1990. While improvements have been made to fleet vehicle fuel efficiency during this time, the resultant decrease in emissions has been offset by increased road traffic and net kilometres driven [25].

In 2015, EU legislation implemented a legally binding CO_2 emissions target on fleet wide average emissions of new vehicles. From 2021 this emissions target is set to be reduced further, from 130 gCO_2/km to 95 gCO_2/km, towards the goal of meeting the EU wide target of a 40% reduction in GHG emissions by 2030 (when compared to 1990 levels) [26]. To meet these targets and the Paris agreement commitments of member nations, the EU published the Renewable Energy Directive II (RED II), which amended, recast and introduced new legally binding renewable energy targets [27]. These targets include an increase of renewables in the

EU energy mix, to a value of 32% by 2030, and a minimum of 14% renewables for all road and rail transport [27]. RED II also limits the share of unsustainable first generation biofuels which may count towards these targets, capping their contribution at 7%, whereas the use of advanced biofuels is promoted, giving specific targets for the use of advanced biofuels periodically for the duration of the directive. The RED II states that the contribution of advanced biofuels, as a share of the consumption of energy within transport, must be a minimum of 0.2% by 2022, 1% by 2025, and 3.5% by 2030. Therefore, advanced biofuels which are determined to be environmentally and economically stable by the EU, as claimed by approved list of feedstocks provided by the RED II (which is updated every two years), are set to play an important role in the future of transport.

Alcohols such as methanol, ethanol, propanol, butanol are identified as possible advanced biofuels, which can be produced through the fermentation of multiple feedstocks listed in the RED II [27]. Such alcohols, along with other oxygenated fuels, have been shown in previous studies to potentially improve engine performance and emissions, due to their unique chemical and physical properties [28–31]. Ethanol is commonly blended with gasoline, typically at concentrations of 5% or 10% by volume, dependent on the region. The high octane rating and latent heat of vaporisation for ethanol when compared to conventional gasoline allows engines to operate at higher compression ratios (CR) when blended fuels are utilised, increasing the thermal efficiency. However, ethanol possesses a number of properties which reduce the viability of higher ethanol blends with gasoline, such as a relatively low energy density (~30% lower than that of gasolines) which limits fuel efficiency, demonstrable hydrophilic behaviour which causes storage issues, and corrosivity which can lead to the corrosion of engine components and fuel supply infrastructure [32–34]. Alternatively, butanols show promise as potential transport fuels in spark ignition (SI) engines; they have higher calorific values than ethanol, are potential octane boosters and when compared to ethanol, butanol is not as hydrophilic and has a lower vapour pressure. Butanol can also be blended to higher ratios in a conventional SI engine without the risk of corrosion. Furthermore, butanol is a more attractive fuel than ethanol for blending with diesel in compression ignition (CI) engines, due to higher cetane numbers, similar viscosity with diesel and a larger degree of miscibility with diesel fuels [35–38]. Of the butanol isomers which may be produced as an advanced biofuel, iso-butanol has been identified as potentially having the greatest octane boosting qualities, with relevance to use in SI engines [39].

1.2 Motivation

To meet the energy needs of an evolving transport sector while achieving the required renewable energy and GHG targets, considerable fuel blending of advanced biofuels such as iso-butanol may be required. Advanced biofuels also require blending with conventional fuels due to both the operational requirements of SI engines and the availability of biofuel components. Individual advanced biofuels are not currently available in large enough quantities to displace conventional fuels and neither would the current production of such fuels be able to keep pace with fuel demands [4]. Therefore, complex blends composed of a mix alternative fuels with conventional fuels are likely to be utilised to meet the needs of the transport sector and associated legislation in the near future. To evaluate the suitability of such blends as alternative transport fuels, the ignition and combustion behaviour needs to be well understood in order to determine if a given fuel blend is compatible with modern engine technologies [35]. Knowledge of this behaviour is also critical for the optimisation of engine operating modes, should a fuel be deemed suitable, as blends of enhanced octane quality may be exploited by higher operating pressures, increasing the thermal efficiency of the engine. This is of particular importance in pressure boosted downsized SI engines, which employ pressure boosting systems such as turbo and superchargers to operate at higher CRs than conventional SI engines, reducing fuel consumption and increasing thermal efficiency without sacrificing power. The degree of boosting in such engine technologies is limited by the presence of engine knock, a potentially damaging abnormal combustion phenomena caused by the induced autoignition of end gases during SI engine operation. Fuels of high octane quality display a higher resistance to this phenomenon and therefore, may be operated at more extreme pressures [40,41]. The penetration of advanced biofuels into the wider transport energy picture therefore requires a thorough understanding of combustion behaviour for the entire blending regime with conventional fuels.

While some research has been conducted into the ignition characteristics of iso-butanol [39,42,43], historically, fewer studies have been conducted into the combustion of larger alcohols when compared to methanol and ethanol, and very little work has been conducted investigating the properties of iso-butanol and gasoline blend fuels, particularly with relevance to turbo/super-charged downsized SI engine technologies. Knowledge of the ignition behaviour of such blends is vital to evaluate the suitability of these fuels for application in modern engine technologies. It is common for fundamental experiments, such as rapid compression machine (RCM) autoignition studies, to be applied in the determination of a fuel's ignition behaviour, at

thermodynamic conditions of relevance to engine combustion [39,44–47]. However, the validity of these findings with respect to a fuel's behaviour in a conventional SI engine is questionable, due to significant differences between the near-homogeneous combustion environment within an RCM and the turbulent environment within an engine combustion cylinder. RCMs are also non-reciprocating, with each test conducted independent of previous tests [48], whereas each engine cycle will be influenced significantly by previous cycles, in terms of both the presence of combustion residuals and changing cylinder temperatures [49,50]. Therefore, fundamental ignition studies may not accurately represent the combustion behaviour of a fuel or a fuel's blending trends under typical SI engine operation, despite taking place under initially similar thermodynamic conditions. Comparisons of the ignition behaviour of fuels at the fundamental and practical engine level have rarely been described in the literature, and when comparisons are made, significant differences between RCM and engine studies have been observed [51,52]. It is therefore important to evaluate the usefulness and validity of applying such fundamental studies under the assumption that results accurately represent practical engine behaviour.

Full characterisation of the combustion behaviour for the entire regime of iso-butanol gasoline blends, for application to the diverse range of SI engine technologies present in the transport fleet, requires detailed investigation at an exhaustive range of conditions. This includes thermodynamic properties such as temperatures, pressures, and stoichiometry. To perform such an analysis would require a prohibitive amount of time, potentially limiting the introduction of viable alternative fuels into the transport energy sector. Computer modelling and simulation provides an opportunity to predict combustion behaviour relatively cheaply and quickly, reducing the need for such an exhaustive regime of potentially expensive and time consuming experiments [53]. Furthermore, computer modelling approaches can be applied to probe conditions wherein experimental measurements are difficult or impossible. These abilities mean that computer modelling of combustion process can be an effective tool for the design, control, testing, and optimisation of combustion technologies (such as new and conventional engine technologies), and the prediction of optimal fuel blends. However, this requires a robust model which accurately represents the fuel chemistry and the effect of the fuel reaction mechanism on combustion processes [7]. Therefore, accurate detailed reaction mechanisms are required, which precisely describe the complex kinetic behaviour of the fuel during combustion, at a series of elementary reaction steps, and accurately represents the thermochemical properties of each species involved in the process. Such models for complex alternative fuels may be subject to considerable degrees of inaccuracy due to uncertainties inherent in input parameters, such as reaction rate parameters and species thermochemical

data [53,54]. This is particularly true for large, detailed mechanisms, which can include several thousand individual elementary reactions and hundreds to thousands of species. Sensitivity analysis techniques can be applied to the predicted targets of a model (such as ignition delay times (IDTs), species concentrations and heat release rates), to identify highly important parameters (such as reaction pre-exponential A-factors and species enthalpies of formation). The results of such analysis help to identify target parameters which require further study through experimental investigation or detailed theoretical calculation. Furthermore, the availability of a comprehensive reaction mechanism does not mean that a chemical process is well understood, particularly for such large, detailed mechanisms. In these cases, the competition between reaction steps and the coupling between species can be difficult to understand. Sensitivity analysis techniques also provide a useful method for developing an understanding of such fine details and the behaviour of complex kinetic processes [53]. This can be applied effectively to investigate the influence of alternative fuels on the chemistry driving ignition behaviour, increasing knowledge of engine relevant combustion phenomena.

The broad research questions that this work seeks to address are:

- What influence does iso-butanol blending with a research grade gasoline fuel have on SI engine performance at different blending levels? Particular focus will be given to engine indicated power and knocking behaviour of the fuel blends.
- How well are measurements from a fundamental combustion system such as an RCM able to represent the trends in autoignition/knocking behaviour shown in practical SI engines i.e. to what extent are fundamental experiments useful in informing how fuel blends will behave in real engines?
- How well can a five component gasoline surrogate fuel represent the auto-ignition behaviour of a research grade gasoline on blending with iso-butanol under experimental conditions? This addresses the question as to whether the surrogate formulation could be used to develop a kinetic mechanism that is representative of the gasoline under the assessed conditions.
- How well does the gasoline surrogate fuel perform in both fundamental systems and practical SI engines in terms of representing trends on blending with iso-butanol? This addresses the question as to whether RCM experiments are sufficient for testing the validity of a surrogate fuel formulation that may be used within engine design.

- How effective are current computer models at predicting the combustion behaviour of the chosen iso-butanol gasoline blends through the use of a five component surrogate for gasoline?

1.3 Research Objectives

This work aims to investigate the influence of iso-butanol blending on the ignition behaviour, heat release and SI engine performance of gasoline and its surrogate, at conditions relevant to application in boosted SI engine technologies. By evaluating this behaviour at both the fundamental and practical engine level, this research also aims to investigate the suitability of RCM experiments for predicting SI engine phenomena. The ability of a detailed chemical kinetic mechanism to predict the autoignitive propensity and low temperature heat release (LTHR) behaviour of iso-butanol blends with a gasoline surrogate is also evaluated in this work. This research aims to utilise this mechanism to investigate the underlying chemistry driving the observed blending influences on combustion behaviour.

The objectives of this research are:

1. To develop the University of Leeds RCM facility to allow the capture of longer homogeneous IDTs, as well as to eliminate the presence of undesirable pre-ignition heat release (PIHR) phenomena.
2. To develop analytical methods for the characterisation and identification of PIHR in RCM datasets.
3. To provide experimental data for the IDTs of iso-butanol, gasoline, a newly developed five component surrogate (5-C), gasoline/iso-butanol blends, and 5-C/iso-butanol blends at a wide range of blending ratios, which may serve as validation targets for the development of chemical kinetic mechanisms.
4. To assess the ability of the proposed surrogate to replicate the autoignition behaviour of gasoline, as both a neat fuel and under iso-butanol blending.
5. To assess the ability of a detailed chemical kinetic mechanism to accurately predict the IDTs of 5-C and 5-C/iso-butanol blends.
6. To apply novel RCM heat release analysis (HRA) techniques to investigate the degree of low temperature exothermicity in the 5-C fuel and the influence of iso-butanol blending on this behaviour.

7. To provide experimental data for the HRRs (heat release rates) of 5-C and 5-C/iso-butanol blends, for a wide range of blending ratios, which may serve as valuable targets for the validation and development of chemical kinetic mechanisms.
8. To evaluate the ability of a detailed kinetic mechanism to accurately predict the heat release behaviour of 5-C and 5-C/iso-butanol blends.
9. To assess the underlying chemistry driving the autoignition of 5-C and 5-C/iso-butanol blends through the application of sensitivity analysis techniques to a detailed chemical kinetic mechanism.
10. To investigate the chemistry driving the LTHR behaviour of 5-C through the application of sensitivity analysis techniques to a detailed chemical kinetic mechanism.
11. To assess the sensitivity of model predictions due to uncertainties in both the thermodynamic properties of species within the mechanism and reaction rate parameters.
12. To investigate the ability of the proposed gasoline surrogate to replicate the combustion behaviour of gasoline in a pressure boosted SI research engine, both as a neat fuel and under iso-butanol blending.
13. To investigate the influence of iso-butanol blending on the normal and knocking combustion properties of gasoline and 5-C in a pressure boosted SI research engine, including knock onsets (KN), knock intensities and indicated mean effective pressure (IMEP).
14. To make comparisons between the combustion behaviour observed within RCM and engine experimental results.

1.4 Thesis Outline

This thesis is divided into eight chapters (including this chapter), as outlined and described briefly here.

Chapter 2: This chapter provides required background knowledge and a literature review of crucial content. Background knowledge is provided within this chapter for the combustion process in SI engines, autoignition and engine knock, RCMs, mild ignition, the autoignition of hydrocarbons and alcohols, chemical kinetics, numerical modelling, biofuels, and iso-butanol.

Chapter 3: This chapter describes the experimental facilities and the associated operating procedures used to collect experimental data, including IDT values, KNs and knock intensities. The modelling approaches utilised in the prediction of IDTs within this study are also thoroughly described here, as are the applied mechanism and sensitivity analysis techniques. HRA methodology of RCM data is detailed within this chapter.

Chapter 4: Techniques for the characterisation and identification of inhomogeneous ignition within the RCM are investigated in this chapter. These include analysis of the RCM pressure gradients and HRR-aHR trajectories. The influence of operational and mechanical improvements to the University of Leeds RCM on the existence of undesirable PIHR and IDT errors are explored within this chapter also. IDTs for iso-butanol captured with flat and creviced piston heads are also presented here.

Chapter 5: The ability of a newly developed five component (5-C) surrogate to represent the ignition behaviour of gasoline within an RCM is evaluated within this chapter, for both “neat” fuels and blends with iso-butanol, at stoichiometric and lean equivalence ratios. The influence of iso-butanol blending, at concentrations of 5-70% by volume, on the IDT and LTHR behaviour of the 5-C surrogate is shown within this chapter. These results are compared to the predictions of a chemical kinetic model and the ability of this model to predict the behaviour of 5-C/iso-butanol blended fuels is evaluated. Local OH sensitivity analysis is applied in this chapter to explore the underlying chemistry driving autoignition behaviour, the influence of iso-butanol blending on this chemistry and to investigate model performance.

Chapter 6: This chapter details further analysis of the applied kinetic mechanism through the enthalpy of formation brute force sensitivity analysis of IDT and characteristic LTHR properties, investigating the impact of uncertainties in species thermodynamic data (estimated through group additivity (GA) methods) on model predictions of IDT, HRRs and start of intermediate temperature heat release (soITHR) accumulated heat release (aHR). Reaction pre-exponential A-factor brute force sensitivity analysis of LTHR HRRs and soITHR aHR is also presented and investigated within this chapter.

Chapter 7: The ability of the 5-C surrogate to accurately represent the normal and knocking combustion properties of the reference gasoline, within a boosted SI research engine, is evaluated in this chapter. The influence of iso-butanol blending on the normal and knocking combustion properties of the 5-C and gasoline fuels is also investigated. These investigations explore the mean pressure cycles of each fuel, cyclic variability, KNs, knock intensities, and IMEP values at various spark advance timings.

Chapter 8: A summary of contributions, final conclusions with relevance to the original research questions, and suggestions for future work are provided in this chapter.

2 Background and Literature Review

2.1 Spark Ignition Engines

It is critically important understand the mechanics of autoignition as it relates to real world SI engines, particularly with the development of new fuels which may not be completely characterised at engine relevant thermodynamic conditions. The ignition behaviours of these fuels not only introduce engine performance changes which must be investigated, but also safety concerns that must be addressed (such as a fuel's knocking propensity and resultant intensity). To understand the implications of a fuel's autoignitive behaviour on SI engines, it is first necessary to understand the basics of SI engines and their operation. Invented in 1876 by Nicolaus Otto, the SI engine has historically been the most popular engine technology, due in part to its comparatively low weight and manufacturing costs [55]. Since its inception, this reciprocating engine design has undergone many modifications and developments, owing to the ever-evolving requirements of transport drive systems and the enactment of stricter regulations and expectations [49]. At the most basic level, the SI engine consists of a reciprocating piston connected to a crank/driveshaft, which converts the linear motion of the piston into a rotational motion. This piston moves within a closed cylinder, compressing a premixed volatile gas charge, which releases stored chemical energy upon the initiation of combustion by a spark. The liberated energy is then converted to mechanical work on the piston, lost due to heat transfer with the engine structure or expelled with exhaust gases. SI engines often utilise a four-stroke engine cycle (however there are situations in which a two-stroke engine is used instead), which can be seen below in Figure 2.1.

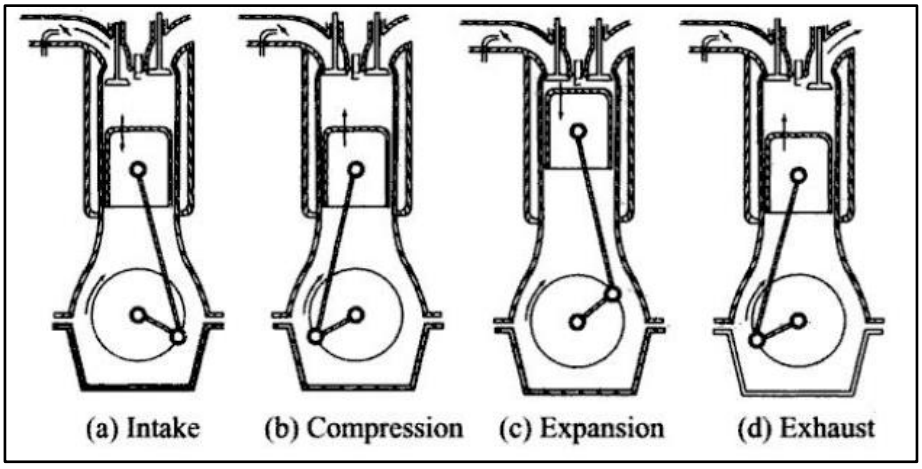

Figure 2.1 The four-stroke cycle in a SI engine [56].

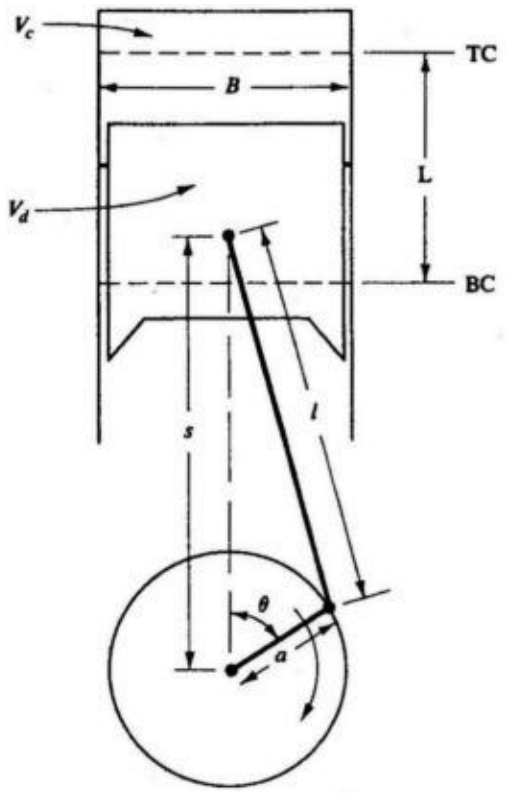

Figure 2.2. Geometry of a piston and cylinder arrangement [49]. In this diagram: *B*=bore, *L*=stroke length, *l*=connecting rod length, *a*=crank radius *θ*=crank angle, V_d=displaced volume and V_c=clearance volume.

The basic geometry of a reciprocating engine can be defined by a set of parameters which describe the piston, cylinder, and crank arrangement. A simple schematic of this system and the associated geometric parameters is shown in figure 2.2. Using these geometric parameters, a series of properties can be defined which characterise a reciprocating engine. The compression ratio (CR) can be defined as the ratio of the maximum cylinder volume (when the piston is at BDC) to the minimum cylinder volume (when this piston is at TDC), as shown in equation 2.1.

$$CR = \frac{V_c + V_d}{V_c} \qquad \text{Equation 2.1}$$

Here V_c is the clearance volume and V_d is the displaced volume or the volume "swept" by the piston during motion from BDC to TDC. The stroke length (*L*) and the crank radius (*a*) are related such that *L*=2*a* and the distance between the crank axis and the piston pin axis can be found at any crank angle by equation 2.2:

$$s = a\cos\theta + (l^2 - a^2\sin^2\theta)^{0.5} \qquad \text{Equation 2.2}$$

where *s* is the distance between the crank and piston axes, *l* is the connecting rod length and θ is the crank angle. From this definition and the geometry of the piston-crank arrangement, the cylinder volume at any crank angle can be calculated:

$$V = V_c + \frac{\pi B^2}{4}(l + a - s) \qquad \text{Equation 2.3}$$

where *B* is the cylinder bore.

SI engines typically operate at much lower CRs (and therefore pressures) than compression ignition (CI) engines to avoid the autoignition of fuels and the associated engine knock (a potentially engine damaging phenomenon caused by the autoignition of fuels as described in section 2.2). While lower operating pressures lead to a lower combustion efficiency, they also mean that the SI engine can have a lightweight construction when compared the CI engine as the engine will undergo less stress. In SI engines, a fuel charge is traditionally produced by the premixing of liquid fuel and air, to create a homogeneous mixture of a known equivalence ratio. The equivalence ratio of this mixture of fuel and air influences the combustion properties of the fuel and engine, such as the power output, efficiency, emissions, and tendency for knocking combustion [55]. Carburettors are commonly applied for the premixing of liquid fuels with combustion air, a mechanism wherein the motion of air through a venturi and the resultant pressure drop, causes the introduction of fuel through an orifice. Ignition of the premixed fuel charge is provided by a spark within the combustion cylinder, prior to the piston reaching TDC, which produces a flame kernel. The kernel then propagates throughout the fuel charge, releasing chemical energy as heat. This heat causes the thermal expansion of combustion cylinder gases and an increase in pressure within the cylinder. The timing of this spark can be optimised for each engine and fuel combination to provide the maximum torque. This optimal spark timing is referred to as the maximum brake torque timing [49]. When timing occurs later than this optimal crank angle, combustion of the entire fuel mixture may not occur before the exhaust valve is opened. This not only reduces the combustion efficiency and power of the engine, by may lead to the overheating of exhaust valves. Also, if the spark timing is too early, ignition may occur before the piston has reached TDC, causing a reduction in the total cycle output power. In these cases, peak pressures and temperatures may be substantial enough to promote the autoignition of any unburnt gases, leading to engine knock [55]. The thermal efficiency of the SI engine is improved in modern engines through several modifications to the cycle, including late valve timing and direct fuel injection, but most importantly to the study of fuels knock properties, engine performance can be improved by running at boosted pressures.

The pressure may be boosted through methods such as supercharging or the operation of a variable CR engine. A more knock resistant fuel can operate at boosted pressures and earlier spark timing, while avoiding the possibility engine knock.

The evolution of the pressure environment within the combustion cylinder can be observed and characterised for a typical SI engine cycle, as shown in figure 2.3. This combustion process can be categorised into three main regimes: the ignition lag stage, flame propagation stage and the afterburning stage [56]. The ignition lag phase defines the time interval between spark discharge (at point A), to the beginning of the pressure rise due to combustion (at point B). This point of pressure rise can be observed in relation to the recorded pressure for a motoring engine cycles, wherein no combustion occurs. During this stage, a self-propagating flame nucleus is developing. The rate of which this process occurs is highly dependent on the fuel used and is driven by the thermodynamic conditions (temperature and pressure) within the cylinder and chemical kinetics. For gasoline fuels, this duration of the ignition lag phase is typically ~0.5 ms [55].

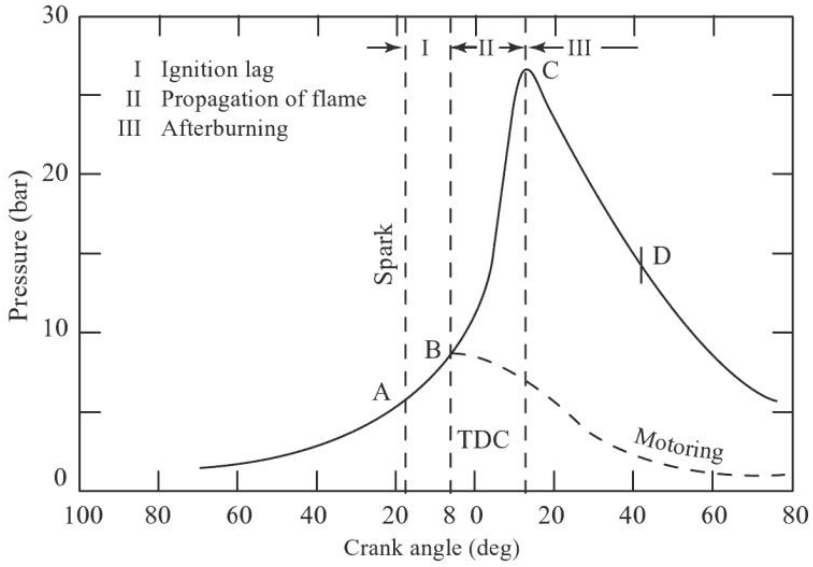

Figure 2.3. Pressure within the combustion chamber of an SI engine during a typical cycle, showing the multiple stages of the combustion process [56].

The flame propagation phase occurs between the point of pressure rise due to combustion (B) and peak pressure (C). During this phase, the flame propagates through the clearance volume at a near constant flame velocity [57]. This process significantly increases temperature and pressure within the combustion cylinder, which in turn forces the piston towards BDC, generating work. As the piston remains near TDC during this phase (as shown by

the crank angle measurements in figure 2.3), heat losses to the cylinder are low, as only a small part of the cylinder is in contact with the flame. The rate of pressure rise during this phase is proportional to the HRR, which is largely dependent on the intensity of turbulence and fuel dependent chemical kinetics, determining the overall reaction rate [56]. Beyond the peak pressure (C), the combustion process has entered the afterburning phase, wherein pressure decreases as the piston (now in the expansion stroke) moves towards BDC. During this phase, flame velocity decreases, causing a subsequent decrease in the rate of combustion [56]. This cycle and phases are characteristic of “normal” combustion in SI engines. However, abnormal combustion phenomena such as autoignition, knock and super-knock produce significantly different pressure behaviour in these regimes.

2.2 Autoignition and Engine Knock

As local temperature and pressure increase, the fuel/air mixture may spontaneously self-ignite in a process known as autoignition. This process is driven by both chemical and physical factors: chemical chain branching reactions produce a thermal feedback effect, wherein exothermicity causes increasing temperature, which in turn accelerates the overall rate of reaction. Initially, chain branching occurs through slow thermal reactions, growing the pool of radicals within the system. These radicals enhance the oxidation of further fuel species and the associated fuel oxidation species, which also produce more radical species through chain branching. Increasing radical concentrations and the resultant increase in total rate of reaction continue to rise, leading to a rapid explosive increase in temperature, radical concentrations, and oxidation rates. At this point, autoignition has occurred. This process is described chemically for general hydrocarbons and alcohols in section 2.5. Many of the reactions associated with the ignition process are exothermic, causing increases in temperature and pressure throughout the fuel mixture. These increasing thermodynamic conditions interact with the rates of individual reactions, which are strongly dependent on temperature and pressure conditions, creating a complex relationship between the overall rate of reaction of the thermodynamic conditions within the reacting mixture. This relationship between reaction rates and temperature/pressure conditions ultimately determines the rate at which autoignition will occur for a given fuel, at a set of thermodynamic conditions [53]. If this phenomenon occurs during the operation of an SI engine, it can cause detrimental abnormal combustion behaviour.

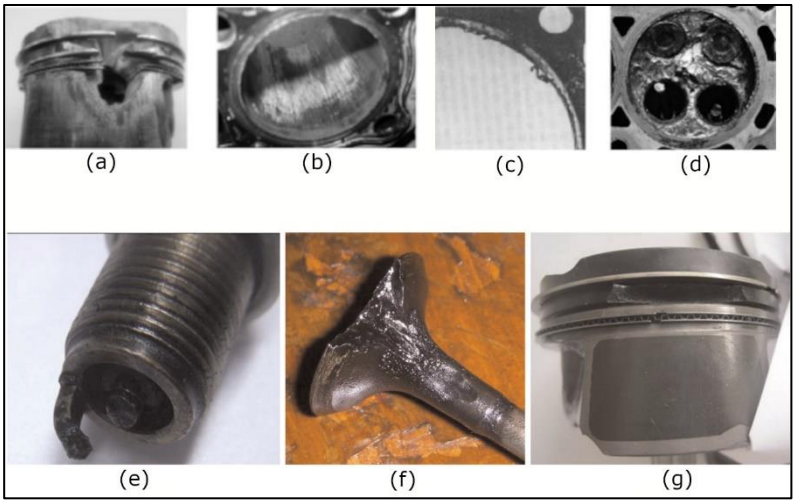

Figure 2.4. Examples of engine component damage causes by exposure to engine knock (a-d) and super-knock (e-g). (a) Piston melt. (b) Cylinder bore scuffing. (c) Gasket deterioration. (d) Cylinder hear erosion. (e) Spark electrode breakage. (f) Exhaust valve melt. (g) Piston ring land cracking. Adapted from [49,58].

When autoignition of the fuel takes place before discharge of the spark, an abnormal combustion process known as preignition occurs [59]. This may be due to high temperature and pressure conditions within the combustion cylinder during engine motoring, but can also be initiated by other sources such as hot interior surfaces, carbon deposits and oil droplets [49,60]. Once this process occurs, it is likely to also occur in subsequent cycles due to the repeatability of the initiation source [61]. This has the potential to lead to engine overheating and causes a relative drop in engine performance. In modern engines preignition is not usually an issue as it can be eliminated through good engine and fuel design, such as an effective cooling system, highly octane rated fuels and deposit prevention additives [62]. In boosted (by supercharging or turbo charging) SI engines, following the initial preignition a secondary autoignition may occur, which can have much more severe consequences. This process leads to a behaviour known as “super-knock”. In these cases, propagating flames generated by preignition hot-spots raise the temperature and pressure of the unburnt gas. A secondary, more reactive hot-spot may then be generated, causing the detonation of the unburnt gas [63] and producing a large pressure increase and subsequent high frequency pressure oscillations. This behaviour has seen much research interest lately, due to the complex processes thought to drive it and the significant engine damage attributed to this phenomenon, as shown in figure 2.4. [58,61,64,65].

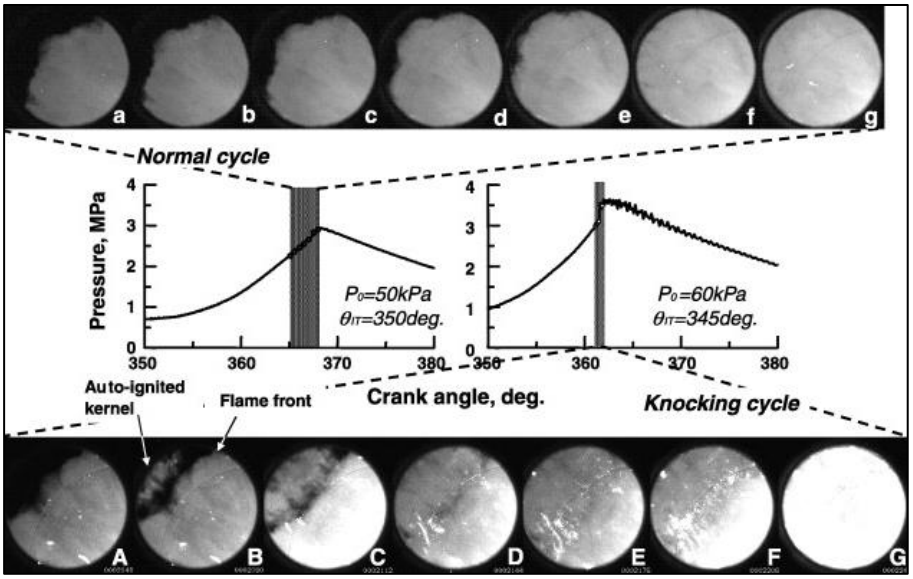

Figure 2.5. Normal and knocking engine cycles, shown by in cylinder pressure measurement and high speed direct imaging [66].

Engine knock describes a phenomenon wherein autoignition occurs post-spark, initiated by increased pressure conditions within the unburnt gas [40]. Under normal SI engine combustion, the discharge of the spark generates a small flame kernel, which propagates through the chamber, consuming fuel. This increases its heat output, raising the rate of propagation further. Under normal combustion, the pressure would rise smoothly to a peak, then decrease smoothly as the piston returns to BDC and the flame dies, with the maximum pressure occurring a few crank angle degrees after TDC. Normal combustion is driven by chemical reactions and molecular transport processes. During engine knock an abnormal combustion process occurs, wherein the fuel beyond the flame boundary is subject to increasing temperatures and pressures caused by the propagating flame front, ultimately leading to the autoignition of the unburnt gas [40]. This process is shown in figure 2.5 by direct imaging of the combustion process [66]. The autoignition of the unburnt gas causes a large increase in pressure followed by high frequency pressure oscillations, as the autoignition front interacts with the propagating flame front. A characteristic “ping” can often be heard during this process, due to the interaction of knock related pressure oscillations with engine cylinder walls, which causes significant vibrations in the cylinder structure. The intensity of the characteristic knocking pressure behaviour (pressure rise followed by high frequency oscillations) is shown in figure 2.6, alongside examples of normal SI engine combustion and super-knocking cases. The regular occurrence of engine knock may cause significant damage to the combustion cylinder and

associated components (e.g. spark plug, piston head, valves), as shown in figure 2.4, and as such this behaviour is highly undesirable.

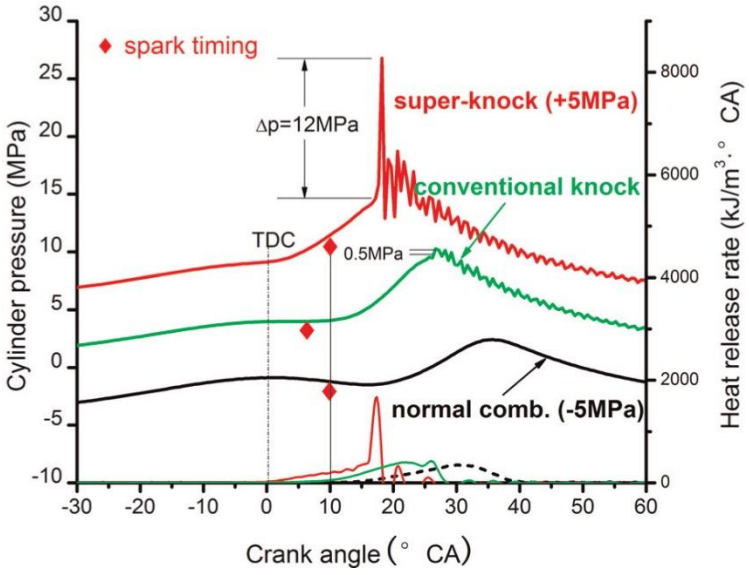

Figure 2.6. In cylinder pressure measurements for typical cases of normal combustion, conventional engine knock and super-knock [58].

To avoid these anomalous SI engine combustion phenomena, it is important that fuels are designed to resist autoignition under SI engine conditions, particularly in the case of boosted engine technologies. A fuel's resistance to autoignition is traditionally indicated by the octane numbers (ON) of the fuel: the research octane number (RON) and motor octane number (MON). ONs for a given fuel can be determined via testing with a single cylinder, overhead valve, variable CR four stroke engine known as a comparative fuel research (CFR) engine. Each ON is determined by investigating the fuels knock resistance at a set of different standard conditions, utilising a standard method, with MON testing occurring at more severe conditions than RON testing, as shown in table 2.1 [67,68]. For each of these testing standards, the ON is measured relative to reference ONs for iso-octane (ON=100) and n-heptane (ON=0), wherein the higher a fuels ON the more resistant it is to autoignition (and therefore engine knock). While such bulk indicators of a fuels octane quality have historically been useful in the characterisation and design of fuels for use in SI engines, as modern engine technologies trend further from the temperature and pressure conditions of such standardised testing regimes and more towards low temperature, high pressure combustion environments, these properties become an incomplete representation of a fuels antiknock properties [69]. IDTs, measured at thermodynamic conditions relevant to the operation of pressure boosted SI engines, allow for the characterisation of a fuels autoignition behaviour throughout the investigated regime, not

just specific standard conditions, identifying the autoignition response of the fuel to changing temperature and pressure conditions. IDT measurements at specific temperature and pressure conditions may also be correlated with bulk octane quality parameters, providing further functionality for such fundamental ignition measurements [69–72].

Table 2.1. RON and MON CFR testing conditions [67,68].

Parameter	**RON**	**MON**
Engine Speed	600 RPM	900 RPM
CR	4-18	4-18
Spark Timing	13 CA° bTDC	14-26 CA° bTDC
Intake Air Temperature	52 °C	149 °C
Intake Air Pressure	Atmospheric	Atmospheric
Coolant Temperature	100 °C	100 °C

Differences in ONs measured at RON and MON conditions can be quantified by fuel's octane sensitivity (*S*). Typically, as temperature and pressure conditions are lower in the RON testing case, the RON is higher than the MON, indicating lower reactivity. For alkane rich fuels, (such as primary reference fuels which are a blend of iso-octane and n-heptane) RON and MON may produce similar ONs due to the negative temperature coefficient (NTC) behaviour exhibited by these fuels, which temporarily causes a reduction in reactivity as temperature increases. The sensitivity parameter describes the change in reactivity of the fuel with respect to temperature and pressure conditions and is defined in equation 2.4, wherein a large value would describe a fuel which is sensitive to changes in operating conditions [73].

$$S = RON - MON \qquad \text{Equation 2.4}$$

The operating regimes of modern SI engines can differ considerably from those described by the CFR RON/MON testing conditions. Therefore, these tests alone cannot provide a sufficient representation of a fuel's knocking propensity under modern SI engine temperatures and pressures [69]. To represent the entire operating regime (from RON to MON conditions), the octane index (OI) is defined, as seen in equation 2.5. An empirical constant, *K* dictates the relationship between the OI and the ONs for a fuel, and is traditionally (1945-2000) given a value of *K*=0.5, making OI the mean of the RON and MON [74]. This OI (where *K*=0.5) is

referred to as the anti-knock index (AKI). However, *K* is dependent solely on the time dependent temperature and pressure conditions experienced by the unburnt gas, displaying a strong correlation with the temperature of the unburnt gas [75,76]. This means that SI engine developments, such as improved cooling systems, pressure boosting (supercharging and turbo charging) and fuel injection advancements, have contributed to a decrease in *K* values by lowering the associated gas temperatures. Typical *K* values were as low as *K*=0 since the year 2000 [74] and now in many cases unburnt gas temperatures exceed the RON boundary, producing *K* values of *K*<0 [65].

$$OI = (1 - K)RON + (K)MON = RON - KS \qquad \text{Equation 2.5}$$

Therefore, if ONs are to be applied for fuels in modern SI engines, they would require extrapolation beyond the RON and MON determined values. However, extrapolating into the -*K* value regime produces values for OI that increase with increasing fuel sensitivity (when *S*>0), indicating that, for a fuel with a high RON, a large sensitivity produces better anti-knock properties than less sensitive fuels under these conditions [75].

Alkanes (paraffins) typically compose 30-80% of gasoline by volume and display very low sensitivities due to characteristic NTC behaviour [77,78]. Of these, normal alkanes (straight-chain alkanes) have the lowest octane ratings, with a decreasing octane quality with increasing chain length. Normal alkanes are not generally found in large amounts in typical gasolines, however iso-alkanes which have a higher relative octane rating are present in much higher quantities [3]. Gasolines and primary reference fuels (PRFs), a gasoline surrogate produced by blending iso-octane and n-heptane to match a gasolines RON/MON, which are largely composed of alkanes, will therefore also display a low sensitivity, indicating poor anti-knock qualities under modern SI engine operating conditions.

Alcohols, aromatics and alkenes (olefins) tend to display much higher sensitivities than alkanes, largely offsetting the adverse impacts of low alkane sensitivity in modern SI engines [75]. Due to pollutant concerns, the gasoline content of aromatics and alkenes is limited by fuel quality legislation. Alkenes have been linked to the formation of photochemical smog through the production of exhaust born intermediate species [79–81]. Aromatics on the other hand, have been shown to increase the emissions of benzene, carbon monoxide and unburnt hydrocarbons [82]. This limits the aromatic content in most common gasolines to <35% by volume, whereas alkenes are generally only found in limited quantities (<20%) due to their poor oxidative stability, which reduces the storage lifetime of the gasoline [3]. The downstream blending of gasoline with

ethanol has also served to increase both RON and sensitivity values. Similarly, the blending of further oxygenated compounds (such as propanol, butanol and pentanol) may achieve further anti-knock enhancements, as well as increasing the biofuel components of modern gasolines. However, the impacts of blending between these oxygenated components and gasolines on the fuels autoignition behaviour is not fully understood, and has seen substantial recent research interest [39,44,47,52,83,84].

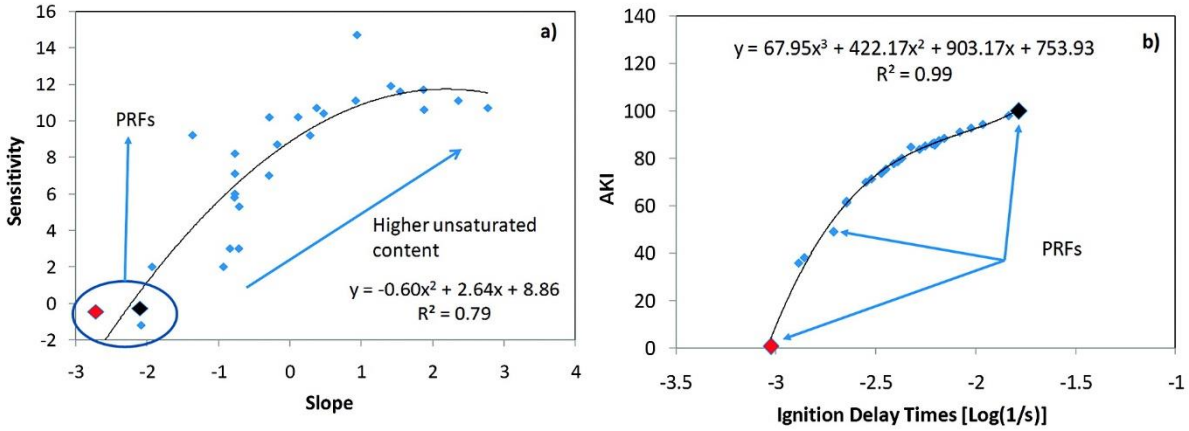

Figure 2.7. Correlations between IDT profile characteristics and octane quality parameters, for a wide range of gasoline surrogates [70].

With relevance to modern engines, it is useful to investigate the autoignition behaviour of a given fuel directly, over a range of engine relevant pressure and temperature conditions which are not completely characterised by bulk octane quality properties (such as ON, S, OI). This can be achieved by measuring the fuel's IDT throughout a temperature and pressure regime [69], where the IDT is defined as the time taken for a fuel to autoignite at a given set of temperature and pressure conditions. The resultant IDT profile displays several characteristics for gasolines and gasoline-like fuels, which can be correlated with octane quality parameters, such as the sensitivity and AKI [65,70]. In the work of Mehl et al. [70], a RON and MON database was produced for a wide range of gasoline surrogate mixtures (containing mixtures of iso-octane, n-heptane, toluene and 1-hexene). IDT simulations were then produced for each of these mixtures, using a zero-dimensional homogeneous constant volume reactor model and a well validated kinetic mechanism [70,85]. From analysis of the RON/MON database and IDT simulations, it was determined that correlations exist between NTC IDT characteristics and octane quality. The slope of the IDT NTC was correlated to the octane sensitivity, as shown in figure 2.7, where a positive slope shows a decrease in IDTs. This correlation shows significant scatter, but a relationship between increasing NTC slope and increasing sensitivity can be observed. This is

due to the sensitivity increasing effect of unsaturated components (aromatics and alkenes), which also suppress the intensity of the NTC [65,70]. A strong correlation was observed in the study between AKI and the IDT at the NTC peak (825 K at 25 bar), as shown in figure 2.7. This establishes a relationship between the octane quality of fuels and their IDT profiles, as well as providing an iterative method for the production of gasoline surrogates [70]. Further work in the literature has shown that bulk octane quality properties, such as RON, MON and OI, can be predicted from both experimental and computationally predicted IDTs at the relevant thermodynamic conditions, for various multi-component gasoline surrogate fuels, whereby the ON can be defined as a linear function of IDT (and coefficients which vary throughout the temperature and pressure regime) [71,72].

2.3 Rapid Compression Machines

Ignition studies can provide important scientific insight into both fuel dependent engine relevant phenomena, such as low temperature combustion and engine knock, and the underlying chemistry which drives these processes. As SI engines trend towards smaller, pressure boosted technologies (engine downsizing), combined with the need for an increase of bio-derived transport fuels and the associated fuel diversity, these studies gain an increased significance. Many fuels which show a high potential for use in SI engines, such as alcohols and their blends with gasoline, are not well characterised under these conditions, driving a need for comprehensive ignition studies of these fuels.

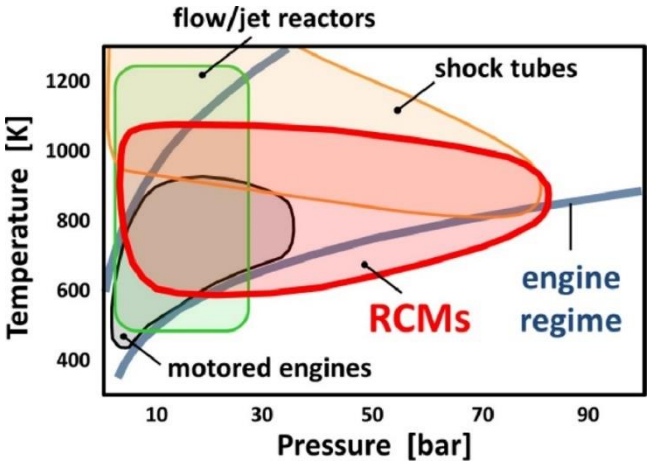

Figure 2.8. Typical temperature and pressure regimes covered by the operating conditions of various experimental devices [86].

A variety of methods can be used to undertake these studies, including: flow/jet reactors [87], motored/skip-fired engines [88], shock tubes [89] and RCMs [48]. These techniques see

such prevalent use as they aim to remove the influence of complex processes such as fuel mixing, evaporation, and turbulence on the autoignition behaviour, allowing studies to focus on the kinetic phenomena of interest. Furthermore, they cover conditions of low temperature and pressure – a region of significant interest due to its relevance to the low temperature, pressure boosted engine combustion environment. RCMs cover a large range of thermodynamic conditions relevant to the engine regime, as shown in figure 2.8, ranging from low to intermediate temperatures (approximately 400-1200 K) and low to high pressures (typically 5-80 bar) [86]. An RCM is, in theory, an ideal homogeneous reactor designed to produce the adiabatic compression of a given fuel/air mixture by a rapidly moving piston, to a predetermined temperature and pressure condition. At the end of compression (EOC), the piston is fixed in place, maintaining the pressure and temperature of the reactor vessel, allowing observation of the fuel mixture's autoignition behaviour by direct measurement of the reaction chamber pressure. This equipment can therefore provide an analogy for a single compression stroke of an IC engine, free of complex engine phenomena such as cyclic variation, residual gas influence and swirl bowl geometry [48]. Due to the temperature and pressure region which RCMs may operate in, they are capable of investigating several fuel specific effects in the low to intermediate temperature regime, including multi-stage ignition behaviour and the IDT NTC region [90–92]. Characteristic examples of these behaviours are shown in figure 2.9, the kinetics of which are explained in section 2.5.

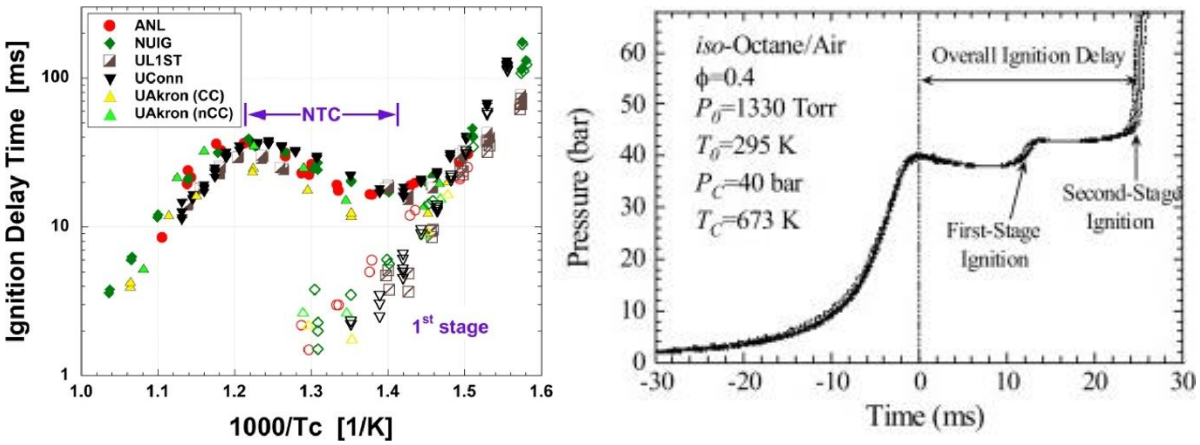

Figure 2.9. Examples of IDT NTC behaviour (left image) and two stage ignition (right image), as captured by RCM experiments [48,86].

By applying the adiabatic core hypothesis, the EOC temperature and pressure conditions in the RCM can be manipulated by control of the initial temperature, pressure and diluent gas composition [93,94]. This hypothesis states that during the compression of the reactive gas,

heat loss only occurs through a thin boundary layer in contact with the reactor walls, while the central core gas is unaffected, with a uniform temperature field. Calculation of the EOC conditions with relevance to the adiabatic core hypothesis are contained in section 3.3.2. IDTs are typically measured relative to the EOC temperatures, pressures, and equivalence ratio, allowing for the production of comprehensive IDT profiles (like that seen in figure 2.8). These profiles provide important information about a fuels autoignitive properties and knock resistance [85], with longer IDTs indicating less propensity for autoignition. They also provide validation targets for the development of chemical kinetic mechanisms in a thermodynamic region of high importance.

While recent shock tube efforts have achieved measurements of IDT up to 50 ms [89], shock tubes are typically used to investigate IDTs of <2 ms [86]. The RCM is capable of experimental durations typically much longer than those seen in shock tubes, with engine applicable fuel loading [95]. This experimental duration for RCMs is typically 2-150 ms, but is largely dependent on the RCM facility used and the ability of this RCM to create and maintain well specified thermochemical conditions within the reaction chamber for a relatively long period of time [86,96]. While the RCM is in theory an ideal, homogeneous reactor, several facility dependent effects and complex fluid mechanics are present in reality. These must be accounted for or minimised to facilitate the production of accurate IDT results and comparisons between RCM facilities.

2.3.1 Facility Effects

Despite the highly repeatable nature of RCM experiments and similarities in operational technique, it can be observed through literature sources that experiments under similar conditions, but produced in different facilities, are significantly different [97–101]. This makes the interpretation of RCM data found in the literature difficult, as it is often not accompanied by the characteristic errors and uncertainties. Heat losses from the combustion chamber post-compression and radical production during compression provide a degree of uncertainty in the final IDT measurement, but these are typically accounted for by the production of “non-reactive” pressure traces [48,86], as described in section 3.3.3. A further large source of uncertainty in IDT measurements is the degree of homogeneity of the combustion chamber environment, which may vary considerably between different RCM designs and is largely affected by complex fluid dynamics initiated by the piston compression event [48,100,102]. The influence of fluid dynamic effects on the measured IDT is more difficult to account for and detect than the presence of heat losses and compression radical formation, as it does not always produce a

clearly observable effect on the RCM pressure trace (a history of transient pressure measurements within the reaction chamber). However, these effects may cause the ultimate failure of the adiabatic core hypothesis due to mixing of the hot core and cool boundary layer gases, making the accurate determination of temperature difficult.

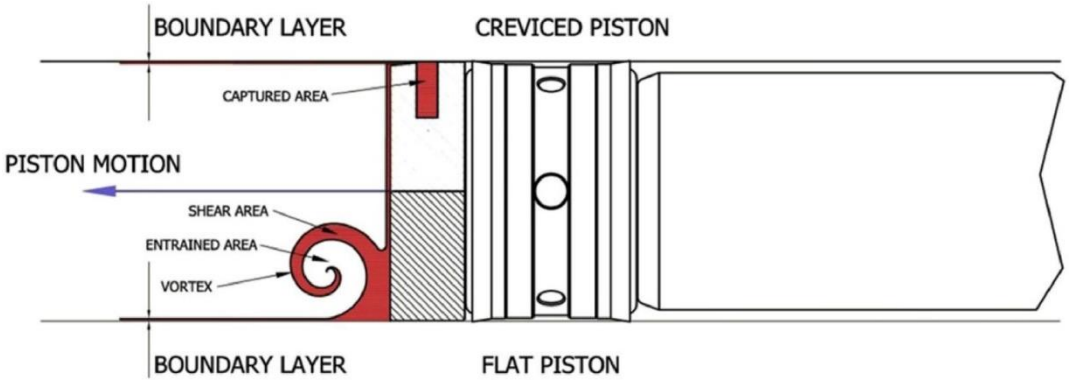

Figure 2.10. An illustration of the formation of roll-up vortices during the compression of a flat piston and containment of the boundary layer by a creviced piston [48].

Inhomogeneities in the reaction chamber, due to fluid motion during the compression stage, have been observed as far back as the 1950's, when Schlieren and direct imaging techniques observed non-uniformities within the reaction chamber due to the interaction of the piston and the boundary layer gas [103,104]. This interaction results in the creation of a roll-up vortex, which mixes cooler gas from the boundary layer with hot gases in the adiabatic core region, as shown in figure 2.10 [105]. In the study of Clarkson et al. [106] it was observed, by the application of Rayleigh scattering and acetone laser induced fluorescence to image the temperature field within the RCM reactor, that by the EOC, roll-up vortices had penetrated the centre of the core gas. The resultant temperature difference between the hot gases and the cool roll-up vortices gases was estimated to be 50 K [106]. It is clear from these results that the influence of these vortices on the homogeneity of the temperature environment is significant. Griffiths et al. [107] showed that, for di-tert-butyl peroxide, reactions proceeded faster in these localised regions of higher temperature. These observations have been reinforced by further experimental measurements [108–110] and multidimensional simulation results [102,111–113], which display the presence of similarly induced inhomogeneities.

To limit the influence of detrimental fluid motion on the development of a uniform reactor environment, Park and Keck [105] made a series of recommendations for RCM design. For the RCM design applied in their study, it was shown through scaling analysis that the piston velocity should be limited to 10-20 m/s to maintain a laminar boundary layer during compression and

avoid any heating of the gas mixture by sound waves, potentially generated by high piston velocities. To reduce the mixing of the boundary layer with the hot core gas, Park and Keck [105] proposed the addition of a crevice around the circumference of the piston head. This crevice provides a volume in which the boundary layer can be captured during the piston motion. An example of this creviced design can be seen, compared to a flat piston head, in figure 2.10. This original crevice design was further developed, for the same RCM configuration, by Lee and Hochgreb [102]. Several design recommendations were given with respect to the geometry of the creviced piston, stating that: the crevice volume should be large enough to contain the boundary layer gas during compression; the crevice should be shaped such that boundary layer gases are quickly cooled upon entering the crevice (preventing reactivity in these gases); and the clearance between the piston bore and reaction chamber wall should be sufficient to capture the full boundary, but small enough to limit the backflow of the boundary into the chamber after compression [102]. Similar recommendations have been validated by the use of computational fluid dynamic (CFD) modelling [100,114]. A novel sabot shaped floating piston head has also been applied to effectively capture the boundary layer gases, utilising similar principles [115].

Crevice geometry was further optimised to improve reactor homogeneity in several studies, including the work of Mittal and Sung [116] and Würmel and Simmie [100], where CFD simulations of several crevice geometries were performed, utilising laminar flow and k-ε models, respectively. From these studies, the optimal crevice volume was found to be between 9-14 % of the reaction chamber volume and was dependent on the diluent gasses used. It was also shown that, increasing the length of the crevice inlet channel does not affect the fluid mechanics of boundary layer capture, but does produce a cooler captured gas. Würmel and Simmie [100] showed that the optimal geometry for this channel (in terms of boundary layer capture) was rectangular, with an optimum depth of 1.0 mm and length of 4 mm. Channel depths greater than 1.5 mm captured more boundary layer gas due to a more unrestricted flow, but the gas captured become hotter with increasing channel depth and a backflow of this gas into the reaction chamber was observed. While an angled design was seen to help somewhat with cooling of the crevice gas, it provided no obvious improvements in the homogeneity of the resultant temperature field [100].

The effectiveness of the creviced piston design was further investigated experimentally. Mittal and Sung [114] applied the recommendations of their CFD modelling study [116] to produce an optimised creviced piston, the influence of which on the temperature environments was investigated. Acetone planar laser induced fluorescence (PLIF) measurements for RCM

compression with a flat and creviced piston head showed that the flat piston head produced significant mixing of the cool boundary layer gas with the hot core gas, as shown in figure 2.11. These PLIF measurements were taken at a compressed pressure of 39.5 bar and a compressed temperature of 770 K. The creviced piston displayed none of this temperature mixing up to a time of 200 ms after the EOC [114], producing a uniform temperature field. However, at timescales longer than 200 ms the uniformity of the temperature field decayed significantly for the creviced piston also, due to mass transfer between the crevice and reaction chamber gases. Furthermore, the introduction of a creviced piston may cause additional multidimensional effects, which impact the integrity of zero dimensional modelling approaches in these cases [48,117–119]. This includes mass flow from the main reaction chamber to the crevice volume during cases of multi-stage ignition, which causes a reduction in the measured pressure rise and may affect the determination of IDT in these cases [117,120,121]. Several studies have applied crevice containment techniques in an effort to eliminate mass transfer between the reactor and crevice post-compression, physically separating the crevice volume from the reaction chamber with a seal [120]. This technique has been shown to produce a significant reduction in the post-compression pressure drop [120,121].

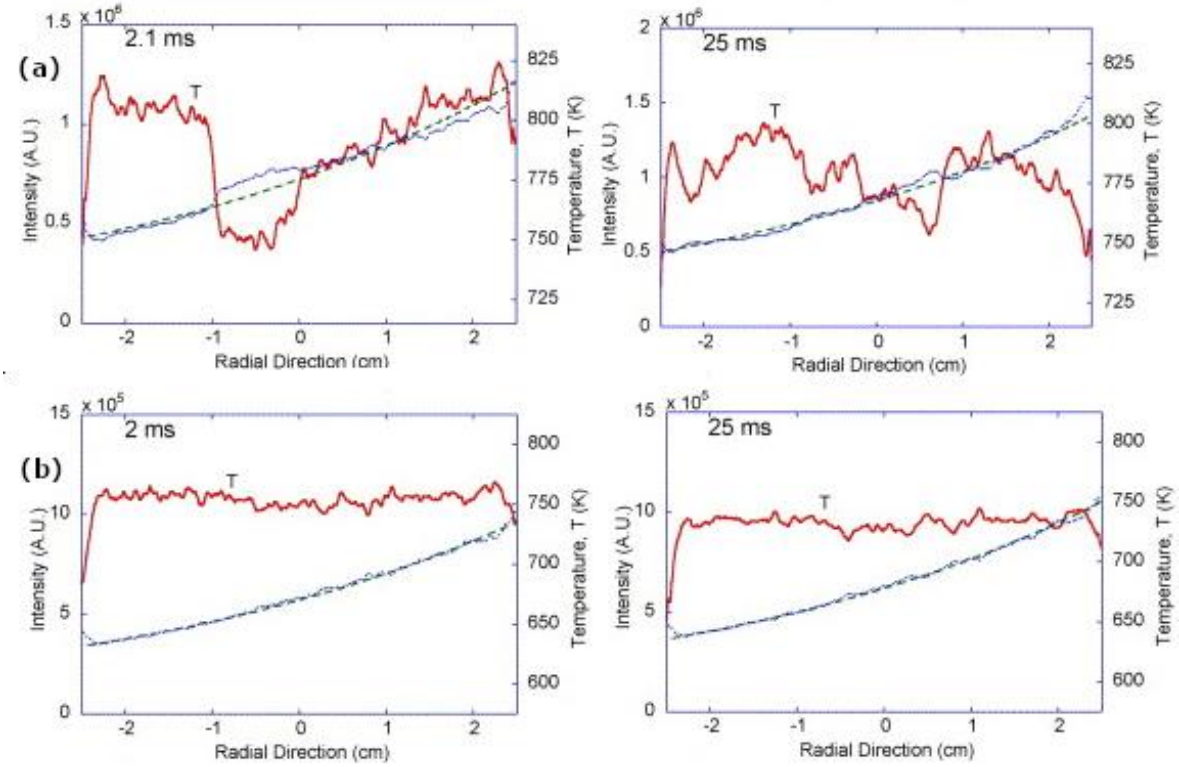

Figure 2.11. Acetone PLIF intensities and the corresponding derived temperature distributions for (a)-a flat piston head and (b)-a creviced piston head, at 2 and 25 ms after the EOC. Solid

grey lines show the measured fluorescence intensities. Dashed grey lines show the fluorescence intensity for a fully homogeneous temperature environment. Red lines show the temperature distribution. Measurements made at T_c=770 K and P_c=39.5 bar. Adapted from [114].

2.4 Mild Ignition

The suppression of roll-up vortices and the generation of a uniform temperature field within the reaction chamber are also important for the prevention of mild ignition within RCMs [103,104]. Mild ignition refers to a process wherein a single or multiple flame kernels develop, producing a distinguishable flame front. This deflagrative process can be observed in RCM pressure measurements and may then transition into an autoignition as the unburnt gas is compressed and heated by propagating flame fronts. The resultant autoignition is characteristically strong, as a result of the elevated pressure and temperature conditions within the chamber, and may result in complex behaviour such as knock, pressure oscillations and detonation [86]. IDT measurements made in the presence mild ignition (also termed as weak ignition or pre-ignition in the literature) are characteristically shorter than homogeneous autoignition cases and may introduce a high degree of variability in IDT measurements [122]. When mild ignition is unaccounted for, or if efforts have not been made to eliminate it, significant IDT discrepancies may be observed between RCMs [86].

Optical access RCMs have been utilised to study the development of mild ignition by high-speed direct imaging of the ignition event [123–127]. Mild ignition was observed intermittently for iso-octane in an RCM, during the investigation of compressed temperatures of 900-1020 K, compressed pressures of 9-15 bar and equivalence ratios of 0.2-2.0 [124], as shown in figure 2.12. Images taken during mild ignition cases of iso-octane displayed a propagating deflagration flame front, corresponding to a preignition pressure rise (also termed pre-ignition heat release). This then transitioned to an autoignition at pressure and temperature conditions higher than the EOC conditions. Similar behaviour was observed for a wide range of syngas blends in the same RCM [123]. For the purpose of modelling and analysis, it was suggested that the deflagrative stage of the mild ignition behaviour be taken into account empirically by using a time integrated average temperature and pressure condition, from the EOC to the time of maximum pressure rise [124,128]. For iso-octane, this produced similar experimental results and kinetic model predictions. Walton et al. [124] also proposed that fuel mixtures with higher thermal diffusivities are less susceptible to mild ignition, as local inhomogeneities can be homogenised more effectively before hot-spots develop.

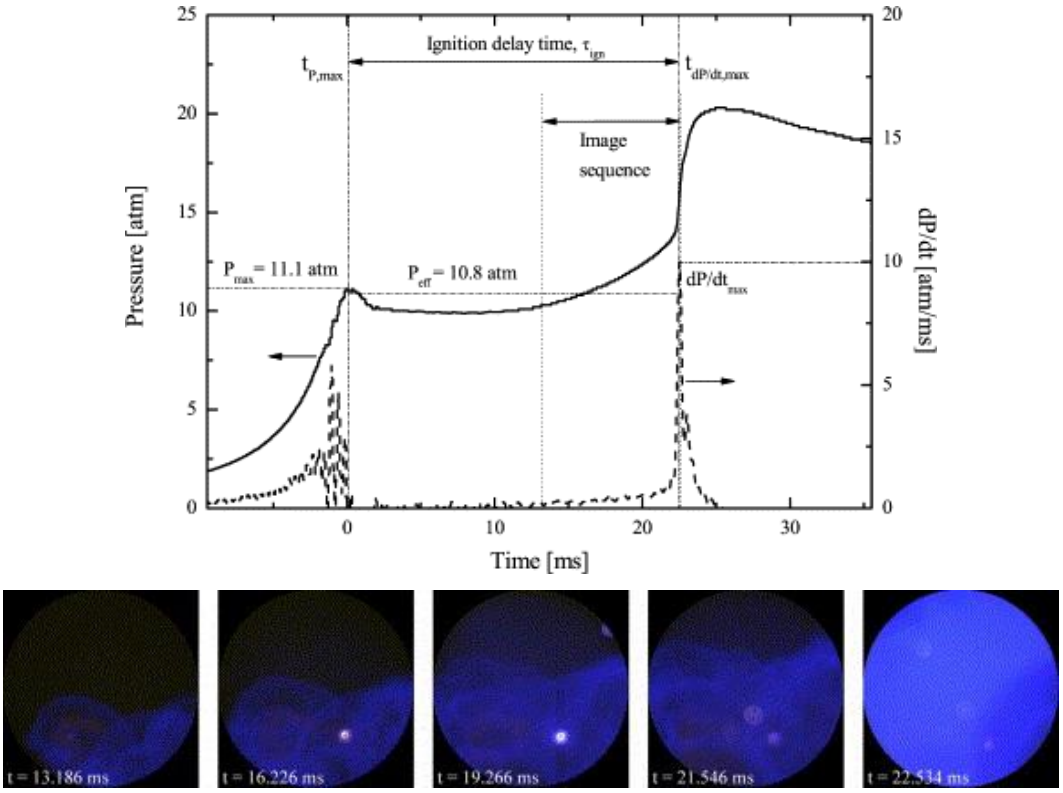

Figure 2.12. RCM pressure-time profile for a mild ignition case of iso-octane fuel and the corresponding image sequence. Compressed conditions of T_c=917 K, P_c=10.8 bar, Φ=0.2. From the study of Walton et al. [124].

The non-uniform thermal gradient within the reaction chamber required to initiate mild ignition was shown in several studies to be quite low. For syngas mixtures in an RCM, at compressed temperatures of 950-1150 K, compressed pressures of 3-15.2 bar and equivalence ratios of 0.1-0.5, Mansfield and Wooldridge [125] found that thermal gradients of approximately 5 K/mm correlated well with the boundary of mild ignition and strong autoignition. In a further investigation of iso-octane mild ignition, over a wide range of RCM operating conditions, it was also found that thermal gradients which facilitated mild ignition were within the region of 5-10 K/mm [126]. This latter study collated three separate datasets for iso-octane, from RCM and shock-tube experiments which exhibited mild ignition and found that this thermal gradient was in good agreement between all datasets [126,128,129]. These ignition boundary thermal gradients are nearing the levels measured within the adiabatic core for well-controlled reaction chambers, that would otherwise be described as homogeneous and apply the use of a creviced piston [86]. Griffiths et al. [130] showed through chemiluminescence imaging of n-pentane autoignition that, at temperature conditions outside of the NTC region, a non-uniform temperature field initiates ignition in local hot regions, whereas in the NTC region reactions may develop faster in cooler

regions of mixed gas. This means that, for fuels which exhibit an NTC, this behaviour can homogenise the temperature field prior to autoignition. A similar smoothing of spatial temperature inhomogeneities due to multistage ignition was witnessed in iso-octane autoignition, by use of direct thermocouple measurements by Desgroux et al. [110]. Based on these findings, it is evident that the measures commonly taken in RCMs to avoid the development of a non-uniform temperature field may not be entirely sufficient, and care must be taken when undertaking experiments under conditions where mild ignition is likely to occur. Particularly in the low temperature, high pressure region, when investigating fuels which display a high degree of temperature sensitivity such as ethanol and toluene, as inhomogeneous ignition cases appear to be more prevalent in this regime [131,132]. During experimentation, it is common to observe non-uniform ignition cases, identified by the distinctive gradual pressure rise prior to ignition. This method is somewhat flawed, as markers directly observed within pressure measurements are not always clear and it relies on the experience of the user conducting experiments. Therefore, analytical methods which are capable of reliably identifying and characterising inhomogeneous ignitions could improve the quality of recorded IDT data. Furthermore, such methods may be applied to historical data to identify the influence of mild ignition on IDT measurements. This is of particularly importance as detailed kinetic mechanism are often validated against such historical datasets, meaning that non-uniform ignition cases may propagate errors in the computational modelling of uniform autoignition.

2.5 Autoignition Chemistry

The oxidation of fuels, and thus the fuel's autoignition, is often a complex chemical process described by several thousand individual elementary reactions. This process is driven by the production and consumption of highly reactive radical species, such as OH, HO_2, CH_3, O and H. The pool of these species evolves during the changing temperatures and pressures of the combustion process through a self-accelerating chain reaction mechanism. Throughout the engine relevant temperature region, reaction exothermicity further accelerates this process, with typically slower fuel oxidation reactions occurring in the low temperature region and faster, explosive reactions occurring once higher temperatures are achieved [133]. Four classifications of radical reactions are often applied to characterise the chain reaction mechanism: chain initiation, chain propagation, chain branching and chain termination.

Chain initiation steps describe the initial generation of radical species through the dissociation of reactants. To initialise the chain mechanism process, energy input into the system must be larger than the minimum activation energy of the primary endothermic initiation

reactions between fuel species and molecular oxygen or radical species [134]. In an RCM or an SI engine, this energy is provided by the compression of the fuel/air mixture, increasing temperature and pressure conditions within the gas. New radicals may also be generated by secondary initiation of stable intermediate products in secondary chain initiation or degenerate branching. In chain propagation steps, an equal number of radicals are both consumed and produced through exothermic reactions, maintaining the current reaction pool. A chain branching reaction produces more radical species than it consumes, increasing the size of the radical pool. These produced radical species can then further propagate or branch the chain mechanism, producing an exponentially increasing pool of radical species. Finally, chain termination reactions remove radicals from the pool, forming stable species from more reactive radical species [53,135]. As chain branching reactions create a sufficiently large radical pool to overwhelm chain termination reactions, oxidation rapidly accelerates and ultimately autoignition occurs. This means that the IDT for a fuel is primarily controlled by low temperature reactions and their influence on the radical pool.

2.5.1 Hydrocarbons

Understanding the low temperature oxidation behaviour of hydrocarbons is important for the determination of end gas autoignition in SI engines and RCMs, due to the important role chain mechanism processes play at these temperatures. When attempting to develop an understanding and unpick the complex chemistry which governs behaviours such as autoignition and LTHR during the analyses produced within this study, knowledge of the general mechanisms driving this behaviour are necessary. This allows for the identification and discussion of key reaction pathways, as identified via sensitivity analysis techniques, which may warrant further research, as well as providing a basis for a kinetic analysis of blending influences on the autoignition behaviour. The low to intermediate temperature region in these cases can be described as 500-1200 K, with the high temperature region describing temperatures >1200 K [136]. Primary low temperature oxidation pathways for hydrocarbons are shown in figure 2.13. The initiation of low temperature autoignition is believed to occur primarily through the hydrogen abstraction of a fuel molecule (denoted RH, where H shows a hydrogen atom bonded to a fuel radical R). Dependent on the size of the fuel molecule, abstraction can occur at many sites, with rates for each site dictated by the bond dissociation energy (BDE) at said sites. Initially, it is thought that these reactions occur through the relatively slow reaction of the fuel molecule with molecular oxygen:

$$RH + O_2 \rightarrow R + H\dot{O}_2 \qquad \text{Equation 2.6}$$

However, as the chain reaction mechanism progresses towards autoignition, hydrogen abstraction through OH and other radical species dominates the generation of a fuel radical pool, due to the much faster rates of reaction. The rate of this hydrogen abstraction is dependent on the strength of the C-H bond (described by the BDE) being attacked by the OH radical, with abstractions for the weaker site typically preferred. This process is why long, straight chain hydrocarbons tend to produce shorter IDTs, as the further the C-H bond gets from the primary site, the weaker the bond tends to be. Branching of the hydrocarbon structure increases the amount of primary C-H sites, typically reducing the species' propensity for autoignition.

$$RH + \dot{O}H \rightarrow R + H_2O \qquad \text{Equation 2.7}$$

In particular, the hydrogen abstraction due to OH radicals is well understood and can be used to predict the relative populations of fuel radical isomers [137]. These fuel radicals (R) (also termed alkyl radicals) may then undergo a chain of reactions which characterise the low temperature autoignition of hydrocarbons.

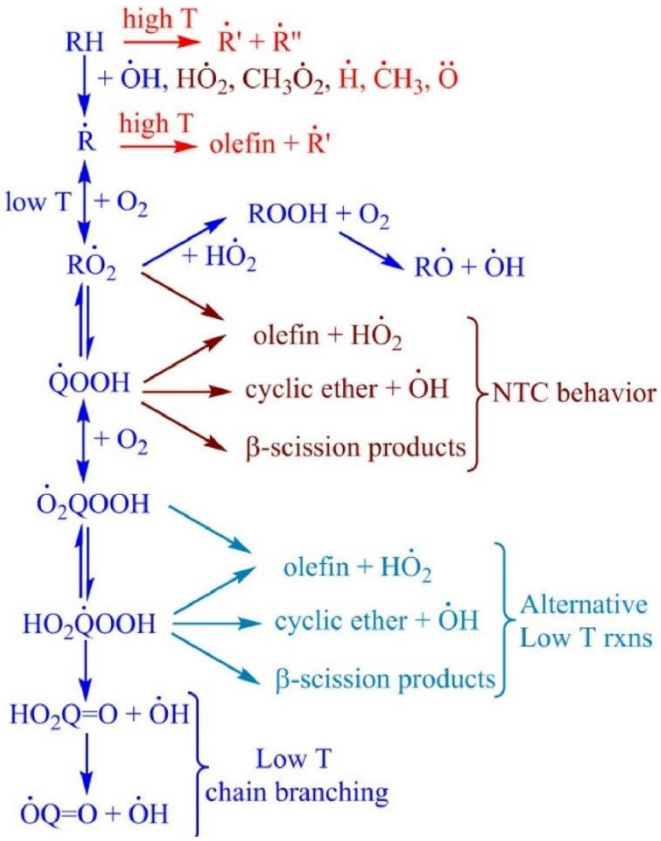

Figure 2.13. A general mechanism of oxidation pathways for hydrocarbons [136].

After the initial hydrogen abstraction reaction, fuel radicals may react with molecular oxygen to produce alkylperoxy radicals, RO_2:

$$\dot{R} + O_2 \leftrightarrow R\dot{O}_2$$ Equation 2.8

At low temperatures, this reaction progresses forwards, towards the production of alkylperoxy radicals. However, as temperatures increase the forward activation energy becomes larger, and equilibrium trends towards the reactants. At intermediate temperatures (850-1200 K), this may lead to the production hydroperoxyl (HO_2) and an alkene/olefin from the reactants. This is considered a chain termination reaction due to the relatively low reactivity of HO_2 at these temperatures, in comparison to OH.

$$\dot{R} + O_2 \leftrightarrow \text{alkene} + H\dot{O}_2$$ Equation 2.9

At these intermediate temperatures, HO_2 radicals typically abstract a further hydrogen to form hydrogen peroxide (H_2O_2), which is largely unreactive at these temperatures. However, H_2O_2 is a critical species as temperatures increase, dissociating into two OH radicals. Alkylperoxy radicals undergo a number of reactions, generally dependent on temperature and pressure conditions. The most relevant reaction for the chain branching process is the isomerisation of the RO_2 species via internal hydrogen abstraction onto the oxygen radical site through a transition state ring. This results in the formation of a hydroperoxyalkyl radical (QOOH, where $Q=R_{H-1}$):

$$R\dot{O}_2 \leftrightarrow \dot{Q}OOH$$ Equation 2.10

This internal isomerisation has a significant impact on the rate of oxidation for a species, as the higher the tendency for isomerisation, the faster the production of radicals from chain branching pathways. However, the alkylperoxy radicals can also proceed through several other reactions, dependent on thermodynamic conditions, which provide access to reactions typical of NTC behaviour. One such reaction is simply the reverse of the formation reaction; dissociating to produce the original fuel radical and molecular oxygen reactants. Also, both the alkylperoxy and QOOH radicals may dissociate to produce alkene and HO_2 species:

$$R\dot{O}_2 \rightarrow \text{alkene} + HO_2$$ Equation 2.11

$$\dot{Q}OOH \rightarrow \text{alkene} + HO_2$$ Equation 2.12

It has been shown that the primary means of HO_2 production during the oxidation process is typically through this decomposition of the alkylperoxy radical [138,139]. This is an important reaction for the low temperature autoignition of hydrocarbons as the channel is chain terminating and partially responsible for the observed NTC region, where increasing temperatures correspond to an increase in IDT. Other reactions important to this behaviour can also be observed in the fate of QOOH radicals, as the formation of cyclic ethers and β-scissions products, combined with the concerted elimination of an alkene and HO_2 from alkylperoxy and QOOH species, only produce one radical species from the previously consumed radical. QOOH species are very weakly bound intermediate species, which were not observed until recently [140].

$$\dot{Q}OOH \rightarrow \beta - \text{scission products} \qquad \text{Equation 2.13}$$

$$\dot{Q}OOH \rightarrow \text{cyclic ether} + OH \qquad \text{Equation 2.14}$$

This makes these pathways chain terminating, reducing reactivity as temperature increases in the NTC region. HO_2 is eliminated to produce H_2O_2 as previously stated, which is stable up to high temperatures, removing radicals from the pool and slowing the overall autoignition reaction. As pressure increases, the importance of this reaction is lessened [141]. The final relevant reaction of the alkylperoxy species is reaction with HO_2 radicals. This reaction forms an alkyl hydroperoxide (ROOH) and molecular oxygen. Again, this reaction is crucial in the determination of ignition phenomena as alkyl hydroperoxide species go on to dissociate into RO radicals and OH radicals, which are important in the chain branching process as they generate multiple radicals.

$$R\dot{O}_2 + HO_2 \rightarrow ROOH + O_2 \qquad \text{Equation 2.15}$$

$$ROOH \rightarrow R\dot{O} + OH \qquad \text{Equation 2.16}$$

QOOH can also progress the chain reaction through a second oxygen addition to produce a O_2QOOH species:

$$\dot{Q}OOH + O_2 \leftrightarrow \dot{O}_2QOOH \qquad \text{Equation 2.17}$$

The O_2QOOH radicals behave similarly to the RO_2 radicals, so far as they can react through the elimination of HO_2 and undergo a further isomerisation. This second isomerisation also propagates through internal hydrogen abstraction via a transition state ring, to form a HO_2POOH (where $P=Q_{H-1}$):

$$\dot{O}_2QOOH \rightarrow \text{alkene} + HO_2 \quad \text{Equation 2.18}$$

$$\dot{O}_2QOOH \leftrightarrow HO_2POOH \quad \text{Equation 2.19}$$

These HO_2POOH radicals react similarly to QOOH radicals. Undergoing HO_2 elimination, β-scission, and the production of cyclic ethers and OH radicals, which have been discussed previously. However, they can also react through dissociation into ketohydroperoxides and more OH radicals, assisting in chain propagation through the creation of highly reactive radicals. The ketohydroperoxides then decompose further to form more OH and fuel radicals.

$$HO_2POOH \rightarrow \text{alkene} + HO_2 \quad \text{Equation 2.20}$$

$$HO_2POOH \rightarrow \beta - \text{scission products} \quad \text{Equation 2.21}$$

$$HO_2POOH \rightarrow \text{cyclic ether} + OH \quad \text{Equation 2.22}$$

$$HO_2POOH \rightarrow \text{ketohydroperoxide} + OH \quad \text{Equation 2.23}$$

$$\text{ketohydroperoxide} \rightarrow \dot{O}PO + OH \quad \text{Equation 2.24}$$

This process is described comprehensively in literature [136,142,143], with recent advancements in understanding [144]. There also exists direct pathways which may skip some of these elementary reactions, such as the direct HO_2 elimination from fuel radicals and molecular oxygen reactions. The proportion of reactions which takes place through these direct pathways is dependent on pressure and temperature conditions.

At high temperatures (>1200 K), the initial fuel species (RH) may undergo thermal decomposition to produce multiple radical species through the breaking of either C-C or C-H bonds [134], as shown in figure 2.13. Alkyl radicals (R) can also further decay into smaller alkyl radicals, which in turn decompose to produce a alkenes and hydrogen atoms. This hydrogen may combine with an oxygen molecule to form OH and O radicals, which further abstract hydrogens from the fuel species. At these temperatures, previously formed hydrogen peroxide (H_2O_2) also decomposes to produce two OH radicals. These steps are largely chain branching and accelerate the combustion to completion [136,145].

2.5.2 Alcohols

While the oxidation mechanism outline given in figure 2.13 is a reasonable approximation for the low temperature autoignition of hydrocarbons, there are key differences between the

mechanism with respect to alkanes and oxygenated hydrocarbons such as alcohols. Blending of alcohols with conventional fuels can alter their combustion behaviour, producing changes in the anti-knock properties of fuel blends. Therefore, it is important to understand the differences in the mechanism for alcohol autoignition, when compared to that of alkanes and other general hydrocarbons. The properties of alcohols open up new reaction pathways and alter the branching ratios of existing pathways during the autoignition of fuel blends, which may produce observable changes in autoignition behaviour due to the influence of alcohol blending agents. This study aims to investigate the impacts of iso-butanol blending on the ignition and heat release behaviour of gasoline and its surrogate, including a kinetic investigation of the chemistry driving the observed blending behaviour. Therefore, an understanding of the general reaction pathways driving the autoignition process for alcohols is required, alongside an understanding of other general fuel hydrocarbon species.

The unique thermochemical properties of alcohols, in comparison to other hydrocarbons, are due to the presence of a hydroxyl moiety (-OH) connected to a hydrocarbon chain. This leads to a weaker C-H bond strength where the carbon is bonded to the –OH and allows for hydrogen bonding interactions when reacting with OH and HO_2 radicals. The strength of each bond in the alcohol structure can be represented through the BDE, which is defined as the standard enthalpy change (per mole) due to the cleaving of a bond through homolysis. The BDEs for the four butanol isomers can be seen below in Figure 2.14.

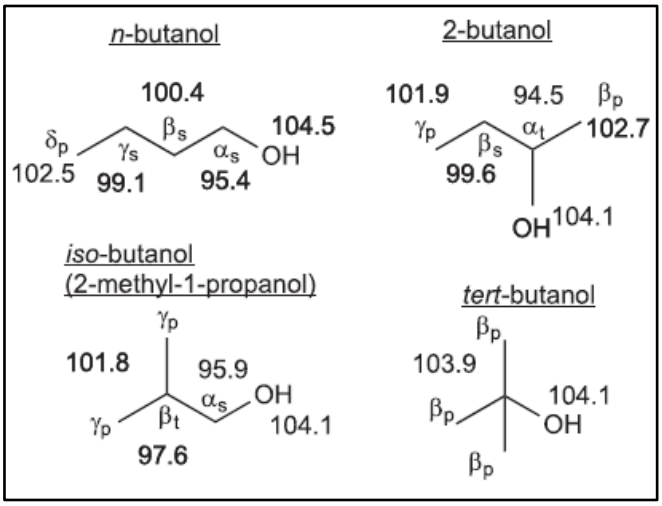

Figure 2.14. Calculated BDEs (at CBS-QB3 level theory) for the four isomers of butanol in kcal/mole [84].

It can be seen that, for alcohols, it is difficult to abstract hydrogen atoms from the O-H site due to the strong BDE. In contrast, the C-H BDE of the carbon connect to the –OH (known as

the adjacent α site) is weakened by the hydroxyl moiety, making the hydrogen atom easier to abstract. As shown in figure 2.14, the hydrogen bonds at the α site have the lowest BDE of all the C-H bonds, making them the easiest to abstract in the molecule. When compared to iso and n-butanol, the BDE for the α site of sec-butanol is lower, meaning that the rate of hydrogen abstraction from this site for sec-butanol will be higher than in n and iso-butanol. This follows the general trend for alcohols that the hydrogen abstraction rates, on a per H atom basis, are described as primary α < secondary α (n and iso-butanol) < tertiary α (sec-butanol). The next H abstraction site, β, exhibits higher BDEs for alcohols than would be expected in other hydrocarbons due to the weakened adjacent α site [146]. Beyond this, the abstraction rates from further sites can be assumed to be established from the same rules as alkane fuels [84].

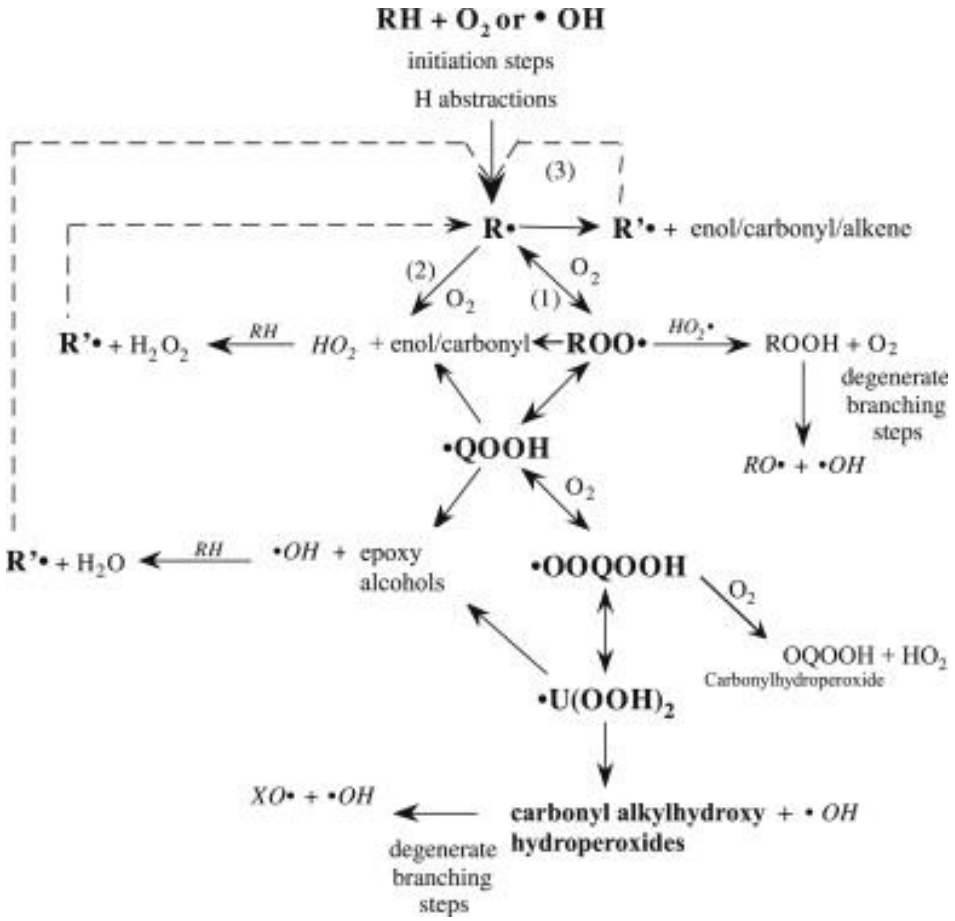

Figure 2.15. A general mechanism of oxidation pathways for alcohols [84,147].

A general oxidation pathway diagram for alcohols can be seen in figure 2.15. Alcohol autoignition proceeds through the formation of hydroxyalkyl radicals (R) and reactions with molecular oxygen. The formation of RO_2 species (hydroxyalkyl peroxy radicals in the case of alcohols) from hydroxyalkyl radicals is analogous to that of alkanes and other hydrocarbons and

is important in the initiation of the chain branching process. The rate at which these reactions progress is dependent on the species radical site, as is also the case for other hydrocarbons [84]. A key feature of alcohol oxidation is that hydroxyalkyl radicals exhibit a lower potential barrier for interactions with molecular oxygen to produce HO_2 and an aldehyde or ketone, than alkylperoxy radicals. This pathway is in competition with low temperature chain branching channels more typical of hydrocarbon oxidations and may explain the characteristically long IDTs of alcohols [148]. Also, the hydroxyl moiety creates an addition internal abstraction site during the isomerisation of RO_2 radicals. This hydroxyl abstraction site can be significantly favourable and abstraction from this site can lead to the decomposition of the QOOH species into an aldehyde and HO_2 radical [149]. The α C-H bonds are also weaker, leading to a preferential formation of enols rather than hydroxyalkenes, via HO_2 elimination, and β-hydroxyalkyl radicals may dissociate at lower temperatures to produce alkenes and OH radicals [143]. This is a further example of the competition between HO_2 elimination and chain branching pathways from RO_2 species, which reduces the overall proportion of reactions along the chain branching pathway and is a cause for the long IDT of alcohols.

For alcohols, the reaction rates for the isomerisation of RO_2 to QOOH radicals are not well studied and as such are estimated through theoretical calculations for feasible transition state rings. The most important isomerisation reactions consist of five to seven member transition rings, with rate coefficients for this step reliant on the C-H bond broken and the ring strain energy barrier [44]. As the chain branching pathway proceeds, there is more competition in the form of the cyclization of QOOH radicals to form epoxy alcohols and OH radicals. This is analogous to the formation of cyclic ethers in the alkane autoignition scheme and competes directly with the second oxygen addition: a critical chain branching channel. Again, these reaction rates are not well studied so rates for the formation of cyclic ethers from alkanes are typically applied. This is acceptable as these reactions are thought to be minor due to a lack of significant cyclic epoxy alcohol measurements during alcohol combustion [84,150,151]. RO_2 may also undergo a concerted elimination of HO_2, in competition with the internal isomerisation pathway and reducing reactivity in the low to intermediate temperature regime [84]. This occurs through a five membered transition state, wherein the OO moiety leaves the RO_2 molecule, abstracting a hydrogen from an adjacent carbon with it, similar to other hydrocarbons [143].

As mentioned, QOOH undergoes a second oxygen addition in a critical step for the low temperature chain branching pathway, to form O_2QOOH radicals. This step is similar to that seen in the alkane low temperature oxidation pathway. For alcohols, the rate of this second

oxygen addition is dependent on if the carbon radical site is an α, primary, secondary, or tertiary site [84]. Similar to the reactions of hydroxyalkyl species with molecular oxygen to produce an aldehyde/ketone and HO_2, the reaction of O_2QOOH with molecular oxygen is important for inhibiting low temperature reactivity in alcohols. This process produces an OQOOH species and a HO_2 radical. In the n-butanol oxidation system, this reaction has been shown to ultimately lead to chain branching, as the OQOOH species decomposes to produce a further OH radical [84,152,153]. The fourth step in the chain branching pathway for alcohols is the isomerisation of O_2QOOH species to form HO_2POOH, analogous to the same process in hydrocarbon low temperature branching. Similarly, this species then decomposes to an OH radical and a carbonyl hydroxyalkyl hydroperoxide species, which undergoes further decomposition to produce another OH radical, a smaller oxygenated radical and a stable oxygenate, such as a ketone or aldehyde. This is the final step of the low temperature chain branching pathway for alcohols, as multiple radical species are formed from a stable reactant [84].

At high temperatures (>1500 K), unimolecular decomposition of the fuel species is an important reaction for alcohol oxidation. This decomposition consists of simple C-C and C-H bond scissions, similar to those seen for other hydrocarbons. However, in alcohols unimolecular water elimination reactions are also important, with four centred reactions involving β site hydrogen atoms being the most favoured. These reactions result in the formation of an alkene and a water molecule [84,154]. Hydrogen abstractions at high temperatures typically occur via H radicals, as opposed to the large amount of abstraction by OH and HO_2 radicals at lower temperatures. The resultant alcohol fuel radicals may then undergo decomposition via β-scission at high temperatures (>900 K), with products dependent on the bond which undergoes scission. Alcohols and alkenes can be formed through the β-scission of a C-C or C-H bond, whereas the scission of the O-H bond results in the formation of an aldehyde species [84]. These unsaturated intermediate species are formed in large quantities and are important to the oxidation of alcohols at high temperatures, reacting through various mechanisms dependent on their structure. Aldehydes are typically subject to hydrogen abstraction from the weakly bound aldehydic site and a subsequent α scission to form an alkyl radical and carbon monoxide. Enols isomerise slowly in the gas phase due to large energy barriers [155], but may undergo isomerisation if catalysed by HO_2 radicals [156], or tautomerization to form an enol-keto tautomer when catalysed by a hydrogen radical [157]. Enol-keto tautomerization may also be catalysed by carboxylic acids [158]. At high concentrations of HO_2 radicals, enols may also isomerise to aldehydes [156]. Enols may also undergo hydrogen abstractions, unimolecular

decomposition, radical decomposition, and hydrogen addition to double bonds, at high temperatures [84,159,160].

2.6 Chemical Kinetics

The study of chemical kinetics can be broadly described as the exploration of reaction rates, through measurement, interpretation and prediction, and the associated reaction mechanisms. This does not only provide information about the rate at which a reaction or process occurs but can provide information about the driving mechanisms of these processes. For a gas phase, chemically reacting process such as autoignition or combustion, behaviour is determined by the rates of several thousand individual chemical reactions. Like every chemical process, the combustion process is not a single, straight-forward reaction; it is composed of many elementary reactions (or intermediate steps). Each reaction rate is dependent on a series of variables which could include parameters such as temperature, pressure and species concentrations [135,161]. Each elementary reaction is defined such that there are no intermediate steps between the reactants and the products. If we consider a reaction of the form:

$$aA + bB \rightarrow cC + dD \qquad \text{Equation 2.25}$$

where the *X* parameters denote the participant substances and the *x* parameters denote the corresponding stoichiometric numbers, it is straight forward to define a parameter which quantifies the rate of reaction. At a given point in time, the concentration of participant *X* is denoted as [*X*]. Therefore, the rates of reaction (in terms of concentration) for the corresponding substances can be determined as such.

$$-\frac{1}{a}\frac{d[A]}{dt} = -\frac{1}{b}\frac{d[B]}{dt} = \frac{1}{c}\frac{d[C]}{dt} = \frac{1}{d}\frac{d[D]}{dt} \qquad \text{Equation 2.26}$$

However, this definition of reaction rate is unwieldy; having many reaction rates to describe the same elementary reaction. This definition can be improved by introducing the extent of reaction, ξ:

$$\xi = \frac{n_X - n_{X_0}}{x} \qquad \text{Equation 2.27}$$

where n_X and n_{Xo} denote the number of moles of *X* at the time of measurement and the start of reaction, respectively. From this, the rate of reaction can be defined as the rate of change of the extent of reaction:

$$r = \frac{1}{V}\frac{d\xi}{dt}$$ Equation 2.28

where *r* is the rate of reaction and *V* is the volume of the reaction system. From this, it follows that:

$$r = \frac{1}{xV}\frac{dn_X}{dt}$$ Equation 2.29

and for a homogenous reaction in a closed vessel of constant volume:

$$r = \frac{1}{x}\frac{d[X]}{dt} \qquad where, [X] = \frac{n_X}{V}$$ Equation 2.30

In each case there is now a single rate for the reaction, in the form of the earlier derived rates. The relationship between the rate of reaction and the production rates of species can be described by a set of ordinary differential equations (ODEs). These equations are coupled and as such, all equations are needed to solve them simultaneously. This is because the number of equations in the series of ODEs is the same as the number of species [54,135,162].

2.6.1 Rate Laws

A rate law is an equation which expresses the relationship between the rates of a reaction with the concentrations of all the species involved. This can be expressed as a function of the species concentrations:

$$r = f([A], [B], \dots)$$ Equation 2.31

This general rate law expresses that the rate of reaction is proportional to the concentration of the reactants, and can be expressed through the assumption of the rule of mass action kinetics [163]:

$$r = k \prod_j^{N_s} [X]_j^{x_j^L}$$ Equation 2.32

where *k* is defined as the rate constant (or coefficient), $[X]_j$ is the molar concentration of species *j*, x_j^L is the reaction order for species *j* for the "left hand side" of the equation (reactants) and N_s is the total number of species in the reaction. Through this assumption, a form of the rate law for a given reaction can be written, such as:

$$r = k[A]^a[B]^b \dots$$ Equation 2.33

Here the letters *a* and *b* denote the reaction order, with respect to the corresponding species. The total reaction order is simply the sum of the individual reaction orders. In order to find the concentrations of species as a function of time, it is necessary to find the integrated rate law. While trivial for simple, first order rate laws, this can become much more difficult for higher order or more complex rate laws, in which cases it is the integrated rate laws are rarely calculated analytically.

2.6.2 The Rate Coefficient

The rate coefficient is independent of the molar concentration but does vary with temperature and, in some cases, pressure, as well as the quantity and quality of the reactants. It is often found experimentally that the natural log of the rate coefficient varies linearly with 1/*T*, where *T* is the temperature. This relationship is described as Arrhenius, and leads to the modelling of the temperature dependent rate coefficient through the Arrhenius equation (equation 2.35):

$$k = A\ exp(-E_a/RT) \qquad \text{Equation 2.34}$$

where the reaction rate *k* is dependent on the temperature *T*, reaction activation energy E_a and pre-exponential factor *A* [145]. From this equation (equation 2.35) and a plot of ln(*k*) against 1/*T*, the Arrhenius parameters (*A* and E_a) can be determined: the y-intercept will be ln(*A*) and the gradient is $-E_a/R$. The activation energy can be formally defined as the minimum kinetic energy that reactants must have in order to form products. To reach this interpretation of the activation energy, it is useful to consider the chemical reaction between two molecules, A and B, and the associated potential energy changes during the reaction. We will assume that the reaction begins when the two molecules collide. They then begin to interact, changing shape and exchanging atoms. In this transition state, the potential energy of the reaction reaches a maximum, and any small energy increase will push the reaction in the direction of forming products, wherein the potential energy will fall. This maximum can be described as the activation energy, as this is the energy needed to reach the height of the potential barrier and begin the formation of products. By assuming a Boltzmann distribution, we know that the fraction of collisions which will have a kinetic energy high enough to pass over this potential barrier is given by: $e^{-E_a/RT}$, as seen in the Arrhenius equations [164]. The rate of collisions is represented by the pre-exponential factor, *A*. Therefore, the expression $Ae^{-E_a/RT}$ represents the rate at which successful collisions occur. This understanding can be applied through transition state theory (TST), to develop an understanding of the rate constant in terms of fundamental

thermodynamic properties and estimate said rate constants. Principally developed by Henry Eyring in the 1930's, TST explores the peak of the potential energy barrier and the transient species in this region. By following the method shown in the literature [164], TST can be used to provide a definition of the rate constant such that:

$$k(T) = \frac{k_B T}{hc^\circ} e^{-\Delta^* G^\circ / RT} \qquad \text{Equation 2.35}$$

where $\Delta^* G^O$ is the standard Gibb's energy of activation between the reactants and the transition state at the peak of the potential barrier, c^O is the standard state concentration, k_B is the Boltzmann constant and h is the Plank constant. The Gibb's energy can be expressed by fundamental thermodynamic properties:

$$\Delta^* G^\circ = \Delta^* H^\circ - T\Delta^* S^\circ \qquad \text{Equation 2.36}$$

where $\Delta^* H^\circ$ is the standard enthalpy of activation and $\Delta^* S^\circ$ is the standard entropy of activation. This definition can be introduced to the rate constant equation to give:

$$k(T) = \frac{k_B T}{hc^\circ} e^{\Delta^* S^\circ / R} e^{-\Delta^* H^\circ / RT} \qquad \text{Equation 2.37}$$

This definition becomes important when we consider a mixture of perfect gases in thermal equilibrium, such that the properties of the mixture can be considered a sum of the constituent gases. At this point, the equilibrium rate constant can be defined as:

$$k_{eq} = \frac{k_{\rightarrow}}{k_{\leftarrow}} = e^{\Delta S^\circ / R} e^{-\Delta H^\circ / RT} \qquad \text{Equation 2.38}$$

where $k_{->}$, $k_{<-}$ and k_{eq} are the forward, reverse and equilibrium rate constants, respectively.

The standard entropy change, and standard enthalpy change may be calculated if the standard entropy and enthalpy of both the reactants and products are known. For the individual species, these can be calculated through the use of the NASA polynomial coefficients. There are a total of 14 coefficients: 7 for the low temperature regime and 7 for the high temperature regime, which can be used to calculate the specific heat at constant pressure as well as the standard enthalpy and entropy [165].

$$\frac{{C_p}^\circ}{R} = a_1 + a_2 T + a_3 T^2 + a_4 T^3 + a_5 T^4 \qquad \text{Equation 2.39}$$

$$\frac{H^\circ}{RT} = a_1 + \frac{a_2}{2} T + \frac{a_3}{3} T^2 + \frac{a_4}{4} T^3 + \frac{a_5}{5} T^4 + \frac{a_6}{T} \qquad \text{Equation 2.40}$$

$$\frac{S^\circ}{R} = a_1 \ln T + a_2 T + \frac{a_3}{2} T^2 + \frac{a_4}{3} T^3 + \frac{a_5}{4} T^4 + a_1 \qquad \text{Equation 2.41}$$

where a_n are the NASA polynomial coefficients. From this it is understood that the thermodynamic properties of the mixture (and the associated NASA polynomial coefficients) are a driving force behind the value of the rate coefficient, and hence the rate of reaction.

It can also be shown in this proof (as performed by [164]) that the pre-exponential factor is not a constant, and is dependent on temperature. This is accounted for in the modified Arrhenius equation:

$$k = A\, T^n exp(-E_a/RT) \qquad \text{Equation 2.42}$$

2.6.3 Pressure Dependence of the Rate Coefficient

Unimolecular reactions, such as thermal decomposition and isomerisation, require collision with another body (the third body, *M*) to take place and proceed to the formation of products. This is shown by the Lindemann mechanism, wherein the unimolecular reaction is described by three elementary reactions, shown in equations 2.44-2.46. The first of these elementary reactions is the forward reaction, which describes the activation of molecule *A* via collision with the third body molecule *M*. This excites the molecule *A* to *A**, an excited reactant which has enough energy to overcome the potential energy barrier required to undergo a given unimolecular reaction.

$$A + M \rightarrow A^* + M \qquad \text{Equation 2.43}$$

The reverse elementary reaction (equation 2.45) describes the loss of energy from the excited *A** molecule through a collision with the third body molecule *M*, to produce the molecule *A*. Whereas equation 2.46 shows the unimolecular reaction of the excited *A** molecule to form reaction products [166].

$$A^* + M \rightarrow A + M \qquad \text{Equation 2.44}$$

$$A^* \rightarrow \text{reaction products}$$

Due to the required presence of a third body (*M*), the rate of these reactions will be dependent on the pressure of this body in the reaction environment [135], as the pressure and concentration of *M* are related ([*M*] = *P*/*RT*). Therefore, it is necessary to produce a rate coefficient expression which illustrates this pressure dependence. This can be determined by using the Lindemann approach to evaluate an intermediate pressure region, utilising Arrhenius

rate parameters for low and high pressure boundary cases. This approach “blends” the two boundary rate expressions to produce a pressure dependent expression [54,161]. This intermediate pressure region may also be referred to as a “fall-off” region and describes a region wherein the reaction rate of unimolecular reactions is neither first nor second order. The boundary Arrhenius expressions are given by:

$$k_0 = A_0 T^{n_0} exp(-E_0/RT) \quad \text{Equation 2.45}$$

at low pressures and

$$k_\infty = A_\infty T^{n_\infty} exp(-E_\infty/RT) \quad \text{Equation 2.46}$$

at high pressures.

The Lindemann expression for the rate coefficient of a fall-off reaction can be written in a general form, such as:

$$k = \frac{k_0[M]}{1+\frac{k_0[M]}{k_\infty}} \quad \text{Equation 2.47}$$

This can be simplified by introducing the dimensionless parameter, reduced pressure (P_r), which can be defined such that:

$$P_r = \frac{k_0[M]}{k_\infty} \quad \text{Equation 2.48}$$

Therefore, the general pressure dependent rate coefficient can be expressed as:

$$k = k_\infty \left(\frac{P_r}{1+P_r}\right) \quad \text{Equation 2.49}$$

While this provides an estimate for the pressure dependent behaviour of some rate coefficients, it is not a sufficient description for applications such as accurate kinetics models. These models need to thoroughly describe the relationship between pressure and the rate of reaction. This can be achieved through the application of the fall-off function, $F(T, P_r)$, such that:

$$k = k_\infty \left(\frac{P_r}{1+P_r}\right) F \quad \text{Equation 2.50}$$

One popular example of a fall-off function is the Troe fall-off function, wherein F is represented as complex expression, seen below.

$$\log F = \log F_{cent} \left[1 + \left[\frac{\log P_r + c}{n - d(\log P_r + c)}\right]^2\right]^{-1} \quad \text{Equation 2.51}$$

where:

$$F_{cent} = (1 - \alpha)\, exp\left(-\frac{T}{T_3}\right) + \alpha\, exp\left(-\frac{T}{T_1}\right) + exp\left(-\frac{T_2}{T}\right)$$

$$c = -0.4 - 0.67 \log F_{cent}$$

$$n = -0.75 - 1.271 \log F_{cent}$$

$$d = 0.14$$

and the parameters α, T_3, T_2 and T_1 are the Troe parameters which must be defined through Troe parameterisation in order to define the fall-off curve properly [54,135]. However, while the Troe fall-off method can accurately represent the pressure dependence of a rate parameter for relatively simple, single well potential energy surface reactions, this method shows an unsatisfactory degree of accuracy for more complex, multiple well, elementary reactions, such as the reactions of molecules which undergo unimolecular isomerisation while fragmenting, to form multiple sets of products [167]. Because of this, in some mechanisms the pressure dependence of rate parameters is calculated using the "PLOG" method.

In the PLOG method, the pressure dependent rate coefficient at a required pressure condition is calculated through the logarithmic interpolation between given Arrhenius rate expressions at discrete pressure conditions, within the pressure range of interest. These Arrhenius rate expressions are defined such that:

$$k(T, P_j) = A_j T^{n_j}\, exp\left(\frac{E_j}{RT}\right) \quad \text{Equation 2.52}$$

for a set of P_j pressures.

When the pressure of interest P lies between the discrete pressure points P_i and P_{i+1}, the pressure of interest can be calculated through the logarithmic interpolation of the specified $k(T,P_j)$ parameters. This can be seen below:

$$\ln k = \ln k_i + (\ln k_{i+1} - \ln k_i)\frac{\ln P - \ln P_i}{\ln P_{i+1} - \ln P_i} \quad \text{Equation 2.53}$$

where k is the rate coefficient for the pressure of interest P and k_i and k_{i+1} are the rate coefficients at the discrete pressure points P_i and P_{i+1} respectively [162,168]. This method is

straight forward to implement and provides an alternative method for determining the pressure dependent rate coefficient of a reaction, particularly for multiple well, multiple channel elementary reactions. However, it should be noted that the accuracy of the calculations performed using the PLOG method is dependent on the number of specified pressures and corresponding rate parameters for each reaction [162]. The mechanism employed in this study (discussed in section 3.5.1) contains pressure dependent rates defined by both the PLOG (11 reactions) and Troe (43 reactions) method, with Troe pressure dependent rate parameters utilised exclusively for third body reactions. PLOG pressure dependent rate parameters are given at six pressures, separated by an order of magnitude in each case, for the associated reactions.

2.6.4 Kinetic Models

The importance of computational modelling, with respect to the study of a fuel's ability to resist engine knock, can be seen in the ability to produce many predicted results and operational data much faster than completing the associated experiments. If the models are sufficiently accurate and robust, this can save a large amount of time in determining the suitability of fuels for use in SI engines. By completing simulations for a large amount of conditions, describing many fuel blends over a wide range of hypothetical conditions, the models can be used to determine the optimal fuel for a given situation, such as specific engine designs, or operating circumstances. A similar approach may be applied to determine the response of a given fuel to changes in engine designs, such as improvements or modifications, which may increase the operating pressures and temperatures. It is also possible, assuming that the underlying theory on which the model is built is correct and the mechanism is thoroughly validated, to explore regions outside of what is possible experimentally [91,145]. This quality may be useful in determining the properties of a fuel under extraordinary circumstances or in "real-world" fringe cases. These models rely on kinetic reaction mechanisms (which define a series of possible elementary reactions and the associated rate parameters), thermochemical data for the species involved and species transport data. Chemical kinetics couples chemical species with the energy equation via the enthalpy of reaction. A series of conservation equations expressed by a kinetic system of ODEs, for species concentrations and energy, are applied to model combustion problems where species transport properties can be ignored, such as autoignition in an RCM [145]. Solvers such as CHEMKIN-PRO [169] and Cantera [168] allow the user to simulate a wide array of combustion processes by combining the reaction mechanism and thermochemical data, allowing the software to calculate the forward and reverse reaction rates based on the microscopic reversibility principle. Historically, interest in

combustion relevant chemical kinetics was largely focused on the investigation of chemical systems driving explosive reactions (such as the high temperature heat release (HTHR) observed in autoignition). Recently, research interest in the reaction rates and mechanisms driving non-explosive chemical reactions has increased drastically, due to the relevance of such kinetic processes in the low temperature combustion of alternative fuels, driven by the emergence of low temperature combustion engine technologies and the associated production of complex pollutant species in this thermodynamic regime [170].

Kinetic models must be tested against experimental data from a range of well understood combustion experiments to determine the validity and accuracy of mechanisms used. This is part of a multi-step process in the production and evaluation of robust chemical kinetic mechanisms. Traditionally, fundamental sets of reactions and the associated rate parameters are produced based on a series of agreed upon reaction classes (as described for alkanes and alcohols in section 2.5), alongside expert knowledge and experience, to predict species which are likely to be present and the associated reactions which are likely to occur. Rate parameters for some reactions which have been previously studied may be sourced from the existing literature, wherein they have been calculated through the application of high-level theoretical calculations or determined via experimental techniques designed to measure elementary reactions (such as discharge flow, flash photolysis and relaxation methods) [135]. The thermodynamic data for each species present in the reaction mechanism must also be supplied. While some of this data is known to a reasonably high degree of certainty, due to high-level theoretical calculation or the experimental derivation of such properties, it is common for this data to be estimated, particularly for complex, short-lived species common during low temperature oxidation. Often, species thermodynamic properties are estimated via Benson's GA method, which considers each species as a set of constituent groups, each representing a polyvalent atom and its ligands. If the contributions of these groups to overall thermodynamic parameters are known, the properties of any species composed of these groups can be estimated. This method is further described in Chapter 6. The ability of such mechanisms to predict target behaviour is then evaluated against experimental results, for example a mechanism designed for the modelling of autoignition behaviour may be evaluated against RCM or shock tube IDT measurements. This process has been described extensively in the literature [53,142,171].

For detailed mechanisms relevant to the combustion behaviour of alternative fuels, such as iso-butanol and gasoline (surrogate) blends, the number of relevant reaction classes and

reactions may become incredibly large, with several thousand species and reactions. The majority of these reactions and species are not well characterised and are likely to be based on estimates, knowledge of smaller species and small amounts of experimental data, introducing potentially thousands of unknown parameters with significant uncertainties. In this case, adding new experimental data for complex fuel species can be extremely useful, as this provides additional knowledge of the fuels combustion behaviour as well as supplying a range of new model validation targets, particularly in cases where such data is scarce. Typically, mechanisms are validated against bulk targets such as IDTs. Sensitivity analysis (detailed more in section 2.6.5) applied to the model's prediction of target parameters can help to locate discrepancies within the model by identifying important species and reactions in driving these behaviours, which warrant further detailed investigations. More insightful model evaluation can be derived through the application of multiple target parameters, which may describe features more subtle than bulk autoignition measurements. For example, by targeting features related to preliminary exothermicity such as HRRs, aHR and temperatures at the soITHR and start of high temperature heat release (soHTHR), sensitivity analysis techniques may be applied to identify model discrepancies as well as develop a further understanding of the kinetic behaviour relevant to LTHR and intermediate temperature heat release (ITHR). This study aims to produce such validation targets by measuring the IDTs of multiple iso-butanol and gasoline surrogate blends and via the application of RCM HRA techniques, as described recently in the literature [172]. Furthermore, this work will evaluate a detailed kinetic mechanism against target heat release parameters as well as bulk IDT predictions, comparing the findings of each analysis to determine if these phenomena are sensitive to similar species and reactions. In the literature, analysis such as this is scarce.

The most expansive and robust mechanisms may be evaluated against a large array of experimental measurements, typically utilising fundamental setups such as RCMs, shock tubes and JSRs, where the influence of complex fluid dynamics is suppressed [62,173,174]. For detailed mechanisms of relevance to the combustion of complex alternative fuels, efforts should be made to evaluate model predictions at a wide range of conditions, covering the regime relevant to the high and low temperature oxidation of the fuel species. This regime is typically representative of the end gas conditions in low temperature, high pressure engines (e.g. pressure boosted SI engines, HCCI engines). Several detailed chemical kinetic models have been developed previously which aim to predict the ignition behaviour of complex alternative fuel blends within fundamental experimental setups, in the context of combustion within engines. However, such models are rarely evaluated against relevant engine combustion measurements,

such as SI engine KNs, the prediction of which must be one of the ultimate goals of practical combustion simulations. This means that, when such mechanisms are applied for the prediction of engine level combustion behaviour, mechanisms and the rate data contained within them may need to be extrapolated to conditions outside of the regime in which they have previously been evaluated. Extrapolating reaction rates outside of the thermodynamic regime which they have been described for is not always accurate, leading to the introduction of significant uncertainties in simulation results [51,176]. Therefore, if a mechanism has only been evaluated and further developed with respect to fundamental measurements, it may be incapable of accurately predicting behaviour at the practical level. In response to a need for more SI engine level validation targets during the combustion of complex alternative fuel blends, this study will provide mean pressure cycles during normal and knocking combustion, KNs, knock intensities, and IMEPs, for a wide range of iso-butanol blends with a gasoline surrogate (5-70% iso-butanol by volume) and spark-advance timings, within a pressure boosted SI engine. The SI engine utilised for this study and the operational methodology employed (described in section 3.4) are designed such that the influence of previous cycles and turbulent fluid motion are minimised, producing measurements which provide convenient model target parameters.

2.6.4.1 Numerical Modelling of a Rapid Compression Machine

For a spatially homogeneous, single zone model, like the zero dimensional homogeneous reactor models used for the simulation of RCM IDTs in this study, a series of coupled governing equations for conservation of mass, species and energy are required. The RCM can be modelled as a closed system (no inlet or outlet during operation). Therefore, the total mass of the system will remain constant throughout the experiment and can be described by:

$$m = \sum_j^n m_j\,, \qquad \frac{dm}{dt} = 0 \qquad \text{Equation 2.54}$$

where m is the mass within the reactor, n is the total number of species, m_j is the mass of the jth species, where j=1,2,3…n and t is the time [168].

For the same model, the rate at which species j is generated through homogeneous phase reactions is:

$$\dot{m}_{j\ gen.} = V\dot{w}_j M_j \qquad \text{Equation 2.55}$$

where V is the volume of the reactor, $\dot{w}_j$ is the molar rate of production of the species j by gas phase reactions per unit volume and M_j is the molecular weight of the species j. The volume will remain unchanged throughout the model in constant volume RCM simulations, but is time

dependent in variable volume simulations (as discussed in section 3.5.2). The rate of change of the mass of each species can be expressed by:

$$m\frac{dY_j}{dt} = \dot{m}_{j\ gen.} = V\dot{w}_j M_j \qquad \text{Equation 2.56}$$

where Y_j is the mass fraction of the species *j*.

In this system, thermal energy is also conserved. For a species in an adiabatic closed system, the first law of thermodynamics states that:

$$\frac{dU}{dt} + P\frac{dV}{dt} = 0 \qquad \text{Equation 2.57}$$

where *U* is the internal energy of the system and *P* is the pressure within the reactor. By assuming the gas within the reactor behaves as an ideal gas, the energy conservation equation for model can be expressed as:

$$mc_v\frac{dT}{dt} = -P\frac{dV}{dt} - \sum_j u_j\dot{m}_{j\ gen.} \qquad \text{Equation 2.58}$$

where c_v is the specific heat at constant volume, *T* is the temperature within the reactor and u_j is the internal energy of the species *j*. This form of the energy equation significantly reduces the cost of evaluating the models system Jacobian, as the derivatives of species equations are taken at constant temperature, as opposed to constant internal energy [168].

Solving the model numerically requires the solving the system of ODEs at each time step, to calculate species concentrations and temperatures which dictate the development of kinetically described reactions. This facilitates the simulation of heat release within the system due to reaction exothermicity, and ultimately the determination of autoignition properties such as the IDT. The integration of the governing equations is performed in time steps (ether fixed or adapted throughout the model problem), through integration control, maintaining convergence of the solution within absolute and relative tolerance limits, ensuring that temperatures, pressures and species concentrations do not change significantly in a single time step [136]. These processes can be completed using solvers such as those described earlier (CHEMKIN-PRO [169] and Cantera [168]).

2.6.5 Sensitivity Analysis

Sensitivity analysis can be used to increase the overall confidence in a model's predictions by allowing the researcher to investigate the influence of uncertainties in input parameters and identify any problems with the underlying kinetics of a model. A thorough

investigation and sensitivity analysis can determine parameters that are negligible and as such, can be reduced out of the model, as well as parameters that require additional research to reduce their uncertainty, with the aim of improving a models representation of chemical kinetic behaviour. Such analysis is of particular use for the evaluation and investigation of large, complex mechanisms wherein (as mentioned in the previous section) model parameters are often estimated from knowledge, experience, and mathematical methods (such as GA). In these cases, sensitivity analysis techniques may be applied to identify parameters which contribute significantly to the uncertainty in the model's prediction of chosen target properties. Influential mechanism parameters that are not known to a high degree of certainty or are misrepresented within the mechanism, may require data with reduced uncertainties to facilitate model improvement. Such data may be located from sources such as high level theory calculations and kinetics experiments. Several online databases are available which aim to compile the kinetic and thermodynamic data available in the literature [175–178]. The choice of target properties for sensitivity analysis is important for the thorough evaluation of a mechanism, as the model's prediction of target properties is sensitive to particular reaction and species parameters. A wide range of targets allows for more of the mechanism to be probed by sensitivity analyses. IDT sensitivity to uncertainties in reaction rate parameters (i.e. pre-exponential A-factors) is commonly investigated in the literature [91,179–181]. However, bulk IDTs are often not particularly sensitive to much of the mechanism, largely being driven by competition between chain branching and termination pathways, as seen in examples of n-butanol and toluene reference fuel (TRF) blends in the literature [47,51]. Sensitivity of IDTs to uncertainties in species thermodynamic data is more uncommon than reaction rate parameters in the literature. For low temperature combustion conditions, sensitive species are typically those associated with the internal isomerisation of fuel oxidation radicals, such as RO_2, QOOH, O_2QOOH, and HO_2POOH species, as shown in the literature through sensitivity analysis of autoignition of di-ethyl ether (DEE) [182,183] and propane [184]. Adding other sensitivity analysis targets, such as characteristic LTHR heat release parameters (HRRs, aHR, temperature) may reveal sensitivities in other areas of the model. The sensitivity of predicted heat release properties to uncertainties in reaction rate parameters has rarely been investigated in the literature [185,186], whereas the impact of uncertainties in the thermodynamic data of species on parameters characteristic of preliminary exothermicity appears to be absent from the literature. This work aims to address this through the application of brute force sensitivity analysis, to independently investigate the impact of uncertainties in species enthalpies of formation and reaction rate A-factors on the predicted IDT, as well as HRR and aHR model

predictions during LTHR, of a gasoline surrogate, identifying differences and similarities between the results. These techniques can also be used to examine the underlying chemistry of a process, determine important reactions within a process and indicate interesting effects of changing conditions, as changes in model input parameters may lead to unexpected results. This study will further apply sensitivity analysis with this aim, to investigate the influence of iso-butanol blending on the chemistry driving the autoignition of a gasoline surrogate.

Local sensitivity analysis techniques are used to investigate the effect that local parameter variations have on kinetics models and to determine the importance of reactions to the overall process. In a local sensitivity analysis, the change in the model's output for a specific parameter (such as a chemical concentration or temperature) is observed due to a small change in an input parameter close to the nominal value of said parameter, keeping all other model parameters consistent. In software, such as CHEMKIN, the Jacobian matrices needed to solve the sensitivity equations are already used in the initial kinetics problem and as such, this simplifies the calculation of sensitivities; the computation of Jacobian matrices can take significant computational time.

The fundamentals of sensitivity analysis can be described through a series of basic equations. Firstly, the rate of concentration change for a given species can be given by the initial value problem:

$$\frac{d\boldsymbol{Y}}{dt} = \boldsymbol{f}(\boldsymbol{Y}, \boldsymbol{x}), \quad \boldsymbol{Y}(t_{\mathbf{0}}) = Y_{\mathbf{0}} \qquad \text{Equation 2.59}$$

where ***Y*** is the vector of molar concentrations, *x* is the parameter vector of *m* elements which may include a range of parameters: rate coefficients, thermodynamic data etc. Solving this problem between the times t=0 and t_1, changing the parameter j by Δx_j and continuing the solution to the ODE described earlier to the time t_2, the sensitivity coefficient can be calculated approximately through the use of the finite difference approximation.

$$\frac{\partial Y_i}{\partial x_j}(t_1, t_2) \approx \frac{\Delta Y_i(t_2)}{\Delta x_j} = \frac{\tilde{Y}_i(t_2) - Y_i(t_2)}{\Delta x_j} \qquad \text{Equation 2.60}$$

where $\tilde{Y}_i$ is the solution when the parameter is modified. Next, the changes in the molar concentration due to the changes of the parameter vector can be shown through a Taylor expansion such that:

$$Y_i(t, x + \Delta x) = Y_i(t, x) + \sum_{j=1}^{m} \frac{\partial Y_i}{\partial x_j} \Delta x_j + \frac{1}{2} \sum_{k=1}^{m} \sum_{j=1}^{m} \frac{\partial^2 Y_i}{\partial_{x_k} \partial_{x_j}} \Delta x_k \Delta x_j + \cdots$$

Equation 2.61

where the first-order partial derivative is known as the first-order local sensitivity coefficient, the second-order partial derivative is the second-order local sensitivity coefficient and so on.

Usually the first-order sensitivity coefficient is sufficient and the other coefficients need not be calculated [54]. This approximation holds true at small changes in the parameter. The matrix of local sensitivity coefficients is known as the sensitivity matrix and is defined as:

$$\mathbf{S} = \left\{ \frac{\partial Y_i}{\partial x_j} \right\}$$

Equation 2.62

where **S** is the sensitivity matrix. As mentioned, it is necessary to normalise these sensitivity coefficients to make them comparable; a sensitivity coefficient may be calculated in different units within the same model, making them not comparable. Normalised sensitivity coefficients are calculated such that they have no units; they are dimensionless. Normalised sensitivity coefficients can be defined as:

$$\frac{\partial \ln Y_i}{\partial \ln x_j}$$

It may be the case that multiple parameters are changed at the same time. In this case the solution for the molar contraction at the modified parameters is:

$$\widetilde{\boldsymbol{Y}}_{\iota}(t_2) = \boldsymbol{Y}(t_2) + \boldsymbol{S}(t_1, t_2) \Delta \boldsymbol{x}(t_1)$$

Equation 2.63

By calculating the partial derivative with respect to the parameter x_j a new series of ODEs can be produced, of the form:

$$\frac{d}{dt} \frac{\partial \boldsymbol{Y}}{\partial x_j} = \mathbf{J} \frac{\partial \boldsymbol{Y}}{\partial x_j} + \frac{\partial \boldsymbol{f}}{\partial x_j}, \quad \frac{\partial \boldsymbol{Y}}{\partial x_j}(t_0) = 0$$

Equation 2.64

where **J** is the Jacobian matrix ($\partial \boldsymbol{f} / \partial \boldsymbol{Y}$). The initial value problem for this set of ODEs is of the form:

$$\dot{\mathbf{S}} = \mathbf{JS} + \mathbf{F}, \quad \mathbf{S}(0) = 0$$

Equation 2.65

where **F** is defined by $\partial \boldsymbol{f} / \partial \boldsymbol{x}$.

Solving these equations above to obtain sensitivity coefficients is known as the direct method. However, this requires prior knowledge of the solutions to the kinetic set of ODEs; **J** and **F** can only be calculated with known variables. Both sets of ODEs can be solved for each parameter out of *m* parameters one at a time, but this requires extensive amounts of calculations and as such, leads to large computational costs. This is often referred to as the brute force method. Multiple methods of local sensitivity analysis have been developed which avoid this problem however, including the decoupled direct method (DDM), and Green's function method (GFM) [54,162].

Brute force sensitivity analysis is (computationally) a relatively simple form of sensitivity analysis which can be used to determine the impact of varying parameters on the overall output of the model. This involves varying each parameter of interest individually and independently by a predetermined amount, then measuring the resultant change in the target model prediction. Model input parameters can then be ranked according to their importance in the determination of the target model output, as described by the measured change in models predicted output value. Of course, this form of analysis is not the most time efficient, as it requires a minimum of *m*+1 individual simulations (where *m* is the number of input parameters which will be modified), but can allow target properties to be accessed which are not easily explored via local, linear methods, such as bulk IDTs and HRRs. For this reason, brute force sensitivity analysis is applied in this study to investigate the sensitivity of various properties which would otherwise be difficult to probe, such as peak HRRs during LTHR and aHR at the soITHR, to uncertainties in enthalpies of formation and reaction rate A-factors. The brute force method has been applied often in the literature to determine the sensitivity of several properties to model input parameters, such as the sensitivity of IDTs to reaction pre-exponential A factors [47,51], sensitivity of IDTs to species thermodynamic properties [183,184] and sensitivity of thermodynamic properties to GA group values [187].

2.7 Biofuels

A biofuel is defined such that the energy of the fuel must be obtained by the conversion of inorganic carbon into organic compounds by living organisms, such as bacteria or plants [188,189]. Suitably, for use in transport, liquid biofuels often have similar properties to conventional transport fuels such as gasoline: an important distinction between biofuels and other alternatives which allows them to be used in engines with minimal modifications in engine design and transport architecture. Because of this, liquid biofuels have garnered a large amount of interest. Biofuels, as an alternative fuels source, are proposed to provide many advantages:

- Renewable – Feedstocks are replenished after harvesting, allowing for a continued supply of biofuels. In contrast, fossil fuels are supplied through a large but finite reservoir.
- GHG emissions – Biofuels are theoretically carbon neutral; the carbon dioxide emissions produced due to combustion are absorbed in the same quantity in the growing phase of the plant based feedstock. In reality, this is not necessarily the case, due to other emissions involved in the production and supply of biofuels. Life cycle emissions can be much lower for advanced (second generation) biofuels than first generation biofuels, as well as largely being influence by the choice of feedstock [190–192].
- Supply infrastructure – Currently, transport fossil fuels utilise a vast network of fuel infrastructure to supply the world with fuel. Biofuels should be able to utilise this same supply network, without the need for modification.
- Combustion – Many liquid biofuels, due to having similar combustion properties as conventional transport fuels, can be used in existing engine technologies with minor modifications. This is a considerable advantage when compared to other alternative fuels such as hydrogen and electricity, which require entirely different transport infrastructure and drive train solutions.
- Availability – A wide range of production pathways (e.g. agriculture, waste, bacteria/algae), with many relatively simple production methods, create the potential for increased availability of biofuels when compared to other alternative fuels and fossil fuels.
- Energy Security – Many countries are dependent on a small number of supply countries to provide fossil fuels. It is possible for a country to produce its own biofuels, rather than relying on pre-existing stocks of fossil fuels or imports. In reality, this is not the case as production requires large amounts of land. Therefore, a country with a small land area but high energy demand (such as the UK), may not be able to supply all its own energy needs.

There are also several disadvantages which come with biofuels (particularly first generation biofuels) when compared to other fuels. While some disadvantages are specific to the fuel or feedstock, most are subject to the following disadvantages in some way:

- Food security – Feedstocks used for biofuel production compete with food as both the feedstock itself (in some cases) and the arable land used. To some degree, however, the impact of this competition is dependent on future agricultural development and technologies which could lead to higher food or biofuel yields from the same land area.
- Water impacts –The production of biofuels requires large amounts of water when compared to other fuels, which is expected to increase significantly as biomass production for biofuel

use increases [193–195]. Biofuel production also impacts water quality as well as consumption; it has been shown that biofuel production can lead to hypoxia issues in local water systems (such as rivers or lakes) by increasing the amount of nitrogen and phosphorus seepage from agriculture. On top of this, biofuel spillages can be devastating for local water systems and wildlife, as seen in 2003 when a spillage caused the death of the Rio Grandes fish population for 95 miles from the spillage site [196,197].

- Land use change – This repurposing of land both impacts biodiversity and increases the lifetime GHG emissions of the biofuel, particularly in cases where forest areas (which have a high carbon stock) are converted for agricultural purposes.
- Biodiversity – As mentioned, biodiversity often suffers due to land use change. In the case of biofuels, vertebrate diversity has been shown to suffer in areas used for biofuel crops when compared to the previous environment [198].
- Monoculture – The growth of a single plant species over a large area of land impacts biodiversity by removing the previous variety of food sources and habitats, as well as creating a fragile crop; the whole yield can be affected by the same pests or diseases [196].
- Invasive species – To minimise the effects of monocultures and improve biofuel yield, genetically modified crops are often used as a feedstock. Potentially, this can introduce an invasive species to a region as the altered crops migrate, causing significant damage to existing agriculture.
- Life cycle emissions – Combustion of the fuel is not the only source for carbon dioxide emissions associated with biofuels: fuel processing, agricultural emissions and fuel transportation all produce emissions which contribute to the lifetime emissions of the fuel. Unlike other fuels, biofuels also produce large amounts of nitrous oxides through the fertilisation of the feedstock crop (in agricultural cases), which is a GHG much more potent than carbon dioxide.

As technology and knowledge progresses, biofuels are reducing the impact of associated negatives. This can be highlighted in the differences between first and second generation biofuels. First generation biofuels have historically shown many of the associated issues with biofuels: land use change (the deforestation of rainforest for palm oil) and competition with food (production of alcohol from food crops) are two well-known examples of this. While these fuels can be easy to produce and process, their environmental impact is considerable and even in some cases worse than the impacts of fossil fuel use. Second generation biofuels however are not produced from food crops and as such address these issues. Instead they are produced

from sources such as waste or crops like grasses, agricultural waste and jatropha which, while not eliminating all issues, certainly limits their impacts. However, second generation biofuels are usually processed differently to first generation biofuels, in some cases requiring several pre-processing steps, increasing the complexity of the production process [189].

Currently, the most popular biofuel for use in SI engines is ethanol (50% of all biofuels supplied in the UK in 2015/16 [189]). This is due to both the ease with which it can be produced and its high ON, which makes it an attractive fuel for blending with gasoline as it acts as an octane booster. However, there are a variety of issues with ethanol use in engines. Ethanol is corrosive to conventional SI engines and as such, can only be blended up to approximately 10-15% without engine modifications [199]. To meet future transport emissions and renewables targets (as set out in the RED II [27]), while continuing to use conventional engine architectures, higher blending ratios of biofuels are required. This is a scenario that cannot be completed in conventional unmodified engines using ethanol. The energy density of ethanol is considerably lower than that of gasoline, meaning that the blending of ethanol with gasoline negatively impacts the total energy density of the fuel and therefore the fuel economy of the engine. This problem increases the larger the blending concentration of ethanol, therefore, as the requirement for higher biofuel blending ratios rises, ethanol becomes a somewhat less attractive fuel choice. Ethanol is also susceptible to water contamination [200]. Longer chain alcohols do not present all the issues seen with ethanol and therefore have the potential to replace ethanol as a fuel. One such alcohol is butanol.

2.7.1 Butanol

Butanol (C_4H_9OH) is a colourless and flammable chain alcohol that has historically been used as a solvent for several applications such as: drugs, detergent, hydraulic fluids, cosmetics and antibiotics [201]. It is often identified as a highly attractive second-generation biofuel, intended to replace or supplement ethanol as an alternative fuel. This is due in part to its more appropriate combustion and physical properties in comparison to ethanol. The four isomers of butanol are n-butanol, sec-butanol, iso-butanol, and tert-butanol, each of which exhibit slightly different properties, which can be seen in table 2.3, due to the different structures of the isomers as dictated by the position of the OH and carbon chain structure.

While, in the above table, it would appear that the tert-butanol is the most suitable butanol for use as a biofuel due to its high ONs, tert-butanol is a petroleum derived product and currently has no viable bio-pathways, and as such it cannot be utilised as a biofuel. Also, of the four butanol isomers, tert-butanol presents the lowest energy density. The energy density of the

three other isomers is very similar and closer to the value for gasoline (although still considerably lower). Of the three bio-derivable isomers, it appears that n-butanol has the lowest ONs and is therefore the least suitable isomer for use in SI engines in terms of knock prevention, whereas sec and iso-butanol have similar ONs, both higher than those seen in n-butanol. However, n-butanol does contain the higher energy density of the isomers, but only marginally. Therefore, it is possible to argue that this is the least suitable bio-derivable isomer for use in SI engines, on the basis of analysis of its chemical properties.

Table 2.2. Comparison of properties for the four isomers of butanol. * = [202], ** = [203], *** = [204].

Fuel	**n-butanol**	**Sec-butanol**	**Iso-butanol**	**Tert-butanol**	**Gasoline**	**Ethanol**
Energy Density (MJ/L)	26.9*	26.7*	26.6*	25.7**	30-33	21.4*
Boiling Point (°C)	118*	99*	108*	83**	27-255	78
RON	98*	105*	105	107**	88-98	109***
MON	85*	93*	90	94**	80-88	90***

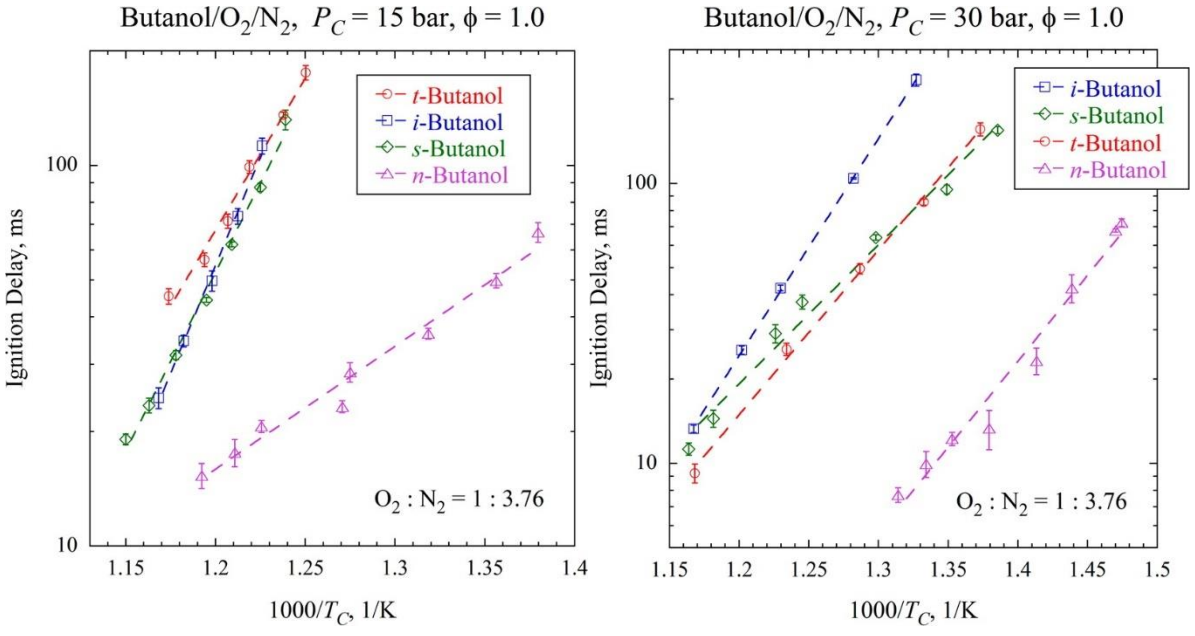

Figure 2.16. Comparative autoignition trends for the four butanol isomers at compressed pressures of 15 (left) and 30 bar (right) [39].

Upon measurement of the IDTs of all four isomers using RCM at engine relevant temperatures and pressures (compressed temperatures of 715-910 K, compressed pressures of 15 and 30 bar and equivalence ratios of 0.5-2.0), Weber and Sung [39] found that the order of reactivity for the butanol isomers was n-butanol > sec-butanol ≈ iso-butanol > tert-butanol at lower pressures and as pressure was increased the order became n-butanol > tert-butanol > sec-butanol > iso-butanol. This complex temperature and pressure dependence of the butanol isomers can be seen below in figure 2.16. These findings highlight the high degree of autoignition resistance exhibited by iso-butanol at SI engine conditions and indicate the molecule's potential as a knock resistant gasoline additive/biofuel blend when compared to the other bioderived butanol isomers, particularly at boosted SI engine pressures (30 bar).

When compared to ethanol, iso-butanol has a much higher energy density (closer to the energy density seen in gasoline) due to a lower ratio of oxygen to carbon in the butanol fuel. This means that the blending of iso-butanol with gasoline will not impact the fuel economy of a vehicle as much as gasoline blending with ethanol to the same degree would. Iso-butanol is more compatible with current fuel supply and engine architecture than ethanol due to its lower degree of corrosiveness and its lower susceptibility to water contamination. This means that iso-butanol can be blended to higher degrees in current engine technologies without the need for any engine modification. Also, iso-butanol may be supplied using the existing petroleum network, unlike ethanol, drastically reducing the cost and emissions of a biofuel economy based on iso-butanol as opposed to ethanol [205,206]. Despite the higher energy density of iso-butanol in comparison to ethanol, the potential benefits of blending iso-butanol with gasoline are unclear due to a lower octane rating. This could potentially reduce the efficiency of pressure boosted SI engines, which are often limited by engine knock. Therefore, it is important to determine the impact of iso-butanol blending on the knocking characteristics of gasoline within a pressure boosted SI engine, particularly as the octane sensitivity of iso-butanol is significantly higher than that of gasoline, which may be beneficial in low temperature combustion engines [207]. RCMs typically operate in the regime characteristic of end gas conditions in such engines and provide a useful proxy for the observation of homogeneous autoignition behaviour of relevance to engine knock. Due to the ease of modelling fundamental setups such as the RCM, such measurements are commonly applied to evaluate detailed kinetic mechanisms designed to be of relevance to the combustion of alternative fuels. However, RCM measurements are rarely compared to the practical engine measurements they are assumed to represents and there is a need to correlate behaviours observed in both fundamental and practical setups.

As a second-generation biofuel, iso-butanol can be produced from a wide variety of feedstocks, many more than first generation ethanol [208]. In terms of bio-pathways, iso-butanol is most commonly produced through fermentation, particularly a process called ABE (acetone-butanol-ethanol) fermentation. Traditionally fermentation produces very low yields of butanol and as such very low yields of the iso-butanol isomer. However, the yield can be improved through modifications to the process and using bacteria specifically engineered to produce iso-butanol [209–212]. As mentioned, using this method butanol can be produced from a wide range of feedstocks, such as:

- Agricultural waste, residues, and by-products – These feedstocks are often easy to process into fermentable sugars. However, the feedstock availability is dependent on the agricultural yield and quality to provide waste [213].
- Food crops – Also dependent on agricultural yield and quality, food crops are easy to process into fermentable sugars. However, this feedstock competes with the food supply and lacks potential for future innovation [213]. Also, the RED II caps the contributions of such biofuels to binding renewables targets [27].
- Non-food crops – Feedstocks such as switchgrass do not compete directly with food (but may compete indirectly through land competition). The processing of these feedstocks often has greater processing costs and energy demands [213].
- Wood – This feedstock is widely available, particularly in the form of sawdust and waste wood. It does not compete with food but is relatively difficult to process into fermentable sugars as well as requiring high degrees of processing and pre-processing [213].
- Industrial by-products – A variety of by-products can be utilised as a potential feedstock for butanol production, including brans, molasses, cheese whey and apple pomace. While this feedstock requires no land use change for the growing of crops, the supply of the feedstock is dependent on industrial production rates. The fuel production process also has high pre-processing costs and a very low product to waste ratio [213].
- Biodegradable municipal waste – Garden waste, parcel packaging and wastewater treatment sludge are a few of the many possible sources for this feedstock. Dependent on the chosen feedstock, supply may vary wildly. It is therefore important to maintain a selection of feedstocks to guarantee a suitable supply [213]. Biofuels sourced from this feedstock are considered to be twice their energy content when determining contributions to RED II requirements [27].

Fermentation processes are susceptible to contamination, especially early in the process through the possible introduction of aerobic bacteria and acid producing anaerobic bacteria. Therefore, measures must be taken to ensure that the fermentation vessels are sterile to avoid periods of extended shut down. This need for a sterile environment drives production costs up and impacts the attractiveness of butanol as an alternative fuel [214]. There is also some concern over the emissions due to the combustion of alcohols, particularly the emission of carbonyl species including: formaldehyde, acetaldehyde, acetone and propenal. All of which are precursors to smog as well as being toxic and irritant [215,216]. The blending of iso-butanol with gasoline in a SI engine was shown to significantly increase the emissions of acetaldehyde but reduced emissions of CO, CO_2 and hydrocarbons as well as providing an increase in overall thermal efficiency [217].

The combustion properties of iso-butanol have been explored exhaustively in the literature due to a growing interest in the fuel as a biofuel target for transport. McEnally and Pfefferle [218] studied the decomposition and hydrocarbon growth process for each of the butanol isomers in 2005. In this study, coflowing methane/air flames were separately doped with 3500 ppm of each of the butanol isomers. Speciation measurements were made by extracting gas samples from the flames, which revealed that the butanol isomers produced much higher concentrations of ketone and aldehyde species than butane did, suggesting that toxic products would be a potential issue with the combustion of butanol isomers as a fuel, as they are for other alcohol fuels [218]. The blending of iso-butanol with gasoline can be applied to minimise the formation of these toxic products, by limiting the quantities of alcohol in the fuel. Grana et al. [219] continued this work, investigating the structure and speciation of non-premixed counterflow flames of n- and iso-butanol, developing a high temperature kinetic mechanism for the combustion of butanol isomers. This study stated that the flame structures and overall high temperature combustion characteristics were similar for all butanol isomers, as well as being similar to n- and iso-propanol [219].

Laminar burning velocities for the butanol isomers and flame instabilities were investigated by Gu et al. [220] using butanol/air premixed spherically expanding flames, at an initial temperature of 428 K and initial pressures of 1-7.5 bar. This study found that laminar burning velocities were generally greater for n-butanol, decreasing further in the order sec-butanol, iso-butanol, tert-butanol. This behaviour was attributed to the presence of functional groups, with branching methyl groups decreasing the laminar burning velocity. Molecular structure had no apparent impact on the flame instability however, with each of the butanol isomers displaying

cellular structures at similar flame radii [220]. These findings were further supported by the work of Veloo and Egolfopoulos [221], which showed the same order of flame speeds at an initial mixture temperature of 343 K, atmospheric pressure and a wide range of equivalence ratios. This would suggest that, within engines, n-butanol and the associated blended fuels may produce higher power output than iso-butanol and its blends but also a greater propensity for knock, given the higher degree of autoignitive propensity of n-butanol. Detailed flame structures for the butanol isomers were measured using molecular beam mass spectrometry (MBMS) by Oßwald et al. [222] for laminar flat premixed low pressure (40 mbar) flames, at Φ=1.7. These measurements found that temperature and species measurements for the butanol isomers were strikingly similar, suggesting global combustion behaviour between the isomers. The intermediate species pools however, displayed significant variation, indicating fuel specific pathways [222]. A further low pressure premixed flame study by Hansen et al. [223] provided further speciation measurements of over 40 individual species for the butanol isomers. These flame studies provide important species measurements during combustion which can be used for the validation of kinetic mechanisms and reveal important quantitative data on the production of aldehydes, enols and alkenes during the combustion process [84].

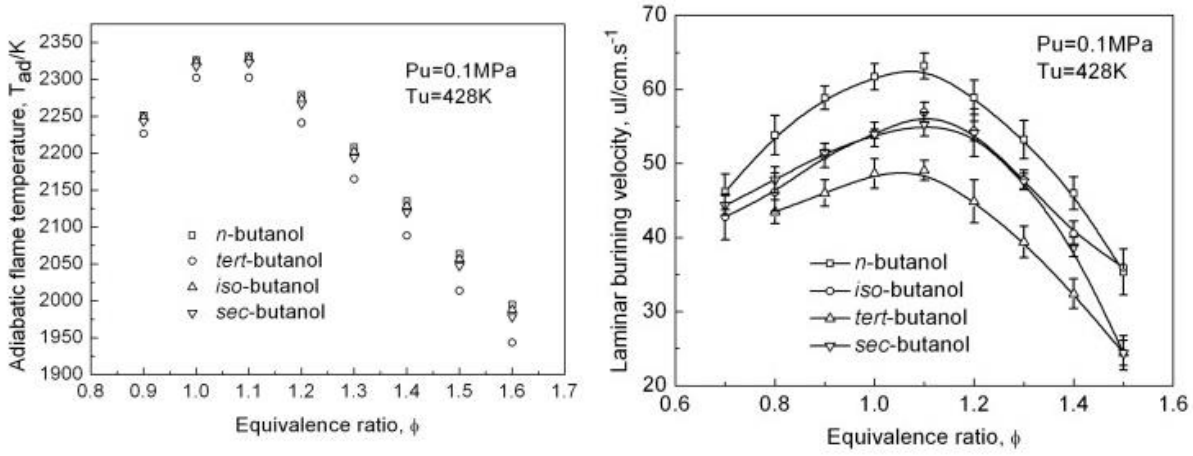

Figure 2.17. Adiabatic flame temperatures and laminar burning velocities for the four butanol isomers, with respect to equivalence ratio, as measured in a spherically expanding flame [200].

Several studies of iso-butanol autoignition have also been produced using RCMs and shocktubes to investigate the molecules IDTs. Moss et al. [42] investigated the high temperature autoignition behaviour of all four butanol isomers in a shock tube, at temperature and pressures of 1200-1800 K and 1-4 bar respectively. Under these conditions, the study determined that n-butanol was the most reactive of the isomers, whereas the other isomers in the order of

decreasing reactivity were iso-butanol, sec-butanol, and tert-butanol. This finding is shown in figure 2.18, for a reflected shock pressure of 1 bar. This supports the findings of Weber and Sung [39] at lower temperatures in an RCM, which showed a similar ordering of reactivity at lower temperatures, with iso-butanol decreasing in reactivity relative to the other isomers as pressure increased and displaying the largest IDTs at a pressure of 30 bar. This indicates that, at the low temperature, high pressure conditions characteristic of modern engine technologies (such as downsized pressure boosted SI engines), iso-butanol displays the greatest potential as an anti-knocking agent when blended with gasoline. However, fundamental ignition studies which investigate this are sparce and the influence of iso-butanol blending on the antiknock properties of gasoline require a thorough characterisation, particularly in the temperature and pressure regime of modern SI engines. This would provide an insight into the behaviour of such blends as well as an array of targets for model evaluation, creating the potential for model improvement in this highly important region. Moss et al. [42] also generated a detailed chemical kinetic mechanism, validated against their shock tube measurements, to describe the oxidation of butanol isomers. Kinetic modelling indicated that, at these high temperature low pressure conditions, iso-butanol was primarily consumed by hydrogen abstraction, resulting in the formation of fuel radicals which decomposed to produce H and OH radicals. Reaction flux and sensitivity analysis of this detailed mechanism demonstrated the importance of three competing classes of consumption reactions in all four of the butanol isomers. The reaction classes identified were hydrogen abstraction, unimolecular decomposition, and dehydration [42].

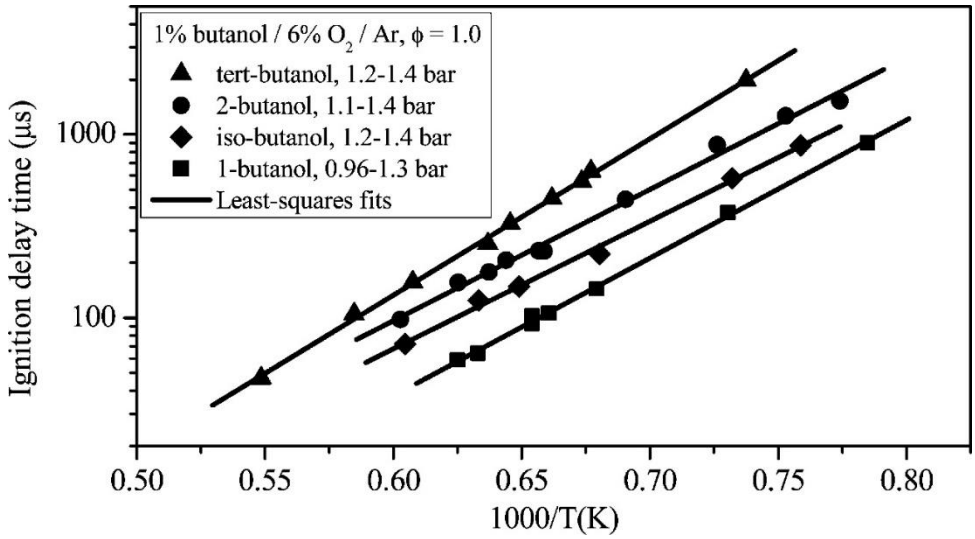

Figure 2.18. Experimental IDT measurements for all four butanol isomers as measured in a shock tube at a reflected shock pressure of 1 bar [42].

Weber et al. [224] extended the range previous iso-butanol RCM IDT measurements by Weber and Sung [39], by investigating compressed temperatures of 800-950 K, compressed pressures of 15-30 bar and an equivalence ratio of 0.5. When compared to previous stoichiometric iso-butanol IDT measurements [39], IDTs at an equivalence ratio of 0.5 were significantly less reactive and also produced no NTC. The original study of Weber et al. [39] also performed variable volume simulations using the mechanism of Sarathy et al. [44], and showed a good IDT agreement between measurements and predictions. It was also concluded in this study that, at the low temperatures and high pressures investigated, peroxy chemistry is important for the oxidation of all the butanol isomers. IDTs of iso-butanol in an RCM, at compressed temperatures of 840-950 K, compressed pressure of 25 bar and equivalence ratio of 0.4, have also been measured by Ji et al. [225]. Intermediate species were also measured for this mixture at 25.3 bar and 905 K, as a further target for kinetic mechanism comparison and validation. Kinetic models produced with several detailed mechanisms found that, while the mechanisms of Merchant et al. [226] and Sarathy et al. [44] predicted the IDT profiles well, the mechanism of Sarathy et al. [44] could not accurately predict the concentrations of ethene, iso-butene and iso-butyl aldehyde. The study then modified the mechanism to include updated rate constants of iso-butanol hydrogen abstractions by OH radicals and β-scissions of hydroxybutyl radicals, which produced a significant improvement in the predictions of ethene and iso-butene concentrations [225]. This study shows that, as previously mentioned, a wider range of available experimental targets for model evaluation allows more of the mechanism to be tested and can produce further improvements than only validating against bulk IDTs. Beyond species measurements, recent analysis methods have made it is possible to extract HRRs describing preliminary exothermicity from RCM pressure measurements. Such analysis provides new model evaluation targets, such as HRRs and aHR, which characterise key low temperature phenomena, such multi-stage ignitions, LTHR, ITHR and the NTC region, which allow for the efficacy of a model and the underlying chemical processes of such behaviour to be probed further.

Blends of butanol isomers with n-heptane were investigated in an RCM, at compressed temperatures and pressures of 650-830 K and 15-30 bar, at stoichiometric conditions, by Yang et al. [227]. IDT measurements for blends under these conditions displayed NTC behaviour, which was suppressed by increasing the butanol blend fraction. IDTs also increased as the butanol mole fraction of the blend increased. Due to the large alkane content in gasoline, similar NTC suppression under iso-butanol blending is expected. However, the degree of suppression and influence of blending on IDTs for the entire blending range is not well characterised in the

literature, particularly for low blending ratios (<20% iso-butanol), where NTC behaviour may dominate over the observed Arrhenius behaviour of iso-butanol. Autoignitive behaviour in this blending region may be important for use in SI engines, as low degrees of blending may be utilised to minimise calorific value impacts on the fuel and reduce the strain on a limited biofuel supply. As such, this blending regime requires thorough characterisation, as well as the parallel iso-butanol blends with a gasoline surrogate, such that modelling and sensitivity analysis techniques can be applied, to develop an understanding of the changes to kinetic behaviour driving the ignition process due to blending. To meet this requirement, this study aims to investigate the autoignition of iso-butanol blends with gasoline and a surrogate, in both an RCM and SI engine. This will also evaluate the ability of a newly developed gasoline surrogate to capture the ignition behaviour of gasoline under blending, at the fundamental and practical level. Computationally modelling of the RCM, through the application of a detailed kinetic mechanism, will facilitate the analysis of the influence of blending on the underlying chemistry.

Chemical analysis of butanol/n-heptane blends showed that these blends exhibited an NTC due to radical pools generated by the low temperature oxidation of n-heptane, accelerating reactivity at low temperatures. Tert-butanol was the least proficient isomer at suppressing the NTC behaviour. A kinetic mechanism was produced by combining the n-heptane mechanism of Curran et al. [228] and the butanol isomers mechanism of Sarathy et al. [44], which produced a good agreement with measured RCM IDTs. Flux analysis also showed that n-heptane addition to the butanol isomers had little impact on the low temperature reaction path, with the main impact being through the hydrogen abstraction radical. With the addition of n-heptane, less hydrogen abstraction occurred due to HO_2 and more occurred via the H radical. At the higher temperature end of the range, OH propagation reactions are reduced under n-heptane blending and a small amount of the hydroxybutyl radicals undergo β-scission. Sensitivity analysis determined that, for pure iso-butanol, hydrogen abstractions from the α carbon site play a major role in inhibiting the total reactivity, whereas abstractions from the γ carbon site promote the reactivity of the fuel. When blended with n-heptane, abstraction from the α site is still inhibiting, but the influence is significantly reduced [227].

Overall, studies of low temperature autoignition of iso-butanol, at conditions relevant to SI engines, are scarce. As such, measurements taken in this region are valuable for developing a complete understanding of the fuel's autoignition behaviour and as model validation targets. Such fundamental studies on the ignition behaviour of iso-butanol and gasoline blends in this low temperature, high pressure region appear to be entirely absent from the literature. While

several studies have investigated the performance and emission impacts of iso-butanol and blends with gasoline on SI engines, there is a lack of studies in the literature which investigate the knocking propensity of these fuels. Autoignition studies generally tend to focus on fuels behaviour within fundamental setups, such as RCMs and shock tubes, wherein the thermodynamic conditions are the same as those experienced by the end gas within engines. However, these setups are largely used to study homogeneous autoignition and as a result, neglect the more complex aspects of the engine in-cylinder environment and, as such, assuming the autoignition trends observed in an RCM are the same as knocking behaviour experienced within an SI engine may not be entirely valid. Evaluating the results of RCM experiments, against measurements made within an SI research engine, allows for the ability of fundamental setups to provide accurate information about the impact of fuel blending on knocking behaviour to be determined. The application of both experiments also provides a larger range and variety of target parameters for the evaluation and investigation of computer models.

The works of Alasfour [229–231], for blends of 30% iso-butanol by volume with gasoline in a single cylinder normally aspirated SI engine, showed that blends typically produce a moderate reduction in engine power (0.2-0.3 kW brake power, ~4%), exhaust temperature and thermal efficiency (7% reduction compared to gasoline) when compared to neat gasoline. However, this blend was also observed to reduce hydrocarbon and NO_x emissions by 12% and 9%, respectively. Bata et al. [232] and Kelkar et al. [233] also observed reductions in engine power, exhaust temperature and thermal efficiencies for 30% iso-butanol blended fuels. In a study of a 50% iso-butanol/gasoline blend, it was found that fuel conversion efficiency increased by 6% with relevance to gasoline, but decreased by 9% when using neat iso-butanol [234]. Brake power, volumetric efficiency, thermal efficiency and specific fuel consumption were all shown to increase in an SI engine for a blend of 5% iso-butanol also [235]. It can be seen from this review that there is a need for further ignition studies of both iso-butanol and blends of iso-butanol with gasoline, at the level of fundamental RCM experiments in the low temperature high pressure region, and also at the level of SI engines, with relevance to the fuels knock resistance. Fundamental RCM results of iso-butanol and blends with gasoline, also produces an opportunity to investigate the fidelity of detailed kinetic mechanisms and serves as a target for future model validation.

3 Experimental, Modelling and Analysis Methodology

3.1 Introduction

Introducing alternative fuels into existing and developing engine technologies, to address the renewables requirements of the transport sector and minimise environmental concerns, warrants a thorough investigation into the combustion behaviour of such fuels. This allows for the identification of optimal fuel blends in terms of engine performance and the determination of blending influences on combustion behaviour. Current advanced SI engine technologies (e.g. downsized pressure boosted engines) are limited by abnormal combustion behaviours such as engine knock, caused by the undesirable autoignition of end gases (section 2.2). Alternative fuel blends which display a boosted octane quality, relative to the conventional fuel (gasoline), may allow for the removal of such a knock limit, facilitating higher engine efficiencies. This study aims to investigate the effects of iso-butanol blending with gasoline (and it's surrogate) on fundamental properties such as IDT, HRRs and gas temperatures during the autoignition process, as well as properties relevant to practical engines, such as mean pressures, cyclic variability, KN, knock intensity and IMEP. Such properties are crucial to the determination of optimal and safe fuel use within modern SI engines. Through the measurement of fundamental and engine level fuel properties, this study will also assess the ability of fundamental measurements to represent trends in behaviour that occur within an engine. Furthermore, the fundamental combustion of iso-butanol blends is studied through computationally modelling, using a gasoline surrogate as a proxy, revealing details about the chemistry driving combustion and heat release behaviour and the associated blending influences. This study also evaluates the predictive capability of such computational modelling, through the application of a current detailed kinetic mechanism, to assess the feasibility of applying such models in their current states for the largescale prediction of combustion behaviour throughout the blending regime.

At the fundamental level, the autoignitive propensity of a fuel is often characterised by the IDT, which may be measured at engine relevant thermodynamic conditions through the use of RCMs. For the fundamental experimental work conducted within this study, the University of Leeds RCM is applied for the measurement of autoignition pressure data. The response of autoignition to changes in the iso-butanol concentration of gasoline/iso-butanol blended fuels is investigated at high pressure, low temperature conditions, most relevant to end gas conditions within pressure boosted SI engines. A detailed description of this equipment, experimental procedure and a list of experimental conditions are shown in section 3.3.

Due to the molecular complexity of gasoline, a surrogate which accurately replicates the combustion behaviour of the reference fuel is required, to facilitate the computational modelling of gasoline (and blends with iso-butanol). In this study, a five component surrogate is developed to closely match the octane quality and molecular composition of the gasoline, in terms of aromatic, olefin and alcohol concentrations. An overview of the details and formulation methodology for this surrogate are given in section 3.2. The suitability of this surrogate as a gasoline proxy is evaluated in the RCM, as a “neat” fuel and under iso-butanol blending. The impact of iso-butanol blending on the autoignition and heat release behaviour of the surrogate is investigated both experimentally and computationally. Heat release behaviour is revealed through the application of novel RCM HRA techniques, as described in section 3.6. Preliminary exothermicity prior to autoignition is vital for the determination of the autoignition phenomena, thus evaluating the influence of blending on this behaviour may reveal further details about the development of autoignition (and the related knocking behaviour) of gasoline/iso-butanol blended fuels. Pressure measurements and the resultant IDT values, as well the results of HRA, also provide targets for the testing and validation of detailed kinetic models. The ability of the chosen kinetic mechanism to mimic these behaviours is evaluated for a large range of blending and thermodynamic conditions. Through the application of sensitivity analysis techniques, the chemistry driving autoignition and LTHR behaviour can be investigated to determine important reactions and species. The modelling approach, the kinetic mechanism applied, and analysis techniques are detailed in section 3.5.

It is necessary to characterise the influence of iso-butanol blending at the practical engine level, to determine the octane quality and indicated power impacts of iso-butanol on gasoline, as well as provide an opportunity for the assessment of fundamental study predictions (at similar thermodynamic conditions). For the future development of engine applicable computational models, the surrogate must also be shown to be a good representation of gasoline’s behaviour during SI engine combustion, both as neat fuels and under the influence of iso-butanol blending. In this research, an engine study is conducted, using a motored, single cylinder, pressure boosted SI engine to investigate the impact of iso-butanol blending on the normal and knocking performance of an SI engine, as well as the surrogates replication of gasoline under these conditions. By measuring the cylinder pressure of each combustion cycle, several key parameters can be investigated including the KN, knock intensity, IMEP and cyclic variability. Knocking behaviour can then be correlated with the autoignition behaviour observed during fundamental experiments. An overview of the SI engine, operating procedure and analysis techniques is given in section 3.4.

Overall, this chapter describes the methods applied, within subsequent chapters, to capture experimental data, produce chemical kinetic models and perform meaningful analysis of these. Fundamental IDT measurements are captured using the University of Leeds RCM, whereas engine-level knock investigations are performed using the Leeds University Ported Optical-access Engine Version 2 ("LUPOE"). Descriptions and operational procedures for this equipment are detailed within this chapter, as are the numerical approaches taken in the processing and analysis of data produced. The modelling techniques applied in the application of kinetic models for the prediction of IDTs in the RCM are also presented in this section, as are the methods used for the evaluation of such models.

3.2 Gasoline Surrogate

Gasoline is often an incredibly complex mixture of several hundred hydrocarbon species [236]. Due to the large amount and variety of hydrocarbons, the degree of complexity for a standard gasoline is too great to kinetically model precisely. Therefore, it is common practice to model the kinetics of gasolines using a less complex gasoline surrogate. These surrogates are designed to match characteristic properties of the reference gasoline, such that the surrogate's behaviour in experiments is similar to that exhibited by the reference gasoline [3]. To match the needs of this study, a five component surrogate (5-C) was produced. This surrogate has been designed to closely match the relevant properties of the PR5801 reference gasoline (supplied by Shell Global Solutions), specifically the RON & MON, hydrogen to carbon (H/C) ratio and molecular composition. Chemical properties such as the RON, MON and H/C ratio are key to describing the auto-ignitive and anti-knocking behaviour of the gasoline, and as such should be matched as closely as possible by any given surrogate.

The molecular composition of the gasoline is responsible for the determination of all subsequent chemical and physical properties, such as ONs, H/C ratio, calorific values, density, vapour pressure etc. Therefore, it is vital that the molecular composition of the surrogate is as close to that of the reference gasoline as possible, while keeping the fuels complexity relatively low, such that it can be modelled kinetically. For the purposes of surrogate development, the molecular composition of gasoline can be categorised into several molecular groups: paraffins (n- and iso-paraffins), naphthenes, aromatics and olefins. It is also now common for commercially available gasolines to include oxygenated compounds, such as alcohols. For the formulation of the 5-C surrogate, iso-paraffins and n-paraffins are represented by iso-octane and n-heptane, respectively. These molecules are well characterised in terms of their autoignition properties and have been applied to a vast amount of studies as surrogate fuels,

either in the form of PRF, which include iso-octane and n-heptane exclusively [228,237–239], or more complex fuel mixtures [240–242]. The aromatic component of the gasoline is represented by toluene, which is also well characterised, leading to commonly used 3-component surrogate mixtures, often titled TRF [47,51]. Olefins are represented here by 1-hexene. This provides a cost-effective and functional emulation of the olefin component of gasolines and has been used in previous studies to similar effect [85,243]. Lastly, alcohols are represented by the addition of ethanol to the surrogate mixture, as this is in direct correlation to the alcohol content of commercially available gasolines.

The surrogate was blended using the methodology of Mehl et al. [70] (with the much appreciated assistance of Dr Scott Wagnon at Lawrence Livermore National Laboratory), whereby the composition of the 5-C surrogate is determined by numerically blending the palette of components (iso-octane, n-heptane, toluene, 1-hexene, ethanol) to match the broad gasoline composition (in terms of fractions of paraffins, olefins, aromatics and alcohols), as well as the RON and MON of the reference gasoline. This methodology then correlates homogeneous gas phase IDT properties to the fuel's octane rating through the use of chemical kinetic modelling. From these model results, the logarithm of IDTs in the NTC region is correlated to the octane sensitivity of the fuel [70,241]. However, this correlation shows significant scatter from the trend proposed in the original study [70]. The second correlated parameter in the formulation model associates the logarithm of IDT at 825 K and 25 bar with the AKI, which shows a much stronger correlation in the original study than the octane sensitivity parameter [70]. Thus, the matching of the reference gasoline's octane rating by the surrogate is dependent on the matching the slope and intensity of the NTC region from simulated IDTs. If the initial surrogate composition fails to match the octane sensitivity of the gasoline, the NTC slope can be manipulated through increasing the aromatic fraction (to flatten the NTC) and increasing the olefin fraction (to make the NTC steeper). The ratio of iso-octane to n-heptane can then be varied to match the reactivity of the fuel (described by the AKI), by controlling the predicted IDT at 825 K and 25 bar.

The comparative properties and compositions of the reference gasoline and the 5-C surrogate can be seen in table 3.1, wherein the 'Octane Sensitivity' refers to the difference between RON and MON values, and the 'Anti-knock Index' is the mean value of the RON and MON. It can be seen that the developed 5-C surrogate matches much of these critical properties closely, particularly values for RON and MON. However, it can also be seen that the 5-C mixture contains a much greater percentage of paraffins than the gasoline. This is due to the lack of naphthenes in the surrogate, which are present in the gasoline. Naphthenic content is

replaced by paraffins to reduce the computational burden of a more complex surrogate mixture, while attempting to maintain a robust emulation of the reference gasoline. While the AKI is closely matched between the gasoline and the surrogate, this would be expected from the strong correlation observed between AKI and the simulated IDT at 825 K 25 bar in the formulation method [70]. However, there is a considerable difference in the octane sensitivities of the two fuels, which may be due to the relatively poor correlation between the sensitivity and the slope of the NTC region [70]. This same discrepancy can be observed in other studies where this formulation method is applied [241].

Table 3.1. A comparison of the compositions and properties of reference gasoline PR5801 and the formulated 5-C surrogate.

Gasoline PR5801 Component	**Gasoline PR5801 (vol%)**	**5-C Surrogate Component**	**5-C Surrogate (vol%)**
Paraffins	47.1	iso-Octane	50.5
		n-Heptane	10.8
Aromatics	26	Toluene	25.9
Naphthenes	8.2		
Olefins	7.9	1-Hexene	8.1
Ethanol	4.7	Ethanol	4.7
Other Oxygenated Compounds	4.4		
Average Molecular Composition	$C_7H_{13.5}O_{0.15}$		$C_{6.8}H_{12.9}O_{0.1}$
RON	95.4		95.1
MON	86.6		87
H/C	1.93		1.9
Octane Sensitivity	8.8		8.1
AKI	91		91.05

3.3 Ignition Delay Time Measurements

At the fundamental level, a fuel's propensity for autoignition is described by IDTs. By measuring the IDT for a range of iso-butanol fuel blending ratios and thermodynamic conditions,

the influence of iso-butanol blending on the autoignition behaviour of gasoline can be investigated. Such measurements are commonly applied to predict energy level combustion behaviour, such as engine knock. The validity of such predictions will be assessed in this study, by evaluating correlations between observed autoignition behaviour within fundamental RCM experiments and knocking combustion within a research SI engine. For the development of computer models which are capable of predicting such fundamental ignition behaviour, accurate gasoline surrogates are required, which are of lower molecular complexity than the reference fuel. Such surrogates must be able to replicate gasoline's IDT behaviour (neat and blended with iso-butanol) if models are to predict the properties of gasoline and the associated blends with iso-butanol effectively. To perform measurements of IDTs, a wide range of blending ratios and thermodynamic condition are investigated within an RCM, the methodology for which is fully detailed in the following sections. The objectives of these experiments are:

- To investigate the influence of iso-butanol blending on the autoignition of gasoline and its surrogate at thermodynamic conditions relevant to end gas conditions within a pressure boosted SI engine.
- To assess the ability of the proposed surrogate to replicate the autoignition behaviour of gasoline, as both a neat fuel and under iso-butanol blending.
- To provide experimental data for the IDTs of iso-butanol, gasoline, a newly developed five component surrogate (5-C), gasoline/iso-butanol blends, and 5-C/iso-butanol blends at a wide range of blending ratios, which may serve as validation targets for the development of chemical kinetic mechanisms and provide a platform for RCM HRA.

3.3.1 Description of the University of Leeds Rapid Compression Machine

All IDT measurements presented in this work were produced using the University of Leeds RCM. Originally designed and built in 1968, by Affleck and Thomas [244] at the Shell Thornton Research Centre, as one half of a dual-opposed piston RCM, this equipment was shortly after acquired by the University of Leeds. While at the University of Leeds, the RCM has undergone many significant changes and improvements (in both previous works and this study) to facilitate the continued production of research relevant to the combustion science community. This has been achieved by extending the operational regime of the original equipment, increasing the EOC pressures and temperatures achievable (making it more suitable for engine relevant research). Also, improvements to piston damping and data acquisition over this time have led to an improvement in the quality of data produced.

Figure 3.1. A photograph of the University of Leeds RCM in the current configuration.

Table 3.2. Key parameters of the University of Leeds RCM.

Parameter	**Value**
Maximum driving pressure	20 bar
Maximum hydraulic locking pressure	50 bar
Maximum mixing chamber pressure	4 bar
Maximum EOC pressure	30 bar
Maximum initial pressure	1.5 bar
Maximum initial temperature	100°C
CR range	9 to 24
Compression time	≤20 ms
Piston bore	44 mm
Piston crevice volume	3 cm^3

The current configuration of the University of Leeds RCM can be seen in figure 3.1. This features a pneumatically driven piston assembly, with hydraulic damping and locking, ensuring that the piston can be fired at high velocity without sustaining any damage or piston-bounce upon reaching TDC. For the purposes of description, the structure of the University of Leeds RCM can be split into several sections: combustion chamber, hydraulic damping and locking, pneumatic driving reservoir, piston displacement measurement, mixing chamber, measurement and auxiliary systems (such as temperature, pressure and operational controls). The following sections of this chapter will provide more details on the design and purpose of each of these sections. For reference, the main operating parameters for the University of Leeds RCM are shown in table 3.2.

3.3.1.1 Combustion Chamber

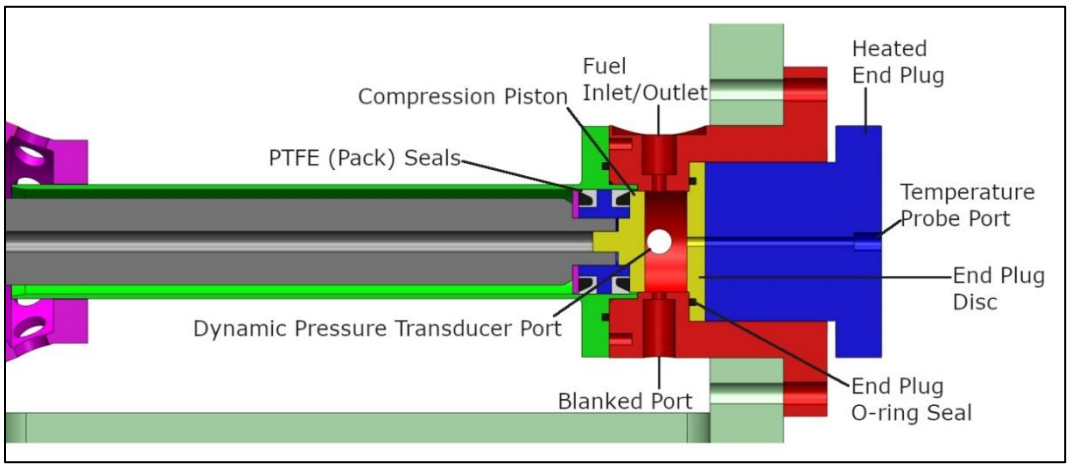

Figure 3.2. A cross-section of the University of Leeds RCM combustion chamber and piston shaft. Adapted from [245].

The stainless steel combustion chamber (and lead-in piston cylinder/shaft) is designed and manufactured to sustain the high temperatures and pressures present during the compression and autoignition of fuel mixtures. A cross-section of this design (with the piston at TDC) is shown in figure 3.2. The cylinder has an internal diameter of 46 mm and a length (at piston BDC) of 228 mm. At TDC, the piston head enters the stepped combustion chamber by 2.25 mm. The combustion chamber has an internal diameter of 44.5 mm and a length of 21.5 mm (at piston BDC), with four access ports located around the circumference of the chamber. Of these four access ports, two are currently blanked and are not used as part of this study, one is occupied by a Kistler 6045A dynamic pressure transducer and the final port is used as a fuel inlet and outlet (controlled by a poppet valve).

A heated end plug is inserted to the combustion chamber, opposite the piston face, and bolted in place to ensure it will not move under high pressure. This plug contains six 300 W cartridge heaters, supplying the main source of pre-heating for the combustion chamber, as well as a thermocouple for temperature monitoring and control. An end-plate containing a rubber O-ring seal sits between the back of the cylinder and the end-plug, which prevents the leaking of air into the chamber when under vacuum, or combustion products from the chamber under pressure. The piston cylinder is also pre-heated through the use of several band-heaters which cover the length of the cylinder, and a single thermocouple. This end-plug design is highly beneficial in a single piston RCM; it provides easy access to the combustion chamber (for cleaning and maintenance purposes) and introduces a degree of modular design. This modularity can be exploited to introduce different end-plug designs, such as optical windows, additional access ports or different dimensions (the CR can be changed by using an end-plug which enters the combustion chamber). Access to the piston head, pack seals and piston cylinder is not possible through the simple removal of the end-plug, meaning that the whole combustion chamber and cylinder assembly must be removed as one piece. However, this process is also straightforward and can be completed quickly. This allows easy access to the piston head for any cleaning or maintenance and the replacement of seals. Upon re-assembly, the cylinder features a tapered lead-in to help avoid damage to the piston head and seals and facilitate an easier assembly.

3.3.1.2 Hydraulic Damping and Locking

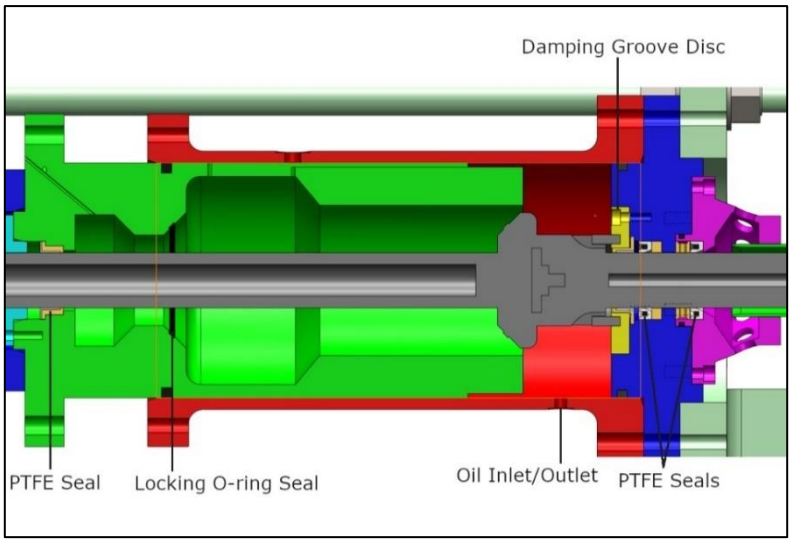

Figure 3.3. A cross-section of the University of Leeds RCM hydraulic damping and locking section. Adapted from [245].

When firing the University of Leeds RCM, large amounts of pneumatic driving pressure (up to 14 bar) act on the piston assembly, allowing the piston to travel the length of the combustion cylinder in <20 ms. It is therefore critical that the piston arrest at the EOC is damped to prevent significant piston bounce. This is achieved through the displacement of hydraulic oil present in the hydraulic damping section of the University of Leeds RCM, a cross-section of which can be seen in figure 3.3.

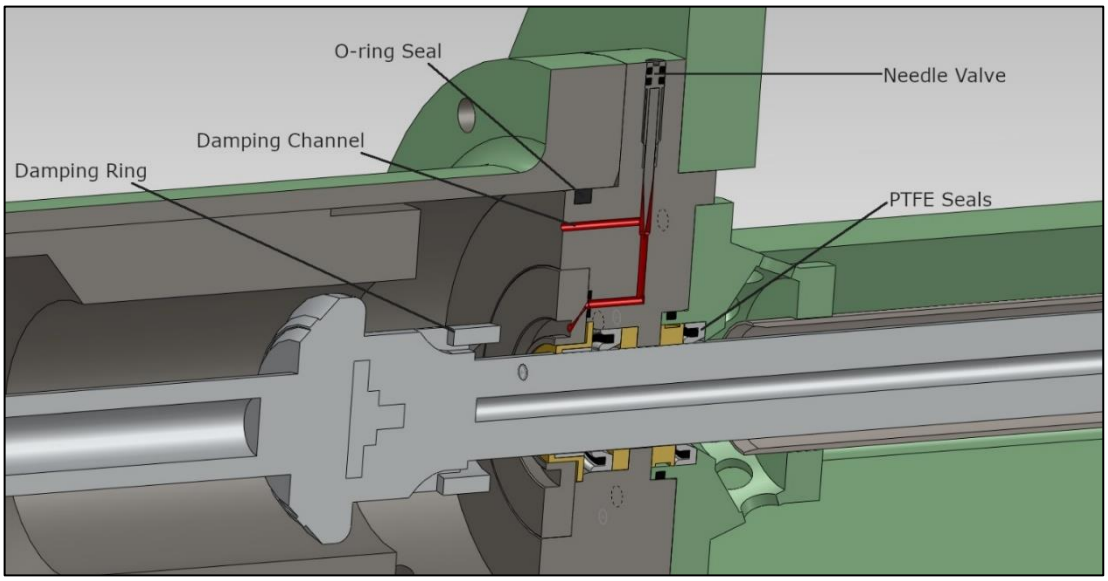

Figure 3.4. A cross-section of the University of Leeds RCM hydraulic damping control and needle valve arrangement. Adapted from [245].

Initially hydraulic oil is pumped into the hydraulic section (through the use of the hand pump seen in figure 3.1). During the movement of the piston assembly towards TDC, the damping ring moves towards the damping groove at high speed. This damping groove provides a very small clearance to the damping ring, meaning that when the two parts of the mechanism come together, oil is forced through the narrow gap between the ring and the groove. The frictional forces caused produced by this cause the damping effect. In the University of Leeds RCM, this damping effect is tuneable. This is possible due to three channels in the back of the damping groove, which lead back around into the hydraulic chamber. Within each of these channels is a needle valve, which can be tightened to restrict the flow of oil through these channels. The design of this system is shown in figure 3.4. With the piston at BDC, hydraulic oil locks the piston in place by forcing the hydraulic section of the piston assembly against the back of the hydraulic chamber. This allows the driving reservoir to be filled to driving pressure and the

piston assembly will not move until a solenoid valve is triggered, releasing much of the hydraulic oil pressure.

3.3.1.3 Driving Air Reservoir

The piston assembly is driven pneumatically by compressed air, stored in the driving air reservoir. Air is supplied by two air lines: a laboratory compressor (limited to 7 bar) and a compressed air cylinder, to save on the amount of compressed air used during operation. The reservoir also contains a pressure relief valve, in case of emergencies, which is set to activate at 19 bar (slightly below the maximum safe pressure of the driving reservoir). When the hydraulic oil in the damping section is released, the compressed air in the driving reservoir forces the driving piston (and therefore the piston assembly) forward. The compressed air in the driving reservoir is also responsible for locking the piston at TDC when compression is complete. A cross-section of this section (and the piston displacement measurement) is shown in figure 3.5.

3.3.1.4 Piston Displacement Measurement

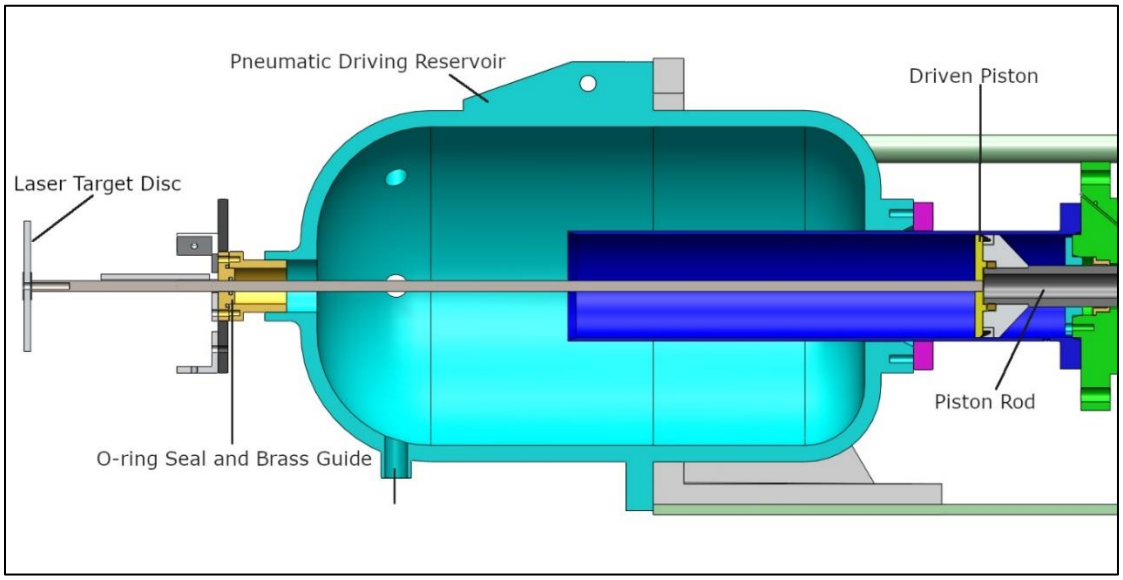

Figure 3.5. A cross-section of the University of Leeds RCM pneumatic driving reservoir and piston displacement measurement system. Adapted from [245].

For the calculation of IDT and for the monitoring of piston bounce, it is beneficial to produce an accurate log of the piston displacement during compression. In the University of Leeds RCM, a 2D linear displacement laser system is utilised to provide this accurate piston displacement data. This method works by reflecting a laser off of a moving end-plate, attached

to the piston assembly. As the end-plate moves with the piston rod, the angle at which the laser is reflected changes, as does the position at which the laser is incident on the sensor. It is then straightforward to calculate the displacement of the end-plate disc (and therefore the piston) from TDC, assuming the system is correctly calibrated.

The University of Leeds RCM uses a Keyence model LK-G82 laser and sensor pack to provide piston displacement measurements. This equipment provides a sampling rate of 20 kHz and provides a measurable range of 30 mm. While this range is much smaller than the stroke length of 230 mm, it is sufficient for the monitoring of piston bounce and indicating when the piston reaches TDC.

3.3.1.5 Piston Rod Assembly

The piston assembly runs through all of the major components in the driving/driven section of the University of Leeds RCM: from piston displacement measurement to the combustion chamber. The assembly features PTFE seals on both the driving and driven piston, serving similar purposes. At the driving end this seal prevents compressed air from leaking out of the pneumatic driving reservoir and into the hydraulic section. Whereas the PTFE pack seals behind the piston head prevent oil from the hydraulic section entering the combustion chamber, air leaking into the combustion chamber when under vacuum, and fuel mixture and combustion products from leaking out of the chamber under compression.

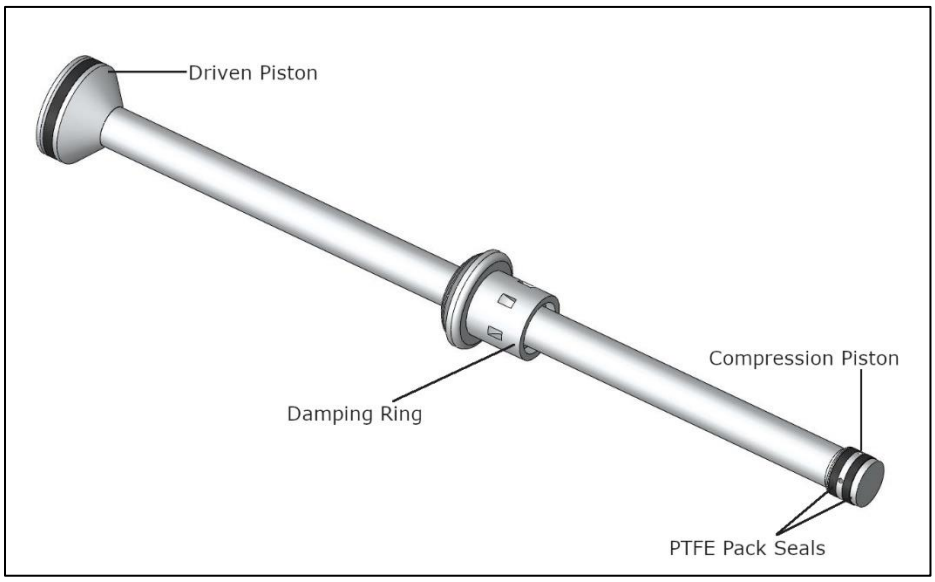

Figure 3.6. A 3D schematic of the University of Leeds RCM piston rod assembly. Adapted from [245].

3.3.1.6 Piston Head

Table 3.3. Dimensions of the flat and creviced piston heads utilised as part of this study.

Parameter	Flat Piston Head	Creviced Piston Head
Face Bore	44 mm	42 mm
Rear Bore	44 mm	44 mm
Length	7 mm	11 mm
Crevice Volume		3 cm^3
Crevice Channel Depth		1 mm
Crevice Channel Length		4 mm

As part of this study the RCM utilises both a creviced and a flat piston head design. A stainless steel flat piston head is applied only in Chapter 4 to investigate and characterise inhomogeneous ignition phenomena. Whereas the creviced piston head is applied for the collection of the bulk of IDT data, as seen in Chapter 5. Each piston head and its associated PTFE seals are screwed onto the end of the piston rod, such that the tension created causes the seals to expand, forming an air-tight seal with the combustion cylinder. The dimensions of each piston head are shown in table 3.3.

3.3.1.7 Mixing Chamber

A separate, heated mixing chamber is used to prepare fuel/air mixtures in the University of Leeds RCM. This method allows for the preparation of a homogeneous mixture at a known temperature, facilitating the accurate calculation of EOC thermodynamic conditions and ensuring the full evaporation of liquid fuel components. The structure of the mixing chamber consists of a central cylindrical tube (composed of 316L stainless steel), sealed at either end by circular caps (303 stainless steel). One of the caps contains 4 ports, for the introduction of the gas inlet, liquid fuel inlet, mixture outlet and pressure transducer to the mixing chamber. The mixing chamber has been designed to a maximum working internal pressure of 0.5 MPa, with an internal volume of 1.77×10^{-3} m^3. This means that (dependent on the fuel used) the mixing chamber can hold enough fuel/air mixture for 15-25 firings of the RCM, if required.

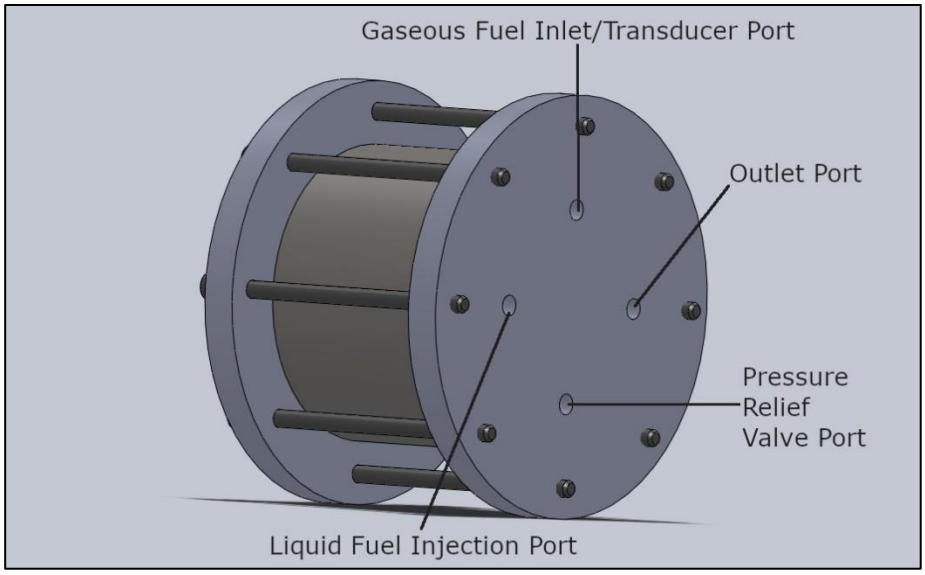

Figure 3.7. A 3D schematic of the University of Leeds RCM mixing chamber. Adapted from [245].

3.3.1.8 Measurement and Auxiliary Systems

- Pressure measurement:
  - Combustion chamber – manometer (COMARK C9557) and dynamic transducer (Kistler 6045A). A differential digital manometer located on the fuel/air inlet of the combustion chamber provides initial pressure measurements, used to accurately transfer the correct amount of fuel from the mixing chamber to the combustion chamber. This manometer measures up to 0.69 MPa gauge pressure, with a resolution of 100 Pa. The dynamic pressure transducer is located on the circumference of the combustion chamber (as mentioned previously) and provides accurate time resolved pressure measurements during the compression and ignition of fuel mixture. During operation, the signal produced by the dynamic pressure transducer is passed through a Kistler 5015 charge amplifier, which produces an output voltage of 0-10 V. This voltage is then digitised by the data acquisition card (DAQ): National Instruments PCI-6110.
  - Mixing chamber – static transducer (UNIK 5000). This transducer allows for the accurate production of the required fuel mixture, as individual components are added on a partial pressure basis. The maximum operating pressure for this transducer is 0.4 MPa. Measured pressure in the mixing chamber is displayed on a digital display with a resolution of 100 Pa.
- Temperature Measurement:

- Temperature is measured throughout the system by a series of exposed tip K-type thermocouples, attached to the desired measurement surfaces. This includes measurement of the mixing chamber, fuel manifold, piston shaft and combustion chamber temperatures. Monitoring these temperatures is necessary to maintain a homogeneous temperature environment throughout the system (preventing inhomogeneous ignition and fuel condensation), and the production of an accurate fuel mixture. Temperature is displayed on a digital display to an accuracy of 0.1 K.

- Temperature Control:
  - Combustion chamber – A series of six 50 W cartridge heaters provide heat for the combustion chamber. These are inserted into an end-plug in a circular arrangement, which is in-turn inserted into the end of the combustion chamber. The piston shaft, which leads into the combustion chamber, is heated by five 75 W band heaters spaced equally between the pistons resting position at BDC and the combustion chamber entrance. The temperatures of these two arrangements can be set separately using their corresponding CAL3200 PID temperature controllers.
  - Mixing chamber - A 2 kW band heater is mounted on the circumference of the central cylinder, with temperature monitoring and control provided by a K-type thermocouple located under the heating element and a CAL3200 PID, respectively.
  - Fuel manifold – To prevent the condensation of fuels within the stainless steel pipework, which delivers fuel from the mixing chamber to the combustion chamber, it is heated by a 50 W/m heating element cable. As with the temperature control of the combustion and mixing chamber, the temperature of this heating element is controlled by combination of a K-type thermocouple and CAL3200 PID.

3.3.2 Fuel Preparation

Each fuel mixture produced for testing in the RCM consists of some combination of the individual components described in table 3.4. As well as liquid fuel components, any RCM test mixture also contains gaseous components which serve the role of both the oxidiser and diluents. Gaseous components are all provided via research grade BOC compressed gas cylinders, connected directly to the RCM mixing chamber by flexible plastic pipe and controlled by individual needle valves. For all test mixtures, oxygen is used as the oxidiser, with a compositional purity of >99.99%. The oxidiser is mixed with liquid fuel components and diluents on a partial pressure basis, with an uncertainty of ±0.5 mbar (0.12% of the total oxidiser pressure). The ratio of diluents varies for each test mixture from an assortment of argon, carbon dioxide and nitrogen.

Table 3.4. Sources for liquid fuel components used in this study.

Component	Reference Code	Purity	Source
Gasoline	PR5801	-	Shell Global Solutions
iso-Butanol	UN1212	>99%	Alfa Aesar
iso-Octane	UN1262	>99%	Merk KGaA
n-Heptane	UN1206	>99%	Fisher Scientific
Toluene	UN1294	99.8%	SA
Ethanol	UN1170	95%	Fisher Scientific
1-Hexene	UN2370	>98%	Alfa Aesar

Mixture compositions are dictated by the required EOC conditions, the capabilities of the RCM and the adiabatic core assumption [93]. The adiabatic core assumption is often applied in RCM studies to estimate the temperature at the EOC (T_c) from pressure measurements, as the direct measurement of these temperatures is difficult [48]. This assumption states that a test gas within the RCM combustion chamber consists of a hot core gas, homogeneous in temperature and composition, surrounded by a cooler boundary layer of gas in contact with the chamber walls. During compression, heat losses occur only from this cooler boundary layer and the hot core gas remains unaffected by heat losses, hence the assumption that the compression of the core gas is adiabatic. This means that for the calculation of test mixture compositions to achieve a desired EOC temperature and pressure condition, it can be assumed that the core region will be compressed isentropically. For the compression of the bulk gas, heat transfer still occurs between the cooler boundary layer and the chamber wall. As such, the compression of the bulk gas is not truly isentropic. However, previous studies have shown that lower than isentropically expected pressure and temperature conditions can be accounted for through the use of the effective CR (P_c/P_i) [108,109]. Hence, the EOC condition can be calculated if the pre-compression temperature (T_i), pressure (P_i) and gas mixtures thermodynamic properties are known, as shown in equation 3.1.

$$\frac{T_c}{T_i} = \left(\frac{P_c}{P_i}\right)^{\frac{\gamma-1}{\gamma}} \qquad \text{Equation 3.1}$$

Here, T_i and T_c are the initial temperature and temperature at the EOC, P_i and P_c are the initial and compressed pressures and γ is the ratio of specific heats for a given fuel/oxidiser mixture. The ratio of specific heats for the fuel mixture requires the calculation of molar heat capacity at constant pressure (C_p) and volume (C_v). The molar heat capacity at constant pressure is calculated for each species via the associated NASA polynomial coefficients [165], as stated by the thermodynamic data presented in the combined mechanism described in section 3.5.1. This is shown in equation 3.2.

$$\frac{C_{pi}}{R} = a_1 + a_2T + a_3T^2 + a_4T^3 + a_5T^4 \qquad \text{Equation 3.2}$$

Here a_n denotes the relevant NASA polynomial coefficient, R is the molar gas constant and c_{pi} is the molar heat capacity at constant pressure for an individual species, i. To calculate the C_p for the entire fuel mixture, the c_{pi} of each species is multiplied by the species molar fraction and summed together, as shown in equation 3.3, where x_i is the molar fraction of the species i, i=0,1,2…n and n is the total number of species.

$$C_p = \sum_0^n x_i c_{p_i} \qquad \text{Equation 3.3}$$

The total molar heat capacity at constant volume for the entire fuel can then be estimated via equation 3.4:

$$C_v = C_p + R \qquad \text{Equation 3.4}$$

where C_v is the total molar heat capacity at constant volume. To calculate the final compressed pressure and temperature of the test mixture, the piston compression is represented as a series of incremental steps, each of stroke length 1 mm. By calculating the CR at each stroke-step, the pressure at each step can also be determined, as shown in equations 3.5 and 3.6.

$$CR_n = \frac{V_i}{V_i + (\pi r^2 l_n)} \qquad \text{Equation 3.5}$$

$$P_{n+1} = P_n + CR_n^{\gamma_n} \qquad \text{Equation 3.6}$$

Here, CR_n is the compression ratio at the n-th step, V_i is the initial combustion chamber volume, r is the radius of the chamber and l_n is the total stroke length travelled by the piston at the n-th step. This calculation continues in incremental steps until the maximum stroke length (230 mm) for the piston is achieved. The temperature at each stroke-step can also be calculated through the application of equation 3.1.

For a fixed initial temperature, a range of EOC conditions can be produced through the manipulation of the initial temperature, pressure, and the ratio of specific heats, which in turn can be controlled through the addition of different diluents in varying amounts. Diluents serve to change the thermodynamic properties of the fuel/air test mixture, such that a wider range of EOC temperatures and pressures can be achieved. Therefore, while the diluents are inert and do not react directly with fuel components, they still produce a significant influence on the measured IDTs in the RCM. A combination gas of argon, carbon dioxide and nitrogen is blended with the liquid fuel mixture, serving as a diluent, with each combination specific to a given EOC temperature and stoichiometry condition. Typically, monatomic gases (such as argon) allow for the investigation of higher temperatures, whereas polyatomic gases (such as carbon dioxide) allow for the probing of lower temperatures [246]. The effects of changing diluent gases have been investigated somewhat in the literature and have shown the diluent gas has a significant impact on the RCM heat loss characteristics and, ultimately, the measured IDT [246,247]. However, due to limitations in the University of Leeds RCM heating arrangement, significant changes to diluent mixtures are required to investigate the desired temperature range.

Before each fuel/oxidiser mixture is prepared, the RCM mixing chamber is heated for a minimum of 2 hours. The pre-heat temperature throughout the mixing chamber must be high enough to ensure that all liquid fuels used are completely in the vapour phase prior to beginning RCM experiments [48,248]. During this time, the RCM manifold and combustion chamber are also heated to provide a uniform temperature throughout the equipment, to ensure the liquid remains in the vapour phase during testing. After the allocated minimum heating time, the mixing chamber is vacuumed to an absolute pressure of less than 5 mbar. The mixing chamber is then purged with compressed air up to an absolute pressure of 2 bar, before repeating the vacuuming process. This ensures the removal of any residuals from previous mixtures.

Liquid fuel components are injected via a valve, directly into the mixing chamber. Each liquid fuel component is measured volumetrically to a pre-determined amount, using a specific syringe reserved for each fuel component, minimising the likelihood of cross-contamination. Each syringe is chosen such that uncertainty in volume measurements is minimised, with an uncertainty of ±0.5 µL for the smallest volumetric fuel component. To illustrate the impact of such an uncertainty, figure 3.8 displays the change in simulated 5-C IDTs as a result of ±1 µL (twice the measurement uncertainty) of ethanol during mixture preparation.

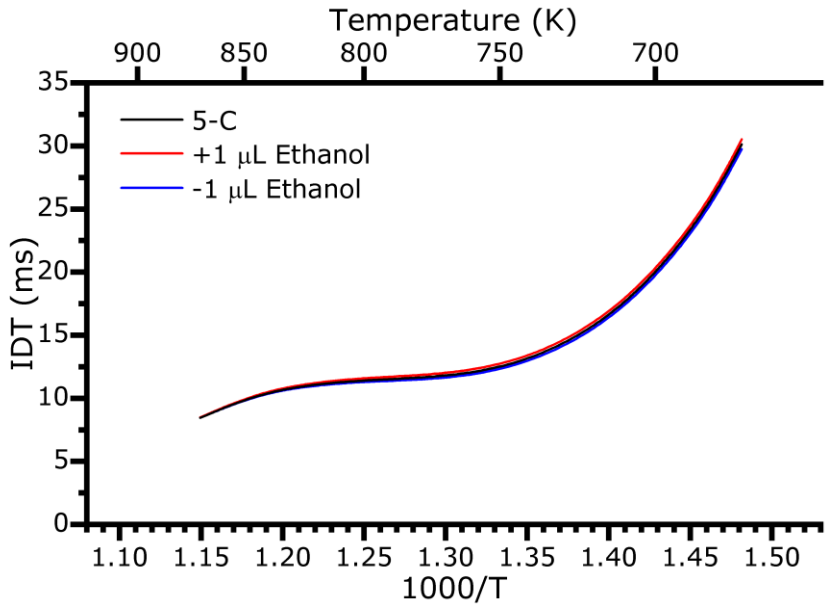

Figure 3.8. The influence of volumetric uncertainty in ethanol during mixture preparation on the simulated IDTs of 5-C. P_c=20 bar. Φ=1.0.

Ethanol is shown in this example as it is the smallest volumetric component and the most temperature sensitive. In this figure, there is no significant observable difference as a result of twice the volumetric measurement uncertainty. As the liquid component is injected, the partial pressure change due to this is measured and compared to a computed partial pressure based on the pre-calculated component volume, as is performed in previous work [248]. This provides a further check that the volume of liquid fuel injected is accurate. Recorded partial pressure readings showed an agreement of <±0.5 mbar for each liquid component. Syringes are screwed onto the valve inlet such that, upon opening the valve and injecting the liquid fuel component, no air enters the mixing chamber. Liquid components of the smallest volume are injected to the mixing chamber first, minimising the potential errors caused by residual mixture becoming trapped in the valve mechanism or small amount of lead-in pipe. Gaseous mixture components, such as oxygen and diluent gases, are supplied to the RCM via individual gas lines and controlled via individual mixing chamber inlet valves. Each gaseous component is added to the mixture on a pre-calculated partial pressure basis. Molecular oxygen is used as the oxidiser in all test mixtures, and some combination of nitrogen (N_2), carbon dioxide (CO_2) and argon (Ar) gases is used as a diluent. Charges are then left to mix diffusively at the pre-determined initial gas temperature (T_i) for 120 minutes minimum (unless stated otherwise), to ensure that the prepared mixture is heated to the required temperature, as well as homogeneous in both temperature and composition.

3.3.3 Operating Technique

Prior to the heating of the combustion chamber (and the preparation of the test mixture), the RCM combustion chamber is thoroughly cleaned. This involves the removal of the combustion chamber end-plug and cartridge heaters (hence why this is completed prior to heating), providing access to the chamber interior and piston face. The end-plug, chamber interior walls and piston face are cleaned thoroughly through using a solvent cleaner (typically acetone). This cleaning procedure is completed firstly with the piston at its EOC condition, providing much easier access to the piston face. The piston is then reset to its start of compression (SOC) position, such that the interior walls of the combustion chamber and piston lead-in shaft can be accessed for cleaning. During this process, the end-plug seal is inspected for damage before being re-inserted into the combustion chamber, at which point the pre-heating of the combustion chamber can begin. The combustion chamber and piston shaft are heated to the same temperatures as the mixing chamber and RCM manifold, to prevent to condensation of fuels throughout the equipment and the introduction of a stratified temperature environment. This preheating is applied for at least the mixing time of the test gas (120 minutes).

After the preparation and homogenisation of the test mixture, RCM testing can begin. Each batch of test mixture provides a number of individual “runs” or “shots” (used interchangeably). For each run, with the piston at the SOC position, the combustion chamber is evacuated to a maximum absolute pressure of 2 mbar. The chamber is then filled with compressed air to a maximum pressure of 2 bar, before repeating the evacuation process. This is repeated several times (typically 3) per run to ensure the removal of any gaseous residuals in the combustion chamber. During this process, the ability of the combustion chamber to hold both a positive and negative gauge pressure is tested through the use of the compressed air and vacuum pump, respectively. In each testing process, the inlet valve is closed, and pressure is measured at both the time of closing the valve and after a period of 5 minutes, generally showing a pressure change of <2 mbar. The presence of a significant pressure change during this test is often evidence of a failed O-ring or piston head pack-seal, which may have degraded through the use of acetone (used for cleaning) or the general wear-and-tear of RCM operation. The same air-flushing and vacuuming technique is applied to RCM manifold sections, ensuring any fuel carrying pipework is also free of gaseous residuals.

Following the evacuation of the combustion chamber, a charge of the test mixture is transferred from the mixing chamber to the combustion chamber and metered slowly through careful control of a high precision needle valve. The quantity of this charge is determined via

pressure measurements of the combustion chamber, such that the partial pressure of the charge is equal to the pre-determined P_i value. Once this value is reached, both the combustion chamber and mixing chamber are isolated by closing the corresponding inlet and outlet valve, and the mixture is left to homogenise in the combustion chamber for 5 minutes. This reduces the influence of turbulence induced through the fluid motion of the test charge as it is introduced to the combustion chamber, which may lead to localised hot and cold gas regions. This effect can be exacerbated by fluid motion during compression, causing significant inhomogeneities and errors in IDT measurement [249]. During this homogenisation period the RCM is prepared for the “firing” of the piston. Hydraulic oil is pumped (using the hand pump seen in figure 3.1) into the damping and locking chamber to a pressure of 40 bar. This pressure locks the piston assembly in place while the pneumatic driving reservoir is filled with bottled compressed air, to a pressure of 13.5 bar.

The firing of the RCM is controlled by a trigger, which opens a solenoid valve, releasing much of the hydraulic oil which locked the piston in place. As the driving force (provided by the compressed air pressure in the driving reservoir) surpasses the locking force (provided by hydraulic oil pressure), the piston is driven at high velocity towards its EOC position. Remaining oil serves to damp the piston’s motion as it enters the combustion chamber, preventing the piston from bouncing back once it reaches TDC. This damping can be controlled by the fine tuning of 3 needle valves, which control the flow rate of oil through damping channels. This piston is held at TDC due to the air pressure in the pneumatic driving reservoir. Piston position is monitored with a Keyence model LK-G82 laser and sensor pack to provide piston displacement measurements, at a rate of 20 kHz. Data from this sensor pack is used in analysis to determine when the piston arrives at TDC. Data collection is triggered by the same electronic trigger which initiates the release of the hydraulic oil solenoid valve. During and after compression, pressure, time, and piston displacement are recorded for the determination of IDT for each run. The driving reservoir is then emptied of compressed air and the piston is reset by introducing compressed air into the combustion chamber, forcing the piston to return to the SOC position. The process is then repeated for the next run, beginning with the evacuation of the combustion chamber.

3.3.4 Ignition Delay Time Measurement

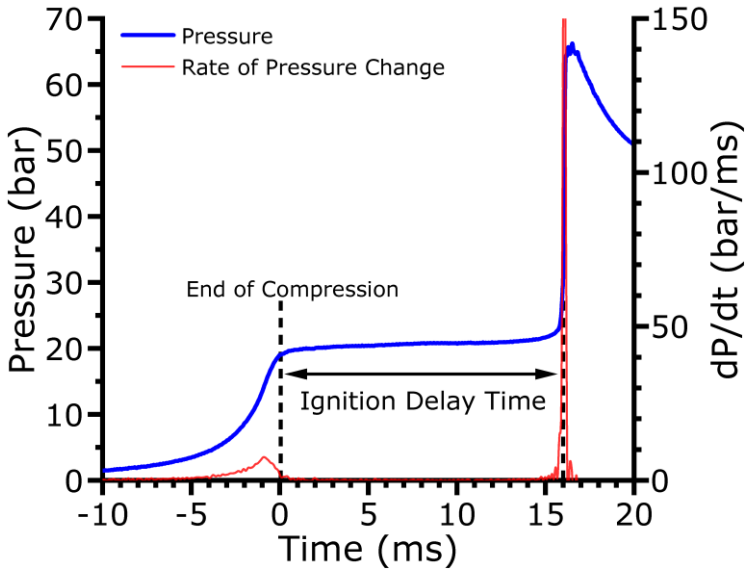

Figure 3.9. The definition of IDT (τ_i) as shown for a typical RCM pressure trace. This pressure trace was recorded for 5-C at conditions of T_c=800 K, P_c=20 bar, Φ=1.0.

The autoignition of a given test can be observed through the evaluation of recorded RCM combustion chamber pressures, during and post-compression. This data provides an RCM "pressure history", which records the development of the pressure environment within the combustion chamber during the experiment. In the case of data collected as part of this study, pressures are recorded at a frequency of 100 kHz, for a time period of 1 second post-initiation of the compression procedure (as controlled by the use of an electronic trigger). The IDT (τ_i) can be defined as the time taken for a given fuel/oxidiser mixture to autoignite at a constant temperature and pressure. With relevance to RCM pressure data, this can be calculated by finding the time difference between the EOC and the time at which autoignition occurs, as shown in figure 3.8. The EOC can be identified by piston displacement measurements, and also by evaluation of the experiments pressure history. In the case of the latter, the EOC can be located by the end of the associated pressure increase, resulting in a local pressure maximum. For the purpose of this study, the point at which autoignition occurs is defined as the time at which a global maximum rate of pressure change occurs. By measuring both of these properties, the RCM can give a direct measurement of IDT. This method is common in previous RCM studies of autoignition [47,48,51]. Other studies have also provided an alternative method, wherein the autoignition point corresponds to a 20% pressure increase in pressure, due to ignition [250,251].

For cases which display two-stage ignition, it is useful to define a first (τ_1) and second (τ_2) stage IDT, as well as the overall IDT (τ_i). An example two-stage ignition case is shown in figure 3.10. This type of ignition is characterised by the presence of a "cool-flame" and an associated LTHR behaviour, as described in detail in section 2.5.1, and is typical of degenerately branched systems [53]. This produces a pressure rise post-compression but before bulk ignition of test gas, as shown in figure 3.10. The first-stage IDT (τ_1) is defined as the time difference between the EOC and the maximum local rate of pressure rise during the LTHR process. The second-stage IDT (τ_2) is therefore defined as the difference between the first-stage IDT (τ_1) and the total IDT (τ_i).

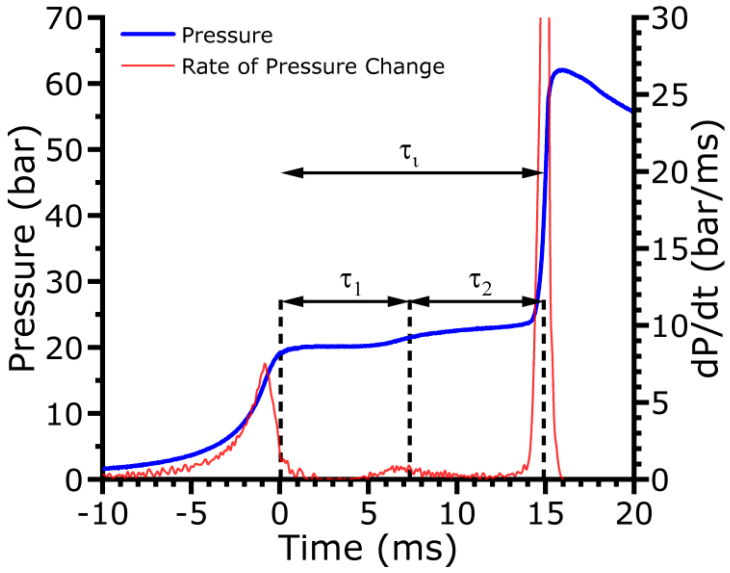

Figure 3.10. The definition of first-stage IDT (τ_1) and second-stage IDT (τ_2), with respect to the total IDT (τ_i), as shown for a typical two-stage ignition RCM pressure trace. This pressure trace was recorded for 5-C at conditions of T_c=710 K, P_c=20 bar, Φ=1.0.

Each IDT value reported in this study is calculated as the mean value of 4-8 individual RCM runs, from the same batch of test mixture. The error in each mean IDT value is then estimated as twice the standard deviation. The standard deviation for each IDT value provided in Chapter 5 was found to be well within 10% of the presented IDT value. For each reactive condition investigated, a corresponding non-reactive pressure history was also produced. Non-reactive cases are produced by replacing the mixture oxygen content with nitrogen and repeating the experiment under the same temperature and pressure conditions as the reactive case. The similar thermophysical properties of oxygen and nitrogen allows for the assumption of consistent heat loss behaviour between the non-reactive and reactive cases. Pressure data provided by these non-reactive tests can be used to determine the temperature at the EOC,

using the adiabatic core assumption shown in equation 3.1. IDTs are presented using this derived temperature and not the pre-calculated temperature, as this better represents the real EOC conditions achieved during the RCM experiment.

3.3.5 Experimental Conditions

Table 3.5. A list of fuel blends and experimental conditions investigated in the RCM as part of this study.

Blend	Iso-Butanol Volume (%)	Equivalence Ratios	Temperatures (K)
Gasoline	0	1.0, 0.5	675-870
Gasoline iB10	10	1.0	710-870
Gasoline iB30	30	1.0, 0.5	
Gasoline iB50	50	1.0	
Gasoline iB70	70	1.0	
5-C Surrogate	0	1.0, 0.5	675-870
5-C iB05	5	1.0	710-870
5-C iB10	10	1.0	
5-C iB20	20	1.0	
5-C iB30	30	1.0, 0.5	
5-C iB50	50	1.0	
5-C iB70	70	1.0	
Iso-Butanol	100	1.0, 0.5	710-870

RCM IDT measurements were conducted for a wide range of compositional and thermodynamic conditions. The representation of gasoline by the developed 5-C surrogate is investigated at conditions of T_c=675-870 K, P_c=20 bar and Φ=1.0 and 0.5. The influence of iso-butanol on the ignition behaviour of gasoline was investigated by blending iso-butanol with the reference gasoline at 10, 30, 50 and 70% by volume iso-butanol. IDTs for each of these individual blends were recorded for conditions of T_c=710-870 K, P_c=20 bar and Φ=1.0. The 30% blend of iso-butanol with gasoline was further investigated at conditions of T_c=710-870 K, P_c=20

bar and Φ=0.5. The same is true for blends of iso-butanol with 5-C. However, this also includes two additional blends of 5% and 20% by volume iso-butanol, to further develop an understanding of the blending behaviour of relatively small iso-butanol volumes. IDT measurements of the "neat" iso-butanol fuel were also recorded at conditions of T_c=710-870 K, P_c=20 bar and Φ=1.0 and 0.5. A full list of experimental conditions is shown in table 3.5 for gasoline and 5-C blends with iso-butanol. Initial temperature, pressure and diluent fractions were varied to produce the required EOC conditions, as discussed previously in section 3.3.2.

3.4 Engine Study

Knowledge of a fuel's combustion behaviour within an SI engine is crucial for the determination of optimal fuel blends, as well as the effective and safe use of alternative fuels in current and developing engine technologies. Boosted SI engines, operating at high pressures, may be limited in their effectiveness by engine knock. Fuel additives and blending components which have the potential to increase the octane quality of the fuel blend, provide an opportunity to operate modern engine technologies at higher in cylinder pressures, without the concern of knocking combustion, improving engine efficiency. However, the benefits of such an octane boosting additive are limited if engine power is significantly impacted. By investigating the influence of iso-butanol blending on the normal and knocking combustion behaviour of gasoline, in terms of mean pressure cycles, cyclic variability, KN, knock intensity and IMEP, at advancing spark timings, this study aims to identify optimal fuel blends for use within SI engines. The results of this investigation will then be compared with the IDT measurements produced through fundamental RCM experiments, assessing the ability of such fundamental experiments in predicting engine level behaviour, at similar thermodynamic conditions. Surrogates must also be able to reproduce the combustion behaviour of gasoline and its blends within SI engines, if models are to be developed which accurately predict engine level gasoline combustion properties. Therefore, the representation of gasoline and iso-butanol blends by the 5-C surrogate within an SI engine is evaluated in this study. In summary, the objectives of the engine study conducted in this research are:

- To investigate the ability of the proposed gasoline surrogate to replicate the combustion behaviour of gasoline in a pressure boosted SI research engine, both as a neat fuel and under iso-butanol blending.
- To investigate the influence of iso-butanol blending on the normal and knocking combustion properties of gasoline and 5-C in a pressure boosted SI research engine (LUPOE), including KNs, knock intensities and IMEP.

- To make comparisons between the combustion behaviour observed within RCM and LUPOE experimental results.

In recent years, the University of Leeds has produced several high quality studies of naturally aspirated SI engine combustion, utilising the Leeds University Ported Optical-access Engine (LUPOE) [57,252,253]. Due to the need to investigate higher compressed pressures, more in line with modern SI engine technologies (such as turbocharging), the LUPOE underwent extensive redesigns and modification. LUPOE modifications are fully detailed in the work of Ling [59] and include: the installation of an independent solenoid valve to the exhaust line (allowing for a controllable exhaust system which may be used to increase charge times), the rearrangement of intake and exhaust ports, and a decrease of 50% in the total number of exhaust holes. These improvements allowed the LUPOE to reach peak motoring pressures of 30 bar, as seen in the several studies which have successfully utilised the updated LUPOE [50,52,254]. The following sections describe the current configuration of the LUPOE facility, the operational procedure followed in this study (Chapter 7) and the analysis techniques applied.

3.4.1 LUPOE Description

The LUPOE was developed on the base of an original, commercially available, Lister Petter-PH1 single-cylinder diesel engine. This original engine was then heavily modified at the University of Leeds for use as a research engine. Firstly, a new cylinder head was developed for the LUPOE to replace the original. This new cylinder head is a flat, disc-shape and contains a compact spark-plug at the centre of the cylinder bore. This shape assists in the generation of a uniform in-cylinder fluid flow, meaning that the impact of turbulence is minimised, whereas the addition of a spark plug is necessary for the conversion of the engine from a diesel (compression-ignition) engine to a gasoline (SI) engine. The compact spark-plug used consists of a 0.5 mm steel anode, housed in a 3 mm diameter alumina sheath. Fuel intake was adapted from an overhead inlet valve, to two diametrically opposed, rectangular shaped intake ports. Each port is inclined by 20% with respect to the cylinder interior, to minimise the turbulent effects such as “swirl” and “tumble” [255]. The exhaust outtake is replaced by a singular exhaust duct, which communicates with the bulk test gas via a void between the cylinder barrel and cylinder liner. This liner contains two rings of circular exhaust holes (of 10 mm diameter each), which allow interaction between the void and the test gas. Port opening for fuel intake and exhaust outtake is controlled by piston motion, which will block the access to exhaust holes and fuel intake ports during motoring. This ported breathing behaviour generates an in-cylinder flow field which is uniform, such that the LUPOE can be described as a featureless flow engine [59].

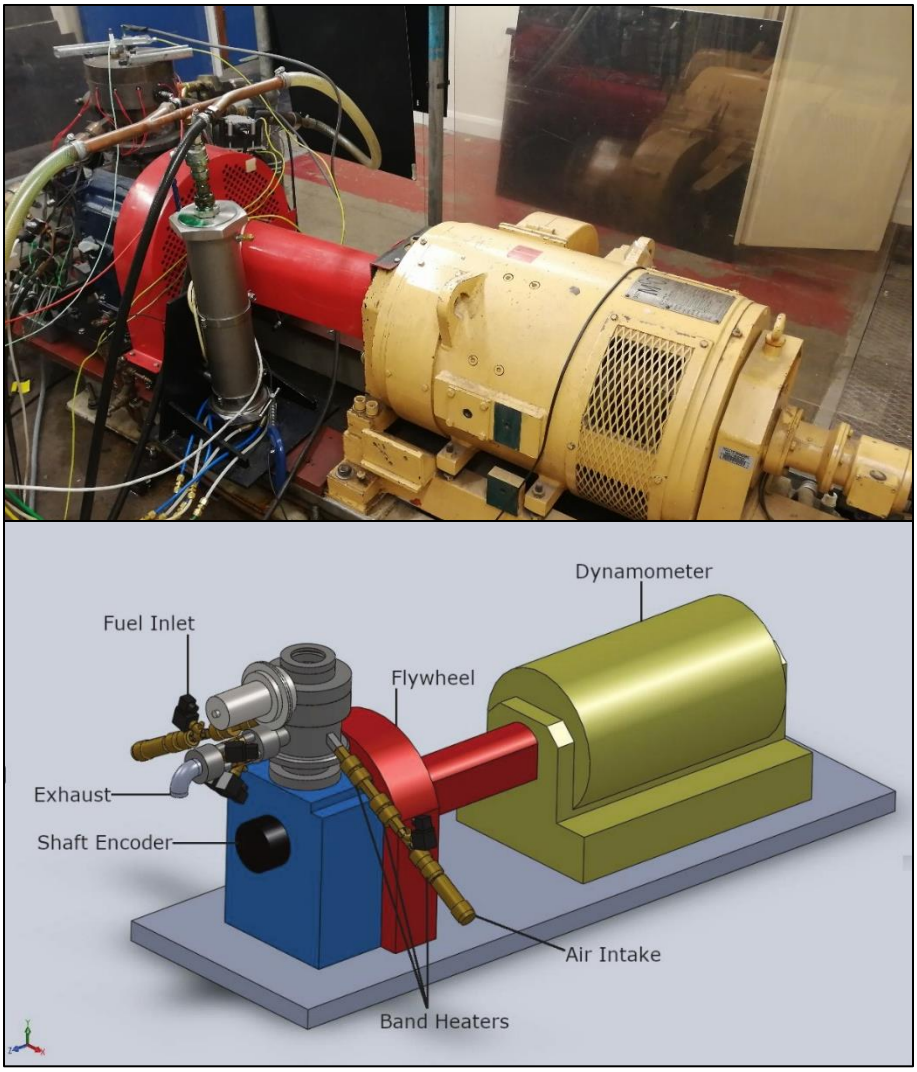

Figure 3.11. A labelled 3D schematic of the LUPOE facility, adapted from [59].

The engine is motor driven, with motion provided by a dynamometer and electric motor, which can be controlled to allow the LUPOE to operate at varying engine speeds. The engine can operate regularly at stable engine speeds of 400-2000 RPM, typically within a variation of -15 to +30 RPM at an engine speed of 750 RPM and -30 to +50 RPM for an engine speed of 1500 RPM. A flywheel is fitted to the engine driveshaft, storing rotational kinetic energy during the operation of the engine. This facilitates the smooth operation of the engine by limiting the influence of fast angular velocity fluctuations due to combustion and the resultant differences in compression and expansion strokes. Reference time signals are provided during the operation of the LUPOE at TDC and fixed crank angle degrees thereafter, by a shaft encoder connected directly to the engine driveshaft. A 3D schematic of the LUPOE facility is shown in figure 3.11. Engine parameters are listed in table 3.6.

Table 3.6. Specifications of the LUPOE, as applied in this study.

Parameter	Value
Cylinder Head Shape	Disc
CR	11.5
Bore	80 mm
Stroke Length	110 mm
Clearance Height	8 mm
Connecting Rod Length	232 mm
Inlet Ports Opening/Closure	107.8 CA°
Exhaust Ports Opening/Closure	127.6 CA°

It should be noted that there are some clear differences between the design and operation of the LUPOE boosted engine and a conventional SI engine, which should be considered during the analysis of any data. Principally, as mentioned, the LUPOE operates on a skip-firing method, whereas a typical SI engine does not. This means that “real” SI engines will be subject to effects which are not considered during the operation of the LUPOE, such as the influence of residual gases on the combustion of a fuel/air mixture and a larger degree of residual heat between combustion cycles. In this sense, the firing-cycle conditions within the LUPOE should be similar to those of the RCM, wherein the presence of post-combustion residuals are ideally eliminated, allowing for a direct comparison of combustion behaviours between the two facilities. The inlet/exhaust architecture is also substantially different between the LUPOE and a conventional SI engine; a conventional SI engine would typically have a single set or pair of overhead inlet and exhaust valves, whereas the LUPOE utilises a pair of diametrically opposed fuel/air inlets on the circumference of the cylinder, and two rings of circular exhaust holes also on the circumference of the cylinder, leading to a single exhaust outtake. The LUPOE has a maximum CR of 11.3 (which can be adjusted if needed, through the use of a series of metal shims, placed between the cylinder head and the top of the engine block). During operation, the in-cylinder pressure reaches as high as 30 bar before ignition, with peak temperatures prior to ignition typically in the range of 620 – 630 K [59]. These conditions differ somewhat from the RCM, which is operated at a compressed pressure of 20 bar and a temperature range of 675-870 K.

3.4.2 Fuel Preparation and Delivery

For the operation of the LUPOE, considerably larger volumes of liquid fuel are required than the operation of the RCM for the completion of a single set of experiments. Typically, a single mixture batch for a set of RCM experiments (several runs at one set of conditions) requires less than 1 ml of total liquid fuel volume, whereas the LUPOE requires at least 1.6 L (two 800 ml tanks, one for line flushing and the other for engine testing) of liquid fuel for the completion of a single experiment (one fuel blend at a range of crank-angle spark advance timings). This is partly due to the necessity of fuel line flushing in the LUPOE, a process which evacuates any previous mixture from all fuel carrying components, ensuring the composition of the tested fuel is homogeneous throughout the equipment. A full 800 ml tank of liquid fuel is required to ensure that this process is completed satisfactorily. Due to the large quantities of fuel required, small errors in the measurement of individual liquid components do not strongly influence the ignition properties of the final blended fuel. As such, the precise syringing of individual liquid components is not required. Instead, liquid fuel mixtures are prepared as 4 L batches, ensuring a consistent mixture between fuel line flushing and experiments, with a reserve of mixture for the completion of repeats/further experiments. Batch fuels for LUPOE experiments are prepared to the same volume percentages as the fuel blends used in RCM experiments. Each individual liquid component is measured volumetrically, using a graduated measuring cylinder appropriate to the required volume of the liquid component. Each measuring cylinder corresponds to an individual fuel for the duration of the mixture preparation process (all glassware is cleaned between the preparation of different batches). Fuel is supplied from an 800 ml fuel tank by to the LUPOE by a standard automotive filter and electrical pump system. The mass flow rate of liquid fuel is controlled by an M53 Bronkhorst Coriolis mass controller and fuel pressure is maintained at 3 bar by a Bosch pressure regulator.

Air is supplied to the LUPOE at a pressure of 4 bar (the compressor supplies air at 7 bar but this is reduced by a filtered regulator). The compressed air line forks into two separate supply lines, each controlled by a Bronkhorst EL-FLOW thermal mass flow meter, with a maximum mass flow rate of 33 g/s, and feedback adaptation to maintain a constant air/fuel ratio during operational pressure fluctuation. To further minimise the influence of air flow oscillations during LUPOE operation, a 5 L surge tank is installed between each inlet pipe and mass flow controller, ensuring a consistent air supply pressure. A series of five 175 W and 200 W band heaters along the length of each intake pipe are used to increase and maintain the air temperature at the required value. The presence of these heaters also supplies the heat flux

required to vaporise liquid fuels during mixing with the supplied air. Fuel in injected 350 mm upstream of the cylinder intake port, wherein it mixes with the combustion air, by a venturi carburettor, ensuring the full vaporisation of liquid fuel prior to entering the cylinder. A schematic of the full LUPOE air/fuel flow control system can be observed in figure 3.12.

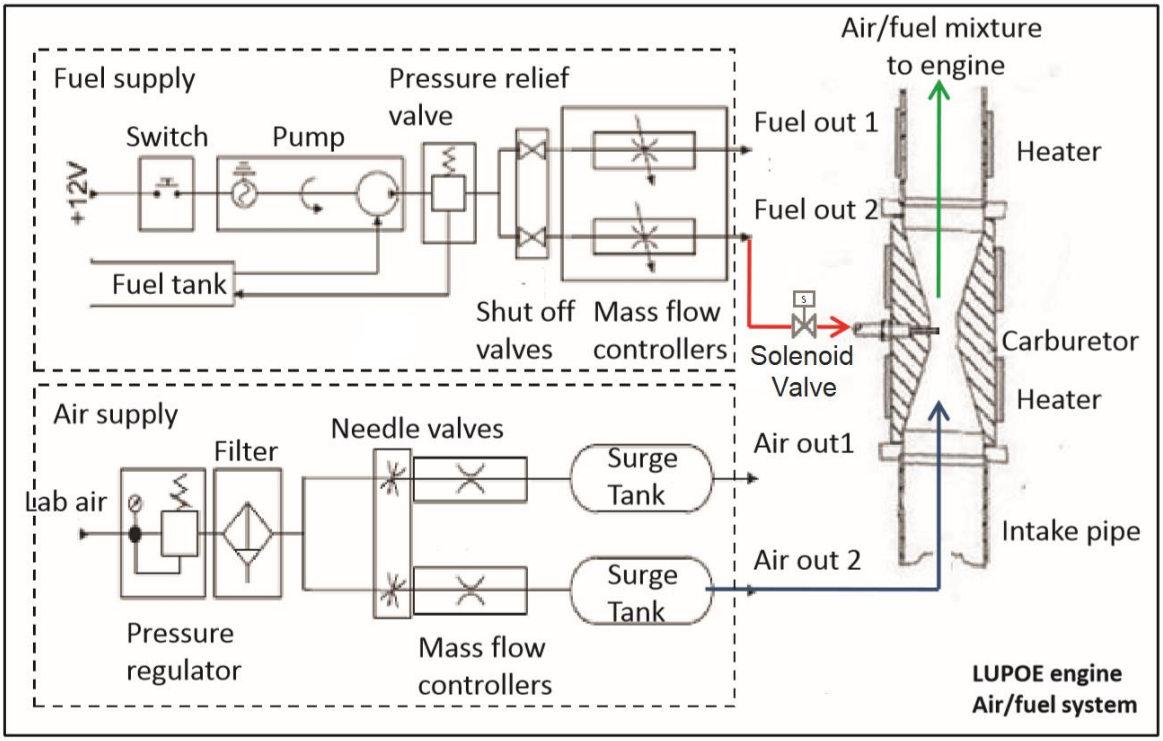

Figure 3.12. A schematic diagram of the full LUPOE air/fuel flow control system, adapted from [59,255].

Cylinder pre-heat temperature is controlled by twelve equally spaced 50 W cartridge heaters, inserted around the circumference of the cylinder, with temperature control provided by a Digitron 4801 control unit. For all LUPOE experiments, the cylinder was preheated to a temperature of 50 °C. Due to the large thermal inertia of the cylinder and the effectiveness of the 50 W cartridge heaters, pre-heating to higher temperatures is not feasible. Increased pre-heat temperatures would also impact the engine resting time between each run, as the cylinder must be left to cool substantially in the absence of an active cooling system.

3.4.3 Operating Procedure

The LUPOE is controlled by a DsPIC 6140A microcontroller, which provides triggering signals for inlet and exhaust valve timing, spark firing and data acquisition, as a function of shaft encoder clock signals. Instructions are provided to the microcontroller via a C script, which can

be easily modified to change experimental parameters (such as spark advance timing and the number of motoring and fuelling cycles). Operation of the LUPOE is initiated by an electronic trigger, which activates the microcontroller and relevant instructions. The microcontroller will terminate the experiments after a given number of firing cycles to reduce the likelihood of extreme knocking conditions (due to increased in-cylinder temperatures from a lack of active cooling), which may cause damage to the equipment or pose a safety risk. The same is also true for conditions which display a peak pressure above a given threshold.

Prior to beginning experiments, the LUPOE cylinder head is removed and inspected for any damage and the presence of soot. The interior of the cylinder head is cleaned in a similar process to RCM cleaning; acetone is applied with a cloth to remove any deposits on the cylinder interior. However, care must be taken when cleaning the spark, which is delicate due to its small diameter (0.5 mm). Black deposits on the spark tip can prevent consistent spark discharge, which can cause a fuel to fail to ignite or ignite at an incorrect time, dependent on the severity of the deposits. After cleaning, the cylinder head O-ring is inspected for any damage before replacing the cylinder head. The engine is then preheated, and temperature is left to homogenise for a minimum of 120 minutes.

For the purpose of this study, the LUPOE was operated at an engine speed (ω) of 750 RPM, an initial pre-heat temperature (T_i) of 323 K, a boosted pressure (P_i) of 1.6 bar and a stoichiometric air/fuel ratio. A list of experimental parameters, as applied at all investigated conditions, is shown in table 3.7. Mass flow rates for each fuel are pre-calculated based on the required stoichiometry. To avoid the presence of post-combustion residuals and exhaust gases, reducing the likelihood of preignition, 24 skip-firing cycles (of which 16 were fuelling cycles) were completed between every firing cycle. This was shown to be effective in previous LUPOE studies [52,255], and also proved so in the completion of this study. Starting at a spark advance crank angle of 2 CA° bTDC (crank-angle degrees before TDC), each fuel is tested for a minimum of 13 sequential firing cycles (with 24 skip-firing cycles between each firing cycle). The engine is then left to cool ambiently for 30 minutes before the next experiment can begin. Spark discharge timing is then advanced by a maximum of 2 CA° and the process is repeated. Once knocking conditions are identified, as oscillations in the recorded in-cylinder pressure history and as a characteristic audible “ping”, spark advance timing is iterated by 1 CA° in either direction to locate the condition at which knock first occurs. Spark discharge timing is then advanced by 1 CA° until the knock limited spark advance (knocking boundary) is found. This point is defined as the latest spark advance timing which generates a minimum of 90% knocking

cases [59]. The spark advance timing may then be advanced further, up until the maximum safe peak pressure of 120 bar is achieved.

Table 3.7. LUPOE operating parameters during all test conditions.

Parameter	**Value**
Engine Speed (ω)	750 RPM
Intake Temperature (T_{in})	323 K
Intake Pressure (P_{in})	1.6 bar
Equivalence Ration (Φ)	1.0
Air Mass Flow Rate ($\dot{m}_{air}$)	10.2 g/sec
Exhaust Gas Recirculation (EGR)	0 %

3.4.4 Data Collection and Analysis

During operation, the in-cylinder pressure was measured using a combination of two pressure transducers: a dynamic pressure transducer (a piezoelectric 0-250 bar Kistler 601A), which is mounted flush to the cylinder wall, and an absolute pressure transducer (0-20 bar Kistler 4045 A20), which is mounted 60° below TDC, at the lower end of the piston barrel. During piston motion, the position of the absolute transducer is such that it is isolated from the combustion chamber as the piston passes a crank angle of 58.6° bTDC, where in-cylinder pressures are typically 2.5-3 bar. Voltage signals from the absolute pressure transducer are amplified by a Kistler 4601A piezoresistive amplifier with a voltage output of 0-10 V, providing a reference pressure for the calculation of the cylinder pressure. The dynamic pressure transducer can be used to measure rapid pressure changes during the experiment, the signals of which are amplified by a Kistler 5007 charge amplifier with a voltage output also of 0-10 V.

The calculation for cylinder pressure (P_{cy}), requires the gauge pressure (P_g), absolute pressure (P_a) and the crank-angle degrees at exhaust port closure (Φ_{EC}):

$$P_{cy} = P_g + \left(P_a(\emptyset_{EC}) - P_g(\emptyset_{EC})\right) \qquad \text{Equation 3.7}$$

where the P_g is provided by dynamic pressure transducer measurements and P_a is provided by absolute pressure transducer measurements.

Pressure traces collected during operation were then analysed to investigate the knocking properties of each fuel blend. The knocking behaviour of a given fuel can be described by its KN and knocking intensity [49]. These properties can be found analytically through the method described in the work of Liu and Chen [173]. This method defines the point of KN as the point at which the first significant pressure inflection is observed in the pressure trace, which then causes a series of pressure oscillations. KN describes the crank angle location at which autoignition of the end gas occurs, producing observable engine knock. The point of inflection can be calculated precisely as shown in equation 3.8.

$$KN = -\frac{dP^2}{d\emptyset^2} = \frac{1}{\Delta\emptyset}\left[\frac{(P_n - P_{n-1})}{\Delta\emptyset} - \frac{(P_{n+1} - P_n)}{\Delta\emptyset}\right] \qquad \text{Equation 3.8}$$

This method calculates the rate of change of the pressure-crank angle gradient, over 3 points of pressure data, where *P* are the pressure parameters at the *n*th crank angle and *Φ* is the crank angle in degrees. As the crank angle is reported in constant steps by the shaft encoder, the change in crank angle is constant. From this, the KN can be determined by finding the first point at which *KN* exceeds a pre-determined knock threshold. This threshold should be less than the maximum amplitude of the knock oscillations but also greater than the amplitude of the noise caused by engine vibrations.

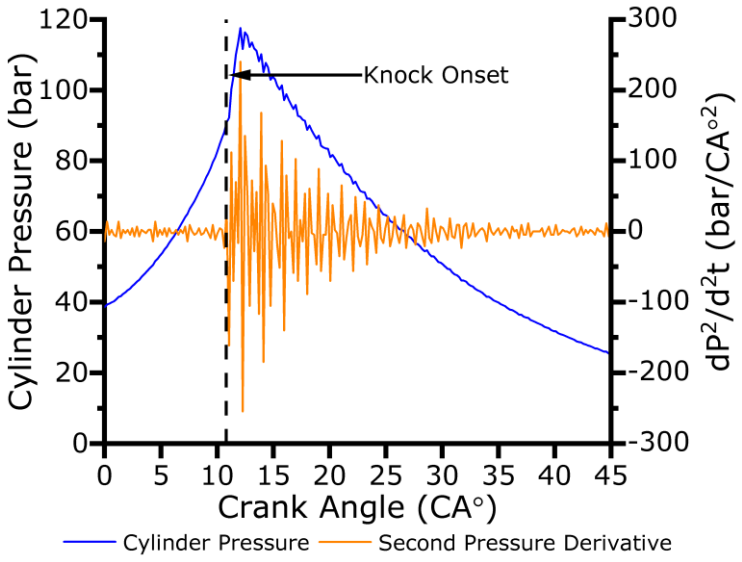

Figure 3.13. An example of analysis performed using the method of Liu and Chen [173], showing the cylinder pressure history, rate of pressure gradient change history and the point of KN. This example is produced using gasoline as the fuel, at a crank angle spark advance timing of 10 CA°.

Due to the influence of characteristic engine non-uniformities and the resultant cyclic variability, selecting a single knock threshold for all investigated conditions may lead to the misidentification of knocking cases. Therefore, a knock threshold is selected on a case by case basis, typically with values of 15-30 bar/CA° [2]. A similar approach has been applied in previous LUPOE work to account for cyclic variability in the determination of KN [52]. This method of KN detection has been shown in a previous study to produce KNs within 0.2 CA° of onsets determined by direct imaging of engine combustion [59]. Knock intensity is defined as the maximum amplitude of the rate of pressure rise. An example of the results derived through this method can be seen below in figure 3.13.

Cycle to cycle variations in peak pressure are typical during LUPOE operation and can provide insight into cyclic variability and the prevalence of engine knock at a given condition. The coefficient of variation (CoV) is a property which characterises these variations and can be defined by equation 3.9, as the ratio of peak pressure standard deviation to the mean peak pressure. Similarly, the CoV for the crank angle location of peak pressure can also be defined in this manner and provides an opportunity for further investigation of the cyclic variability and knocking propensity at a given condition. This statistical parameter is often applied to evaluate cyclic variability within engine studies [50,256–259].

$$CoV = \frac{\sigma_{P_{max}}}{\bar{P}_{max}} \qquad \text{Equation 3.9}$$

3.5 Simulations and Sensitivity Analysis

In this study, each RCM condition investigated experimentally is also simulated via chemical kinetic modelling (as described in detail in section 2.6), to evaluate the model's ability in reproducing the fuel's ignition behaviour and to develop an understanding of the ignition behaviour of blended fuels. Chemical kinetic modelling, in theory, has the potential to accurately predict the ignition behaviour of a wide variety of fuels at a large amount of thermodynamic conditions. This predictive ability could provide a low cost alternative (both financially and in terms of time) to an extensive series of experiments studying ignition, which can aid in the generation of optimal fuel mixtures and the determination of such a fuel's combustion behaviour. However, to provide predictions to a high degree of certainty, a robust and comprehensively validated chemical kinetic mechanism is required. The need for a highly detailed kinetic mechanism to facilitate the prediction of combustion for complex fuel mixtures, introduces significant challenges, as these mechanisms may require the accurate description of hundreds to thousands of species and several thousands of reactions. Uncertainties in these parameters

may propagate throughout the model, causing inaccuracies in model predictions. The accurate determination of each reaction rate parameter and species thermodynamic data within a detailed mechanism, through experimental or theoretical means, is not feasible. Sensitivity analysis techniques allow for the identification of highly important reactions and species which would warrant such evaluation, allowing for the estimation of parameters which are not as important, based on previous knowledge and experience. The objectives of the modelling study and associated analysis conducted within this work are:

- To assess the ability of a detailed chemical kinetic mechanism to accurately predict the IDTs of 5-C and 5-C/iso-butanol blends, such that computer models may be applied to predict the behaviour of gasoline blends.
- To evaluate the ability of a detailed kinetic mechanism to accurately predict the heat release behaviour of 5-C and 5-C/iso-butanol blends.
- To assess the underlying chemistry driving the autoignition of 5-C and 5-C/iso-butanol blends through the application of sensitivity analysis techniques to a detailed chemical kinetic mechanism.
- To investigate the chemistry driving the LTHR behaviour of 5-C through the application of sensitivity analysis techniques to a detailed chemical kinetic mechanism.
- To assess the sensitivity of model predictions due to uncertainties in both the thermodynamic properties of species within the mechanism and reaction rate parameters.

The CHEMKIN-PRO [169] software is utilised to predict the ignition behaviour of the full range of 5-C and iso-butanol blends (as listed in section 3.3.5), wherein the RCM is modelled as a closed, zero-dimensional homogeneous batch reactor. A variable volume approach was applied for the prediction of IDTs, which takes account of characteristic RCM heat losses post-compression and any exothermicity during the compression phase. This process is described in full in section 3.5.2 and has been shown in a previous study of H_2 autoignition to perform well when compared to more computationally expensive CFD simulations of the RCM [260]. Constant volume simulations, which do not account for the effects of compression and RCM heat losses, are also completed using the same modelling technique. These simulations serve as a platform for sensitivity analysis performed in this study, due to the lower computational requirements when compared to variable volume simulations (which are vastly increased by the application of the sensitivity analysis techniques detailed in this chapter), while predicting similar IDTs (as shown in figure 3.15). Local OH concentration sensitivity analysis is produced using the CHEMKIN-PRO [169], whereas enthalpy of formation and A-factor brute force sensitivity

analyses are completed using the Cantera [168] Python library (Cantera version 2.4.0, Python version 3.7).

3.5.1 Mechanism Description

A combined mechanism of the Sarathy et al. butanol isomers mechanism [84] and Lawrence Livermore National Laboratories (LLNL) “Gasoline Surrogate” mechanism [85] is applied to produce modelling results. It is understood that some improvements have been made to the LLNL “Gasoline Surrogate” mechanism in recent studies. These changes include the replacement of the original C_0-C_4 sub mechanism with the AramcoMech 2.0 mechanism [261], the updating of C_5-C_8 alkane chemistry in line with recent studies [46,90,91,262,263], the revision of aromatic and cyclical species chemistry [264–269] and the updating of the ethanol sub mechanism to reflect recent studies [270]. However, this updated mechanism has not been made publicly available and detailed changes to kinetic and thermodynamic data have not been thoroughly described in the literature sources [271,272]. As such, this study applies the original LLNL gasoline surrogate mechanism, which was shown in the original study to be validated for several individual species and blends of relevance to gasoline surrogates, and at a wide range of appropriate thermodynamic conditions [85]. Appendix A outlines the structure of the combined mechanism and the constituent sub-mechanisms used in this study. The thermodynamic properties for all species included in the combined mechanism are predicted via Benson’s GA method as implemented by the THERM program developed by Ritter and Bozzelli [273]. This is documented in the sources for the gasoline surrogate and butanol mechanism components [84,85]. The work of Agbro et al. [51,274] highlighted the importance of the reaction $C_6H_5OH+CH_3=C_6H_5CH_3+OH$, through local and global sensitivity analysis of the gasoline surrogate mechanism. The mechanism was updated such that the rate constant for this reaction was consistent with that provided by Seta et al. [275], which is the source for much of the other toluene oxidation chemistry present in the surrogate mechanism. Reverse and equilibrium rate constants for the reaction were implemented into the gasoline surrogate mechanism. This update increased the IDTs observed for a surrogate mixture (57.5% iso-octane, 11.25% n-heptane, 31.25% toluene by volume), particularly at temperatures <800 K, while the IDTs at the high temperature end remained relatively consistent [51].

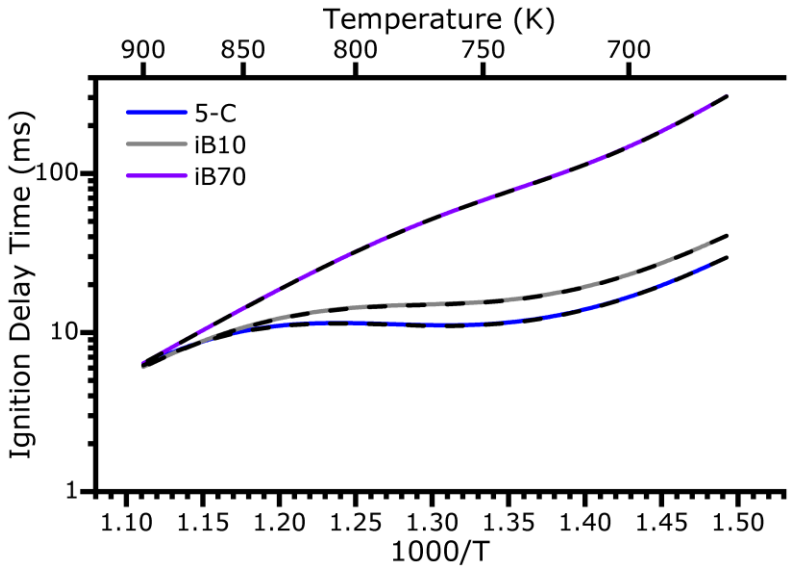

Figure 3.14. Constant volume simulation IDTs for the full and "reduced" mechanism, showing no difference between the predictions at blends of 5-C, iB10 and iB70. The solid coloured lines show simulation results for the reduced mechanism. The dashed black lines show simulation results for the corresponding full mechanism cases. P_c=20 bar, Φ=1.0.

The full combined mechanism consists of 8396 (6524 reversible of which 5624 have defined reverse rate parameters) reactions and 1983 species. Using mechanism reduction techniques as an autonomous tool, unaccessed species and reactions which, while part of the original mechanism, do not take part in the determination of IDTs for the investigated mixtures, are eliminated from the mechanism. This was performed using the Reaction Workbench software [276], applying the Direct Relation Graph with Error Propagation (DRGEP) reduction method [277]. The IDTs at all investigated conditions for the 5-C, iB10 and iB70 fuels were selected as the reduction targets, with a relative tolerance of 0%, such that only species and reactions not involved in the autoignition chemistry of the surrogate and iso-butanol blends were removed from the mechanism. This simple elimination of irrelevant species and reactions produced a mechanism of a more manageable size of 4322 reactions (3643 reversible of which 2403 have defined rate parameters) and 872 species, which was observed to produce no observable difference in simulated IDTs when compared to the full mechanism, as shown in figure 3.14.

3.5.2 Rapid Compression Machine Modelling

Both constant volume and variable volume simulations are performed as part of this study. Constant volume simulations are analogous to initiating the simulation once the RCM piston has

reached the EOC. These simulations do not represent reactor physics characteristic of RCMs, such as heat losses from the test gas post compression and exothermicity or radical production during the compression phase. As such, these simulations take place in a constant volume, zero-dimensional homogeneous batch reactor model, representing the RCM test gas as a single homogeneous zone. While these simulations do not account RCM physics, they are much less computationally expensive that the variable volume counterpart.

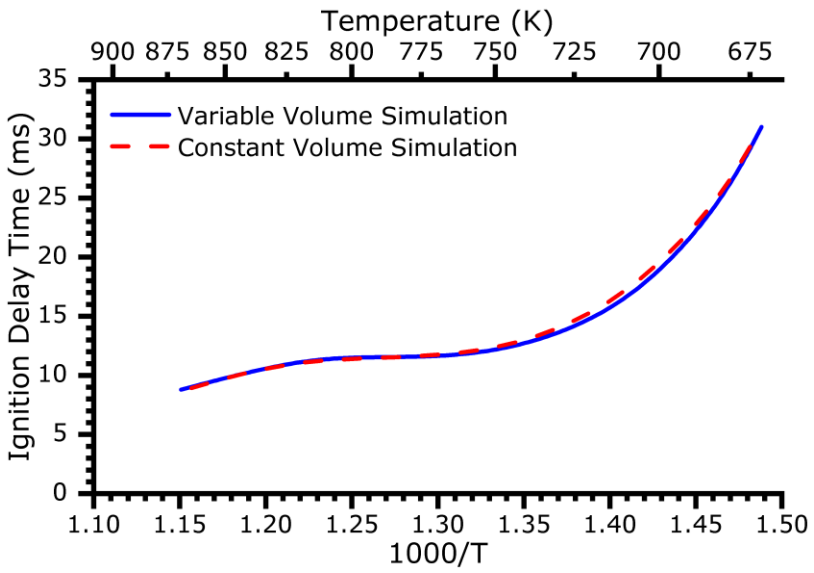

Figure 3.15. Similarities between predicted IDTs from constant volume and variable volume simulations for 5-C at P_c=20 bar, Φ=1.0.

In this study, a typical constant volume simulation can be completed in 2-5 minutes, which is much less than the 30-90 minutes required for each variable volume simulation. Because of this, constant volume simulations are applied when computationally expensive sensitivity analysis are required to limit excessive computation timescales. This approach is justified due to the similar IDTs predicted under constant and variable volume simulations at most conditions, as shown in an example comparing the two simulations for the 5-C fuel (figure 3.15). However, differences between the two methods are magnified at longer IDTs due to the increased influence of RCM heat losses. The initial conditions for the constant volume simulation are set such that the starting temperature and pressure are equal to the EOC RCM temperature and pressure of the investigated mixture. Mixture compositions are set according to initial molar fractions of RCM test mixtures.

While an RCM would ideally represent a fully homogeneous reactor, with instantaneous compression to the desired T_c and P_c and limited heat losses, this is not the case in reality.

Each RCM facility is subjected to unique facility effects which produce significant variations in results between different RCMs [101]. These facility effects are typically defined by the compression phase and post-compression heat losses. The kinetic implications for accurately representing these phenomena in models are clear, due to the exponential temperature dependence of reaction rates and the influence of heat losses on gas temperature, and the potential initiation of radical production during compression. The build-up of radicals during the compression stroke can play a substantial role in the evolution of the radical pool post-compression, producing significantly shorter IDTs. This is evidenced in the work of Mittal et al. [278], which modelled the ignition of dimethyl ether (DME)/oxidiser mixtures under separate conditions, accounting for heat losses post-compression in one case and accounting for the compression stroke and heat losses in another case. At a condition of T_c=639 K and P_c=20.1 bar, accounting for the compression stroke was shown to reduce the IDT by 7% from the case which did not. As temperature was increased to T_c=720 K, this difference increased to a 60% shorter IDT. While concentrations of the main radicals during the compression stroke was small (<1 ppm), this was nonetheless sufficient to produce a substantial reduction in IDTs [278].

The representation of post-EOC heat losses can be represented by specifying the volume expansion of the core gas post-compression, through pressure measurement of non-reactive RCM experiments (described in section 3.3.4). While the bulk gas is maintained at a constant volume during the RCM experiment, the boundary layer between the core gas and the wall cools post-compression, allowing the core gas to experience an effective volume expansion. This method is commonly applied to produce variable volume simulation results in the literature [47,51,116,132,250,260]. The effective volume is calculated at each timestep based on the pressure recorded from non-reactive RCM tests, following the method shown in equation 3.10, as applied in previous studies [39,47,51].

$$V(t) = V_0 \left(\frac{P(t)}{P_0}\right)^{\frac{1}{\gamma}} \qquad t \geq 0 \qquad \text{Equation 3.10}$$

Here $V(t)$ is the effective volume at time t, V_0 is the initial volume, $P(t)$ is the measured pressure of the non-reactive case at time t, P_0 is the initial pressure and γ is the ratio of specific heats for the gas. By evaluating the volume for all relevant points in time, a tabulated volume history of the non-reactive RCM experiment is produced, which can justifiably be used to represent the volume history of the reactive case during compression due to their similar thermodynamic properties. Time dependent gas temperature can also be derived using the

adiabatic core assumption (equation 3.1). Temperatures derived in this manner have been shown to closely agree with those predicted by CFD simulations of RCMs [48].

Simulations are produced using both constant and variable volume methods for the 5-C surrogate, iso-butanol fuel, and blends of 5, 10, 20, 30, 50 and 70% iso-butanol by volume. IDT predictions are made for all the above listed fuels for conditions of T_c=710-870 K, P_c=20 bar and Φ=1.0, using the same fuel composition as in the RCM experiments. The 5-C, iso-butanol and 30% iso-butanol blend (iB30) are also simulated at conditions of T_c=710-870 K, P_c=20 bar and Φ=0.5, in the same manner. In each simulation, the predicted IDT is defined as the time difference from the EOC to the maximum peak in OH concentration, which often serves as an analogue for the point of ignition in models of this kind.

3.5.3 Sensitivity Analysis

To investigate discrepancies between experimental IDTs and simulated results, as well as to highlight important reactions and the driving thermochemical behaviour, sensitivity analysis was conducted at several modelled conditions. Investigated targets for sensitivity analysis include the IDT (using peak OH concentration as a proxy), HRRs, aHR and gas temperatures at the soITHR and soHTHR.

A local A-factor sensitivity analysis on peak OH concentration was performed using the CHEMKIN-PRO software [169], to determine the sensitivity and potential influence of each reaction on the peak concentration of OH. The radical OH was selected as the target for this analysis as it is known to serve as the main chain carrier for hydrocarbon autoignition and oxidation, with a rate of production which is closely linked to the overall reaction rate [279,280]. For local A-factor sensitivity analysis, CHEMKIN-PRO [169] utilises a modified version of DASPK [281] which applies backward differentiation formula methods to solve the system of ODEs and produce the desired sensitivity coefficients [162]. For a local A-factor sensitivity analysis on OH concentration, the system of ordinary differential equations can be defined in the form:

$$\frac{dZ_{OH}}{dA_i} = f(Z_{OH}, A_i) \qquad \text{Equation 3.11}$$

where Z_{OH} is the mass fraction of OH radicals in the total gas, A_i is the pre-exponential factor of the reaction i and i=0,1,2…n, where n is the total number of reactions in the mechanism. The first order sensitivity coefficient is therefore defined as:

$$S_i(t) = \frac{\partial Z_{OH}(t)}{\partial A_i}$$ Equation 3.12

where S_i is the first order local sensitivity coefficient of the OH concentration relative to the A-factor of reaction *i* and at time *t* [162,280]). For the full matrix of model variables, the differential of equation 3.12 with respect to A_i gives the equation:

$$\frac{d\boldsymbol{S_{j,i}}}{dt} = \frac{\partial \boldsymbol{f}}{\partial \boldsymbol{y}} \cdot \boldsymbol{S_{j,i}} + \frac{\partial \boldsymbol{f}}{\partial A_i} = \mathbf{JS} + \mathbf{F}$$ Equation 3.13

where **J** is the Jacobian matrix with respect to the system variable, **F** is the derivative with respect to the system parameters (parametric Jacobian matrix) and *j* refers to the dependent variables of the system (such as species mass fractions, molar fractions and gas temperatures) [162,282]. This Jacobian matrix is the same as that required by CHEMKIN-PRO [169] in the solution to the original model problem by backwards-differentiation. As such, it is readily available for sensitivity computations. This analysis produces a tabulated list of time integrated sensitivity coefficients for each reaction [162]. By evaluating the sensitivity coefficient at the time of peak OH concentration, an analogue for the sensitivity of IDTs to the A-factor of each reaction can be determined. Sensitivity coefficients are then normalised by the largest sensitivity magnitude (such that normalised negative sensitivities remain negative), to produce normalised sensitivity values.

For the study of sensitivity for key heat release parameters (such as aHR and temperature at soITHR/soHTHR) to changes in reaction pre-exponential A-factors, a brute-force sensitivity analysis method is applied, as no clear chemical markers exist to define these points precisely and consistently. In this method, the A-factor of each reaction in the mechanism is perturbed independently and the change in a global variable due to each perturbation is investigated. For the purposes of this study, pre-exponential A-factors were increased by a factor of 1.5 (50% increase) from their nominal values, while other model parameters were maintained at their original values. This method was applied using the Cantera [168] Python library, for constant volume simulations. Sensitivity coefficients for the various heat release parameters were calculated using equation 3.14.

$$S_i = \frac{(y_0 - y_1)}{y_0}$$ Equation 3.14

Here, S_i is the sensitivity coefficient of the parameter *y* relative to reaction *i*, and y_0 and y_1 the predicted parameter values for the base and perturbed case, respectively. Again, sensitivity coefficients were normalised by the magnitude of the largest sensitivity, to produce a list of

normalised sensitivities. This method has been applied in previous studies in the A-factor sensitivity analysis of global IDTs [47,51].

Furthermore, a brute force sensitivity analysis was performed to assess the impact of uncertainties in the thermodynamic properties of each species (namely the enthalpy of formation) on the overall IDT and key heat release parameters (HRRs, aHR and temperatures at soITHR/soHTHR). When not specified within the kinetic mechanism, reverse and equilibrium rate constants are calculated using species thermodynamic data, expressed as NASA polynomial functions [165]. Thus, the values of species' thermodynamic properties and their relevant uncertainties, may produce a significant influence on global model predictions. To investigate this, the NASA polynomial coefficient [165] a_6 was modified for each species, ensuring that only the enthalpy of formation (h_f) for the species was affected, without influencing the species entropy or specific heat. The standard enthalpy of formation was modified individually and independently for each species by a constant value of +5 kJ mol^{-1}, similar to previous studies of thermodynamic property sensitivities [183,184]. Using the same method as A-factor brute force sensitivity analysis, the sensitivity coefficient corresponding to this change can be calculated via equation 3.14. Diluent species and molecular oxygen are excluded from thermodynamic sensitivity analysis. The high sensitivity of molecular oxygen is known, due to its presence in many important reactions such as initiation oxygen additions, and the molecule's thermodynamic data is assumed to be known with absolute certainty [183]. Therefore, this value is discounted to prevent the dilution of further normalised sensitivity values. In addition, it is acknowledged that in reality, correlations exist between enthalpy values for different species. This behaviour is neglected in this analysis as correlations are only described for smaller species present within Active Thermochemical Tables (ATcT) [175,283]. Such information is not known for the larger fuel related species within the mechanism and therefore it is not possible to account for such correlations. The aim of these enthalpy of formation sensitivity analyses, is to identify important species that are key to the observed ignition and heat release behaviour, rather than attempting to assess the overall uncertainty in the chosen targets, which would necessitate taking correlations into account. As part of the analysis, heats of formation for the key identified species from the mechanism were compared with values available in Burcat's latest thermochemical tables, based on experimental, ab initio calculation and more recently ATcT methods [176]. Values derived from brute force enthalpy sensitivity analysis were also normalised by the largest derived sensitivity coefficient values in each case, to produce lists of normalised sensitivity coefficients.

3.6 Heat Release Rate Analysis

HRA provides an opportunity to investigate the development of multi-stage ignition phenomena and provide further fundamental data on the autoignition behaviour of fuels, as well as to evaluate the influence of fuel blending on such behaviours. LTHR behaviour is a crucial driving factor in the development of autoignition, particularly at low temperatures and within the NTC region. By evaluating the influence of iso-butanol blending on such heat release behaviour, greater insight can be gained into the overall impacts of blending on ignition behaviour. A robust computer model should also accurately predict such behaviour, else the prediction of global ignition behaviour (such as IDT) is fundamentally flawed. The research objectives for HRA conducted within this study are:

- To apply novel RCM HRA techniques to investigate the degree of low temperature exothermicity in the 5-C fuel and the influence of iso-butanol blending on this behaviour.
- To provide experimental data for the HRRs of 5-C and 5-C/iso-butanol blends, for a wide range of blending ratios, which may serve as valuable targets for the validation and development of chemical kinetic mechanisms.
- To evaluate the ability of a detailed kinetic mechanism to accurately predict the heat release behaviour of 5-C and 5-C/iso-butanol blends.

Goldsborough et al. [172] have shown in previous work that HRA can be applied effectively to RCM experiments, facilitating the investigation of LTHR behaviour for a wide range of thermodynamic conditions. This study applies similar methods for the calculation of HRRs from experimental RCM reactive pressure histories. Initially, the energy conservation equation (equation 3.15) is applied to the gas in the RCM reaction chamber:

$$\frac{dU_s}{dt} = \dot{Q}_{chem} - \dot{Q}_{wall} - \dot{W}_{piston} - \dot{H}_{out} + \dot{H}_{\text{in}} \qquad \text{Equation 3.15}$$

where U_s is the total sensible internal energy, $\dot{Q}_{chem}$ is the rate of heat released, $\dot{Q}_{wall}$ is the rate of heat exchange with the chamber walls, $\dot{W}_{piston}$ is the rate of work done by the piston on the gas and $\dot{H}_{out}$ and $\dot{H}_{\text{in}}$ are the rates of enthalpy flow out and in of the reaction chamber respectively. The adiabatic core assumption is applied to define the simplified RCM system, such that it is composed of a single volume consisting of both burnt and unburnt gases. In this simple system, any reactivity that may be present in the cool boundary layer is neglected. It is assumed that the contents of the combustion chamber are fully homogeneous in terms of pressure and that the contents behave as an ideal gas. Non-reactive RCM tests provide

pressure (and volume) histories, which are applied to empirically account for heat losses from the RCM system over the course of a test. By applying equation 3.15 under these conditions, and assuming that the piston trajectory is identical between both reactive and non-reactive cases, it can be shown that [172]:

$$HRR = \frac{\gamma}{\gamma - 1}\frac{dV}{dt}(P - P_{nr}) + \frac{1}{\gamma - 1}V\left(\frac{dP}{dt} - \left.\frac{dP}{dt}\right|_{nr}\right) - \frac{PV}{(\gamma - 1)^2}\left(\frac{d\gamma}{dt} - \left.\frac{d\gamma}{dt}\right|_{nr}\right)$$

Equation 3.16

where, *HRR* is the heat release rate, *γ* is the ratio of specific heats, *V* is the reaction chamber volume (as calculated from the non-reactive pressure history for the given experiment case), *P* is the pressure in the chamber and the suffix 'nr' denotes properties of the non-reactive case. From this equation it is possible to calculate the HRR at any time step, given the appropriate reactive and non-reactive pressure histories.

The Cantera [168] python library and the combined iso-butanol/gasoline surrogates mechanism (detailed in section 3.5.1) is applied to each RCM experiment case to calculate the temperature dependent specific heats at each time step, as required to solve equation 3.16. Specific heats for each species are determined using the NASA 7-coefficient polynomial parameterisation, as dictated by mechanism thermodynamic data. This allows the model to account for the changing gas properties during the experiments. Pressure traces are aligned for this model at the EOC, as determined by the RCM piston displacement measurements, such that the EOC is equivalent to piston TDC. The aHR is calculated as the time integrated HRR. All HRRs and aHRs presented in this study are normalised by the lower heating value (LHV) of the fuel mixture for each blend, allowing for comparisons between blends of their proportional heat release behaviour. Estimates of instantaneous gas temperatures can be made, based on the extent of exothermicity, using equation 3.17:

$$T_{gas} = T_u + x_b \cdot \frac{LHV}{c_v}$$

Equation 3.17

where T_{gas} is the gas temperature, *LHV* is the fuel's lower heating value, T_u is the unburnt temperature and x_b is the extent of exothermicity, as described by equation 3.18.

$$x_b = \int \frac{HRR}{LHV}dt$$

Equation 3.18

This novel method of HRA for RCMs has been applied in several recent studies to investigate heat release behaviour of both experiments and simulation predictions

[172,186,284,285]. RCM pressure traces are captured at a frequency of 100 kHz, which is sufficient to resolve low and ITHR behaviour. However, to resolve rapid HTHR behaviour a higher capture frequency (~1 MHz) would be required [172]. As such, HTHR behaviour as deduced by HRA is rarely discussed in this study, unless the fuels ignition duration is long enough to warrant it (for example, in the case of iso-butanol analysis in Chapter 4). In future work, it may be possible to resolve the high, low, and ITHR behaviour by splitting the dynamic pressure signal from the RCM and simultaneously recording the signal through a high and low frequency data acquisition card. For the processing of HRA, RCM reactive and non-reactive pressure traces are subject to a 5 kHz low bandpass filter to eliminate high frequency noise from pressure measurements. This is vital for the investigation of LTHR, due to the relatively small pressure changes associated with the relevant cool-flame phenomenon.

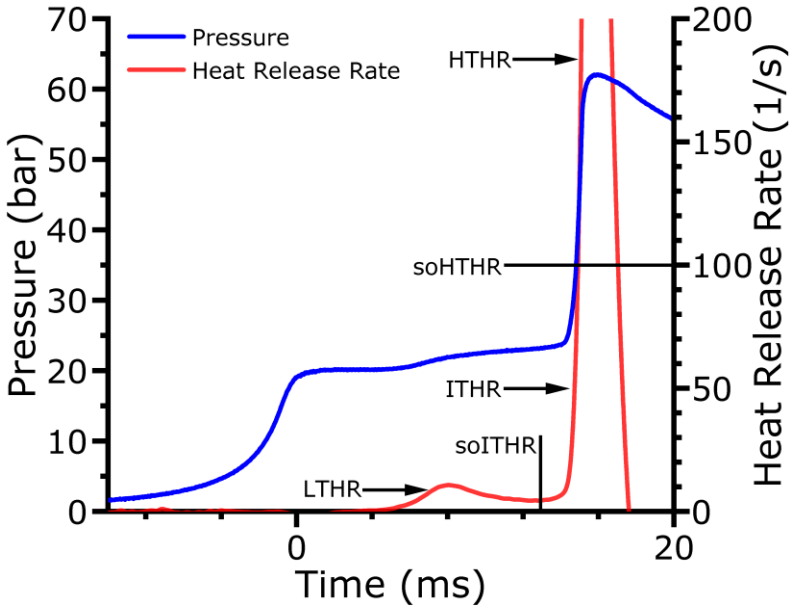

Figure 3.16. The definition of LTHR, ITHR, HTHR, soITHR and soHTHR, as shown for a typical two-stage ignition RCM pressure trace. This pressure trace was recorded for 5-C at conditions of T_c=710 K, P_c=20 bar, Φ=1.0.

LTHR, ITHR and anomalous PIHR are the focus of much of the HRA in this study. Definitions for each of these regimes can be seen in figure 3.16, wherein LTHR is described by exothermicity following the EOC, through the peak HRR at first stage ignition (in multi-stage ignition cases), up to the inflection point in HRR prior to autoignition [284]. This process is typical of degenerate branching systems [53]. For fuels which display ITHR behaviour, this begins at the described post-LTHR HRR inflection point (soITHR) and continues until the soHTHR, which is defined as the point at which the HRR exceeds 100/s ($HRR > 100/s$) [172].

PIHR cases are displayed in Chapter 4 HRA and are described by a slowly evolving pressure rise prior to autoignition, characteristic of a deflagration. This may consume a considerable amount of the fuel's chemical energy, increasing the pressure and temperature within the combustion chamber considerably, before inducing a strong autoignition. This heat release is defined by any heat release from the EOC until the transition to rapid autoignition [284].

Errors in HRA are difficult to estimate precisely, due in part to complex sources of uncertainty in RCM operation [248]. However, the largest source of errors in this analysis is likely to be due to the use of a single zone approximation in the determination of the HRR, and the application of the adiabatic core assumption in the calculation of temperatures and gas properties. Also, during reactive RCM experiments, exothermic processes can lead to greater heat losses than those experienced by non-reactive cases, leading to errors in the determination of HRR from these two pressure traces. The determination of these errors is beyond the scope of this study but should be considered in any future work.

4 Characterisation and Elimination of Inhomogeneous Ignition in a Rapid Compression Machine

4.1 Introduction

Pre-ignition heat release (PIHR) is a form of inhomogeneous (or spatially non-uniform) ignition behaviour observed in many RCM and shock-tube studies of IDT [124,131,132,286–289]. This phenomenon describes a process whereby flame/reaction fronts are initiated by inhomogeneities in the test charge [86,95]. This can be observed experimentally as a significant heat release prior to the main stage ignition event, which coincides with the propagation of reaction fronts throughout the test environment [123,125–127]. This propagation develops a significantly increased temperature and pressure environment within the reactor in comparison with a case unaffected by PIHR. Due to the nature of this behaviour, it can cause inaccurate uniform IDT measurements by generating times much shorter than those captured under homogeneous conditions, producing a mean IDT with a high degree of uncertainty. It is therefore beneficial to both characterise and eliminate this phenomenon, removing its influence on uniform RCM IDT measurements. It is not the purpose of this chapter to provide a thorough description PIHR or fully document previous literature on the topic, as this is covered in section 2.4. Traditionally, optical techniques are applied to determine the presence of PIHR by identifying the formation and evolution of the characteristic flames and flame fronts [124]. However, the experimental requirements for such setups often impose limitations on the achievable experimental conditions, such as EOC temperature and pressure conditions, and stoichiometries. This is due to the structural constraints applied to the RCM by the addition of optical access. Such access and diagnostic equipment can also provide a large financial cost, making such analysis infeasible for some facilities.

This chapter applies alternative, analytical methods to characterise PIHR in experimental RCM data, distinguishing such cases from a set of iso-butanol IDTs, which contains a large number of PIHR cases. An investigation of the relationships between the rate of pressure change (dP/dt) with pressure (P) and time from ignition (t_{-i}) in individual RCM pressure histories, aims to display the feasibility of PIHR determination from relatively simple and low-cost techniques. This method is then applied to identify and remove PIHR cases from existing data sets. Novel RCM HRA techniques are also applied to distinguish the key heat release features of PIHR and provide a further alternative, low cost and low (experimental) impact method of PIHR determination and removal. This technique is presented in previous literature, wherein it

proved an effective method for the determination of PIHR in a series of hot-spot pre-ignition induced IDT simulations for syngas mixtures [172]. Operational changes and mechanical modifications to the RCM are then made in an attempt to eliminate PIHR cases. Modifications focus on the elimination of turbulence induced gas inhomogeneities, while operational changes aim to improve the uniformity of test mixtures and produce a higher standard of maintenance and operation for the University of Leeds RCM. Additionally, the influence of these modifications on the overall uncertainty in IDT measurements is explored.

4.2 Inhomogeneous Ignition Characterisation

Under adiabatic conditions, it would be reasonable to expect a high degree of repeatability between RCM experiments and facilities. However, this is not always the case [97–99], which can make the interpretation of RCM captured IDTs found in literature difficult. The adiabatic core assumption provides a significant source of uncertainty in RCM experiments, as the homogeneous nature of the combustion environment cannot be guaranteed; “roll-up” vortices can be generated by the high velocity motion of the piston into the gaseous fuel/air mixture during compression [102]. These vortices mix the cool boundary layer into the hot adiabatic core, leading to a breakdown of the adiabatic core assumption [48,100,102]. This process and further descriptions of RCM turbulence are described in more detail in sections 2.3 and 2.4. It has been proposed in literature that, as a result of this turbulent mixing, a non-uniform distribution of temperature is generated within the gas, which may then lead to the generation of inhomogeneous ignition phenomena such as PIHR through the creation of localised high temperature zones (or “hot-spots”) [102,105,290].

Multiple literature sources have experienced and documented PIHR (or mild ignition) behaviour to varying degrees, providing several further rational explanations for its presence in each case. Dependent on the fuel and conditions investigated, the general consensus is that PIHR behaviour is commonly caused by non-ideal fluid dynamics as described previously [48,86,95,291,292]. Walton et al. showed that, for iso-octane mixtures, the rate of PIHR reaction front propagation was dependent on the degree of thermal stratification of the test gas [124], further evidencing the influence of a temperature inhomogeneities on the development of non-uniform autoignition. Others propose that the presence of particulates, oil droplets and residual combustion products in the combustion chamber are also a likely cause of PIHR [132,293–295], particularly when inducing a behaviour which is not highly repeatable, due to the variation in particle dimensions. Particles may ignite more rapidly than the surrounding gaseous fuel/air mixture. If the energy released by the combustion of these particles is high enough to accelerate

local gas reactions, it can cause the fuel/air mixture to ignite early [295]. Particulate generated hotspots and those caused by turbulent mixing of relatively hot and cold gases may both influence RCM operation simultaneously, increasing the propensity for induced PIHR and imposing significant uncertainties on the determination of uniform IDTs. For fuels which experience NTC behaviour, the turbulent mixing of test gas has been shown to accelerate first stage ignition in the vortex affected region. This leads to shorter measured IDTs (in the NTC regions) from RCMs which suffer with this non-uniform fluid behaviour, such as those utilising a flat piston head [296].

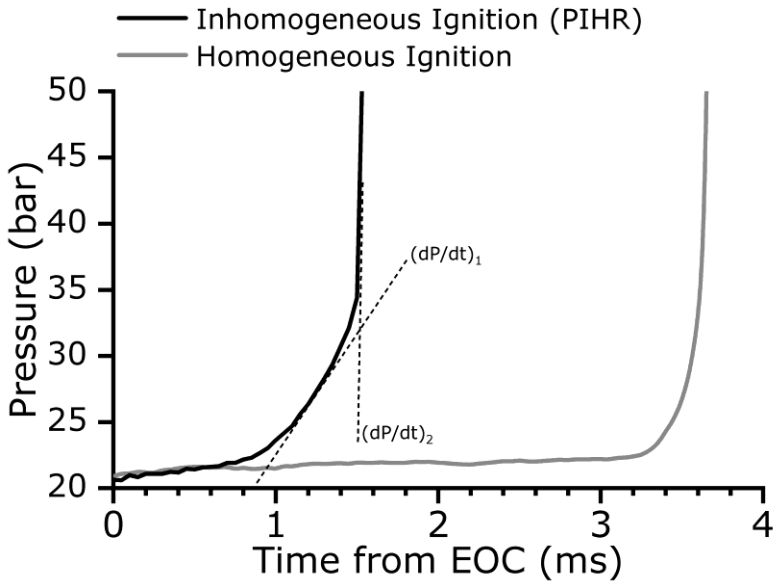

Figure 4.1. An example of a characteristic PIHR RCM pressure trace compared to that of a homogeneous ignition case. Pressure histories displayed are for iso-butanol at conditions: T_c=881K, P_c=20 bar and Φ=1. The solid lines show experimental RCM pressure traces. The dashed lines display the gradient change in the PIHR pressure trace.

An example pair of pressure traces, illustrating the impact of PIHR on development of main stage ignition in iso-butanol, can be seen in figure 4.1. These pressure traces are taken from RCM experiments for iso-butanol, at a compressed temperature of 881 K, and they show the development of autoignition at the time after EOC. The homogeneous ignition (or strong ignition) pressure trace shown in this figure provides a good example of the main stage ignition profile which is expected for an RCM operating at uniform conditions, under the assumption of an adiabatic core. The pressure trace displayed here for the homogeneous ignition of iso-butanol, is similar to that presented in the literature for this fuel [224,225]. Little to no pressure rise is displayed by the homogeneous ignition case prior to the IDT, and ignition in this case can

be described as a near instantaneous and large pressure rise. Similar observations can be made for homogeneous ignition in terms of the rate of pressure change (d*P*/d*t*) during ignition, which shows near zero values prior to a large and abrupt increase. This behaviour is shown in figure 4.2, which displays the pressure gradients with respect to time after EOC, for the iso-butanol RCM experimental pressure traces exhibited in figure 4.1.

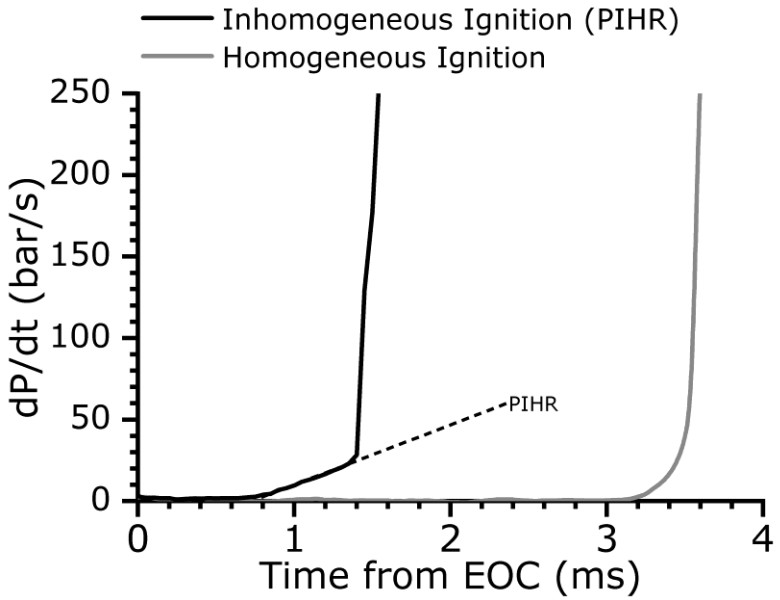

Figure 4.2. Pressure gradients with respect to time from EOC for the example pressure traces shown in figure 4.1. Iso-butanol fuel at conditions: T_c=881K, P_c=20 bar and Φ=1. Solid lines show experimental RCM pressure traces. The dashed line shows a forward forecast of the PIHR pressure gradient.

The behaviours displayed by the inhomogeneous/PIHR ignition case in figure 4.2 are observably different to those produced by the homogeneous case. The main stage ignition shown by the PIHR case can be categorised into two distinct regions: a relatively slow pressure change which elevates pressure conditions above the EOC conditions, and a rapid pressure increase similar to that exhibited by homogeneous ignition. However, identifying the presence of these two regimes by simple observation of pressure traces can prove difficult. As such, pressure gradients at points tangential to each regime are displayed in figure 4.1 by dashed lines, to aid the readers ability to distinguish between the PIHR and homogeneous case. The difference between the two ignition regimes in the PIHR case can be observed further in the pressure gradient trace shown in figure 4.2, wherein the PIHR regime is clearly visible prior to the “strong-ignition” regime. Pressure and d*P*/d*t* traces, similar to those shown by the PIHR case in figures 4.1 and 4.2, are also present in the autoignition and knock literature [64,127].

The work of Assanis et al. [127] investigated the autoignition of iso-octane using the University of Michigan optical access RCM, initiating the evolution of PIHR via the discharge of a sparkplug, generating a local hotspot. As the flame front propagates from this hotspot (as shown by sequence of still images taken through the optical access port), the pressure within the reaction chamber rises as the unburnt gas is compressed by the reaction front. This generates the typical PIHR “slow” pressure rise. As the front propagates further, the unburnt gas autoignites and the characteristic “strong” ignition (as seen in the homogeneous ignition case in figure 4.1) occurs. It should also be noted that both inhomogeneous and homogeneous ignition are (in the case shown in figure 4.1) present at the same condition, for the same fuel (iso-butanol) and using the same batch of prepared test mixture. Therefore, it can be determined that the PIHR present in this iso-butanol example is not an intrinsic property of the fuels autoignition development under these conditions, but a behaviour induced by non-uniformities present during RCM operation.

Also observable in figure 4.1 is the EOC pressure (P_c) for both the homogeneous and inhomogeneous ignition cases, which is above the pre-calculated P_c for this mixture of 20 bar. The P_c also appears to increase steadily prior to ignition. In the homogeneous case, this plateaus at a pressure of ~21 bar. A possible cause for this divergence between the calculated P_c and that experienced in the RCM, is the presence of radical initiation processes during the piston compression stroke, which may accelerate the development of the radical pool [48]. Naturally, while there is little reactivity overall during the compression phase, this may lead to a mild heat release and an associated increase in temperature and pressure. An example of the influence of pre-EOC reactivity can be seen in the literature [278] wherein the IDT of a DME/oxidiser mixture in an RCM is simulated, accounting for both reactivity pre-EOC and heat loss post-EOC in one case, and only accounting for post-EOC heat losses in the other. This work showed a significantly reduced IDT for the case accounting for pre-EOC reactivity, particularly at conditions with a characteristically short IDT, and an increasing concentration of the radical species during compression. However, it is also likely that the observable P_c difference between calculations and RCM results is due to the accumulation of small errors during the preparation of fuel/oxidiser test mixtures and operation of the RCM. This accumulation is then manifested as an observable error in the P_c (and thus T_c also). These characteristic RCM errors are explored further later in this chapter (section 4.4).

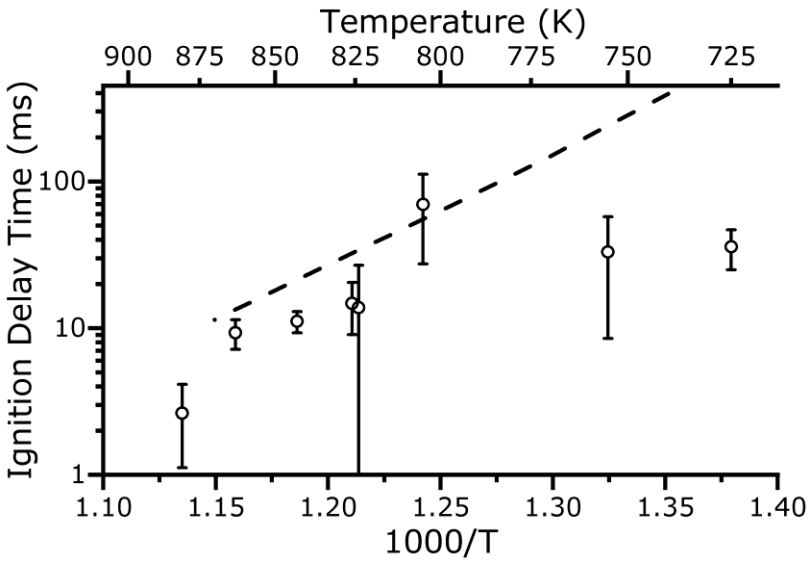

Figure 4.3. IDTs for iso-butanol, taken with a flat RCM piston head. Symbols show mean IDTs of 4-6 individual RCM measurements and error bars represent twice the standard deviation. The dashed line shows variable volume IDT simulation results. T_c=725-881 K, P_c=20 bar, Φ=1.0.

Prior to developments made in this chapter of work, the University of Leeds RCM was fitted with a flat piston head or 44 mm bore. Otherwise (unless stated differently), the RCM used for the collection of data presented in this chapter is as described in section 3.3.1. This configuration of the RCM facility was used for the collection of data presented in figure 4.3, showing iso-butanol IDTs captured at a range of temperature conditions from T_c=725-881 K, a P_c=20 bar and stoichiometric fuel/diluent mixtures. Error bars show twice the standard deviation of IDTs at each point. Also presented in this figure are variable volume simulations of the iso-butanol fuel, modelled using the method described in section 3.5.2 and the Sarathy et al. butanol isomers mechanism [84]. This mechanism is described further in section 3.5.1. IDT measurements displayed in figure 4.3, for the intermediate and high temperature end of the conditions investigated, could be said to follow the general Arrhenius trend expected for iso-butanol under these conditions [39,44,224]. This same trend is seen in variable volume simulations but with longer IDTs estimated throughout (except for the condition at T_c≈805 K). However, this trend is not followed for RCM IDT measurements at the low temperature end of the investigated region (<800 K). In this low temperature region, IDTs are much shorter than would be expected. It is also clear that for many of the RCM IDTs shown in figure 4.3, the uncertainty in the IDT point value (as determined by twice the standard deviation of multiple individual RCM experiments) is far too great to state that the IDTs are valid. The largest error bars can be observed for RCM IDTs at conditions of T_c=805 K and 755 K, which give

measurements for IDT of 70±42 ms and 33±25 ms (percentage errors of 61 and 74%), respectively. It is proposed that this unreasonably high degree of uncertainty in the reported IDTs is due to the influence of the previously described PIHR phenomenon for a significant amount of individual iso-butanol experiments. To investigate this, the rate of pressure change (d*P*/d*t*) for each individual RCM experiment is analysed as a method for the identification and subsequent removal of inhomogeneous PIHR cases in the data set shown in figure 4.3.

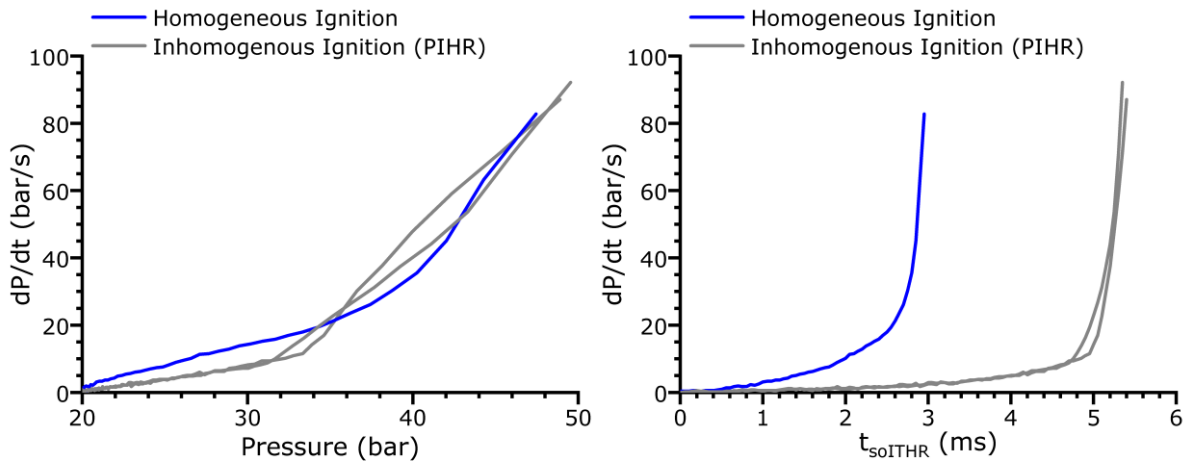

Figure 4.4. Characterisation of pre-ignition through the d*P*/d*t* analysis. Example of iso-butanol fuel at conditions: T_c=826 K, P_c=20 bar, Φ=1.

The evolution of d*P*/d*t* with respect to pressure and time after the start of intermediate temperature heat release (t_{soITHR}) is shown for an example set of iso-butanol RCM cases in figure 4.4. The soITHR is defined in detail in section 3.6 but briefly, for the purposes of this analysis, this point can be described as the beginning of the local continuous pressure rise, leading to ignition. In this example, d*P*/d*t* is displayed as a five-point moving average to remove the presence of pressure transducer noise, which can otherwise make analysis difficult.

There are several trends displayed in figure 4.4, which clearly distinguish PIHR cases from cases of homogenous ignition when applying this method of pressure history analysis. Firstly, in the relationship between d*P*/d*t* and pressure, PIHR cases display an observably slower rate of pressure change at the same pressures as the homogeneous case, during the development of the PIHR behaviour. This can be observed clearly at pressures below 30 bar. These lower values of d*P*/d*t* then abruptly transition to a regime of rapidly increasing pressure and d*P*/d*t*. Homogeneous ignition on the other hand, displays a gradually rising d*P*/d*t* with increasing pressure until the maximum d*P*/d*t* value is reached. This simple analysis also allows

for the precise determination of the pressure of the gas mixture at the end of PIHR, which may otherwise be difficult to determine through the observation of RCM pressure histories.

Similar behaviour can be seen in the relationship between dP/dt and t_{soITHR} for the PIHR examples: a slow rate of pressure rise occurs and for a much longer period of time than the homogeneous ignition, leading into an abrupt transition to a rapid increase in dP/dt. This would appear to indicate a difference in the initial heat release behaviour between the PIHR and homogeneous ignition cases, which is investigated in the following section. Secondly, it appears that, while PIHR cases provide a shorter IDT, the duration of the ignition process is longer due to the initially slow pressure rise and relatively early soITHR. This feature is not present in the homogeneous ignition cases and clearly distinguishes PIHR cases. The second regime observable for PIHR, which represents the ignition of the fuel at elevated temperature and pressure conditions, also occurs at a considerably faster rate than the ignition observed in the homogeneous case, which may have implications for the knock intensity in PIHR cases. The work of Wang et al. [64] has shown the relationship between pre-ignition (PIHR) and super-knock in an RCM, with relevance to SI engines. It was demonstrated in the study, through the use of RCM pressure measurements and high-speed direct photography of the ignition event, that the evolution of super-knock occurred in three main stages. Initially, a pre-ignition hot-spot causes a deflagration, evidenced by a gradual pressure rise as shown by the primary PIHR pressure regime. This pressure rise causes the detonation of unburnt gases and displays a strong pressure discontinuity (the secondary PIHR regime). Finally, this produces strong pressure oscillations, which are evidence of super-knock [64]. Therefore, there are engine performance and safety implications from the presence of PIHR. For fuels with a higher than average propensity for such behaviour, these implications should be considered when discussing the feasibility of such fuels in SI engines.

The same trends observed using this analysis for iso-butanol examples can also be observed in other fuels, as shown in figures 4.5 and 4.6 for examples of iso-butanol and gasoline blended fuels, indicating that this method is effective at identifying PIHR for multiple fuel blends in RCMs.

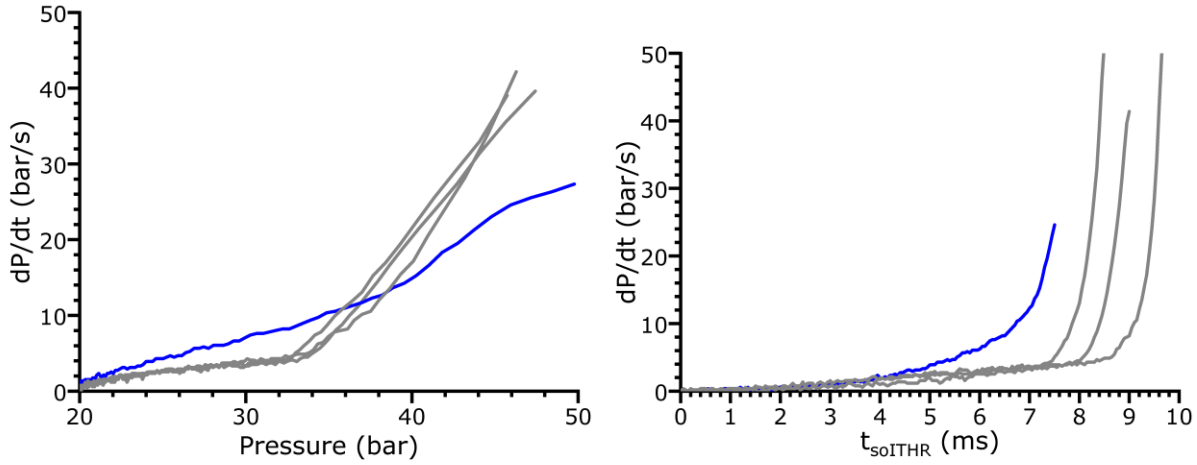

Figure 4.5. Examples of pre-ignition characterisation applied to iB50 fuel (50% iso-butanol, 50% gasoline blend by volume). Blue lines show homogeneous ignition cases. Grey lines show PIHR cases. T_c=805 K, P_c=20 bar, Φ=1.

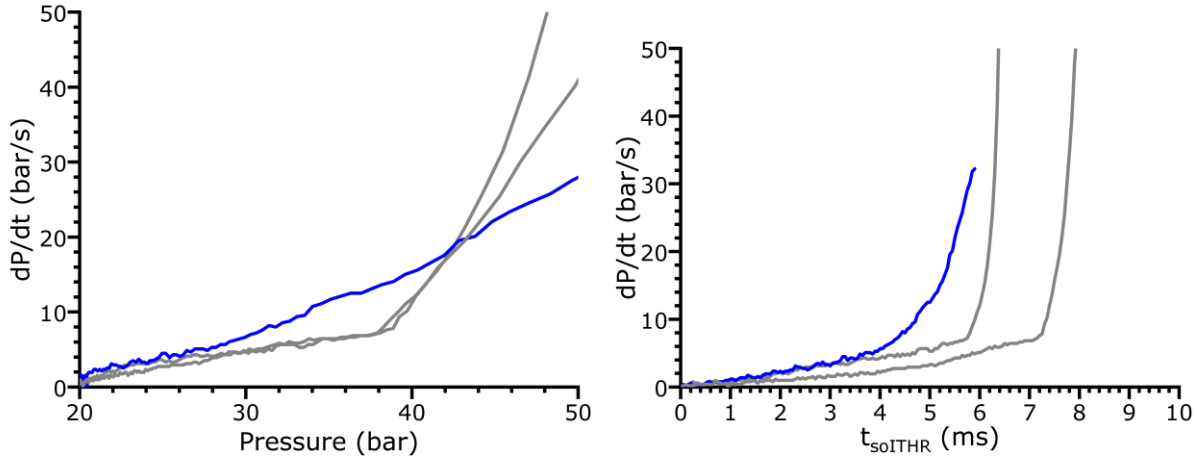

Figure 4.6. Examples of pre-ignition characterisation applied to iB90 fuel (90% iso-butanol, 10% gasoline blend by volume). Blue lines show homogeneous ignition cases. Grey lines show PIHR cases. T_c=805 K, P_c=20 bar, Φ=1.

The characterisation of facility induced PIHR cases has been demonstrated through the use of d*P*/d*t* RCM pressure trace analysis. By applying this simple analytical method to the iso-butanol data collected by the University of Leeds RCM with a flat piston (figure 4.3), multiple PIHR cases were identified. These cases are shown in table 4.1. By removing these identified cases, the degree of uncertainty improves significantly, and the IDT trend is more similar to that observed in literature [39,44,224], as shown in figure 4.7. However, this also means that there are no longer any IDT measurements at temperatures below ~820 K, as there were no homogeneous ignition cases below this temperature. This is due to the breakdown of the

adiabatic core assumption at long test times, meaning that longer IDTs cannot be measured accurately. Many of the extracted IDTs in table 4.1 at a given temperature show significant differences between the longest and shortest values for PIHR cases, particularly at relatively low temperatures. This indicates a behaviour that, at these conditions, is not highly repeatable for iso-butanol fuel and may be induced via inadequacies in RCM operation and maintenance.

Table 4.1. A list of PIHR cases identified in the original iso-butanol dataset, as determined through the use of the d*P*/d*t* PIHR characterisation method shown in figures 4.4-4.6.

T_c (K)	Ignition Delay Times (ms)			
725	31.5	34.2	42	
755	24.4	41.7		
805	53.8	57.8	67	100
824	8	8.4	11.2	
826	10.8	12.3	12.9	
863	7.9			
881	1.7	2.1		

The d*P*/d*t* analysis method described has proven useful for the characterisation the detrimental PIHR behaviour and the removal of such cases from the relevant data sets. As part of a project to provide a useful, searchable database of accurate data, the ReSpecTh database contains a large amount of RCM data including pressure traces of many reactive experiments [297]. Analysis such as that described in this section may be applied autonomously to identify PIHR cases in a database, like that of ReSpecTh, and may help to determine the influence of this phenomenon on historic IDT measurements. These measurements serve as targets for the development of kinetic models, and IDT errors induced by non-uniform ignition such as PIHR can therefore propagate through to the predictions of such models. Due to the simplicity of the analytical method and the intensity of the pressure gradient discontinuity observed (for example in figures 4.4-4.6), the method described above could also be applied to crudely identify PIHR cases automatically during the collection of RCM data, aiding in the detection of PIHR identification by the RCM operator. This would also provide the operator information that may elucidate any maintenance and operational issues early.

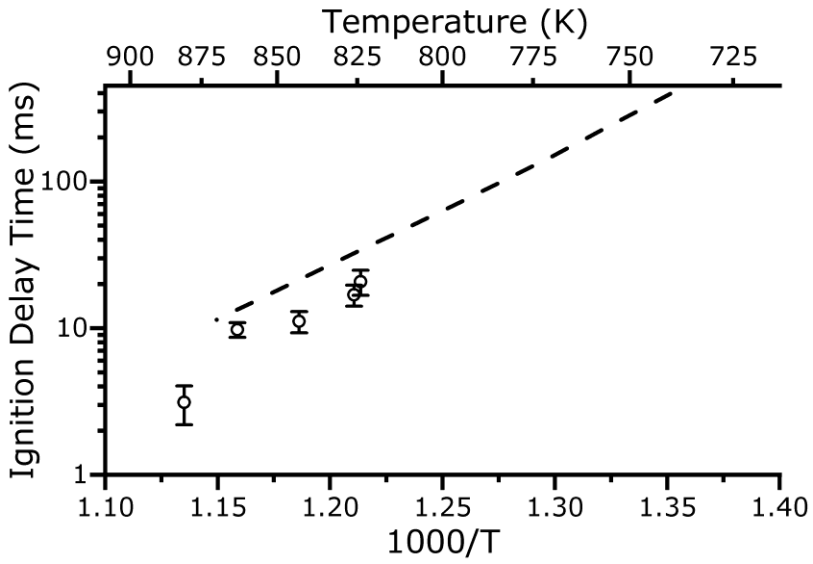

Figure 4.7. IDTs for iso-butanol, taken with a flat RCM piston head, with identified PIHR cases removed. Symbols show IDTs captured in the RCM. The dashed line shows variable volume IDT simulation results. T_c=725-881 K, P_c=20 bar, Φ=1.0.

4.3 Heat Release Analysis of Ignition Regimes

HRA is an alternative method which may be able to distinguish PIHR and homogeneous ignition test cases in suspect sets of experimental data. While historically, HRA has not consistently been applied to RCM results, recent studies have developed a novel method for such analysis (as described thoroughly in section 3.6) and shown that there is significant potential to develop a deeper understanding of autoignition and the associated preliminary exothermicity [172,186,284]. This method has been applied previously to investigate the PIHR phenomena in both RCM experiments of cyclopentane [284] and numerical simulations of hot-spot induced mild ignition of syngas [172,298]. In these studies, RCM HRA proved an effective tool for the identification and investigation of PIHR ignition cases. Therefore, this analytical method is applied to the pressure histories for iso-butanol results presented in figure 4.3, as a relatively cheap method for the identification of PIHR cases in RCM datasets.

An example of HRA applied to both a homogeneous ignition and inhomogeneous ignition (PIHR) case is shown in figure 4.8. In this figure, the HRR is plotted in relation with the associated aHR. As described in section 3.6, the HRR and aHR are normalised by the LHV of the fuel. The HRR-aHR trajectory provides an indication of the developing heat release behaviour during the ignition stage. Both the homogeneous and inhomogeneous iso-butanol analysis presented in figure 4.8, are the result of HRA applied to the respective pressure traces

shown in figure 4.1. This allows for a direct comparison between observations made for PIHR and homogeneous ignition pressure traces and heat release behaviour.

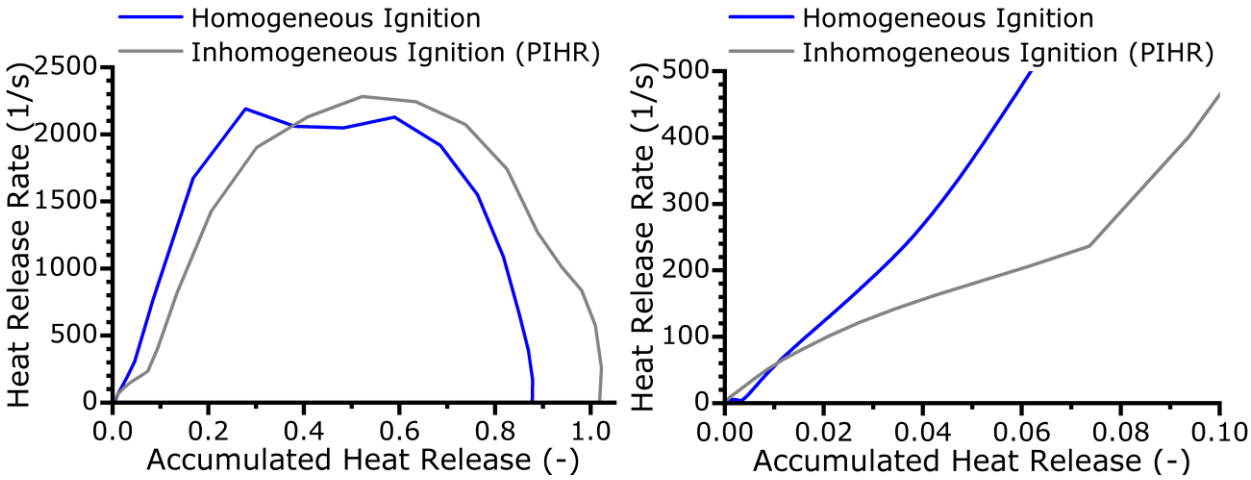

Figure 4.8. HRA applied to RCM pressure histories for iso-butanol fuel at conditions: T_c=881K, P_c=20 bar and Φ=1. Left figure shows the HRRs and aHR for the full pressure trace. Right figure shows only the PIHR region.

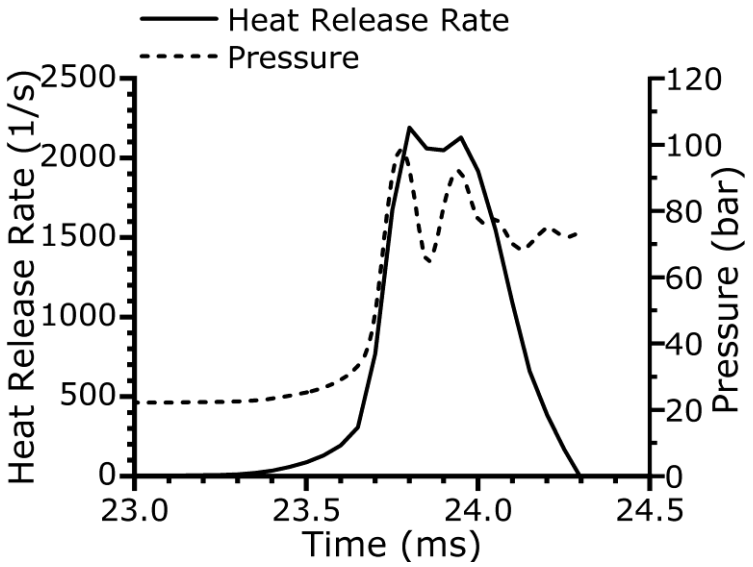

Figure 4.9. The influence of autoignition induced pressure oscillations on the derivation of HRRs from experimental RCM pressure traces, as seen in the homogeneous ignition case shown in figure 4.8. Iso-butanol at conditions of T_c=881K, P_c=20 bar and Φ=1.

For the homogeneous iso-butanol ignition case shown in figure 4.8, a clear and near immediate, rapid heat release occurs, as shown by the HRR-aHR trajectory. This regime characterises high-temperature heat release (HTHR) (strong ignition) and correlates strongly

with the pressure behaviour witnessed in figures 4.1 and 4.2. The HRR of the homogeneous ignition in this case quickly reaches a peak HRR (at approximately aHR=0.25) due to the intensity of iso-butanol autoignition at this temperature (T_c=881K). The resultant pressure oscillations were not successfully filtered from the pressure signal (as described in section 3.6) due to their intensity and are manifest in the HRA analysis as a drop in HRR prior to this initial peak value in this case, as shown by figure 4.9. A characteristic homogeneous ignition case at a lower temperature can be seen in figure 4.10, which will be described in more detail shortly. HRR for the homogeneous case in figure 4.8 begins to continuously decrease at an aHR of approximately 0.6, before heat release ends at aHR≈0.9. This profile is similar to that shown in the RCM HRA produced for the uniform ignition of an ethanol/oxidiser mixture at similar conditions [172].

In the case of the PIHR ignition shown in figure 4.8, the bulk behaviour is very similar to that shown by the homogeneous ignition case. HRR quickly rises to a peak value, before continuously decreasing, at an aHR equal to roughly half of the fuels total LHV. However, unlike the homogeneous case, the PIHR case displays an additional exothermic regime prior to the characteristic HTHR. This primary regime defines PIHR cases in HRA and can be seen most clearly in the right hand side image of figure 4.8. As was shown in the simple dP/dt analysis displayed in figures 4.4-4.6, this regime abruptly transitions, showing a significant discontinuity before and after the transition, and a delayed transition to HTHR behaviour. PIHR characteristics displayed in the HRA show a high degree of correlation with those exhibited in figure 4.2, associating this lower rate of heat release with the gradual pressure rise observed, and the driving deflagration behaviour described in literature [64,123,124]. The resultant detonation of compressed unburnt gases due to this deflagration, as reported in the literature [64], is supported by the rapid HRR after the primary PIHR regime, similar to that shown for the HTHR of uniform autoignition. In the example shown in figure 4.8, it can be seen that this PIHR behaviour consumes 0.07-0.08 of the total fuel LHV, for iso-butanol. In other words, 7-8% of the fuel's total chemical heat energy is released via flame propagation, as opposed to autoignition. A similar heat release behaviour is witnessed in the literature, for the same ethanol/oxidiser mixture discussed previously [172]. This literature example shows the same separation of heat release regimes, with a primary, relatively slow rate of HRR which transitions to a delayed HTHR profile after consuming a substantial portion of the fuels total LHV. The aHR value post-heat release for the PIHR case is observed to be slightly above aHR=1.0. This, similar to the case of an HRR "dip" in the homogenous ignition analysis, is due to the influence of large pressure oscillations during auto-ignition and the resultant impact on the HRA calculation.

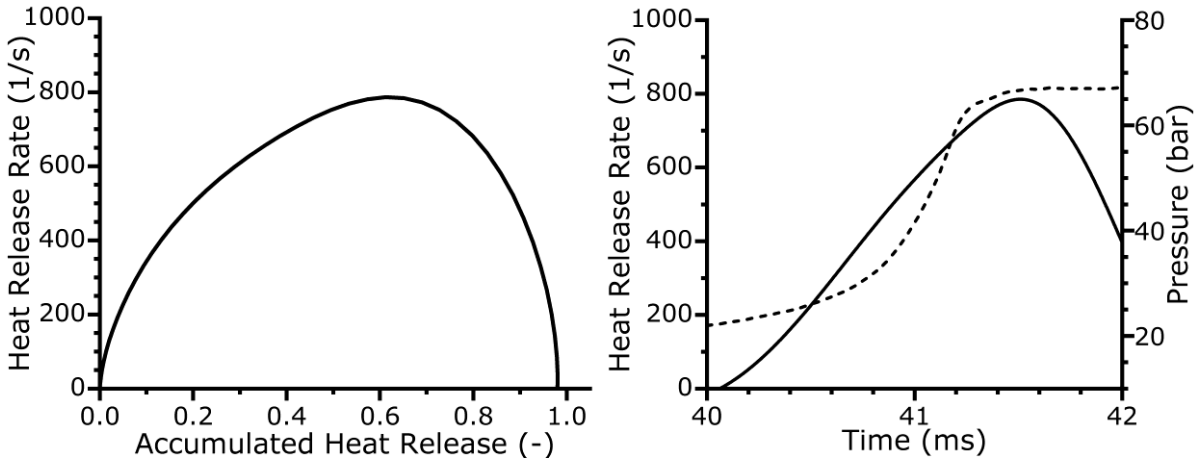

Figure 4.10. An example of HRA for a homogeneous ignition case of iso-butanol. Left image shows the HRR-aHR trajectory during autoignition. Right image shows the HRR behaviour with time, and the associated pressure history. Solid lines show the derived HRR. Dashed line shows the recorded RCM pressure history. T_c=830 K, P_c=20 bar, Φ=1.

HRA for a homogeneous ignition case free of the influence of significant pressure oscillations is shown in figure 4.10. The lower temperature investigated in this case for iso-butanol, produces a less intense autoignition than that shown in figure 4.9, and thus a much lower amplitude of the resultant pressure oscillations. As for the homogeneous example shown in figure 4.9, the earliest stages of the HRR-aHR trajectory show the immediate presence of HTHR. Peak HRR is achieved for the condition in figure 4.10 at an aHR≈0.6, similar to that shown for the PIHR ignition case, further indicating the influence of pressure oscillations at peak pressure on the determination of HRRs from RCM pressure histories. Peak HRR and peak pressure are also significantly lower for the lower temperature iso-butanol condition, which is to be expected given the less intense autoignition, with peak HRRs of 2050 and 790 s^{-1} and peak pressures of 100 and 67 bar for the T_c=881 and 830 K conditions, respectively. Also, due to the lack of significant pressure oscillations, more of the fuels LHV is represented in the HRA, as shown by the increase in total aHR from 0.9 in the homogeneous case of figure 4.8, to an aHR approaching 1.0 in the case shown in figure 4.10.

Heat release analyses of multiple PIHR cases for iso-butanol, at a similar temperature to that shown in figure 4.10, are shown in figure 4.11. The same features which distinguish the PIHR case from the homogeneous ignition case shown in figure 4.8 can be seen in each of the cases present in this example. However, there are some notable differences at this lower temperature condition. Firstly, each of the cases presented in figure 4.11 shows a larger degree of aHR at the transition point between PIHR and HTHR, than that shown in figure 4.8.

Temperature conditions of 881 K and 830 K display an aHR at the transition between PIHR and HTHR of 0.07-0.08 and 0.15-0.25, respectively. This is due to the lower reactivity of the fuel at this lower temperature, as evidenced by IDT measurements in both this study (figure 4.7) and in the literature [39,224], which means that more exothermicity is required to reach conditions which will induce the autoignition of unburnt gas. Also, the peak HRRs reached by the lower temperature conditions are significantly lower than those reached by the example in figure 4.8, indicating a less intense autoignition when it does occur despite a greater extent of deflagration (as defined by the proportion of fuel LHV consumed as PIHR).

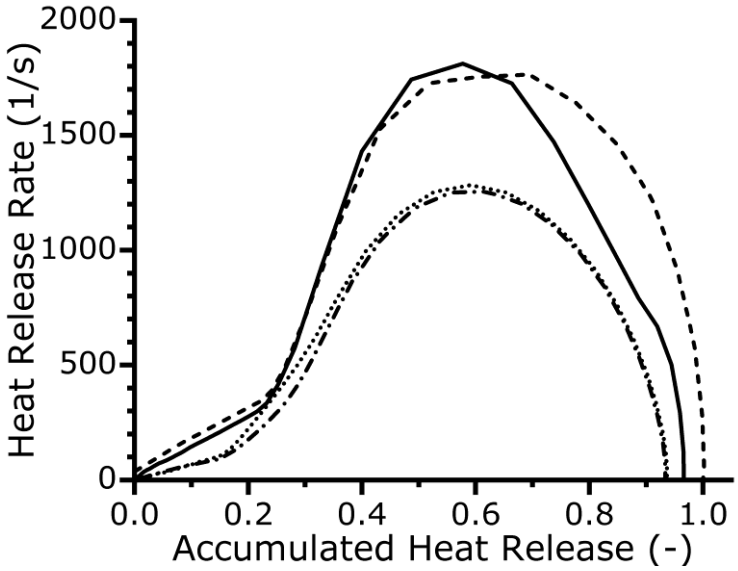

Figure 4.11. Multiple examples of PIHR (mild ignition) HRA for iso-butanol fuel, showing the HRR-aHR trajectories during the ignition process. T_c=826 K, P_c=20 bar, Φ=1.

Due to less intense post-ignition pressure oscillations, the PIHR example cases shown in figure 4.11 also do not misrepresent the bulk ignition HRR behaviour to the degree seen in figure 4.8, producing reasonable values for aHR (i.e. <1.0). Interestingly, HRA of iso-butanol PIHR conditions (figure 4.11) appears to show two distinct profiles, each showing a pair of analyses. One profile shows a larger degree of degree of pre-ignition exothermicity, with HTHR (bulk autoignition) delayed until aHR>0.2. Whereas the other profile shows a slower rate of heat release during the primary PIHR, with HTHR delayed until 0.1<aHR<0.2. This shows that, at least for this case, that the PIHR behaviour of iso-butanol is not highly repeatable. It is useful to hypothesise as to why these two distinct profiles occur. Perhaps the presence of both particulates and an inhomogeneous temperature environment within the combustion chamber induces PIHR to different degrees of intensity, dependent on the driving phenomenon and the associated hot-spot geometry. Further work will be required to determine this if this statement is

accurate, however CFD simulations by Goldsborough et al. [172,298], wherein the effect of a centrally located hot-spots radius on the heat release of non-uniform RCM ignition of syngas was investigated, have shown that an increase in such a hot-spot radius caused an increase in the aHR at which the predicted PIHR to HTHR transition occurred. This would support the hypothesis that particulate and turbulence induced hot-spots can produce varying degrees of PIHR in the same set of RCM experiments, causing the characteristically large uncertainties observed in the IDT measurements shown previously (figure 4.3).

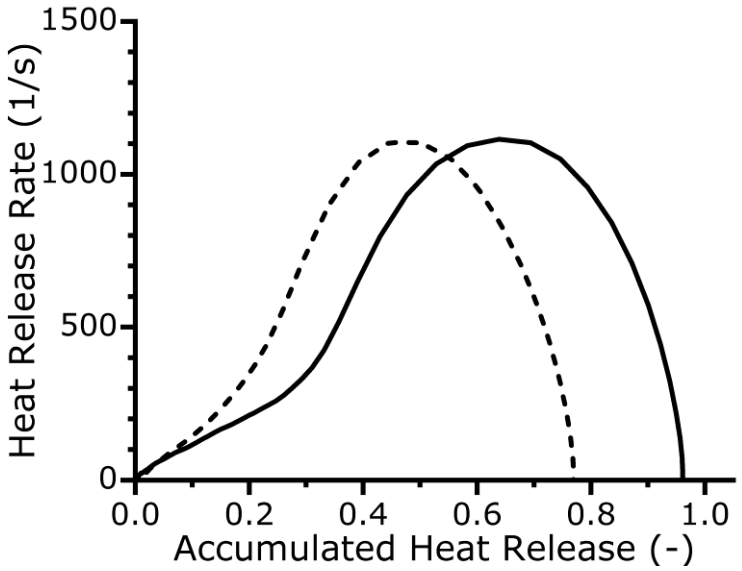

Figure 4.12. An example of HRA for two “subtle-PIHR” ignition case of iso-butanol, which was not identified by d*P*/d*t* analysis, showing the HRR-aHR trajectory during autoignition. T_c=826 K, P_c=20 bar, Φ=1.

Interestingly, the RCM HRA techniques applied in this chapter appear capable of identifying PIHR cases which were not clearly identified through the use of the simpler d*P*/d*t* analysis. An example of one such cases is seen in figure 4.12, which shows the HRR-aHR trajectories for two “subtle” PIHR cases: one trajectory for the same RCM pressure history defined as homogeneous ignition in figure 4.4 (solid line), and another “subtle” PIHR case at the same temperature (dashed line). It is clear from the HRA shown, that these experiments are subject to substantial PIHR, showing a similar HRR-aHR trajectory to that seen in figure 4.11. However, the PIHR regime shown for these case (figure 4.12), do not appear to show a clearly definable transition point. Instead, the PIHR regimes transition gradually into a delayed HTHR regime. While HRA is demonstrably a more powerful tool for the identification of PIHR markers than d*P*/d*t* analysis, it is more computationally expensive, requires significant pre-processing of inputs (pressure histories) and is sensitive to pressure oscillations and transducer noise (as

discussed in section 3.6). This means that the application of such analysis as an autonomous PIHR identification method would be difficult. However, it is clearly a robust tool for the dedicated investigation of RCM heat release behaviour, particularly in PIHR cases.

4.4 Rapid Compression Machine Modification and Ideal Operation

Like all experimental setups, there are multiple sources of random and systematic uncertainties which influence the quality of data collected from RCMs, which are described thoroughly in the literature [48,248]. In the case of the RCM results displayed in figures 4.1-4.7, the University of Leeds RCM utilised a flat piston head. This induces significant fluid motion during the compression of the test gas, potentially mixing the adiabatic core gas with the cool boundary layer. If the adiabatic core assumption is no longer true under these circumstances, a significant source of uncertainty is introduced to measurements made by the RCM [248]. Previous work has also shown that the turbulence induced by piston motion (which is amplified by the use of a flat piston head) can amplify any pre-existing turbulence present within the test gas, such as that caused by the injection of the test gas into the combustion chamber [249]. Therefore, the reduction of initial turbulence induced by RCM handling of test mixtures should also reduce overall uncertainties.

Further sources of uncertainty in RCM IDT measurements can be found in the concentrations of initial reactants in the test batch mixture, as well the methods utilised in mixture preparation [48]. During the preparation of a given fuel/oxidiser test mixture (as described in section 3.3.2), the partial pressure measurement of gaseous components and the handling of liquid reactants (such as syringing) may introduce uncertainties into the fractional composition of a test mixture. Many liquid components also require significant heating to ensure the fuel is entirely in the vapour phase, but care should be taken to account for fuel volatility. Heating must be uniform throughout both the mixing chamber and any fuel carrying components of the RCM, to prevent the condensation of fuel during transition to the combustion chamber and to ensure that the test mixture arrives at the combustion chamber in a homogeneous state. Studies have made an effort to apply in-situ analytical techniques to measure the composition of test mixtures within the combustion chamber prior to compression, ensuring their homogeneity [299,300]. Furthermore, the uniform heating of the mixing chamber prevents potential mixture stratification. RCM maintenance standards may also introduce a degree of uncertainty in IDT measurements [48]. The presence of black deposits (i.e. soot), reaction products and hydraulic oil may contaminate a poorly maintained RCM combustion chamber after a series of successive RCM experiments. PIHR phenomena has been witnessed as a symptom of this, as shown in a

study of aromatic fuels by Mittal and Sung [132], in which tests were completed in both a contaminated and uncontaminated test chamber. The presence of fuel mixture remnants in the mixing chamber and fuel carrying feed lines will influence the composition of any subsequent test mixtures.

To facilitate an improvement in the quality of IDT data produced by the University of Leeds RCM, comprehensive operational changes were enacted in response to the series of uncertainty sources described previously. Experiments presented in figure 4.3 were conducted using a mixture preparation procedure as described in section 3.3.2, except for the mixing time. The mixing time used in the acquisition of these IDTs for iso-butanol was as low as 30 minutes. Due to the use of an un-stirred mixing chamber, longer mixing times are required to ensure the homogeneity of the batch test mixture in terms of both composition and temperature. As such, the minimum mixing time was increased to 120 minutes. Many other RCM studies continuously stir the fuel mixture within the mixing chamber, through the use of a magnetic stirrer for example [39,179,301–306]. However, in the case of the University of Leeds RCM, this would have required extensive modification to the facility and was ultimately deemed unnecessary, due to the relatively small size of the mixing chamber and results displayed in this chapter. To further reduce the uncertainty associated with batch mixture production, the quantity of each individual batch mixture was increased from an absolute pressure of 1 bar, to a minimum absolute pressure of 2 bar. This minimised the influence of instrument error in the partial pressure measurement of gas components and the volumetric measurement of liquid components. Volumetric liquid fuel measurements were also checked against the corresponding partial pressure measurement during the addition of liquid fuels to the mixing chamber.

RCM care previously consisted of sporadic cleaning of the combustion chamber, often dictated by the observable deterioration of IDT pressure histories. To ensure the elimination of contaminants and the associated IDT uncertainty from RCM experiments, a daily regime of combustion chamber cleaning was introduced, as was a weekly “deep-clean” of the combustion chamber and piston assembly. Daily cleaning consists of the removal of the combustion chamber end plug to provide access to the chamber interior, with the piston at BDC to allow access to the entire piston shaft. The interior, piston face and end plug are cleaned thoroughly with a liberal amount of acetone and a clean cloth, taking care to ensure any recesses are free of black deposits. This cleaning technique is common [48]. Deep cleaning requires the dismantling of the RCM combustion chamber, providing access behind the piston head. This also provides an opportunity to assess the piston assembly for any damage which may induce

non-uniform piston compression. To ensure optimal cleanliness between individual RCM tests, multiple non-reactive air tests are completed between each reactive test. This reduces the likelihood of the presence of residual combustion products and deposits as they are dislodged by these tests. Cleanliness is further ensured by the thorough vacuuming and air flushing procedures documented in sections 3.3.2 and 3.3.3.

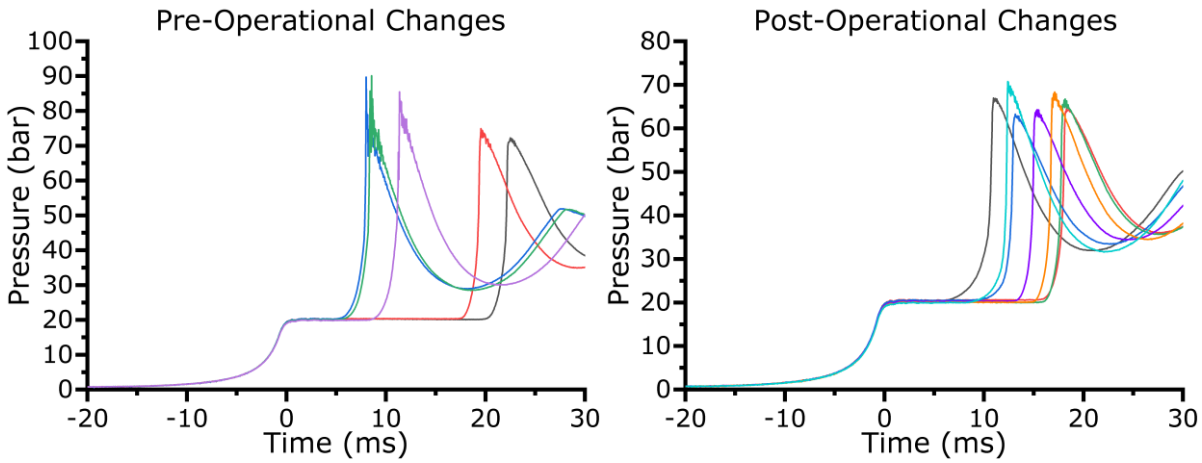

Figure 4.13. RCM pressure histories highlighting the impact of operational changes. Each coloured line signifies a separate "run" of the RCM. Conditions reported: iso-butanol fuel, T_c=826 K, P_c=20 bar, Φ=1.

The influence of the application of these operational changes is shown in figure 4.8, wherein examples of iso-butanol RCM pressure traces are shown for both pre and post-operational changes. Each set of pressure traces are taken from single and separate mixture batches. Prior to the implementation of operational changes there are multiple clear PIHR cases, as shown by tests 3, 4 and 5. These tests exhibit the characteristic gradual pressure rise and pressure discontinuity. Also shown by these cases is a large degree of pressure oscillation post-ignition, characteristic of a strong detonation leading to knock [64]. The range of measured IDTs is also incredibly large for the same batch of fuel/oxidiser mixture at the same thermodynamic conditions, with a IDTs ranging from 8 ms to 22 ms (a difference of 14 ms). Post-operational IDT measurements show a significant improve in repeatability, with a tighter clustering of individual autoignition pressure traces. However, the presence of PIHR cases is still apparent in tests 1, 3 and 7. Interestingly, despite the mixture composition and thermodynamic conditions being the same as the pre-operation change experiment, these PIHR cases display significantly different behaviour. Post-operational changes PIHR cases appear to show a slower primary pressure rise, reaching a peak at lower pressures prior to the change in dP/dt regime. Also, the resultant pressure oscillations are muted in comparison to pre-operational change PIHR cases, as is the

global peak pressure. These changes may be due to a reduced possibility of particulate induced hot-spots caused by the improved RCM maintenance regime, leading to the assumption that these PIHR cases are caused by fluid motion. HRR-aHR trajectories for test 3 and 7 PIHR cases, post-operational changes, can be seen in figure 4.14. While more examples are clearly required to draw any definitive conclusions, only one PIHR regime can be seen, supporting the suggestion that particulate hot-spots have largely been removed. Heat release accumulated during PIHR is also significantly less than that which occurred prior to HTHR pre-operational changes, indicating that the severity of PIHR has largely been reduced by these changes. The range of IDTs is improved post-operational changes, with a shortest measured IDT of 10.8 ms and a longest measured IDT of 18 ms (a difference of 7.2 ms, approximately half the pre-operational change case).

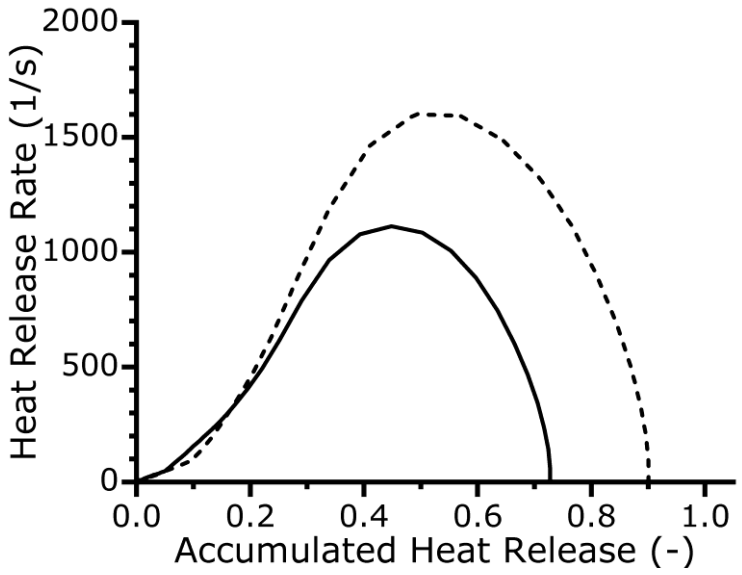

Figure 4.14. HRR-aHR trajectories for PIHR cases post-operation changes for iso-butanol. The solid line shows test 3. The dashed line shows test 7. T_c=826 K, P_c=20 bar, Φ=1.

While the issue of pre-ignition has not been eliminated and the degree of uncertainty in both cases is not acceptable, there is a clear improvement in the scatter of IDTs due to the operational changes. The average IDT pre operational changes is 13.8 ms with an error (represented by twice the standard deviation) of ±13 ms, whereas the average IDT post operational changes is 14.8 ms with an error of ±5.7 ms, which is a significant improvement but still a fractional uncertainty >1/3 of the total IDT. Therefore, it is concluded that the operational changes enacted can produce a drastic improvement in the quality of RCM produced IDTs. However, there are still improvements to be made, and these may lie in the suppression of fluid motion during piston compression within the University of Leeds RCM.

Modification of the University of Leeds RCM through the introduction of a creviced piston head is the final method investigated for the elimination of detrimental PIHR cases and the improvement of IDT uncertainty. The introduction of creviced piston heads has been shown in the literature to significantly improve the temperature homogeneity of the post-compression environment, through the capture of the cool boundary layer and resultant prevention of turbulent mixing through swirl vortices [102,116].

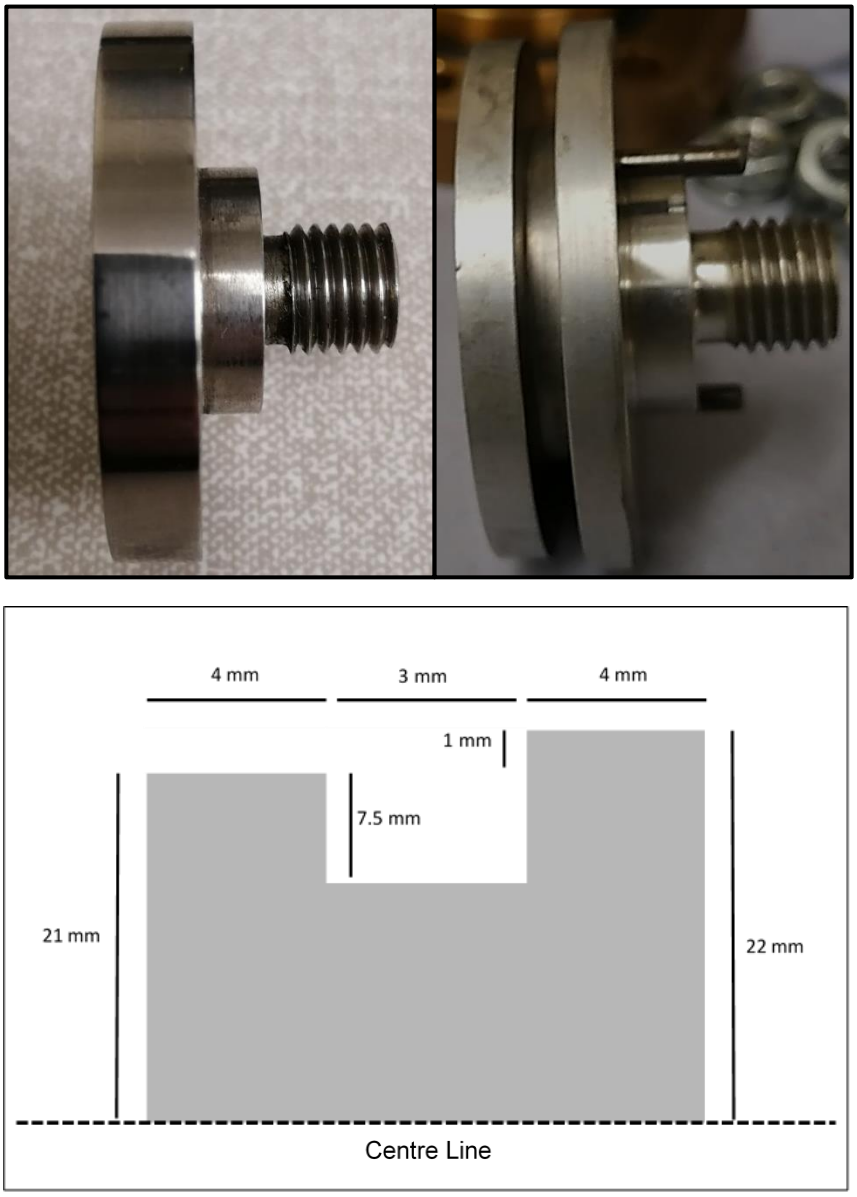

Figure 4.15. Geometry of the University of Leeds RCM creviced piston head. Top left image shows a photograph of the previous flat piston head. Top right image shows a photograph of the

newly manufactured creviced piston head. Bottom image shows the dimensions of this creviced piston head.

The design of the creviced piston head can be seen in figure 4.15. Several design creviced piston design recommendations have been suggested in the literature, for the efficient suppression of fluid mixing during RCM piston compression [100,102,116,307]. These state that the crevice should be large enough to contain the boundary layer gas during compression, the crevice geometry should facilitate the cooling of gases which enter the crevice and the crevice channel depth should be sufficient to capture the entire boundary layer. It has been shown in the literature, through the application of CFD simulations, that optimal crevice volumes are between 9-14% of the total combustion chamber volume at TDC [100,116]. Also, optimal channel geometry was shown to be rectangular, with an optimal channel depth of 1 mm and length of 4 mm. This channel geometry was shown to effectively capture boundary layer gas, facilitate the effective cooling of crevice gases, and limit the backflow of gasses back into the reaction chamber, when compared to other geometries [100]. These recommendations are also discussed in section 2.3.1. Following the recommendations of the literature [100,102,116,307] and minimising the impact on the operation of the RCM, the piston head was designed with a crevice channel length of 4 mm, channel depth of 1 mm, a rectangular crevice geometry and a crevice volume of 3 cm^3 (10% of combustion chamber volume at the EOC). While the use of an angled channel geometry may have assisted in the extended capture and cooling of the boundary layer gas [100], machining proved impractical, given that this was shown to produce no obvious improvements in the spatial homogeneity of the temperature field [100]. CFD simulations performed by Würmel and Simmie [100] showed that a crevice volume of up to 8% of the total reaction chamber volume (at the EOC) was insufficient for capturing the boundary layer and generating a homogeneous temperature environment. However, homogeneous temperature environments were generated by crevices of volume 8.5-12.5% of the total volume, for argon, carbon dioxide, nitrogen, and oxygen gases. These gases make up the oxidiser fraction of investigated mixtures in the RCM studies applied in this chapter and chapter 5, as described in section 3.3.2. Therefore, a crevice volume within this region would be most beneficial for maintaining the homogeneity of the temperature field within this study. The piston geometry described here allows the creviced piston head to operate at the same CR as the previous flat piston head and avoid any impact on in-cylinder measurement instruments, while attempting to improve the homogeneity of the temperature environment.

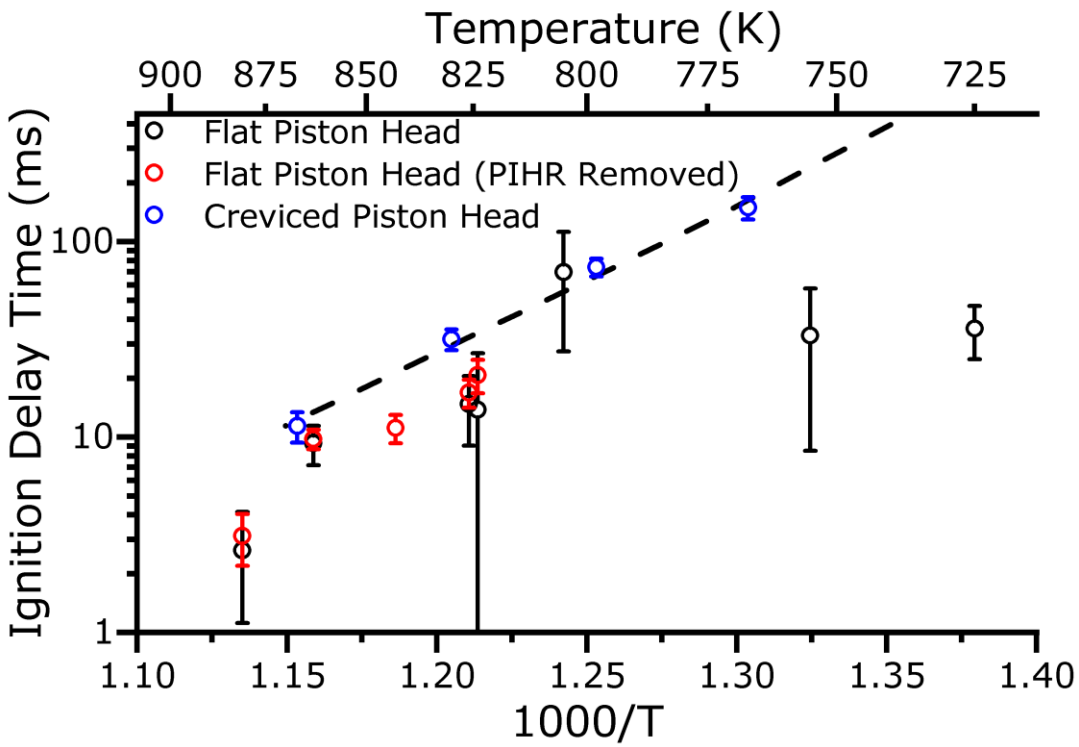

Figure 4.16. IDTs for iso-butanol, highlighting the difference between data captured with different RCM configurations. The dashed line represents variable volume simulations of iso-butanol. P_c=20 bar, Φ=1.

As observed in figure 4.16, the impact of the creviced piston head design is considerable. This figure shows IDTs for iso-butanol with both flat and creviced piston head RCM configurations. Also shown are the flat piston head IDTs but with PIHR cases removed via dP/dt analysis. It is clear that the use of the creviced piston head provides both a drastic improvement in relative IDT uncertainties and a more consistently Arrhenius behaviour, which is expected for iso-butanol [39,180,224]. IDTs are also consistently longer in the case of the creviced piston head, implying the existence of subtle PIHR (as identified by HRR analysis in figure 4.12) in the flat piston head cases with PIHR removed by dP/dt analysis. The creviced piston head also allows for the probing of lower temperatures than the simple removal of PIHR cases, with IDTs captured at T_c=798 and 767 K. Temperatures <800 K demonstrated a large degree of PIHR with the flat piston head, making the capture of IDTs under uniform conditions impossible. However, due to the impact of RCM heat losses and the nature of iso-butanol's Arrhenius IDT relationship with temperature [39,44,224], IDTs for iso-butanol below compressed temperatures of 767 K have proven difficult to measure, as even with addition of the creviced piston head, the adiabatic core assumption will break down at extremely long IDTs as boundary layer gas flows from the

crevice back into the combustion chamber. To prevent this, some studies apply crevice containment, wherein the crevice is sealed at the EOC, sealing the boundary gases away from the combustion chamber [115,118,119,121]. A physical barrier is commonly applied to achieve this containment. However, pseudo-crevice containment through the use of triangular crevice geometries, with a narrow entrance, has not fully been investigated. This pseudo containment may provide a relatively cheap solution, which can be applied to existing RCMs without the need for extensive redesigns. A number of these designs have been produced at the University of Leeds but are currently awaiting testing in future work.

PIHR cases have been completely eliminated in the measured IDTs of iso-butanol, through the introduction of mechanical and operational improvements to the University of Leeds RCM. This can be seen in figures 4.17 and 4.18, which show examples of the PIHR identification techniques utilised in this chapter applied to iso-butanol pressure measurements made post-changes. Figure 4.17 shows d*P*/d*t* analysis techniques applied to five individual RCM tests of iso-butanol, completed after RCM changes, at a compressed temperature of 830 K, exhibiting none of the characteristics typical of PIHR in any test (examples shown in figures 4.4-4.6). The ignition process also displays a large degree of repeatability in these cases, with a similar duration between all tests and a single, consistent regime produced in both d*P*/d*t* vs *P* and d*P*/d*t* vs t_{solTHR} analyses. This repeatability and lack of PIHR cases indicates a significant improvement in the spatial temperature homogeneity within the reaction chamber, consistent throughout a series of experiments. Further analysis, through the evaluation of HRR-aHR trajectories is shown in figure 4.18, for iso-butanol IDTs taken after RCM improvements, at temperatures of 770 K (left) and 830 K (right). At 830 K, each test shows a highly repeatable heat release profile, featuring a single regime of heat release during early ignition and does not exhibit the observed discontinuity or lower rate of heat release during early exothermicity characteristic of PIHR cases (figure 4.11). The same trends can be seen for all tests completed at a compressed temperature of 770 K, albeit with observably more noise during the bulk heat release, as the duration of the pressure rise due to ignition is longer at this lower temperature. Also, HRRs are much lower at this temperature, signifying a less intense autoignition event. The RCM failed to capture homogeneous IDTs at this temperature prior to operational and mechanical improvements, due to the influence of PIHR. These improvements have facilitated not only the accurate production of homogeneous IDTs, improving data quality, but they have also extended the range of RCM conditions, allowing for the production of accurate, low temperature measurements, which provide further targets for the evaluation of computational models.

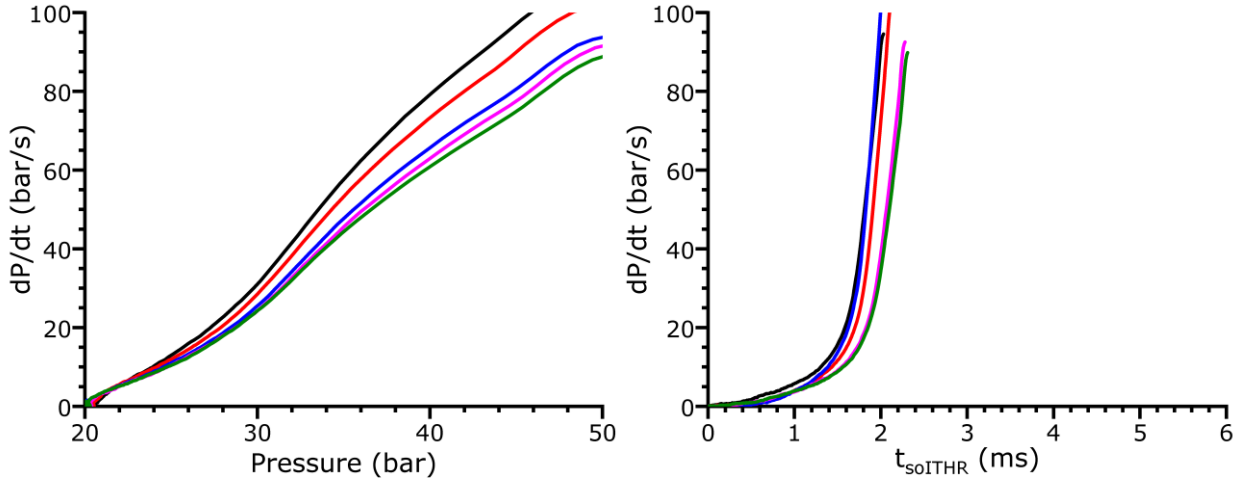

Figure 4.17. An example of the lack of PIHR cases after operational and mechanical improvements to the RCM, as shown through d*P*/d*t* analysis. Each line shows an individual RCM test of iso-butanol fuel at conditions: T_c=830 K, P_c=20 bar, Φ=1.

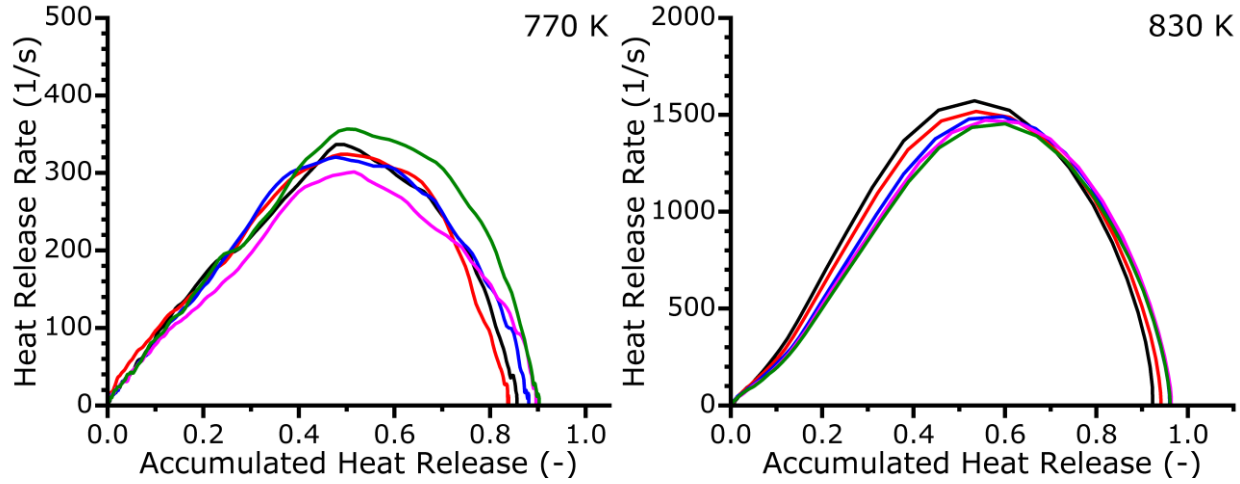

Figure 4.18. HRR-aHR trajectories showing the development of homogeneous heat release during iso-butanol autoignition, at compressed temperatures of 770 K (left) and 830 K (right). P_c=20 bar, Φ=1.

4.5 Summary

The identification and characterisation of PIHR has been achieved through the application of analytical methods to RCM pressure histories. Initially, a simple d*P*/d*t* analysis, which investigated the relationships between d*P*/d*t* with pressure and time post-soITHR (t_{soITHR}), was applied. This analysis proved somewhat effective for distinguishing between PIHR and homogenous ignition case, producing several markers for the identification of PIHR cases. While homogeneous cases displayed a near constant increase in d*P*/d*t* with increasing pressure

during ignition, PIHR cases displayed two clear regimes. The primary regime is defined as the PIHR region and showed a gradual rise in d*P*/d*t* with pressure, lower than that associated with homogeneous ignition. This regime then abruptly transitioned, at a transition point, to a regime displaying a much larger d*P*/d*t* with pressure. This discontinuity is characteristic of PIHR cases in d*P*/d*t* analysis. In terms of t_{50ITHR}, PIHR cases display a transition to bulk HTHR much later than homogeneous cases (figures 4.4-4.6). PIHR cases were removed from IDTs taken with a flat piston headed RCM using the d*P*/d*t* method, as shown in figure 4.16. This provided a significant improvement in both the uncertainty of mean IDT values and the overall IDT profile observed for iso-butanol, bringing it closer to that expected form literature sources [39,44,84,224]. However, this removed all iso-butanol IDT measurements below <800 K. Simple analysis such as this is not computationally expensive and may be applied in future studies, to autonomously identify PIHR cases during the capture of RCM pressure data.

HRA was also investigated as a method for PIHR identification and characterisation. Similar to d*P*/d*t* analysis, HRA of RCM pressure histories proved effective at identifying key markers of PIHR cases. While homogeneous ignition HRR-aHR trajectories showed a near immediate transition to HTHR behaviour, PIHR cases displayed a primary regime of gradual, relatively low HRRs. At a transition aHR value dependent on the intensity of the PIHR phenomenon, the delayed HTHR was initiated. Two clear PIHR regimes were observed for iso-butanol ignition at T_c=826 K (figure 4.11). It was proposed that this may indicate multiple sources of PIHR behaviour (such as particulates and temperature inhomogeneities), which may produce associated hot-spots of varying geometry. This would support findings in the literature, that showed that increasing hot-spot radius in CFD simulations of syngas autoignition, caused an increase in the aHR produced by PIHR [172,298]. This delayed HTHR displayed a large HRR discontinuity with the primary PIHR regime. It was also demonstrated that HRA was capable of identifying “subtle” PIHR cases, which were otherwise difficult to locate via d*P*/d*t* analysis, as shown in figure 4.12. These subtle cases showed the same gradual primary PIHR and strong HTHR regimes, however, the determination of a clear transition point was not as obvious as in “strong” PIHR cases. While this method is demonstrably a more powerful tool than d*P*/d*t* analysis for the determination of PIHR cases from RCM pressure data, it is significantly more computationally expensive, limiting the use as a method of autonomous PIHR detection during data collection. However, the tool provides significantly more insight into the evolution of PIHR and other heat release behaviour than the simple d*P*/d*t* analyses.

The impacts of operational changes and mechanical modification of the University of Leeds RCM on the presence of PIHR cases and overall IDT errors, was investigated. A number of operational changes were made to raise the standard of University of Leeds RCM maintenance and operation, including: an increase in mixture preparation time (from 30 minutes to 120 minutes), daily cleaning of the combustion chamber and non-reactive compressions between reactive experiments. These changes provided a significant improvement in the repeatability of RCM IDT experiments on a run-to-run basis, as seen in figure 4.13. However, the degree of variation in individual pressure histories was still unacceptable post-changes. As such, the RCM underwent mechanical modification through the replacement of the previous flat piston head with a creviced piston head (as shown in figure 4.15). This modification provided a drastic improvement in IDT errors when compared to both flat piston head results and PIHR removed flat piston head results (figure 4.16). Creviced piston IDT measurements showed generally longer IDT measurements than flat piston head iso-butanol measurements and allowed for the probing of lower temperatures due to the extended existence of the adiabatic core. The combination of the operational and mechanical changes made to the RCM in this chapter appear to have eliminated the presence of PIHR and, as a result of this, IDT associated errors have been drastically reduced, providing iso-butanol measurements which appear consistent with previous studies [39,44,84,224]. There is scope for further work in this area, as the containment of crevice captured gases may extend the existence of an adiabatic core, allowing the investigation of longer IDTs and lower compressed temperatures [48,118,119]. Generally, crevice containment operates by providing a physical barrier to the crevice gas at the EOC, which may require significant modification to the RCM combustion chamber. Pseudo-crevice containment, through the design of crevice geometry to effectively capture boundary layer gas for longer time periods, may provide a cost-effective solution which requires less intrusive modification.

5 The Influence of iso-Butanol on the Ignition Delay Times and Low Temperature Heat Release of Gasoline and its Surrogate: An Experimental and Kinetic Modelling Study

5.1 Introduction

Bio-derived fuels, including bio-alcohols, are an attractive alternative to fossil derived fuels, either as single fuels or as supplementary components. Strategies for the limitation of climate change impacts mandate the reduction of transport emissions, including the use of a wide range of fossil fuel alternatives and supplements. The attractiveness of alcohols in this case is due in part to the physical and thermodynamic similarities they share with conventional fossil fuels, such as gasoline. This allows for possible applications in SI engine technologies and fuel distribution infrastructure with little to no modification [84,258]. Iso-butanol has been identified in the literature as a potential fuel component to satisfy the need for a bio-derivable fuel component as it provides the greatest knock resistant ignition properties over a range of reasonable conditions of the bio-derivable butanol isomers [39]. The ignition characteristics of iso-butanol as a single component have been investigated in previous works [39,42,43]. However, it is vital to also understand the ignition characteristics of any alternative fuel or fuel supplement blend fully with gasoline, such that the feasibility of the fuel blending can be determined. The feasibility of a given blend is dependent on satisfying engine performance concerns, such as a fuel's knock resistance. This is not only important for use in current SI engines, but also for emergent technologies such as turbo-charged, downsized engines and homogeneous compression charge ignition (HCCI) engines. A thorough ignition study is necessary for developing an understanding of fuels which are not well characterised at engine relevant conditions. RCMs can be used to investigate this regime, producing IDT data over a range of realistic, engine relevant, thermodynamic conditions [48]. IDTs describe the time taken for a given fuel/oxidiser mixture to auto-ignite at a given set of thermodynamic conditions, which can provide an analogue for the fuel's knock resistance. When IDTs are investigated for a range of conditions, a comprehensive profile of a given fuel's autoignition behaviour can be determined.

Due to the relatively simple physical conditions of an RCM, cases can be modelled though the application of detailed chemical kinetics. Where investigatory experiments would otherwise be prohibited (perhaps due to their difficulty or the cost of experiments), computer developed models provide a relatively cheap and quick alternative [308]. The application of numerical

models in this way provides a platform for a thorough investigation of the underlying chemistry which drives the autoignition process, with the aim of developing a deeper understanding of a given fuel and its characteristics on blending. Fundamental experiments, such as RCM IDT investigations, provide a range of validation targets for a model, that are often relevant to real world engine conditions. By providing the data from these experiments, numerical models can be further developed to increase their validity at all relevant conditions. This is especially true for new fuels, which may have been exposed to little investigation and analysis. Gasoline is, unfortunately, too complex to model effectively, due to the large amount and variety of hydrocarbons of which the fuel is composed. Thus, a surrogate fuel consisting of less components but designed to match the relevant gasoline properties is often developed to facilitate the modelling of the reference gasolines behaviour. In this chapter, the ability of the five-component surrogate described in section 3.2 to mimic the autoignition behaviour of the reference gasoline is investigated. This is performed using the University of Leeds RCM (described thoroughly in section 3.3.1), at conditions of T_c=675-870 K, P_c=20 bar and Φ=1.0. The influence of iso-butanol on the autoignition behaviour of this surrogate is also investigated for blends of 5-70 % iso-butanol by volume, at conditions of T_c=710-870 K, P_c=20 bar and Φ=1.0. Simulations are produced for each of these conditions using the combined iso-butanol and gasoline surrogate mechanism described in section 3.5.1 [84,85], following the methods thoroughly described in sections 3.5.2 and 3.5.3.

A novel HRA technique for RCMs is applied to experimental and modelling results, facilitating a deeper investigation into the influence of iso-butanol on the autoignition of the 5-C surrogate and the representation of LTHR behaviour by the model. Due to an array of challenges concerning the use of RCMs, such as significant heat losses, fuel transfer into piston crevices and the difficulty in acquiring suitable transducer measurements, HRA has not traditionally been applied to RCM studies. However, recent studies have developed a method through which HRA may be applied to RCM experimental data [172]. This technique provides an avenue for significant further exploration of fuels and their ignition behaviour. To further the investigation of blending behaviour and model representation, local OH sensitivity analyses are completed. This serves to identify important reactions at a range of conditions, providing insight into the underlying chemistry responsible for observed changes in the IDT behaviour of fuels. Analysis such as this can also be applied to locate areas of potential model uncertainties, which can be isolated for future model development.

5.2 Surrogate Performance

Figure 5.1 shows RCM IDTs of the reference gasoline, its 5-C surrogate, and the variable volume simulated IDTs for 5-C. All IDTs are captured at a pre-calculated compressed pressure of 20 bar, Φ=1 (stoichiometric) and at pre-calculated compressed temperatures of 675 – 870 K. Displayed temperatures are taken from the EOC, as calculated from real RCM pressure traces. IDTs are presented as the mean of 4-6 individual experiments, errors bars are displayed representing twice the standard deviation of each case.

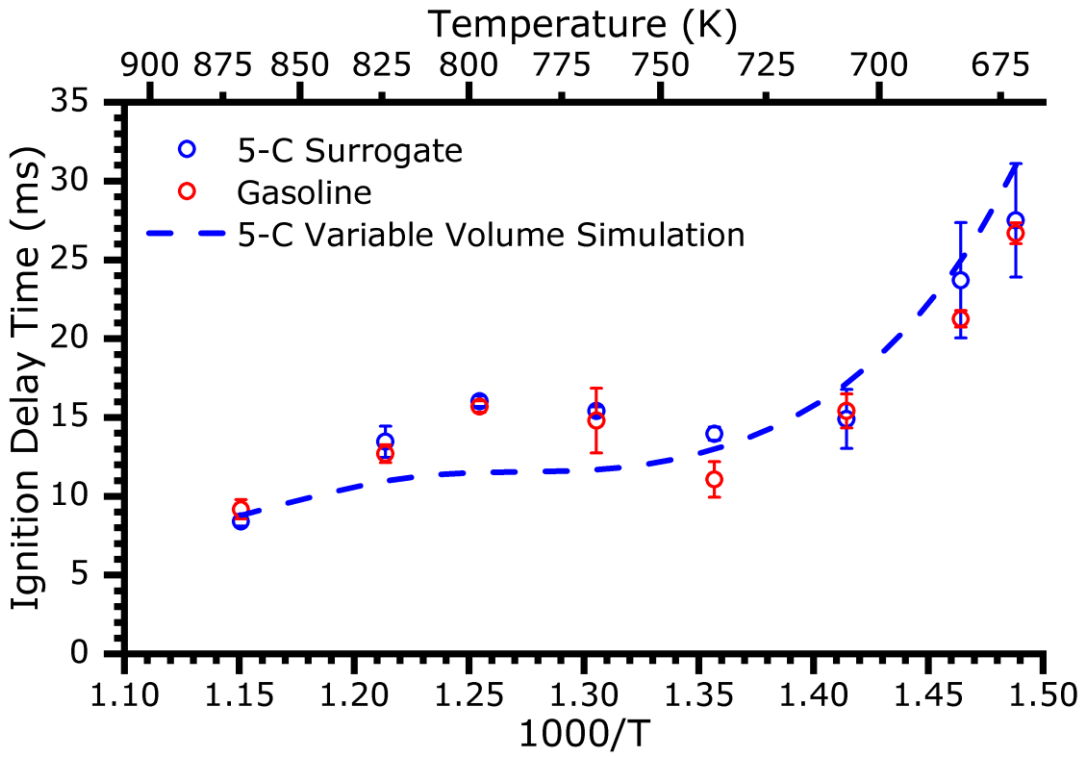

Figure 5.1. Surrogate representation of the reference gasoline IDT profile, including variable volume simulation predictions. P_c=20 bar, Φ=1.

Experimentally, the 5-C surrogate provides an excellent representation of the reference gasoline. The general IDT profiles appear very similar for the two fuels, including similar values at the low and high temperatures, as well as within the negative temperature coefficient (NTC) region. An exception to this relationship can be found at 740 K. At this condition, the 5-C surrogate shows a significantly longer IDT (~3 ms longer) than the reference gasoline leading to the appearance of a less intense NTC region. This behaviour is somewhat predicted by the 5-C variable volume simulation, which shows an NTC region much shallower than that of the reference gasoline. However, under these conditions, the NTC behaviour predicted by the

variable volume simulation substantially under-predicts the IDTs displayed by the 5-C surrogate. In contrast, at the lower end of the temperature regime, the model slightly over-predicts the IDT of the 5-C surrogate. These differences indicate the combined mechanism applied does not accurately reproduce the ignition behaviour of one or multiple of the 5-C surrogate components. This is investigated further in this study, through the application of sensitivity analysis techniques. It should also be noted that, in general, the 5-C surrogate displays a larger uncertainty in IDT measurements, than the reference gasoline. This is to be expected due to the added complexity of the preparation of the 5-C mixture, which requires the injection and mixing of five individual liquid components. At low temperatures, where the error bars appear largest for 5-C, the influence of ethanol (which displays an Arrhenius relationship between IDTs and temperature) may be significant. Percentage uncertainties in the ethanol concentration during mixture preparation are the largest of all the components, due to the small volume required, but the influence of this is minimal, as shown in figure 3.8. However, test-to-test mixture variations due to limitations in the University of Leeds mixing chamber (non-stirred), as well as small variations in initial temperature and pressure, will produce variations in the EOC conditions and fuel compositions which produce a larger variation in IDT measurements for the same condition. Such test-to-test mixture changes are particularly important for 5-C, which requires more time to homogenise than the single component gasoline. This would produce larger degrees of error in regions which are the most temperature sensitive (e.g. <710 K), like those observed. In future, efforts should be made to improve the University of Leeds RCM fuel mixing facilities, particularly for the investigation of more complex fuel mixtures (more components) and lower temperatures.

Pressure traces for individual RCM experiments, across the temperature range can be seen in figure 5.2, providing a comparison of the ignition development for the reference gasoline and 5-C surrogate. At temperatures of both 675 and 686 K, gasoline produces shorter IDTs than the 5-C surrogate. Upon investigating the pressure traces for these cases, the development of profiles is similar between the two fuels. However, the gasoline clearly undergoes a first-stage ignition (or cool-flame) earlier than the 5-C in both cases. This causes temperature and pressure to be elevated earlier for gasoline, leading to shorter IDTs. Interestingly, at 740 K, both fuels undergo a first-stage ignition at the same time, but the reference gasoline undergoes main-stage ignition much earlier than the surrogate. These observations indicate that, while the surrogate provides a good representation of gasoline IDTs, it is failing to sufficiently represent the cool-flame behaviour in some cases. This is likely due to the significant over-abundance of alkanes in the surrogate, which contribute largely to this behaviour [85]. At conditions of 710 K and 800 – 870 K, the surrogate provides an accurate representation of the gasoline's IDTs,

which is reflected in the pressure traces of each case. At 710 K the two fuels display similar cool-flame behaviour, in terms of profile, intensity and timing. Whereas, at higher temperatures neither fuel displays significant multi-stage ignition behaviour.

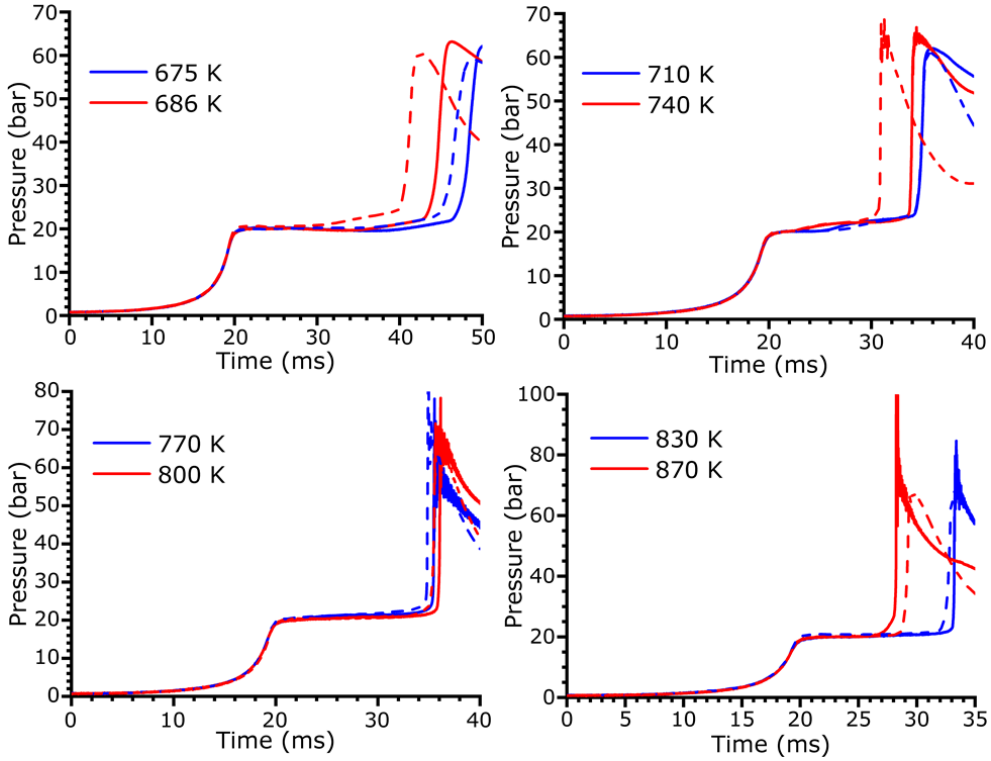

Figure 5.2. Comparisons of 5-C surrogate and gasoline experimental RCM pressure traces. Solid lines show 5-C surrogate pressure traces. Dashed lines show gasoline pressure traces. P_c=20 bar, Φ=1.

Figure 5.3 shows the experimentally derived IDTs for the blended conditions iB10, iB30 and iB50, for the 5-C surrogate and reference gasoline, as well as variable volume simulation results for these 5-C and iso-butanol blends. It can be seen in this figure that the 5-C surrogate continues to provide a reasonable analogue for the reference gasoline under blended conditions, providing a good representation of the trends on blending to higher levels of iso-butanol. As expected, based on the ONs of the fuels, increasing the volume percentage of iso-butanol leads to longer IDTs, particularly at lower temperatures. However, at 710 K, the 5-C iB10 IDT is significantly shorter than that observed in gasoline iB10, and at high and low temperatures there are notable differences between the IDTs for iB50 blends. There is also a significant difference between iB30 IDTs for the two fuels at 740 K, and generally shorter IDTs for the 5-C iB30 than the gasoline blend. Error bars, shown as twice the standard deviation, are presented for all conditions in figure 5.3 but are mostly too small to be observed over such a large IDT scale. In

the shown temperature region (710-870 K), errors for 5-C and gasoline blends are similar, as seen for the same temperature region in the “neat” fuels. In general, variable volume simulations continue to under-predict the NTC intensity for each blend, which is consistent with an under-prediction of IDTs for the unblended surrogate. This general failure of the model becomes more pronounced with increasing percentage of iso-butanol in the blend.

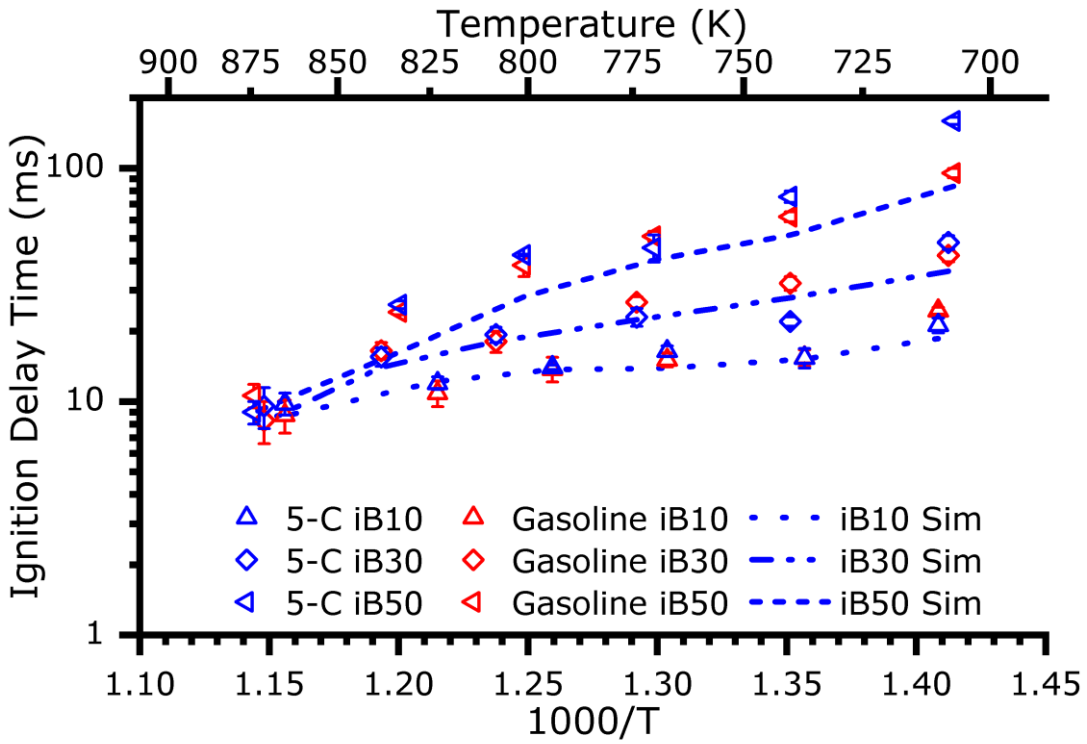

Figure 5.3. Surrogate representation of the reference gasoline IDT profile at blends of 10, 30 and 50% iso-butanol by volume, including variable volume simulation predictions. P_c=20 bar, Φ=1.

IDTs for iB70 gasoline and surrogate blends can be seen in figure 5.4. At temperatures of 770 – 870 K, the surrogate blend again provides a reasonable representation of the gasoline blend, with both fuels exhibiting no sign of NTC behaviour. However, at low temperatures (710, 740 K) the surrogate blend did not ignite, as heat loss effects at long experiment timescales prevented the fuel from achieving ignition. This is contrary to the gasoline blend which did ignite, although with long IDTs, indicating again a difference in low temperature reactivity between the surrogate blend and the gasoline blend.

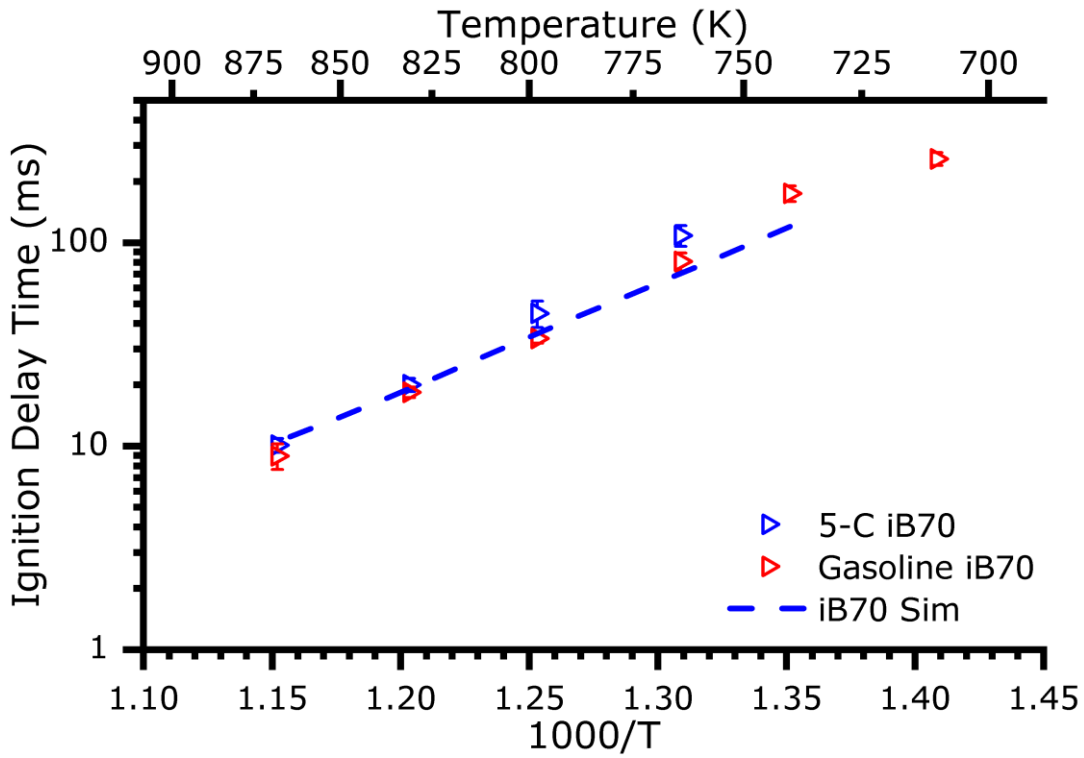

Figure 5.4. Surrogate representation of the reference gasoline IDT profile at a 70% iso-butanol blend, including variable volume simulation predictions. P_c=20 bar, Φ=1.

Pressure traces for a selection of 5-C and gasoline blended conditions are highlighted in figure 5.5, providing an example of ignition behaviour similarity and differences for the investigated blends. At a temperature of 770 K, the 5-C iB10 and gasoline iB10 show approximately the same IDTs (as seen in figure 5.3), which is represented in the example pressure traces. Both the 5-C iB10 and gasoline iB10 show very mild two-stage ignition, with the first stage occurring at approximately the same time for each fuel. This is followed by a strong autoignition, as shown by a large pressure rise over an extremely short period of time, producing a large pressure gradient. This strong autoignition is not apparent for the iB30 cases at a temperature of 740 K, where both the 5-C and gasoline iB30 fuels produce a gradual rise in pressure before the ignition event. This behaviour is characteristic of inhomogeneous ignition phenomena, such as pre-ignition [124,131,132,286–289]. However, unlike pre-ignition, these pressure traces are highly repeatable as seen in the pressure traces displayed in figure 5.6, indicating that this behaviour is a consistent feature of the iB30 blend.

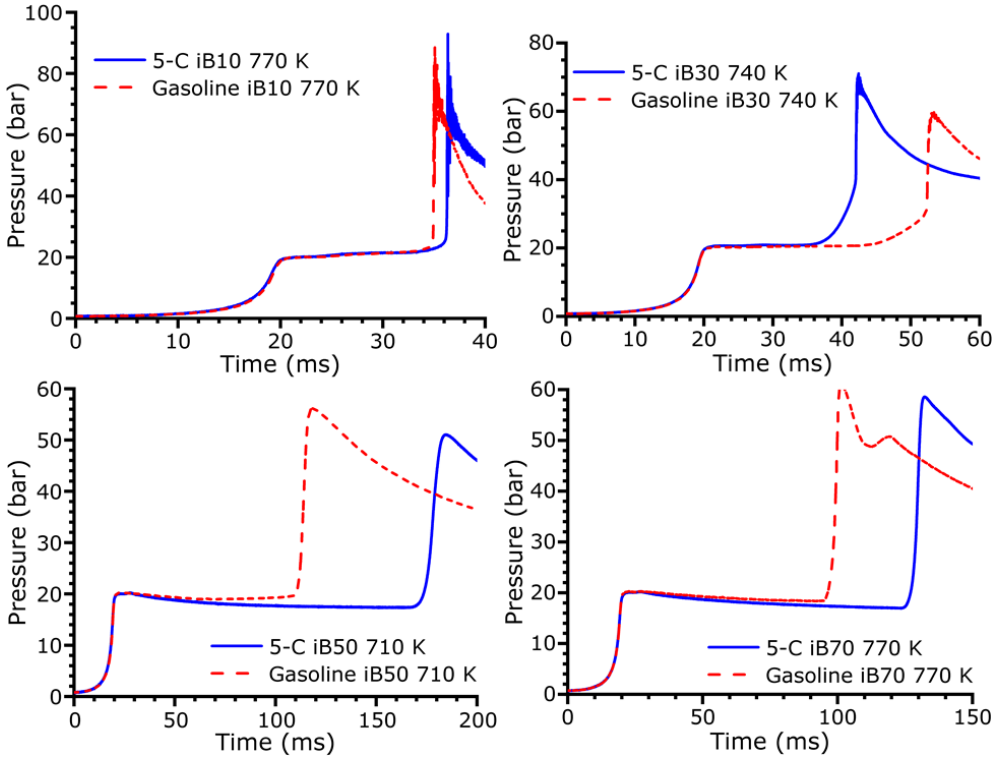

Figure 5.5. A selection of pressure traces, providing a comparison between gasoline and surrogate iso-butanol blends. P_c=20 bar, Φ=1.

There are clear differences in the pressure traces for the 5-C and gasoline iB30 fuels, which are consistent which a significant difference in IDTs between the two fuels. The 5-C iB30 fuel at 740 K auto-ignites much earlier than the gasoline iB30 blend, due to a gradual pressure rise which occurs earlier than the same phenomena in the gasoline iB30 blend. This pressure rise is also larger and faster for the 5-C iB30 blend, as is the peak pressure reached after ignition. At an EOC temperature of 710 K, the 5-C and gasoline iB50 blends do not produce any of the multistage ignition phenomena displayed by the iB10 and iB30 blends at temperatures of 770 K and 740 K, respectively. Significant heat loss can be observed for the 5-C iB50 fuel before ignition, leading to long IDTs. This is not as apparent in the gasoline iB50 case, which produces much shorter IDTs than the surrogate and butanol blend at the same temperature. The gasoline iB50 blend produces a small amount of heat release prior to ignition, which appears to limit the impact of characteristic RCM heat losses. This same heat release is not observed prior to ignition for the 5-C iB50 case. Example pressure traces for iB70 fuels at 770 K also show extremely long IDTs, which are influenced by extensive heat losses. Again, the gasoline blend produces significantly shorter IDTs, displaying less sensitivity to the influence of

RCM losses. However, unlike in the iB50 710 K case, neither the gasoline iB70 nor 5-C iB70 display significant heat release before the ignition event.

Examples of RCM repeatability for each blend are shown in figures 5.6 and 5.7. As previously mentioned, despite the appearance of the iB30 740 K pressure traces as characteristic of pre-ignition, both the gasoline and surrogate blend show high degrees of repeatability, making it unlikely that this behaviour is due to inhomogeneous ignition. Other blends continue to show a high degree of repeatability, at the conditions highlighted in figure 5.7. Not only is the IDT largely consistent for each collection of individual experiments, the peak post-ignition pressures of individual cases are also approximately the same (neglecting any post-ignition transducer noise), at a given blend/condition. Compression profiles (pressure change due to piston motion) and EOC pressures are also observed to be identical for each individual experiment, for a given blend and condition. This is due to the high repeatability of RCM operation, particularly when following specific operating procedures (as detailed in Methodology). Furthermore, the heat loss profiles post-compression are also consistent between individual experiments. There are no observable differences in repeatability between gasoline and 5-C cases (and the associated blends with iso-butanol) shown in these examples. For the iB70 blend cases shown, the magnitude of IDT deviation for experiments is larger than for blends of lower iso-butanol volume percentage, which is to be expected at longer IDTs.

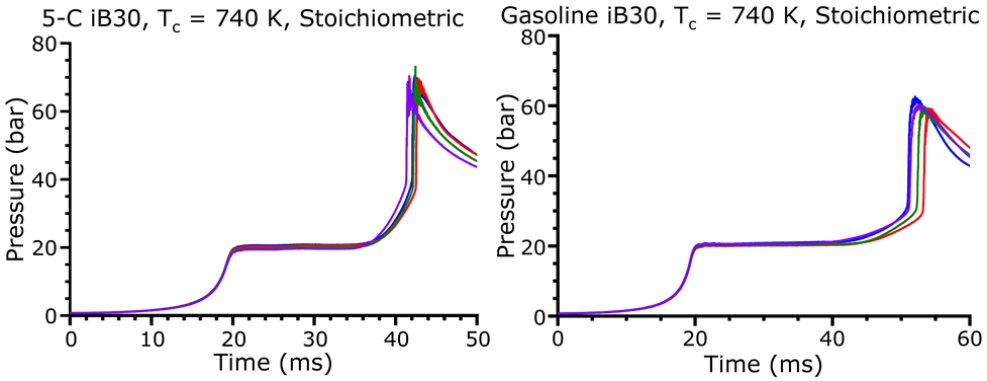

Figure 5.6. Demonstration of RCM repeatability for iB30 740 K conditions. Each coloured line represents the pressure trace for an individual experiment. P_c=20 bar, Φ=1.

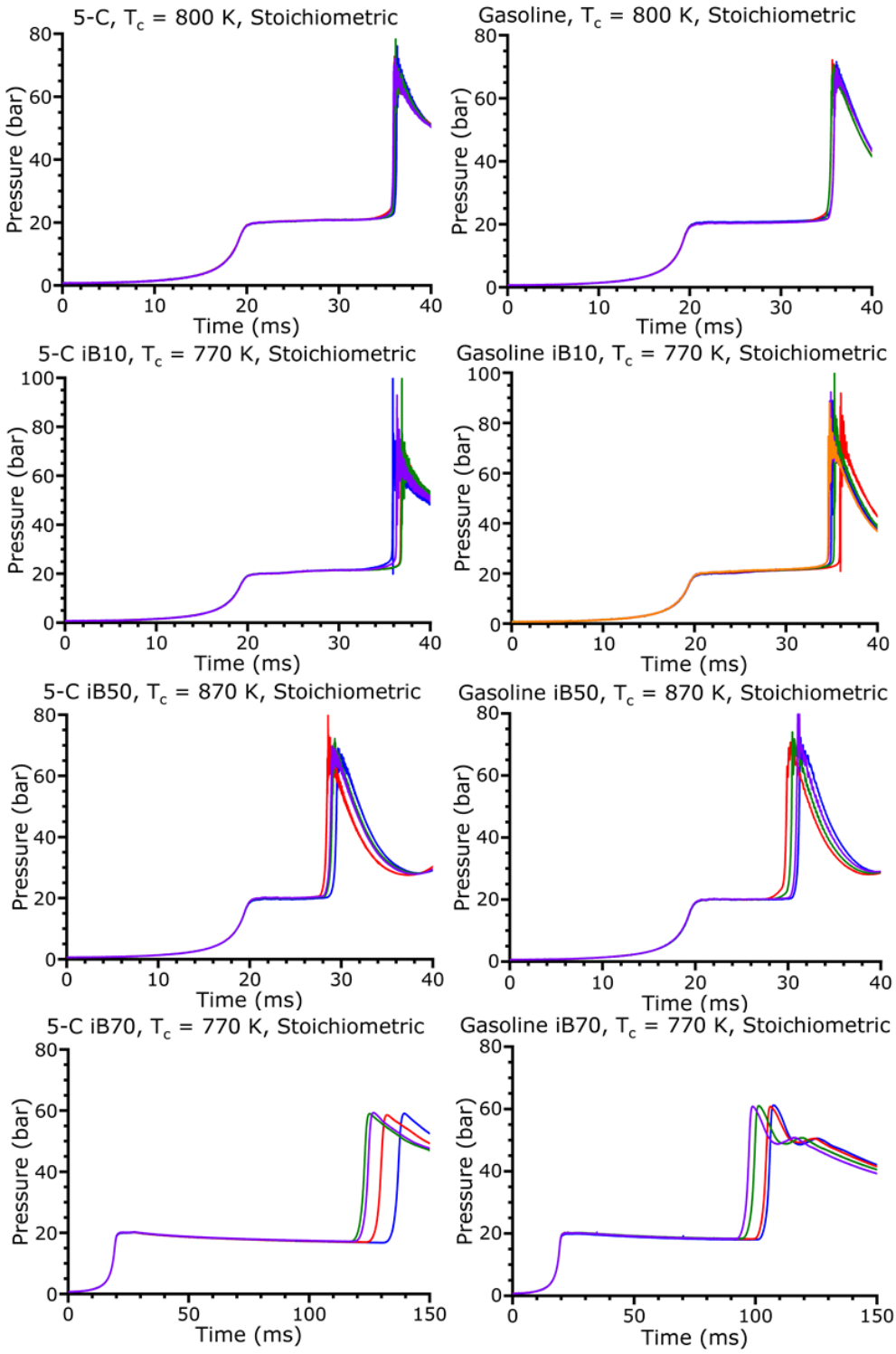

Figure 5.7. Further examples of RCM repeatability for a selection of conditions (5-C 800 K, gasoline 800 K, 5-C iB10 770 K, gasoline iB10 770 K, 5-C iB50 870 K, gasoline iB50 870 K, 5-C iB70 770 K and gasoline iB70 770 K). Each coloured line represents the pressure trace for an individual experiment. P_c=20 bar, Φ=1.

5.3 Blending Behaviour

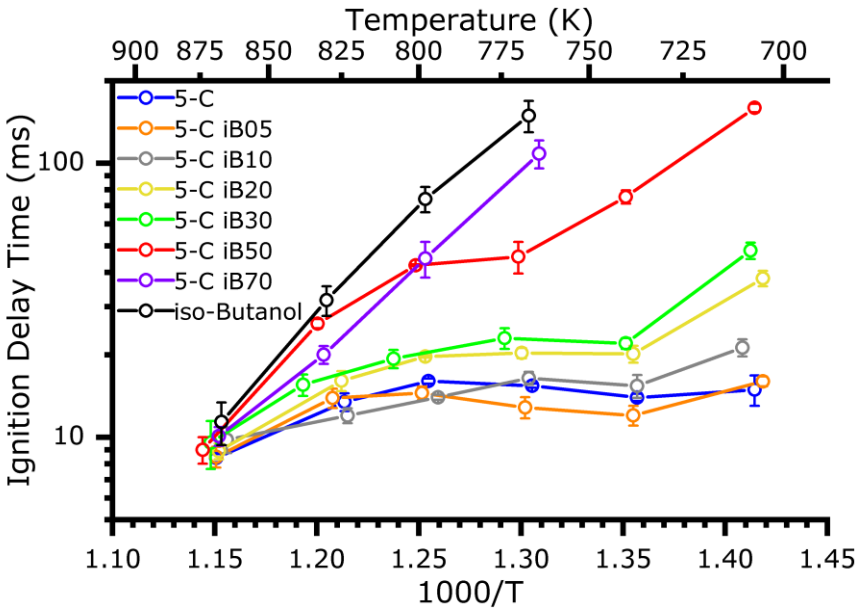

Figure 5.8. Experimental IDTs for 5-C and iso-butanol blends. Symbols show mean IDTs at each condition. Lines between each point are displayed to aid in the distinction of blending behaviour. P_c=20 bar, Φ=1.

The influence of increasing iso-butanol volume percentage on the IDTs of blends, can be seen in figures 5.8-5.10, which shows IDT profiles for all blending ratios for the 5-C/iso-butanol (figure 5.8) and gasoline/iso-butanol (figure 5.9) blends. Variable volume simulations for 5-C/iso-butanol blends can be seen in figure 5.10. Unlike the 5-C surrogate and reference gasoline, the IDTs of iso-butanol exhibit no NTC behaviour. Instead, an Arrhenius behaviour is observed, where the IDTs increase exponentially with decreasing temperature. This behaviour is consistent with literature examples of iso-butanol IDTs [39]. At temperatures below 770 K, IDTs for iso-butanol could not feasibly be recorded in the University of Leeds RCM, due to the excessively long delay times. At conditions with long times between the EOC and ignition, the adiabatic core assumption breaks down, even with the use of a creviced piston head. This break down leads to a higher likelihood of inhomogeneous ignition events (such as pre-ignition) and drastically increased degrees of heat loss, which cause unreliable IDT measurements, with a low degree of repeatability [48,120]. Figure 5.10 shows that variable volume simulations provide a good prediction of the iso-butanol ignition delay behaviour, accurately capturing the Arrhenius behaviour and providing a relatively good estimate of real IDTs across the studied temperature range.

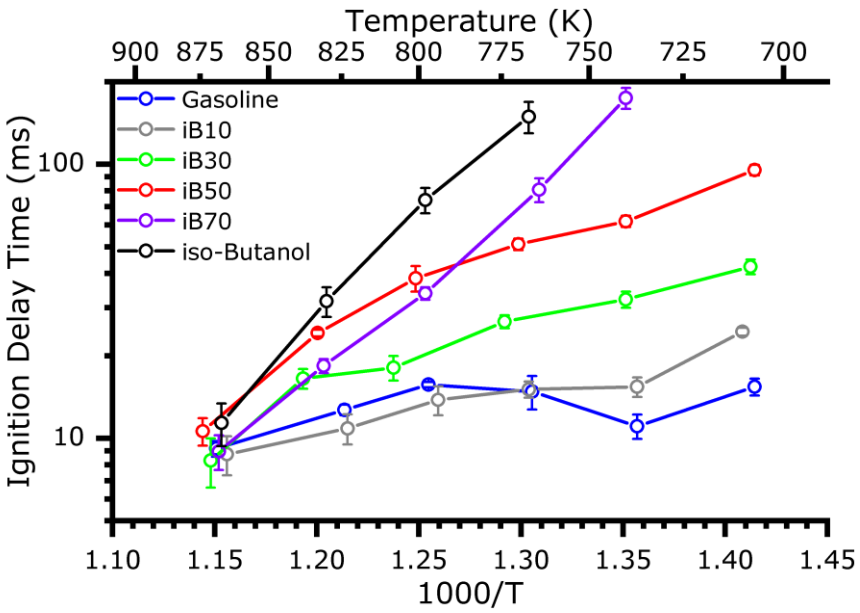

Figure 5.9. Experimental IDTs for gasoline and iso-butanol blends. Symbols show mean IDTs at each condition. Lines between each point are displayed for clarity. P_c=20 bar, Φ=1.

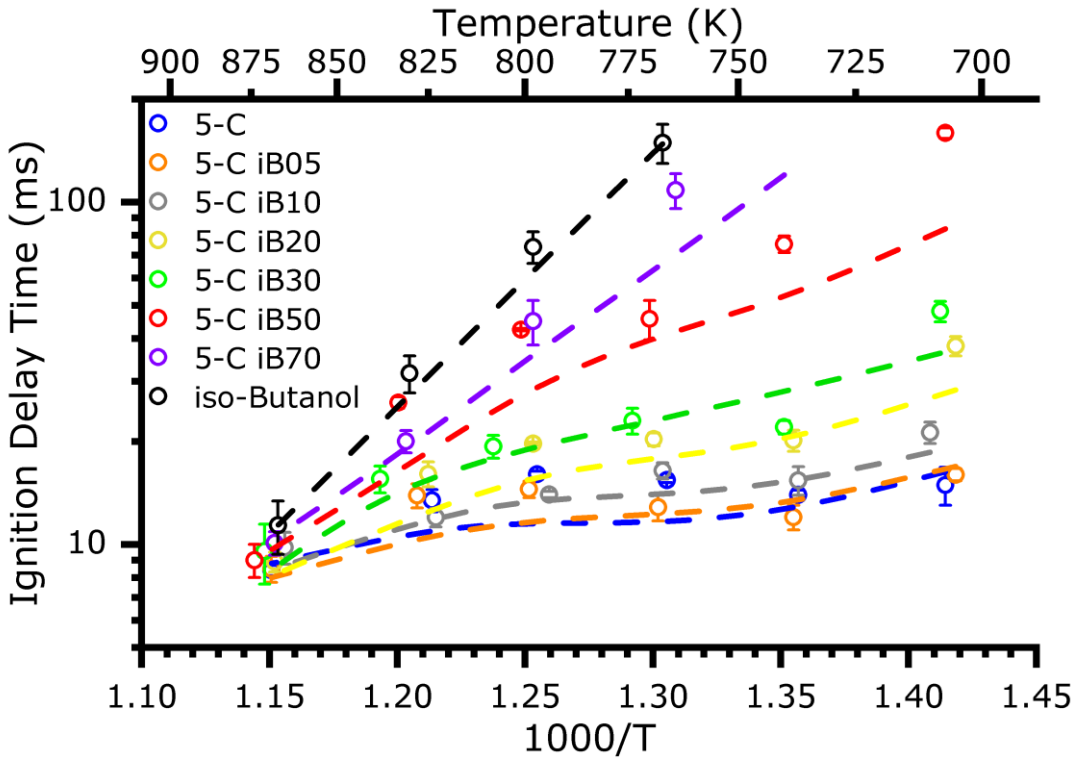

Figure 5.10. Comparison of experimentally derived IDTs for all investigated 5-C and iso-butanol blends. Symbols show IDTs collected from RCM experiments. Dashed lines show variable volume simulation results. P_c=20 bar, Φ=1.

In general, at temperatures of and below 770 K, the influence of iso-butanol blending on the IDTs appears to be monotonic: increasing iso-butanol volume fraction leads to a longer IDT. The exception to this generality can be seen for the 5-C iB05 blend (figure 5.8), wherein IDTs at temperatures of 740-800 K are shorter than those observed for the 5-C surrogate. At higher temperatures (>800 K), the IDTs for iB05 are practically the same as those for the 5-C surrogate (within reasonable uncertainty). However, there is an apparent cross-over in autoignition susceptibility between the iB05 and iB10 blends at these temperatures, where the higher degree of iso-butanol blending produces shorter IDTs. At these conditions (800, 830 K), the 5-C iB10 blend also displays shorter IDTs than the 5-C, making it the most reactive fuel blend at these conditions. This same cross-over behaviour is also observed for gasoline and the iB10 blend, as seen in figure 5.9, supporting the existence of such blending behaviour and minimising the likelihood that the observed error is induced by small uncertainties in mixture preparation, as the gasoline iB10 blend only consists of two components. At these low iso-butanol blends, this non-linear blending behaviour may be due to the suppression of the typical NTC behaviour by small amounts of alcohol. While this suppression of the NTC by iso-butanol is also present in the larger iso-butanol content (e.g. iB50, iB70) conditions, the influence of the larger amounts of iso-butanol is such that the IDTs have increased drastically beyond those of the 5-C surrogate and gasoline, suppressing the overall reactivity of the fuel. Similar behaviour has been observed in the blending of n-butanol with gasoline [47,51], where suppression of the fuels NTC region by n-butanol was observed to produce an IDT cross-over at 20% n-butanol. Given the longer ignition times and Arrhenius profile of iso-butanol when compared to n-butanol [39], it is not unreasonable to speculate that this cross-over would appear at blends of lower iso-butanol volume. Pressure traces for conditions which highlight this crossover behaviour can be seen in figure 5.11, showing the 5-C surrogate, iB05 and iB10 blends at EOC temperature conditions of 770, 800 and 830 K. At 800 K, all three of these blends produce similar IDTs (as shown in figure 5.12). Pressure traces at this condition are also similar for all the blends, showing no discernible multi-stage ignition and a strong, sharp pressure rise due to auto-ignition.

As described previously, the iB05 blend produces the shortest IDTs of all blends at 770 K. Upon examination of the pressure traces at this temperature, 5-C and iB10 again show a strong, sharp ignition. However, the iB05 case shows a significant degree of intermediate heat release prior to the main ignition event, as characterised by a gradual pressure rise. This raises the temperature and pressure of the mixture, leading to shorter IDTs. Similarly, to the intermediate heat release displayed by iB30 (as shown in figure 5.6), this behaviour is highly repeatable, indicating that this is not evidence of inhomogeneous ignition and is instead a feature of the

blend, introduced by the blending of iso-butanol. The same heat release behaviour is observed for both iB10 and iB05 at 830 K, where the iB10 now produces the shortest IDT for all blends. Again, the behaviour is repeatable, indicating further that the heat release behaviour (which appears responsible for this IDT cross-over) is caused by the blending with iso-butanol.

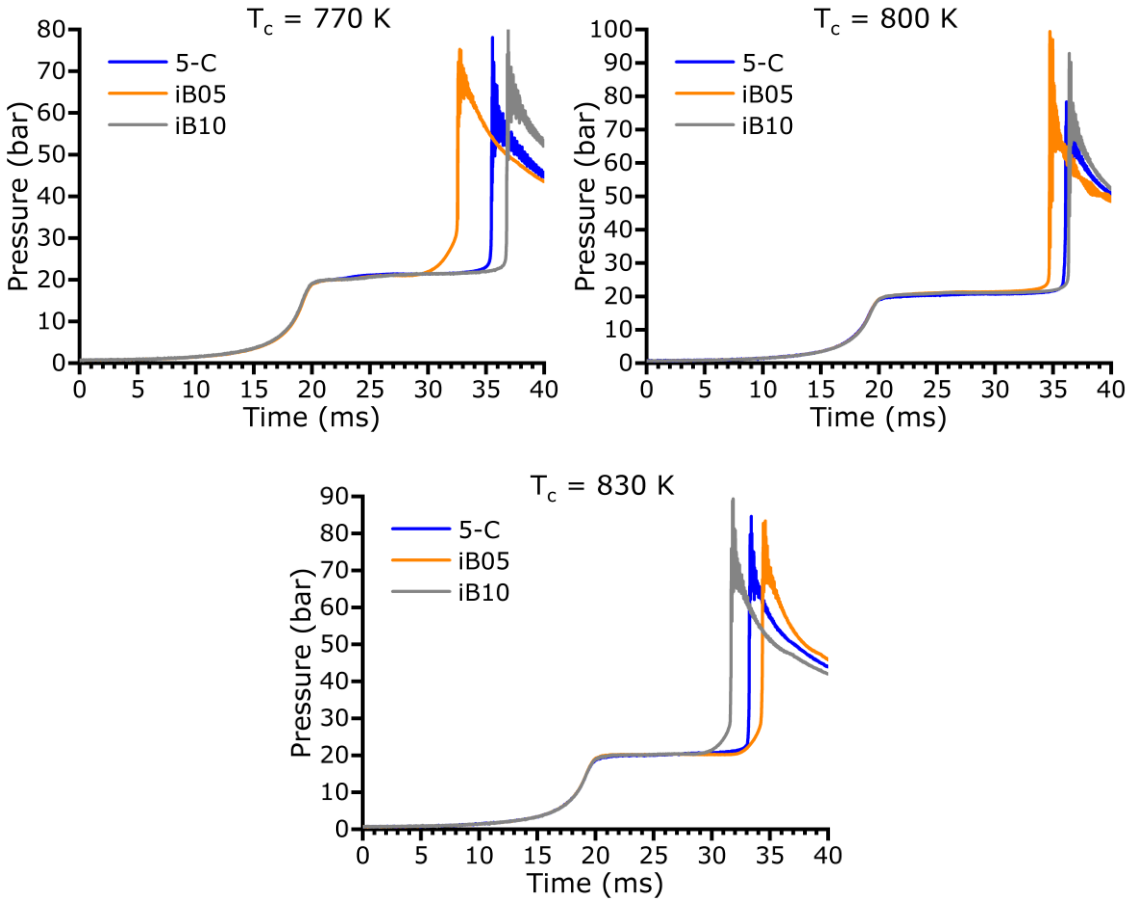

Figure 5.11. Comparison of single RCM pressure traces for the 5-C surrogate, iB05 and iB10, at cross-over conditions. P_c=20 bar, Φ=1.

As the blend's iso-butanol volume fraction is increased to 20, 30 and 50%, IDTs increase across the temperature regime. The NTC behaviour observed for the 5-C surrogate and gasoline slowly shallows out, with only a mild indicator of this behaviour at the iB50 blend conditions. Also, perhaps due to this shallowing of the NTC, IDTs for iB20 and iB30 conditions (apart from the lowest temperature condition) are very similar, particularly in the NTC region. This impacts on the choice of blends that would be most appropriate for use in a SI engine based on this data, as the marginal knock resistance gains must be balanced against any changes in the overall calorific value of the fuel blend, due to the addition of 10% more iso-butanol by volume. The iB50 blend shows a drastic increase in IDTs from the iB30 blend, with

IDTs at higher temperatures very similar to those seen in the pure iso-butanol fuel. However, the iB70 blend produces IDTs shorter than those of the iB50 blend at these same temperatures, for both gasoline and 5-C blends with iso-butanol. These iB70 blends display an Arrhenius IDT behaviour characteristic of the iso-butanol fuel, with no distinguishable NTC region. Like iso-butanol, IDTs at the lowest temperatures could not be captured due to the exceedingly long delays and associated heat loss effects. In the mid-temperature range, iB70 does produce longer IDTs than iB50, but due to the mild NTC present in the iB50 fuel the two IDT profiles cross-over, leading to the aforementioned shorter iB70 IDTs. This provides a further example to the effects of NTC suppression by the iso-butanol fuel component.

While variable volume simulations correctly predict the ignition delay behaviour at the lowest investigated temperatures (increasing iso-butanol volume at these conditions increases IDT), they fail to predict several other features of these blends. The failure of the mechanism to predict the 5-C NTC region has been mentioned previously, and this is a common feature for all the lower iso-butanol blends (iB05, iB10, iB20). Similarly, to the 5-C surrogate, variable volume simulations also show a slight over-prediction at the lowest temperatures for the iB05 blend. However, as the iso-butanol volume percentage increases beyond 5%, simulations begin to under-predict IDTs at these same temperature conditions, with an increasing degree respective to the iso-butanol volume percentage of the blend. At iB50, simulations under-predict IDTs throughout the regime, and provide little indication of any NTC. While it seems logical to attribute some of this difference to experimental heat losses at longer IDTs, it should be noted that not only should variable volume simulations provide a sufficient account of this, but also pure iso-butanol does not show such a disparity. This may indicate that the gasoline surrogate's aspect of the mechanism [85] is the source of simulation issues, which is further supported by the mechanisms inability to reproduce the NTC region.

The representation of a selection of individual RCM pressure traces by variable volume simulations is shown in figure 5.12. These conditions have been chosen as they represent points of significant difference between experimentally derived IDTs and those predicted through variable volume simulations. For the iB50 blend at a compressed temperature of 710 K, simulations underpredicted the IDT by the largest amount of any point investigated. The pressure trace for the variable volume simulation reveals that the model predicts significant heat release prior to the main ignition event, which is not present in the experimental pressure trace. Instead, the RCM pressure trace displays continued heat losses until the eventual ignition over 70 ms later. Whereas, for the iB30 blend at 740 K it is the RCM pressure trace which displays

significant heat release prior to ignition (as mentioned previously), and the simulation which displays none. In this case, the variable volume simulation largely over-predicts the IDT for iB30 due to its failure to replicate this multi-stage ignition behaviour.

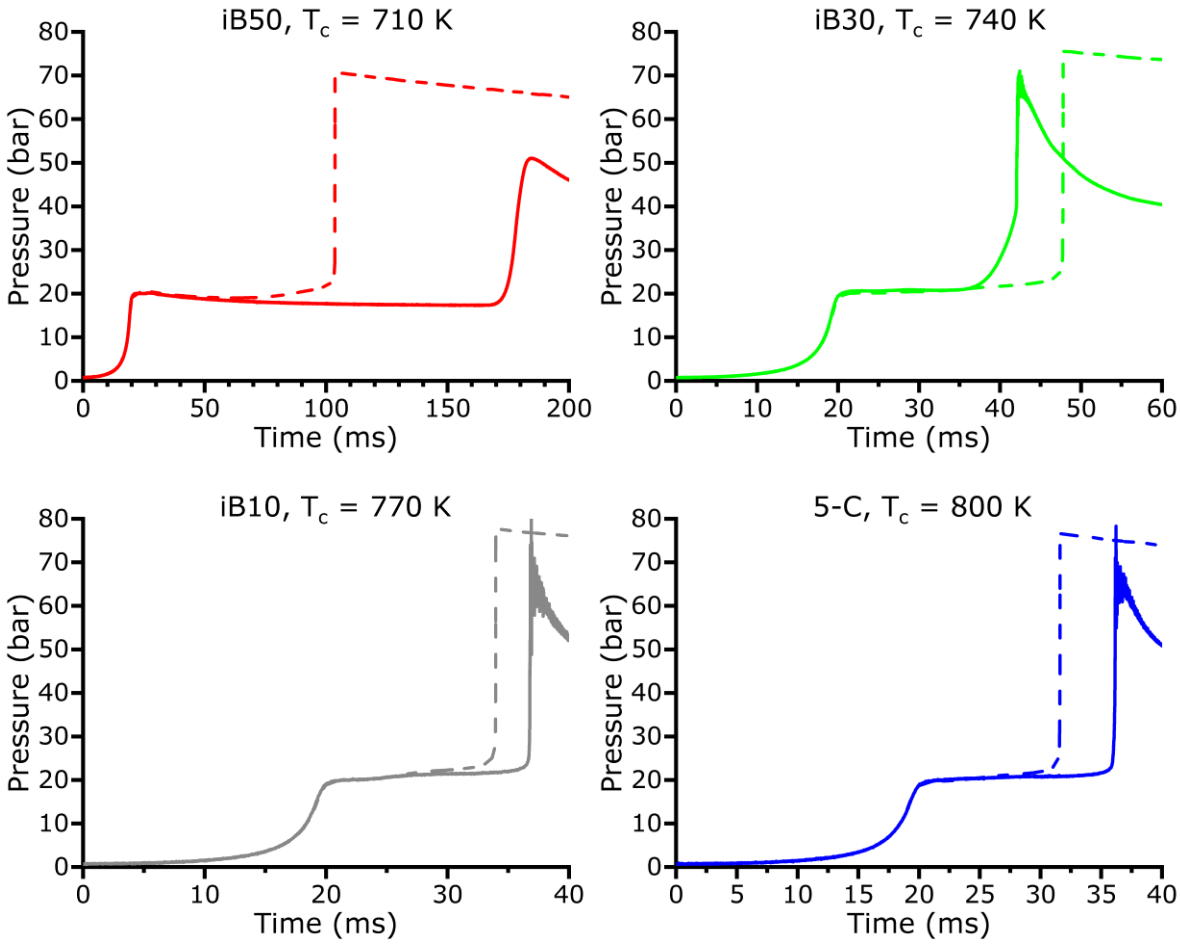

Figure 5.12. Pressure traces for a selection of cases with significant IDT differences between simulated and experimental results. Solid lines represent RCM pressure traces. Dashed lines represent variable volume simulation pressure. P_c=20 bar, Φ=1.

Failures of the model to accurately predict IDTs under iso-butanol blending and the complex blending behaviour observed in RCM measurements, may indicate a lack of or misrepresentation of fuel interactions. However, recent work by Gorbatenko et al. [47] has shown for n-butanol and surrogate blends, that the impact of cross-reactions between fuel species and their associated oxidation radicals was negligible, producing IDT differences of less than 0.1 ms throughout the testing regime (which is similar to the regime studied in this work). The interaction of fuels and the associated radical species is more likely to occur through interactions with the radical pool and it is important that the mechanism represents such

reactions accurately. This will be investigated further in section 5.6 through sensitivity analysis of the model for multiple 5-C/iso-butanol fuel blends.

At temperatures of 770 and 800 K, the simulation predicts shorter IDTs than the RCM experiments for the iB10 blend and 5-C, respectively. Upon investigating the first stage ignition behaviour of these conditions (as shown in more detail in figure 5.13), it is apparent that the simulation is significantly over-predicting the intensity of this phenomenon. This is leading to higher temperature and pressure conditions within the reactor, ultimately causing a shorter IDT. While the original surrogate mechanism provides evidence for the accurate representation of fuel interaction, in the form of IDT predictions for multiple blends of traditional surrogate components, it does not account for component interactions with ethanol [85]. Ethanol is a common component in gasoline mixtures available to the consumer, and as such the blending behaviour of gasoline and ethanol should be chemically represented by the gasoline surrogate. The lack of representation of this blending behaviour is a potential cause for models' inability to represent much of the surrogate and low-butanol blends ignition behaviours, which will require further investigation. These observations mandate further investigation into the underlying chemistry and thermodynamics governing the auto-ignition of these fuels, to determine the root cause of such major differences between model predictions and experimental results. This will include comprehensive HRA and reaction sensitivity analysis.

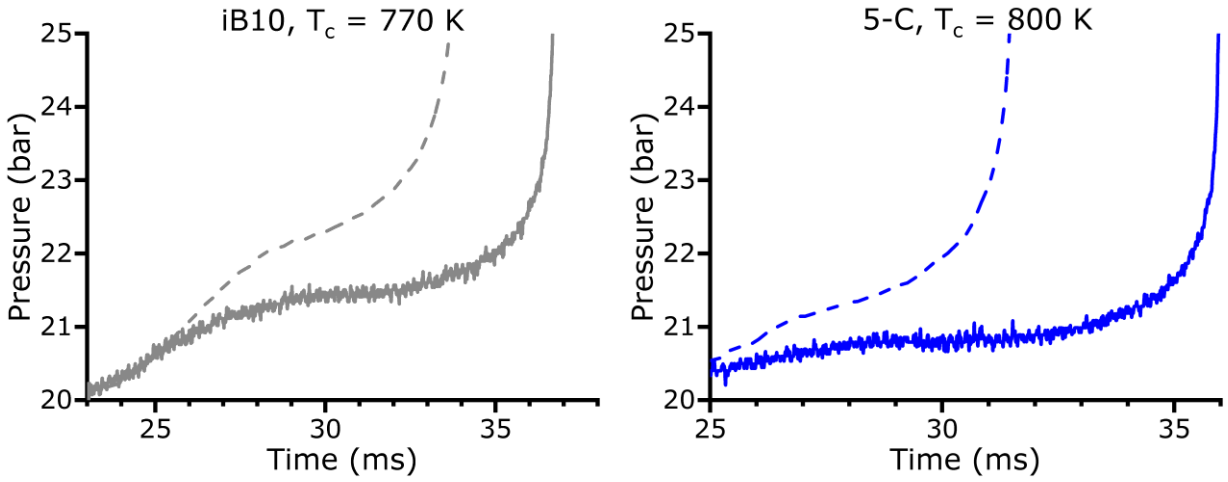

Figure 5.13. Enlarged pressure traces showing first stage ignition differences between experimental and simulated results. Solid lines represent RCM pressure traces. Dashed lines represent variable volume simulation pressure history. P_c=20 bar, Φ=1.

5.4 Influence of Equivalence Ratio

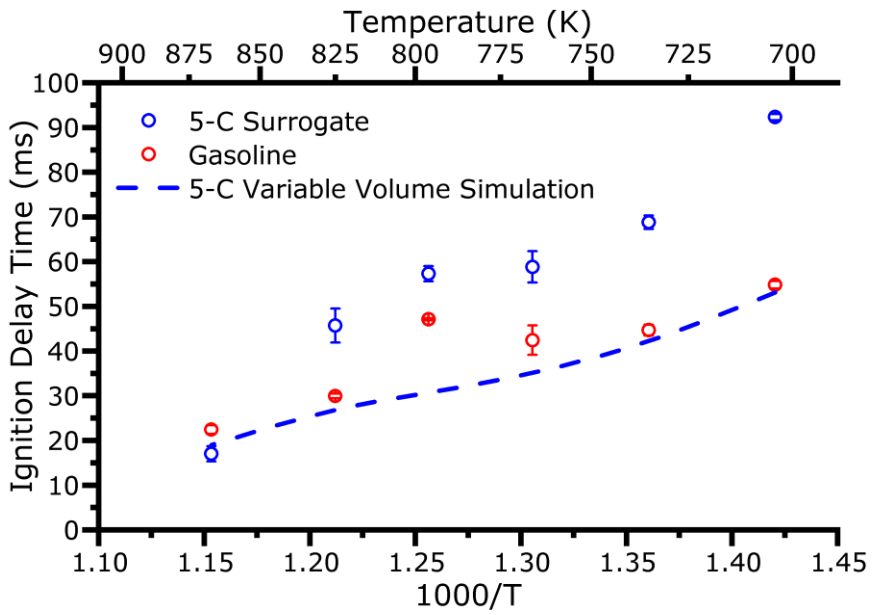

Figure 5.14. Surrogate representation of the reference gasoline IDTs at lean conditions, including variable volume simulation predictions. P_c=20 bar, Φ=1.

The reference gasoline and its representation by the 5-C surrogate were also investigated at the lean air/fuel condition of Φ = 0.5. The IDT profiles associated with this investigation can be seen in figure 5.14, alongside variable volume simulations for the 5-C lean experiments. Both the reference gasoline and the 5-C display a clear NTC behaviour, however, there are significant differences between the ignition behaviour of these two fuels. The largest difference in IDTs can be observed at the lowest temperature (~710 K), wherein the 5-C surrogate produces IDTs which are much longer than those produced by the reference gasoline (92.3 and 54.8 ms, respectively). Errors at this condition are approximately the same for the 5-C and gasoline (±0.7 and ±0.8 ms, respectively), indicating a high degree of repeatability for both fuels and allowing for confidence in the validity of these measurements. The 5-C surrogate also showed some small increases in IDT (over the reference gasoline) at stoichiometric conditions, which decreasing the equivalence ratio has exaggerated. Variable volume simulations fail to predict the long IDT observed for the 5-C surrogate, but estimates are close to the measured gasoline value. This is contrary to variable volume predictions at stoichiometric conditions, which produce a slight over-prediction of IDTs. Longer IDTs for the 5-C surrogate continue throughout the IDT profile, with a generally decreasing magnitude as EOC temperature increases. An exception to this trend can be seen shortly after the NTC peak (~830 K), where the difference between 5-C and gasoline IDTs increases. This appears to be due to a

significantly more intense NTC for the reference gasoline, which is not fully replicated by the developed surrogate. This lack of intensity can be further observed at temperatures of 770-800 K for the 5-C surrogate. The same behaviour is also observed at stoichiometric conditions, where the NTC for the 5-C is shallower than that observed in gasoline, which is again exaggerated by the lower equivalence ratio. Variable volume simulations fail to reproduce any meaningful NTC; a similar failure of the model as that witnessed at stoichiometric conditions. At the highest temperature of 870 K, IDTs for both fuels have converged, as also appears to be the case for all fuels investigated at stoichiometric conditions. Overall, variable volume simulations vastly under-predict IDT for the 5-C surrogate across the temperature range, except for at the 870 K condition, and fail to produce any NTC. Therefore, the model is not suitable for the prediction of surrogate ignition behaviour under lean stoichiometry conditions.

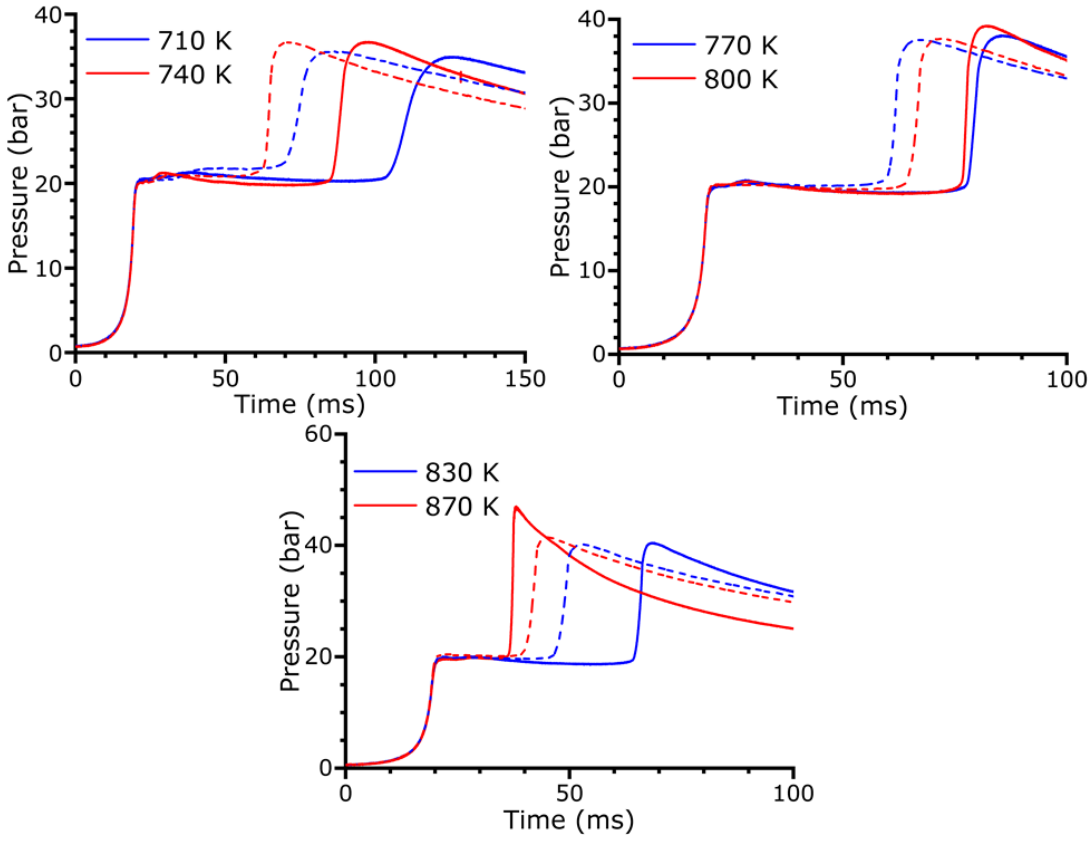

Figure 5.15. Individual RCM pressure traces for 5-C and gasoline fuels. Solid lines = 5-C surrogate pressure trace. Dashed lines = Reference gasoline pressure trace. P_c=20 bar, Φ=1.

IDT differences between the 5-C surrogate and reference gasoline (at lean conditions) can be further explored through the investigation of RCM pressure traces, as shown in figure 5.15. Clear differences in the pressure trace for each fuel are evident at the lowest investigated

temperature (710 K). Both fuels at this temperature display two stage ignition, with the first stage occurring at the same time in each fuel (relatively shortly after the EOC). However, the resultant pressure rise from this event is more pronounced in the reference gasoline, leading to higher temperature and pressure conditions within the reactor: a potential cause of the shorter IDT. The 5-C fuel is also subject to more substantial heat loss effects at 710 K than the gasoline, as less heat release occurs for the surrogate post first stage ignition, extending the IDT as temperature and pressure conditions within the reactor are reduced. Similarly, while the intensity of first stage ignition is approximately the same at 740 K, the 5-C pressure trace again shows an increased effect of heat losses, leading to a longer IDT.

Temperatures of 770 – 830 K continue to show increased degrees of heat loss for the surrogate, leading to longer IDTs. The increased influence of heat losses on the 5-C surrogate was also observed at long IDTs for blended stoichiometric conditions, such as the iB50 710 K pressure trace displayed in figure 5.5. Coupled with 5-C surrogates' observable failure to fully reproduce the low temperature behaviour of the reference gasoline, it is possible that small differences in the surrogate and gasoline composition and properties (such as RON, MON and alkane content) are leading to observable ignition behaviour differences. While the surrogate provides an excellent representation of gasoline at stoichiometric conditions, lean experiments have displayed the need for improvement of the surrogate (as did large degrees of iso-butanol blending), potentially through the addition of an additional naphthenic component or the re-evaluation of alkane content to more accurately reproduce the gasoline composition.

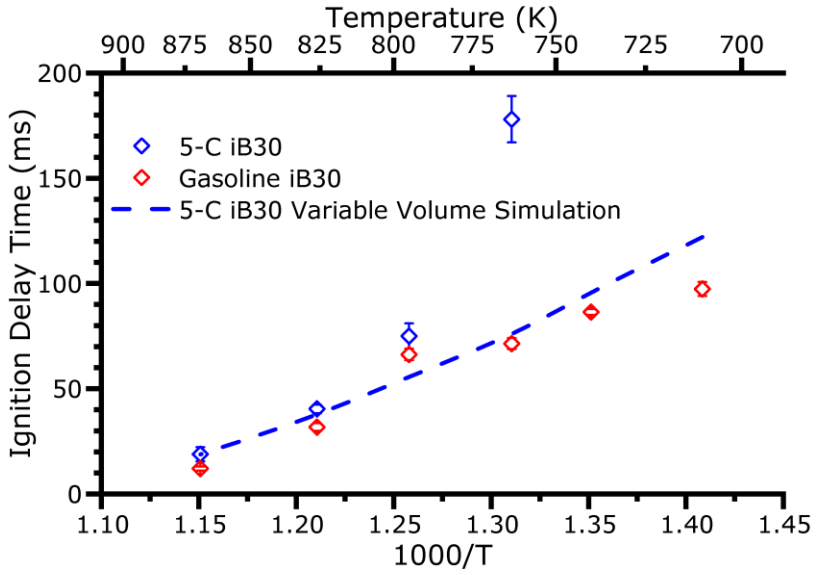

Figure 5.16. Surrogate representation of the reference gasoline IDT profile at a 30% iso-butanol blend and a lean air-fuel ratio, including variable volume simulation predictions. P_c=20 bar, Φ=1.

The representation of the gasoline iB30 blends ignition behaviour by the 5-C iB30 blend, at lean stoichiometry conditions, can be seen in figure 5.16. Also included in this figure are the variable volume simulation results for 5-C iB30 experiments. Gasoline iB30 RCM results display a very mild NTC, around 770-800 K, which is not reproduced by 5-C iB30 RCM results, which display more Arrhenius behaviour. Due to long IDTs associated with this behaviour, it was not possible to collect IDTs for the 5-C iB30 blend below temperatures of ~770 K. Results captured for 5-C iB30 at 770 K display a much longer IDT than that exhibited by the gasoline iB30 at the same temperature, again displaying the lack of low temperature representation by the surrogate at lean stoichiometry. Such a stark difference in measured IDTs at this temperature warrants further investigation in future RCM work, as small uncertainties present during mixture preparation will produce a greater influence on mixture composition and therefore, lead to potential errors in IDT measurement. However, IDTs at temperatures below 770 K could not be captured as they did not autoignite, which appears to support that the IDT at 770 K is not an error induced anomaly. Due to the long IDT of 5-C iB30 at 770 K, the associated IDT error is larger than for any other IDT measurements for the iB30 blends. At this temperature, variable volume simulation predictions for the 5-C iB30 are more similar to the gasoline iB30 IDTs, vastly under-predicting the IDTs of the 5-C iB30 RCM results at lean conditions. At temperatures of 800-870 K, the 5-C iB30 and gasoline iB30 RCM results produce similar IDTs and variable volume simulations produce a reasonable reproduction of these high temperature RCM results.

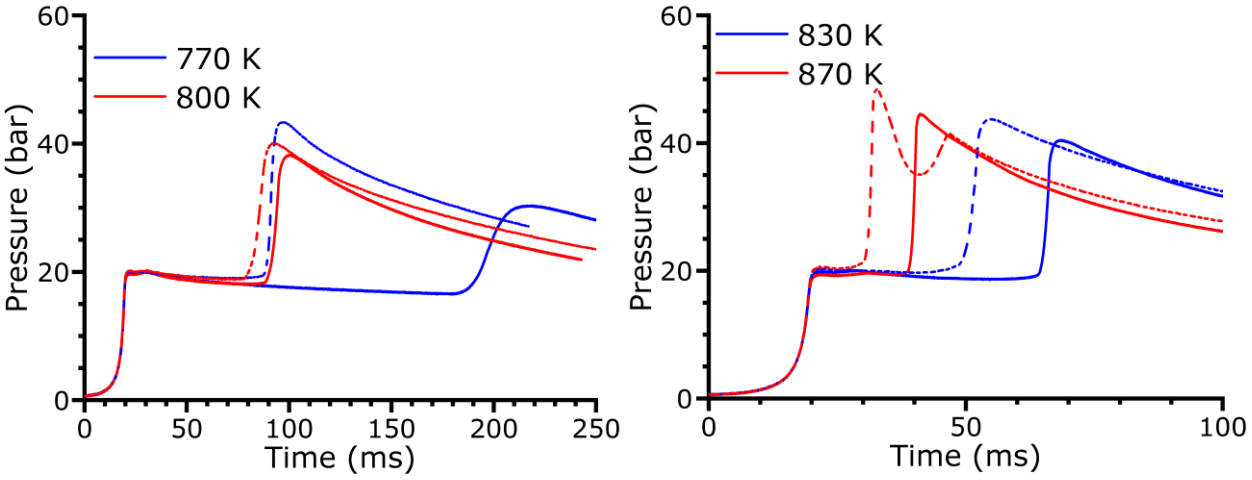

Figure 5.17. Individual RCM pressure traces for 5-C iB30 and gasoline iB30 fuels. Solid lines = 5-C surrogate pressure trace. Dashed lines = Reference gasoline pressure trace. P_c=20 bar, Φ=1.

Pressure traces for 5-C iB30 and gasoline iB30 RCM experiments are shown in figure 5.17. RCM pressure traces for the 770 K lean condition again show that the surrogate blend experiences longer IDTs and an increased amount of heat losses (as shown by greater degrees of pressure loss post-EOC and prior to ignition), when compared to gasoline iB30 at the same temperature. This may be due to larger amounts of LTHR in the gasoline fuel that are not reproduced by the 5-C blend (due to compositional differences), which combat the pressure and temperature reductions associated with characteristic RCM heat losses. Differences in the first stage ignition and LTHR behaviour of gasoline and 5-C was also observed under stoichiometric conditions, indicating this aspect of the surrogate requires addressing. This behaviour is characteristic of alkanes, such as n-heptane and iso-octane, which are significantly over-represented in the surrogate [46,85,91,136]. In future work, it may be useful to evaluate to ability of a six component surrogate, which can account for gasoline's naphthene content and limit the concentration of alkanes in the surrogate, with the aim of more accurately representing first stage IDT and LTHR behaviour. In the literature, a seven component surrogate produced some success in matching the first stage IDT of a reference gasoline but largely over-predicted the intensity of first stage ignition. Four and three component surrogates have also proven ineffective at matching these cool flame properties at stoichiometric and lean conditions [45,70,181,309,310]. At temperatures of 800 and 830 K, the 5-C iB30 blend also shows relatively high heat losses post-compression. At 830 K, the gasoline iB30 blend also shows a degree of mild heat release prior to the main ignition event which is not evident in the 5-C iB30 pressure trace. At stoichiometric conditions, heat release prior to ignition was common in both 5-C and gasoline iB30 cases, but only a very mild form appears at lean conditions, and only for the gasoline iB30 cases at 830 and 870 K.

IDT profiles for blends of 5-C, iB30 and iB100 (iso-butanol), at both stoichiometric (Φ = 1.0) and Φ = 0.5 equivalence ratios, providing a direct comparison of ignition behaviours for each stoichiometry, are presented in figure 5.18. Variable volume simulations for each blend and stoichiometry are also visible in figure 5.18. The influence of lean conditions on IDT magnitudes is apparent for all fuel blends: a 0.5 decrease in equivalence ratio causes a drastic increase in IDTs. Also, for fuel blends which exhibit an NTC at stoichiometric conditions (5-C and 5-C iB30), reducing the equivalence ratio leads to suppression of the NTC. In the case of iB30, the NTC is eliminated entirely, due to both the concentration of iso-butanol and the lean equivalence ratio. Suppression of the NTC under lean conditions can also be seen in the literature for multiple gasolines and their surrogates [311–313], as well as individual surrogate fuel components [46,314]. IDTs for each blend converge at the high temperature end of the

scale into two separate points, dependent on the equivalence ratio, showing that reducing the equivalence ratio produces an increase in IDT, regardless of temperature (for the temperature range and pressure investigated). The model also predicts this basic trend. Iso-butanol IDTs appear to be the least impacted by changing stoichiometry, with the smallest difference between stoichiometric and lean measurements. However, variable volume simulations predict a more substantial difference, significantly over-predicting lean IDTs.

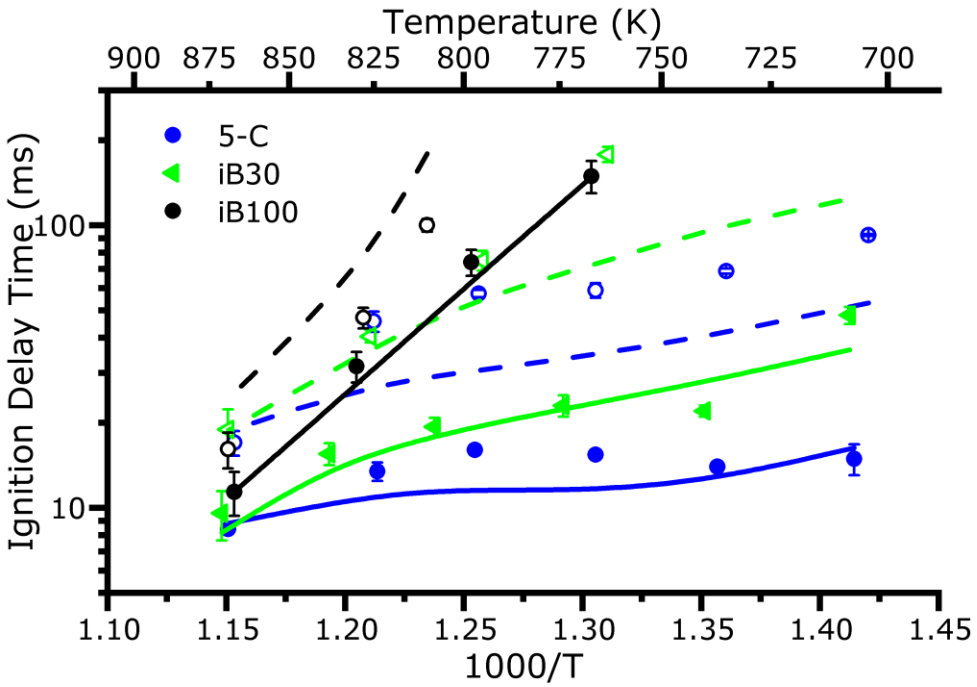

Figure 5.18. A comparison between the IDTs of the 5-C surrogate, iB30 blend and iso-butanol (iB100) fuels, at lean and stoichiometric conditions, showing RCM results and variable volume simulations. Filled symbols = RCM results at the stoichiometric air/fuel ratio (Φ = 1.0). Unfilled symbols = RCM results at the lean air/fuel ratio (Φ = 0.5). Solid lines = variable volume simulation results at the stoichiometric air/fuel ratio (Φ = 1.0). Dashed lines = variable volume simulation results at the lean air/fuel ratio (Φ = 0.5).

Simulations for iB30 are consistent at high temperatures (>800 K), producing accurate predictions for both lean and stoichiometric equivalence ratios but failing to represent low temperature ignition behaviour. In a general sense, simulations fail to accurately represent the effect of changing equivalence ratio on IDTs. These simulations predict a vertical translation of the IDT profile for lean conditions, which is not an accurate representation of the fuels changing ignition behaviour at low temperatures. For iso-butanol, a reduction in equivalence ratio produces an increase in IDTs, with no autoignition observed in the RCM at temperatures below

~800 K due to the low reactivity of the fuel at these conditions. This decrease in reactivity at lean conditions is similar to that seen for iso-butanol in the literature, as is the inability to capture low temperature IDTs [224]. While the model predicts this increase in iso-butanol IDTs, it overpredicts IDTs for the lean conditions, whereas iso-butanol predictions at stoichiometric conditions were very good. Further analysis would be required to determine why the model fails to represent this change in ignition behaviour, including the further exploration of equivalence ratio on surrogate and iso-butanol blended fuels IDT behaviour and extensive sensitivity analysis of the applied mechanism.

5.5 Heat Release Analysis

To further investigate the non-linear blending behaviour observed and provide targets for further model investigation, HRRs are extracted and analysed from the RCM experiments. Figures 5.19-5.29 show the experimental and simulated HRRs prior to the main ignition event plotted against the aHR and time from the maximum pressure gradient, at temperatures of 710-870 K. LTHR is common in degenerately branched systems and describes exothermic events that occur before the main stage of heat release, which describes the auto-ignition event [53]. LTHR is indicated by a relatively sharp peak in HRR and an associated rise in pressure, which also produces a visible CH_2O^* chemiluminescence, and is considered to be chemically due to the decomposition of ketohydroperoxides to produce multiple OH radicals [172]. In some cases, LTHR may be followed by an intermediate stage of heat release (ITHR), which also occurs before the auto-ignition event. ITHR is less well understood but can be described as a gradual rise in HRR (and therefore pressure), due to coupled self-heating processes. The driving chemistry of ITHR is less well understood than LTHR but it is thought to be due to RO_2 direct elimination reactions, producing an alkene/carbonyl/ether species + HO_2, followed by the recombination reactions of HO_2. This leads to an accumulation of large amounts of H_2O_2, which, as temperature slowly increases, will ultimately decompose into OH radicals, causing the main stage of heat release and auto-ignition [315]. For the purpose of the following analyses: the soITHR is defined as the inflection point of the HRR gradient post LTHR, and the soHTHR is defined as the point at which the HRR exceeds 100/s. Various methods have been suggested to define the end of ITHR/soHTHR, based on threshold HRR and dHRR/dt values, but these produce similar thresholds [315]. As such, a similar has approach has been taken in this study as the previous RCM heat release literature in defining the soHTHR as the point at which HRR>100/s [172,186,284,285].

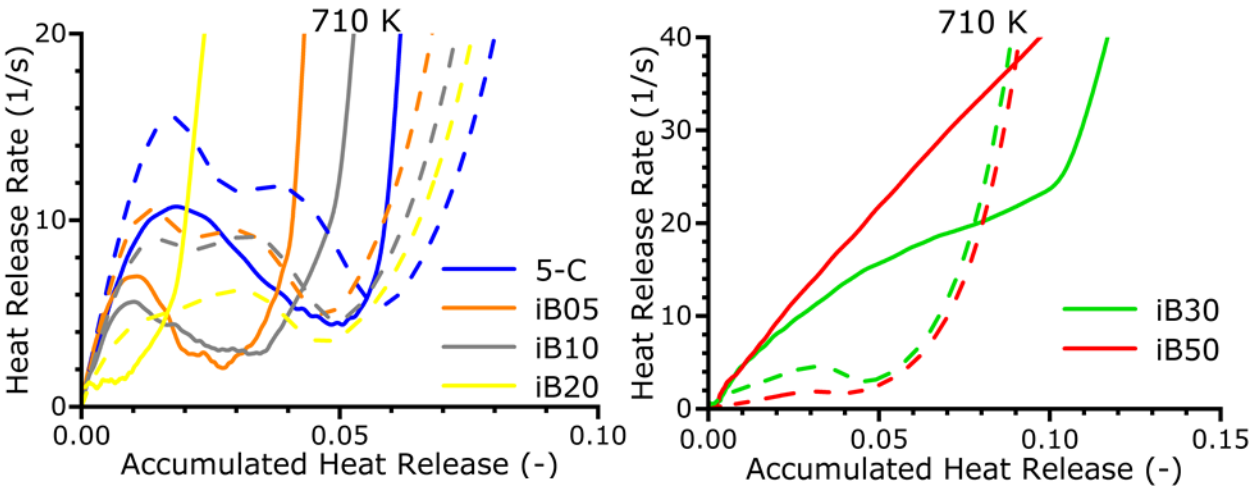

Figure 5.19. LTHR behaviour as calculated from RCM and variable volume simulation data, showing the relationship between HRR and aHR at a compressed temperature of 710 K. Solid lines = RCM analysis. Dashed lines = simulation analysis. P_c=20 bar, Φ=1.

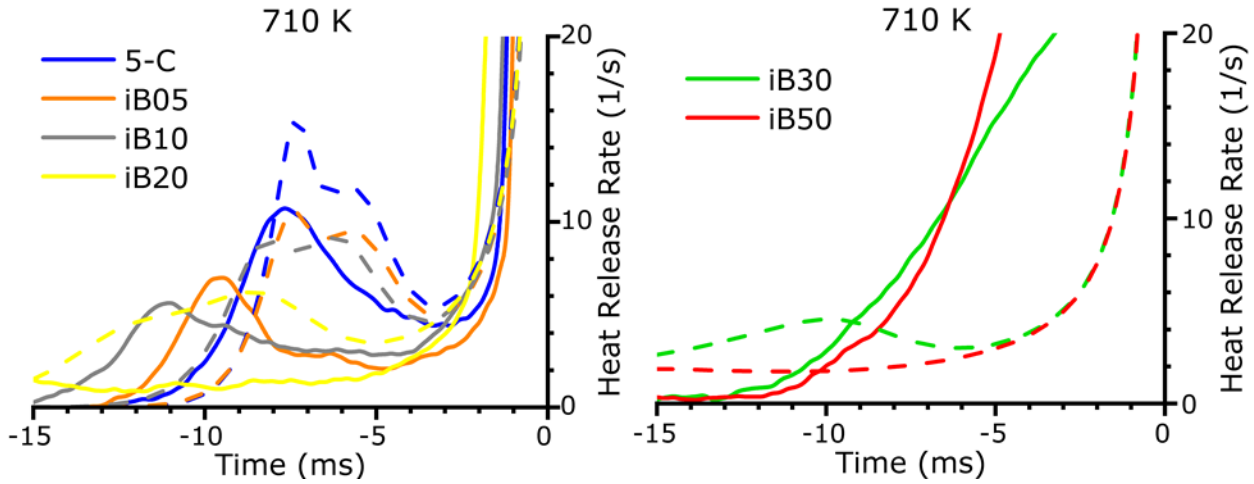

Figure 5.20. LTHR behaviour as calculated from RCM and variable volume simulation data, showing the relationship between HRR and time from point of ignition at a compressed temperature of 710 K. Solid lines = RCM analysis. Dashed lines = simulation analysis. P_c=20 bar, Φ=1.

At 710 K, the experimentally derived data in figures 5.19 and 5.20 shows a clear single LTHR peak for the 5-C surrogate. This LTHR is similar, in intensity of profile, to that seen for a PRF (RON 90) in the literature, at a pressure of 20 bar and temperature of 735 K [172]. The model, however, predicts two stages of LTHR, with the second stage appearing as a small peak, shouldering an initial larger peak. Multiple stages of heat release have been observed in the literature [92,315–317], however, many of these behaviours do not correlate well with that

shown by the model in figures 5.19 and 5.20, with many sources discussing multistage heat release in terms of the presence of LTHR and ITHR [315,318–320], or as a delayed/multi-phase HTHR [316,321–323]. AlRamadan et al. [317] did show a similar two-phase LTHR during n-heptane autoignition under extremely conditions at a temperature of 600 K. However, this phenomena was not further investigated in the original study, other than pointing out its existence, as it was only present at low initial temperatures and long ignition timescales, limiting its relevance to engine conditions [317]. Machrafi and Cavadias [324] also showed two distinct stages of LTHR in their study of a reference gasoline and TRF at lean equivalence ratios within a HCCI engine. This study determined that this delayed LTHR was due to radical scavenging caused by toluene in the TRF and aromatics in the gasoline: the formation of relatively stable benzyl radicals and HO_2 (which goes on to form the less reactive H_2O_2) is in competition with the consumption of alkanes through hydrogen abstraction, until HO_2 radicals reach a critical concentration. At this critical HO_2 concentration, much of the relatively unreactive benzyl radicals react to form the more reactive benzaldehyde radicals, removing the stability caused by the presence of significant benzyl concentrations. This causes the formation of H_2O_2 to become less important than its decomposition, promoting the formation two OH radicals, which in turn facilitate the chain branching pathways of the remaining fuel, leading to autoignition [324]. Similar two stage LTHR has also been seen in the HRA of TRF simulations, at P_c=20 bar and T_c=700-765 K [325]. The determination of the underlying chemistry driving two stage LTHR observed for simulation of 5-C will require further analysis of the model including sensitivity analysis, as completed in Chapter 6. The results presented here provide important evaluation targets for such analysis and for future model development.

The experimentally derived peak HRR for 5-C is somewhat lower in magnitude than the model peak and both the LTHR initiation and the peak LTHR occur earlier than predicted by the model. The addition of small amounts of iso-butanol produces a clear impact on the LTHR behaviour of the fuels, reducing the peak HRR in the LTHR region and flattening the LTHR profile. Similar behaviour has also been observed in a previous study on the blending of n-butanol with a TRF, wherein the addition of 10% n-butanol by volume produced a significant reduction in LTHR peaks HRRs at a temperature of ~700 K [325]. Even for iB05 experimental results, there is a clear LTHR peak reduction and the appearance of a mild shoulder to the LTHR peak, indicating a possible second, much smaller phase of LTHR. However, this shoulder displays very low HRRs, so its presence is certainly not definitive. When compared to the experimental 5-C surrogate results, the HRR profile is extended, with LTHR beginning earlier and continuing longer, but at lower magnitudes. This is also true for iB10, which further reduces

the peak LTHR value at an earlier time, and displays a flatter, more constant HRR profile. These lower peak LTHR values coincide with an increase in IDTs between blends. As in the 5-C surrogate simulations, iB05 and iB10 peak LTHR is over-predicted by the model and begins later than the experimentally derived heat release. The simulations display two distinct LTHR humps, which are clearly not present in the experimentally derived data, with much higher peak heat release than that calculated from experimental pressure traces. In the modelling results, the reduction of LTHR due to increasing iso-butanol concentrations appears to be largely focused on the initial LTHR peak, with the secondary peak reduced significantly less. In terms of aHR, simulations predict that ignition occurs at a slightly higher aHR for 5-C than iB05 and iB10, which coincides with an increased rate of HRR for the surrogate. From observing higher iso-butanol blends, it appears that accumulating more heat release prior to ignition indicates shorter IDTs, which is intuitive as this would also indicate elevated temperature and pressure conditions. Main stage ignition also occurs at much smaller values of aHR in experiments than the simulations predict. At blends of higher iso-butanol volume percentage, LTHR is completely absent at 710 K in the experimental data, despite the prediction of small amounts of LTHR by the model. The model prediction also shifts at these higher blending ratios, from predicting a two stage LTHR dominated by the first stage, to being dominated by the second stage before almost entirely disappearing. A region of ITHR can be observed in the HRR analysis of iB30 and iB50, leading into the main phase HRR. Initially, it was thought that this may represent inhomogeneous ignition events (such as pre-ignition) but due to the high degree of repeatability and the certainty with which PIHR was removed in the previous chapter, it was concluded that the phenomena are part of the blend's homogeneous ignition behaviour.

Heat release analyses for each blend at 740 K can be seen in figures 5.21 and 5.22, showing HRRs with respect to aHR and time from the point of ignition, respectively. When compared to the HRR analysis of blends at 710 K, analysis of simulations also predicts two stage LTHR for the 5-C fuel at 740 K. In this case however, the first stage of LTHR displays a significantly reduced HRR magnitude, whereas the second stage of LTHR produces an HRR similar to the lower temperature case. Also, the distance between the two simulated LTHR peaks is reduced (in terms of both aHR and time), when compared to 710 K. Furthermore, the aHR at the soITHR for the simulated 5-C case is less at 740 K, likely due to the reduction in LTHR peak one intensity. This reduction in soITHR aHR and peak one HRR magnitude is also present in the RCM HRA for the 5-C surrogate. At 740 K, RCM HRA also appears to show a small second stage of LTHR, but this is a speculative observation given the relatively small magnitude of this second peak. Again, simulations over-predict the intensity of LTHR intensity

for the 5-C fuel, as well as the aHR at soITHR. In figure 5.22 it can be seen that, for variable volume simulations, the LTHR peaks occur much closer to the point of ignition, indicating that the significantly larger HRR magnitude (and resultant amount of aHR) causes ignition to occur sooner. This same phenomenon is also observed at conditions of 770 and 800 K, as shown in figures 5.28 and 5.30, and correlates with significant under prediction of RCM IDT measurements for the 5-C fuel in the NTC region. LTHR is vital for the determination of the overall IDT in this region, indicating a misrepresentation of the chemistry which drives low temperature behaviour may be a cause of global model failures [326]. RCM analyses for iB05 shows a larger amount of LTHR in terms of both peak magnitude and aHR, at 740 K than at any other iB05 temperature condition. This coincides with the lowest IDT measured for all blends, excluding the highest temperature of 870 K. While the simulation matches this initial LTHR peak well for iB05, a second peak is also predicted that is not present in the experimental case, causing a larger amount of heat release to accumulate in simulation predictions before ITHR. Despite this, simulation and RCM HRA both show an initial LTHR peak at approximately the same time prior to ignition, and simulations provide a reasonable prediction for the IDT (over-estimating the value slightly). Similarly, LTHR for iB10 also occurs at a similar time in RCM and simulation analysis, coinciding with a good IDT prediction. However, simulations do not fully capture the intensity of iB10 LTHR, particularly over predicting the second stage of LTHR (which is present in simulations as a 'shoulder' to the initial peak, but much clearer in RCM analysis).

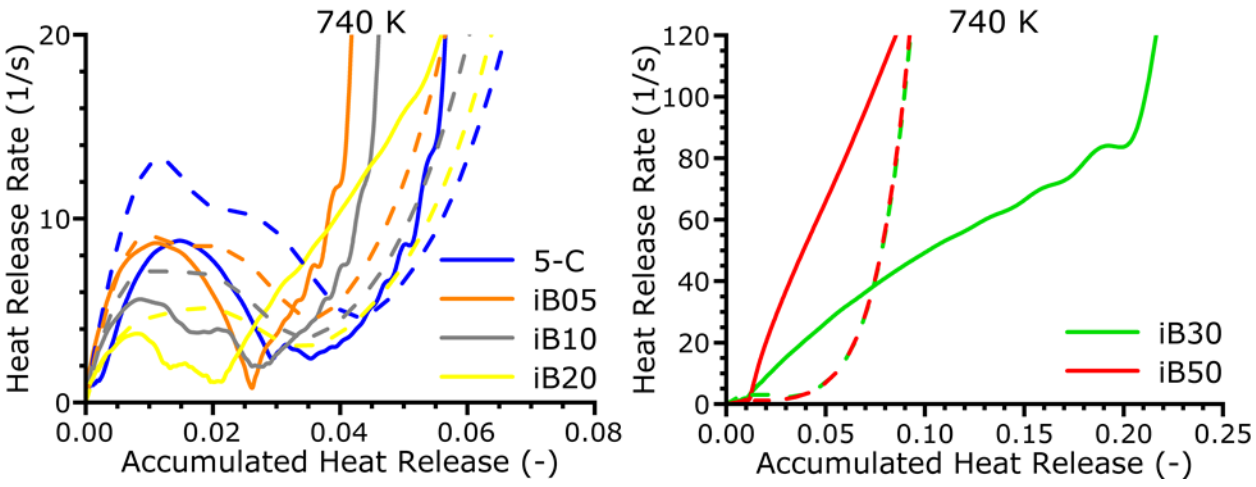

Figure 5.21. LTHR behaviour as calculated from RCM and variable volume simulation data, showing the relationship between HRR and aHR at a compressed temperature of 740 K. Solid lines = RCM analysis. Dashed lines = simulation analysis. P_c=20 bar, Φ=1.

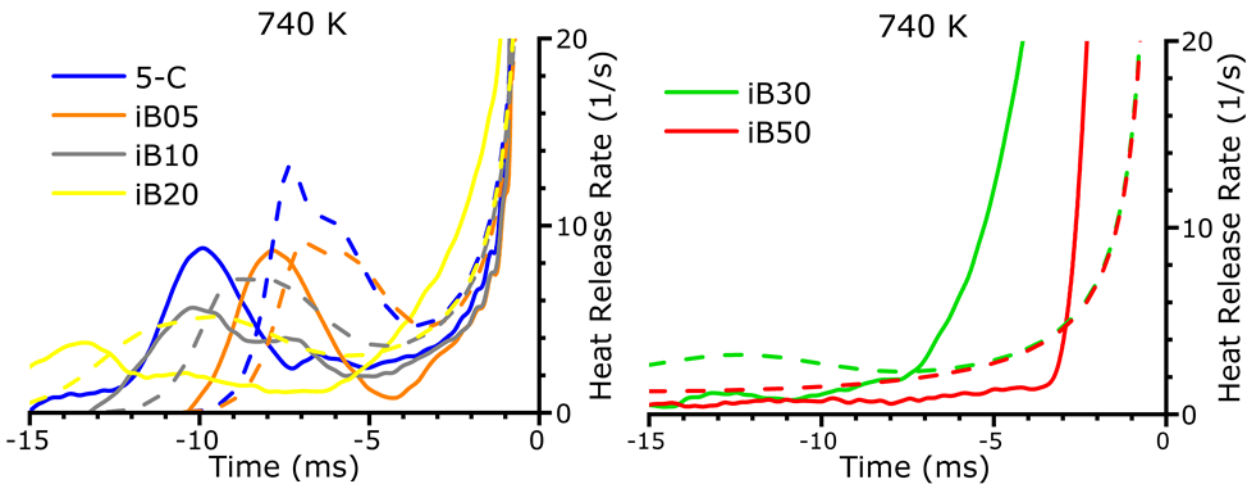

Figure 5.22. LTHR behaviour as calculated from RCM and variable volume simulation data, showing the relationship between HRR and time from point of ignition at a compressed temperature of 740 K. Solid lines = RCM analysis. Dashed lines = simulation analysis. P_c=20 bar, Φ=1.

In general, at these low temperatures the suppression of LTHR by iso-butanol blending is similar to that observed in a recent study ethanol blending with a FACE-F gasoline and its surrogate (FGF-LLNL), which displayed an approximately 50% reduction in peak HRR due to the addition of 10% ethanol (at T_c=760 bar and P_c=43 bar) [186]. Similar degrees of HRR suppression can be seen in the HRA presented in this thesis, where iB10 produces roughly a 50% reduction in peak HRRs at temperatures of 710-770 K. Interestingly, for iB20, RCM and simulation HRR analyses display significantly different LTHR profiles, yet simulations provide a good prediction of the iB20 IDT at 740 K. Simulations predict more LTHR than is observed for iB20 at 740 K, which was also the case at 710 K. However, as is shown in figure 5.31, RCM analysis for iB20 at 740 K displays a gradual rate of heat release post-LTHR and prior to HTHR, which leads to elevated pressure and temperature conditions. This appears to negate the overprediction of LTHR by the simulation as this ITHR profile is not reproduced by the model, indicating that there may be a cancellation of errors within the model. While this leads to prediction of global IDT which gives a reasonable match with RCM measurements, the model is failing to accurately represent preliminary exothermicity. The iB30 blend RCM analysis also produces a large amount of ITHR at 740 K (to a greater degree than that observed at 710 K for the same fuel), which is not represented by simulations. Due to this lack of representation, and the absence of a notable LTHR, the model predicted IDT is much higher than that produced in the RCM for iB30 at 740 K. It is thought that formaldehyde (CH_2O) is important in the generation of ITHR behaviour, as it is present in large concentrations during the process and is quickly

consumed as a precursor to HO_2 formation [327,328]. During oxidation, iso-butanol is known to form significant quantities of CH_2O [84], which may induce the observed ITHR behaviour.

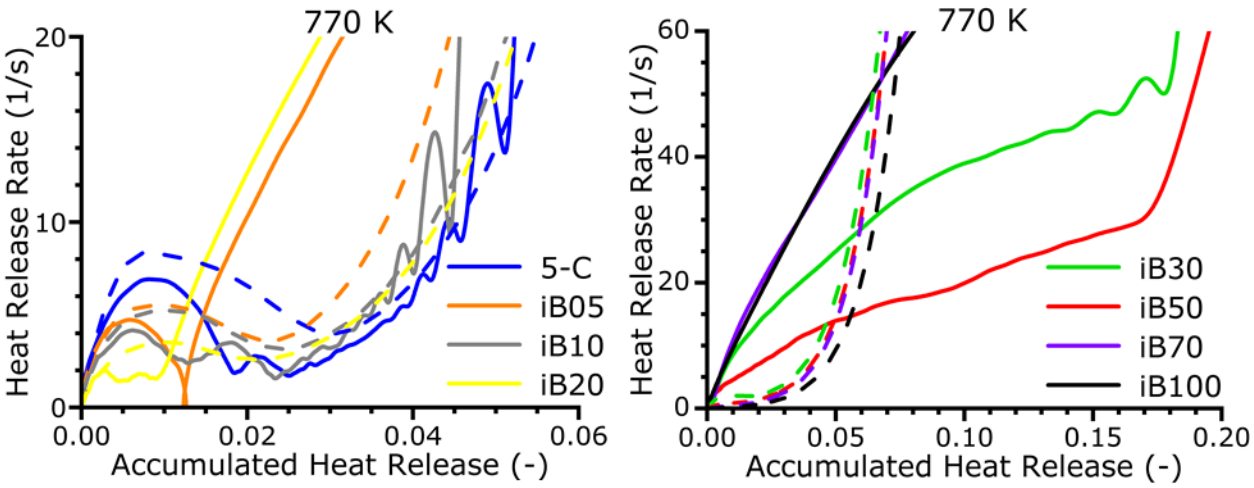

Figure 5.23. LTHR behaviour as calculated from RCM and variable volume simulation data, showing the relationship between HRR and aHR at a compressed temperature of 770 K. Solid lines = RCM analysis. Dashed lines = simulation analysis. P_c=20 bar, Φ=1.

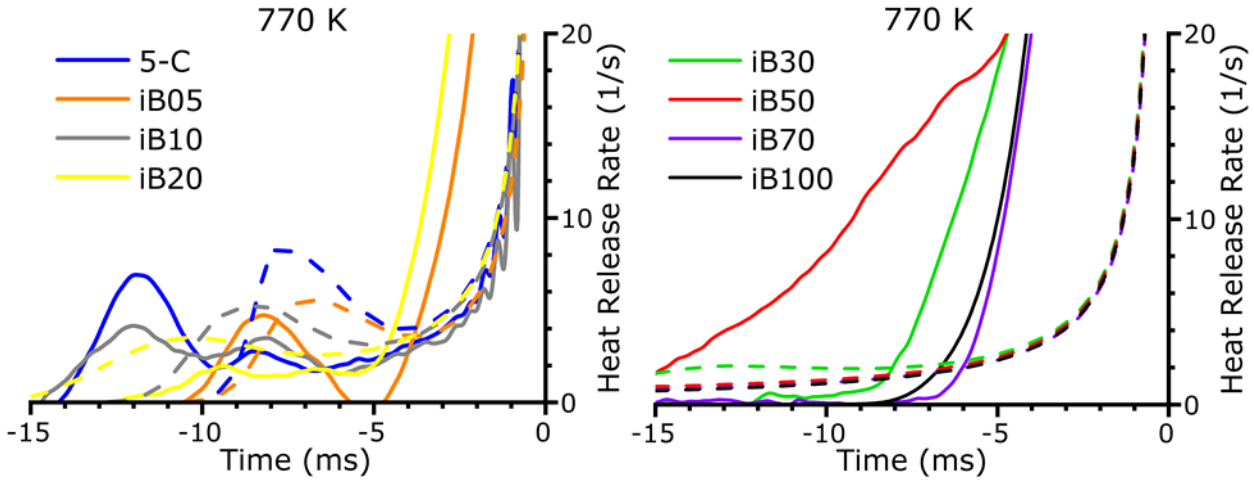

Figure 5.24. LTHR behaviour as calculated from RCM and variable volume simulation data, showing the relationship between HRR and time from point of ignition at a compressed temperature of 770 K. Solid lines = RCM analysis. Dashed lines = simulation analysis. P_c=20 bar, Φ=1.

At 770 K (within the NTC region for many of the investigated fuels), as shown in figures 5.23 and 5.24, both the 5-C surrogate and iB10 RCM analyses display two distinct stages of LTHR, unlike the lower temperature of 710 K. For the 5-C surrogate, the first LTHR peak is the most prominent (as was the case to a more pronounced degree at 740 K), whereas both peaks

show equal prominence in iB10. This behaviour is not predicted by the model, which produces only one stage of LTHR. However, iB05 does only show one LTHR peak, consistent with simulations. At this condition, iB05 also produces shorter IDTs than both the iB10 and 5-C surrogate (a behaviour not predicted by simulations). This would appear to indicate that the delayed release of total LTHR due to two distinct stages of initial exothermicity, as opposed to a single stage, reduces the auto-ignitive propensity of the fuel, increasing IDTs. This is further validated by comparison with simulated results, which display large under-predictions of IDT for the 5-C surrogate and iB10 at this condition, while also predicting a single stage of rapid heat release. On the other hand, the prediction of iB05 IDT is relatively good, as is the prediction of the LTHR profile. For all these results however, once again simulations over-predict the magnitude of the LTHR peak and under-predict the time (from the maximum HRR) at which this peak occurs.

The unusual behaviour of iB05 (when compared to its neighbouring blends) can be further identified in the relation of HRR and aHR. While the 5-C surrogate and iB05 show distinct phases of LTHR leading into a sharp main phase HRR, this transition is somewhat muted for iB05, which does not show such a sharp rise in heat release. Instead, iB05 appears to show a phase of ITHR (as shown in figure 5.31), as well as LTHR. This ITHR shows a much shallower gradient than that seen in the main phase heat release but will lead to more highly elevated temperature and pressure conditions than if the ITHR did not occur, causing the main phase heat release to occur earlier. Calculated results for iB20 show some small LTHR at this condition, which is predicted by simulations but largely over-predicted in terms of intensity. This then transitions into a gradual ITHR region, similar to that observed for iB20 at 740 K, but to a more significant degree. Ignition for iB20 occurs at a much larger aHR than for iB05 because of the fuel's higher auto-ignitive resistance, due to the higher proportion of the less reactive iso-butanol. This gradual ITHR behaviour displays more similarities to the heat release profiles observed in neat iso-butanol fuel, which produces a much slower main phase of heat release during ignition, as observed most clearly in figures 5.27 and 5.29. Blends of 30% and 50% iso-butanol show no LTHR but do show ITHR of progressively lower intensity, whereas iB70 and iso-butanol (which show the longest IDTs at this condition) only show a main stage heat release of relatively low HRR. This would appear to indicate that, as predicted, the addition of iso-butanol suppresses the typical alkane chemistry, entirely removing the characteristic LTHR behaviour at blends of 30% iso-butanol and above at this condition. Instead, the behaviour transitions to an ITHR behaviour, which is not characteristic of either pure iso-butanol or the 5-C surrogate. It should also be noted that, at the low temperatures discussed, the addition of even

a small amount of iso-butanol (5% by volume), clearly reduces the amount of aHR at soITHR. This observation applies to both simulated and experimentally derived results.

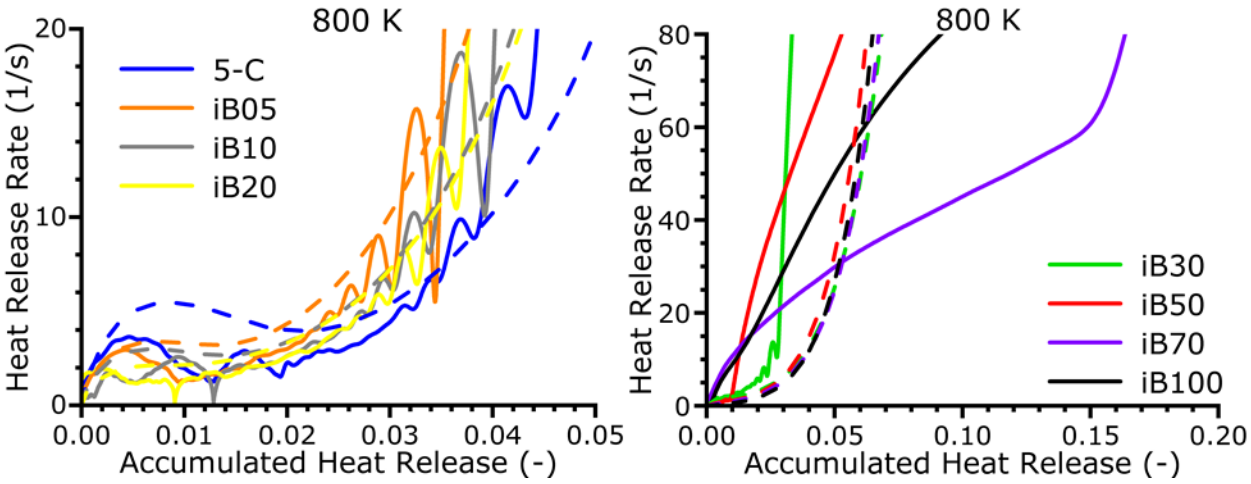

Figure 5.25. LTHR behaviour as calculated from RCM and variable volume simulation data, showing the relationship between HRR and aHR at a compressed temperature of 800 K. Solid lines = RCM analysis. Dashed lines = simulation analysis. P_c=20 bar, Φ=1.

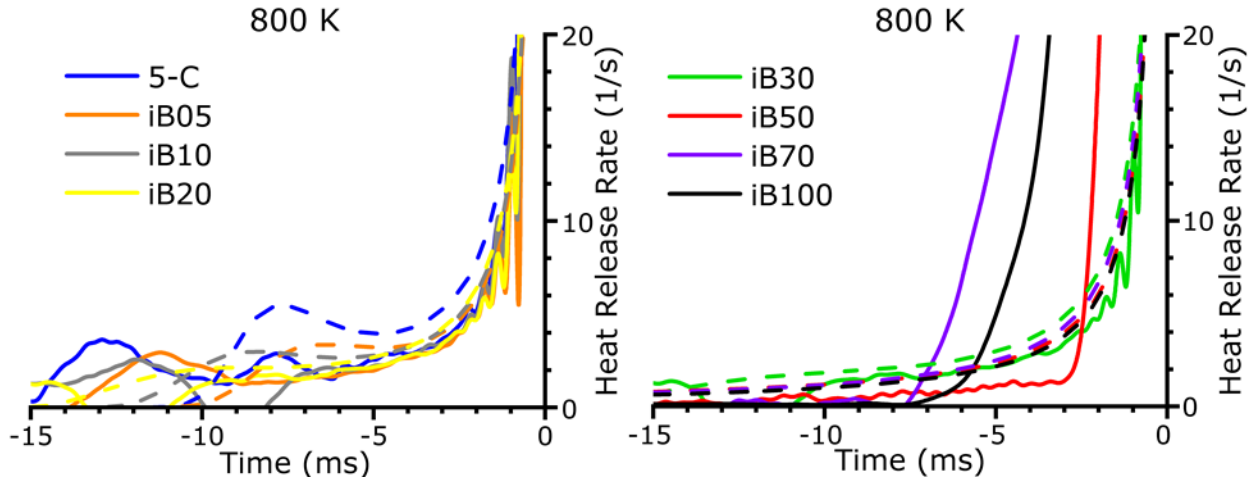

Figure 5.26. LTHR behaviour as calculated from RCM and variable volume simulation data, showing the relationship between HRR and time from point of ignition at a compressed temperature of 800 K. Solid lines = RCM analysis. Dashed lines = simulation analysis. P_c=20 bar, Φ=1.

At a compressed temperature of 800 K (seen in figures 5.25 and 5.26), much of the LTHR intensity observed at lower temperatures is absent, for both RCM and variable volume simulation results. RCM derived HRRs for the 5-C, iB05 and iB10 fuels all display a similar magnitude for the initial LTHR peak. This corresponds with similar IDTs for these fuels at 800 K.

Simulations do not predict such a clustering, instead estimating a significantly larger LTHR peak for 5-C than the butanol blends. Also, while simulations appear to provide a reasonable representation of HRR behaviour with respect to aHR (figure 5.25), for blends of iB05 and iB10, simulated LTHR peaks occur much closer to the point of ignition than those observed in the RCM. Similarly to observations made at lower temperatures, LTHR in variable volume simulations appears to initiate bulk ignition at a faster rate than that observed in the RCM, indicating that the mechanism is misrepresenting LTHR kinetics and the chemical relationships between LTHR and ITHR/HTHR, particularly in the NTC region. While RCM results show that, at 800 K, iB50 no longer displays a gradual ITHR behaviour, iB70 now does. This causes the IDT for the lower blend (iB50) at this temperature, to be similar to that displayed by the blend with a higher volume of iso-butanol (iB70). Simulated HRRs fail to reproduce this, as they also fail to predict the apparent NTC behaviour of the iB50 blend.

Again, at 830 K (shown in figures 5.27 and 5.28) the 5-C surrogate experiments show two distinct phases of LTHR, whereas simulations predict only one small phase of LTHR. This, as was the case for the 770 K condition, coincides with a significant under-prediction of the IDT by the model, further indicating that the lack of two stage LTHR representation at these temperatures is a cause of the simulations inability to reasonably predict the NTC IDT behaviour. Similarly, the simulations fail to reproduce the LTHR behaviour of iB05. The blend shows an early LTHR peak in experiments, but simulations predict some small LTHR just prior to ignition. This coincides with a large under-prediction of iB05 IDT, as has been a common feature within the NTC region. For iB10, the simulation and experimental results produce a similar LTHR profile, with the heat release occurring at roughly the same time. As would be consistent with observations for other blends, this coincides with a correct prediction of the IDT by the simulation. Furthermore, at this condition the IDTs of iB10 have crossed over with the 5-C surrogate and iB05, producing the lowest IDTs out of all the blends at 830 K. Upon investigation of the aHR, similar behaviour can be observed as was seen for iB05 at 770 K: a phase of ITHR follows the LTHR, elevating temperature and pressure conditions within the reactor, which is not present in the other lower iso-butanol content blends (shown in figure 5.31). For higher blends, the behaviour is similar as reported for 770 K. At 830 K however, IDT results show a continuation of the crossover between iB50 and iB70 blends, wherein iB50 IDTs become longer than the higher blending ratio. This does not coincide with any increase in ITHR propensity for iB70, which produces no distinguishable LTHR or ITHR, and does not undergo any NTC behaviour as iB50 does. On the other hand, iB50 now again displays a gradual ITHR profile (which was absent for this fuel at 800 K) similar to that seen for iB30 at the same temperature.

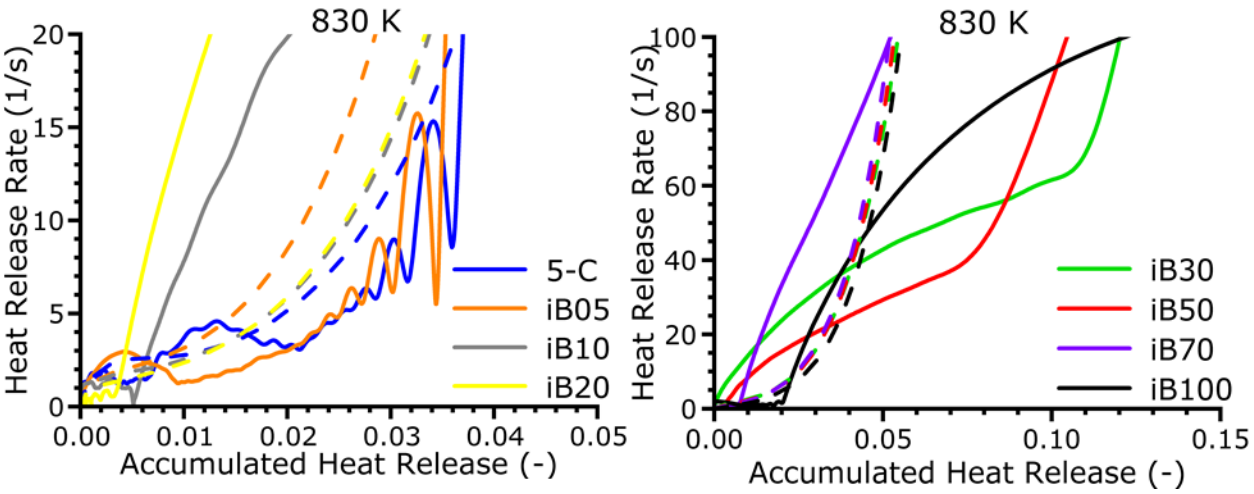

Figure 5.27. LTHR behaviour as calculated from RCM and variable volume simulation data, showing the relationship between HRR and aHR at a compressed temperature of 830 K. Solid lines = RCM analysis. Dashed lines = simulation analysis. P_c=20 bar, Φ=1.

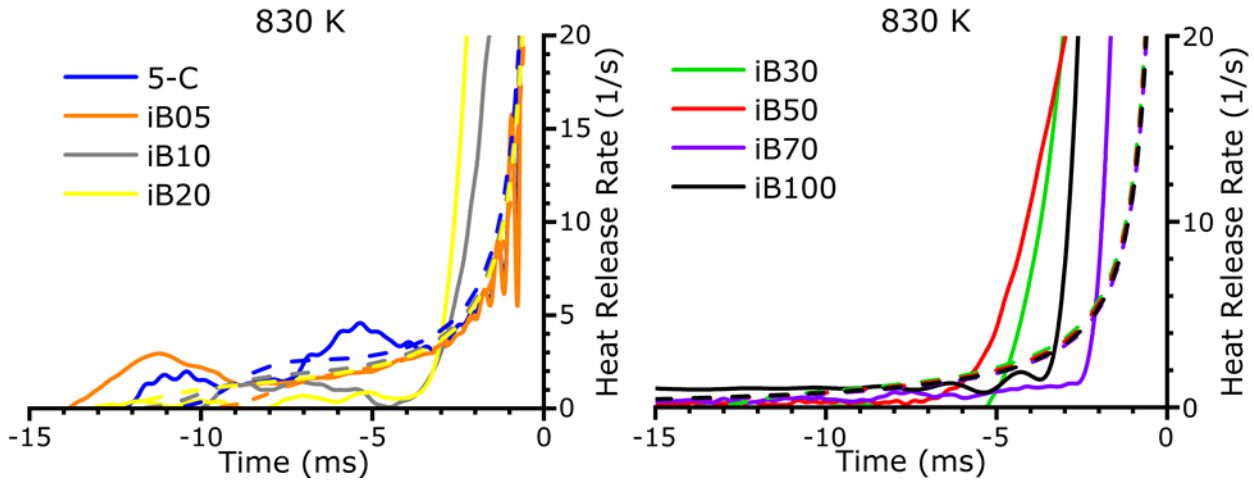

Figure 5.28. LTHR behaviour as calculated from RCM and variable volume simulation data, showing the relationship between HRR and time from point of ignition at a compressed temperature of 830 K. Solid lines = RCM analysis. Dashed lines = simulation analysis. P_c=20 bar, Φ=1.

At the highest investigated temperature of 870 K (shown in figures 5.29 and 5.30), no distinguishable LTHR is present for any of the fuel blends. This would be expected as the fuel transitions out of the NTC behaviour which characterises the low to intermediate temperatures of those investigated. IDTs at this temperature cluster together (as seen in figure 5.10), displaying a similar reactivity regardless of the fuel, and this is reproduced well by variable volume simulations as is the LTHR HRR behaviour.

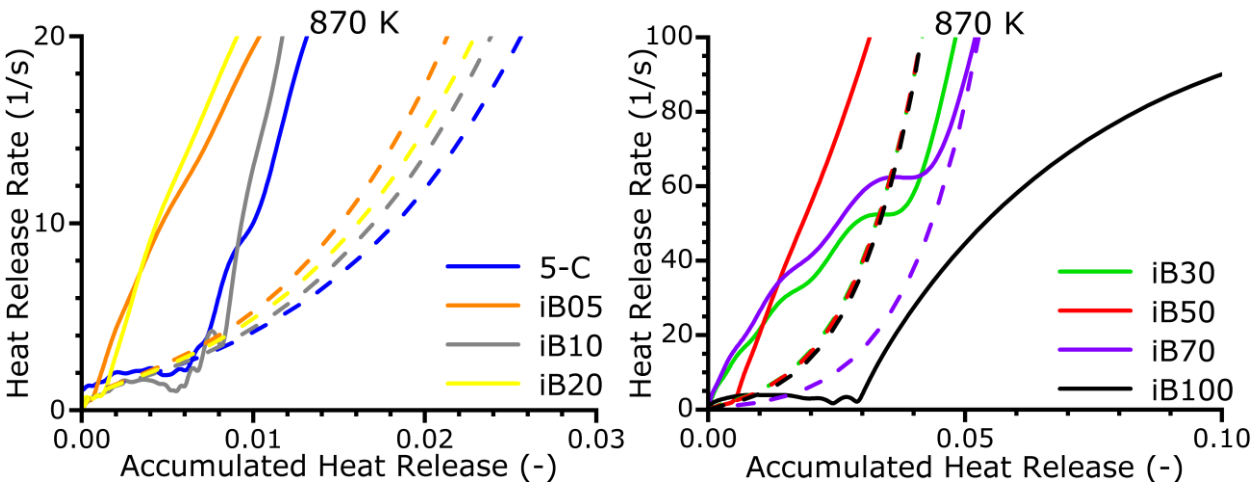

Figure 5.29. LTHR behaviour as calculated from RCM and variable volume simulation data, showing the relationship between HRR and aHR at a compressed temperature of 870 K. Solid lines = RCM analysis. Dashed lines = simulation analysis. P_c=20 bar, Φ=1.

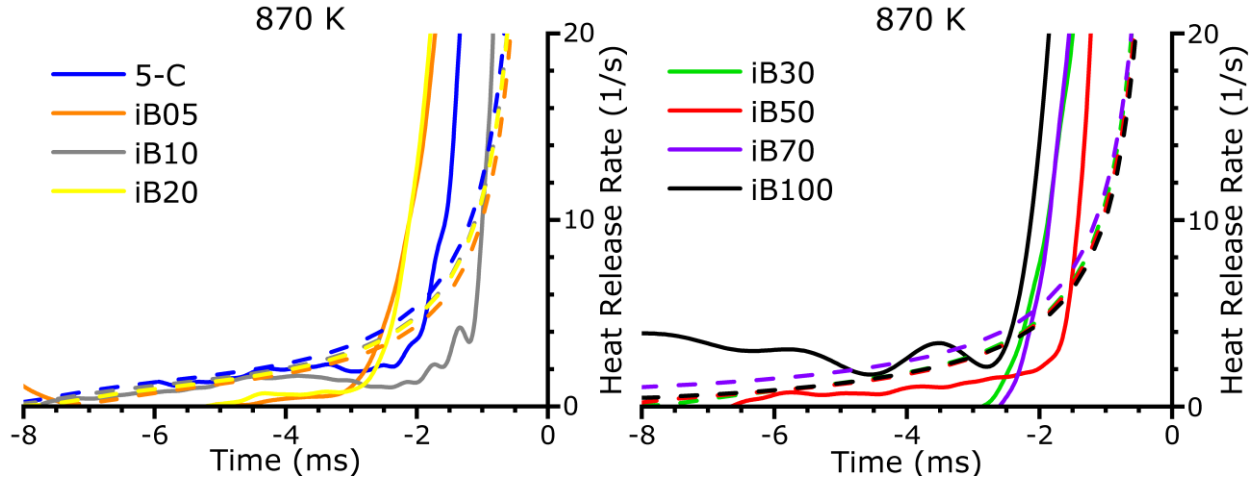

Figure 5.30. LTHR behaviour as calculated from RCM and variable volume simulation data, showing the relationship between HRR and time from point of ignition at a compressed temperature of 870 K. Solid lines = RCM analysis. Dashed lines = simulation analysis. P_c=20 bar, Φ=1.

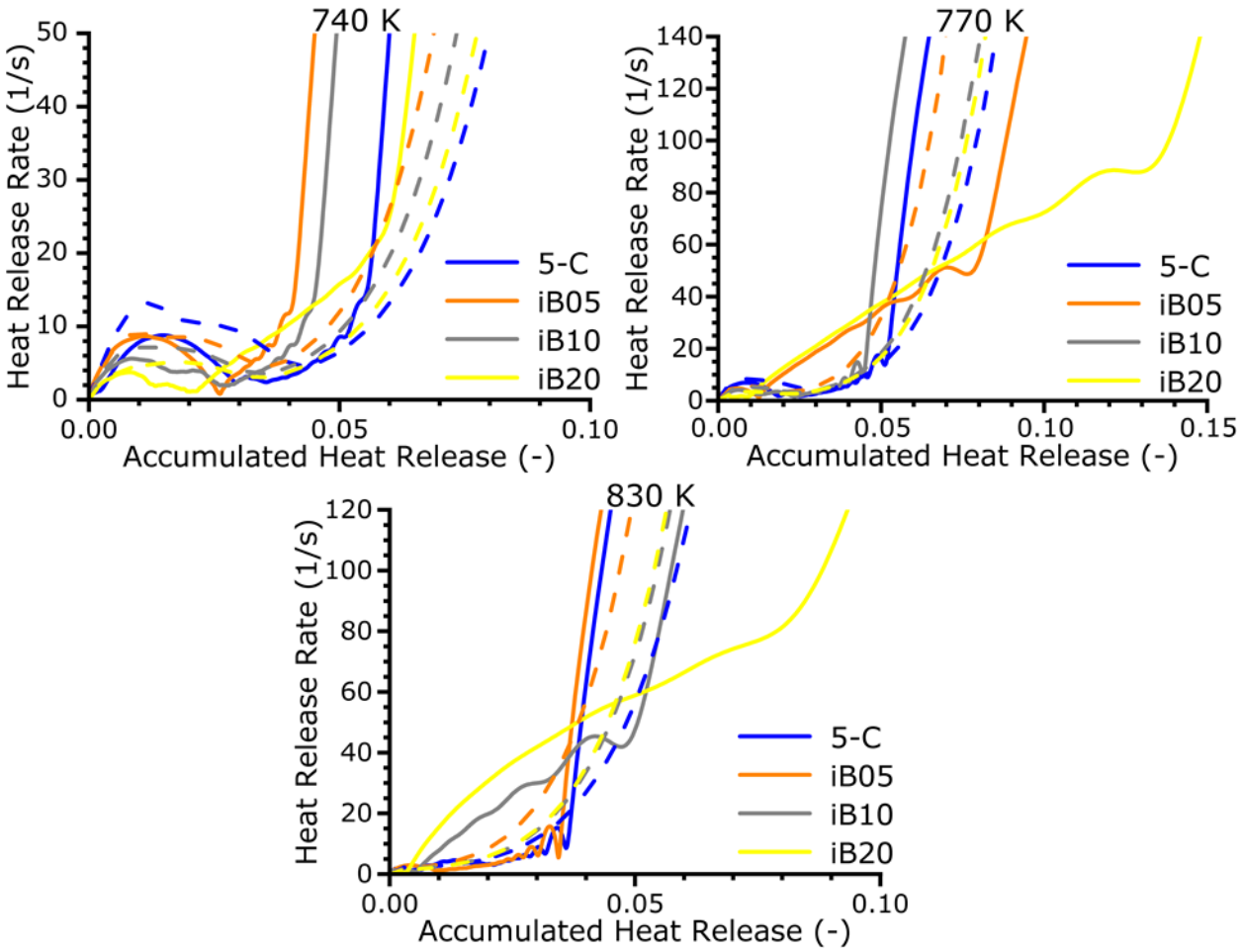

Figure 5.31. ITHR behaviour for the 'lower' iso-butanol volume fraction fuel blends, showing the relationship between HRR and aHR. Solid lines = RCM analysis. Dashed lines = simulation analysis. P_c=20 bar, Φ=1.

Temperatures at the soITHR and soHTHR give a further indication of the extent of exothermicity as a result of LTHR and ITHR, respectively. Figure 5.32 shows the temperatures at the soITHR (T_{soITHR}) and soHTHR (T_{soHTHR}) for the 5-C surrogate, as well as the temperatures at the soHTHR for iB30 and iB100. Values are determined for both RCM data and variable volume simulations, using the definitions for soITHR and soHTHR previously described. Experimentally derived RCM temperatures at the soITHR for 5-C produce a profile which clearly correlates with the IDT profile for the same fuel. The similarity is such that the NTC region displayed by the IDT profile is also present in T_{soITHR}. This is not the case for simulated conditions however, which predict essentially constant T_{soITHR} values. It is not surprising that 5-C simulations do not reproduce this behaviour, given that they also fail to reproduce the NTC apparent in the IDT profile. The lack of complex low temperature exothermicity representation

by the model further indicates that failures lie in the model's ability to accurately represent the low temperature chemistry. In general however, the predicted values for T_{soITHR} are similar to those derived through RCM HRA, at compressed temperatures below 800 K. Historically, experimental measurements have proposed a homogenising effect of the LTHR on spatial temperature non-uniformities generated during piston motion and gas compression [110]. While the experimentally derived results displayed in this chapter for 5-C can be described as somewhat constant (similar to results shown in the literature [172]) and therefore are in corroboration of the historical assumption, T_{soITHR} and IDT also appear to be somewhat correlated. Therefore, given new experimental data for the evaluation of kinetic mechanisms, novel methods of analysis and the apparent importance of LTHR in the determination of global values such as IDT, the assumption of a constant T_{soITHR} may not be sufficient for the development of kinetic mechanisms. It has also been suggested in previous studies of RCM heat release, that targets such as T_{soITHR} and T_{soHTHR} be applied as model evaluation and sensitivity analysis targets, to develop a better understanding of kinetic features which occur during preliminary exothermicity, such as HO_2 chemistry, and to investigate model failures in the prediction of LTHR and ITHR behaviour [172,185]. Real T_{soITHR} from RCM experiments, while non-trivial to determine, is a feasible target for the further development of kinetic models.

Simulations do reproduce soHTHR temperatures well for the 5-C surrogate, producing a steadily increasing T_{soHTHR} with increasing T_c. This is a similar profile to 5-C RCM data and a reasonable set of predictions for T_{soHTHR} point values. HTHR behaviour is largely dependent on small molecule chemistry, which is known to a greater degree of accuracy than the complex low temperature oxidation processes associated with LTHR [325,329]. Therefore, without the presence of significant ITHR behaviour, the model would be expected to produce a good representation of this behaviour, if thermodynamic conditions at the end of LTHR are also predicted accurately, as they generally appear to be for 5-C. Similar behaviour has been shown in previous RCM HRA studies of a PRF (RON 90) [172,285]. Excluding the case at ~870 K, it appears that generally, greater preliminary exothermicity occurs at lower compressed temperatures. A larger amount of LTHR is expected at lower temperatures, due to the influence of alkane content on the bulk behaviour of the fuel, and the increase in total heat release prior to soHTHR appears to be largely dependent on this increased LTHR.

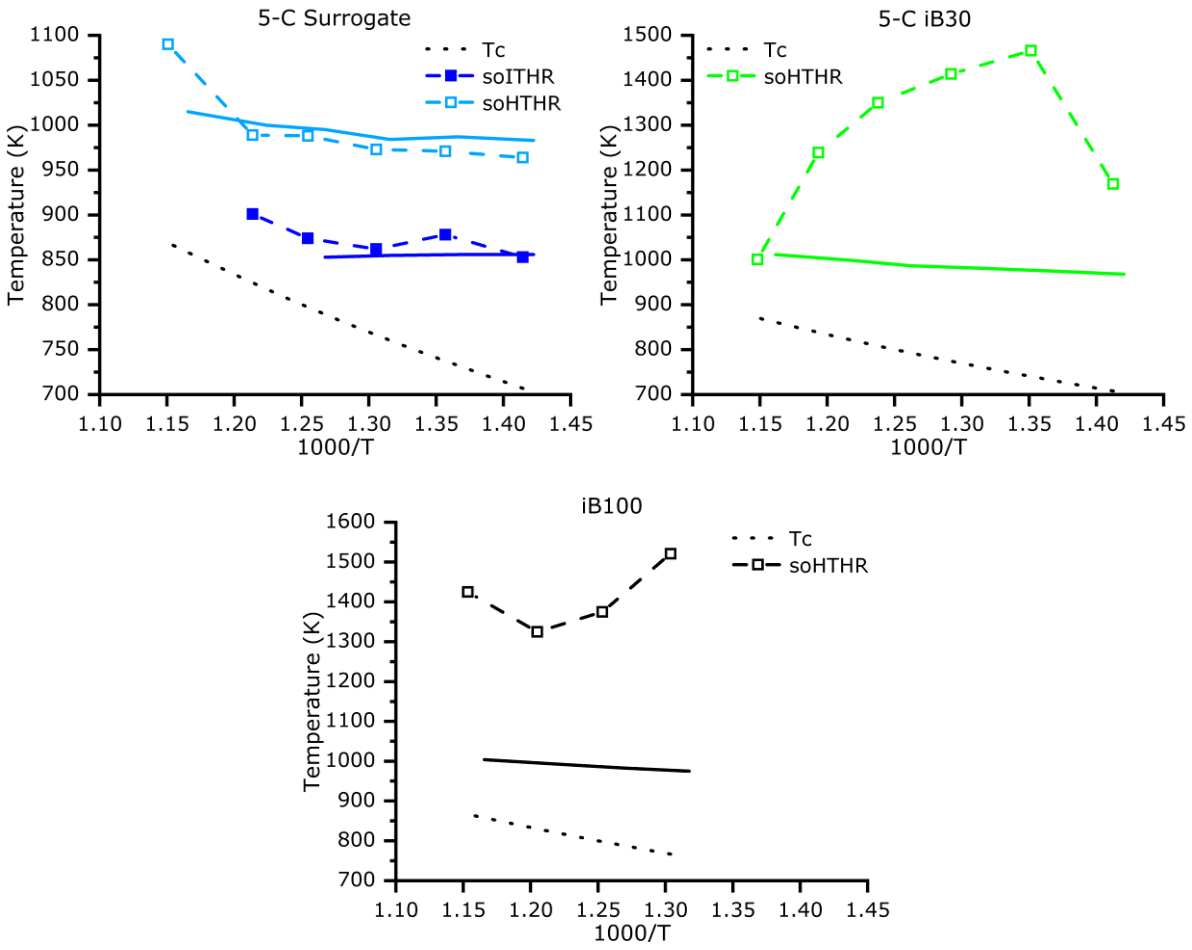

Figure 5.32. Temperatures at the soITHR (when applicable) and soHTHR for the fuels 5-C, iB30 and iB100 (iso-butanol). Symbols joined by dashed lines = RCM derived results. Solid lines = Simulation derived results. Dotted line = Temperature at the EOC. P_c=20 bar, Φ=1.

Blends of iB30 and iB100 (iso-butanol) do not produce any distinguishable LTHR (as shown previously), therefore only T_{soHTHR} profiles can be investigated. However, unlike the 5-C case there are significant differences between results calculated from experimental and simulation data for the iB30 and iB100 fuels. The iB30 blend displays much higher temperatures at soHTHR than those observed for 5-C due to the presence of a gradual ITHR witnessed in both pressure traces and HRA. This behaviour leads to a large amount of aHR prior to ignition, causing elevated temperatures (and pressures), as evidenced in figure 5.32. As a result of this phenomenon, IDTs for iB30 are only marginally longer than those observed for iB20, but with the additional 10% volumetric iso-butanol, cause a significant reduction in fuel calorific values. Variable volume simulations predict T_{soHTHR} similar to those exhibited by the 5-C simulations, showing little increase with increasing temperature. This misrepresentation of the iB30 blend

gas temperatures is a result of the model's failure to replicate the ITHR phenomenon observed for this fuel, as shown in the previous HRA. Iso-butanol RCM results also show a set of extremely high T_{soHTHR} values. However, unlike iB30 this is not due to a gradual ITHR phenomenon, but the definition used for soHTHR. As stated previously, soHTHR is defined as the point which HRR is greater than 100/s, which is appropriate for fuels which produce a strong ignition, with main stage heat release occurring in a very short period of time. However, due to the low reactivity of iso-butanol, the rate of pressure rise (and HRR) during the main stage of ignition is relatively slow. It is because of this different heat release profile that HRRs of over 100/s are achieved much later into the main ignition stage, producing larger gas temperatures. Simulations of iB100 predict a much faster bulk heat release and as such, simulated values for T_{soHTHR} are significantly lower than those calculated from RCM data.

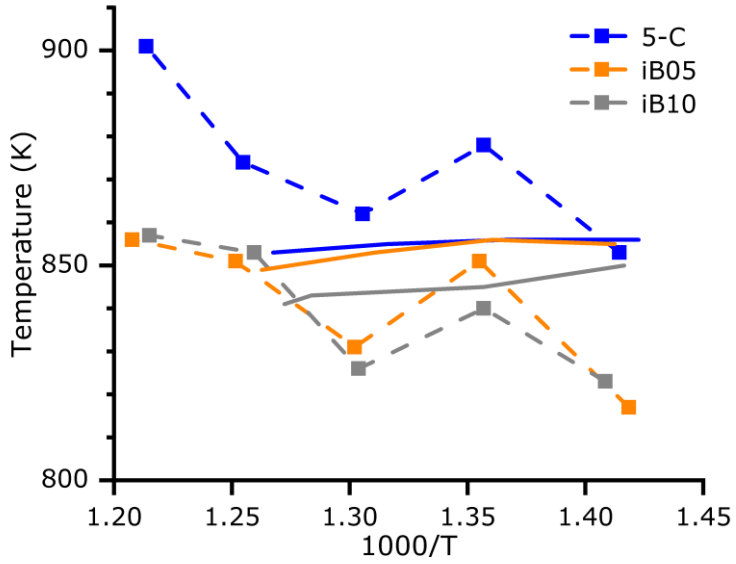

Figure 5.33. Temperature at soITHR for the 5-C surrogate and blends of iB05 and iB10, as calculated from RCM and variable volume HRR analysis, plotted against the temperature at the EOC. Symbols joined by dashed lines = RCM derived results. Solid lines = Simulation derived results. P_c=20 bar, Φ=1.

Fuel blends of 5-C, iB05 and iB10 have displayed the most prominent examples of LTHR behaviour in the applied HRA but showed significant differences between RCM and simulated heat release profiles. These differences are stipulated to be a cause of the IDT prediction failures by the model. Figure 5.33 shows T_{soITHR} values for 5-C, iB05 and iB10 RCM and variable volume simulation results. It is clear from this analysis that even the addition of small volumes of iso-butanol to the blend drastically affects the low temperature behaviour of the fuel, with a 5% volume of iso-butanol decreasing T_{soITHR} by 32.5 K on average. As iso-butanol volume is

increased to 10%, the same drop in T_{solTHR} is not observed due to IDT crossover behaviour between iB05 and iB10, which is manifest in the T_{solTHR} profiles. This crossover in T_{solTHR} occurs at the same EOC temperatures as the observed crossover in IDT, with shorter IDTs correlating with marginally higher soITHR temperatures. As shown for 5-C in figure 5.32, both the iB05 and iB10 display behaviour reminiscent of their respective IDT profiles, including an NTC region. None of the behaviour described for iB05 and iB10 is represented by simulated results for T_{solTHR}, which again predicts near constant temperatures regardless of T_c.

There is little real-world experimental data from fundamental experiments (such as from RCMs) available, which could help to quantify preliminary exothermicity events such as LTHR and ITHR. Heat release analyses such as those produced in this chapter and in other work [172,186,284] provide an opportunity for this and for the improvement of kinetic models by serving as an additional validation target. Goldsborough et al. [172] concluded in their study of RCM HRA, that significant trends could be identified using this technique, particularly during the early regions of HRR-aHR trajectories, wherein LTHR and ITHR phenomena are present. Previous studies have largely focused on the impacts of temperature and pressure on heat release behaviour, showing that as pressure increases, the intensity of LTHR and the resultant aHR increases [172,285]. This study has applied these same analysis techniques to investigate the influence of iso-butanol blending on the preliminary exothermicity of the 5-C surrogate, identifying general trends and apparent complex blending behaviour. For the 5-C at low temperatures, HRA results are generally consistent with previous literature results for the LTHR of a PRF (RON 90), showing similar peak HRRs, aHR at soITHR, and LTHR profiles for low temperatures (<740 K) [172,285]. However, the addition of even small concentrations of iso-butanol appears to suppress this LTHR substantially. A similar impact of alcohol blending can be seen in the literature, where blends of ethanol (0-30%) with the FGF-LLNL gasoline surrogate displayed a large reduction in LTHR at blends as low as 10% ethanol (the lowest concentration investigated), coinciding with the suppression of NTC behaviour [186]. The same study also simulated the LTHR by applying an updated version of the gasoline surrogate mechanism utilised in this study, which was not made available. However, this updated mechanism also appears to fail in its representation of LTHR behaviour, significantly underpredicting the intensity of LTHR and misrepresenting ITHR behaviour, for the gasoline surrogate and blends with ethanol, at conditions of T_c=760 K and P_c=43 bar, indicating that the model still requires considerable evaluation and improvement in this area. HRA of iB05 and iB10 cases reveal the presence of a gradual ITHR post-LTHR, which elevates temperature and pressure conditions within the combustion chamber, coinciding with the low IDT values for the

iB05 and iB10 fuels. The presence of substantial ITHR even at low iso-butanol concentrations may be due to an increase in formaldehyde production via iso-butanol oxidation, which is thought to contribute significantly to the ITHR process [84,327,328]. Simulations largely fail to predict heat release behaviour prior to HTHR, predicting two stages of LTHR in some cases where this is not present in experimental analysis, which will be investigated further in Chapter 6. Properties such as peak LTHR HRRs, soITHR and soHTHR temperatures, times and aHR provide critical information about the potency of LTHR in a fuel but are rarely considered in the development of kinetic mechanisms. The current work shows that the chosen model fails to reproduce the experimentally derived heat release profiles to lesser or greater extents in different temperature regions and that this failure may underlie further global model failures, such as the under-prediction of IDTs.

5.6 Sensitivity Analyses

Potential kinetic reasons that may underlie the inability of the model to accurately predict IDTs for the investigated fuels are further investigated in this chapter through the application of sensitivity analyses of reaction rate parameters. Figures 5.34-5.36 show the normalised local OH sensitivity analysis results for the three temperature conditions: 710 K, 770 K and 830 K, for the 5-C surrogate, iB30 and iso-butanol, respectively. Here, a positive value indicates that an increase in the rate constant leads to an increase in OH concentration, which serves as an analogue for reactivity. Each of these are limited to displaying the top 20 values (at each temperature investigated) in terms of normalised sensitivity for local OH sensitivity analyses, for the sake of brevity.

At the lowest temperature of 710 K, 5-C surrogate simulations provided a reasonable representation of measured IDTs. As can be observed in the local OH sensitivity analysis in figure 5.34, reactivity at this condition is dictated by typical low temperature alkane oxidation chemistry, with hydrogen abstraction by OH from n-heptane and iso-octane (primarily via the primary and secondary sites) promoting reactivity. The hydrogen abstraction of ethanol and toluene by OH radicals are key to the reduction of reactivity at this temperature, due to the consumption of OH radicals producing relatively unreactive fuel radicals and water. Also, hydrogen abstraction at the tertiary iso-octane site is highly negatively sensitive due to the lack of low temperature chain branching pathways from the resultant radical and production of relatively unreactive olefin species [91]. Hydrogen abstraction from 1-hexene appears as a positively sensitive reaction at this relatively low temperature. This is expected as the relatively high reactivity of 1-hexene is thought to initiate low temperature reactivity [85]. The large

negative sensitivity of formaldehyde reacting with OH radicals to produce a water molecule and formyl is apparent at all temperatures for the 5-C surrogate, due to the termination of relatively highly reactive OH. The production of $2HO_2$ from the reaction of H_2O_2 and molecular oxygen is also highly negatively sensitive. The reverse of this reaction is important for the generation of the H_2O_2 pool which will ultimately decay into 2OH radicals, leading to the main ignition event.

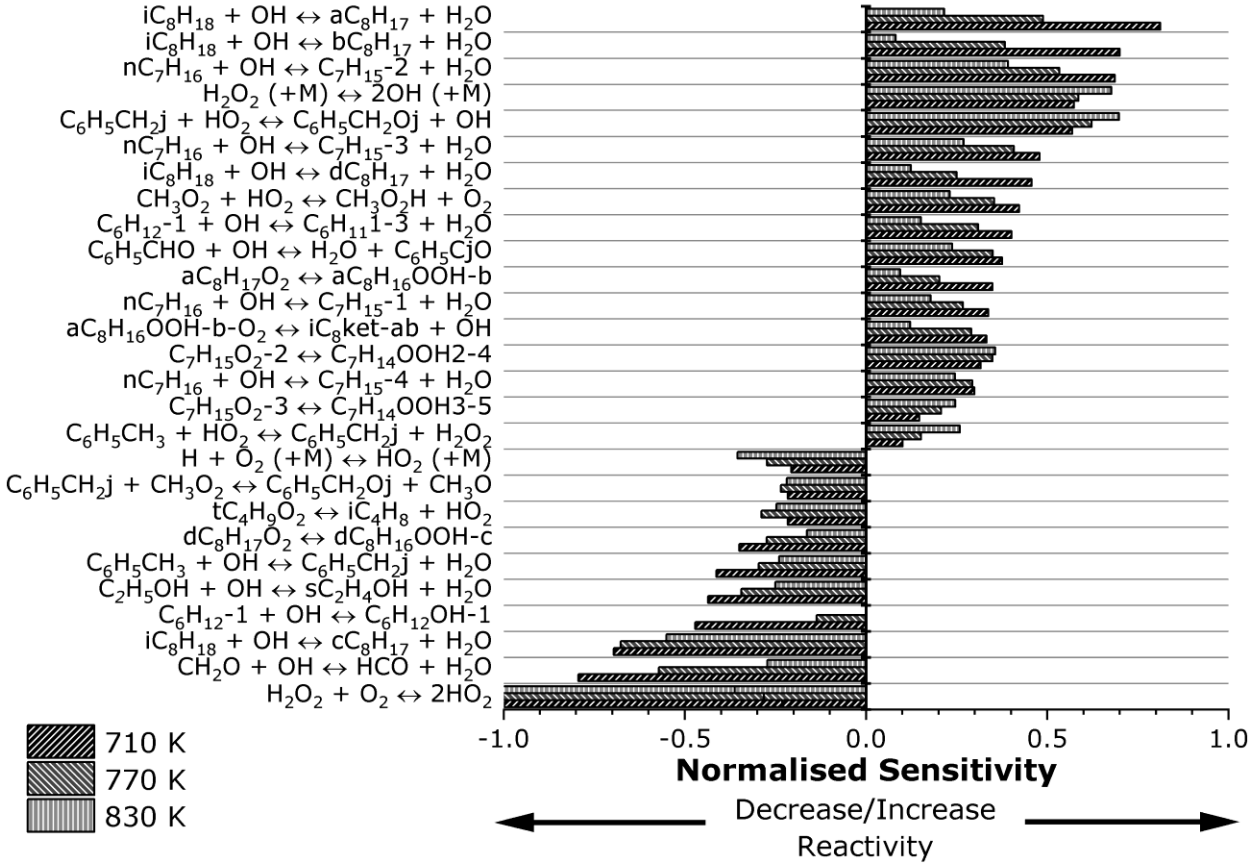

Figure 5.34. Normalised local OH sensitivity analysis results for the 5-C surrogate. P_c=20 bar, Φ=1.

For iB30 it can be seen that iso-butanol oxidation reactions now dominate at 710 K, with the hydrogen abstraction from iso-butanol's primary carbon site by OH radicals being the most sensitive reaction, reducing reactivity. Further hydrogen abstraction from the resultant radical's alcohol site is also highly negatively sensitive due to the production of a relatively unreactive aldehyde, as well as the generation of the less reactive HO_2 radical from the initial OH. This coincides with a large under-prediction of IDT by the model and this pathway has been identified as a controlling aspect of high pressure, low temperature oxidation [39]. Alternatively, the first oxygen addition to the primary fuel radical species is sensitive in the positive direction as this

opens a pathway to low temperature chain branching. Hydrogen abstraction/initiation is favoured from one of the tertiary iso-butanol sites, due to an increased propensity for low temperature chain branching from this site. However, particularly at temperatures as low as 710 K, the elevated BDE at the tertiary site compared to primary and secondary sites makes abstraction from this site more difficult. This behaviour is a root cause of the low reactivity of iso-butanol and therefore leads to its octane boosting quality, even when compared to other butanol isomers [84]. Similar alkane reactions are seen for iB30 as with the 5-C surrogate, but their importance is reduced due to the relative dominance of iso-butanol reactions.

As temperature is increased to 770 K, it would be expected that sensitivity analysis of the 5-C surrogate begins to identify reactions which are typical of NTC behaviour, such as the production of olefins and HO_2 radicals from RO_2 and QOOH species, and other chain propagation and termination routes [90,228,262]. However, few of these negatively sensitive reactions appear, while simulations largely under-predict the intensity of the NTC region. Instead, reactivity is largely dominated again by the hydrogen abstraction of alkanes, with the tertiary iso-octane abstraction again displaying a highly negative sensitivity as opposed to abstractions from the alternative sites. Hydrogen abstractions from n-heptane continue to display highly positive sensitivities, owing to the fuel's importance in the driving of first-stage ignition (cool flame) at low temperatures. Given the considerable recent updates to the n-heptane sub mechanism [46], which are not included in the combined mechanism applied here, updating the n-heptane scheme in the mechanism may provide an avenue for model improvement. The reaction of benzyl radicals with HO_2 to produce benzoxy and OH radicals ($C_6H_5CH_2j+HO_2=C_6H_5CH_2Oj+OH$) appears as more positively sensitive than at 710 K. This reaction has been identified in literature as playing a key role in the low to intermediate temperature oxidation of toluene [85,330], which makes up a large amount of the 5-C surrogate, so its importance is not unexpected.

Sensitivity analysis for iB30 at 770 K shows that the importance of hydrogen abstraction from the tertiary iso-butanol site has increased relatively, as increasing temperatures reduce the importance of the tertiary site's high BDE. As would be expected, the dissociation of H_2O_2 into two OH radicals shows an increase in sensitivity as the initial temperature increases. For the pure iso-butanol fuel, the production of H_2O_2 via hydrogen abstraction from the primary iso-butanol site by HO_2 appears highly sensitive in driving positive reactivity, much more so than for the blended fuel. This is likely due to the consumption of a relatively unreactive HO_2 radical ultimately leading to the production of two OH radicals once temperatures become high enough

for the dissociation of H_2O_2. This process is key for driving the production of OH radicals at this condition, as the lower reactivity of the iso-butanol fuel will struggle to develop a large pool of OH radicals, without the assistance of the alkanes present in the blend, as indicated by much larger radical pools of HO_2 and H_2O_2. These concentrations are both an order of magnitude larger than those seen for the iB30 blend, which are in turn larger than the 5-C surrogates.

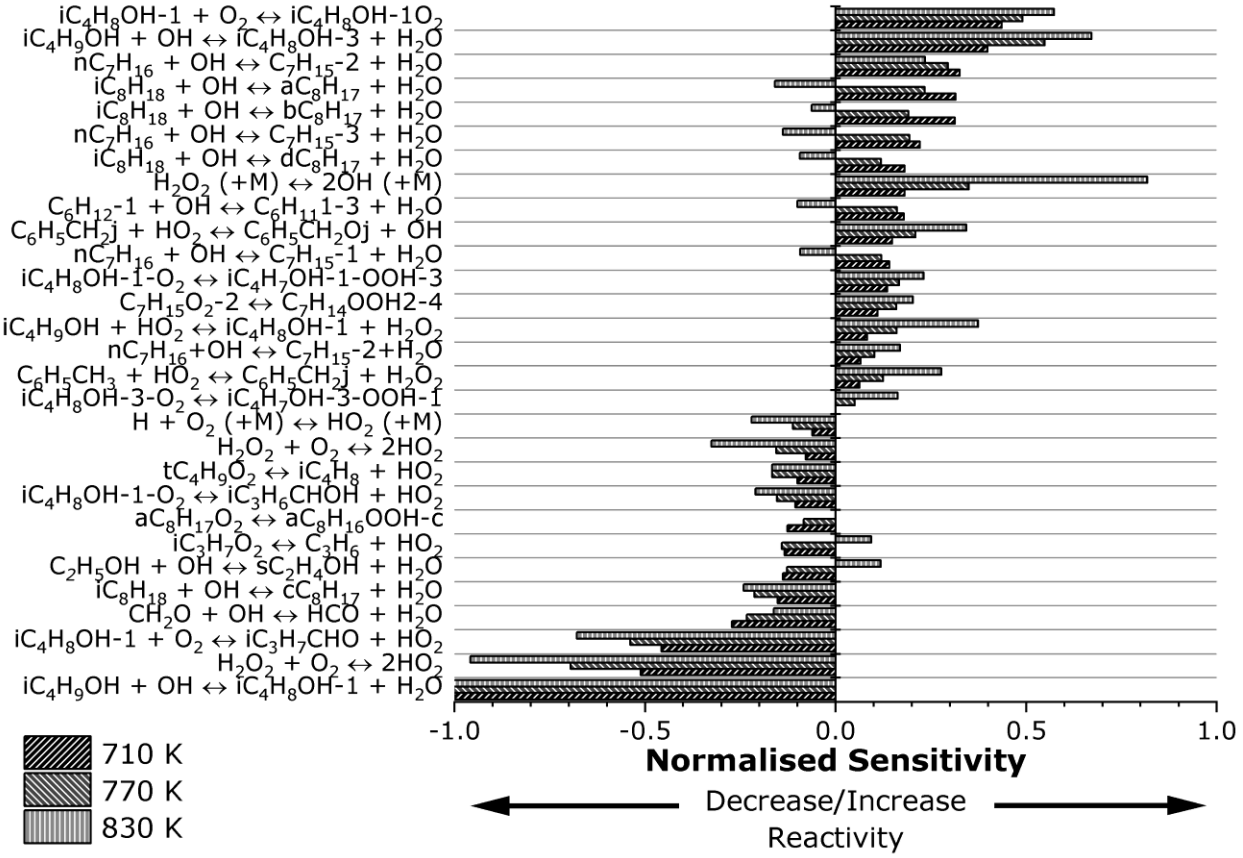

Figure 5.35. Normalised local OH sensitivity analysis results for the iB30 blend. P_c=20 bar, Φ=1.

Similar features can be observed for iso-butanol at 830 K, however the previously mentioned production of H_2O_2 directly through hydrogen abstraction is now the most sensitive reaction, due to an increase in temperatures. Also, reactions indicative of low temperature branching pathways begin to display less relative importance. The iB30 blend displays high sensitivities for the same iso-butanol reactions as the raw iso-butanol fuel at this temperature but is dominated by the dissociation and oxidation of H_2O_2 to form 2OH and $2HO_2$ radicals, respectively. The former of these reactions dominates the positive sensitivities as two highly reactive radicals are produced from a largely unreactive species, whereas the latter dominates the negative sensitivities at 830 K, as the HO_2 radicals formed are relatively less reactive than

the OH radicals, causing an overall loss of reactivity. The oxidation of toluene increases in significance at higher temperatures also. At this condition, simulations produce a good estimate for iso-butanol and iB30 IDTs, as they did for 770 K.

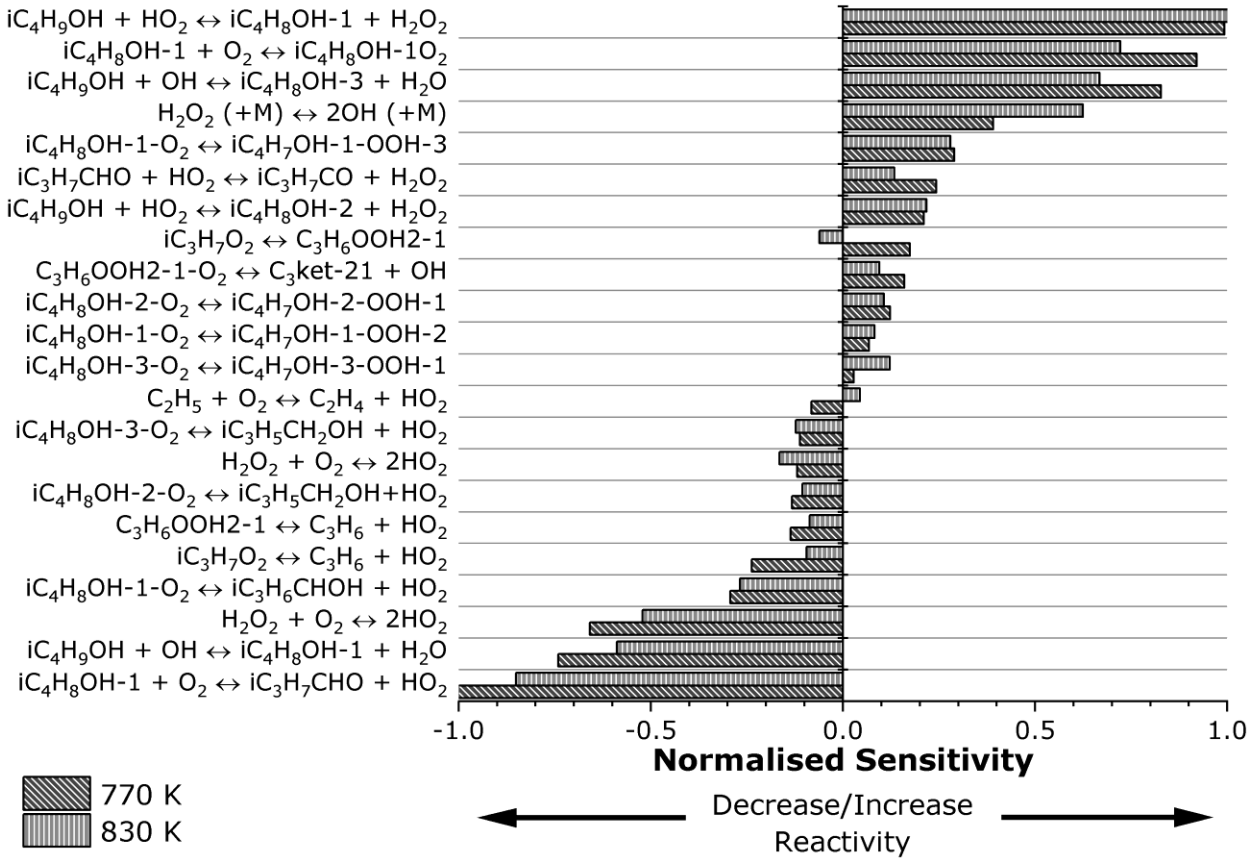

Figure 5.36. Normalised local OH sensitivity analysis results for iso-Butanol fuel. P_c=20 bar, Φ=1.

Meanwhile, sensitivity analysis results of the 5-C surrogate continue to show little indication of NTC behaviour, contrary to the trends seen experimentally. The only indication of this is the decomposition of the RO_2 species $tC_4H_9O_2$ to produce iso-butene and a HO_2 radical. This reaction was also present in results for 770 K at a similar relative sensitivity. The reaction $C_6H_5CH_2j+HO_2=C_6H_5CH_2Oj+OH$ is again highly positively sensitive, as is H_2O_2 decomposition. As the OH concentration for the 5-C surrogate seems highly dependent on this benzyl reaction at conditions where the model largely fails to represent experimental data, and there is little data for rates of reactions associated with toluene oxidation at these temperatures, this would appear to be a potentially large source of model uncertainty [85,331]. It should also be noted that this reaction is much less sensitive at iB30, wherein the model produces a much better

representation of the IDT profile. The model sources the reaction rate for this HO_2 radical activation to OH on the recommendation of Ellis et al. [330] which provides a rate via experimental methods. However, this produces a constant, temperature independent rate of reaction within the model which is significantly different to the temperature dependent rates proposed later in theory based calculations [332]. The apparent high sensitivity of this reaction in the 5-C and iB30 cases, paired with this uncertainty in the rate constant may propagate significant uncertainty into model predictions. In further support of this statement, recent studies have made substantial changes to aromatic sub mechanisms and display significantly improved model representation, particularly at low temperatures [264,268,269]. Updating the mechanism using these resources may provide a source for model improvement.

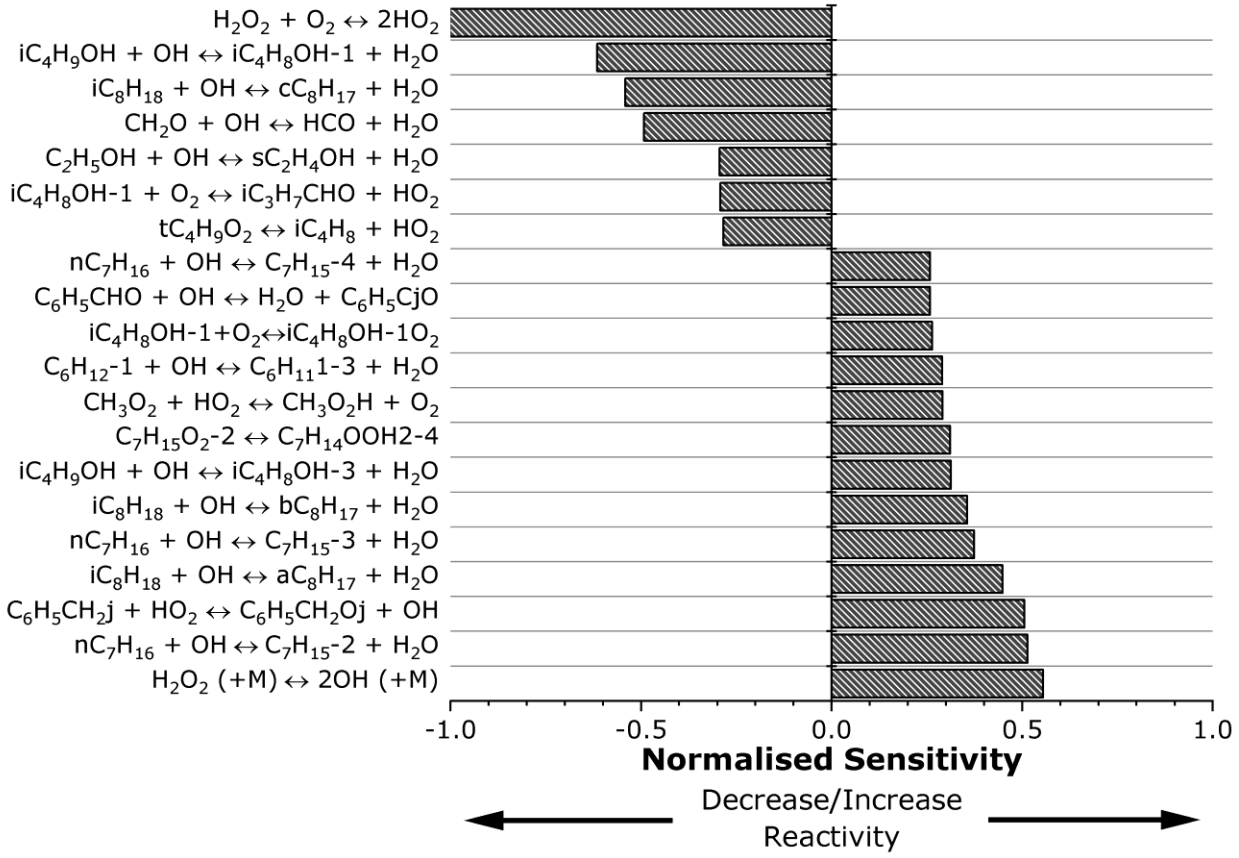

Figure 5.37. Normalised local OH sensitivity analysis results for iB10 at 770 K. P_c=20 bar, Φ=1.

An interesting feature of the blending of iso-butanol with the 5-C surrogate is that, even at small volumes of iso-butanol, iso-butanol oxidation chemistry reactions become highly sensitive. An example of this can be seen in figure 5.37, which shows the normalised local OH sensitivity analysis for iB10 at 770 K. In this example, the hydrogen abstraction from the primary iso-

butanol abstraction site is the most dominant fuel reaction, despite only contributing 10% of the blend volume. As mentioned during the discussion of the iB30 sensitivity analysis, this reaction reduces reactivity due to the fuel radical's tendency to produce relatively unreactive aldehydes and HO_2 radicals. This behaviour is similar to that witnessed for blends of n-butanol, which has been shown to display a high degree of sensitivity for butanol initiation reactions at blends of 10 and 20% n-butanol by volume [47,51]. The presence of highly sensitive iso-butanol chemistry at such low volumetric blends provides an explanation for HRA features such as the significant reduction in T_{soITHR} and peak LTHR HRRs, due to the addition of relatively small volumes of iso-butanol (such as that observed between 5-C and iB05 in figures 5.31 and 5.17).

5.7 Summary

The ability of a newly developed five-component surrogate (5-C) to reproduce the IDTs of a reference gasoline with RON 95 in an RCM, at conditions of T_c=675-870 K, P_c=20 bar and Φ=1.0 was investigated. This investigation showed that the 5-C surrogate produced an accurate representation of the gasoline throughout the temperature regime, with the only exception occurring at T_c≈740 K, wherein 5-C displayed a mildly longer IDT than the gasoline. This caused a slightly shallower NTC region for the 5-C than that produced by the gasoline. Variable volume simulations were completed in an attempt to replicate IDTs captured by the RCM, using a combined iso-butanol and gasoline surrogate mechanism [84,85]. While these simulations provided a reasonable prediction at the lowest and highest temperatures investigated, they failed to represent the intensity of the NTC in the 5-C fuel, significantly underpredicting IDTs in this region. HRA of the LTHR and ITHR for 5-C also showed distinct differences between RCM results and simulation predictions, with simulated LTHR often overpredicting the rate and amount of heat release prior to soITHR. Simulations also failed to represent the LTHR profile of experimental data, such as at 770 K, where simulations predicted a single stage of LTHR, whereas RCM results produced two distinct stages. At many of the investigated conditions, this LTHR occurred much closer to the point of ignition for variable volume simulations than in experimentally derived results, particularly at temperatures where simulations predicted shorter IDTs than the RCM.

An investigation of T_{soITHR} for 5-C results showed that these temperatures mirrored the T_c dependent behaviour of the overall IDT profile of the fuel, including the NTC region. Simulations failed to predict this behaviour, instead producing a near constant T_{soITHR} at all temperatures. From these observations it was postulated that the mechanism's failures may lie in the representation of the fuel's low temperature behaviour. Local OH analysis for the 5-C surrogate

at temperatures of 710, 770 and 830 K appeared to support this, singling out multiple n-heptane hydrogen abstraction reactions as highly sensitive, the importance of which in the formation of the first stage ignition (cool flame) is understood [46,228]. This analysis also identified the reaction $C_6H_5CH_2j+HO_2=C_6H_5CH_2Oj+OH$ as highly sensitive. This reaction was determined to be important during the development of low temperature behaviour and is a source of potentially large model uncertainty due to the source of rate parameters used by the gasoline surrogate mechanism component [85,330]. While rate parameters for this reaction are sourced from experimental data, this produces a constant, temperature independent rate of reaction within the model. This is significantly different to the temperature dependent rates proposed in more recent theory based calculations [332]. Future work on the representation of the 5-C surrogate by the model should focus on the development of the mechanism to accurately reproduce the observable LTHR behaviour, with the aim of improving IDT prediction. It is proposed that this can be achieved by updating much of the gasoline surrogate sub mechanism to account for recent work, particularly for the n-heptane and aromatic sub mechanisms [46,264,268,269]. Targets derived through the application of HRA, such a LTHR peak HRRs, T_{solTHR}, T_{soHTHR} and aHR may also serve as validation targets for the further development of such a model to facilitate the accurate representation of LTHR behaviour.

The influence of iso-butanol blending on the IDTs of the developed surrogate was investigated at blends of 5-70% by volume, T_c=710-870 K, P_c=20 bar and Φ=1.0. Many interesting features emerged from this blending. At the lowest investigated temperature (710 K), increasing the volume fraction of iso-butanol also produced an increase in measured IDT. This was consistent with the predictions of variable volume simulations. However, as temperature is increased to 740 K and 770 K, iB05 displays a shorter IDT than the original 5-C surrogate. As temperature is increased further (>800 K), iB10 now produces the shortest IDTs of all fuels investigated, producing a cross-over effect with both the 5-C and iB05 fuels. Similar behaviour is present in n-butanol literature, at blends of 20% n-butanol by volume [47]. Simulations failed to accurately predict this cross-over behaviour but did provide reasonable predictions for iB10 and iB05 outside of the NTC region. HRA of these cases revealed the impact of a gradual ITHR post-LTHR, which elevated temperature and pressure conditions within the combustion chamber, coinciding with the low IDT values for the iB05 and iB10 fuels. The observed IDT cross-over behaviour was also present in an analysis of T_{solTHR}, as was the NTC behaviour apparent in the IDT profile. Interestingly, the addition of small volumes of iso-butanol was shown to provide a dramatic change in LTHR behaviour, causing significant drops in T_{solTHR} and peak LTHR HRR values. This suppression of LTHR at low concentrations is similar to that observed

in the literature for blends of FACE-F gasoline and its surrogate with ethanol, which showed a roughly 50% reduction in peak LTHR HRR at a temperature of 760 K with the addition of only 10% ethanol [186]. Similar degrees of peak LTHR HRR reduction were observed in this chapter through the addition of 10% iso-butanol at temperatures of 710-770 K. Local OH sensitivity analysis revealed that with the addition of only 10% iso-butanol, the hydrogen abstraction from the primary iso-butanol site was the dominant fuel reaction at a temperature of 770 K, further indicating the immediate impact that iso-butanol blending has on the ignition driving chemistry. Blends of iB20 and iB30 produced largely similar IDT profiles due to the presence of a unique heat release profile for iB30 in which gradual ITHR was present in every condition. The high degree of repeatability shown in these cases ruled out the presence of inhomogeneous ignition phenomena such as pre-ignition. While simulations did not reproduce the heat release behaviour of iB30, IDT predictions were largely accurate. This was likely coincidental, due to the unusual ignition behaviour of the blend producing shorter than expected IDTs negating the IDT underprediction which has characterised the model at other blends. Predictions for the neat iso-butanol fuel and iB70 blend are reasonably accurate, indicating that iso-butanol chemistry is well represented, and fault is most likely to lie in the gasoline surrogate component of the mechanism and its representation of LTHR behaviour.

6 Influence of Thermodynamic Properties and their Uncertainties on Kinetic Models

6.1 Introduction

Due to the relatively simple physical conditions of an RCM, cases can be modelled though the application of detailed chemical kinetics. Where investigatory experiments would otherwise be prohibited (perhaps due to their difficulty or the cost of experiments), computer developed models provide a relatively cheap and quick alternative [308]. The application of numerical models in this way provides a platform for a thorough investigation of the underlying chemistry which drives the autoignition process, with the aim of developing a deeper understanding of a given fuel and its characteristics on blending. Fundamental experiments, such as RCM IDT investigations, provide a range of validation targets for a model, that are often relevant to real world engine conditions. By providing the data from these experiments, numerical models can be further developed to increase their validity at all relevant conditions. This is especially true for new fuels, which may have been exposed to little investigation and analysis. However, the validity of a given model is determined largely by the inaccuracies and uncertainties of the underlying thermodynamic and kinetic data of each species and reaction.

Thermochemical properties, such as species enthalpy of formation, impact on energy balances and the position of chemical equilibria within a kinetic system. As such, these properties play an important role in the accurate prediction of ignition characteristics by chemical kinetic models. This importance results mostly from the direct impact of thermochemical properties on the determination of the equilibrium rate constant, k_{eq} (equation 2.39), and the subsequent calculation of backwards reaction rates. While some species and reactions are relatively well understood and as such have a low degree of uncertainty associated with them, much data (particularly for longer chain fuel radicals) is based on assumptions and estimates derived from experience and knowledge of similar species. Small species are often well characterised, either through experimental validation [333], quantum chemical calculations [334] or through statistical optimisation approaches incorporating combined sets of data [335,336]. However, in the case of thermodynamic data, estimates for larger species are often calculated via Benson's GA [337], which serves as an alternative and less resource intensive method.

By considering a species as a set of constituent groups, each representing a polyvalent atom and its ligands, Benson's GA method provides estimates for the thermochemical

properties of the species [337,338]. This method is considered a second order approximation of species properties, as nearest neighbour atoms are also considered in a given group definition. Non-nearest neighbour interactions, which may contribute significantly to species properties, can also be accounted for throughout the species through the addition of correction groups. An example of this can be seen in the gauche correction group, which accounts for the gauche effect [339], which describes an intramolecular interaction between two groups or atoms with a dihedral angle of 0-120°. Using this method, thermodynamic parameters (y_i=$\Delta h_{f,i}$ (298 K), $s^0_{int,i}$ (298 K) $c_{p,i}$) of a given molecule (*i*) can be estimated based on the corresponding thermodynamic parameters of the individual groups ($x_{ij=}$ $\Delta h_{f,ij}$ (298 K), s^0_{ij} (298 K) $c_{p,ij}$), as shown in equation 6.1.

$$y_i = \sum_j n_{ij} x_{ij} \qquad \text{Equation 6.1}$$

Here n_{ij} is the number of groups (*j*) in the species (*i*) and $s^0_{int,i}$ (298 K) is the intrinsic standard entropy [339]. To calculate the standard entropy, molecular symmetry and optical isomerisation much be accounted for, as described in the literature [339]. For the estimation of radical species thermochemistry, the hydrogen bond increment approach (as applied in computational solvers such as THERM [273]) can be implemented. Thermochemical properties for the radical species are computed in respect to the parent (non-radical) molecule, through the addition of a bond dissociation group. This group accounts for the broken hydrogen bond in the radical species and the resultant differences in thermochemical properties. Once the thermodynamic properties of a species have been determined, they can be expressed in the form of NASA polynomial coefficients [165], for use in kinetic modelling applications. While this method provides an opportunity for the estimation of complex species thermochemical properties, which may otherwise be prohibitively expensive to calculate or are currently not possible to determine experimentally, it introduces unavoidable parameter uncertainties [187,340].

Previous studies have investigated the impact of uncertainties in species thermodynamic data on the overall IDT and they have been shown to produce a substantial overall uncertainty [183,184] in predicted outputs such as IDTs. This has also been shown to be the case for uncertainties in individual GA group values [187]. However, knowledge of the impact of thermodynamic property uncertainties, such as those in enthalpies of formation (particularly when derived via GA estimations), on global properties such as IDT, is still limited. The literature is also lacking studies which investigate the sensitivity of characteristic LTHR parameters (such as HRRs, aHR and temperatures) to uncertainties in species thermodynamic properties. This

chapter aims to apply brute force sensitivity analysis techniques, to investigate the sensitivity of IDTs and LTHR properties to uncertainties in species enthalpy of formation. Many oxygenated species are produced and consumed during the low temperature oxidation process, the formation and structure of which are dependent on the structure of the parent fuel molecule. The required thermodynamic parameters of such species are commonly estimated by applying Benson's GA methods, as it is impractical to consider the application of high level quantum chemistry calculations for the derivation of thermochemical parameters of long chain molecules [136].

6.2 Thermodynamic Sensitivity Analysis of Ignition Delay Times

Brute force sensitivity analysis was performed to assess the impact of uncertainties in the thermodynamic properties of each species (namely the enthalpy of formation) on the overall IDT. To achieve this, the NASA polynomial [165] a_6 was modified, ensuring that only the enthalpy of formation for the species was affected, without influencing the species entropy or specific heat. The standard enthalpy of formation was modified individually and independently for each species by a constant value of +5 kJ mol^{-1}, which is well within the uncertainty bounds proposed for many oxygenated fuel radical species [176] but large enough to facilitate the identification of significantly important species. The previous work of Hughes et al. [184] similarly investigated the influence of species enthalpies of formation on propane IDTs, by applying a +1 kJ mol^{-1} increase in enthalpies. This proved effective in the identification of a small number of species, which had a significant impact on the prediction of IDT targets. However, an increase in this parameter value change (within common uncertainty values for species of interest) may identify further influential species, or species which display a non-linear relationship with target properties, which are only identified by extending the investigated enthalpy boundary conditions. The sensitivity coefficient corresponding to this change can be calculated via $SC = (\tau_{mod} - \tau_i)/\tau_i$, where *SC* is the sensitivity coefficient for a given species, τ_{mod} is the IDT after the enthalpy modification for this species and τ_i is the initial (unmodified) IDT for this condition. Diluent species and molecular oxygen are excluded from thermodynamic sensitivity analysis. The high sensitivity of molecular oxygen is known, due to its presence in many important reactions such as initiation oxygen additions, and the molecule's thermodynamic data is assumed to be known with absolute certainty [183]. Therefore, this value is discounted to prevent the dilution of further normalised sensitivity values. In addition, whilst it is acknowledged that in reality, correlations exist between enthalpy values for different species, they have been neglected here as they are only known for smaller species present within Active

Thermochemical Tables (ATcT) [175,283]. Such information is not known for the larger fuel related species within the mechanism and therefore it is not possible to account for such correlations. The aim of this work is to identify important species that are key to the observed ignition behaviour, rather than attempting to assess the overall uncertainty in the chosen targets, which would necessitate taking correlations into account.

Kinetic mechanisms require accurate values of thermodynamic properties for each species within the system, for the calculation of accurate backwards reaction rates (where not explicitly stated in the kinetic mechanism). To facilitate the availability of such thermodynamic data, several online resources serve as compilations and databases of species thermochemical parameters. The National Institute of Standards and Technology (NIST) Chemistry Webbook database [178] compiles a large amount of species physical and thermodynamic properties, as sourced from the literature, as well as providing GA estimation tools. Similarly, the Third Millennium Ideal Gas and Condensed Phase Database (Burcat's tables) are also available [176]. As part of the analysis presented within this chapter, enthalpies of formation for the key identified species from the mechanism are compared with values available in Burcat's latest thermochemical tables, based on experimental, ab initio calculation and more recently ATcT methods [176]. Enthalpies of formation and uncertainties may also be compared to values found in the literature and the NIST database, where appropriate [178]. Values for brute force enthalpy of formation sensitivity analysis are normalised by the largest corresponding values at each investigated condition, to produce lists of normalised sensitivity coefficients.

Potential kinetic and thermodynamic reasons that may underlie the inability of the model to accurately predict IDTs for the investigated fuels is further investigated here through the application of sensitivity analyses of thermodynamic model input parameters. As the localised OH sensitivity analysis (section 5.6, figure 5.34) appears to have indicated that the failures of the model can be found in the gasoline surrogate component of the mechanism, brute force thermodynamic sensitivity analysis is focused on the surrogate modelling only. Figure 6.1 shows the percentage changes in IDT which resulted from a +5 kJ mol^{-1} standard enthalpy of formation change for each species in the kinetic mechanism, for the 5-C fuel at temperatures of 710, 770 and 830 K. Figure 6.2 shows brute force normalised sensitivity analysis results for the species thermodynamic sensitivity analysis of the 5-C surrogate at temperatures of 710 K, 770 K and 830 K. For figures 6.1 and 6.2, a positive value (both IDT percentage change and normalised sensitivity coefficient) indicates an increase in IDT, and therefore a decrease in reactivity. IDT percentage changes are shown for every species in the mechanisms, whereas normalised brute

force sensitivities are limited to displaying the top 20 species (as determined by the magnitude of normalised sensitivities) at each temperature investigated (31 total species), highlighting only the most sensitive species.

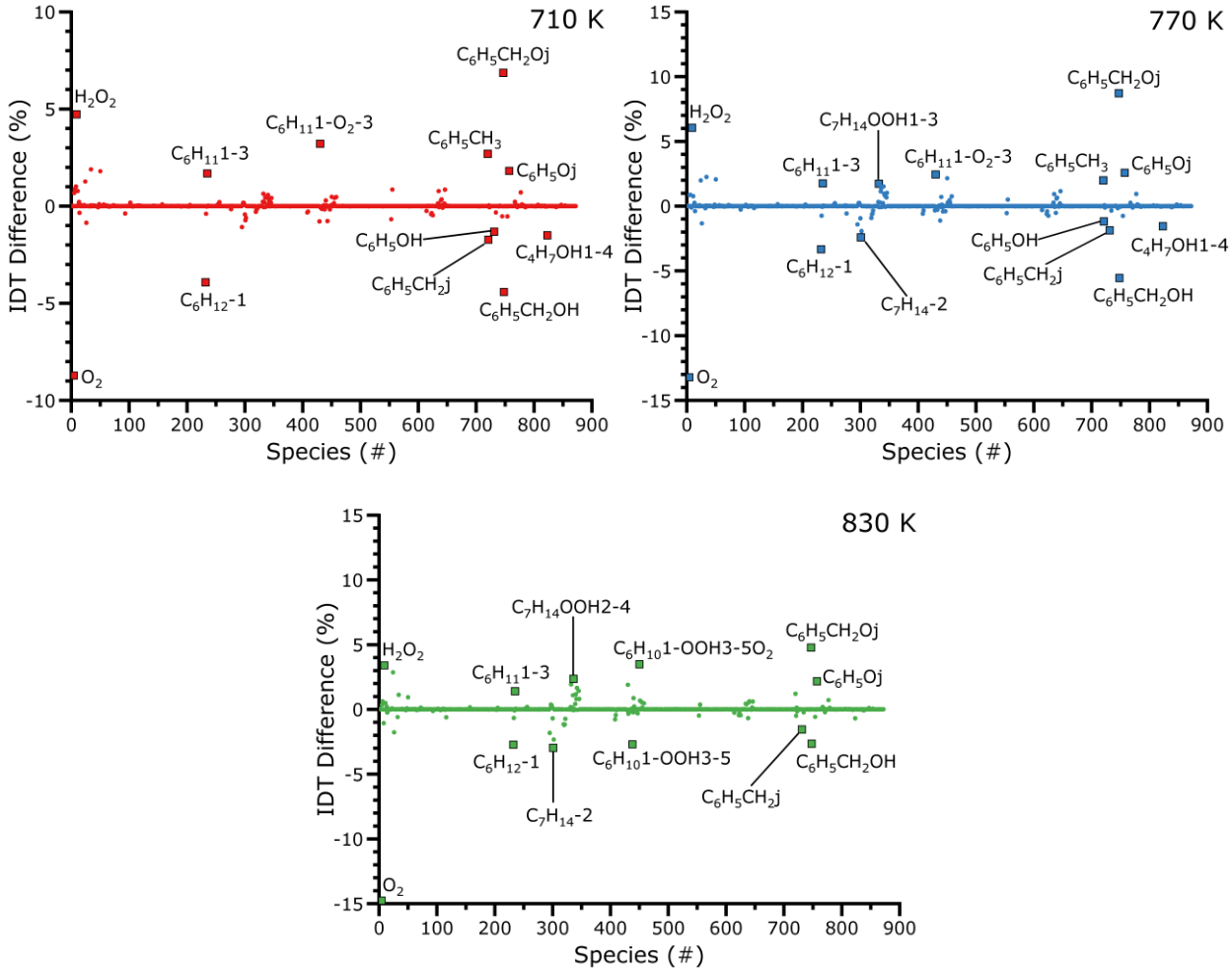

Figure 6.1. Percentage differences in the predicted IDT for 5-C constant volume simulations, due to a +5 kJ mol^{-1} change in species enthalpy of formation. P_c=20 bar, Φ=1.

Several trends can be observed in figure 6.1, which show the percentage difference in IDT due to a +5 kJ mol^{-1} change in species enthalpy of formation, for each species in the combined mechanism independently. At each temperature investigated, only a fraction of the total number of species display a significant change in IDT. This can largely be attributed to the presence of specified reverse rates, which remove the need for calculation of backwards rate of reactions via species thermodynamic properties (2403 reverse reaction rates are given, meaning 1240 reverse rates are calculated from thermodynamic data). Therefore, the significance of changes in the enthalpy of formation for several species are largely reduced. Reaction sensitivity

analyses, such as those in the Chapter 5 for local OH sensitivity analysis and the brute force A-factor sensitivity analyses provided in this chapters, allow for the investigation of species and reactions which do not appear as sensitive in enthalpy of formation sensitivity analysis. The observed change in IDT is large for changes in the enthalpy of formation of O2 and H2O2 at all temperatures, due to the importance of these species in the oxidation and chain reaction mechanism which drives autoignition. However, the characteristic uncertainties for these species are relatively low (or non-existent in the case of O2, by definition), and as such the change in IDT is not representative of the actual influence of uncertainties in these species. At the low temperature (710 K) and NTC region (770 K) conditions, percentage IDT changes are generally larger than those observed at the high temperature (830 K) condition, due to the increased importance of complex low temperature oxidation pathways at these temperatures (section 5.6) [53,136].

Figure 6.2 shows that the thermodynamic sensitivity at all investigated temperatures is largely dominated by the enthalpies of formation of toluene and 1-hexene and their associated low temperature oxidation intermediate species. This is expected for 1-hexene and its associated species, and is consistent with the understanding that the relatively high reactivity of olefins drives low temperature reactivity, as observed in the local OH sensitivity of the 5-C surrogate at 710 K (figure 5.34). Increasing the enthalpy of formation for 1-hexene reduces the energy barrier of initiation reactions, raising the overall reactivity of the fuel. While the temperature dependent profile of the heat of formation for 1-hexene used in the LLNL mechanism employed here largely agrees with that derived from NASA polynomials in the most recent Burcat table, Burcat proposes a high uncertainty of ±8 kJmol^{-1} in Δh_f (298 K) for this species (as calculated via G3B3 quantum chemistry calculations). The standard enthalpy of formation for 1-hexene is given as -41.7 kJmol^{-1} in the utilised mechanism, as determined via GA methodology [85], -39.4 kJmol^{-1} in Burcat's tables, and an average of ten literature sourced values (determined experimentally through calorimetry hydrogenation) provided by the NIST database gives a standard enthalpy of -42.3±2.6 kJmol^{-1}, with maximum and minimum literature source values of -44.8 and -41.4 kJmol^{-1}, respectively [341–349]. It is clear from these values that there is some uncertainty in the standard enthalpy of formation for this highly sensitive fuel species, which may be of particular importance for the initiation of low temperature hexene oxidation. As shown in figure 6.1, small uncertainties in the standard enthalpy of formation for 1-hexene may translate to considerable changes in the global IDT, with a +5 kJmol^{-1} change producing an approximately 4% decrease in IDT at 710 K. Alkenes such as 1-hexene typically display much shorter IDTs in the NTC region than similar alkanes, but a longer IDT at lower

temperatures (<700 K) due to the presence of the double bond. This double bond may undergo radical additions, with a low required activation energy, which causes the removal of highly reactive radical species from the system and competes with reaction promoting hydrogen abstraction routes.

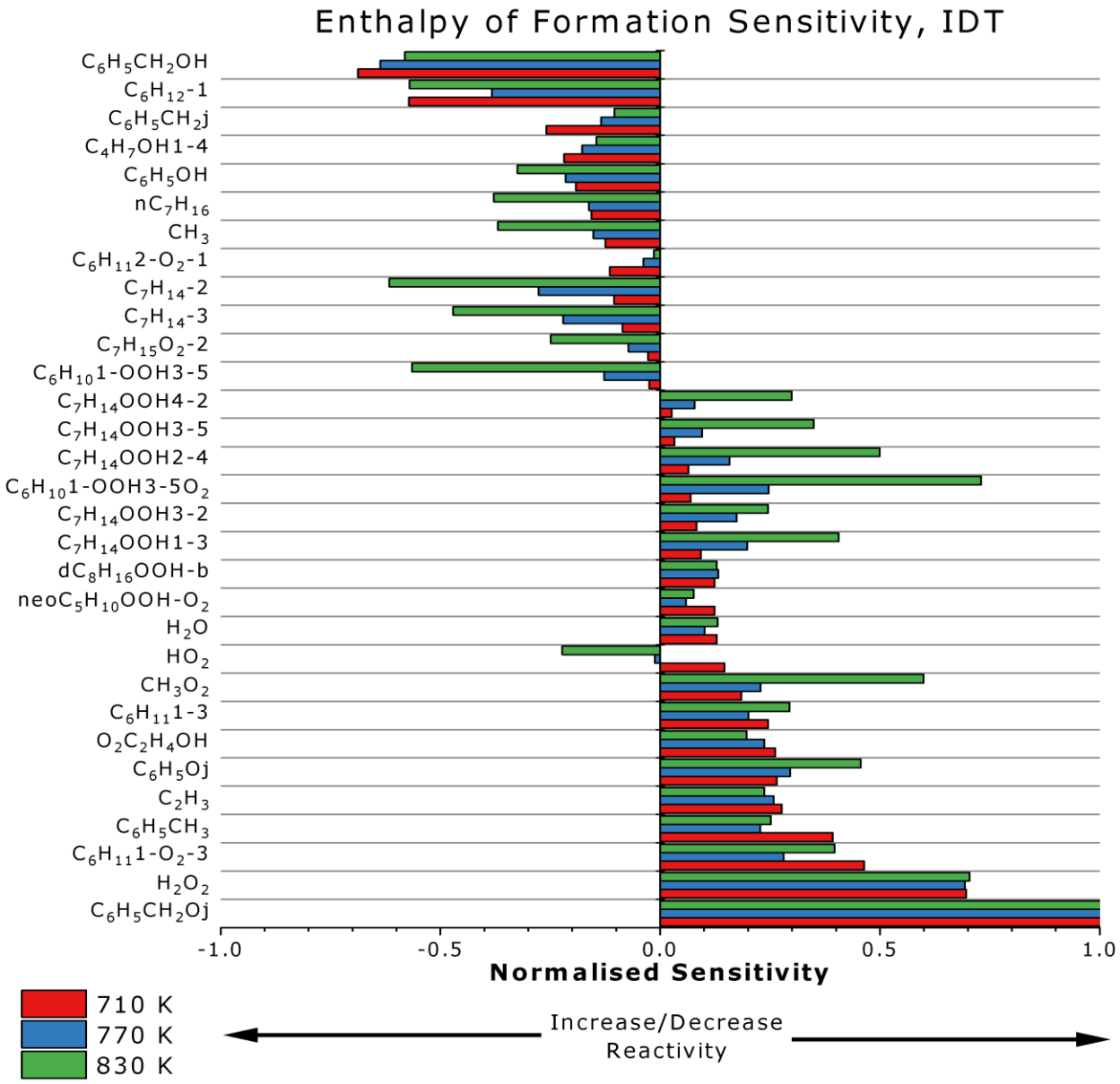

Figure 6.2. Normalised sensitivity coefficients for IDT due to a +5 kJ mol^{-1} change in the enthalpy of formation of each species, for the 5-C surrogate at temperatures of 710, 770 and 830 K. P_c=20 bar, Φ=1.0.

Of the hexene oxidation intermediate species, highly positive sensitivities are also shown for RO_2 and O_2QOOH species, specifically $C_6H_{11}1\text{-}O_2\text{-}3$ and $C_6H_{10}1\text{-}OOH3\text{-}5O_2$. The positive

sensitivities of these species are representative of a decrease in reactivity, due to a shift in the primary and secondary oxygen addition equilibria reducing the production of the species, leading to an overall decrease in the rate of low temperature chain branching. Alternatively, the 1-hexene QOOH species C_6H_{10}1-OOH3-5 produces a large negative sensitivity, indicating in increase in reactivity, as an increase in the enthalpy of this species promotes chain branching through the secondary oxidation equilibrium. These QOOH and O_2QOOH species are particularly sensitive at the highest temperature of 830 K, as the production of the hex-1-en-3-yl which initiates this chain increases significantly at post-NTC region temperatures [350,351]. A slight reduction in the relative normalised sensitivities of the 1-hexene fuel species and C_6H_{11}1-O_2-3 can also be observed in the NTC region (T_c=770 K), likely due to the lower degree of NTC behaviour exhibited by 1-hexene when compared to alkanes. Uncertainties in the heats of formation for these intermediate species may contribute to significant changes in the IDT, as shown in figure 6.1.

The presence of heptene isomers as highly negatively sensitive species, increasing reactivity, is due to the oxidation of n-heptane, wherein alkenes are formed via the concerted elimination of RO_2 radical species [46,85]. An increase in the enthalpy of formation for these alkene species shifts the equilibrium position of their formation back towards reactants, maintaining larger concentrations of the more reactive RO_2 radicals, hence the observed large negative sensitivities. The rate of formation for these alkenes increases significantly as temperature increases from 650-850 K, as indicated by the increasing degree of sensitivity [46]. Several n-heptane oxidation intermediates are also present as highly sensitive species, including the RO_2 radical $C_7H_{15}O_2$-2 and several QOOH species (C_7H_{14}OOH1-3, C_7H_{14}OOH2-4, C_7H_{14}OOH3-2, C_7H_{14}OOH3-5, and C_7H_{14}OOH4-2). The general presence of RO_2 and QOOH as highly sensitive species in the determination of IDT is also observed in previous literature studies. During the study of propane autoignition, brute force sensitivity analysis identified that species involved in the first and second internal isomerisation reactions (i.e. RO_2, QOOH, O_2QOOH and HO_2POOH) were highly important for the determination of first and total IDTs [184]. Similar observations have also been made in the literature for the autoignition of DEE, where IDT is highly sensitive to the enthalpies of formation of such fuel radical species, showing the largest potential for optimisation when compared with other thermodynamic and reaction rate parameters [182,183]. The identified isomerisation reactions of n-heptane (and iso-octane) RO_2 species also appear as highly sensitive in local OH sensitive analysis produced in the previous chapter, as well as in previous sensitivity analysis studies [47,51]. The observed negative and positive heats of formation sensitivities for the RO_2 and QOOH species,

respectively, are largely due to shifts in the internal isomerisation equilibrium. This reaction, and the subsequent chain mechanisms, drive the NTC behaviour observed for alkanes [53,136]. Moving the equilibrium towards reactants (RO_2), by increasing the enthalpy of formation for QOOH species, causes a reduction in the reactivity, whereas the reverse is true for an increase in RO_2 enthalpy of formation. This is shown most clearly in figure 6.1c, wherein a +5 kJmol^{-1} change in the enthalpy of formation of $C_7H_{14}OOH2$-4 produces an ~2% increase in IDT, at 830 K.

The large presence of toluene oxidation chemistry is also expected at all investigated temperatures, as toluene is known to suppress low temperature reactivity and delay both the cool flame (in two-stage ignition) and the main ignition phase [85]. Toluene oxidation intermediates identified in the mechanism through enthalpy of formation sensitivity analysis, often produce temperature dependent behaviour for enthalpies of formation which differs considerably from that presented by Burcat's table, which provides enthalpies of formation for these species based on G3B3 quantum chemistry calculations ($C_6H_5CH_2$j, C_6H_5OH, $C_6H_5CH_2Oj$ and $C_6H_5CH_2OH$). An increase in the enthalpy of benzyl alcohol ($C_6H_5CH_2OH$), leads to a decrease in IDT at all temperatures, as this increases the barrier to the production of this relatively stable species from toluene fuel radical species [352]. Furthermore, the low temperature oxidation of benzyl alcohol is accelerated by an increase in the enthalpy of formation for the species, due to the resultant promotion of hydrogen abstraction reactions. The standard enthalpy of formation given for benzyl alcohol within the mechanism (as determined via GA) is -100.4 kJmol^{-1}, whereas both Burcat's tables and the literature [353] (as determined experimentally in a rotating bomb calorimeter) give the value as -94.6±3.0 kJmol^{-1}. As such, there is a significant degree of uncertainty in this parameter, which can propagate through the system, producing considerable changes in the predicted IDT. This can be seen clearly at all investigated temperatures in figure 6.1, with the most significant change occurring at 770 K, wherein a +5 kJmol^{-1} change in the benzyl alcohol enthalpy of formations causes a ~6% decrease in IDT. Alternatively, the large positive sensitivities displayed for the benzyloxy radical ($C_6H_5CH_2Oj$) are due to the resultant decrease in the formation of this critical low temperature oxidation species, which occurs in large concentrations during the oxidation of toluene [264,269]. IDTs have been shown to be highly sensitive to the formation reaction of the benzyloxy radical, both in local OH analysis shown in the previous chapter (figure 5.34) and in previous studies of the gasoline surrogate mechanism employed here [47,51,85], further indicating the importance of this species in determining autoignition behaviour. The combined mechanism attributes a standard enthalpy of formation of 117 kJmol^{-1} for this species, through GA methods. This is

significantly different to the standard enthalpy of formation provided by G3B3 quantum chemistry calculations in Burcat's tables, which is 125.9±8 kJmol^{-1}. The significant influence of such uncertainties on the predicted IDT can be seen in figure 6.1, with the largest IDT percentage change due to a +5 kJmol^{-1} occurring at 770 K (~8.5% increase in predicted IDT). It should also be noted that the latest Burcat table presents significant uncertainties for the enthalpies of formation for further intermediate toluene oxidation species of up to ±8 kJmol-1 [176]. The observed dominance of toluene and 1-hexene low temperature oxidation species in this analysis echoes the statements presented in the HRA of experimental RCM data (section 5.5), further emphasising the importance of correctly representing LTHR behaviour for predicting ignition behaviour.

Small radical species such as HO_2 and CH_3 are present as sensitive species in figure 6.2, due to the prevalence of these species in multiple oxidation chain mechanism reactions. However, the enthalpies of formation for these species are known with relatively small uncertainties, as shown in the Active Thermochemical Tables [175]. This is similarly the case for other common species, such as H_2O_2, H_2O and CH_3O_2, which while important for the low and high temperature oxidation mechanism, also display small degrees of uncertainty in the heats of formation (relative to larger fuel radical and intermediate species). Therefore, an increase in enthalpy of formation as great as 5 kJmol^{-1} is unrepresentative of the true uncertainty for the species. The resultant sensitivities and change in IDT are also not representative of the influence of the actual uncertainties for these species. Significant uncertainties in highly sensitive species, which are also chemically important in the development of this low temperature behaviour, may propagate strongly into model predictions (figure 6.1). Therefore, it is necessary that the associated thermochemical uncertainties be minimised.

Since the production of the mechanisms used in this study, work by Zhang et al. [46] has developed the underlying n-heptane mechanism to account for new reaction classes and rate rules, as well as updating thermodynamic data based on newly optimised group values [354]. These changes were deemed by the study to produce reasonably good IDT and mole fraction predictions, while maintaining parity with rate rules applied to other alkanes such as pentane and n-hexane [90,144]. Similar thermochemistry and kinetic updates were also produced by Atef et al. [91] for the iso-octane sub mechanism. Thermochemistry for the majority of presented species is calculated via Benson's GA (as stated in the mechanism source) [85]. Recent work by vom Lehn et al. [187,355] has shown a high sensitivity in species enthalpy of formation for groups such as OO/C/H, C/C$_2$/H/OO and C/C/H$_2$/OO, which represent the OO and OOH

moieties and their adjacent groups, as seen in alkyl hydroperoxide, peroxy and peroxy hydroperoxide radical species (typical of low temperature chain branching pathways). This supports the results of previous studies which have identified the enthalpies of formation for RO_2, QOOH, O_2QOOH and HO_2POOH species as highly important for the determination of IDTs [182–184], as well the results shown in figures 6.1 and 6.2, wherein the enthalpies of many oxygenated species predicted by GA are also highly sensitive. Therefore, small errors in the associated group values have the potential to cause significant changes in enthalpy and therefore IDTs for such species. To avoid these characteristic uncertainties of the GA method, where possible, species thermochemical properties should be determined through experimental and quantum chemical calculation methods, as has occurred to facilitate the characterisation of small molecules [333,334,356]. However, where this is not feasible (due to the complexity of longer fuel radical species and oxidation intermediates), future work should be motivated towards the reduction of group uncertainties to improve the accuracy of the GA method.

6.3 Thermodynamic Sensitivity Analysis for Heat Release Properties

The importance of LTHR in the determination of the IDT has been discussed in the prior chapter (Chapter 5), wherein HRA techniques [172] were applied to both measured RCM data and the predictions of kinetic modelling. In this analysis (section 5.5) for the 5-C surrogate, significant differences were observed in characteristic LTHR properties between the analysis of RCM data and model predictions, which correlate well with further failures of the model in the prediction of IDT. LTHR describes a process of slowly evolving exothermicity prior to autoignition (and HTHR), common in degenerately branched systems [53], the properties of which are dependent on the chemical kinetic pathways followed during low temperature oxidation [357]. Chemically, the LTHR process is due to the decomposition of ketohydroperoxides formed during the low temperature oxidation of fuel species, which leads to the production of multiple OH radicals. ITHR may also occur, with or without the presence of LTHR, and is characterised by a gradual pressure rise (when compared to autoignition/HTHR) due to self-heating processes. Chemically, it is thought that ITHR is largely reliant on the production of alkenes, ethers, carbonyl species, and HO_2 via the elimination of RO_2 radicals, followed by the recombination of HO_2 with either HO_2 or CH_3 radicals [315]. ITHR behaviour can be induced in a fuel mixture through the addition of small amounts of fuel which display LTHR behaviour [315]. Large concentrations of H_2O_2 develop during increasing temperature and pressure conditions, until conditions are sufficient to induce the decomposition of H_2O_2 into two OH radicals, causing the degenerate branching associated with HTHR.

Multiple stages of LTHR were observed in section 5.5 during the HRA of the 5-C kinetic modelling results, which was largely absent from the analysis of RCM results. Multiple stages of heat release have been observed in several RCM and HCCI engine studies, for individual and blended fuels, with several descriptions of the underlying governing phenomena, dependent on the nature of the multiple stage heat release behaviour [92,315–317]. However, many of the multi-stage heat release behaviours observed in the literature do not correlate well with those observed in this study, wherein an apparent additional stage of LTHR is observed. Much of the literature sources discuss multi-stage heat release in relevance to the presence of ITHR [315,318–320] or multi-phase/delayed HTHR [316,321–323]. Previous work has observed the presence of an additional stage of heat release, similar in appearance and intensity to LTHR, for gasoline and a surrogate fuel of iso-octane, n-heptane and toluene, at lean equivalence ratios within a HCCI engine [324]. This additional heat release occurs between the initial cool flame and final ignition of the fuel and is attributed to the influence of toluene. The presence of toluene in the surrogate (and aromatics in the gasoline) leads to competition between the consumption of alkane fuel components (increasing reactivity) and the formation of relatively stable benzyl radicals ($C_6H_5CH_2j$) (decreasing reactivity), as temperatures increase post-LTHR. At extremely lean conditions (Φ=0.3) and a pressure of 10 bar, the work of AlRamadan et al. [317] showed for chemical kinetic simulations, the presence of a small “kink” in the first heat release stage of n-heptane at a temperature of 600 K and, to a much lesser extent, at a temperature of 700 K. The profile of this two-staged or delayed LTHR behaviour is similar to that observed in the HRA of 5-C simulations presented in section 5.5. However, the study did not investigate this phenomenon further, as it was only present low initial temperatures and long ignition timescales, limiting its relevance to engine conditions [317].

The presence of two-stage LTHR at SI engine relevant conditions, as experienced in kinetics simulations of 5-C in section 5.5, and the underlying processes which drive this phenomenon are of interest for the further understanding of the autoignition behaviour. This may be particularly relevant for the representation of heat release behaviour prior to HTHR, by chemical kinetic models, which has been observably poor when compared to RCM HRA (section 5.5). This poor representation of LTHR behaviour by the mechanism coincides with failures of the model to accurately predict 5-C IDTs. By performing brute force sensitivity analysis for multiple target parameters characteristic of LTHR (HRRs, aHR and temperature), this section aims to investigate the impact of uncertainties in species thermodynamic properties on the predicted LTHR behaviour. Uncertainties in the thermodynamic properties of a majority of fuel oxidation species present within the mechanism may be large, due to the use of GA

methodology in the determination of such properties. Analyses in the section are unique, as the direct influence of species enthalpy of formation uncertainties on LTHR behaviour, correlated with the influence on global IDTs, has not been investigated in previous studies.

6.3.1 Low Temperature Heat Release Rates

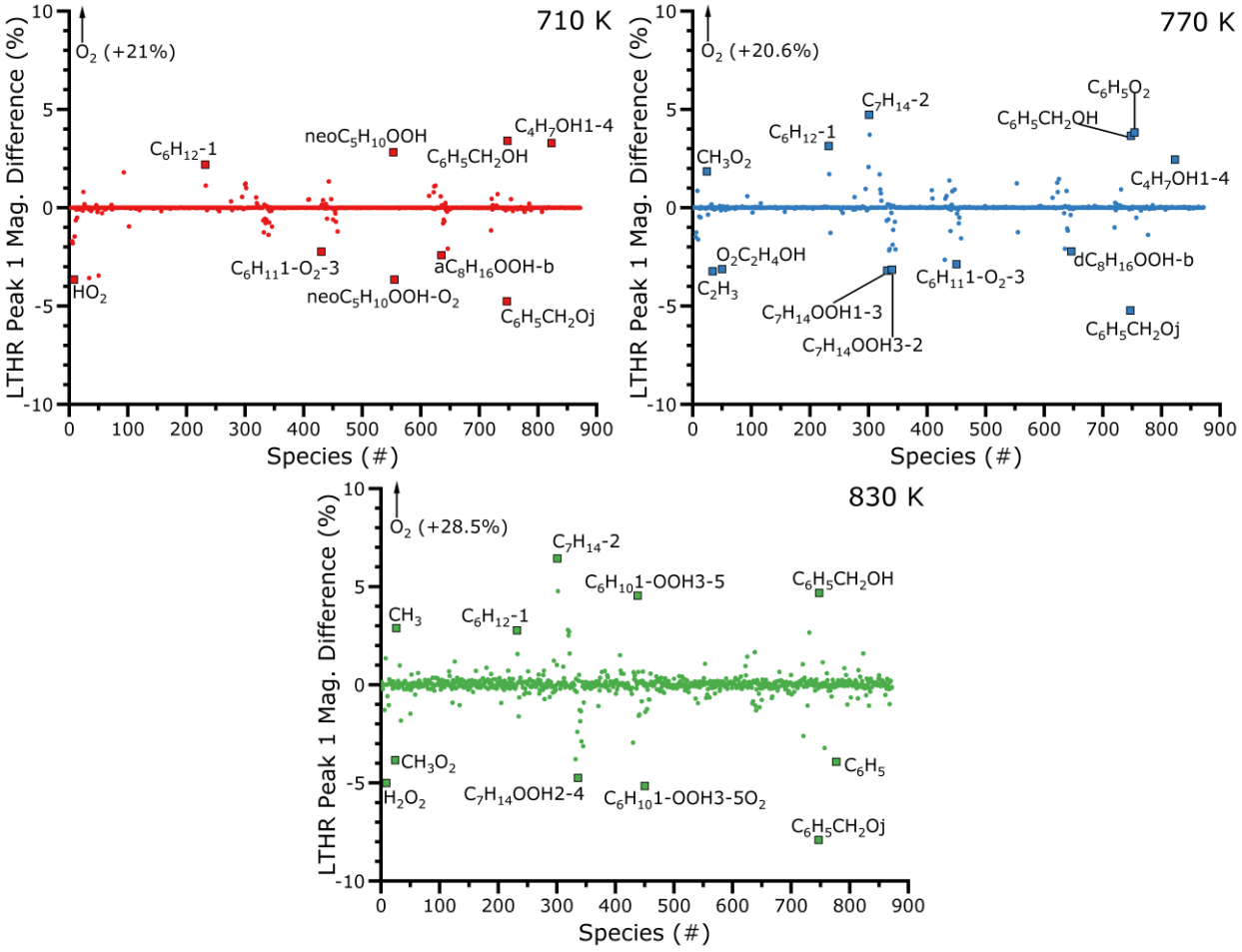

Figure 6.3. Percentage differences in the predicted magnitude of the first LTHR peak for 5-C constant volume simulations, due to a +5 kJ mol^{-1} change in species enthalpy of formation. P_c=20 bar, Φ=1.0.

The influence of a +5 kJmol^{-1} change to species enthalpies of formation on the predicted peak HRR, for the first LTHR peak, is shown in figure 6.3 for compressed temperatures of 710 K, 770 K and 830 K. The corresponding normalised sensitivity coefficients, as determined through a brute force sensitivity analysis, due to this change are shown in figure 6.4. In this sensitivity analysis, a positive normalised sensitivity value describes an increase in the peak HRR, whereas a negative value corresponds to a decrease in HRR. This changing intensity of LTHR may not correspond to an overall increase in the amount of LTHR however, as the duration of

LTHR is not represented by peak HRRs. This analysis must therefore be coupled with an investigation into the sensitivity of the aHR due to LTHR to provide a full overview of the sensitivity of LTHR behaviour to species enthalpy of formation. As shown in HRA of 5-C model prediction, two stages of LTHR are observed at 710 K (figures 5.17 and 5.23), whereas 770 K displays only a single clear LTHR HRR peak (figures 5.19 and 5.25). At a compressed temperature of 830 K (figures 5.21 and 5.27), a small amount of heat release is evident prior to HTHR, but it is difficult to distinguish these as the HTHR behaviour evolves rapidly. For the purpose of this analysis, a LTHR peak is defined for the 830 K at the point at which the HRR plateaus, after the first stage heat release and prior to autoignition. This point can be determined by the local minimum in HRR gradient. A significantly larger degree of scatter can be observed for percentage changes at 830 K due to this difficulty in the separation of LTHR and HTHR at this condition, and the resultant location of a LTHR peak. At all investigated conditions, a significant percentage change to the magnitude of LTHR peak HRR values can be seen for changes in the enthalpy of formation for many species, indicating general importance of accurate species thermochemical parameters on the evolution of LTHR.

Similarly to results observed for the sensitivity of IDTs to changes in enthalpy of formation (figure 6.2), the most sensitive species for the peak HRR at LTHR peak one are benzyl alcohol (which is highly positively sensitive) and the benzyloxy radical (highly negatively sensitive). An increase in the enthalpy of the benzyl alcohol limits the formation of the relatively stable species from more reactive radicals, for example through the addition of OH to benzyl radicals ($C_6H_5CH_2j+OH=C_6H_5CH_2OH$), while lowering the boundary to the formation of the benzyloxy radical via hydrogen abstraction (e.g. $C_6H_5CH_2OH+O_2=HO_2+C_6H_5CH_2Oj$). The more reactive benzyloxy radical, which is present in large concentrations during the low temperature oxidation of toluene, may then go on to form more reactive radical species [264,269,352]. Increasing the enthalpy of formation for the benzyloxy radical reduces the rate of production for this species, which is important for driving the low temperature oxidation of toluene. One highly sensitive reaction impacted by this change is the formation of more reactive benzyloxy and OH radicals from benzyl and HO_2 radicals ($C_6H_5CH_2j+HO_2=C_6H_5CH_2Oj+OH$), as seen in figure 6.5. This is in competition with the formation of benzyl alcohol from benzyl species, which is a likely cause for the large sensitivities observed for these oxygenated benzyl species. These results show that an increase in the intensity of LTHR, as caused by enthalpy of formation changes for these species, correlates with a decrease in the overall IDT. The significant influence of these species on the percentage change in HRR peak magnitude can be observed at all temperatures win figure 6.3. Also, large, normalised sensitivity values can again be observed for 1-hexene and

several of the fuel's low temperature oxidation species, as was the case for the IDT sensitivity analysis observed in figure 6.2. The long saturated carbon chain present in the 1-hexene molecule, allows for the presence of two stage ignition and mild NTC behaviour, meaning that the oxidation of this species can contribute significantly to LTHR [350]. Hydrogen abstraction of the 1-hexene fuel molecule is promoted by an increase in the enthalpy of formation, leading to an increase in peak low temperature HRR, wherein the low temperature oxidation pathways of fuel species are critical [357]. The importance of 1-hexene abstraction reactions is supported by reaction A-factor sensitivity analysis, which also highlights the importance of this pathway in driving LTHR behaviour (C_6H_{12}-1+OH=C_6H_{11}1-3+H_2O). These results further indicate the importance of toluene and 1-hexene oxidation in the prediction of LTHR and the IDT, due to the respective inhibiting and promoting natures of these processes [85].

Several heptene species are present in the most sensitive species of both IDT (figure 6.2) and LTHR HRR (figure 6.4) enthalpy of formation sensitivity analysis. For the latter, the observed positive sensitivity of these species describes an increase in peak HRR, caused by decrease in the elimination of QOOH species (e.g. C_7H_{14}-1+HO_2=$C_7H_{14}OOH_1$-2) through a shift in the equilibrium of this reaction towards QOOH. This increases the production of radical species from the relatively unreactive alkenes, causing an increase in LTHR. These species appear particularly sensitive in the NTC region (770 K) due to the increase in RO_2 concerted elimination in this region, as do further n-heptane oxidation intermediates, such as several QOOH species (C_7H_{14}OOH1-3, C_7H_{14}OOH2-4, C_7H_{14}OOH3-2, C_7H_{14}OOH3-5, C_7H_{14}OOH4-2), which were also highly sensitive in the prediction of IDT shown previously. An increase in the enthalpy of formation of n-heptane QOOH species increases the boundary to internal isomerisation reactions (e.g. $C_7H_{15}O_2$-3=$C_7H_{14}OOH_3$-2) and lowers the boundary to chain terminating pathways typical of NTC behaviour, such as the elimination of QOOH species (e.g. C_7H_{14}-1+HO_2=$C_7H_{14}OOH_1$-2), producing the observed largely negative sensitivities for these species. N-heptane is known to produce significant NTC behaviour, even when blended with species which would aim to suppress this behaviour, such as toluene [46,85]. Therefore, uncertainties present in the enthalpies of formation for these species, introduced by the application of GA to determine species properties, may produce significant changes in LTHR (and ultimately IDT) behaviour. This can be seen in figure 6.3.

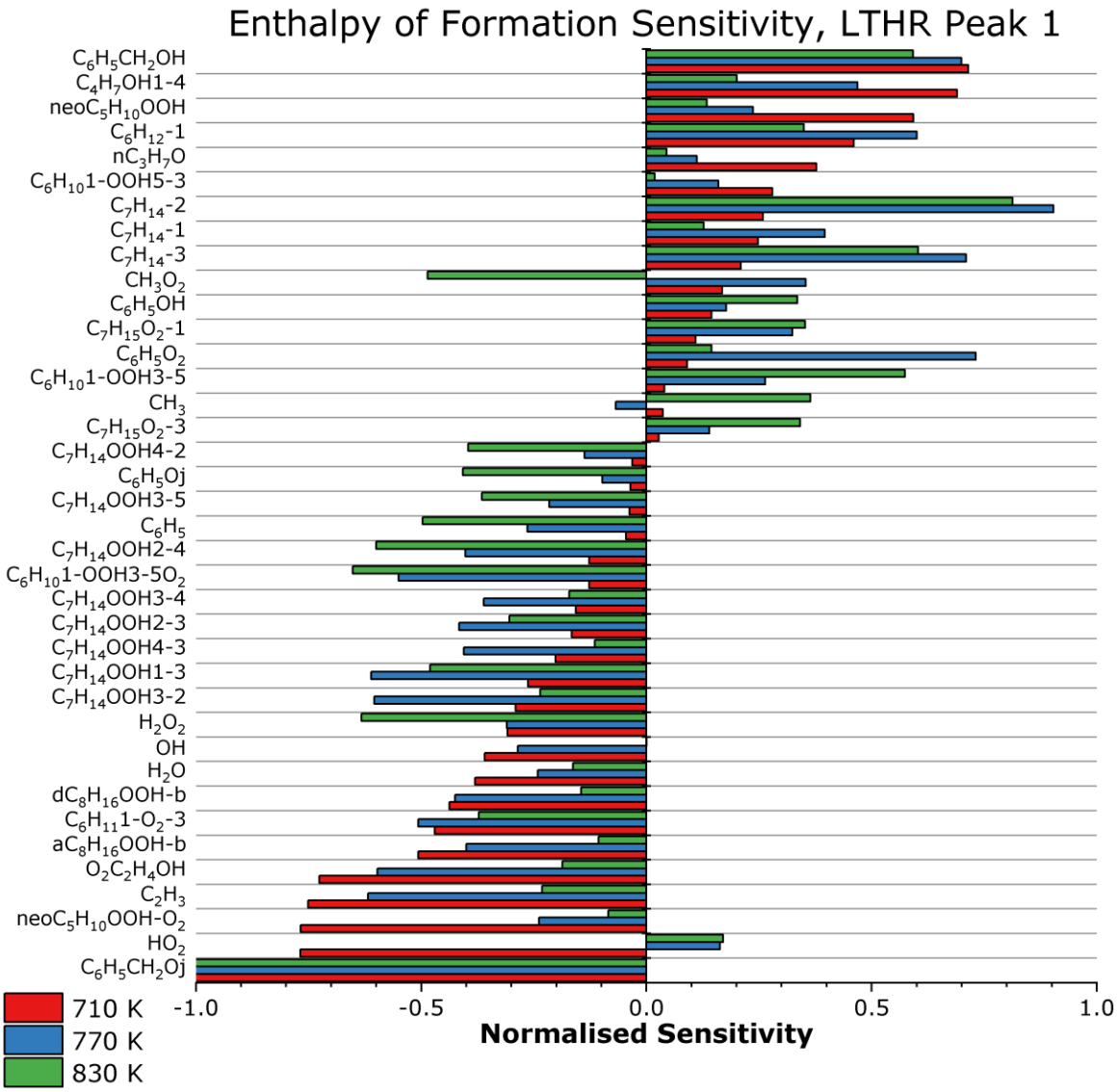

Figure 6.4. Normalised sensitivity coefficients for the magnitude of LTHR peak one due to a +5 kJ mol^{-1} change in the enthalpy of formation of each species, for the 5-C surrogate at temperatures of 710, 770 and 830 K. P_c=20 bar, Φ=1.0.

At the lowest investigated temperature of 710 K, large degrees of sensitivity can be observed in figure 6.4 for the oxidation intermediate species of neo-pentane, specifically the QOOH species $neoC_5H_{10}OOH$ and the O_2QOOH species $neoC_5H_{10}OOH\text{-}O_2$. The presence of these species is attributed to neo-pentyl radicals formed during the low temperature oxidation of iso-octane. Iso-butene, pentenes and neo-pentyl radicals are commonly observed products of iso-octane oxidation [91,238]. Iso-butene may undergo a methyl addition to the internal carbon site, leading to the formation of neopentyl radicals [358]. Increasing the enthalpy of formation for the QOOH species, produces an increase in LTHR peak HRR (for the first observed LTHR peak

at 710 K), and the progression of low temperature oxidation of neopentane is promoted via the second oxygen addition. This addition forms neo$C_5H_{10}OOH$-O_2, of which an increase in enthalpy of formation understandably decreases the rate of formation. An increase in the enthalpy of formation for the O_2QOOH species is also likely to further inhibit low temperature reactivity (and this the LTHR rate), as it encourages competition from typical NTC chain termination and propagation pathways of the QOOH species, as opposed to branching. As temperatures increase, concentrations of these species decrease and as such, so does the sensitivity to changes in the species enthalpy of formation [262].

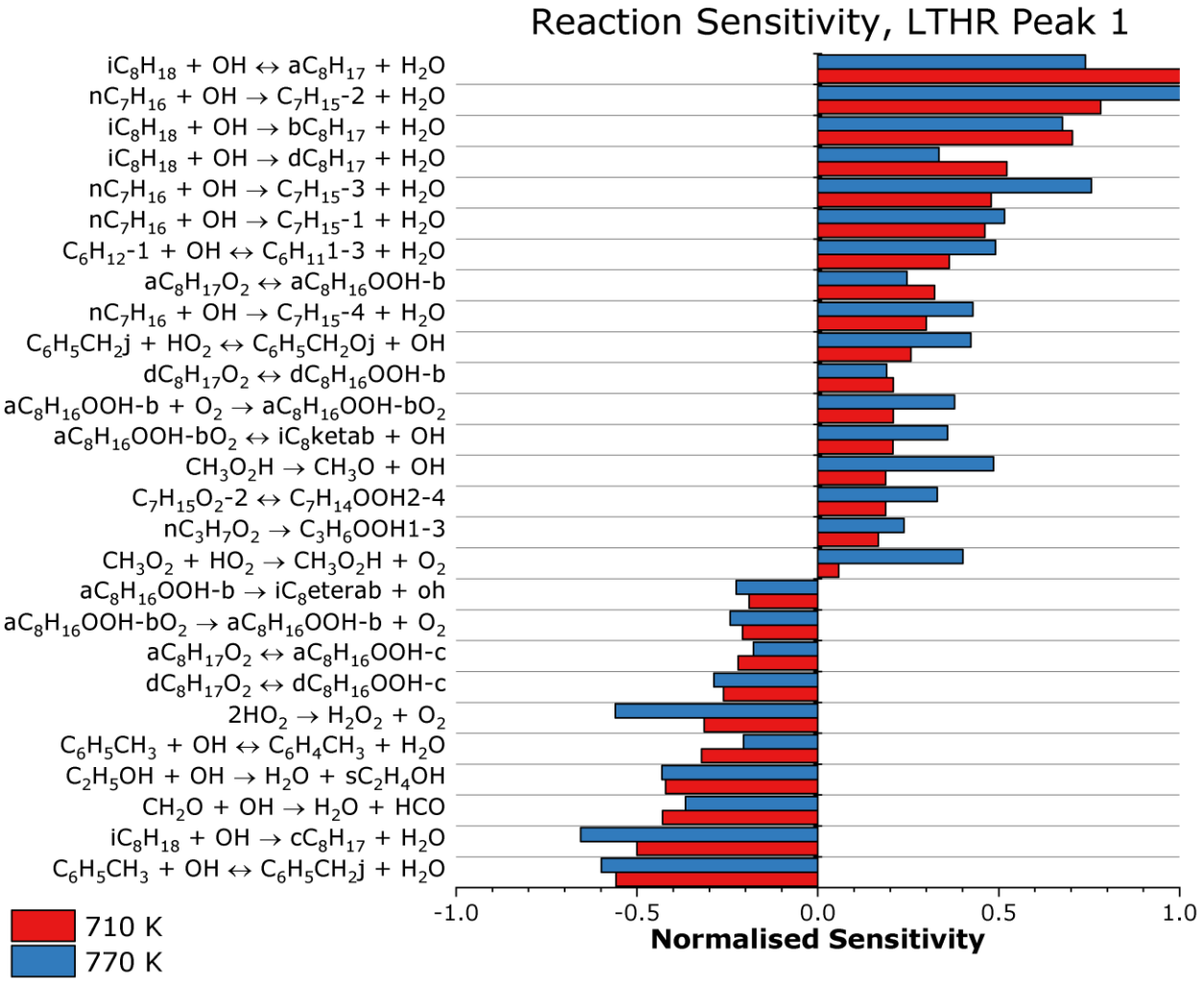

Figure 6.5. Normalised sensitivity coefficients for the magnitude of LTHR peak one due to a 2 factor increase in the pre-exponential A-factor of each reaction, for the 5-C surrogate at temperatures of 710, 770 and 830 K. P_c=20 bar, Φ=1.0.

Butenol (C_4H_7OH1-4/1-buten-4-ol/3-buten-1-ol) is also present as a highly positively sensitive species, particularly at temperatures of 710 and 770 K, as seen in figure 6.4. This species also appeared to be highly sensitive in the determination of IDTs (figure 6.2) but appears more highly sensitive during LTHR, indicating that this species may be less important during HTHR. This observation is further supported by the larger degree of sensitivity for butenol at lower temperatures and reducing sensitivity as temperature increases, in terms of both LTHR and IDTs. Similarly, to the observed neo-pentyl oxidation species, butenol may be formed via the interactions of small oxidation products, such as ethenyl radicals which are generated largely through the low temperature oxidation of 1-hexene, with C_2H_4OH produced during the oxidation of ethanol. Dependent on the abstraction site, the C_2H_4OH radical site can be located at the primary carbon, secondary carbon, or oxygen sites, leading to the formation of pC_2H_4OH, sC_2H_4OH or C_2H_5O. The formation of the observed butenol species is dependent on the presence of the pC_2H_4OH radical, the formation of which is not heavily favoured at 710 K [292,359]. As temperature increases, the ethanol hydrogen abstraction branching ratio shifts further towards the formation of the other radicals, whereas the branching ratio of pC_2H_4OH formation decreases [292,359]. This is a likely cause for the reduction in sensitivity for the butenol species as temperature increases, as well as the increased sensitivity during LTHR when compared to IDTs. Work by Sivaramakrishnan et al. [360] and Mittal et al. [292] has made efforts to update the temperature dependence of the hydrogen abstraction branching ratios and have shown near constant branching ratios throughout the temperature regime. Given the high sensitivity of the butenol species, this may produce a significant impact on the development of LTHR behaviour within the mechanism. It should be noted that this species is not present in the original LLNL gasoline surrogates mechanism [85] utilised as part of the combined mechanism applied in this study, but is in the butanol isomers mechanism [84]. As no butanols are present in the investigated fuel (5-C), the species must be formed due to interactions between the two kinetic mechanisms. An increase in the enthalpy of formation for 1-buten-4-ol promotes several important reactions for the consumption of enols, including hydrogen abstraction, addition of H radicals to double bonds and unimolecular decomposition [84,159,160]. Such an increase also causes a shift in the equilibrium of the reaction $C_4H_7OH1\text{-}4=C_2H_3+pC_2H_4OH$, towards the more reactive ethenyl radical. Within the combined mechanism, the standard enthalpy of formation for 1-buten-4-ol, as determined via GA, is given as -151 $kJmol^{-1}$. Literature sources for this property are sparse, however the study of Vélez et al. [361] experimentally determined the gas-phase standard enthalpy to be -147.3±1.8 $kJmol^{-1}$, whereas the theoretical quantum calculation of Kondo et al. [362], at the G2(MP2) level with an atom additive type correction, obtained a

corrected value of -142.3 $kJmol^{-1}$. Clearly there is a significant degree of uncertainty in the enthalpy of formation for this species, with both literature sources displaying considerably smaller enthalpies than the GA derived value in the mechanism. Such a change would propagate to the intensity of LTHR, reducing the magnitude of HRR significantly, as seen in figure 6.3.

In general, this analysis highlights the importance of low temperature oxidation pathways and the associated accurate description of the species involved in these reactions, for the prediction of LTHR HRRs. This is further supported by brute force sensitivity analysis of reaction pre-exponential A-factors on the LTHR peak HRR, as shown in figure 6.5. In this reaction sensitivity analysis, A-factors were increased by a factor of two, for each reaction within the combined mechanism independently, and the resultant change in the predicted LTHR HRR was recorded. This analysis highlights further reactions which are not identified by the enthalpy of formation sensitivity analysis, as in many cases backwards reaction rates are specified within the kinetic mechanism, highlighting the necessity of applying both rate parameter and thermodynamic data sensitivity analysis to provide a more substantial evaluation of the model, particularly in cases where the mechanism is mix of defined and undefined reverse reaction rates. In future work, the simultaneous investigation of the models response to changes in species thermodynamic data and reaction rate parameters should be applied using global sensitivity and uncertainty analysis techniques, to explore the interrelationships which exist between reaction rate and thermodynamic parameters and provide a full quantitative assessment of the model with regards to these parameters. Such analysis would be computationally expensive and time consuming. Therefore, it is currently beyond the scope of this study but is recommended for future research in this area. Unsurprisingly, the results shown in figure 6.5 display the dominance of hydrogen abstraction reactions from fuel species which produce substantial low temperature reactivity, such as iso-octane, n-heptane and 1-hexene, which is consistent with the finding of previous studies of first stage IDTs [181,325,363,364]. As discussed for local OH sensitivity analysis of 5-C simulations in section 5.6, these abstraction reactions demonstrate abstraction site influences on low temperature reactivity. Abstraction from the tertiary iso-octane site, leading to the formation of cC_8H_{17}, results in a largely negative sensitivity and a resultant decrease in peak LTHR values, extending first stage ignition. Other iso-octyl radicals, formed through hydrogen abstraction from other iso-octane sites, proceed with low temperature oxidation through oxygen addition to form RO_2 species, followed by internal isomerisation to QOOH and so forth (as detailed in section 2.5.1), until the formation and subsequent decomposition of ketohydroperoxides resulting in chain branching. This

contributes considerably to early stages of heat release during autoignition, as shown by the large positive sensitivities for the initiation of these pathways through hydrogen abstraction. This is not the case for the oxidation of cC_8H_{17}, which mostly progresses via the formation of di-isobutylene and a HO_2 radical from the RO_2 species $cC_8H_{17}O_2$. Effectively, the cC_8H_{17} radical acts as an OH scavenger, inhibiting the low temperature reactivity of the fuel [181].

A large negative sensitivity can be seen at temperatures of 710 and 770 K in figure 6.5, for the hydrogen abstraction of toluene by an OH radical, as this consumes an OH to form a relatively unreactive benzyl radical. This formation of the benzyl radical, through the OH scavenging of the toluene fuel species, competes with the low temperature oxidation of alkane and olefin species, reducing the bulk low temperature reactivity of the 5-C fuel [324]. Benzyl radicals may react further with HO_2 to radicals to form more reactive OH and benzyloxy radicals. The importance of this reaction increases with increasing temperature, as observed by the increase in sensitivity between 710 and 770 K cases. By combining reaction rate sensitivity analysis and thermodynamic sensitivity analysis, the importance of toluene low temperature oxidation in the development of LTHR can be observed clearly. In summary, A-factor sensitivity analysis shows the importance of hydrogen abstraction (as it does for all fuel species) from toluene to form benzyl radicals and initiate the low temperature oxidation process ($C_6H_5CH_3+OH=C_6H_5CH_{2j}+H_2O$). This abstraction largely occurs from the methyl site at low temperature conditions, as indicated by the high sensitivity of this reaction [264]. The benzyl radical then tends to react with HO_2 radicals to form benzyloxy and OH radicals ($C_6H_5CH_2j+HO_2=C_6H_5CH_2Oj+OH$) [264,269], as identified by A-factor sensitivity analysis. However, small amounts of the benzyl radical may undergo OH addition, to form the relatively unreactive benzyl alcohol ($C_6H_5CH_2j+OH=C_6H_5CH_2OH$) [269]. Enthalpy of formation sensitivity analysis identifies competition between these two benzyl reaction pathways, with an increase in the enthalpy of formation for the relatively unreactive benzyl alcohol species ($C_6H_5CH_2OH$) producing an increase in LTHR HRRs and a decrease in IDT, as benzyl formation shifts more towards the production of the more reactive $C_6H_5CH_2Oj$. Likewise, the reverse of this is true for an increase in the enthalpy of formation for the benzyloxy radical. Benzyl alcohol may also form benzyloxy radicals through hydrogen abstraction ($C_6H_5CH_2OH+OH=C_6H_5CH_2Oj+H_2O$) and an increase in the enthalpy of the benzyl alcohol will increase the forwards rate of this reaction. $C_6H_5CH_2Oj$ may then decompose ($C_6H_5CH_2Oj=C_6H_5CHO+H$), producing benzaldehyde (C_6H_5CHO) and highly reactive H radicals, increasing the reactivity of the fuel [264,269]. Small amounts of the benzyloxy radicals may also decompose ($C_6H_5CH_2Oj=C_6H_5+CH_2O$) to produce phenyl radicals (C_6H_5) and formaldehyde (CH_2O). Benzaldehyde than continues through the

oxidation process, producing C_6H_5CjO radicals via hydrogen abstraction ($C_6H_5CHO+OH=C_6H_5CjO+H_2O$), which then decompose to produce phenyl radicals and CO ($C_6H_5CjO=C_6H_5+CO$) [269]. This process seems to be largely dependent on the rate of initial hydrogen abstraction of toluene, as identified by A-factor sensitivity analysis, and competition between the formation of benzyloxy and benzyl alcohol species from the resultant benzyl radical, as identified by enthalpy of formation sensitivity analysis. This process is important for the development of both LTHR and global IDT predictions, as indicated by the combined sensitivity analysis techniques shown in this chapter. The benefits of a combination of enthalpy of formation and reaction rate A-factor sensitivity analysis is well highlighted in this section, as it allows for the identification of sensitive parameters which are not shown by the analyses individually, facilitating an investigation of more of the models underlying chemistry.

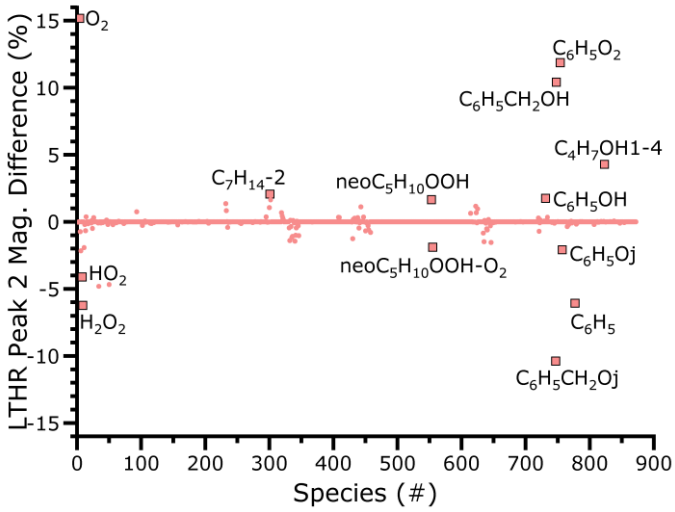

Figure 6.6. Percentage differences in the predicted magnitude of the second LTHR peak for 5-C constant volume simulations, due to a +5 kJ mol^{-1} change in species enthalpy of formation, at a temperature of 710 K. P_c=20 bar, Φ=1.0.

At a temperature of 710 K, a second stage of LTHR is observed for the 5-C fuel in chemical kinetic simulations, which is not apparent in HRA of RCM results (section 5.5). Figure 6.6 shows the change in the magnitude of this second stage LTHR as a result of a +5 $kJmol^{-1}$ change to species enthalpies of formation and figure 6.7 shows the corresponding normalised sensitivity coefficients. While several of the species which appeared sensitive in the first stage of heat release (figure 6.4) also display significant degrees of sensitivity at the second peak (which would be expected due to the proximity of the two peaks to each other), the dominance of toluene oxidation chemistry has increased. Of particular note are the large sensitivities of the

peroxy phenyl radical ($C_6H_5O_2$) and the phenyl radical (C_6H_5), which were not as highly sensitive for the first stage of LTHR at 710 K. Large sensitivities can also be observed for the benzyl alcohol and benzyloxy radical species, as seen in thermodynamic sensitivity analysis results for the first stage LTHR (figure 6.4) and IDT (figure 6.2).

During LTHR, large concentrations of $C_6H_5O_2$ are formed, reaching a peak value which coincides with the secondary peak of LTHR, as shown in figure 6.8. This species is largely formed through oxygen addition to the phenyl radical, resultant from the low temperature oxidation of toluene. As temperatures increase due to the first stage of LTHR, the equilibrium of this reaction shifts from $C_6H_5O_2$ towards formation of the phenyl radical and oxygen. In the literature, the recombination of phenyl with O_2 displays a negative temperature dependence at temperatures relevant to LTHR, which then becomes a positive temperature dependence at higher temperatures characteristic of HTHR [365,366]. However, in the mechanism applied in this study, a constant reaction rate is attributed to this reaction, which is not representative of the temperature dependent behaviour of the reaction rate in the temperature region of interest to this study. The peroxy phenyl radical may also decompose to form C_6H_5Oj (phenoxy) radicals, but the formation of this species is largely dominated by the oxidation of the phenyl radical to form a phenoxy radical and an O radical, ultimately leading to final combustion products through the decomposition of the phenoxy radical [324,367]. This process frees up radicals (particularly H, O and HO_2), which may then consume fuel species through low temperature oxidation pathways, without further obstruction. The obstruction of LTHR by toluene oxidation and the formation of relative unreactive, radical scavenging species, followed by this process (as temperatures increase enough to shift the peroxy phenyl-phenyl equilibrium but not enough to cause the decomposition of H_2O_2 and the associated degenerate branching), causes the observed delayed stage of LTHR. A similar behaviour, termed “obstructed pre-ignition” has been observed in the literature for a surrogate fuel containing 30% toluene by volume, at lean (Φ=0.3-0.54) HCCI engine conditions [324], but with observably more distinct heat release phases. An increase in the enthalpy of formation for the peroxy phenyl radical shifts the equilibrium further in the direction of the phenyl radical, initiating a larger degree of delayed LTHR, as shown by the resultant percentage change presented in figure 6.6. In this figure, a +5 kJmol-1 change in the enthalpy of formation of the peroxy phenyl radical produces a +11.8% change in the peak HRR.

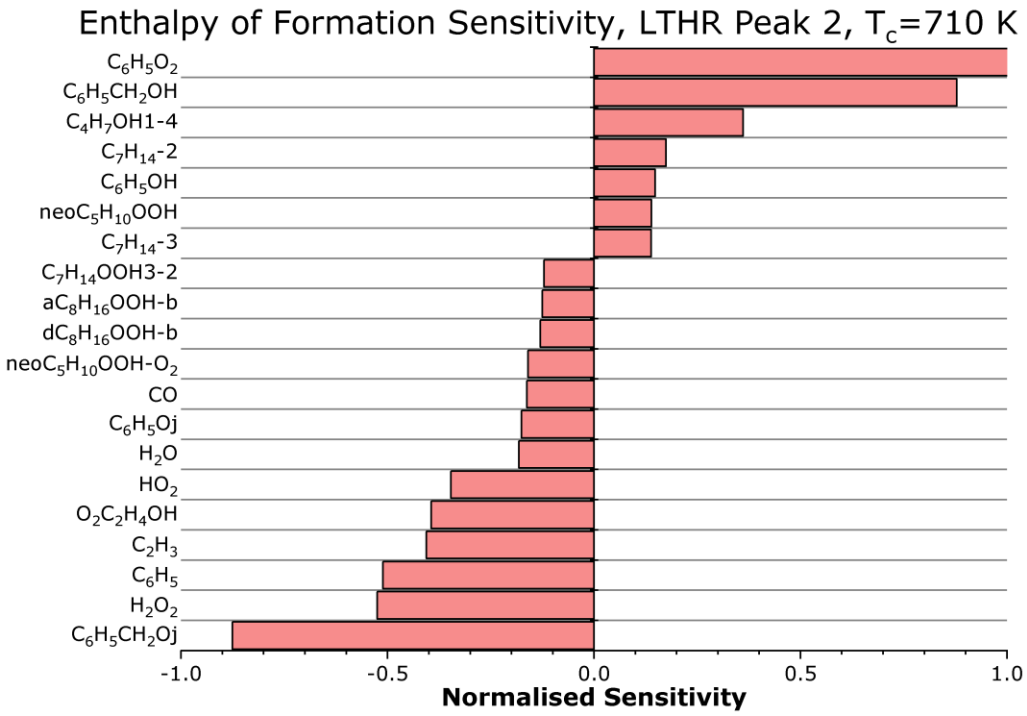

Figure 6.7. Normalised sensitivity coefficients for the magnitude of LTHR peak two due to a +5 kJ mol^{-1} change in the enthalpy of formation of each species, for the 5-C surrogate at a temperature of 710 K. P_c=20 bar, Φ=1.0.

While the standard enthalpy of formation for the phenyl radical is known with reasonable uncertainty (336.88±0.54 kJmol^{-1}), as shown in the Active Thermochemical Tables resource [175], this shows some mild disagreement with the value determined via GA within the mechanism (339.7 kJmol^{-1}). As LTHR peak heat release, specifically for second stage LTHR at 710 K and total LTHR at 770 and 830 K, appears highly sensitive to this species, small changes such as this may significantly impact model predictions. This can be seen in figures 6.3 and 6.6, wherein a +5 kJ mol^{-1} change in the enthalpy of formation for the phenyl radical produces a -6.1% and -3.9% change in peak LTHR values for second phase LTHR at 710 K and total LTHR at 830 K, respectively. Uncertainties for both peroxy phenyl and phenoxy enthalpies of formation are much larger, with the G3B3 level quantum calculations presented in Burcat's tables giving values of 141.6±8 kJmol^{-1} and 61.6±8 kJmol^{-1} [176], respectively, whereas GA derived values within the mechanism are given as 151 kJmol^{-1} and 50.62 kJmol^{-1}. Further standard enthalpies of formation have been attributed to the phenoxy radical in the literature, with a value of 54.0 ± 6.0 kJ mol^{-1} determined experimentally [368] and a value of 60.51 kJ mol^{-1} calculated at the G3MP2B3 level of theory [369]. Therefore, the uncertainty in the enthalpy of formation for these

highly sensitive species is substantial and may produce changes in model predictions larger than those observed the +5 kJ mol^{-1} change in the enthalpy applied in this study.

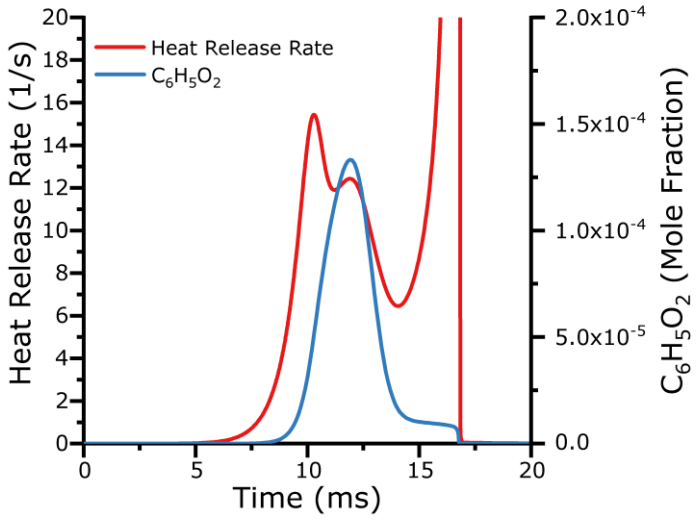

Figure 6.8. Simulated HRRs and concentrations of the peroxy phenyl radical, showing the correlation between the concentration and the presence of second stage LTHR, for 5-C at 710 K. P_c=20 bar, Φ=1.0.

By modifying the species enthalpies of formation for the toluene oxidation intermediate species identified in this analysis (figure 6.7), such that they are aligned with values given by the latest version of Burcat's tables [176], considerable changes can be observed in the LTHR behaviour at 710 and 770 K (figure 6.9). When compared to previous heat release predictions of the model (shown in figure 6.9 and section 5.5), at 710 K the second stage of LTHR is much less pronounced, appearing here as a "shoulder" to the first stage LTHR. A similar observation can be made at 770 K, wherein the originally present "shoulder" has largely disappeared, leaving only the primary LTHR peak. These profiles also appear to be somewhat more consistent with those presented by the HRA of RCM experiments, indicating that the applied modifications to thermodynamic data have made slight improvements towards the accurate representation of LTHR behaviour. However, there are still clear differences between the RCM derived and simulation predicted LTHR behaviour at 710 K, whereby simulations still overpredict the intensity of LTHR peak HRR, which is initiated later than the LTHR of 5-C within the RCM. Simulation predictions are significantly improved at 770 K, where the modification of the thermodynamic data associated with second stage of LTHR has reduced peak HRR and delayed HTHR, which coincides with an improved prediction of IDT (figure 10). A reduction in the intensity and amount of LTHR translates to an increase in IDT, as shown in figure 6.10.

Significant increases can be observed for IDT throughout the low temperature and NTC regions, due to changes in the thermodynamic properties of species identified as sensitive in second stage LTHR. This modification is not intended to provide accuracy improvements to the combined mechanism, but simply highlight the importance of uncertainties in these species in the prediction of IDT and LTHR properties.

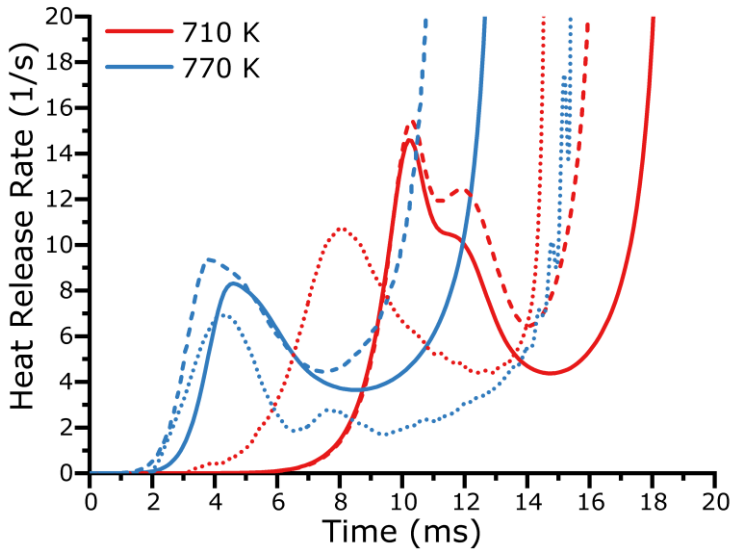

Figure 6.9. Predicted HRRs for the LTHR of 5-C, obtained after the modification of thermodynamic data for toluene intermediate species identified in figure 6.7, compared against predicted HRRs prior to modification and experimental HRRs (as shown in section 5.5). Solid lines show model predictions with modified thermodynamic data. Dashed lines show model predictions prior to modifications. Dotted lines show experimentally derived HRRs. P_c=20 bar, Φ=1.0.

Also shown in figure 10 are IDTs for an example of “tuned” thermochemistry, wherein the enthalpies of sensitive species associated with the low temperature oxidation of n-heptane and 1-hexene (RO_2, QOOH, O_2QOOH and alkene species) have been modified to provide the desired IDT profile. This example is not a demonstration of model improvement and mechanisms should not be tuned in the method utilised for this example. Thermodynamic properties and reaction rate parameters should be based in high level theoretical calculations and experimental results where possible or estimated using up to date methods and data. However, these IDTs are displayed as an example of how uncertainties in the thermodynamic data of species can dramatically impact the IDT profile. In this example, the enthalpies of formation for several species identified through enthalpy of formation sensitivity analysis for IDTs and LTHR are modified within uncertainty limits to produce an IDT profile much more

similar to that shown by experimental IDT measurements, including a significant improvement in the NTC intensity predictions of the model. Towards improving the combined mechanism, a thorough evaluation of thermodynamic data for all sensitive species and the associated rate rules should be performed, as the impact of these parameters is clear, particularly in the presence of LTHR. Discrepancies between thermodynamic data and reaction rates have been observed between the current literature and those present in the combined mechanism, of importance to the prediction of IDT and LTHR behaviour. These will need to be assessed and thoroughly accounted for in future work, towards the development of the model to accurately predict preliminary exothermicity.

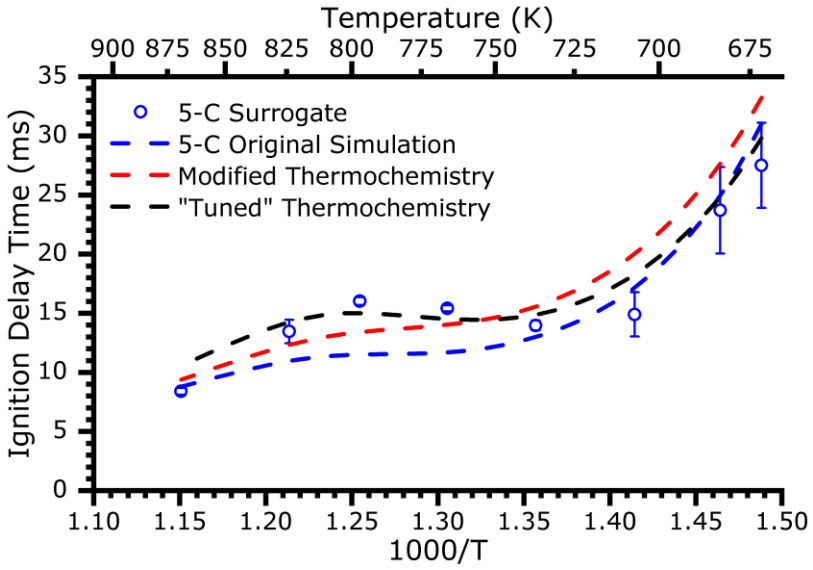

Figure 6.10. The impact of modifying thermodynamic data, for toluene oxidation species identified as sensitive at second stage LTHR, on the predicted IDT for 5-C. P_c=20 bar, Φ=1.0.

Normalised sensitivity coefficients for a brute force sensitivity analysis of the peak HRRs in the second stage LTHR, due to changes in reaction pre-exponential A-factors, can be seen in figure 6.11. Again, the hydrogen abstraction of fuel species displays a high degree of sensitivity, highlighting the importance of low temperature oxidation pathways at these conditions. Also, the oxidation of benzyl radicals ($C_6H_5CH_2j$) by HO_2 to produce benzyloxy ($C_6H_5CH_2Oj$) and reactive OH radicals can be observed as highly positively sensitive, as the radical scavenging of the benzyl species is overcome and more free radicals become available for the oxidation of further fuel species. Radical scavenging by the toluene fuel can be observed as significantly negatively sensitive in figure 6.11, forming benzyl radicals via hydrogen abstraction. The production of a phenoxy radical and an O radical, due to oxygen addition to phenyl radicals, also appears as a

sensitive reaction at these conditions, supporting the observations of enthalpy of formation sensitivity analysis for the second phase LTHR peak (figure 6.7).

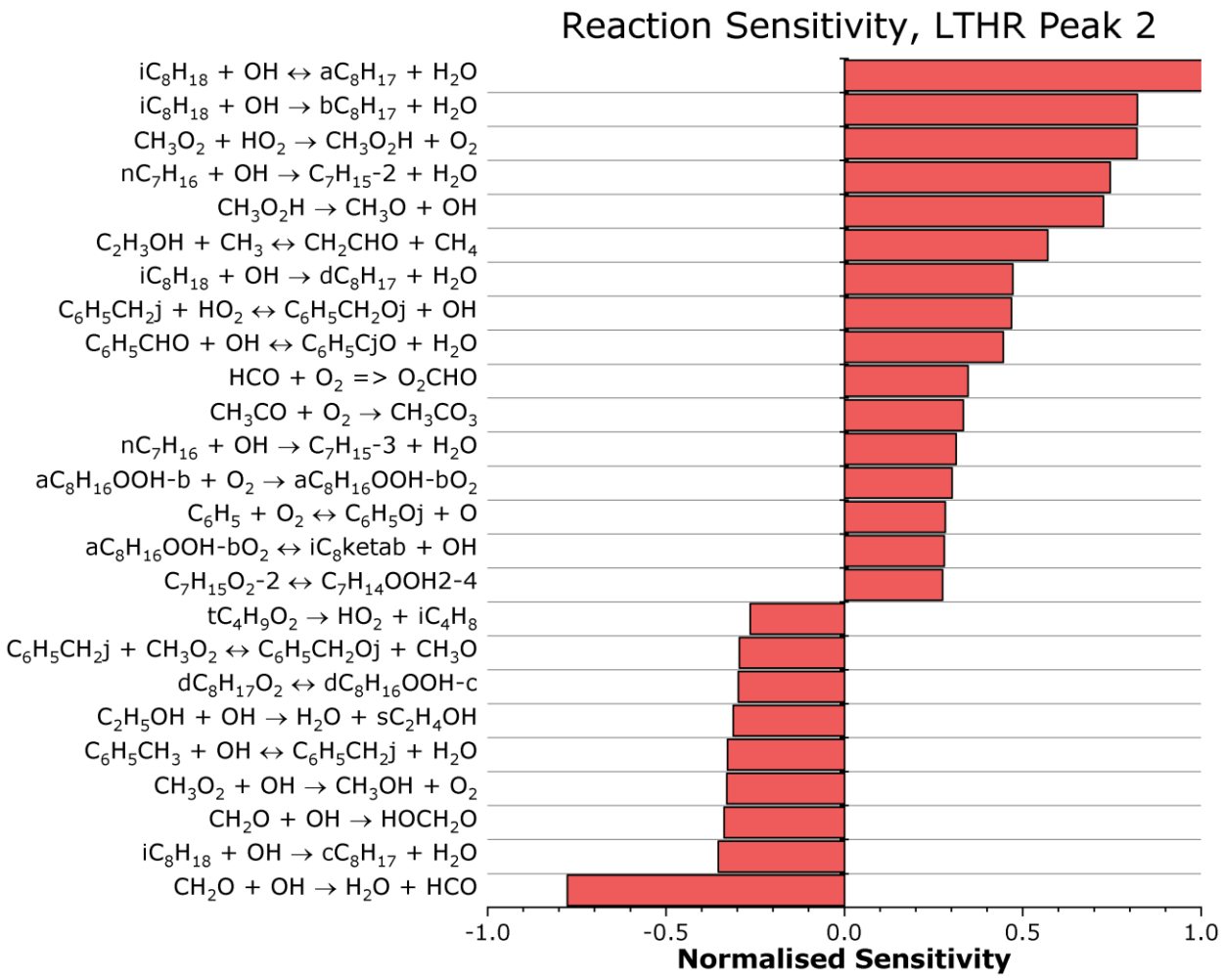

Figure 6.11. Normalised sensitivity coefficients for the magnitude of LTHR peak two due to a 2 factor increase in the pre-exponential A-factor of each reaction, for the 5-C surrogate at temperatures of 710, 770 and 830 K. P_c=20 bar, Φ=1.0.

Heat release during second phase LTHR is inhibited largely by the reaction of $CH_2O+OH=H_2O+HCO$, which consumes formaldehyde and a highly reactive OH radical, in a chain termination. Similar OH termination reactions also appear highly negatively sensitive at this condition ($CH_2O+OH=HOCH_2O$, $CH_3O_2+OH=CH_3OH+O_2$). As hydrocarbons structures break down, such as the decomposition of ketohydroperoxides, several similar primary molecules and intermediates are formed, including CH3O and formaldehyde [172]. The significant presence of reactions involving these small hydrocarbon species is observably

greater at the second stage of LTHR, due to increased concentrations formed during the initial stage of LTHR, which may now react with the increasing radical pool. The hydrogen addition to CH_3O_2 ($CH_3O_2+HO_2=CH_3O_2H+O_2$) appears largely promoting of second stage LTHR, as the resultant CH3O2H may decompose to produce methoxy and OH radicals. Methoxy radicals rapidly decompose to produce formaldehyde and a H atom [370].

At a temperature of 770 K, a distinct second phase of LTHR is no longer present in 5-C simulations. However, the total LTHR shows a large “shoulder” (as seen in figures 5.19 and 5.25) at this condition, indicating that the two stages of LTHR have largely merged together at this higher temperature condition, as the peroxy phenyl-phenyl equilibrium shifts earlier in the autoignition process. This can be observed in the enthalpy of formation brute force sensitivity analysis at 770 K, wherein the phenyl and peroxy phenyl radicals increase significantly in sensitivity when compared to the first stage LTHR at 710 K (figure 6.4). At 770 K the peroxy phenyl radical is the most positively sensitive species, similar to that seen for the second stage of LTHR at 710 K (figure 6.7), increasing from the 23rd most positively sensitive species for the first stage of LTHR HRR at 710 K. As temperature is increased further to 830 K, the sensitivity of HRR to the peroxy phenyl radical is reduced. Much lower concentrations of the species are present, as the increased temperatures limit the radical formation from the oxygen addition to phenyl radicals, which largely forms phenoxy radicals, followed by phenol. This can be seen in the increasing sensitivities of these species at 830 K, opposed to the large reduction in sensitivity for the peroxy phenyl radical (figure 6.4). Reaction sensitivity analysis results display large negative sensitivities for the formation of H_2O_2 from HO_2 radicals ($2HO_2=H_2O_2+O_2$), for the first stage LTHR at 710 K and total LTHR at 770 K. However, this reaction is absent from analysis results of the second stage LTHR. This is not due to a lack of importance, as a two factor increase in the pre-exponential A-factor for this reaction removes this secondary peak entirely, indicating the importance of HO_2 radicals (which are present in large concentrations during the second stage LTHR) in oxidation reactions at these conditions.

6.3.2 Accumulated Heat Release

An increase in peak LTHR HRR may not necessarily translate to an overall increase in the amount of heat released, and the duration of the heat release must be considered. The amount of heat released during LTHR can be quantified by the aHR at soITHR, wherein the soITHR is defined as the inflection point of the HRR gradient, after peak LTHR (or peak second stage LTHR) is observed. No clear end to LTHR is present at the 830 K condition, as the peak LTHR leads directly into higher temperature heat release behaviour. Therefore, no point can easily be

defined which consistently marks the end of LTHR for the calculation of soITHR aHR. Percentage differences in the soITHR aHR at temperatures of 710 and 770 K (wherein clear LTHR is present), resulting from a +5 kJmol-1 change in the enthalpy of formation for each species, can be seen in figure 6.12. Species which produce significant changes in the aHR soITHR are near identical to those highlighted for producing changes in the soITHR temperature, as seen in figures 6.12 and 6.13. As such, the normalised sensitivity coefficients for both characteristic heat release properties are not displayed here, as this would be largely redundant. Normalised sensitivity coefficients for the brute force sensitivity analysis of soITHR aHR, due to a +5 kJmol-1 change in the enthalpy of formation for each species, are shown in figure 6.14 for temperatures of 710 and 770 K. Figures 6.12 and 6.13 display a significant amount of scatter in percentage differences for all species, which was not observed for the analysis of HRRs and IDT at temperatures of 710 and 770 K. This is potentially due to a combination of the analysis methodology, wherein chemical kinetic simulations applied an adaptive time-step, and the determination of the soITHR location.

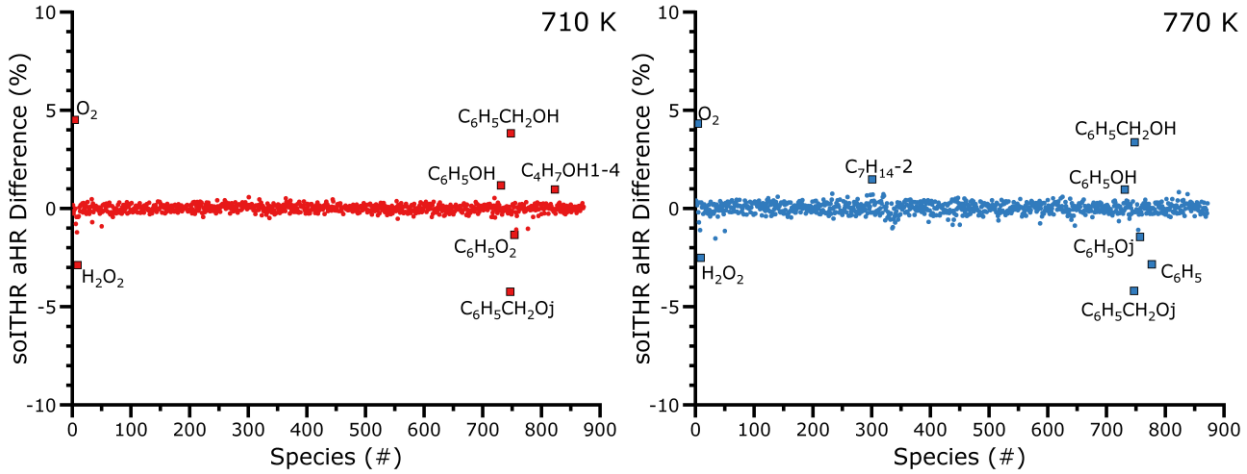

Figure 6.12. Percentage differences in the predicted aHR at the soITHR for 5-C constant volume simulations, due to a +5 kJ mol^{-1} change in species enthalpy of formation, at a temperature of 710 K. P_c=20 bar, Φ=1.0.

The most positively and negatively sensitive species observed for the sensitivity analysis of soITHR aHR (figure 6.14) are again benzyl alcohol and the benzyloxy radical, respectively. This is expected due to the apparent high degree of importance of these species in the determination of the rapidity of both LTHR phases (figures 6.4 and 6.7) and the prediction of IDTs (figure 6.2). Increasing the enthalpy of formation for benzyl alcohol encourages the forward progression of low temperature oxidation of this species, ultimately towards chain branching

reactions. These pathways are critical at all stages of LTHR, as shown in the previous analysis presented in this chapter. Therefore, this increase in enthalpy produces an increase in soITHR aHR. Alternatively, increasing the enthalpy of the benzyloxy radical limits the progression of low temperature oxidation for benzyl alcohol species, as the boundary for hydrogen abstraction is increased, causing a resultant decrease in the amount of LTHR and thus the soITHR aHR. The influence of uncertainties for the enthalpies of formation of these species has been discussed previously in the context of IDTs, but a large influence on the intensity and integrated heat release can also be observed in figures 6.3 and 6.12.

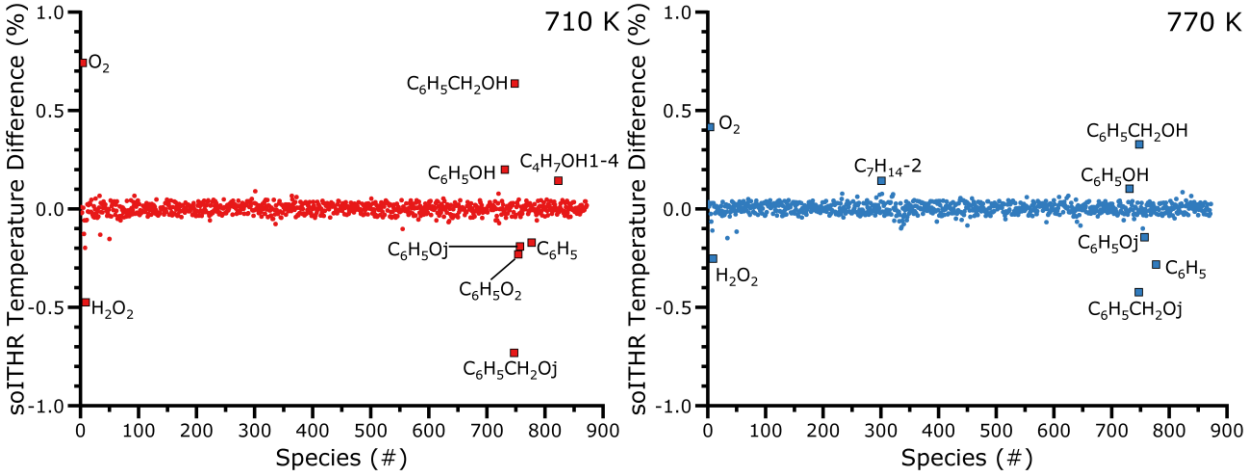

Figure 6.13. Percentage differences in the predicted temperature at the soITHR for 5-C constant volume simulations, due to a +5 kJ mol^{-1} change in species enthalpy of formation, at a temperature of 710 K. P_c=20 bar, Φ=1.0.

Contrary to sensitivity analysis for the HRR of the secondary LTHR peak at 710 K and the total LTHR at 770 K, soITHR aHR sensitivity analysis results show that the peroxy phenyl radical ($C_6H_5O_2$) is highly negatively sensitive for both 710 and 770 K conditions. Therefore, while an increase in the enthalpy of formation of this species causes an increase in the rapidity of second stage heat release, it produces a decrease in the total heat released. An increase in the peroxy phenyl enthalpy of formation increases the rate of production of phenyl radicals during the second stage of LTHR, leading to the further oxidation of aromatic species, increasing fuel reactivity. However, this same increase limits the formation of the peroxy phenyl radical at lower temperatures (such as the first stage LTHR), producing lower concentrations of the species to engage in second stage LTHR. Therefore, the second stage LTHR may appear more rapid (as phenyl radical formation is promoted from peroxy phenyl), but does not last as long, causing HRRs to decay faster and reducing the aHR for the LTHR process. The sensitivity

of aHR to this species at soITHR is somewhat limited however, due to the lack of sensitivity during the first stage of LTHR.

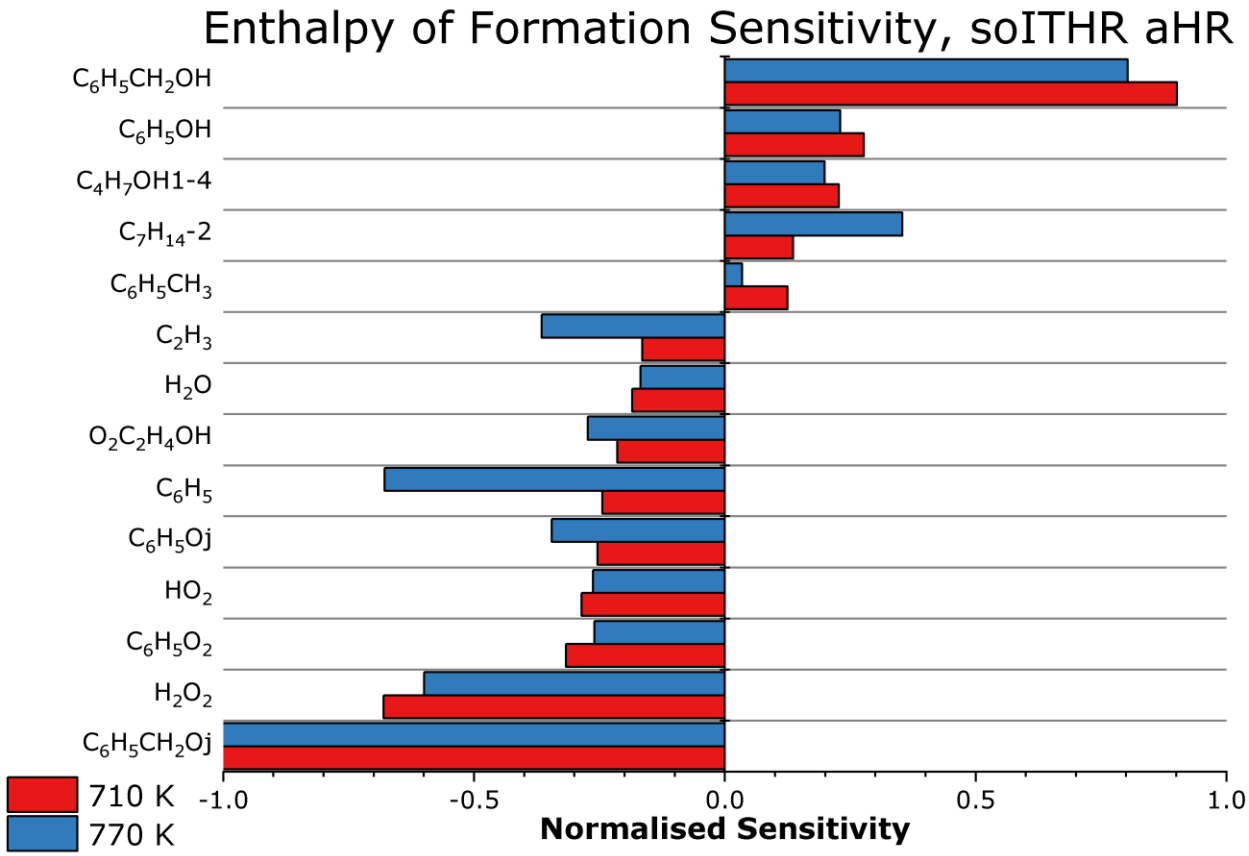

Figure 6.14. Normalised sensitivity coefficients for the soITHR aHR due to a +5 kJ mol^{-1} change in the enthalpy of formation of each species, for the 5-C surrogate at temperatures of 710, 770 and 830 K. P_c=20 bar, Φ=1.0.

Dominant reactions which influence the accumulation of LTHR, as determined via brute force sensitivity analysis of pre-exponential A-factors, are shown in figure 6.15 for 5-C simulations at temperatures of 710 and 770 K. These results show consistency with the corresponding sensitivity analysis results for LTHR peak values. Specifically, the hydrogen abstraction of fuel species again displays a high degree of sensitivity at both temperatures, as well as reactions characteristic of the resultant low temperature oxidation such as oxygen addition and internal isomerisation. Notably, the decomposition of H_2O_2 to produce 2OH radicals appears as negatively sensitive in this analysis, which is contrary to results observed for local OH sensitivity analysis at the same conditions (section 5.6). Significant quantities of H_2O_2 accumulate during LTHR due to the recombination of HO_2 radicals, which are generated in large concentrations. As temperature and pressure increase, a critical point is reached at which H_2O_2

decomposition into 2OH is initiated, causing degenerate chain branching and HTHR characteristic of autoignition [172]. Therefore, an increase in rate of this reaction initiates HTHR earlier, producing a more reactive fuel and shorter IDT. However, this earlier initiation brings HTHR forward and reduces the amount of observable LTHR prior to HTHR, thus reducing the amount of aHR at the soITHR. HO_2 recombination to form H_2O_2 is the most negatively sensitive reaction at both temperatures as this removes important HO_2 radicals from the system, reducing peak HRRs considerably (eliminating second stage LTHR at 710 K).

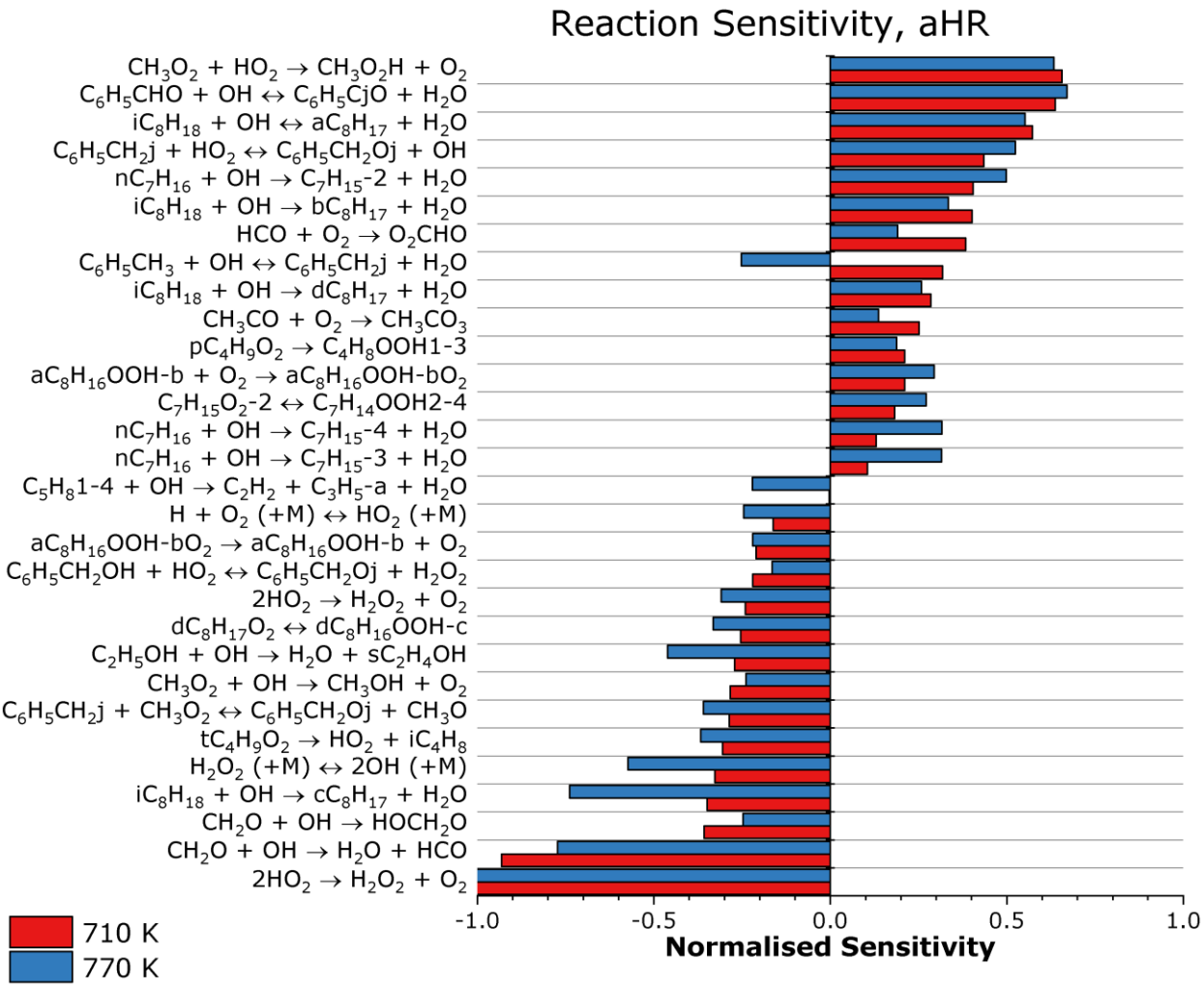

Figure 6.15. Normalised sensitivity coefficients for the soITHR aHR due to a 2 factor increase in the pre-exponential A-factor of each reaction, for the 5-C surrogate at temperatures of 710, 770 and 830 K. P_c=20 bar, Φ=1.0.

The presence of multiple reactions characteristic of the low temperature oxidation of fuel species, particularly for toluene oxidation, aligns with the results of enthalpy of formation sensitivity analysis for characteristic LTHR properties. This highlights the importance of correctly representing the thermodynamic properties of such species for the accurate prediction of LTHR behaviour by kinetic models. This is particularly the case for two stage LTHR, where the presence of this behaviour seems dependent on the equilibrium position of oxygen addition to the phenyl radical, where both forward and backward reaction rate parameters are not specified.

6.4 Summary

In this study, the sensitivity of model predictions for the IDT and characteristic LTHR properties to uncertainties in species enthalpy of formation has been evaluated, for chemical kinetic simulations of constant volume 5-C autoignition at temperatures of 710, 770 and 830 K, P_c=20 bar, Φ=1.0. Due to the importance of the enthalpy of formation in the calculation of reverse rates of reaction (where they are not explicitly stated within the kinetic mechanism), it is essential that the thermochemical properties of important species are accurately represented within a given model [371]. Small species are often well characterised through a variety of methods including experimental validation [333], quantum chemical calculations [334] and statistical optimisation approaches incorporating combined sets of data [335,336]. However, for larger more complex species, parameters are often derived from small numbers of experimental and theoretical studies, or estimated through methods such as Benson's GA [54,337].

For the combined mechanism applied within this study, the thermodynamic properties of each species are estimated via GA methodology [84,85]. This mechanism largely failed to represent the IDT behaviour of the 5-C surrogate, particularly within the NTC region, and predicted multi-stage LTHR behaviour for the fuel which was not observed in RCM HRA. Brute force sensitivity analysis of the IDT with respect to species enthalpies of formation (figure 6.2) revealed the importance of species associated with the low temperature oxidation of toluene and 1-hexene, which are known to suppress and promote low temperature reactivity, respectively [85]. The most sensitive species at temperatures which feature significant LTHR (710 and 770 K) were shown to be benzyl alcohol and the benzyloxy radical resultant from the hydrogen abstraction from the alcohol site. An increase in the enthalpy of formation of benzyl alcohol encourages this hydrogen abstraction, promoting the low temperature oxidation pathways associated with toluene, thus increasing reactivity, and decreasing IDT. An increase in the enthalpy of formation for the benzyloxy radical counteracts this, reducing the rate of hydrogen abstraction. Several low temperature oxidation associated species displayed

significant degrees of enthalpy of formation uncertainty, and differences between the values estimated by GA and those present in the literature were observed throughout. For the benzyloxy radical, the GA derived standard enthalpy of formation is given within the mechanism as 117 $kJmol^{-1}$, whereas G3B3 quantum chemistry calculation results available in Burcat's tables give a value of 125.9±8 $kJmol^{-1}$ for the standard enthalpy of formation for this species [176]. There is clearly a significant degree of uncertainty in the enthalpy of formation of this species which appears as highly sensitive in the prediction of the IDT and occurs in large concentrations during the oxidation of toluene [264,269]. Significant differences between GA derived enthalpies and those presented in Burcat's tables are also present for many species associated with the low temperature oxidation of toluene. Furthermore, the latest Burcat table presents significant uncertainties for the enthalpies of formation of many of these species of up to ±8 kJmol-1 [176]. These enthalpy uncertainties may propagate throughout the system and manifest in the global IDT as significant percentage changes to IDT predictions (figure 6.1).

Similar species appear as highly sensitive for the prediction of peak HRRs during the first phase of LTHR at 710 K and total LTHR at 770 and 830 K. In addition to toluene, hexene and alkane low temperature oxidation intermediates, an interaction between the LLNL gasoline surrogates mechanism [85] and the butanol isomers mechanism [84] lead to the formation of the sensitive 1-buten-4-ol. This species is formed through the interaction of small oxidation products, such as ethenyl radicals generated through the low temperature oxidation of 1-hexene, with C_2H_4OH produced during the oxidation of ethanol. This species is not present in the original gasoline surrogate mechanism and is introduced by the butanol isomers mechanism. This species displays particularly high sensitivity at 710 K, where an increase in the enthalpy of formation causes a significant increase in the magnitude of first stage LTHR (figure 6.3). A large degree of uncertainty in the enthalpy of formation of this species is observed, with significant differences between the GA derived value provided by the combined mechanism and values provided in the literature [361,362]. In general, brute force sensitivity analysis results for peak LTHR values due to changes in reaction pre-exponential A-factors highlighted the importance hydrogen abstraction reactions of the fuel species, showing significant site specificity. It is therefore important that the site relative reaction rates are accurately represented within the mechanism to facilitate the prediction of LTHR behaviour.

At 710 K, the model predicts a second delayed stage of LTHR which is not observed in the experimentally derived RCM HRA. Enthalpy of formation sensitivity analysis highlighted the importance of toluene low temperature oxidation intermediates in the determination of the peak

HRR for this behaviour. From these results, it is proposed that this behaviour arises largely due to shifts in the equilibrium of oxygen addition to the phenyl radical, forming peroxy phenyl. At low temperatures, large concentrations of the relatively unreactive peroxy phenyl radical are formed. As temperature increases, the equilibrium moves towards the phenyl radical and oxygen, which proceeds to final combustion products, increasing the radical pool. The increased radical concentrations promote the further low temperature reactivity of fuel species, which was previously inhibited by the formation of relatively stable species, creating a delayed stage of LTHR. Large uncertainties are present in the standard enthalpy of formation for many toluene intermediate species involved in this behaviour. A similar delayed heat release effect induced by toluene has been observed in a lean condition HCCI engine study of a TRF and gasoline [324]. Reaction sensitivity analysis again highlighted the importance of hydrogen abstraction reactions, initiating low temperature oxidation pathways. A large amount of small species reactions are also shown to be highly sensitive during the second phase LTHR, which are present in larger concentrations than the first stage heat release due to the prior low temperature oxidation and chain branching. Hydrogen abstraction of formaldehyde by OH radicals is the most negatively sensitive reaction in this case, due to the termination of OH, whereas the formation of CH_3O_2H and its subsequent decomposition show a high degree of positive sensitivity due to the generation of multiple radical species.

In general, these results highlight the need for the accurate thermochemical data of many species of relevance to prediction of surrogate autoignition behaviour. Accurate predictions of this behaviour are required if chemical kinetic models are to provide a suitable alternative to extensive ignition studies, with relevance to the investigation of alternative fuels. Species such as the oxygenated intermediates formed during low temperature degenerate chain branching, hydrocarbon species with similar molecular weights to liquid fuels, enols, ketones, and esters, largely lack reliable enthalpy of formation data [176,371]. Where possible, efforts should be made towards the determination these values through experimental means or through the application of high level theoretical calculations. The application of GA methodology provides an alternative method for the estimation of thermochemical parameters which are otherwise difficult to determine but relies on accurate group values. Groups which represent the OO and OOH moieties and their adjacent groups, typical of alkyl hydroperoxide, peroxy and peroxy hydroperoxide radical species, have been shown to produce large degrees of sensitivity in the derivation of enthalpy of formation values [184,187,355], which may propagate into model predictions such as IDT and LTHR properties. Recent efforts have been made to update individual group values for a wide range of species [354,372–374] and future efforts should

continue to focus in this area towards the reduction individual group uncertainties. However, currently no reliable database of up-to-date group values exists, which would serve as a useful resource for the development of accurate kinetic models.

7 Knocking Properties of iso-Butanol and Gasoline Blended Fuels in a Boosted Spark-Ignition Engine

7.1 Introduction

Currently, there is a demand for fuels of high anti-knocking quality, and a renewed interest in the knocking behaviour of alternative fuels, such as biofuels and their blends with conventional fossil fuels [41,47,51,52]. This is due to the potential of pressure boosted, downsized engines for the reduction of transport related GHG emissions. These engines reduce fuel consumption without sacrificing the output power, by employing pressure boosting systems such as turbo and superchargers, operating at higher CRs than conventional SI engines. However, the degree of pressure boosting and thus the effectiveness of downsized engines is limited by the problem of engine knock [41]. As discussed in section 2.2, conventional engine knock is initiated by the compression of unburnt gases during the combustion process by the propagating flame front, to temperature and pressure conditions high enough to accelerate chemical reactions in the unburnt gas, leading to autoignition [40]. This autoignition induces sonic pressure waves which further interact with the flame front, producing high frequency pressure oscillations within the engine cylinder, which interact with the cylinder surfaces. This causes the cylinder to vibrate, producing an audible ping, and potentially causing serious damage to the cylinder and piston head [40,49,58]. Engine knock and autoignition behaviours are dependent on the fuel composition and the evolution thermodynamic conditions during engine operation, and are governed chemical kinetics [375].

A thorough understanding of potential alternative fuels and their anti-knocking quality and autoignitive behaviour is required to facilitate the sensible use of such fuels in modern SI engine technologies. However, ignition and SI performance studies for alternative fuels such as iso-butanol and blends with gasoline in SI engines are uncommon [229,376–379], and studies of blends at boosted engine pressure conditions appear to be absent in the literature. There is therefore a need to determine the influence of iso-butanol blending on boosted SI engine performance and knocking behaviour. This chapter aims to characterise this by blending iso-butanol with a reference gasoline, at blending ratios of 5-70% iso-butanol by volume, investigating the onset of knock and the associated intensity for each blend by progressively

advancing spark timing further from TDC. The influence of iso-butanol blending on non-knocking ("normal") combustion is also investigated within the same boosted single cylinder research engine (LUPOE). The ability of the five component (5-C) surrogate to replicate the combustion and knocking behaviour of the reference gasoline within an SI engine is also investigated, as previous surrogates have proven ineffective at representing the reference gasoline under these conditions [52,255,274]. If models are to be developed for the accurate and consistent prediction of combustion behaviour within SI engines, surrogate fuels need to provide a robust representation of the combustion behaviour of gasoline. Such behaviour will need to be well represented by the surrogate under normal and knocking combustion, for neat fuels and blends with alternative fuels. If a surrogate can be produced which closely matches the blending behaviour of gasoline under these conditions and a detailed model is developed to replicate the trends of this surrogate, then computational modelling may be effectively utilised for optimisation of engine and fuel blends designs. While there are many RCM studies which test the fidelity of gasoline surrogate fuels [45,309,311,312,380], studies within SI engines are less common [241,381], while studies of low temperature combustion pressure boosted SI engines are rarer still [52]. Therefore, the results presented in this chapter, for the combustion behaviour of 5-C and iso-butanol blends also provide valuable data for the evaluation of detailed models.

7.2 Surrogate Representation of Gasoline

7.2.1 Normal Combustion

For the purposes of this study, normal combustion is classified as a combustion process wherein no anomalous engine phenomena such as knock, or pre-ignition are observed. Under these conditions, the representation of the reference gasoline by the developed 5-C surrogate can be seen in figure 7.1. This figure shows a comparison of the mean in-cylinder pressures for 5-C and gasoline, at spark advance timings of 2, 4, 6 and 8 CA°, with all knocking cases removed prior to the calculation of the mean pressure cycle. At spark advance timings of 2 CA° and 4 CA°, no knocking cases were observed for either fuel, thus the displayed mean pressure cycle is the average of all collected pressure cycles for each fuel. However, spark advance timings of 6 CA° and 8 CA° produced some knocking cases in each fuel, and these were removed before calculating the mean from only the normal combustion pressure cycles. For the 6 CA° cases, the influence of knock was minor and only three and four cycles were removed from a total of 24-26 firing cycles for the gasoline and 5-C, respectively. Therefore, the mean displayed in this case is a reasonable representation of the bulk behaviour of each fuel under normal combustion conditions. At 8 CA°, the presence of knocking combustion is much greater,

with only five normal combustion firing cycles observed for both gasoline and 5-C. Beyond 8 CA° no mean normal combustion pressure cycle is shown, as all firing cycles displayed some degree of engine knock.

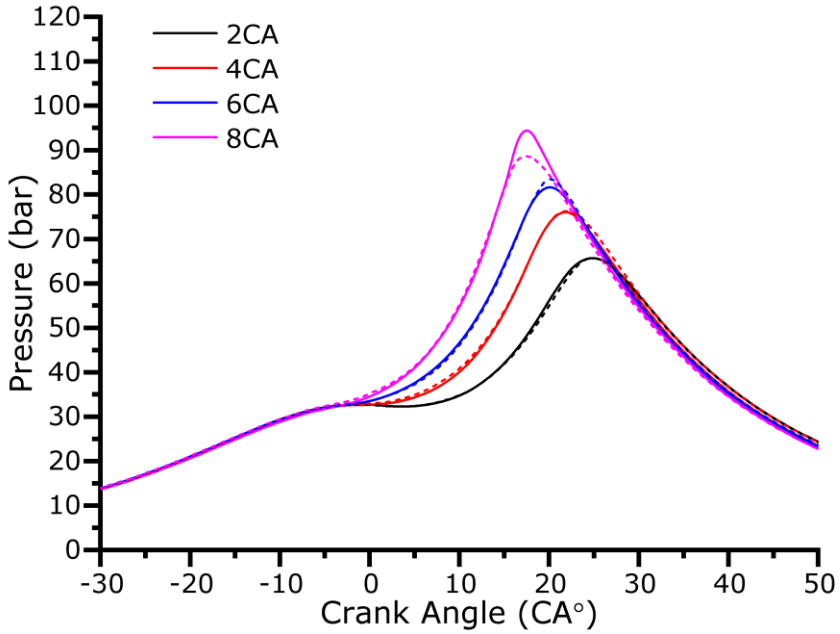

Figure 7.1. Mean in-cylinder pressure measurements under normal combustion, at spark advance timings of 2-8 CA°. Solid lines show mean 5-C pressures. Dashed lines show mean gasoline pressures. Engine speed=750 RPM, intake temperature=323 K, intake pressure=1.6 bar and Φ=1.0.

For a spark advance of 2 CA°, the mean pressure profile for the 5-C shows no significant differences with that of the gasoline. The surrogate matches the gasoline well in terms of the mean peak pressure (65.7 bar for both fuels), the crank angle location of the peak pressure (24.8 CA° for both fuels) and the evolution of the pressure rise due to combustion, as shown by the gradient of the mean pressure profile in figure 7.2. In previous studies, the peak pressure has been applied as a proxy value for the burning rate when investigating fuels of comparable calorific values [50,52,254]. A previous study investigated the representation of the same reference gasoline by a three component, TRF surrogate [52]. This previous study showed that, at a spark advance timing of 2 CA°, the TRF produced a significantly lower peak pressure and pressure rise rate during normal combustion, indicating a lower burning velocity than the reference gasoline. This behaviour was attributed to the composition of the TRF, which contained much more paraffins, particularly the relatively slow burning iso-octane. The TRF also contained no ethanol or olefinic components, which are present in the reference gasoline and

have been shown to have higher burning velocities than iso-octane and toluene [382]. The 5-C surrogate has been designed to represent the volume fractions of ethanol, olefins, and aromatics in the reference gasoline (as described in section 3.2), producing an accurate representation of the gasolines burning rate and pressure evolution during normal combustion.

The mean pressure cycles for 5-C and gasoline are also near-identical at a spark timing of 4 CA° bTDC. Mean peak pressures for the 5-C and gasoline are 76.1 bar and 76.3 bar, respectively, located at a crank angle of 21.9 CA° after top dead centre (aTDC) for both fuels. The development of the pressure rise due to combustion is shown for this condition in figure 7.2 and is again strikingly similar between the reference gasoline and the surrogate. The previous work of Agbro et al. [52], showed that, at these same conditions, the TRF surrogate gave a somewhat better representation of the mean gasoline pressures at 4 CA°, as opposed to 2 CA°. However, the TRF produced several knocking cycles at this spark timing which were not removed from the mean pressure cycle, as stated in the original study and observable in the faster burning rate and higher peak pressure of the TRF with respect to the other investigated fuels [52]. In the work displayed in this chapter, neither the 5-C or gasoline displayed any knocking cycles at this spark timing, and the representation is significantly better than that seen in the previous TRF studies [52,255,274].

As spark timing is advanced further (to 6 CA° bTDC), a small amount of knocking cycles are observed for both the 5-C and gasoline fuels. By discounting these cases in the calculation of the mean pressure cycles, only the normal combustion cycles are accounted for. It can be seen in figure 7.1 that, at these conditions, the 5-C and gasoline again produce a largely similar mean cylinder pressure profile. However, gasoline does display a larger mean peak pressure than the 5-C in this case, with values of 83.5 bar and 81.7 bar, respectively (an increase of ~2%), indicating a slightly faster burn rate for gasoline. The crank angle location of these peak pressures is the same for each fuel (20.1 CA°), and the first pressure derivatives for each fuel only show minor differences (figure 7.2). As such, the 5-C surrogate continues to provide an accurate representation of the normal combustion of gasoline, in terms of the evolution of the mean pressure profile. While the difference in peak pressure is minor, it may be indicative of the lower octane sensitivity (*S*) of the 5-C fuel (8.1 as compared to 8.8 for the reference gasoline), which indicates a slower increase in reactivity as temperature and pressure conditions increase, relative to the reference gasoline. As spark timing is advanced, the temperature of the unburnt gas post-spark increases [255], thus an advancement of spark timing from 4 CA° to 6 CA° bTDC would see a greater increase in reactivity for the gasoline than the 5-C, as illustrated by a

faster burning rate or a larger mean peak pressure for normal combustion conditions. This difference may also be attributed to a large fraction of iso-octane in the surrogate, which is larger than the total fraction of all paraffins in the reference gasoline. Branched alkanes typically display slower burning velocities than straight chain alkanes of similar length. Also, the naphthenic content of the gasoline is not represented at all in the surrogate, which has been shown in the literature to produce similar burning velocities to straight chain alkanes [383,384]. Therefore, differences in the bulk burning velocity of the surrogate and the gasoline may exist, which become apparent at advanced spark timings. The burning velocity of a fuel affects the engine efficiency and the burn rate of the fuel, therefore impacting the peak pressure also [385].

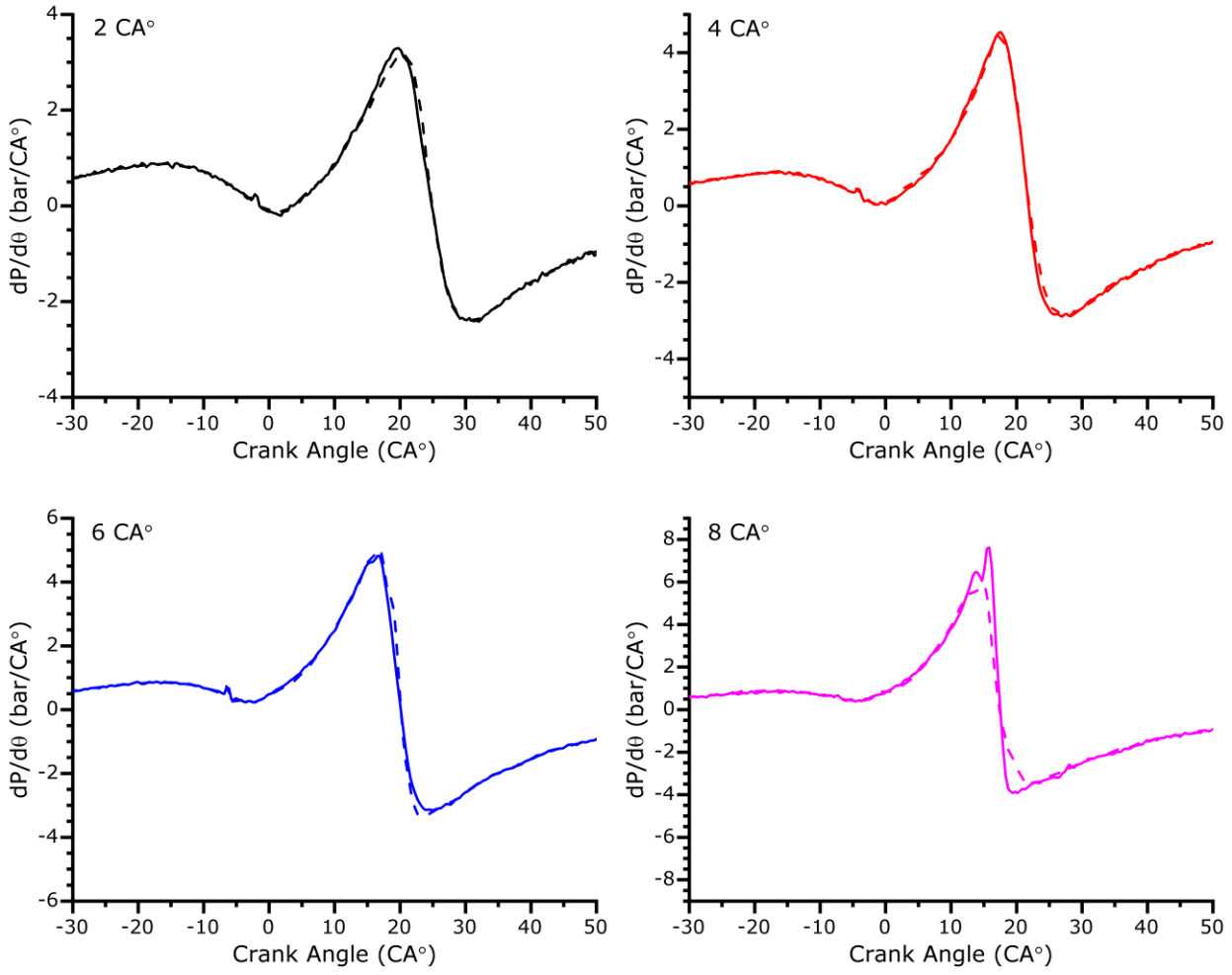

Figure 7.2. First pressure derivatives for the mean pressure cycles of 5-C and gasoline, for normal combustion cases. Solid lines show mean 5-C pressures. Dashed lines show mean gasoline pressures. Engine speed=750 RPM, intake temperature=323 K, intake pressure=1.6 bar and Φ=1.0.

At the final spark advance timing condition in which normal combustion can be observed (8 CA°), the majority of cases demonstrate knocking behaviour. These knocking cases are identified by calculating the second pressure derivative at each crank angle step, for each firing cycle, and scanning this data for values which exceed a pre-defined knock boundary value, as discussed in section 3.4.4. At this condition, the mean peak pressure achieved by the 5-C is significantly larger than that achieved by the gasoline, with values of 94.5 bar and 88.7 bar (an increase of 6.5%) occurring at crank angles of 17.6 CA° and 17.3 CA° aTDC, respectively. The pressure gradients also display differences, with a higher peak gradient for the 5-C, as well as the presence of two distinct peaks. This latter observation indicates the presence of a secondary pressure regime, which may be attributed to autoignition of unburnt gases, which was not intense enough to achieve the minimum second pressure derivative boundary value required to be distinguished as a knocking cycle during analysis. The presence of such cases in the calculation of the mean pressure cycle may also explain the higher peak pressure observed for the 5-C, particularly as this is contrary to the behaviour observed in the transition from 4 to 6 CA° spark advance timing.

In general, as spark timing is advanced further from TDC, several trends relating to the mean normal combustion pressure cycles can be observed for both gasoline and 5-C. Mean peak pressure increases as the spark timing advances, whereas the crank angle of this peak decreases, moving closer towards TDC. This increase in mean peak pressure and rate of burning can be attributed somewhat to the increase in unburnt gas temperatures as spark timing is advanced [255]. While the crank angle location of the mean peak pressure appears to move earlier in the cycle with respect to TDC, when investigated relative to the spark firing, the location is roughly constant between 4 and 6 CA° bTDC spark timing, as shown in table 7.1. This may be due to the removal of knocking cases at 6 CA° bTDC spark timing, which tend to occur in “fast” cycles. These fast cycles are defined as any cycle with a peak pressure greater than the mean peak pressure plus one standard deviation, whereas slow cycles are the mean peak pressure minus a standard deviation. Similar definitions have been applied to characterise SI engine cycles in the literature [50,52,57,386]. The removal of fast cycles could decrease the calculated mean peak pressure and retard the crank angle location of this peak. This can be observed in the small increase in the difference between the peak pressure crank angle location and spark timing, from 4 to 6 CA°, as well as the smaller comparative peak pressure increase due to this change, when compared to the peak pressure change displayed by a transition from 2 to 4 CA° and 6 to 8 CA°. Also, the peak positive and negative pressure gradients can be seen to increase with advancing spark timing, indicating a more rapid pressure rise and decrease,

and a faster rate of burning. At a spark timing of 8 CA° bTDC, mean peak pressure occurs earlier for the gasoline than 5-C, which may indicate a higher degree of reactivity for gasoline. However, due to the prevalence of knocking combustion at this condition, few normal combustion cycles are seen for both fuels. Therefore, this difference cannot definitely be attributed to the mean combustion behaviour of the fuels at this condition and would require the collection of more normal combustion cases before conclusions can be made based on these results. In general, the 5-C surrogate produced a good representation of the reference gasoline's mean pressure development during normal SI combustion, particularly when compared to a three component TRF surrogate investigated in the literature [52,255,274,381]. This high degree of accuracy in the representation of gasoline by the surrogate was also observed in the fuels autoignition behaviour, as shown in RCM IDT measurements shown in section 5.2.

Table 7.1. Mean peak pressures and the associated crank angle locations for the normal combustion of gasoline and the 5-C surrogate, as well as the associated coefficients of variation. The crank angle change from ignition is the difference between the spark timing (bTDC) and the crank angle location of the peak pressure (aTDC).

Fuel	**Spark Timing (CA° bTDC)**	**Mean Peak Pressure (bar)**	**Crank Angle Location (CA° aTDC)**	**CoV_{Pmax} (%)**	**Crank Angle Change from Ignition (CA°)**	**CoV_{CA} (%)**
Gasoline	2	65.7	24.8	7.5	26.8	6.2
	4	76.3	21.9	6.9	25.9	5.7
	6	83.5	20.1	5.4	26.1	7.6
	8	88.7	17.3	6.6	25.3	9.1
5-C	2	65.7	24.8	7.2	26.8	10.0
	4	76.1	21.9	7.3	25.9	6.7
	6	81.7	20.1	7.6	26.1	8.1
	8	94.5	17.6	2.6	25.6	4.2

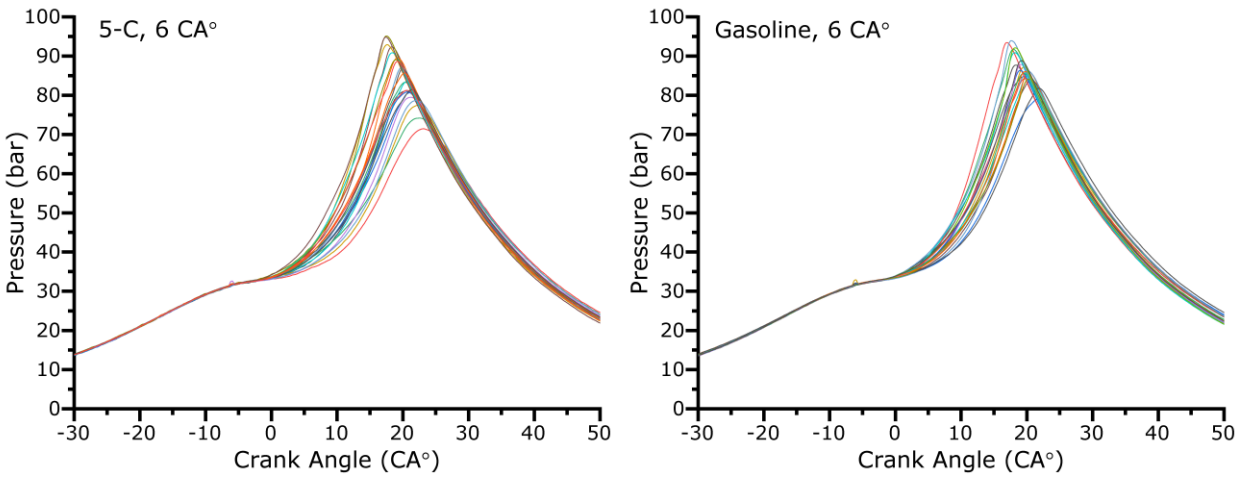

Figure 7.3. An example of the cycle to cycle variation for 5-C and gasoline normal combustion cases at a spark advance timing of 6 CA°. Engine speed=750 RPM, intake temperature=323 K, intake pressure=1.6 bar and Φ=1.0.

Cyclic variability in SI engine combustion describes the difference between in cylinder pressure evolution (and thus the power generated) on a cycle to cycle basis. Large degrees of cyclic variability can negatively impact SI engine performance, as it is common for spark timing to be optimised for the heat release profile of the most common cycle. Therefore, any significant deviation from this optimum cycle will cause a reduction in engine power and efficiency [49,50]. Furthermore, a large enough degree of cyclic variability (greater than 10% in terms of IMEP variability) causes a large degree of variability in engine speed, which is manifest as a deterioration in vehicle driveability which is noticeable to the driver [49]. This behaviour is observed when the engine is operated at nominally identical conditions and caused by variations in instantaneous rates of combustion between each cycle, with may be due to a number of potential sources [49,50,386,387]. These sources include mixture inhomogeneity within the cylinder (particularly near to the spark plug), spark discharge characteristics, trapped amounts of fuel, air and combustion residuals from previous cycles, and turbulence and charge motion during combustion. It has been suggested in the literature that the elimination of cyclic variability would have largely positive effects on SI engine performance, including a 10% increase in brake power output for the same rate of fuel consumption [388]. Examples of the cyclic variability for the 5-C and gasoline fuels, for normal combustion cases only at a spark timing of 6 CA° bTDC, can be seen in figure 7.3. At this condition, while the derived mean peak pressures are similar between the two fuels, the 5-C surrogate clearly displays a larger degree

of cyclic variability than gasoline. This behaviour is consistent with the increased degrees of uncertainty in IDT measurements of the 5-C with respect to gasoline, particularly at low temperatures (as seen in section 5.2).

The cyclic variability of 5-C and gasoline at each spark timing condition, for normal combustion cases, can be seen in table 7.1 as described by the CoV for the peak pressure and the crank angle location of the peak pressure. The CoV is equal to the standard deviation of the target property, divided by the mean of the target property, as described in section 3.4.4. At a spark advance timing of 2 CA°, the cyclic variability of peak pressure is similar for both 5-C and gasoline, with a slightly lower degree of variability for the surrogate. However, the degree of variability in the crank angle location of peak pressure is significantly higher for 5-C. As spark timing is advanced from 2 to 6 CA°, the degree of cyclic variability of peak pressure decreases for gasoline, but increases for the 5-C. Also, the 5-C continues to display a higher degree of variability in the crank angle location of peak pressure at all three of these spark timings. CoV values at 8 CA° bTDC spark advance are unreliable due to the small amount of normal (non-knocking) combustion cases at this spark timing. These results indicate that, for normal combustion, the 5-C generally displays a larger cyclic variability than the reference gasoline. A possible source of this increased variability may be the large amounts of toluene (>25 % by volume) in the surrogate blend, which has been shown to be sensitive to non-uniformities within temperature environments during RCM experiments [132]. It was also observed during LUPOE experiments, that the use of large amounts of toluene caused considerable carbon deposits within the engine cylinder which required regular cleaning. The presence of post-combustion residuals is known to increase cyclic variability [49,50,386]. These findings limit the viability of surrogates composed of large quantities of toluene within SI engines, such as those proposed by the formulation methods of Morgan et al. [389] and in the work of Kalghatgi et al. [390]. These high toluene concentration surrogates matched the RON and MON of the reference gasoline well but neglected the molecular composition. Morgan et al. [389] showed a reasonably good agreement between high toluene concentration surrogates and the reference gasoline in a HCCI engine. However, experience with such surrogates in the LUPOE and the knowledge that toluene combustion can rapidly form multiple soot precursors [391–394], dictates that these surrogates would lead to an increased propensity for soot formation, which is known to increase cyclic variability. A large degree of cyclic variability can be observed for such surrogates in an SI engine in the work of Kalghatgi et al. [390]. Therefore, for a surrogate to accurately represent the cyclic variability of gasoline, the aromatic content of the gasoline should be considered as a target during for surrogate formulation.

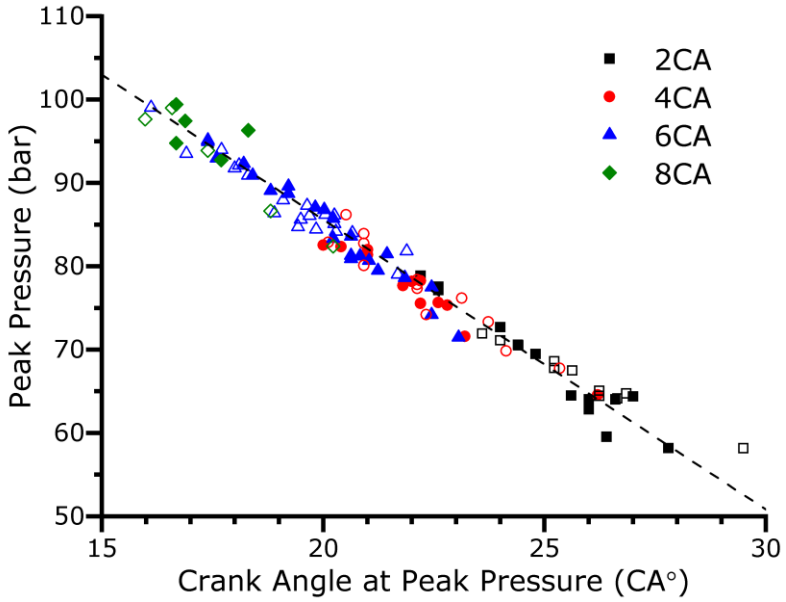

Figure 7.4. The correlation of peak pressures and the crank angle location of peak pressures for each normal combustion cycle of 5-C and gasoline. Solid symbols show 5-C measurements. Empty symbols show gasoline measurements. The dashed line shows a linear trendline drawn through all values for both fuels. Engine speed=750 RPM, intake temperature=323 K, intake pressure=1.6 bar and Φ=1.0.

The relationship between peak pressure and the crank angle location of peak pressure is largely linear, as outlined in previous studies [50,52,274]. This relationship can be seen in figure 7.4 for normal combustion cases of the 5-C and gasoline fuels. While the peak pressure and crank angle ranges for the two fuels are similar, some differences are apparent. At a spark timing of 2 CA° bTDC, a large degree of variability can be observed for both fuels. However, the 5-C displays several cycles which achieve a higher peak pressure earlier. Both fuels also display at least one case at this spark timing which produces a relatively low peak pressure at a large crank angle aTDC. In each case, these cycles occur early during the experimental procedure, when the engine is at its coolest. As the engine is operated, cylinder temperature increases due to the lack of any dedicated cooling system. Pressure and crank angle ranges for the two fuels at 4 CA° are similar, with a slightly larger crank angle range for the 5-C (as shown by a larger CoV). The range of peak pressures extends significantly lower for the 5-C than gasoline at a spark timing of 6 CA° bTDC, but achieves a similar range top-end, indicating that at this condition, the gasoline exhibits a faster burning rate than the 5-C, as shown by the mean peak pressure in figure 7.1. This behaviour correlates with an increased reactivity of gasoline at

low temperature RCM conditions, with respect to the 5-C, as seen in IDT measurements displayed in section 5.2 (figure 5.1).

7.2.2 Knocking Combustion

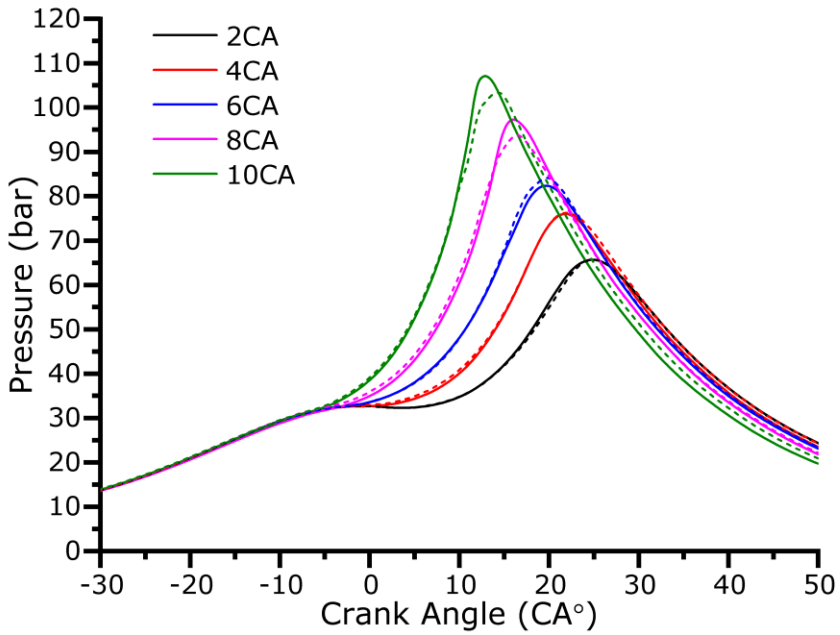

Figure 7.5. Mean in-cylinder pressure measurements for all combustion cases (normal and knocking), at spark advance timings of 2-10 CA°. Solid lines show mean 5-C pressures. Dashed lines show mean gasoline pressures. Engine speed=750 RPM, intake temperature=323 K, intake pressure=1.6 bar and Φ=1.0.

The influence of knocking combustion on the mean pressure cycles for 5-C and gasoline can be seen in figure 7.5, wherein the previously removed knocking cases exhibited at spark timings of 6 and 8 CA° have been included in the calculation of the mean cycle. Also presented are the mean pressure cycles at 10 CA° spark advance, which are composed entirely of knocking cycles. No knocking cycles are present at spark timings of 2 and 4 CA° bTDC, so the mean pressure cycles shown for these cases in figure 7.5 are identical to those displayed for the same spark timings in figure 7.1. Slight differences can be observed in the total mean pressure cycle, when compared to that for normal combustion cases only, at a spark timing of 6 CA° bTDC. The difference in peak pressures at this condition is the same as that displayed under exclusively normal combustion, but the magnitude of mean peak pressure is increased for both fuels due to the influence of high peak pressures associated with knock. The crank angle location of this mean peak pressure is also closer to TDC, due to the rapid pressure rise of knocking combustion cases. Values for mean peak pressure and the crank angle location of

mean peak pressure for the total combustion cases can be seen in table 7.2. This same trend can be seen to a higher extent at a spark timing of 8 CA°. This disparity in mean peak pressures observed at this spark timing for normal combustion cases is also present when the influence of knock is considered and continues to be present at a spark timing of 10 CA° bTDC. This indicates that the advancement of spark timing, and the associated increase in unburnt gas temperatures during the cycle [59,255], leads to a degradation in the surrogate's representation of gasoline. This is contrary to behaviour observed in the literature for a three component TRF surrogate, which saw an improvement in the representation of the mean pressure cycle of gasoline as spark timing was advanced [52].

Table 7.2. Mean peak pressures and the associated crank angle locations for the combustion (normal and knocking) of gasoline and the 5-C surrogate. The crank angle change from ignition is the difference between the spark timing (bTDC) and the crank angle location of the peak pressure (aTDC).

Fuel	**Spark Timing (CA° bTDC)**	**Mean Peak Pressure (bar)**	**Crank Angle Location (CA° aTDC)**	**CoV_{Pmax} (%)**	**Crank Angle Change from Ignition (CA°)**	**CoV_{CA} (%)**
Gasoline	6	84.2	19.8	5.9	25.8	12.7
	8	93.8	16.5	7.7	24.5	12.1
	10	103.4	14.4	5.9	24.4	13.5
5-C	6	82.4	19.8	8.6	25.8	9.7
	8	97.3	16.2	4.5	24.2	8.1
	10	107.2	12.9	3.4	22.9	8.6

For knocking conditions, the mean peak pressure is no longer a reliable proxy for the burning rate of the fuel due to the presence of autoignition [52]. However, for fuels with a similar burning rate (as determined for the gasoline and 5-C normal combustion cases) the crank angle location of the peak pressure in knocking cycles may indicate the susceptibility of the fuel to autoignition. In this regard, while the crank angle location of peak pressure is largely similar for the gasoline and 5-C fuels at 6 and 8 CA°, the 5-C reaches a peak pressure 1.5 CA° earlier than gasoline at a spark timing of 10 CA° bTDC. This variation is minor and correlates with a shorter measured IDT for the 5-C than gasoline, at the highest investigated temperature of 870

K within the RCM, as shown in section 5.2 (figure 5.1). While temperature is not directly measured within the engine as part of this study, a previous modelling study of the LUPOE indicates that temperatures at the beginning of first stage heat release are approximately 750 K and 800 K, for spark timings of 6 and 8 CA° bTDC, respectively [395]. Intuitively, the temperature at this point for a spark timing of 10 CA° bTDC will be significantly higher. However, in general the representation of the gasoline's mean pressure cycle development by the 5-C is good, with or without the inclusion of knocking cycles.

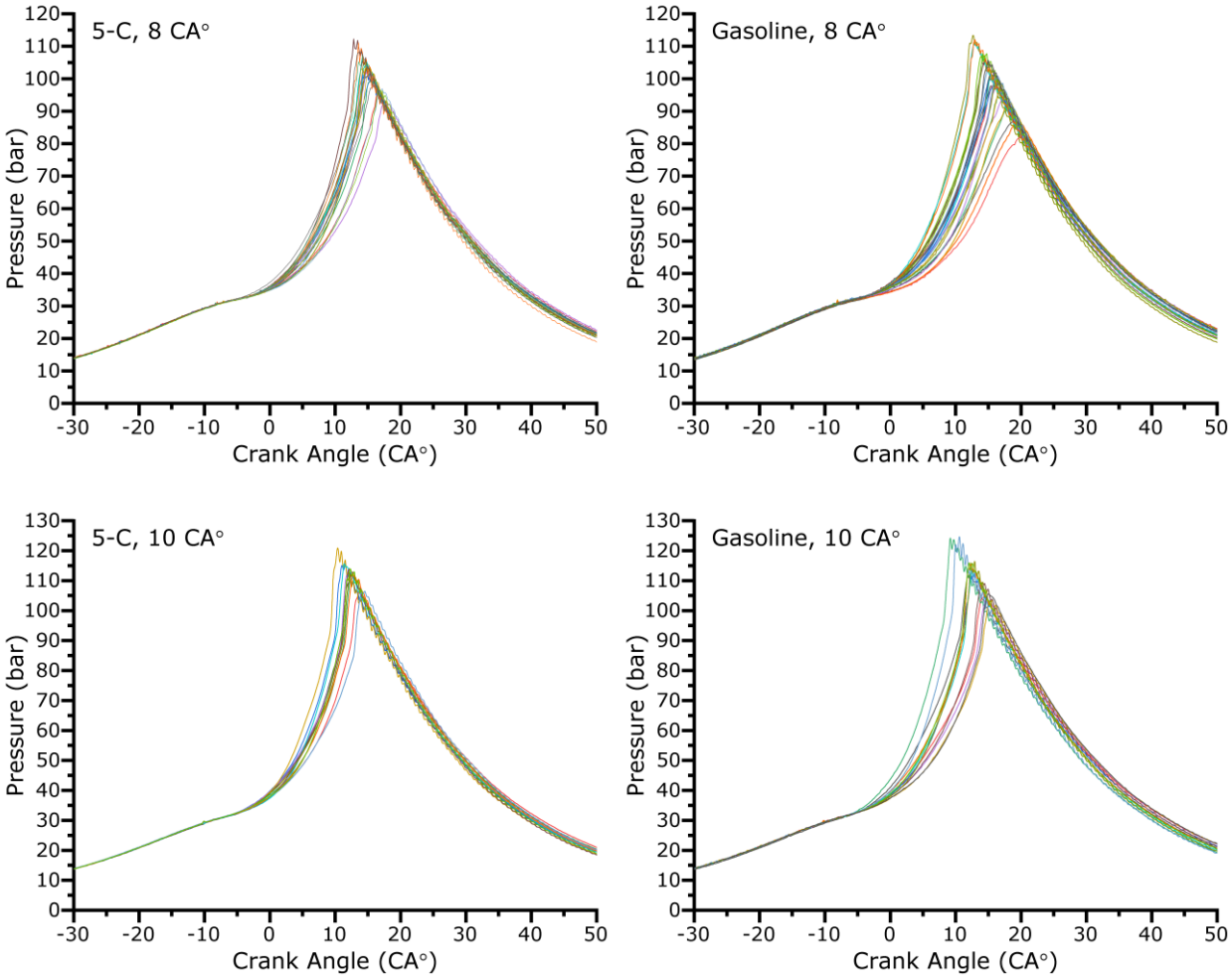

Figure 7.6. Examples of the cycle to cycle variation for 5-C and gasoline combustion cases, including prevalent knocking combustion, at a spark advance timing of 8 and 10 CA° bTDC. Engine speed=750 RPM, intake temperature=323 K, intake pressure=1.6 bar and Φ=1.0.

The cycle to cycle variation in pressures can be seen in figure 7.6, for spark timings which induce a large degree of knocking cycles. At spark timings of both 8 and 10 CA° the 5-C displays significantly less cyclic variability than the gasoline, which appears to be due to an

increase in the amount of slower gasoline cycles. This is contradictory to trends observed under normal combustion, wherein the 5-C typically displays a greater degree of cyclic variability. This appears to have also been the case for the previous study of a TRF mixture to represent the same reference gasoline at a spark timing of 8 CA° bTDC, with a large degree of engine knock [274]. Furthermore, this behaviour agrees with RCM measurements for the 5-C, which showed a small error in IDT measurements at the intermediate to high temperature range (~740-870 K), indicating a high degree of repeatability in the induction of autoignition. The degree of cyclic variability in peak pressure decreases as the spark timing is advanced further from TDC for both the gasoline and 5-C fuels, as shown by the CoV displayed in table 7.2. An increase can be observed in the CoV of the crank angle location of the peak pressure, when the spark timing is advanced from 8 to 10 CA° bTDC, despite an apparent reduction in the range and standard deviation of this value over all cycles, due to significant decrease in the mean location of peak pressure.

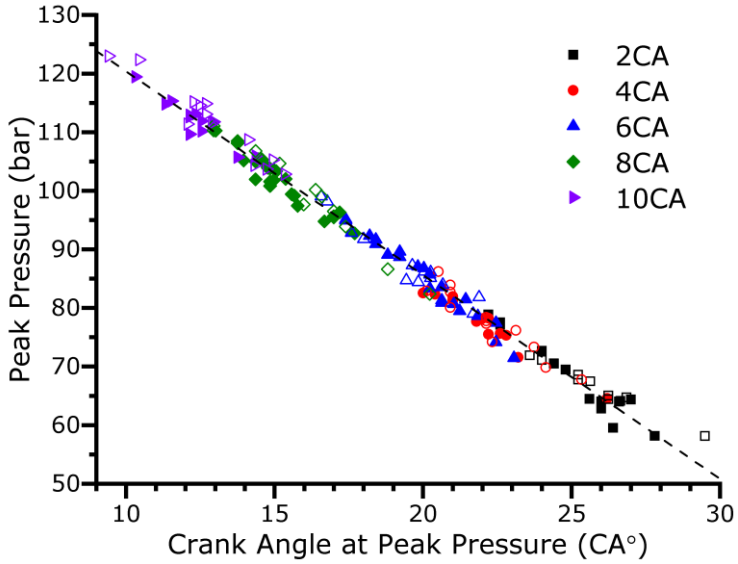

Figure 7.7. The correlation of peak pressures and the crank angle location of peak pressures for each combustion cycle (including knocking cycles) of 5-C and gasoline. Solid symbols show 5-C measurements. Empty symbols show gasoline measurements. The dashed line shows a linear trendline drawn through all values for both fuels. Engine speed=750 RPM, intake temperature=323 K, intake pressure=1.6 bar and Φ=1.0.

The relationship between peak pressure and the crank angle location of peak pressure is also linear when knocking cases are considered (shown in figure 7.7), as was the case for normal combustion cycles (figure 7.4). Both the 5-C and gasoline display similar ranges for peak pressures and the associated crank angle location. Higher peak pressures can be observed

closer to TDC for 5-C than gasoline at a spark timing of 8 CA°, whereas gasoline displays a lower range of peak pressures further from TDC, indicating a larger amount of slow cycles for gasoline. At a spark timing of 10 CA°, 5-C displays a smaller range of both peak pressures and the associated crank angle locations than gasoline, as reflected in the lower CoV values of the surrogate, indicating an increase in the amount of both fast and slow gasoline cycles.

KNs and knock intensities were calculated for both the gasoline and 5-C fuels, following the method described in section 3.4.4. The mean KNs and intensities are shown for spark timings of 6, 8 and 10 CA° bTDC in figure 7.8. Throughout all spark timing conditions, the 5-C produces an accurate representation of the reference gasoline in terms of both the KN and the knock intensity. At spark timings of 6 and 8 CA°, the KNs of the two fuels are near-identical, whereas at a spark timing of 10 CA°, there is a small under-representation of the gasolines KN by the surrogate. This indicates that, at the furthest spark advance timing, the 5-C surrogate autoignites marginally earlier in the engine cycle than the reference gasoline. This behaviour correlates well with RCM IDT measurements, which also showed a good representation of the autoignition behaviour of the reference gasoline (section 5.2). Small differences in RCM measured IDT times, such as 1-2 ms, may translate into differences as large as tens of crank angle degrees in SI engine KN. Therefore, the development of a surrogate that accurately matches both autoignition behaviour in an RCM and knocking propensity in an SI engine can be difficult. When compared to the previous TRF study [52,274], the 5-C produces a much better representation of the gasolines knocking propensity, particularly at a spark timing of 6 CA°, where the TRF was seen to autoignite much earlier in the cycle. This shows that the representation the gasolines composition by key species groups, such as paraffins, olefins, aromatics, and alcohols, produces a more accurate surrogate. Sources in the literature have also shown that the surrogates which represent more gasoline components tend to produce a more accurate representation of ignition behaviour, as shown for four, five and seven component surrogates in RCMs [45,309,380].

In the study of Khan et al. [396], the ability of a PRF and TRF to represent the KN behaviour of gasoline was evaluated within a normally aspirated SI engine. It was shown for these gasoline surrogates, that the TRF provided a reasonable representation of the gasoline's KN at a spark advance timing of 20 CA° bTDC but the PRF was significantly more reactive than the reference gasoline and the TRF, as well as displaying a larger variability in KNs. The TRF surrogate used in this study was designed to match the RON, MON and H/C ratio of the reference gasoline and not provide an exact match for the aromatic content. Modelling

predictions made for more complex four component surrogates in the study of Khan et aI. [396] showed that a surrogate designed to match the composition of the reference gasoline, in terms of matching iso-paraffin, n-paraffin, aromatic and naphthene concentrations, predicted KNs closest to those observed in the engine, when compared to the TRF and a four component surrogate based on the matching of octane quality properties. In the study of Sarathy et al. [241], surrogates of seven and eight components were developed to match multiple properties of reference FACE-F and FACE-G gasolines, respectively. The matched properties include RON, MON, H/C ratio, density, distillation characteristics, average molecular weight, carbon types and hydrocarbon groups (iso-paraffins, n-paraffins, olefins, naphthenes and aromatics). These surrogates were formulated using computational methodology described previously in the literature [397]. Knock intensities were measured at multiple spark timings for the seven and eight component surrogates (FGF-KAUST and FGG-KAUST, respectively), as well as the reference gasolines, within a CFR engine at RON-like and MON-like conditions. Both surrogates were capable of accurately capturing the knock intensity trends with advancing spark timing, with the eight component surrogate producing a more highly accurate reproduction of the reference gasoline behaviour [241]. While these previous studies display the importance of matching the broad chemical composition of gasoline in replicating knocking behaviour, generally, studies of surrogate behaviour within SI engines are rare, particularly when compared to studies produced in fundamental setups such as RCMs. Also, studies at boosted SI engine pressure conditions relevant to low temperature combustion appear to be mostly absent from the literature, making the results presented in this section for the representation of gasoline's knocking behaviour by a five component surrogate, at boosted SI engine conditions, unique. When compared with the IDT measurements presented in section 5.2 (figure 5.1), it would appear that a good representation of gasolines knocking behaviour in the engine, correlates with a good representation of homogeneous IDTs in the RCM. Spark advance timings of 6-10 CA° bTDC correlate with end gas temperatures during the onset of first stage heat release of ~750-850 K [52,395]. Within this temperature range, IDTs for the gasoline and 5-C are very closely matched, which coincides with an excellent representation of knocking behaviour within the engine. At a compressed temperature of 870 K, gasoline displayed slightly longer IDTs than 5-C, whereas from ~770-830 K the two fuels produced IDTs within uncertainty limits of each other. This lower reactivity for gasoline at the higher temperature end of the scale is also present in KN measurements. These trends indicate that the RCM is a useful tool for assessing the capabilities of a surrogate for use in an SI engine, at least under the conditions investigated in this study.

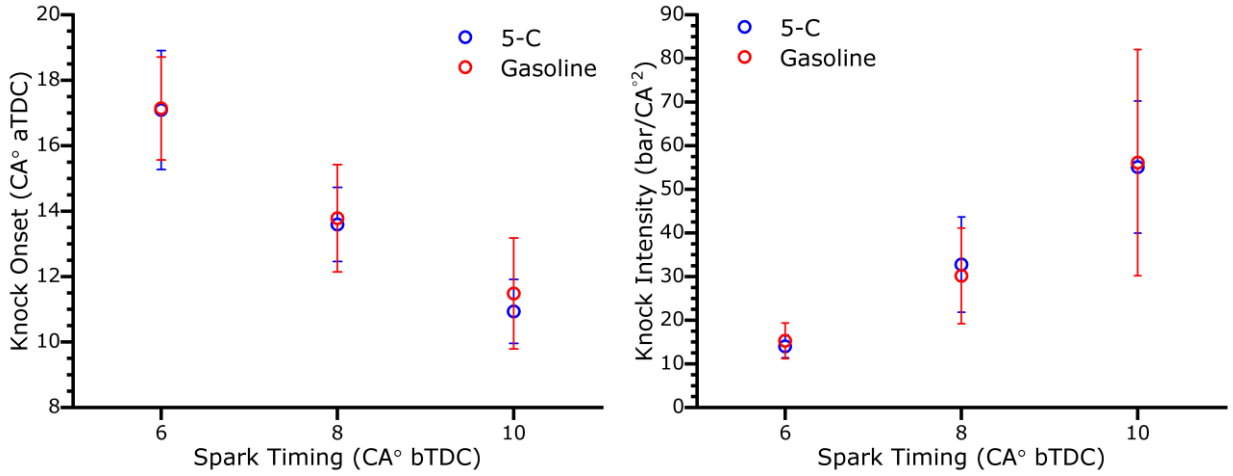

Figure 7.8. Mean KNs (left) and intensities (right) for 5-C and gasoline fuels, at all spark timings which displayed knocking cases. Error bars represent the standard deviation of values for each condition. Engine speed=750 RPM, intake temperature=323 K, intake pressure=1.6 bar and Φ=1.0.

At spark timings of 6 and 10 CA° bTDC, the mean knock intensity for gasoline and the surrogate are practically identical, with a slightly more intense mean intensity for the 5-C at a spark timing of 8 CA° bTDC. For both fuels, as the spark is advanced further from TDC, the mean knock intensity increases and so does the standard deviation of knock intensities. This is due to both the intrinsic difficulty in the analysis of the amplitude of highly transient pressure waves, caused by autoignition of the end gas, and the increasing severity of these pressure waves with earlier autoignition [52]. Significant departure from the mean value for knock intensity will occur at severely knocking cases, as autoignition of the end gas can occur at spatially random points (the location of autoignition is not consistent on a cycle to cycle basis), and the location of this autoignition site influences the measured knocking pressure amplitude [40,59].

The relationship between knock intensity and KN can be seen in figure 7.9 for each knocking cycle of the 5-C and gasoline fuels. Also seen in this figure is the relationship between peak pressure and KN for the same set of knocking cycles. Both the knocking intensity and peak pressures increase with spark advancement further from TDC and with decreasing KNs, for both the gasoline and 5-C. Therefore, as the occurrence of autoignition of the end gas moves earlier (towards TDC), the piston is closer to TDC and autoignition will occur under higher pressure conditions. While the relationship between knock intensity and onset, at a given spark timing appears to be linear, as seen in previous studies [52,255,274], the overall trend

(totalling all spark timings for both gasoline and 5-C) is clearly non-linear, with the knock intensity increasing by greater amounts as the KN decreases and spark timing is advanced. The range of KNs, peak pressures and knock intensities is generally consistent between the surrogate and gasoline, however, at 10 CA° spark advance bTDC the gasoline displays a larger range of values at both the range top and bottom, but still produces mean values similar to those of 5-C. This is representative of the larger degrees of error seen for gasoline in figure 7.8 at this spark timings, as well as the larger cyclic variability observed for the gasoline in figure 7.6 and table 7.2. Overall, the 5-C provides an excellent representation of the reference gasoline under both normal and knocking combustion, accurately reproducing KNs, knock intensities and mean firing cycle behaviour. This supports similar conclusions on the surrogate's proficiency made on the basis of RCM IDT measurements, as seen in section 5.2.

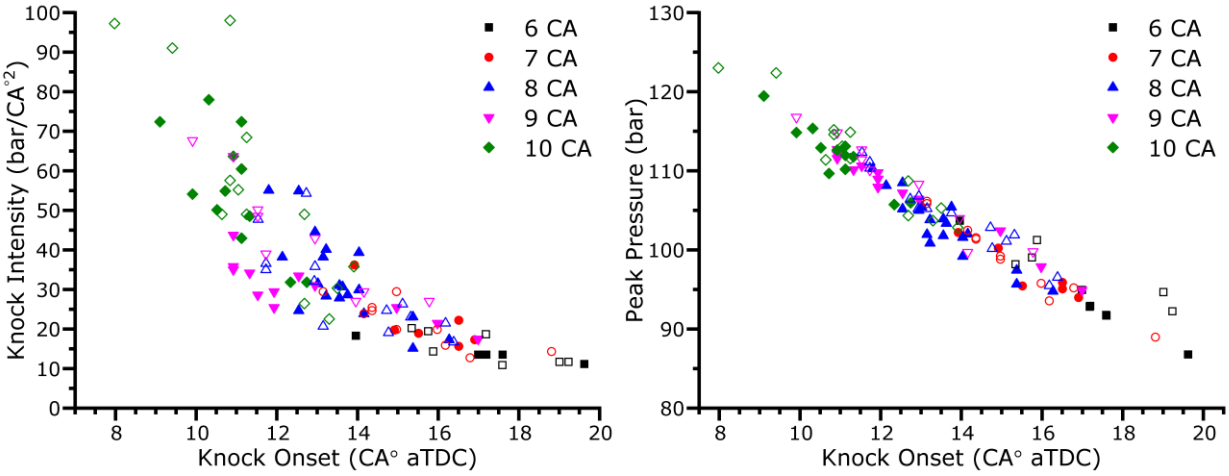

Figure 7.9. The relationship between KN and knock intensity (left), and peak pressure (right), for each firing cycle of the 5-C and gasoline fuels. Engine speed=750 RPM, intake temperature=323 K, intake pressure=1.6 bar and Φ=1.0.

7.2.3 Indicated Mean Effective Pressure

The indicated mean effective pressure (IMEP) is a fundamental engine parameter, independent of engine speed, number of cylinders and displacement of the engine. This property is a measure of the work output during a single piston cycle and can be calculated directly from cylinder pressure and volume data [398]. IMEP is defined as the indicated work per cycle per unit volume [49], it is a hypothetical pressure which when acting on the piston during the expansion stroke, results in the indicated work of the engine. For the purpose of this study IMEP can be determined by the integral of in cylinder pressure, as shown in equation 7.1 [399].

$$IMEP = \frac{1}{V_d}\int_{-180°}^{180°} P\, dV \qquad \text{Equation 7.1}$$

In this equation, P is the in cylinder pressure and V_d is the displaced volume. This calculation is essentially the determination of the area enclosed by the cycles *P-V* diagram. IMEP values are calculated for each firing cycle, using the measured in cylinder pressure and derived engine volume at each crank angle step. From knowledge of the IMEP and the geometry of the engine, the indicated power (IP) can be calculated as shown in equation 7.2.

$$IP = IMEP \times \frac{\pi B^2 L}{4} \times \frac{N}{60} \times \frac{n}{x} \qquad \text{Equation 7.2}$$

In this equation, B is the cylinder bore, L is the stroke length, N is the engine speed in RPM, n is the number of cylinders and x is the number of revolutions for one engine cycles (e.g. 1 for a two-stroke engine and 2 for a four-stroke engine). All of these parameters are fixed for the LUPOE as it is applied in this study, therefore, IP is simply equal to IMEP multiplied by a constant. For a given IMEP in units of Pa, $IP = IMEP \times c$, where $c = 6.11 \times 10^{-3}$.

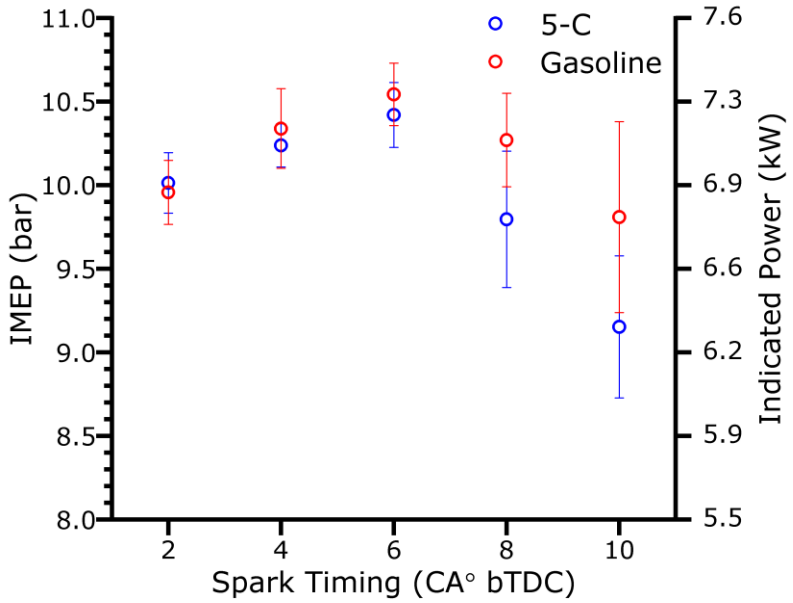

Figure 7.10. Mean IMEP values for 5-C and gasoline fuels at each spark timing condition. Error bars represent the standard deviation of IMEP values in each case. Engine speed=750 RPM, intake temperature=323 K, intake pressure=1.6 bar and Φ=1.0.

The mean IMEP values for 5-C and gasoline, at each spark advance timing (including both normal combustion and knocking cases) can be seen in figure 7.10. At spark timings of 6 CA° bTDC and below, the 5-C again gives a good representation of the reference gasoline, as

would be expected from the similar mean pressure behaviour at these conditions. As the presence of knocking cycles increases, at spark timings of 8 and 10 CA° bTDC, the 5-C displays significantly shorter IMEP values than gasoline, with both fuels displaying large error bars. This may be due to the intensity of knock induced pressure oscillations, which will impact the calculation of IMEP through the integral of the pressure cycle. Practically, this region is of limited relevance to the operation of SI engines, as optimal engine operation is designed to avoid these areas of significant knock. Therefore, an indication of the IMEP in this region would be of limited benefit for the design of optimal, non-knocking, engine modes or for the optimisation of fuel blends to achieve maximum power during normal combustion.

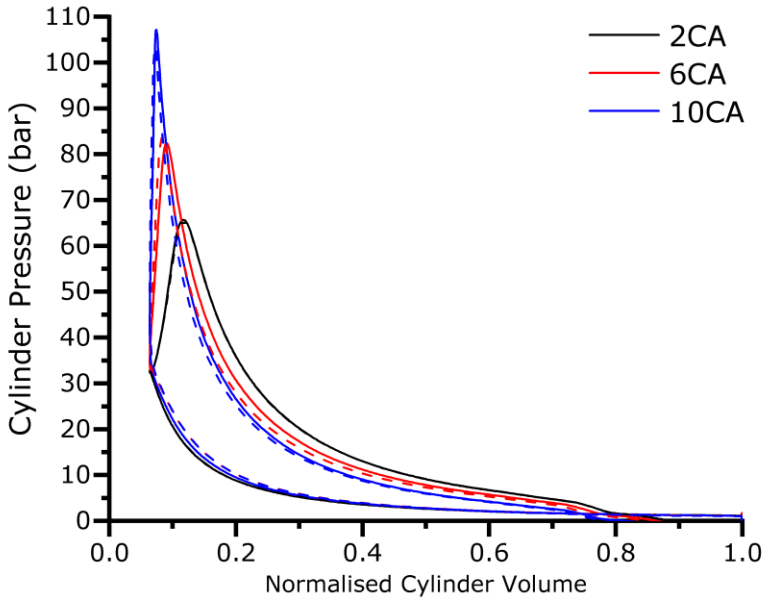

Figure 7.11. Mean *P-V* diagrams for 5-C and gasoline at spark timings of 2, 6 and 10 CA° bTDC. Solid lines show mean *P-V* diagrams for 5-C. Dashed lines show *P-V* diagrams for gasoline. Engine speed = 750 RPM, intake temperature = 323 K, intake pressure = 1.6 bar and Φ = 1.0.

For both fuels, IMEP increases with advancing spark timing until a spark timing of 6 CA°, decreasing thereafter. As spark timing is advanced further from TDC and the peak pressure occurs at a crank angle closer to TDC, a critical point is reached wherein a significant amount of the work done by the combustion of the fuel gas mixture occurs before the piston reaches TDC, working against the motion of the piston. An increase in this pre-TDC work due to further increases in spark advancements, causes a decrease in the total work output per cycle despite a larger peak pressure. This decrease in IMEP with increasing spark advancement beyond the optimal can also be demonstrated by the *P-V* diagrams of each case, as shown in figure 7.11. In this figure the mean *P-V* diagrams for 5-C and gasoline are shown at spark timings of 2, 6 and

10 CA° bTDC. It can be seen in figure 7.11, that the area enclosed by the cycle (which is equal to the IMEP) decreases marginally from a spark timing of 6 CA° to 10 CA°. While the peak pressure at a spark timing of 10 CA° is significantly larger, much of this occurs during piston compression (decreasing volume), whereas for spark timings of 2 and 6 CA° bTDC, the majority of the pressure rise due to combustion occurs post-compression (increasing volume).

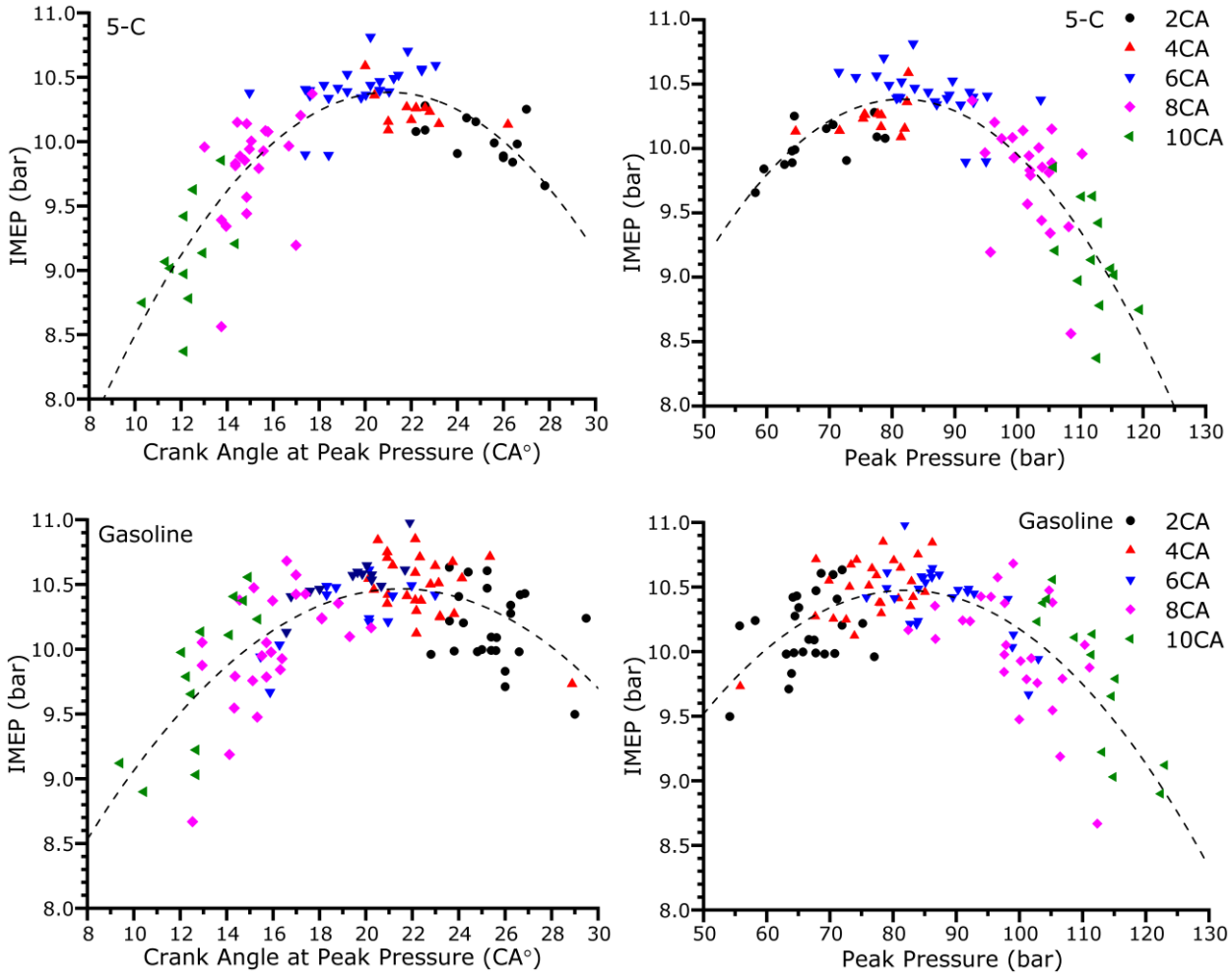

Figure 7.12. The relationships of IMEP to crank angle at peak pressure and peak pressure, for each firing cycle of 5-C and gasoline. Dashed lines show a polynomial trendline plotted through all cycles for the given fuel. Engine speed=750 RPM, intake temperature=323 K, intake pressure=1.6 bar and Φ=1.0.

The cyclic variability of the IMEP for 5-C and gasoline at all investigated spark advance timings can be seen in figure 7.12, which displays the relationship of IMEP to peak pressure and the crank angle location of peak pressure for each cycle. The non-linearity of the relationship between IMEP and the peak pressure can also be observed in this figure. For 5-C and gasoline,

the optimal peak pressure and crank angle location of peak pressure are similar and occur at spark advance timings of 4-6 CA° bTDC. The optimal peak pressures (to achieve the highest IMEP) for 5-C and gasoline are 81.5 and 82.0 bar, respectively, whereas the optimal locations of peak pressure are 21.0 and 21.5 CA° aTDC. Gasoline appears to display a larger cyclic variability in terms of IMEP, particularly at knocking conditions, which reflects the larger cyclic variability of gasoline in terms of peak pressures (seen in figure 7.6).

The 5-C surrogate has been shown in the above sections to provide an excellent reproduction of the normal and knocking combustion behaviour of the reference gasoline within an SI engine. Mean pressure cycles at all spark advance timings for 5-C produced a reasonable representation of the gasoline, with near identical mean cycles observed for normal combustion at spark advance timings of 2 and 4 CA° (figure 7.1, 7.5). The knocking propensity and intensity of the reference gasoline was also closely matched by the surrogate, reflecting the behaviour observed in RCM IDT measurements, which also showed a good representation of the gasoline's autoignition behaviour by the 5-C, at similar thermodynamic conditions (section 5.2). Finally, the IMEP of the 5-C (a measure of the work done by the combustion of the fuel mixture per cycle) produced a good representation of the reference gasoline up to spark timings of 6 CA° bTDC, and similar optimal values of peak pressure and the associated crank angle location were also largely similar. At more advanced spark timings, the influence of knock produced a large degree of variance in the IMEP calculated from in cylinder pressure trace. As such, it is difficult to compare the mean IMEP values under these conditions.

7.3 Influence of iso-Butanol Blending on Engine Performance

7.3.1 Normal Combustion

The influence of iso-butanol blending on the normal combustion of 5-C and gasoline within the LUPOE can be seen in figure 7.13, at a spark timing of 2 CA° bTDC, in terms of the mean pressure cycle for each fuel. It is necessary to evaluate the impact of iso-butanol blending on the combustion behaviour of gasoline under both normal and knocking conditions, to evaluate the viability of such blends for use in pressure boosted SI engines and determine the anti-knock capabilities of these blends. The ability of the surrogate to replicate the blending behaviour of gasoline under normal and knocking conditions also requires investigation, as the ultimate goal of such a surrogate would be to facilitate the modelling of gasoline/iso-butanol blend combustion within an SI engine. A surrogate which can accurately replicate the blending behaviour of gasoline would enable computational modelling to effectively optimise fuel blends, as well as engine design and operation. When assessing the ability of the surrogate to reproduce the

combustion behaviour of neat gasoline (section 7.2), RCM IDT measurements provided an accurate proxy for behaviour observed in the engine. The blending of iso-butanol with the base fuels provides an opportunity for further evaluation of RCM predictions, which showed complex fuel blending behaviour, particularly for blends of iB05 and iB10, as seen in section 5.3 (figures 5.8 and 5.9).

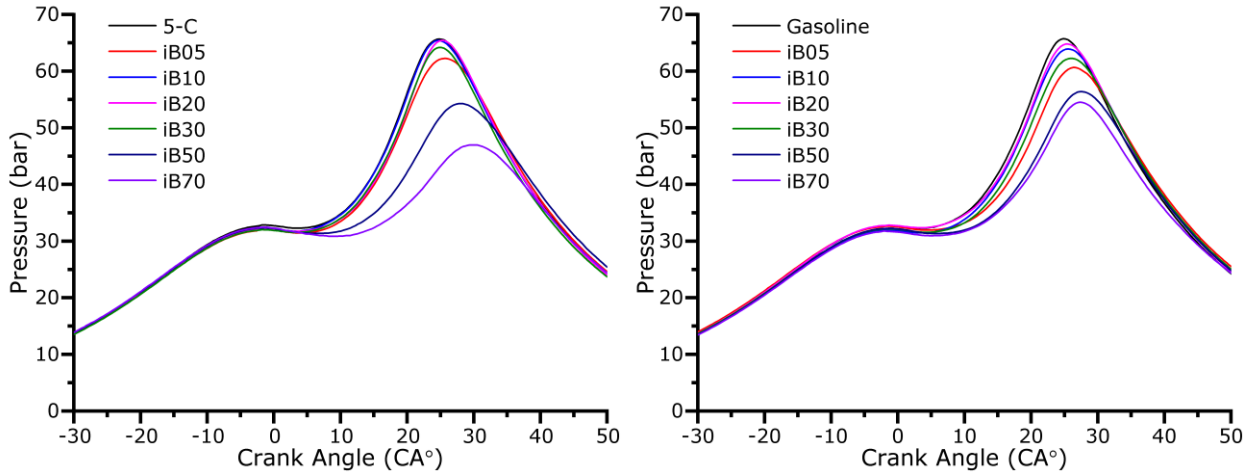

Figure 7.13. Mean pressure cycles for the normal combustion of iso-butanol blends with 5-C (left) and gasoline (right), at a spark timing of 2 CA° bTDC. Engine speed=750 RPM, intake temperature=323 K, intake pressure=1.6 bar and Φ=1.0.

Interestingly, increasing the blending level of iso-butanol appears to induce a non-linear response in the mean peak pressure for blends with both 5-C and gasoline. This can also be seen in table 7.3. A volume of 5% iso-butanol (iB05) produces a significant decrease in the mean peak pressure and an increase in the crank angle location of peak pressure, when compared to the neat 5-C and gasoline fuels. Generally, alcohols have been reported in the literature to display faster burning velocities than iso-octane and toluene (large components of the 5-C surrogate), which would cause an increase in the maximum pressure for fuels with similar calorific values [52,59,62,254,382,400]. In the literature, iso-butanol has been shown to produce laminar burning velocities similar but slightly faster than those of gasoline, iso-octane and toluene, at similar conditions [44,221,401,402]. Therefore, a blend of 5% iso-butanol may be expected to produce a slightly higher peak pressure than the unblended fuels, which is the opposite to the observed behaviour. In the RCM study presented in Chapter 5, the iB05 blend produced a significant reduction in the LTHR at the lowest investigated temperature of 710 K, when compared to 5-C. This suppression of LTHR at low temperatures may lead to a reduction in the charge heating of the end gas during normal combustion. While this process is beneficial

in terms of a fuels knock resistance (by lowering the end gas temperature and pressure) [403–405], under normal combustion peak pressures may be reduced. The suppression of LTHR and the increased burning rates due to iso-butanol blending are in direct competition, and the interplay between these behaviours due to blending may warrant further research for the determination of optimal fuel blends.

Table 7.3. Mean peak pressures and the associated crank angle locations of the peaks, for blends of iso-butanol with 5-C and gasoline at a spark timing of 2 CA° bTDC.

Base Fuel	**Iso-Butanol Content (vol%)**	**Mean Peak Pressure (bar)**	**CoV_{Pmax} (%)**	**Crank Angle Location (CA° aTDC)**	**CoV_{CA} (%)**
Gasoline	5	60.6	8.8	26.6	10.0
	10	63.9	7.6	25.5	7.6
	20	64.8	7.8	25.5	6.8
	30	62.3	8.3	25.9	7.9
	50	56.4	10.5	27.3	8.0
	70	54.5	18.3	27.3	18.9
5-C	5	62.3	10.4	25.5	9.7
	10	65.4	8.2	24.8	7.8
	20	65.4	5.9	25.2	5.2
	30	64.2	6.2	24.8	4.5
	50	54.3	17.1	28.1	11.7
	70	47.0	16.1	29.5	10.2

As the volume of iso-butanol is increased to 10% (iB10), the mean peak pressure increases relative to iB05, and the mean crank angle location decreases, as the increase in the blend's burning rate appears to impart significant influence. These mean values are similar to those displayed by the 5-C and gasoline fuels, as well as blends of 20% iso-butanol by volume. Previous studies of n-butanol blending with gasoline displayed similar behaviour for an investigated blend of 20% n-butanol [52,255,274]. Increasing the volume of iso-butanol further,

to 30% of the fuels total volume (iB30), produces a reduction in the mean peak pressure for both 5-C and gasoline blends. At blending ratios as large as this, the decrease is likely due to a significant decrease in the blends calorific value, due to the lower calorific value of iso-butanol in comparison to the reference gasoline [406,407]. The lower calorific value of the blends is in competition with the increase in burning rate of the pure iso-butanol, as a faster burning rate means that combustion can be completed at smaller cylinder volumes, earlier in the piston stroke [52]. This explains the near constant mean properties of iB10 and iB20 before the decrease in mean peak pressures when the blending ratio is increased to iB30.

Blends of 50 and 70% iso-butanol by volume (iB50 and iB70), continue the trend shown by iB30, decreasing the mean peak pressure with increasing iso-butanol content. This is most clearly seen for the 5-C blends in figure 7.13, wherein the iB70 blend clearly produced the lowest value for mean peak pressure, at the furthest crank angle from TDC. However, for the blends of iso-butanol with gasoline, iB70 only produces a marginally lower peak pressure than the iB50 case. The reason for this stark difference between gasoline and surrogate iB70 is unclear, as any compositional differences between the surrogate and gasoline will be minimised as the butanol blending ratio increases. A previous study of the blending of n-butanol with a TRF surrogate also displayed a lower peak pressure for a blend of 20% n-butanol, than that exhibited by the same blend of n-butanol and gasoline [52]. In this study it was proposed that peak pressure decreased for the TRF and n-butanol blend due to the slightly lower calorific value when compared to the same gasoline blend, which was amplified as more of combustion volume becomes significant later in the piston cycle. This may also be the case for 5-C blends of iB50 and iB70, which both display lower mean pressures than the gasoline equivalents at a later crank angle location, indicating more of the combustion process occurs at larger cylinder volumes. The significant reduction in mean peak pressures observed for large concentrations of iso-butanol would lead to a reduction in engine power for these blends, limiting their viability for use in SI engines at this spark timing. However, advancing spark timing further from TDC results in larger peak pressures (as shown previously for the neat gasoline and 5-C fuels in figures 7.1 and 7.5) and more engine power, providing that no knock occurs. An increase in the fuels knock resistance due to increased iso-butanol blending would facilitate the advancement of spark timing further, allowing for engine powers comparable to those of gasoline. This will be explored further in the following sections, which investigate the knock resistance of fuel blends and IMEP at various spark timings.

The cyclic variability of each fuel blend, for normal combustion at a spark timing of 2 CA°, can be seen in figure 7.14, which displays the relationship between peak pressure and the crank angle location of peak pressure for each firing cycle, and in table 7.3, which quantifies the cyclic variability by the CoV of peak pressure and the crank angle location. These target parameters are commonly investigated to quantify the cyclic variability [49,259,386]. The degree of cyclic variability at blends of 5-30% iso-butanol by volume, is similar to that exhibited by the neat 5-C and gasoline fuels, as seen in table 7.1 and figure 7.2. A reduction in cyclic has been shown in the literature for blends of gasoline and a TRF with n-butanol, which showed a reduction in cyclic variability at 20% n-butanol by volume [52]. This reduction appears to be absent in the blending of iso-butanol with gasoline, possibly due to the larger temperature sensitivity of iso-butanol in comparison with n-butanol. However, at blends of iB50 and iB70, the cyclic variability increases significantly, in terms of both the peak pressure and the crank angle location of peak pressure. This reflects behaviour exhibited by iso-butanol in the RCM (see Chapter 4), which displayed a large degree of sensitivity to temperature inhomogeneities within the RCM combustion chamber, as shown by the fuel's propensity for pre-ignition in the presence of turbulent mixing. The non-linear blending behaviour of iso-butanol with 5-C and gasoline can also be observed for the individual pressure cycles shown in figure 7.14, as cycles at iB05 display lower peak pressures, at crank angles further from TDC than the neat gasoline fuels. Peak values for iB10 and iB20 per cycle are then similar to the neat gasoline fuels, whereas blends of iB50 and iB70 decrease peak pressure at larger crank angle locations. For iB70, the 5-C blend displays several cycles which produce significantly lower peak pressures at larger crank angles than the matching gasoline blend, whereas the single lowest peak pressure for gasoline blends can be seen at a blending ratio of 50% iso-butanol. This increased cyclic variability at large iso-butanol concentrations limits their use in SI engines, as large cycle to cycle variations can limit engine performance. In SI engines, spark timing is usually optimised for the heat release profile of the most frequent cycle. Large deviations from this optimum cycle can lead to decreases in engine power and efficiency, with substantially large variations producing noticeable deterioration in vehicle driveability [49,50]. Therefore, it is important that fuel blends target the minimisation of cyclic variability, as well as improvements in knock resistance and engine power. In this regard, blends of 10-30% iso-butanol produce similar degrees of cyclic variability to the base gasoline.

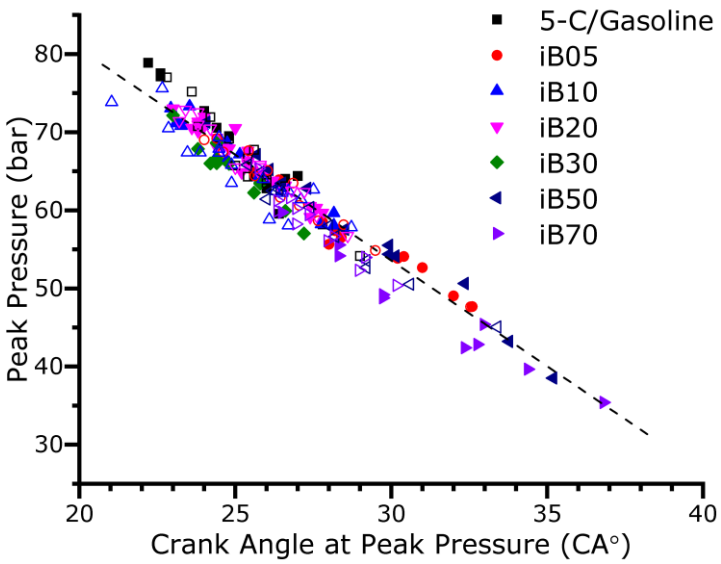

Figure 7.14. The correlation of peak pressures and the crank angle location of peak pressures for each normal combustion cycle of iso-butanol blends with 5-C and gasoline fuels, at a spark timing of 2 CA° bTDC. Solid symbols show 5-C blend measurements. Empty symbols show gasoline blend measurements. The dashed line shows a linear trendline drawn through all values for both fuels. Engine speed=750 RPM, intake temperature=323 K, intake pressure=1.6 bar and Φ=1.0.

7.3.2 Knocking Combustion

The influence of iso-butanol concentration on the KN, as spark timing is advanced further from TDC, can be seen in figure 7.15. Blends of iB30, iB50 and iB70 are not represented in this figure, as they did not display any knocking cases at the investigated spark timings before the maximum safe in cylinder peak pressure of 120 bar was achieved, indicating a high degree of knock resistance for these blends. Such blends would allow an engine to operate at high pressures, increasing engine efficiency. Also, for 5-C blends of iB05 and iB10 no knocking cases were observed below a spark timing of 8 CA° bTDC. However, knocking cases were observed at spark timings as low as 6 CA° for gasoline iB05, and 7 CA° for gasoline iB10, indicating a difference in the blending behaviour of gasoline and the surrogate. This is consistent with RCM results shown for iB10 blends in Chapter 5, which displayed slightly longer IDTs for the 5-C iB10, at a compressed temperature of ~770 K, which correlates well with the temperature expected at a spark advance timing of 7 CA° [52,395]. As previously discussed, small differences in IDT (1-2 ms) can translate to several tens of crank angle degrees, which may account for the lack of knock for the 5-C blends.

In general, it appears that increasing the concentration of iso-butanol causes an increase in the fuels knock resistance. However, non-linear behaviour is once again apparent at the lower blending ratios (iB05 and iB10), as was also observed for mean cycle peak pressures under normal combustion and RCM IDT measurements. At spark timings up to 8 CA° bTDC, iB05 displays a greater resistance to knock than the neat fuels, with iB10 displaying a further increase. At a spark timing of 9 CA° bTDC, the KNs of the iB05 and iB10 fuels crossover, with iB05 now displaying the greatest knock resistance. This behaviour is apparent for both 5-C and gasoline blends with iso-butanol, at the same spark timing. Measurements of IDT in the RCM also reflect this crossover behaviour between iB05 and iB10 (figure 5.8), at compressed temperatures of ~800-830 K, which correlates well with predicted end gas temperatures at these spark timings [395]. As spark timing is increased further (to 10 CA° bTDC, ~850 K in the RCM), a second crossover occurs and iB10 now displays the later KN of both the 5-C and gasoline blends, while the iB05 displays the earliest KN of gasoline blends. In general, at 10 CA° spark advance timing, the KNs of the neat fuels, iB05 and iB10 blends converge. Also, blends of 20% iso-butanol by volume display knocking cycles with an onset similar to this converged onset value, despite displaying no knocking cycles at shorter spark advance timings. This is representative of autoignition behaviour observed within the RCM, whereby measured IDTs for all blends converged at the highest investigated compressed temperature of ~870 K.

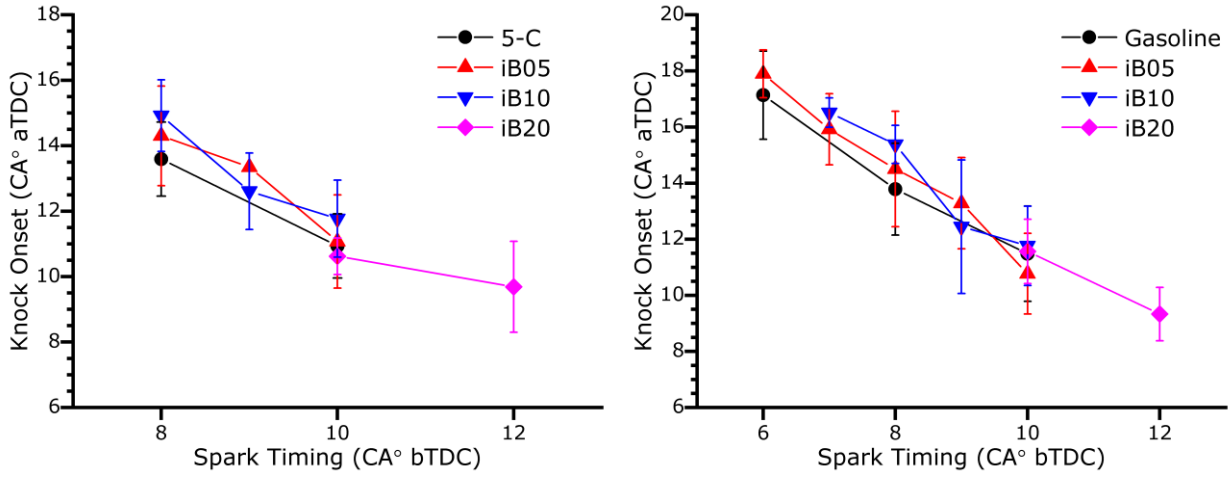

Figure 7.15. Mean KNs for iso-butanol blends with 5-C (left) and gasoline (right) fuels, at all spark timings which displayed knocking cases. Error bars represent the standard deviation of values for each condition. Engine speed=750 RPM, intake temperature=323 K, intake pressure=1.6 bar and Φ=1.0.

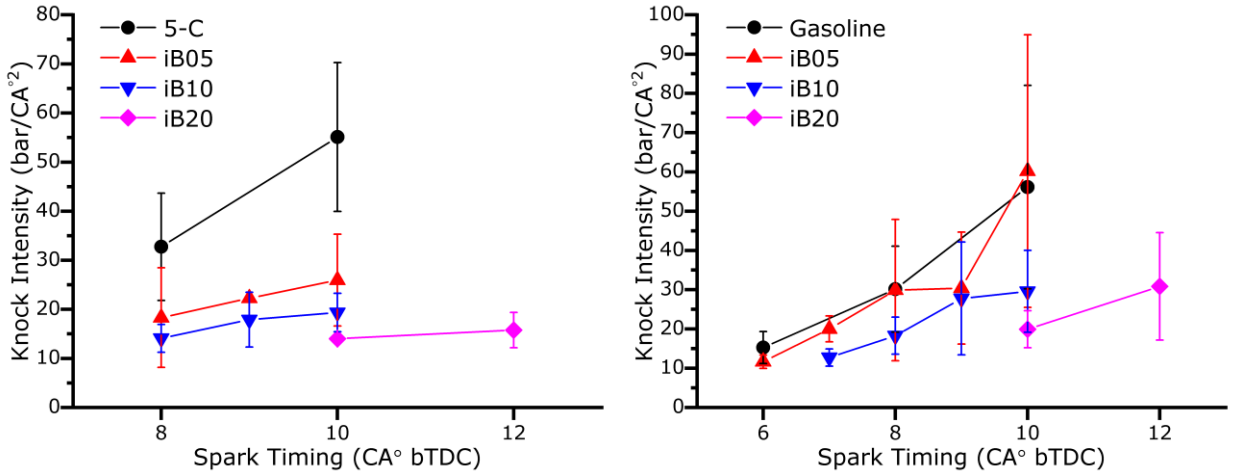

Figure 7.16. Mean knock intensities for iso-butanol blends with 5-C (left) and gasoline (right) fuels, at all spark timings which displayed knocking cases. Error bars represent the standard deviation of values for each condition. Engine speed=750 RPM, intake temperature=323 K, intake pressure=1.6 bar and Φ=1.0.

The influence of iso-butanol blending on knock intensity for blends with 5-C and gasoline can be seen in figure 7.16. In general, increasing the iso-butanol concentration of the blend causes a decrease in the observed knock intensity, across all spark advance timings, and the cross-over behaviours witnessed for iB05 and iB10 in the mean pressure cycles and KN are not present in the knock intensity. This is due to the suppression of LTHR (or first stage ignition) common in alkane fuels by the iso-butanol. LTHR in an engine can cause the enhancement of knock, increasing the intensity of the second stage ignition [395]. It has been shown in the literature that suppression of the fuels LTHR by the application of fuel blending and additives, can alter the knocking propensity of the fuel [408]. It was observed in HRA of RCM experiments, that the addition of as little of 5% iso-butanol by volume produced significant suppression of the LTHR behaviour of the 5-C (section 5.5).

Blends of the 5-C with iso-butanol tend to produce lower knocking intensities than the corresponding gasoline blends at the same conditions. A similar behaviour has been shown in the literature for blends of 20% n-butanol with the same reference gasoline and a TRF surrogate, wherein knock intensities for the n-butanol/TRF were considerably lower than the corresponding gasoline blend [52,255,274]. This is likely due to the higher resistance to engine knock at higher iso-butanol concentrations, which suppresses the intensity of pressure oscillations associated with engine knock. Knocking intensities for the gasoline iB05 blend are significantly higher than the corresponding 5-C iB05 values, with intensities similar to those exhibited by the neat

gasoline. Gasoline/iso-butanol blends also tend to display a larger standard deviation of knocking intensities throughout all conditions and blending ratios. The cyclic variability of peak pressures and the associated crank angle locations, for blends of iB05, iB10 and iB20 is shown in table 7.4. This similarly shows that the gasoline/iso-butanol blends tend to display larger cyclic variability, as was also observed for knocking cases of the neat gasoline and 5-C. The degree of cycle to cycle variation in both properties decreases with increasing iso-butanol concentration for both 5-C and gasoline blends. While the surrogate represents the general trend of cyclic variability decreasing as iso-butanol concentration increases in this case, the representation of the degrees of cyclic variability is an aspect which may need improvement in future work, as the cyclic variability is an important engine property which will need to be accounted for if computational models are to accurately predict the behaviour of gasoline blends and provide an opportunity for optimisation.

Table 7.4. Cyclic variability for the knocking combustion of iso-butanol blends with 5-C and gasoline fuels, at a spark timing condition of 10 CA°, as represented by the CoV of peak pressure and the crank angle location of the peak pressure. Engine speed = 750 RPM, intake temperature = 323 K, intake pressure = 1.6 bar and Φ = 1.0.

Base Fuel	Iso-Butanol Content (vol%)	CoVPmax (%)	CoVCA (%)
Gasoline	5	7.1	15
	10	5.3	11.6
	20	4.8	9.9
5-C	5	8.8	14
	10	4.9	10.1
	20	4.1	7.1

The relationship between peak pressures and the crank angle locations of peak pressure, on a per cycle basis, for blends of iB05, iB10 and iB20 can be seen in figure 7.17, and continues to show the same linear relationship as observed previously. For a spark timing 10 CA° bTDC, the gasoline iB05 blend produces several cycles which display higher peak pressures, closer to TDC. This trend is also apparent at blends of iB10 and iB20 and is likely responsible for the larger knock intensities observed for gasoline blends, as autoignition occurs closer to the cylinder roof, under higher pressure conditions. For iB20, the gasoline/iso-butanol blend also

displays higher peak pressures at the same crank angle as the 5-C/iso-butanol blend, for spark timings of 8 and 10 CA° bTDC.

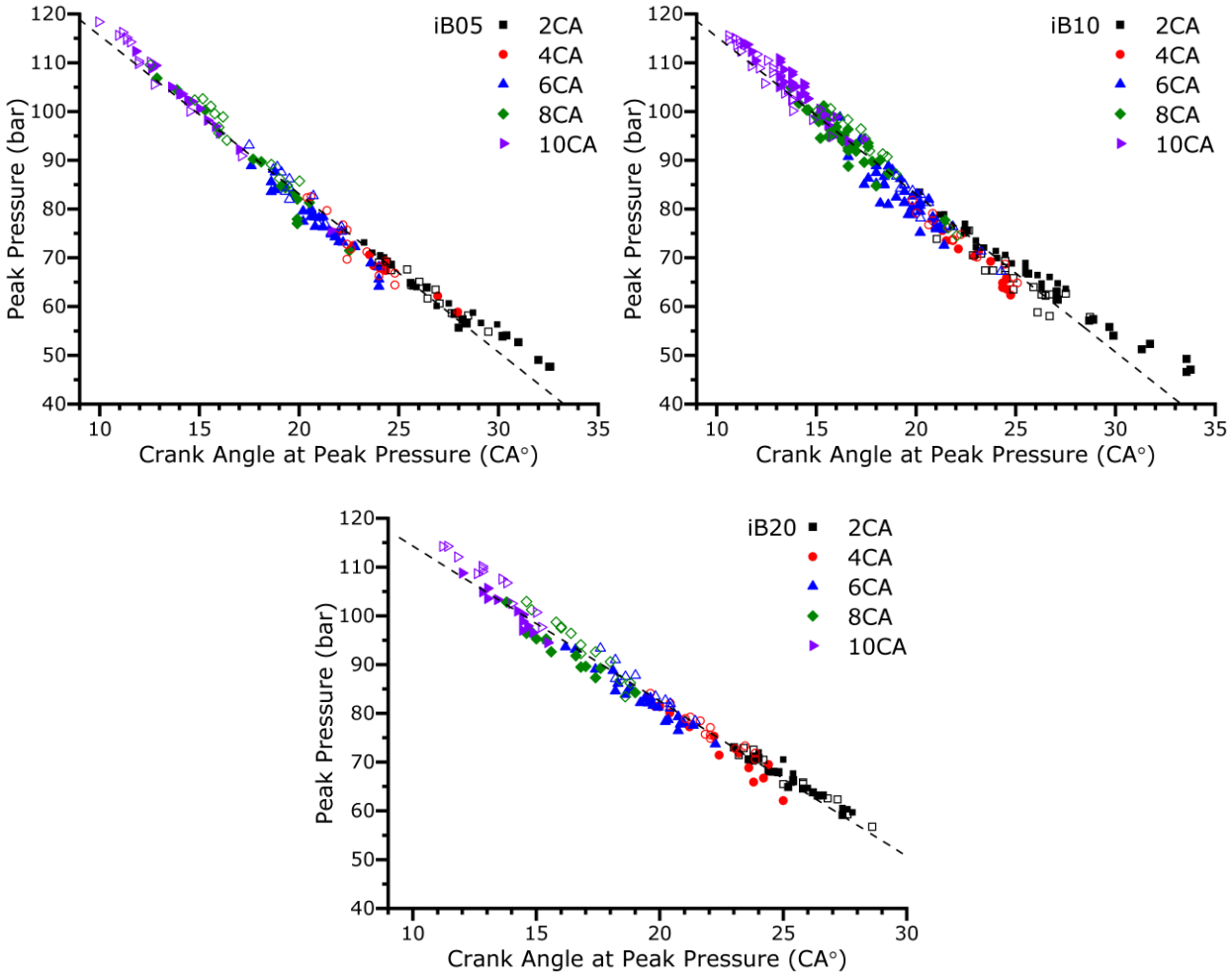

Figure 7.17. The correlation of peak pressures and the crank angle location of peak pressures for each combustion cycle (including knocking and normal cycles) of iB05, iB10 and iB20. Solid symbols show 5-C/iso-butanol blend measurements. Empty symbols show gasoline/iso-butanol blend measurements. Engine speed=750 RPM, intake temperature=323 K, intake pressure=1.6 bar and Φ=1.0.

It has been shown in the above section that the advancement of spark timing further from TDC leads to a decrease in KN (figure 7.15), an increase in knock intensity (figure 7.16) and an increase in peak pressures (figure 7.17). Increasing the fuel concentration of iso-butanol generally produces an increase in knock resistance and a reduction in knock intensity, with no knocking cases observed for concentrations greater than 20% iso-butanol by volume, without exceeding the maximum safe peak pressure of 120 bar. However, at a spark timing of 8-9 CA°

bTDC a cross-over can be observed between iB05 and iB10, wherein iB05 produces the longest KN. This corresponds with similar cross-over behaviour observed during autoignition in the RCM (section 5.4), at a compressed gas temperature of ~800-830 K. This means that, at a spark timing of 9 CA° bTDC iB05 displays a higher degree of knock resistance than both the base fuels and iB10 blends. This enables octane enhancement of the fuel blend through the addition of only a small amount of iso-butanol (if the engine is optimised to operate at this condition). Blending to such a small degree would meet the minimum requirements of the RED II, which states that 3.5% of all road transport fuel must be sourced from advanced biofuels by 2030 [27], if blending of gasoline with iso-butanol was introduced on a large scale similar to that of ethanol blending (i.e. blended at the pump). However, when compared to the base gasoline fuel, iB05 produces a larger degree of cyclic variability and slightly lower peak pressures during normal combustion.

7.3.3 Indicated Mean Effective Pressure

The influence of iso-butanol blending on the mean IMEP at various spark advance timings can be seen in figure 7.18 (for blends of 5-C and iso-butanol) and figure 7.19 (for blends of gasoline and iso-butanol). For blends of iB05 and iB10, mean IMEP values remain somewhat constant as spark timing is advanced from 2 to 6 CA° bTDC, while IMEP values for the 5-C and gasoline increase gradually. At these spark timings, IMEP values for iB05 and iB10 blends are lower than the corresponding values for 5-C and gasoline. As the blending ratio is increased to iB20, the IMEP observably increases with spark advancement up to a timing of 6 CA° bTDC, for both 5-C and gasoline blends, but does not produce a mean IMEP larger than those displayed by the neat fuels. As spark timing is advanced further the mean IMEPs of 5-C and gasoline reduce significantly. Due to this, at a spark advance timing of 8 CA°, a cross-over can be observed whereby the IMEPs of iB05 and iB20 are larger than the IMEP values of 5-C and gasoline. This is due to the increased knock resistance of these fuel blends, which allows for combustion to occur later in the engine cycle, minimising the work done by the combustion of the gas on the piston during compression. A marginal increase in IMEP has also been observed in the literature for blends of 20% iso-butanol with gasoline [379], which would lead to an increase in engine power as well as the increased knock resistance of the fuel. At a spark timing of 10 CA° bTDC, significant differences can be observed between 5-C and gasoline blended fuels. Gasoline iB05 produces a much lower value for IMEP than that seen for 5-C iB05, which may be due to the prevalence of high intensity knock at this condition, as shown in figure 7.16. Also, in general IMEP values are lower for 5-C blends than gasoline blends, particularly at normal combustion conditions (spark timings < 6 CA° bTDC). The increased knock resistance of

iB20 blends produces IMEP values equivalent to or larger than the corresponding neat fuel value at a spark timing of 10 CA° bTDC.

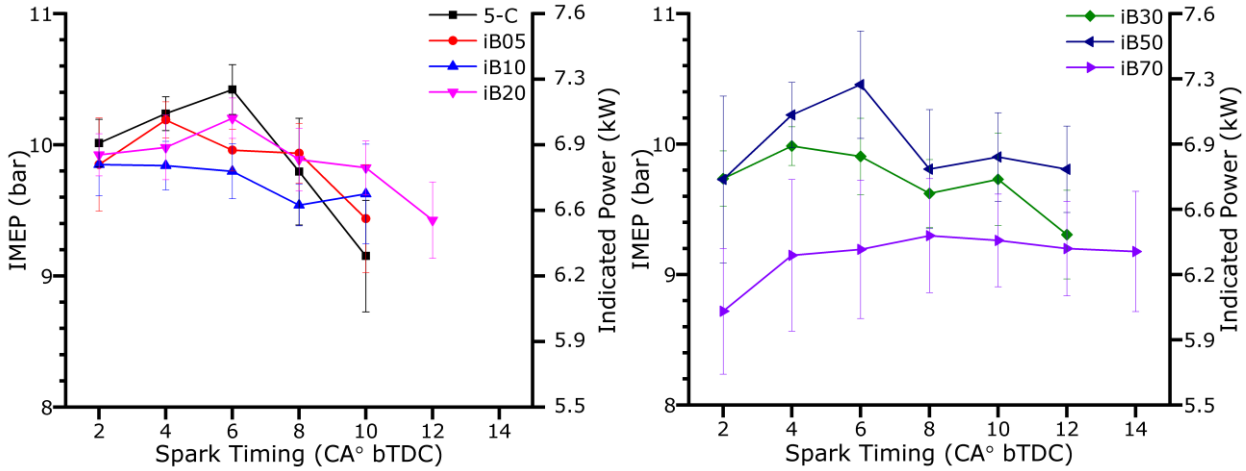

Figure 7.18. Mean IMEP values for 5-C/iso-butanol blends at each spark timing condition. Error bars represent the standard deviation of IMEP values in each case. Engine speed=750 RPM, intake temperature=323 K, intake pressure=1.6 bar and Φ=1.0.

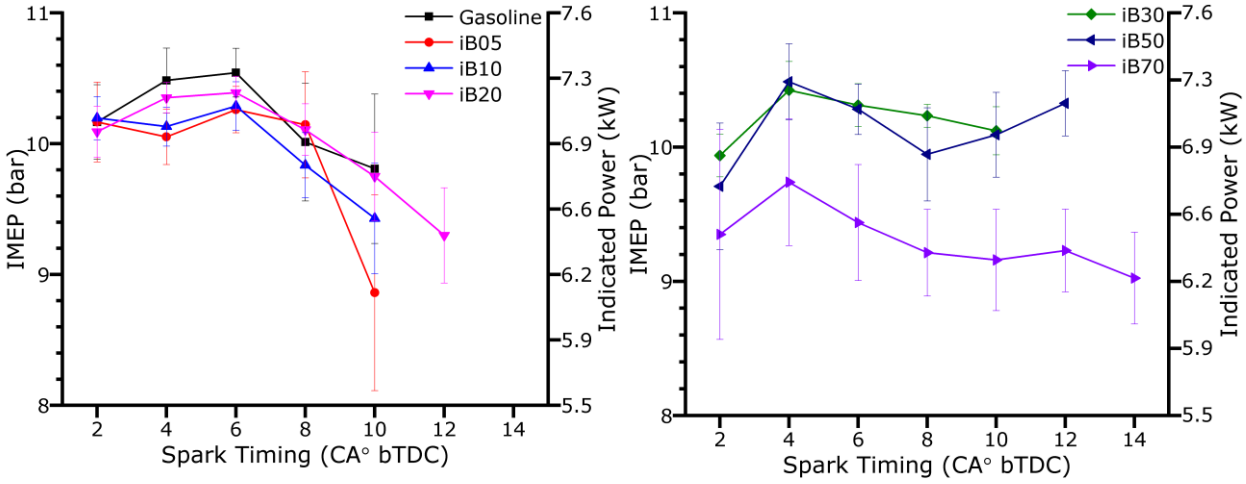

Figure 7.19. Mean IMEP values for gasoline/iso-butanol blends at each spark timing condition. Error bars represent the standard deviation of IMEP values in each case. Engine speed=750 RPM, intake temperature=323 K, intake pressure=1.6 bar and Φ=1.0.

For 5-C, the blend of 30% iso-butanol (iB30) produces similar IMEPs to iB20 at spark timings of 2 and 4 CA° but appears to show lower mean IMEP values at longer spark advance timings. A reduction in brake power for blends of 30% iso-butanol with gasoline has also been observed in the literature [229]. Gasoline blends also display a marginal reduction in IMEP for the iB30, when compared to gasoline, at spark advance timings of 4 and 6 CA° bTDC.

Otherwise, the gasoline iB30 produces IMEPs consistently larger than the neat gasoline, whereas 5-C iB30 only displays larger mean IMEPs at spark timings of 10 and 12 CA° bTDC. At these timings, the enhanced knock resistance of the iB30 delays the development of high combustion pressures until later in the piston cycle.

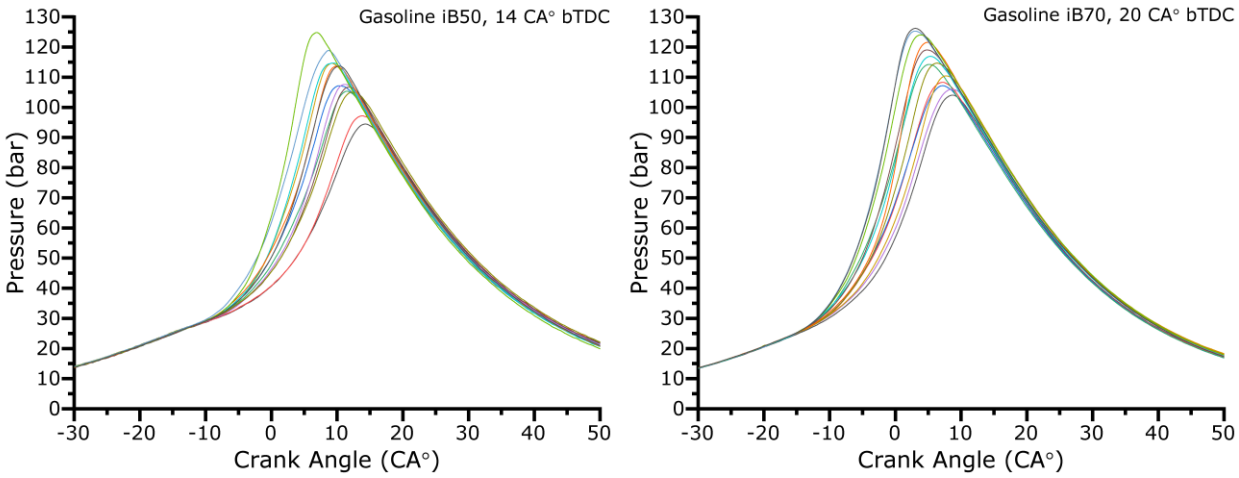

Figure 7.20. In cylinder pressure measurements for each cycle of gasoline iB50 (left) and iB70 (right) blends, at spark advance timings of 14 CA° and 20 CA° bTDC, respectively. Engine speed=750 RPM, intake temperature=323 K, intake pressure=1.6 bar and Φ=1.0.

For blends of 50% iso-butanol, IMEPs at a spark advance timing of 2 CA° bTDC are considerably lower than those for the neat fuels and blends of low iso-butanol concentration, which is indicative of the much lower peak pressures observed at this blending ratio (figures 7.13 and 7.14). This is also the case for iB70 blends, which decrease the IMEP at this condition even further. At spark timings of 4 and 6 CA° bTDC, iB50 displays IMEPs larger than or approximately equivalent to those displayed by the neat fuels. As spark timing is advanced further, IMEPs for iB50 are considerably larger than those displayed by the neat fuels due to the influence of knock and the high knocking resistance of the iB50 blends. Blends of iB50 were investigated at spark advance timings of up to 14 CA° bTDC (until the maximum safe peak pressure was achieved) and no knocking cases were observed, as seen in figure 7.20. IMEPs displayed for iB70 blends are significantly lower than those displayed by blends of lower iso-butanol concentration, however, the blend is capable of operating at much earlier spark advance timings than the neat fuels and lower concentration iso-butanol blends. This can be seen in figure 7.20, wherein the iB70 gasoline blend is shown to operate at a spark advance timing of 20 CA° bTDC without the presence of any knocking cycles. The capability of a fuel to operate effectively at large spark advance timings is important for SI engine performance. If the

knock limited spark advance is closer to TDC than the maximum brake torque timing, engine performance is limited by knock. Therefore, a fuel with a high degree of knock resistance allows for the further advancement of spark timing towards the maximum brake torque timing.

High degrees of iso-butanol blending cause an increase in the knock resistant properties of the fuel, allowing the engine to be operated at further advanced spark timings, increasing the temperature and pressure within the cylinder, allowing for more efficient engine operation. However, at a blend of 70% iso-butanol by volume, significant reductions in engine power can be observed (figure 7.19) due to the influence of iso-butanol on the calorific value of the fuel, even at spark timings advanced far from TDC. The use of such a high blending ratio would require the consumption of additional fuel to produce the same power output, which may have a negative impact on total vehicle emissions, as well as the requirements for additional fuel production to meet the consumption needs. A blend of 50% iso-butanol appears to produce a large degree of knock resistance, displaying no knocking cases throughout the study (up to spark timings of 12 CA° bTDC), while producing an indicated engine power comparable to that of gasoline when operating at sufficiently advanced spark timings. Like iB70, the iB50 blend produces a large increase in cyclic variability when compared to gasoline, particularly at short spark advance timings. However, as spark timing is advanced further from TDC, this variability decreases, meaning that this fuel may be viable if operated at such spark timings. Operating at large spark advance timings would also need to occur to maximise the benefit of the fuel's large degree of knock resistance and reasonable engine power at these conditions.

At low degrees of iso-butanol blending, some octane enhancement can be observed (figure 7.15) but this coincides with a reduction in engine power during normal combustion. Cyclic variability is also increased for the iB05 blend relative to gasoline, which may have impacts on engine optimisation and performance. On the other hand, for iB10 cyclic variability is similar to that of the base gasoline but this blend displays complex blending behaviour, showing a crossover in KNs with the iB05 blend wherein iB10 becomes the least knock resistant at a spark timing of 9 CA° bTDC. The advancement of spark timings is limited by knock at the same spark advance as gasoline for the iB05 blend, whereas iB10 can only advance 1 CA° before experiencing knock. Blends of 20% and 30% iso-butanol display considerable degrees of knock resistance, with iB30 showing no knocking cycles up to a spark timing of 10 CA° bTDC (wherein the maximum safe operating pressure of the LUPOE was achieved), as well as IMEPs comparable to those of gasoline under normal combustion and similar degrees of cyclic variability. From the trends in this study, due to the influence of iso-butanol blending on the

combustion behaviour of gasoline, 20-50% iso-butanol by volume appears to produce a range of fuels suitable for use in pressure boosted SI engines. The widescale use of any blend in this range would impact significantly on the requirements of the RED II, which requires a minimum of 14% renewable fuels for all road and rail transport, with at least 3.5% coming from advanced biofuels, by 2030 [27]. However, meeting the production needs for large quantities of iso-butanol would be difficult currently, as iso-butanol yields are limited due to both process and economic constraints [208,409]. Therefore, it is recommended that blends of 20-30% be implemented as these provide many of the benefits of higher iso-butanol concentrations but with lower biofuel quantities required.

7.4 Summary

In this study, the effectiveness of a five component surrogate (5-C) in the representation of the normal and knocking combustion properties of a reference gasoline in a boosted SI engine has been evaluated. It was shown that, for normal combustion at spark advance timings of 2-6 CA° bTDC, the 5-C and reference gasoline produce near identical mean pressure cycles (figure 7.1), quantified by the mean peak pressure, the crank angle location of the mean peak pressure (table 7.1) and the evolution of the pressure gradient during combustion (figure 7.2). When compared to the representation of the reference gasoline by a previous three component TRF surrogate [52], the five component provided a much better representation of the gasoline under normal combustion. The cyclic variability, as quantified by the CoV for peak pressure and the associated crank angle location, was larger for the 5-C than the gasoline at these conditions. Under knocking conditions, the representation of the reference gasoline by the 5-C was excellent, with the 5-C accurately representing mean KNs and related knocking intensities (figure 7.8). This reflects similar results obtained for the measurement of IDTs within the RCM, wherein the surrogate's representation of the gasoline was also very good. Minor differences were observed between the fuels in the mean pressure cycles at spark advance timings of 8 and 10 CA° bTDC (figure 7.5). 5-C reached a peak pressure 1.5 CA° earlier than gasoline at a spark timing of 10 CA°, which while only a minor variation, correlates with a shorter measured IDT for the 5-C than gasoline, at the highest investigated temperature of 870 K within the RCM. Based on previous predictions of end gas temperatures within the LUPOE, this temperature correlates well with the approximate temperatures during engine operation at a spark timing of 10 CA° bTDC [395]. It was also observed that, at knocking conditions, the 5-C displayed a lower degree of cyclic variability, which decreased with increasing spark advance timing. At spark timings of 2-6 CA° bTDC, the 5-C also produced a reasonable representation of the gasolines

IMEP. However, this representation broke down somewhat due to the presence of knocking cycles, wherein intense pressure oscillations impacted the calculation IMEP from the measured in cylinder pressure.

The influence of iso-butanol blending on the normal and knocking combustion properties of the 5-C and gasoline fuels was investigated for blends of 5-70% iso-butanol by volume. Under normal combustion, at a spark timing of 2 CA° bTDC, non-linear blending effects were observed in the mean pressure cycles for each blend. The addition of a small amount of iso-butanol (iB05) produced a decrease in the mean peak pressure, when compared to the neat 5-C and gasoline fuels. As iso-butanol concentration was increased further (to iB10), mean peak pressures increased to similar values as those shown by the neat fuels. This non-linear behaviour was attributed to competition between the suppression of LTHR and the increase in burning rate due to the increase in iso-butanol content. Suppression of the LTHR was observed for blends as low as iB05 in RCM HRA, particularly at low compressed temperatures. This suppression of LTHR at low temperatures is proposed to cause a reduction in the charge heating of the end gas during normal combustion, reducing in cylinder temperature and pressure conditions. The interplay between these phenomena warrants further research, as it has implications for the production of optimal fuel blends and the associated SI engine performance. A further non-linear behaviour is observed during normal combustion, as blending ratios greater than 20% iso-butanol by volume displayed a reduction in the mean peak pressures observed. This behaviour was attributed to the lower calorific value of iso-butanol [406,407], which is in competition with the slightly faster burning rates of iso-butanol when compared to iso-octane, toluene and gasoline [44,221,401,402].

Generally, iso-butanol blending produced a greater degree of knock resistance with increasing iso-butanol concentration (figure 7.16). Blends of larger than 30% iso-butanol content by volume produced no knocking cases at all spark advance timings that could be safely investigated. Blending of iso-butanol with both 5-C and gasoline displayed a further non-linear behaviour at a spark timing of 9 CA° bTDC, wherein iB05 displayed a longer KN than the iB10 blends. This correlated well with RCM measurements of IDT for iB05 and iB10 blends, at compressed temperatures of ~800-830 K, which correlates well with predicted end gas temperatures at a spark timing of 9 CA° bTDC [395]. Increasing iso-butanol concentration also produced a decrease in the apparent knock intensities (figure 7.17) and cyclic variability (table 7.4). Blends with a greater knock resistance were shown to produce larger IMEP values, particularly at spark advance timings longer than 6 CA° bTDC. The iB50 blend displayed IMEP

values close to those for the neat fuels under normal combustion, at spark advance timings of up to 14 CA° bTDC. At this condition, all cycles were free of knock, and the maximum safe working pressure of 120 bar was achieved. The ability to advance the spark timing further from TDC towards the maximum brake torque timing, with minimal impacts on the work done per cycle, may lead to improvements in SI engine performance.

8 Conclusions and Directions for Future Research

This work has investigated the combustion characteristics of conventional and alternative fuels with relevance to boosted SI engines, focusing largely on the influence of iso-butanol blending on the autoignitive behaviour of gasoline and a newly developed five-component surrogate (5-C). Investigations of this behaviour for gasoline, gasoline/iso-butanol blends, 5-C and 5-C/iso-butanol blends, at the fundamental level (RCM) and practical engine level (LUPOE), applying the methodology described in Chapter 3, have developed an improved understanding of the influence of iso-butanol blending on key combustion characteristics. This includes insight into single and multistage autoignition, characteristic LTHR behaviour and the associated HRRs, PIHR, and the onset and intensity of engine knock. The ability of chemical kinetic modelling to predict the global ignition behaviour and underlying heat release phenomena of the investigated fuels was evaluated, applying a combined blend mechanism based on the LLNL gasoline surrogates mechanism [85] and Sarathy et al. butanol isomers mechanism [84]. Further knowledge of the model and an understanding of the chemistry driving autoignition and LTHR behaviour were developed through the application of sensitivity analysis techniques (described in Chapters 2 and 3), for both reaction A-factors and species enthalpies of formation. The following sections describe the contributions arising from this work, a summary of the conclusions and research findings of each chapter in this thesis, general conclusions encompassing the project as a whole, and recommendations for the direction of future research.

8.1 Summary of Contributions

As part of this work, the University of Leeds RCM facility was developed via the implementation of operation changes and mechanical modification, bringing the facility up to the standard of other high quality RCM research facilities. These changes improve the quality of data provided by the facility, with standardised operational requirements ensuring the consistency of data quality between studies. This was achieved for the study of homogeneous IDTs by the prevention of undesirable PIHR, due to the elimination of inhomogeneities introduced by poor RCM operational and maintenance standards, and the reduction of complex fluid flow phenomena induced by high velocity piston motion. This latter improvement is attributed to the development of a bespoke creviced piston head, which leads to a prolonged lifetime of the spatially homogeneous hot core gas (and thus the adiabatic core assumption), allowing the facility to probe longer IDTs (~200 ms). This is particularly important for fuels of high octane sensitivity which display a larger propensity for PIHR, such as iso-butanol, ethanol, and toluene. As part of these improvements, a simplistic method for the determination of RCM

PIHR cases through pressure gradient analysis was developed, which proved effective at identifying PIHR cases which may otherwise be difficult to locate in the RCM pressure data.

A newly developed five component surrogate (5-C) designed to closely match the octane quality of the reference gasoline as well as represent the aromatic, olefin, and ethanol content, was evaluated for the first time. The 5-C closely matched the ignition behaviour of the gasoline in both RCM and LUPOE studies. The capability of 5-C to act as a suitable surrogate under iso-butanol blending was also examined. Good quality surrogates provide an opportunity for the development and validation of chemical kinetic models to predict the ignition behaviour of highly complex gasoline fuels, using the surrogate as a proxy. For the development of biofuels, such as iso-butanol, as a “drop-in” gasoline additive/blending agent, the representation of gasoline blending behaviour by the surrogate is important as this allows models to facilitate the development of optimal fuel blends, engine operating parameters and further knowledge of the underlying chemical processes driving combustion behaviour.

Valuable RCM data are provided in this study for a wide range of iso-butanol blends with gasoline and 5-C. This includes IDTs at boosted SI engine relevant conditions, HRRs and aHRs for LTHR, which may serve as validation targets for the further development and improvement of detailed chemical kinetic models. Heat release properties were determined through the application of recent HRA methods for RCMs [172], showing that this methodology can be applied to investigate preliminary exothermicity for a range of fuels, thermodynamic conditions, and is applicable to multiple RCM facilities (as long as facility effects are accounted for).

Through the application of local OH sensitivity analysis, this work investigated the influence of iso-butanol blending on autoignition, developing an improved understanding of the chemical kinetics which drive observed changes in ignition behaviour as a result of iso-butanol blending. Further brute force sensitivity analysis of IDT and characteristic LTHR properties, due to changes in species enthalpy of formation, highlighted the importance of accurate thermodynamic data for many critical species, which may not be accurately estimated by GA values within the combined mechanism. Such analysis, applied to examine the presence of two stage LTHR, identified the importance of toluene oxidation chemistry in the production of this phenomenon, effectively creating a delayed phase of LTHR.

This work provides valuable practical engine data, using a boosted SI research engine (LUPOE), for a wide range of 5-C and gasoline blends with iso-butanol, at several spark advance timings. These results provide information about the influence of iso-butanol as a biofuel additive on several important engine properties such as cyclic variability, in-cylinder

pressure, KN, knock intensity and IMEP, highlighting optimal fuel blends for SI engine operation. Results for the combustion of 5-C and 5-C/iso-butanol blends may also serve as validation targets for the modelling of SI engine combustion.

8.2 Concluding Remarks

During the introduction to this thesis (Chapter 1), motivation for the subsequent work was framed in the form of five research questions, each of significant importance for furthering knowledge towards the understanding of alternative fuel (iso-butanol/gasoline blends) combustion in SI engines. In this section, conclusions are drawn from the results and discussions displayed in this thesis and presented in the context of the original research questions. This section is structured such that these questions are outlined briefly below, followed by the relevant conclusions.

- What influence does iso-butanol blending with a research grade gasoline fuel have on SI engine performance?

By investigating the influence of iso-butanol blending on SI engine performance, with particular focus given to knocking behaviour and indicated power, this work aimed to evaluate iso-butanol/gasoline blends as viable fuels for use in pressure boosted, downsized SI engines. Given the results presented in Chapter 7, blends of 20-50% iso-butanol by volume with gasoline appear to be the most viable for use in boosted SI engines, producing significant anti-knock benefits, with blends above 20% iso-butanol displaying no knocking cases during experiments. While significant indicated power reductions (shown by IMEP) could be observed at low spark advance timings for some fuels, these blends could operate at much higher spark timings without incurring engine knock. Therefore, while the fuel blends have a lower calorific value than gasoline, the advancement of spark timing towards the maximum brake torque timing without being knock limited allows these blends to produce a reasonable indicated power, comparable to that of gasoline under normal combustion. A previous study on the influence of butanol blending with gasoline (RON 95) for each of the butanol isomers, in a normally aspirated 1.6 L four cylinder SI engine, found that a blend of 20% iso-butanol gave the highest engine torque, brake power and brake thermal efficiency among all of the blends tested [410], showing that iso-butanol blends in this region are viable fuels in both turbocharged downsized and conventional SI engines.

Blending to a higher volume of iso-butanol continued to produce anti-knock improvements over gasoline but added limited benefits when compared to blends of 30% iso-butanol or more,

as none of these fuels displayed any cases of engine knock. The significantly lower calorific value also drastically reduced indicated power output, limiting the viability of such blends. The introduction of iso-butanol blends of 20-50% to the European transport fleet could contribute significantly to meeting the requirements of the RED II, which requires a minimum of 14% renewable fuels for all road and rail transport, with at least 3.5% coming from advanced biofuels, by 2030 [27]. However, to meet the fuel requirements of such a high degree of blending, large quantities of advanced iso-butanol fuel would be required, which are not feasible with current rates of production due to economic and process constraints [208,409]. Therefore, blending to lower degrees may be required. At lower blending ratios (iB05-iB10), complex non-linear behaviour was observed and, while blends with low volumes of iso-butanol did display some moderate knock resistance improvements, the indicated power was typically lower for these blends than gasoline and iB20, comparatively limiting the viability of such blends. While a blend of 50% iso-butanol appears to be optimal for boosted SI engine performance, this is unlikely to see wide-scale implementation due to the requirement for large volumes of iso-butanol, although improvements in production processes and the resultant yields are areas of high degrees of research interest [212,409,411–413]. A good compromise appears to be in the blending of 20-30% iso-butanol, which produces significant anti-knock benefits with comparable indicated power when compared to gasoline, while limiting the barrier to largescale implementation.

- To what extent are fundamental experiments useful in informing us on the behaviour of fuel blends in real engines?

It is common for fundamental experiments, such as RCM ignition studies, to be conducted under the assumption that such studies provide a satisfactory proxy for the investigation of a fuel's behaviour under real engine conditions. The validity of such an assumption was questioned in section 1.2 of this thesis, motivating an investigation into the behaviour of several iso-butanol and gasoline fuel blends at the fundamental (RCM) and practical engine (LUPOE) level. While the investigated pressure was lower in the RCM (20 bar) than the boosted engine (30 bar), similar temperature ranges are present in the corresponding end gasses for each case [52,395]. From the results presented in Chapters 5 and 7, several trends can be observed in both RCM and LUPOE experiments due to increased iso-butanol blending. Generally, at low end gas temperatures, as the iso-butanol concentration increases so does the knock resistance of the fuel. This can be seen in RCM temperatures below 750 K, and spark advance timings of 6 CA°. Engine experiments, however, do not display a higher reactivity for iB05 blends in this

region (6 CA°/~750 K) than the neat fuel, which was observed during RCM experiments. The lower peak pressures observed for iB05 relative to gasoline and iB10 during normal combustion may be somewhat responsible this behaviour, as end gas pressures and temperatures will be lower than those predicted, leading to higher knock resistance at the same spark advance timing. This behaviour could not have been predicted by IDT measurements and was attributed to the suppression of LTHR, causing a reduction in the charge heating of the end gas, which was shown during RCM HRA at the same temperature conditions. To determine the end gas temperatures of iB05 in this case and facilitate the comparison between RCM and LUPOE experiments, modelling of these conditions would be required to predict said temperatures or direct temperature measurement within the engine cylinder is needed. The increased reactivity of the iB10 blend relative to gasoline is apparent in both sets of experiments at higher temperatures (9 CA°/~850 K), as is the cross-over behaviour observed between iB05 and iB10. At the highest investigated RCM temperatures, IDTs appear to converge, becoming similar regardless of the fuel blend. Similarly, at a spark advance timing of 10 CA°, all gasoline blends which displayed knocking behaviour produce a similar KN. At blends of iB50 and iB70, the cyclic variability increased significantly with respect to other blends, which reflects the high sensitivity of iso-butanol to temperature inhomogeneities within the RCM combustion chamber, as shown by the fuel's propensity for pre-ignition in the presence of turbulent mixing in Chapter 4.

These similarities, which arise at similar end gas temperature conditions, show that measurements made in fundamental RCM experiments produce a good representation of knocking trends in an SI engine. However, it should be noted that the research engine used in this study applies a skip-firing mode, wherein several motoring cycles are completed between each firing cycle, minimising the influence of previous firing cycles on each subsequent firing cycle. This is clearly not representative of "real" SI engine operation, wherein each cycle is influenced significantly by the previous one, and as such the relevance of RCM measurements to such operating conditions cannot be fully evaluated at this point.

- How well can a five component gasoline surrogate fuel represent the autoignition behaviour of a research grade gasoline on blending with iso-butanol under ideal experimental conditions?

The accurate representation of gasoline by the current surrogate formula is vital for assessing the possibility of developing chemical kinetic models that are representative of chemically complex gasoline fuels. By investigating the autoignition behaviour of the newly developed 5-C surrogate and surrogate within the RCM, this study has shown that the current

surrogate provides an excellent representation of gasoline in terms of IDTs. This representation was good throughout the investigated temperature regime (675-870 K) at a pressure of 20 bar and a stoichiometric equivalence ratio, with the only significant difference observed at 740 K, wherein the gasoline displayed a higher degree of reactivity than the surrogate. However, upon investigation of RCM pressure measurements, the 5-C was found to misrepresent the first stage ignition (and thus LTHR) behaviour of the gasoline in some cases, particularly at temperatures displaying the largest IDT discrepancies. This behaviour may be due to the over-abundance of alkanes in the surrogate, which may be remedied through the introduction of a sixth component to represent the naphthene content of the gasoline and limit the paraffinic content. Under blending with iso-butanol the representation of gasoline blends by the 5-C blends was also very good. However, significant differences were observed for low temperature conditions under high degrees of iso-butanol blending (iB50-70), with 5-C blends producing significantly longer IDTs. When compared to a previous three component TRF, designed to represent the same gasoline by matching the RON and H/C ratio, the 5-C displays a much better representation throughout the temperature regime [51]. From these observations, it can be seen that matching the aromatic, olefin and ethanol content, as well as the RON and MON of the reference gasoline, is beneficial for the formulation of a robust, accurate surrogate fuel, and this can be completed through the use of five components (iso-octane, n-heptane, toluene, 1-hexene and ethanol). Based on the results presented in this thesis, at stoichiometric conditions, in the thermodynamic regime investigated, a kinetic mechanism developed to replicate the behaviour of the 5-C surrogate and blends with iso-butanol would provide an accurate representation of the more complex gasoline/iso-butanol blends.

While at stoichiometric conditions, the 5-C surrogate provided an overall very good representation of the reference gasoline's IDT behaviour (neat and under iso-butanol blending), at an equivalence ratio of 0.5 the surrogate largely failed to replicate the IDT measurements of gasoline and gasoline-iB30. At these lean conditions, the surrogate was generally significantly less reactive than the corresponding gasoline measurements, producing much longer IDTs. The surrogate produced less heat release during first stage ignition in these cases, as observed by a smaller pressure rise, and was impacted by larger degrees of heat loss than gasoline cases as a result. It may be that the addition of a further component to the surrogate, to accurately represent the naphthene and alkane content, would produce a better representation of LTHR behaviour and IDTs at lean conditions. However, more research is required in this regard and the representation of gasoline by the surrogate at less extreme equivalence ratios should also be investigated, in relation to practical SI engines.

- How well does the gasoline surrogate represent the blending performance with iso-butanol in both fundamental systems and practical SI engines?

The formulation method applied in the production of the 5-C surrogate correlates the octane quality of the fuel to parameters derived from the IDT profile (particularly in the NTC region) [70]. Therefore, an accurate representation of gasoline in the RCM should coincide with a similar degree of accuracy in the LUPOE, if the correlations made in the formulation method are valid. This was shown to be the case for the neat 5-C and gasoline fuels. Following on from a very good representation of the gasoline in the RCM, the 5-C continued to produce an excellent representation of the neat gasoline in the LUPOE, for both normal and knocking combustion cases. Mean pressure measurements, KNs, knock intensities and IMEP values (during normal combustion) for gasoline were all well represented by the 5-C surrogate, particularly when compared to the previously investigated TRF [52]. A number of minor differences observed between the 5-C and gasoline IDTs in the RCM correlated well with small differences observed in the LUPOE. These included a slightly earlier KN for the 5-C fuel at a spark advance timing of 10 CA° bTDC, which agreed with a slightly higher degree of reactivity for 5-C at the highest investigated temperature within the RCM. Under blending with iso-butanol, some differences between the 5-C and gasoline blends emerged within the LUPOE, including a lower propensity for knock for the 5-C iB10 at a spark timing of 6 CA° bTDC. This correlates with a lower degree of reactivity observed during RCM experiments at 770 K. Small differences in RCM IDT times, such as 1-2 ms, may translate into differences of several crank angles within an engine, thus a slightly lower degree of reactivity for the 5-C at 770 K may manifest as a significant reduction in knocking propensity within the LUPOE. The representation of gasoline by the surrogate appears to be similar in both fundamental RCM experiments and practical engine level LUPOE experiments, highlighting the ability of the surrogate to represent gasoline in both environments, which facilitates the development of computer models to accurately represent the combustion behaviour of gasoline/iso-butanol blends in both cases. This also provides further support for the validity of fundamental experiment measurements for predicting the behaviour of fuels at the level of practical engines, at least in the case of a skip-firing research engine.

- How effective are current computer models at predicting the combustion behaviour of iso-butanol and gasoline blends?

While the representation of gasoline by the newly developed 5-C surrogate is generally very good for both neat fuels and blends with iso-butanol, facilitating the development of kinetic

models to represent the behaviour of gasoline in fundamental systems and SI engines, the mechanism chosen [84,85] for the modelling of these fuels in this study largely fails to reproduce their combustion behaviour. For the 5-C fuel, variable volume simulations provide a reasonable prediction for IDTs at the lowest and highest temperatures but significantly underpredict the intensity of the NTC region. Simulations also fail to represent the form and intensity of LTHR, which is important for the development of the main stage ignition. These same model failures in the representation of IDT and heat release behaviour were also apparent under blending with iso-butanol. Furthermore, variable volume simulations failed to predict the observed cross-over behaviour for iso-butanol blends, between iB05 and iB10, and between iB50 and iB70. These findings lead to conclusion that current computer models, utilising the combined mechanism applied in this study, are not effective at predicting the combustion behaviour of iso-butanol and gasoline blended fuels (through the prediction of surrogate behaviour), particularly in the NTC region, and the mechanism requires significant improvement if a good representation is to be achieved. The previous conclusions made in this section have described the validity of RCM experiments in the prediction of practical engine combustion behaviour. Therefore, a model which accurately reproduces RCM measurements would be useful for the prediction of SI engine combustion, allowing for the determination of optimal engine operation parameters and fuel blends without the need for expensive and time consuming experiments. Further development of the mechanism to produce a highly accurate model would therefore be highly beneficial.

It was proposed during this study that model failures may propagate from the incorrect representation of heat release behaviour prior to HTHR. This was supported by a local OH sensitivity analysis, which identified multiple reactions known to be important during the development of first stage ignition. Similarly, an enthalpy of formation sensitivity analysis on IDTs identified species typical of the low temperature oxidation of toluene, n-heptane and 1-hexene. Characteristic LTHR properties were also highly sensitive to many of these same species, identifying their importance in the development of heat release prior to HTHR. From these findings it is proposed that not only should efforts continue towards the accurate representation of species thermodynamic data and reaction rate parameters within the mechanism, but chemical kinetic models should be developed to match typical LTHR properties as additional target parameters, such as HRRs, aHR and temperature at soITHR and soHTHR.

8.3 Directions for Future Work

- Due to limitations in production, and the requirement for largescale advanced biofuel blending (as set out in the RED II), the diversification of the transport energy sector through the blending of multiple biofuels into a single mixture is likely to be required. This includes mixtures of multiple butanol isomers, mixtures of alcohols and also complex biofuel mixtures which include many varying bioderived species (such as ethanol, ethyl levulinate and bioethers). This may also allow for the unique properties of each constituent fuel component to be exploited through the optimisation of fuel blends. Further research should be conducted into the properties of such complex fuel blends, towards the determination of blending rules for the design of optimal fuel blends, as well as the combustion behaviour of such blends. Research is required for such blends in both fundamental systems and practical engines. Fundamental research provides an indication of the fuel's behaviour at the practical level and facilitates the development of accurate, detailed computer models, which may see an increased significance in the design of optimal blends for highly complex fuel mixtures.
- During this study, iso-butanol/gasoline blends were investigated within an RCM and a motored SI engine, operating under skip-firing, with correlations described between the two facilities. However, neither facility fully represents the combustion environment present in an engine during "real-world" operation, as previously described. To determine the usefulness of such studies (RCM and skip-fired engine) for predicting combustion behaviour within real engines, the results of this study may be compared with a study on the combustion of iso-butanol/gasoline blends in a full-scale laboratory based commercial SI engine, operating under "driving" conditions. Furthermore, the properties of such blends require investigation at a larger range of engine operating parameters, such as equivalence ratios and engine speeds, to fully characterise their combustion behaviour.
- The impact of iso-butanol blending on SI engine performance, particularly in terms of knocking behaviour and indicated power, has been evaluated in this study. However, no research has been conducted within this work into the associated impact of blending on emissions. While some studies have been conducted into the emissions characteristics of iso-butanol/gasoline blends, these tend to focus on a narrow range of blends and engine operating parameters [378,379,414,415]. These laboratory emissions test also do not provide a full picture of the fuel's emission behaviour during real driving conditions. To develop an understanding of the impact of iso-butanol on practical emissions, there is a need to investigate each blend over a wide range of conditions relevant to the conditions

observed during real world vehicle use [416]. Therefore, future emissions testing of iso-butanol/gasoline blended fuels should evaluate the impact of blending on real driving emissions, through the use of a research vehicle and real driving emissions (RDE) tests [416], as well as laboratory based emissions test cycles.

- While the IDT representation of the reference gasoline by the 5-C surrogate was good for both the neat and iso-butanol blended fuels at stoichiometric conditions, large differences were observed at Φ=0.5. Further investigation of the surrogate and gasoline under lean conditions is required to determine the cause of these differences and the influence of stoichiometry on ignition behaviour of gasoline and surrogate blends with iso-butanol.
- Chemical kinetic modelling largely failed to represent ignition behaviour of 5-C within the NTC region, as well as generally misrepresenting the LTHR behaviour of 5-C and blends with low concentrations of iso-butanol. Future work on the representation of the 5-C surrogate by the model should focus on the accurate reproduction of LTHR behaviour, with the aim of improving IDT predictions at low temperatures and in the NTC region. It is proposed that this can be achieved by updating much of the gasoline surrogate sub mechanisms to account for recent updates to n-heptane and aromatic sub mechanisms [46,264,268,269]. The HRA of RCM pressure data provides a range of new validation targets for such an improved mechanism, such a LTHR peak HRRs, TsoITHR, TsoHTHR and aHR.
- Enthalpy of formation sensitivity analysis revealed the importance of several species of complex structures in the determination of IDT and characteristic LTHR properties. Where possible, efforts should be made towards the determination of the thermodynamic properties of these species through experimental means or high-level quantum calculations. However, where this is impossible or unreasonable, GA estimates need to apply accurate and up to date group values. Recently, significant efforts have been made to update individual group values for a wide range of species [354,372–374]. A database of state of the art GA values would facilitate the generation of consistent estimates to the highest possible quality within the community, towards the general improvement of detailed kinetic mechanisms, as significant sensitivities have been observed in species thermodynamic data to several individual groups typical of oxygenated species observed during low temperature oxidation and autoignition [355].
- Detailed mechanisms, such as the combined mechanism investigated in this study, are often a combination of reversible and irreversible reactions which are further complicated by the presences of specified reverse reaction rates in some cases but not in others. Therefore,

neither sensitivity analysis of species thermodynamic properties nor reaction rate parameters is entirely sufficient to fully investigate the influence of uncertainties on global parameters. Future work should focus sensitivity analysis efforts on global techniques to investigate changes to both species thermodynamic properties and reaction rate parameters simultaneously.

Appendix A

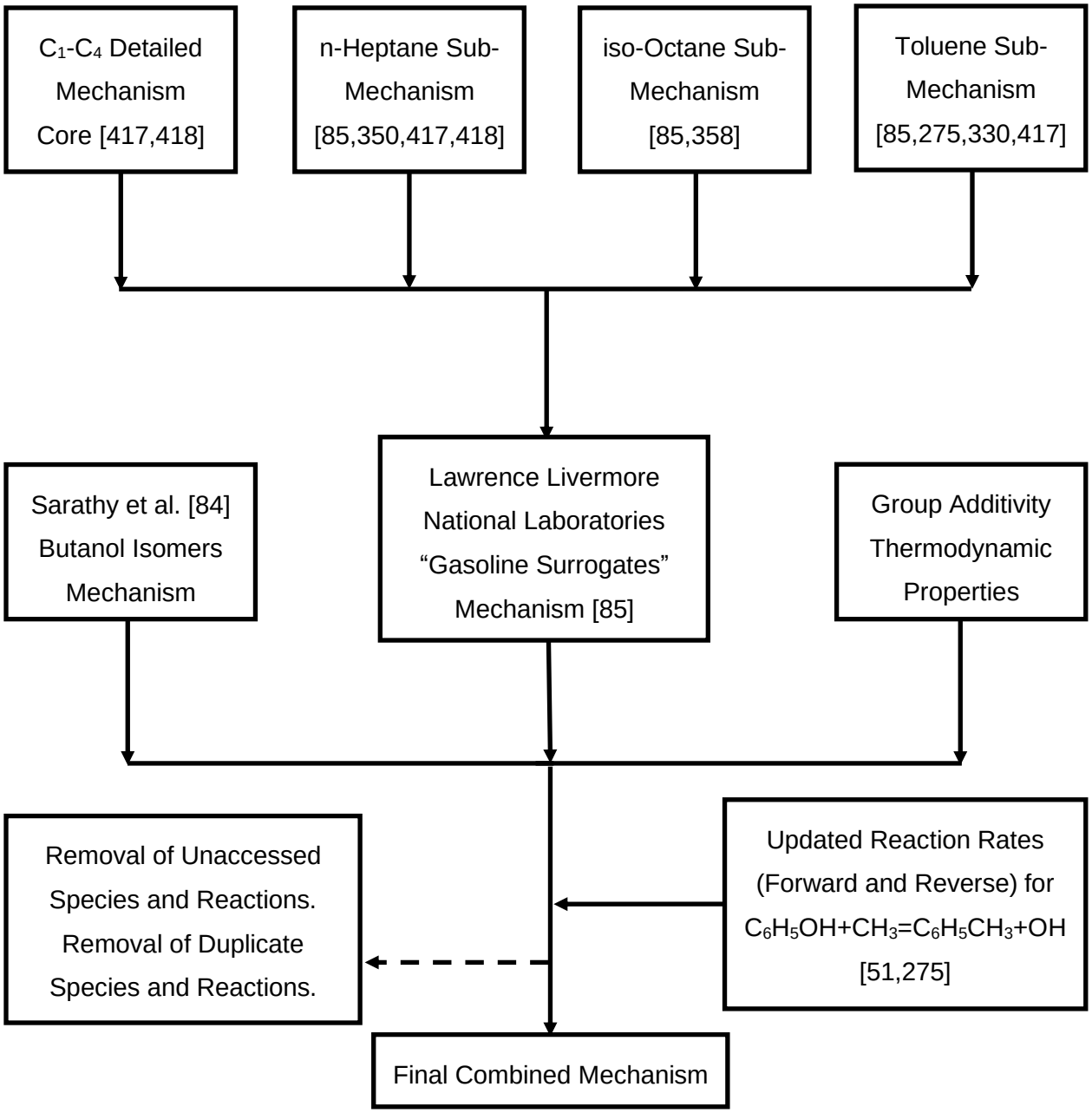

Figure A.1. A flow diagram showing the constituent elements and structure of the combined mechanism utilised for modelling purposes in this study.

References

[1] British Petroleum. Statistical Review of World Energy - 2019, 68th Edition 2019. https://www.bp.com/content/dam/bp/business-sites/en/global/corporate/pdfs/energy-economics/statistical-review/bp-stats-review-2019-full-report.pdf (accessed September 14, 2020).

[2] British Petroleum. Statistical Review of World Energy - 2020, 69th Edition 2020. https://www.bp.com/content/dam/bp/business-sites/en/global/corporate/pdfs/energy-economics/statistical-review/bp-stats-review-2020-full-report.pdf (accessed September 14, 2020).

[3] Sarathy SM, Farooq A, Kalghatgi GT. Recent progress in gasoline surrogate fuels. Progress in Energy and Combustion Science 2018;65:67–108. https://doi.org/10.1016/j.pecs.2017.09.004.

[4] Kalghatgi G. Is it really the end of internal combustion engines and petroleum in transport? Applied Energy 2018;225:965–74. https://doi.org/10.1016/j.apenergy.2018.05.076.

[5] International Energy Agency. World Energy Outlook 2019 – Analysis. IEA 2019. https://www.iea.org/reports/world-energy-outlook-2019 (accessed September 14, 2020).

[6] Exxon Mobil. Outlook for Energy. ExxonMobil 2019. https://corporate.exxonmobil.com:443/Energy-and-environment/Looking-forward/Outlook-for-Energy (accessed September 14, 2020).

[7] Vancoillie J, Verhelst S. Modeling the combustion of light alcohols in SI engines : a preliminary study. FISITA World Automotive Congress. Student Congress, Proceedings, International Federation of Automotive Engineering Societies; 2010.

[8] Sharma TK, Rao GAP, Murthy KM. Homogeneous Charge Compression Ignition (HCCI) Engines: A Review. Arch Computat Methods Eng 2016;23:623–57. https://doi.org/10.1007/s11831-015-9153-0.

[9] Krishnamoorthi M, Malayalamurthi R, He Z, Kandasamy S. A review on low temperature combustion engines: Performance, combustion and emission characteristics. Renewable and Sustainable Energy Reviews 2019;116:109404. https://doi.org/10.1016/j.rser.2019.109404.

[10] Bright Hub Engineering. HCCI - Reliable, Efficient and Cost Effective Ignition Technology 2009. https://www.brighthubengineering.com/machine-design/23906-everything-you-should-know-about-homogeneous-charge-engines/ (accessed September 14, 2020).

[11] Mazda Motor Corporation. MAZDA: SKYACTIV-X | We are Engineers 2017. https://www.mazda.com/en/innovation/mazda-stories/engineers/skyactiv-x/ (accessed September 14, 2020).

[12] MacLean HL, Lave LB. Evaluating automobile fuel/propulsion system technologies. Progress in Energy and Combustion Science 2003:69.

[13] Bergthorson JM, Thomson MJ. A review of the combustion and emissions properties of advanced transportation biofuels and their impact on existing and future engines. Renewable and Sustainable Energy Reviews 2015;42:1393–417. https://doi.org/10.1016/j.rser.2014.10.034.

[14] Malins C. What role is there for electrofuel technologies in European transport's low carbon future? 2017.

[15] Royal Society (Great Britain). Sustainable synthetic carbon based fuels for transport. 2019.

[16] NGV Global Knowledgebase. Current Natural Gas Vehicle Statistics 2019. http://www.iangv.org/current-ngv-stats/ (accessed September 14, 2020).

[17] International Energy Agency. Technology Collaboration Programme on Advanced Motor Fuels 2012. https://www.iea-amf.org/content/fuel_information/lpg (accessed September 14, 2020).

[18] Sims REH, Mabee W, Saddler JN, Taylor M. An overview of second generation biofuel technologies. Bioresource Technology 2010;101:1570–80. https://doi.org/10.1016/j.biortech.2009.11.046.

[19] International Energy Agency. Transport Biofuels – Analysis. IEA 2019. https://www.iea.org/reports/transport-biofuels (accessed September 14, 2020).

[20] Council of the European Union. 2002/358/EC: Council Decision of 25 April 2002 concerning the approval, on behalf of the European Community, of the Kyoto Protocol to the United Nations Framework Convention on Climate Change and the joint fulfilment of commitments thereunder. Council of the European Union; 2002.

[21] HM UK Government. Climate Change Act 2008 (As Enacted). HM UK Government; 2008.

[22] United Nations. Paris Agreement 2015.

[23] IPCC. Global Warming of 1.5 °C. mental Panel on Climate Change; 2018.

[24] HM UK Government. Climate Change Act 2008 - (Amended). HM UK Government; 2019.

[25] Department for Business, Energy and Industrial Strategy. 2018 UK Greenhouse Gas Emissions, Final figures. 2020.

[26] European Commission. 2030 climate & energy framework. Climate Action - European Commission 2016. https://ec.europa.eu/clima/policies/strategies/2030_en (accessed September 14, 2020).

[27] European Commission. DIRECTIVE (EU) 2018/ 2001 OF THE EUROPEAN PARLIAMENT AND OF THE COUNCIL - of 11 December 2018 - on the promotion of the use of energy from renewable sources. Official Journal of the European Union 2018:128.

[28] Srinivasan CA, Saravanan CG. Study of Combustion Characteristics of an SI Engine fuelled with Ethanol. Journal of Sustainable Energy & Environment 2010;1:7.

[29] Gravalos I, Moshou D, Gialamas T, Xyradakis P, Kateris D, Tsiropoulos Z. Performance and Emission Characteristics of Spark Ignition Engine Fuelled with Ethanol and Methanol Gasoline Blended Fuels. Alternative Fuel 2011. https://doi.org/10.5772/23176.

[30] Farkade HS, Pathre AP. Experimental investigation of methanol, ethanol and butanol blendswith gasoline on SI engine. IJETAE 2012;2.

[31] Gopal M, Rajendra D. Experimental Study on SI Engine At Different Ignition Timing Using CNG And Gasoline-20 % n Butanol Blend. International Journal of Emerging Technology and Advanced Engineering 2013;3.

[32] Wallner T, Miers SA, McConnell S. A Comparison of Ethanol and Butanol as Oxygenates Using a Direct-Injection, Spark-Ignition (DISI) Engine, American Society of Mechanical Engineers Digital Collection; 2009, p. 129–39. https://doi.org/10.1115/ICES2008-1690.

[33] Szulczyk K. Which is a better transportation fuel - Butanol or ethanol? International Journal of Energy and Environment 2010;1.

[34] Wigg BR. A study on the emissions of butanol using a spark ignition engine and their reduction using electrostatically assisted injection. University of Illinois at Urbana-Champaign, 2011.

[35] Skevis G. Liquid Biofuels: Biodiesel and Bioalcohols, 2010. https://doi.org/10.1002/9783527628148.hoc051.

[36] Lapuerta M, García-Contreras R, Campos-Fernández J, Dorado MP. Stability, Lubricity, Viscosity, and Cold-Flow Properties of Alcohol−Diesel Blends. Energy Fuels 2010;24:4497–502. https://doi.org/10.1021/ef100498u.

[37] Kumar V, Gupta D, Naseer Siddiquee MW, Nagpal A, Kumar N. Performance and Emission Characteristics of n-Butanol and Iso-Butanol Diesel Blend Comparison, 2015, p. 2015-01–2819. https://doi.org/10.4271/2015-01-2819.

[38] Lapuerta M, Hernández JJ, Fernández-Rodríguez D, Cova-Bonillo A. Autoignition of blends of n-butanol and ethanol with diesel or biodiesel fuels in a constant-volume combustion chamber. Energy 2017;118:613–21. https://doi.org/10.1016/j.energy.2016.10.090.

[39] Weber BW, Sung C-J. Comparative Autoignition Trends in Butanol Isomers at Elevated Pressure. Energy Fuels 2013;27:1688–98. https://doi.org/10.1021/ef302195c.

[40] Konig G, Sheppard CGW. End Gas Autoignition and Knock in a Spark Ignition Engine, 1990, p. 902135. https://doi.org/10.4271/902135.

[41] AlRamadan AS, Badra J, Javed T, Al-Abbad M, Bokhumseen N, Gaillard P, et al. Mixed butanols addition to gasoline surrogates: Shock tube ignition delay time measurements and chemical kinetic modeling. Combustion and Flame 2015;162:3971–9. https://doi.org/10.1016/j.combustflame.2015.07.035.

[42] Moss JT, Berkowitz AM, Oehlschlaeger MA, Biet J, Warth V, Glaude P-A, et al. An Experimental and Kinetic Modeling Study of the Oxidation of the Four Isomers of Butanol. J Phys Chem A 2008;112:10843–55. https://doi.org/10.1021/jp806464p.

[43] Stranic I, Chase DP, Harmon JT, Yang S, Davidson DF, Hanson RK. Shock tube measurements of ignition delay times for the butanol isomers. Combustion and Flame 2012;159:516–27. https://doi.org/10.1016/j.combustflame.2011.08.014.

[44] Sarathy SM, Vranckx S, Yasunaga K, Mehl M, Oßwald P, Metcalfe WK, et al. A comprehensive chemical kinetic combustion model for the four butanol isomers. Combustion and Flame 2012;159:2028–55. https://doi.org/10.1016/j.combustflame.2011.12.017.

[45] Kukkadapu G, Kumar K, Sung C-J, Mehl M, Pitz WJ. Autoignition of gasoline and its surrogates in a rapid compression machine. Proceedings of the Combustion Institute 2013;34:345–52. https://doi.org/10.1016/j.proci.2012.06.135.

[46] Zhang K, Banyon C, Bugler J, Curran HJ, Rodriguez A, Herbinet O, et al. An updated experimental and kinetic modeling study of n-heptane oxidation. Combustion and Flame 2016;172:116–35. https://doi.org/10.1016/j.combustflame.2016.06.028.

[47] Gorbatenko I, Tomlin AS, Lawes M, Cracknell RF. Experimental and modelling study of the impacts of n-butanol blending on the auto-ignition behaviour of gasoline and its surrogate at low temperatures. Proceedings of the Combustion Institute 2019;37:501–9. https://doi.org/10.1016/j.proci.2018.05.089.

[48] Sung C-J, Curran HJ. Using rapid compression machines for chemical kinetics studies. Progress in Energy and Combustion Science 2014;44:1–18. https://doi.org/10.1016/j.pecs.2014.04.001.

[49] Heywood J. Internal Combustion Engine Fundamentals. McGraw-Hill Education; 1988.

[50] Burluka AA, El-Dein Hussin AMTA, Ling Z-Y, Sheppard CGW. Effects of large-scale turbulence on cyclic variability in spark-ignition engine. Experimental Thermal and Fluid Science 2012;43:13–22. https://doi.org/10.1016/j.expthermflusci.2012.04.012.

[51] Agbro E, Tomlin AS, Lawes M, Park S, Sarathy SM. The influence of n -butanol blending on the ignition delay times of gasoline and its surrogate at high pressures. Fuel 2017;187:211–9. https://doi.org/10.1016/j.fuel.2016.09.052.

[52] Agbro E, Zhang W, Tomlin AS, Burluka A. Experimental Study on the Influence of *n* -Butanol Blending on the Combustion, Autoignition, and Knock Properties of Gasoline and Its Surrogate in a Spark-Ignition Engine. Energy Fuels 2018;32:10052–64. https://doi.org/10.1021/acs.energyfuels.8b00713.

[53] Pilling MJ. Low-temperature Combustion and Autoignition. Elsevier; 1997.

[54] Turányi T, Tomlin AS. Analysis of Kinetic Reaction Mechanisms. Berlin: Springer; 2014.

[55] Stone R. Introduction to Internal Combustion Engines. Basingstoke: Macmillan International Higher Education; 2012.

[56] Ganesan V. Internal Combustion Engines. New York: McGraw-Hill; 1996.

[57] Liu K, Burluka AA, Sheppard CGW. Turbulent flame and mass burning rate in a spark ignition engine. Fuel 2013;107:202–8. https://doi.org/10.1016/j.fuel.2013.01.042.

[58] Wang Z, Liu H, Song T, Qi Y, He X, Shuai S, et al. Relationship between super-knock and pre-ignition. International Journal of Engine Research 2015;16:166–80. https://doi.org/10.1177/1468087414530388.

[59] Ling Z. Flame propagation and autoignition in a high pressure optical engine. phd. University of Leeds, 2014.

[60] Dahnz C, Han K-M, Spicher U, Magar M, Schießl R, Maas U. Investigations on Pre-Ignition in Highly Supercharged SI Engines. SAE International Journal of Engines 2010;3:214–24.

[61] Kalghatgi GT, Bradley D. Pre-ignition and ‘super-knock’ in turbo-charged spark-ignition engines: International Journal of Engine Research 2012. https://doi.org/10.1177/1468087411431890.

[62] Khan AF. Chemical kinetics modelling of combustion processes in SI engines. PhD. University of Leeds, 2014.

[63] Bates L, Bradley D, Paczko G, Peters N. Engine hot spots: Modes of auto-ignition and reaction propagation. Combustion and Flame 2016;166:80–5. https://doi.org/10.1016/j.combustflame.2016.01.002.

[64] Wang Z, Qi Y, He X, Wang J, Shuai S, Law CK. Analysis of pre-ignition to super-knock: Hotspot-induced deflagration to detonation. Fuel 2015;144:222–7. https://doi.org/10.1016/j.fuel.2014.12.061.

[65] Wang Z, Liu H, Reitz RD. Knocking combustion in spark-ignition engines. Progress in Energy and Combustion Science 2017;61:78–112. https://doi.org/10.1016/j.pecs.2017.03.004.

[66] Kawahara N, Tomita E, Sakata Y. Auto-ignited kernels during knocking combustion in a spark-ignition engine. Proceedings of the Combustion Institute 2007;31:2999–3006. https://doi.org/10.1016/j.proci.2006.07.210.

[67] ASTM International. ASTM D2699-19, Test Method for Research Octane Number of Spark-Ignition Engine Fuel. West Conshohocken, PA,: ASTM International; 2019. https://doi.org/10.1520/D2699-19.

[68] ASTM International. ASTM D2700-19, Standard Test Method for Motor Octane Number of Spark-Ignition Engine Fuel. West Conshohocken, PA: ASTM International; 2019. https://doi.org/10.1520/D2700-19.

[69] Bradley D, Head RA. Engine autoignition: The relationship between octane numbers and autoignition delay times. Combustion and Flame 2006;147:171–84. https://doi.org/10.1016/j.combustflame.2006.09.001.

[70] Mehl M, Chen JY, Pitz WJ, Sarathy SM, Westbrook CK. An Approach for Formulating Surrogates for Gasoline with Application toward a Reduced Surrogate Mechanism for CFD Engine Modeling. Energy Fuels 2011;25:5215–23. https://doi.org/10.1021/ef201099y.

[71] Naser N, Sarathy SM, Chung SH. Estimating fuel octane numbers from homogeneous gas-phase ignition delay times. Combustion and Flame 2018;188:307–23. https://doi.org/10.1016/j.combustflame.2017.09.037.

[72] Naser N, Yang SY, Kalghatgi G, Chung SH. Relating the octane numbers of fuels to ignition delay times measured in an ignition quality tester (IQT). Fuel 2017;187:117–27. https://doi.org/10.1016/j.fuel.2016.09.013.

[73] Kalghatgi GT. The outlook for fuels for internal combustion engines. International Journal of Engine Research 2014;15:383–98. https://doi.org/10.1177/1468087414526189.

[74] Mittal V, Heywood JB. The Shift in Relevance of Fuel RON and MON to Knock Onset in Modern SI Engines Over the Last 70 Years. SAE International Journal of Engines 2010;2:1–10.

[75] Boot MD, Tian M, Hensen EJM, Mani Sarathy S. Impact of fuel molecular structure on auto-ignition behavior – Design rules for future high performance gasolines. Progress in Energy and Combustion Science 2017;60:1–25. https://doi.org/10.1016/j.pecs.2016.12.001.

[76] Somers KP, Cracknell RF, Curran HJ. A chemical kinetic interpretation of the octane appetite of modern gasoline engines. Proceedings of the Combustion Institute 2019;37:4857–64. https://doi.org/10.1016/j.proci.2018.05.123.

[77] Leppard WR. The Chemical Origin of Fuel Octane Sensitivity, 1990, p. 902137. https://doi.org/10.4271/902137.

[78] Pitz WJ, Cernansky NP, Dryer FL, Egolfopoulos FN, Farrell JT, Friend DG, et al. Development of an Experimental Database and Chemical Kinetic Models for Surrogate Gasoline Fuels, 2007, p. 2007-01–0175. https://doi.org/10.4271/2007-01-0175.

[79] Atkinson R. Gas-phase tropospheric chemistry of organic compounds: A review. Atmospheric Environment Part A General Topics 1990;24:1–41. https://doi.org/10.1016/0960-1686(90)90438-S.

[80] Perry R, Gee IL. Vehicle emissions in relation to fuel composition. Science of The Total Environment 1995;169:149–56. https://doi.org/10.1016/0048-9697(95)04643-F.

[81] Hajbabaei M, Karavalakis G, Miller JW, Villela M, Xu KH, Durbin TD. Impact of olefin content on criteria and toxic emissions from modern gasoline vehicles. Fuel 2013;107:671–9. https://doi.org/10.1016/j.fuel.2012.12.031.

[82] Hochhauser AM. Review of Prior Studies of Fuel Effects on Vehicle Emissions. SAE Int J Fuels Lubr 2009;2:541–67. https://doi.org/10.4271/2009-01-1181.

[83] Sarathy SM, Park S, Weber BW, Wang W, Veloo PS, Davis AC, et al. A comprehensive experimental and modeling study of iso-pentanol combustion. Combustion and Flame 2013;160:2712–28. https://doi.org/10.1016/j.combustflame.2013.06.022.

[84] Sarathy SM, Oßwald P, Hansen N, Kohse-Höinghaus K. Alcohol combustion chemistry. Progress in Energy and Combustion Science 2014;44:40–102. https://doi.org/10.1016/j.pecs.2014.04.003.

[85] Mehl M, Pitz WJ, Westbrook CK, Curran HJ. Kinetic modeling of gasoline surrogate components and mixtures under engine conditions. Proceedings of the Combustion Institute 2011;33:193–200. https://doi.org/10.1016/j.proci.2010.05.027.

[86] Goldsborough SS, Hochgreb S, Vanhove G, Wooldridge MS, Curran HJ, Sung C-J. Advances in rapid compression machine studies of low- and intermediate-temperature autoignition phenomena. Progress in Energy and Combustion Science 2017;63:1–78. https://doi.org/10.1016/j.pecs.2017.05.002.

[87] Dryer FL, Haas FM, Santner J, Farouk TI, Chaos M. Interpreting chemical kinetics from complex reaction–advection–diffusion systems: Modeling of flow reactors and related experiments. Progress in Energy and Combustion Science 2014;44:19–39. https://doi.org/10.1016/j.pecs.2014.04.002.

[88] Kang D, Lilik G, Dillstrom V, Agudelo J, Lapuerta M, Al-Qurashi K, et al. Impact of branched structures on cycloalkane ignition in a motored engine: Detailed product and conformational analyses. Combustion and Flame 2015;162:877–92. https://doi.org/10.1016/j.combustflame.2014.09.009.

[89] Hanson RK, Davidson DF. Recent advances in laser absorption and shock tube methods for studies of combustion chemistry. Progress in Energy and Combustion Science 2014;44:103–14. https://doi.org/10.1016/j.pecs.2014.05.001.

[90] Zhang K, Banyon C, Togbé C, Dagaut P, Bugler J, Curran HJ. An experimental and kinetic modeling study of n-hexane oxidation. Combustion and Flame 2015;162:4194–207. https://doi.org/10.1016/j.combustflame.2015.08.001.

[91] Atef N, Kukkadapu G, Mohamed SY, Rashidi MA, Banyon C, Mehl M, et al. A comprehensive iso-octane combustion model with improved thermochemistry and chemical kinetics. Combustion and Flame 2017;178:111–34. https://doi.org/10.1016/j.combustflame.2016.12.029.

[92] Sarathy SM, Tingas E-Al, Nasir EF, Detogni A, Wang Z, Farooq A, et al. Three-stage heat release in n-heptane auto-ignition. Proceedings of the Combustion Institute 2019;37:485–92. https://doi.org/10.1016/j.proci.2018.07.075.

[93] Hu H, Keck J. Autoignition of Adiabatically Compressed Combustible Gas Mixtures, 1987. https://doi.org/10.4271/872110.

[94] Mittal G, Sung C-J, Yetter RA. Autoignition of H2/CO at elevated pressures in a rapid compression machine. International Journal of Chemical Kinetics 2006;38:516–29. https://doi.org/10.1002/kin.20180.

[95] Grogan KP, Scott Goldsborough S, Ihme M. Ignition regimes in rapid compression machines. Combustion and Flame 2015;162:3071–80. https://doi.org/10.1016/j.combustflame.2015.03.020.

[96] Battin-Leclerc F, Blurock E, Bounaceur R, Fournet R, Glaude P-A, Herbinet O, et al. Towards cleaner combustion engines through groundbreaking detailed chemical kinetic models. Chem Soc Rev 2011;40:4762–82. https://doi.org/10.1039/C0CS00207K.

[97] Minetti R, Carlier M, Ribaucour M, Therssen E, Sochet LR. Comparison of oxidation and autoignition of the two primary reference fuels by rapid compression. Symposium (International) on Combustion 1996;26:747–53. https://doi.org/10.1016/S0082-0784(96)80283-9.

[98] Griffiths JF, Halford-Maw PA, Mohamed C. Spontaneous ignition delays as a diagnostic of the propensity of alkanes to cause engine knock. Combustion and Flame 1997;111:327–37. https://doi.org/10.1016/S0010-2180(97)00004-7.

[99] Silke EJ, Curran HJ, Simmie JM. The influence of fuel structure on combustion as demonstrated by the isomers of heptane: a rapid compression machine study. Proceedings of the Combustion Institute 2005;30:2639–47. https://doi.org/10.1016/j.proci.2004.08.180.

[100] Wurmel J, Simmie J. CFD studies of a twin-piston rapid compression machine. Combustion and Flame 2005;141:417–30. https://doi.org/10.1016/j.combustflame.2005.01.015.

[101] Bradley D, Lawes M, Materego M. Interpretation of Auto-ignition Delay Times Measured in Different Rapid Compression Machines. 25th International Colloquium on the Dynamics of Explosions and Reactive systems, Leeds: Leeds; 2015.

[102] Lee D, Hochgreb S. Rapid Compression Machines: Heat Transfer and Suppression of Corner Vortex. Combustion and Flame 1998;114:531–45. https://doi.org/10.1016/S0010-2180(97)00327-1.

[103] Taylor CF, Taylor ES, Livengood JC, Russell WA, Leary WA. Ignition of Fuels by Rapid Compression, 1950, p. 500178. https://doi.org/10.4271/500178.

[104] Livengood JC, Leary WA. Autoignition by Rapid Compression. Ind Eng Chem 1951;43:2797–805. https://doi.org/10.1021/ie50504a046.

[105] Park P, Keck JC. Rapid Compression Machine Measurements of Ignition Delays for Primary Reference Fuels. SAE Transactions 1990;99:11–23.

[106] Clarkson J, Griffiths JF, MacNamara JP, Whitaker BJ. Temperature fields during the development of combustion in a rapid compression machine. Combustion and Flame 2001;125:1162–75. https://doi.org/10.1016/S0010-2180(01)00236-X.

[107] Griffiths JF, MacNamara JP, Mohamed C, Whitaker BJ, Pan J, Sheppard CGW. Temperature fields during the development of autoignition in a rapid compression machine. Faraday Discuss 2002;119:287–303. https://doi.org/10.1039/B102002L.

[108] Griffiths JF, Jiao Q, Kordylewski W, Schreiber M, Meyer J, Knoche KF. Experimental and numerical studies of ditertiary butyl peroxide combustion at high pressures in a rapid compression machine. Combustion and Flame 1993;93:303–15. https://doi.org/10.1016/0010-2180(93)90111-F.

[109] Desgroux P, Gasnot L, Sochet LR. Instantaneous temperature measurement in a rapid-compression machine using laser Rayleigh scattering. Appl Phys B 1995;61:69–72. https://doi.org/10.1007/BF01090974.

[110] Desgroux P, Minetti R, Sochet LR. Temperature Distribution Induced by Pre-Ignition Reactions in a Rapid Compression Machine. Combustion Science and Technology 1996;113:193–203. https://doi.org/10.1080/00102209608935494.

[111] Guézet J, Kageyama T. Étude aérodynamique dans une machine à compression rapide. Revue Générale de Thermique 1997;36:17–25. https://doi.org/10.1016/S0035-3159(99)80062-2.

[112] Chen K, Karim GA. An Examination of the Effects of Charge Inhomogeneity on the Compression Ignition of Fuel-Air Mixtures, 1998, p. 982614. https://doi.org/10.4271/982614.

[113] Frolov SM, Emans M, Ivanov VS, Basara B, Leshevich VV, Penyazkov OG. 3D simulation of hydrogen ignition in a rapid compression machine. Journal of Loss Prevention in the Process Industries 2013;26:1558–68. https://doi.org/10.1016/j.jlp.2013.08.013.

[114] Mittal G, Sung C-J. Aerodynamics inside a rapid compression machine. Combustion and Flame 2006;145:160–80. https://doi.org/10.1016/j.combustflame.2005.10.019.

[115] Donovan MT, He X, Zigler BT, Palmer TR, Wooldridge MS, Atreya A. Demonstration of a free-piston rapid compression facility for the study of high temperature combustion phenomena. Combustion and Flame 2004;137:351–65. https://doi.org/10.1016/j.combustflame.2004.02.006.

[116] Mittal G, Sung C-J. A Rapid Compression Machine for Chemical Kinetics Studies at Elevated Pressures and Temperatures. Combustion Science and Technology 2007;179:497–530. https://doi.org/10.1080/00102200600671898.

[117] Mittal G, Raju MP, Sung C-J. CFD modeling of two-stage ignition in a rapid compression machine: Assessment of zero-dimensional approach. Combustion and Flame 2010;157:1316–24. https://doi.org/10.1016/j.combustflame.2010.02.019.

[118] Mittal G, Raju MP, Bhari A. A numerical assessment of the novel concept of crevice containment in a rapid compression machine. Combustion and Flame 2011;158:2420–7. https://doi.org/10.1016/j.combustflame.2011.04.013.

[119] Mittal G, Gupta S. Computational assessment of an approach for implementing crevice containment in rapid compression machines. Fuel 2012;102:536–44. https://doi.org/10.1016/j.fuel.2012.07.026.

[120] Mittal G, Bhari A. A rapid compression machine with crevice containment. Combustion and Flame 2013;160:2975–81. https://doi.org/10.1016/j.combustflame.2013.06.027.

[121] Mittal G, Chomier M. Effect of crevice mass transfer in a rapid compression machine. Combustion and Flame 2014;161:398–404. https://doi.org/10.1016/j.combustflame.2013.09.008.

[122] Petersen EL, Kalitan DM, Barrett AB, Reehal SC, Mertens JD, Beerer DJ, et al. New syngas/air ignition data at lower temperature and elevated pressure and comparison to current kinetics models. Combustion and Flame 2007;149:244–7. https://doi.org/10.1016/j.combustflame.2006.12.007.

[123] Walton SM, He X, Zigler BT, Wooldridge MS. An experimental investigation of the ignition properties of hydrogen and carbon monoxide mixtures for syngas turbine applications. Proceedings of the Combustion Institute 2007;31:3147–54. https://doi.org/10.1016/j.proci.2006.08.059.

[124] Walton S, He X, Zigler B, Wooldridge M, Atreya A. An experimental investigation of iso-octane ignition phenomena. Combustion and Flame 2007;150:246–62. https://doi.org/10.1016/j.combustflame.2006.07.016.

[125] Mansfield AB, Wooldridge MS. High-pressure low-temperature ignition behavior of syngas mixtures. Combustion and Flame 2014;161:2242–51. https://doi.org/10.1016/j.combustflame.2014.03.001.

[126] Mansfield AB, Wooldridge MS, Di H, He X. Low-temperature ignition behavior of iso-octane. Fuel 2015;139:79–86. https://doi.org/10.1016/j.fuel.2014.08.019.

[127] Assanis D, Wagnon SW, Wooldridge MS. An experimental study of flame and autoignition interactions of iso-octane and air mixtures. Combustion and Flame 2015;162:1214–24. https://doi.org/10.1016/j.combustflame.2014.10.012.

[128] Fieweger K, Blumenthal R, Adomeit G. Self-ignition of S.I. engine model fuels: A shock tube investigation at high pressure. Combustion and Flame 1997;109:599–619. https://doi.org/10.1016/S0010-2180(97)00049-7.

[129] Vermeer DJ, Meyer JW, Oppenheim AK. Auto-ignition of hydrocarbons behind reflected shock waves. Combustion and Flame 1972;18:327–36. https://doi.org/10.1016/S0010-2180(72)80183-4.

[130] Griffiths JF, MacNamara JP, Sheppard CGW, Turton DA, Whitaker BJ. The relationship of knock during controlled autoignition to temperature inhomogeneities and fuel reactivity. Fuel 2002;81:2219–25. https://doi.org/10.1016/S0016-2361(02)00134-5.

[131] Büttgen RD, Raffius T, Grünefeld G, Koß H-J, Heufer A. High-speed imaging of the ignition of ethanol at engine relevant conditions in a rapid compression machine. Proceedings of the Combustion Institute 2019;37:1471–8. https://doi.org/10.1016/j.proci.2018.05.001.

[132] Mittal G, Sung C-J. Autoignition of toluene and benzene at elevated pressures in a rapid compression machine. Combustion and Flame 2007;150:355–68. https://doi.org/10.1016/j.combustflame.2007.04.014.

[133] Griffiths JF, Barnard JA. Flame and Combustion, 3rd Edition. CRC Press; 1995.

[134] Koivisto EK. Ignition and combustion of future oxygenated fuels in compression-ignition engines. Doctoral. UCL (University College of London), 2016.

[135] Pilling MJ, Seakins PW. Reaction Kinetics. Second Edition. Oxford, New York: Oxford University Press; 1995.

[136] Curran HJ. Developing detailed chemical kinetic mechanisms for fuel combustion. Proceedings of the Combustion Institute 2019;37:57–81. https://doi.org/10.1016/j.proci.2018.06.054.

[137] Sivaramakrishnan R, Michael JV. Rate constants for OH with selected large alkanes: shock-tube measurements and an improved group scheme. J Phys Chem A 2009;113:5047–60. https://doi.org/10.1021/jp810987u.

[138] Miller JA, Klippenstein SJ. The reaction between ethyl and molecular oxygen II: Further analysis. International Journal of Chemical Kinetics 2001;33:654–68. https://doi.org/10.1002/kin.1063.

[139] Estupiñán EG, Smith JD, Tezaki A, Klippenstein SJ, Taatjes CA. Measurements and Modeling of DO2 Formation in the Reactions of C2D5 and C3D7 Radicals with O2. J Phys Chem A 2007;111:4015–30. https://doi.org/10.1021/jp067602a.

[140] Savee JD, Papajak E, Rotavera B, Huang H, Eskola AJ, Welz O, et al. Direct observation and kinetics of a hydroperoxyalkyl radical (QOOH). Science 2015;347:643–6. https://doi.org/10.1126/science.aaa1495.

[141] Kaiser EW. Temperature and Pressure Dependence of the C2H4 Yield from the Reaction C2H5 + O2. J Phys Chem 1995;99:707–11. https://doi.org/10.1021/j100002a039.

[142] Simmie JM. Detailed chemical kinetic models for the combustion of hydrocarbon fuels. Progress in Energy and Combustion Science 2003;29:599–634. https://doi.org/10.1016/S0360-1285(03)00060-1.

[143] Zádor J, Taatjes CA, Fernandes RX. Kinetics of elementary reactions in low-temperature autoignition chemistry. Progress in Energy and Combustion Science 2011;37:371–421. https://doi.org/10.1016/j.pecs.2010.06.006.

[144] Bugler J, Somers KP, Silke EJ, Curran HJ. Revisiting the Kinetics and Thermodynamics of the Low-Temperature Oxidation Pathways of Alkanes: A Case Study of the Three Pentane Isomers. J Phys Chem A 2015;119:7510–27. https://doi.org/10.1021/acs.jpca.5b00837.

[145] Westbrook CK, Dryer FL. Chemical kinetic modeling of hydrocarbon combustion. Progress in Energy and Combustion Science 1984;10:1–57. https://doi.org/10.1016/0360-1285(84)90118-7.

[146] Carstensen H-H, Dean AM. Development of Detailed Kinetic Models for the Thermal Conversion of Biomass via First Principle Methods and Rate Estimation Rules. Computational Modeling in Lignocellulosic Biofuel Production, vol. 1052, American Chemical Society; 2010, p. 201–43. https://doi.org/10.1021/bk-2010-1052.ch010.

[147] Battin-Leclerc F. Detailed chemical kinetic models for the low-temperature combustion of hydrocarbons with application to gasoline and diesel fuel surrogates. Progress in Energy and Combustion Science 2008;34:440–98. https://doi.org/10.1016/j.pecs.2007.10.002.

[148] Pelucchi M, Bissoli M, Rizzo C, Zhang Y, Somers K, Frassoldati A, et al. A Kinetic Modelling Study of Alcohols Operating Regimes in a HCCI Engine. SAE Int J Engines 2017;10:2354–70. https://doi.org/10.4271/2017-24-0077.

[149] Zádor J, Fernandes RX, Georgievskii Y, Meloni G, Taatjes CA, Miller JA. The reaction of hydroxyethyl radicals with O2: A theoretical analysis and experimental product study. Proceedings of the Combustion Institute 2009;32:271–7. https://doi.org/10.1016/j.proci.2008.05.020.

[150] Welz O, Savee JD, Eskola AJ, Sheps L, Osborn DL, Taatjes CA. Low-temperature combustion chemistry of biofuels: Pathways in the low-temperature (550–700K) oxidation chemistry of isobutanol and tert-butanol. Proceedings of the Combustion Institute 2013;34:493–500. https://doi.org/10.1016/j.proci.2012.05.058.

[151] Welz O, Zádor J, Savee JD, Sheps L, Osborn DL, Taatjes CA. Low-Temperature Combustion Chemistry of n-Butanol: Principal Oxidation Pathways of Hydroxybutyl Radicals. J Phys Chem A 2013;117:11983–2001. https://doi.org/10.1021/jp403792t.

[152] Heiss A, Sahetchian K. Isomerization reactions of the n-C4H9O and n-OOC4H8OH radicals in oxygen. International Journal of Chemical Kinetics 1996;28:531–44. https://doi.org/10.1002/(SICI)1097-4601(1996)28:7<531::AID-KIN5>3.0.CO;2-W.

[153] Jorand F, Heiss A, Sahetchian K, Kerhoas L, Einhorn J. Identification of an unexpected peroxide formed by successive isomerization reactions of the n-butoxy radical in oxygen. J Chem Soc, Faraday Trans 1996;92:4167–71. https://doi.org/10.1039/FT9969204167.

[154] Moc J, Simmie JM, Curran HJ. The elimination of water from a conformationally complex alcohol: A computational study of the gas phase dehydration of n-butanol. Journal of Molecular Structure 2009;928:149–57. https://doi.org/10.1016/j.molstruc.2009.03.026.

[155] da Silva G, Kim C-H, Bozzelli JW. Thermodynamic Properties (Enthalpy, Bond Energy, Entropy, and Heat Capacity) and Internal Rotor Potentials of Vinyl Alcohol, Methyl Vinyl Ether, and Their Corresponding Radicals. J Phys Chem A 2006;110:7925–34. https://doi.org/10.1021/jp0602878.

[156] da Silva G, Bozzelli JW. Role of the α-hydroxyethylperoxy radical in the reactions of acetaldehyde and vinyl alcohol with HO2. Chemical Physics Letters 2009;483:25–9. https://doi.org/10.1016/j.cplett.2009.10.045.

[157] Hansen N, Harper MR, Green WH. High-temperature oxidation chemistry of n-butanol – experiments in low-pressure premixed flames and detailed kinetic modeling. Phys Chem Chem Phys 2011;13:20262–74. https://doi.org/10.1039/C1CP21663E.

[158] da Silva G. Carboxylic Acid Catalyzed Keto-Enol Tautomerizations in the Gas Phase. Angewandte Chemie International Edition 2010;49:7523–5. https://doi.org/10.1002/anie.201003530.

[159] Altarawneh M, Al-Muhtaseb AH, Dlugogorski BZ, Kennedy EM, Mackie JC. Rate constants for hydrogen abstraction reactions by the hydroperoxyl radical from methanol, ethenol, acetaldehyde, toluene, and phenol. Journal of Computational Chemistry 2011;32:1725–33. https://doi.org/10.1002/jcc.21756.

[160] Rao H-B, Zeng X-Y, He H, Li Z-R. Theoretical Investigations on Removal Reactions of Ethenol by H Atom. J Phys Chem A 2011;115:1602–8. https://doi.org/10.1021/jp111407d.

[161] Atkins P, Paula J de. Atkins' Physical Chemistry. OUP Oxford; 2010.

[162] Reaction Design. ANSYS Chemkin-Pro 17.2 Theory Manual 2016:414.

[163] Waage P, Gulberg CM. Studies concerning affinity. J Chem Educ 1986;63:1044. https://doi.org/10.1021/ed063p1044.

[164] McQuarrie DA, Simon JD. Physical Chemistry: A Molecular Approach. University Science Books; 1997.

[165] McBride BJ, Gordon S, Reno MA. Coefficients for Calculating Thermodynamic and Transport Properties of Individual Species. NASA Technical Memorandum 1993;4513.

[166] Fernandes, R. Combustion Chemistry. *In:* M.W. Lackner, F; Agarwal, A. K, ed. Handbook of Combustion. Weinheim: Wiley-VCH Verlag GmbH and Co, 2010.

[167] Venkatesh PK, Chang AY, Dean AM, Cohen MH, Carr RW. Parameterization of pressure- and temperature-dependent kinetics in multiple well reactions. AIChE Journal 1997;43:1331–40. https://doi.org/10.1002/aic.690430522.

[168] Goodwin DG, Speth RL, Moffat HK, Weber BW. Cantera: An Object-oriented Software Toolkit for Chemical Kinetics, Thermodynamics, and Transport Processes. 2018. https://doi.org/10.5281/zenodo.1174508.

[169] Reaction Design. CHEMKIN-PRO 15112. San Diego: Reaction Design; 2011.

[170] Glassman I, Yetter RA, Glumac NG. Combustion. Academic Press; 2014.

[171] Frenklach M, Wang H, Rabinowitz MJ. Optimization and analysis of large chemical kinetic mechanisms using the solution mapping method—combustion of methane. Progress in Energy and Combustion Science 1992;18:47–73. https://doi.org/10.1016/0360-1285(92)90032-V.

[172] Goldsborough SS, Santner J, Kang D, Fridlyand A, Rockstroh T, Jespersen MC. Heat release analysis for rapid compression machines: Challenges and opportunities. Proceedings of the Combustion Institute 2019;37:603–11. https://doi.org/10.1016/j.proci.2018.05.128.

[173] Liu Z, Chen R. A Zero-Dimensional Combustion Model with Reduced Kinetics for SI Engine Knock Simulation. Combustion Science and Technology 2009;181:828–52. https://doi.org/10.1080/00102200902864704.

[174] Liu Z. Chemical kinetics modelling study on fuel autoignition in internal combustion engines. thesis. Loughborough University, 2010.

[175] Ruscic B, Pinzon RE, Laszewski G von, Kodeboyina D, Burcat A, Leahy D, et al. Active Thermochemical Tables: thermochemistry for the 21st century. J Phys: Conf Ser 2005;16:561–570. https://doi.org/10.1088/1742-6596/16/1/078.

[176] Goos E, Burcat A, Ruscic B. Extended Third Millennium Ideal Gas and Condensed Phase Thermochemical Database for Combustion with Updates from Active Thermochemical Tables 2020.

[177] NIST Chemical Kinetics Database n.d. https://kinetics.nist.gov/kinetics/citation.jsp (accessed September 23, 2020).

[178] NIST. NIST Database. NIST Chemistry WebBook, SRD 69 2018. https://doi.org/10.18434/T4D303.

[179] Weber BW, Kumar K, Zhang Y, Sung C-J. Autoignition of n-butanol at elevated pressure and low-to-intermediate temperature. Combustion and Flame 2011;158:809–19. https://doi.org/10.1016/j.combustflame.2011.02.005.

[180] Pan L, Zhang Y, Tian Z, Yang F, Huang Z. Experimental and Kinetic Study on Ignition Delay Times of iso-Butanol. Energy Fuels 2014;28:2160–9. https://doi.org/10.1021/ef4021069.

[181] Kukkadapu G, Kumar K, Sung C-J, Mehl M, Pitz WJ. Autoignition of gasoline surrogates at low temperature combustion conditions. Combustion and Flame 2015;162:2272–85. https://doi.org/10.1016/j.combustflame.2015.01.025.

[182] vom Lehn F, Cai L, Pitsch H. Impact of thermochemistry on optimized kinetic model predictions: Auto-ignition of diethyl ether. Combustion and Flame 2019;210:454–66. https://doi.org/10.1016/j.combustflame.2019.09.011.

[183] vom Lehn F, Cai L, Pitsch H. Sensitivity analysis, uncertainty quantification, and optimization for thermochemical properties in chemical kinetic combustion models. Proceedings of the Combustion Institute 2019;37:771–9. https://doi.org/10.1016/j.proci.2018.06.188.

[184] Hughes KJ, Griffiths JF, Fairweather M, Tomlin AS. Evaluation of models for the low temperature combustion of alkanes through interpretation of pressure–temperature ignition diagrams. Phys Chem Chem Phys 2006;8:3197–210. https://doi.org/10.1039/B605379C.

[185] Wilson D, Allen C. A comparison of sensitivity metrics for two-stage ignition behavior in rapid compression machines. Fuel 2017;208:305–13. https://doi.org/10.1016/j.fuel.2017.07.002.

[186] Cheng S, Kang D, Fridlyand A, Goldsborough SS, Saggese C, Wagnon S, et al. Autoignition behavior of gasoline/ethanol blends at engine-relevant conditions. Combustion and Flame 2020;216:369–84. https://doi.org/10.1016/j.combustflame.2020.02.032.

[187] vom Lehn F, Cai L, Pitsch H. Thermochemical property estimation based on group additivity method: Impact of groups on kinetic model predictions. *In*: Proceedings of the 9th European Combustion Meeting, 14-17 April 2019, Lisbon.

[188] Mueller L, Schindler U, Mirschel W, Shepherd T, Ball B, Helming K, et al. Sustainable Agriculture Volume 2. Http://DxDoiOrg/101051/Agro/2009057 2010;30. https://doi.org/10.1051/agro/2009057.

[189] Royal Academy Of Engineering. Sustainability of Liquid Biofuels. Royal Academy Of Engineering; 2017.

[190] Pereira LG, Cavalett O, Bonomi A, Zhang Y, Warner E, Chum HL. Comparison of biofuel life-cycle GHG emissions assessment tools: The case studies of ethanol produced from sugarcane, corn, and wheat. Renewable and Sustainable Energy Reviews 2019;110:1–12. https://doi.org/10.1016/j.rser.2019.04.043.

[191] Hanaki K, Portugal-Pereira J. The Effect of Biofuel Production on Greenhouse Gas Emission Reductions. In: Takeuchi K, Shiroyama H, Saito O, Matsuura M, editors. Biofuels and Sustainability: Holistic Perspectives for Policy-making, Tokyo: Springer Japan; 2018, p. 53–71. https://doi.org/10.1007/978-4-431-54895-9_6.

[192] Maga D, Thonemann N, Hiebel M, Sebastião D, Lopes TF, Fonseca C, et al. Comparative life cycle assessment of first- and second-generation ethanol from sugarcane in Brazil. Int J Life Cycle Assess 2019;24:266–80. https://doi.org/10.1007/s11367-018-1505-1.

[193] Dominguez-Faus R, Powers SE, Burken JG, Alvarez PJ. The Water Footprint of Biofuels: A Drink or Drive Issue? Environ Sci Technol 2009;43:3005–10. https://doi.org/10.1021/es802162x.

[194] Elbehri A, Segerstedt A, Liu P. Biofuels and the Sustainability Challenge: A Global Assessment of Sustainability Issues, Trends and Policies for Biofuels and Related Feedstocks. Trade and Markets Division, Food and Agriculture Organization of the United Nations; 2013.

[195] Hammond GP, Li B. Environmental and resource burdens associated with world biofuel production out to 2050: footprint components from carbon emissions and land use to waste arisings and water consumption. Global Change Biology Bioenergy 2016;8:894–908. https://doi.org/10.1111/gcbb.12300.

[196] Ottinger RL. Biofuels - Potential, Problems and Solutions. Fordham Environmental Law Review 2009;19.

[197] Programme UNE. Towards Sustainable Production and Use of Resources: Assessing Biofuels. UNEP/Earthprint; 2009.

[198] Fletcher RJ, Robertson BA, Evans J, Doran PJ, Alavalapati JR, Schemske DW. Biodiversity conservation in the era of biofuels: risks and opportunities. Frontiers in Ecology and the Environment 2011;9:161–8. https://doi.org/10.1890/090091.

[199] Abel J, Virtanen S. Corrosion of martensitic stainless steel in ethanol-containing gasoline: Influence of contamination by chloride, H2O and acetic acid. Corrosion Science 2015;98:318–26. https://doi.org/10.1016/j.corsci.2015.05.027.

[200] Gu X, Huang Z, Li Q, Tang C. Measurements of Laminar Burning Velocities and Markstein Lengths of n-Butanol−Air Premixed Mixtures at Elevated Temperatures and Pressures. Energy Fuels 2009;23:4900–7. https://doi.org/10.1021/ef900378s.

[201] Liu H, Wang G, Zhang J. The Promising Fuel-Biobutanol. *In*: Fang Z. Liquid, Gaseous and Solid Biofuels - Conversion Techniques. Rijeka: InTech; 2013. https://doi.org/10.5772/52535.

[202] Christensen E, Yanowitz J, Ratcliff M, McCormick RL. Renewable Oxygenate Blending Effects on Gasoline Properties. Energy Fuels 2011;25:4723–33. https://doi.org/10.1021/ef2010089.

[203] Hamadi A. Selective additives for improvement of gasoline octane number. Tikrit J Eng Sci (TJES) 2010;17:22–35.

[204] Hunwartzen I. Modification of CFR Test Engine Unit to Determine Octane Numbers of Pure Alcohols and Gasoline-Alcohol Blends, 1982, p. 820002. https://doi.org/10.4271/820002.

[205] Merola SS, Tornatore C, Marchitto L, Valentino G, Corcione FE. Experimental investigations of butanol-gasoline blends effects on the combustion process in a SI engine. Int J Energy Environ Eng 2012;3:6. https://doi.org/10.1186/2251-6832-3-6.

[206] Kass MD, Janke C, Theiss T, Baustian J, Wolf L, Koch W. Compatibility Assessment of Plastic Infrastructure Materials with Test Fuels Representing E10 and iBu16. SAE Int J Fuels Lubr 2015;8:95–110. https://doi.org/10.4271/2015-01-0894.

[207] Wang C, Prakash A, Aradi A, Cracknell R, Xu H. Significance of RON and MON to a modern DISI engine. Fuel 2017;209:172–83. https://doi.org/10.1016/j.fuel.2017.07.071.

[208] Nigam PS, Singh A. Production of liquid biofuels from renewable resources. Progress in Energy and Combustion Science 2011;37:52–68. https://doi.org/10.1016/j.pecs.2010.01.003.

[209] Jones DT, Woods DR. Acetone-butanol fermentation revisited. Microbiol Rev 1986;50:484–524.

[210] Smith KM, Cho K-M, Liao JC. Engineering Corynebacterium glutamicum for isobutanol production. Appl Microbiol Biotechnol 2010;87:1045–55. https://doi.org/10.1007/s00253-010-2522-6.

[211] Tashiro Y, Yoshida T, Noguchi T, Sonomoto K. Recent advances and future prospects for increased butanol production by acetone-butanol-ethanol fermentation. Engineering in Life Sciences 2013;13:432–45. https://doi.org/10.1002/elsc.201200128.

[212] Akita H, Nakashima N, Hoshino T. Bacterial production of isobutanol without expensive reagents. Appl Microbiol Biotechnol 2015;99:991–9. https://doi.org/10.1007/s00253-014-6173-x.

[213] Niemisto J, Saavalainen P, Pongracz E, Keiski RL. Biobutanol as a Potential Sustainable Biofuel - Assessment of Lignocellulosic and Waste-based Feedstocks. J Sustain Dev Energy Water Environ Syst 2013;1:58–77. https://doi.org/10.13044/j.sdewes.2013.01.0005.

[214] Pfromm PH, Amanor-Boadu V, Nelson R, Vadlani P, Madl R. Bio-butanol vs. bio-ethanol: A technical and economic assessment for corn and switchgrass fermented by yeast or Clostridium acetobutylicum. Biomass and Bioenergy 2010;34:515–24. https://doi.org/10.1016/j.biombioe.2009.12.017.

[215] Grosjean E, Grosjean D, Fraser MP, Cass GR. Air Quality Model Evaluation Data for Organics. 2. C1−C14 Carbonyls in Los Angeles Air. Environ Sci Technol 1996;30:2687–703. https://doi.org/10.1021/es950758w.

[216] Grosjean D, Grosjean E, Gertler AW. On-Road Emissions of Carbonyls from Light-Duty and Heavy-Duty Vehicles. Environ Sci Technol 2001;35:45–53. https://doi.org/10.1021/es001326a.

[217] Poitras M-J, Rosenblatt D, Goodman J. Impact of Ethanol and Isobutanol Gasoline Blends on Emissions from a Closed-Loop Small Spark-Ignited Engine, 2015, p. 2015-01–1732. https://doi.org/10.4271/2015-01-1732.

[218] McEnally CS, Pfefferle LD. Fuel decomposition and hydrocarbon growth processes for oxygenated hydrocarbons: butyl alcohols. Proceedings of the Combustion Institute 2005;30:1363–70. https://doi.org/10.1016/j.proci.2004.07.033.

[219] Grana R, Frassoldati A, Faravelli T, Niemann U, Ranzi E, Seiser R, et al. An experimental and kinetic modeling study of combustion of isomers of butanol. Combustion and Flame 2010;157:2137–54. https://doi.org/10.1016/j.combustflame.2010.05.009.

[220] Gu X, Huang Z, Wu S, Li Q. Laminar burning velocities and flame instabilities of butanol isomers–air mixtures. Combustion and Flame 2010;157:2318–25. https://doi.org/10.1016/j.combustflame.2010.07.003.

[221] Veloo PS, Egolfopoulos FN. Flame propagation of butanol isomers/air mixtures. Proceedings of the Combustion Institute 2011;33:987–93. https://doi.org/10.1016/j.proci.2010.06.163.

[222] Oßwald P, Güldenberg H, Kohse-Höinghaus K, Yang B, Yuan T, Qi F. Combustion of butanol isomers – A detailed molecular beam mass spectrometry investigation of their flame chemistry. Combustion and Flame 2011;158:2–15. https://doi.org/10.1016/j.combustflame.2010.06.003.

[223] Hansen N, Merchant SS, Harper MR, Green WH. The predictive capability of an automatically generated combustion chemistry mechanism: Chemical structures of premixed iso-butanol flames. Combustion and Flame 2013;160:2343–51. https://doi.org/10.1016/j.combustflame.2013.05.013.

[224] Weber BW, Merchant S, Sung C-J, Green WH. An Autoignition Study of iso-Butanol: Experiments and Modeling. ArXiv:170601827 [Physics] 2013.

[225] Ji W, Zhang P, He T, Wang Z, Tao L, He X, et al. Intermediate species measurement during iso-butanol auto-ignition. Combustion and Flame 2015;162:3541–53. https://doi.org/10.1016/j.combustflame.2015.06.010.

[226] Merchant SS, Zanoelo EF, Speth RL, Harper MR, Van Geem KM, Green WH. Combustion and pyrolysis of iso-butanol: Experimental and chemical kinetic modeling study. Combustion and Flame 2013;160:1907–29. https://doi.org/10.1016/j.combustflame.2013.04.023.

[227] Yang Z, Wang Y, Yang X, Qian Y, Lu X, Huang Z. Autoignition of butanol isomers/n-heptane blend fuels on a rapid compression machine in N2/O2/Ar mixtures. Sci China Technol Sci 2014;57:461–70. https://doi.org/10.1007/s11431-014-5475-7.

[228] Curran HJ, Gaffuri P, Pitz WJ, Westbrook CK. A Comprehensive Modeling Study of n-Heptane Oxidation. Combustion and Flame 1998;114:149–77. https://doi.org/10.1016/S0010-2180(97)00282-4.

[229] Alasfour FN. Butanol—A single-cylinder engine study: availability analysis. Applied Thermal Engineering 1997;17:537–49. https://doi.org/10.1016/S1359-4311(96)00069-5.

[230] Alasfour FN. NOx Emission from a spark ignition engine using 30% Iso-butanol–gasoline blend: Part 1—Preheating inlet air. Applied Thermal Engineering 1998;18:245–56. https://doi.org/10.1016/S1359-4311(97)00081-1.

[231] Alasfour FN. NOx Emission from A Spark Ignition Engine Using 30% Iso-Butanol–Gasoline Blend: Part 2—Ignition Timing. Applied Thermal Engineering 1998;18:609–18. https://doi.org/10.1016/S1359-4311(97)00082-3.

[232] Bata R, Elrod A, Lewandowski T. Evaluation of butanol as an alternative fuel, Houston, Texas: 1989.

[233] Kelkar A. Comparative Study of Methanol, Ethanol, Isopropanol, and Butanol as Motor Fuels, Either Pure or Blended with Gasoline. Electronic Theses and Dissertations 1981.

[234] Irimescu A. Fuel conversion efficiency of a port injection engine fueled with gasoline–isobutanol blends. Energy 2011;36:3030–5. https://doi.org/10.1016/j.energy.2011.02.047.

[235] Balaji D, Govindarajan P, Venkatesan J. Influence of isobutanol blend in spark ignition engine performance and emissions operated with gasoline and ethanol. International Journal of Engineering Science and Technology 2010;2(7):2859-68.

[236] Wallington TJ, Kaiser EW, Farrell JT. Automotive fuels and internal combustion engines: a chemical perspective. Chem Soc Rev 2006;35:335–47. https://doi.org/10.1039/B410469M.

[237] Curran HJ, Pitz WJ, Westbrook CK, Callahan GV, Dryer FL. Oxidation of automotive primary reference fuels at elevated pressures. Symposium (International) on Combustion 1998;27:379–87. https://doi.org/10.1016/S0082-0784(98)80426-8.

[238] Curran H. A comprehensive modeling study of iso-octane oxidation. Combustion and Flame 2002;129:253–80. https://doi.org/10.1016/S0010-2180(01)00373-X.

[239] Westbrook CK, Pitz WJ, Mehl M, Curran HJ. Detailed chemical kinetic reaction mechanisms for primary reference fuels for diesel cetane number and spark-ignition octane number. Proceedings of the Combustion Institute 2011;33:185–92. https://doi.org/10.1016/j.proci.2010.05.087.

[240] Andrae JCG. Development of a detailed kinetic model for gasoline surrogate fuels. Fuel 2008;87:2013–22. https://doi.org/10.1016/j.fuel.2007.09.010.

[241] Sarathy SM, Kukkadapu G, Mehl M, Javed T, Ahmed A, Naser N, et al. Compositional effects on the ignition of FACE gasolines. Combustion and Flame 2016;169:171–93. https://doi.org/10.1016/j.combustflame.2016.04.010.

[242] Park S, Wang Y, Chung SH, Sarathy SM. Compositional effects on PAH and soot formation in counterflow diffusion flames of gasoline surrogate fuels. Combustion and Flame 2017;178:46–60. https://doi.org/10.1016/j.combustflame.2017.01.001.

[243] Singh E, Badra J, Mehl M, Sarathy SM. Chemical Kinetic Insights into the Octane Number and Octane Sensitivity of Gasoline Surrogate Mixtures. Energy Fuels 2017;31:1945–60. https://doi.org/10.1021/acs.energyfuels.6b02659.

[244] Affleck WS, Thomas A. An Opposed Piston Rapid Compression Machine for Preflame Reaction Studies. Proceedings of the Institution of Mechanical Engineers 1968;183:365–87. https://doi.org/10.1243/PIME_PROC_1968_183_034_02.

[245] Mumby RD. Experimental Characterisation of Fuel Blends. phd. University of Leeds, 2016.

[246] Würmel J, Silke EJ, Curran HJ, Ó Conaire MS, Simmie JM. The effect of diluent gases on ignition delay times in the shock tube and in the rapid compression machine. Combustion and Flame 2007;151:289–302. https://doi.org/10.1016/j.combustflame.2007.06.010.

[247] Wagnon SW, Wooldridge MS. Effects of buffer gas composition on autoignition. Combustion and Flame 2014;161:898–907. https://doi.org/10.1016/j.combustflame.2013.09.022.

[248] Weber BW, Sung C-J, Renfro MW. On the uncertainty of temperature estimation in a rapid compression machine. Combustion and Flame 2015;162:2518–28. https://doi.org/10.1016/j.combustflame.2015.03.001.

[249] Ihme M. On the role of turbulence and compositional fluctuations in rapid compression machines: Autoignition of syngas mixtures. Combustion and Flame 2012;159:1592–604. https://doi.org/10.1016/j.combustflame.2011.11.022.

[250] Tanaka S, Ayala F, Keck JC. A reduced chemical kinetic model for HCCI combustion of primary reference fuels in a rapid compression machine. Combustion and Flame 2003;133:467–81. https://doi.org/10.1016/S0010-2180(03)00057-9.

[251] Di Sante R. Measurements of the auto-ignition of n-heptane/toluene mixtures using a rapid compression machine. Combustion and Flame 2012;159:55–63. https://doi.org/10.1016/j.combustflame.2011.05.020.

[252] Murad AEMA. Flow and combustion in disc and pent-roof SI engines. phd. University of Leeds, 2006.

[253] Roberts PJ, Sheppard CGW. The Influence of Residual Gas NO Content on Knock Onset of Iso-Octane, PRF, TRF and ULG Mixtures in SI Engines. SAE Int J Engines 2013;6:2028–43. https://doi.org/10.4271/2013-01-9046.

[254] Ling Z, Burluka A, Azimov U. Knock Properties of Oxygenated Blends in Strongly Charged and Variable Compression Ratio Engines, 2014, p. 2014-01–2608. https://doi.org/10.4271/2014-01-2608.

[255] Zhang W. Measurements of flow and combustion in a strongly charged spark ignition engine. phd. University of Leeds, 2018.

[256] Jaramillo J, Zapata J, Bedoya ID. Interactive control of combustion stability and operating limits in a biogas-fueled spark ignition engine with high compression ratio. Int J Interact Des Manuf 2018;12:929–42. https://doi.org/10.1007/s12008-017-0446-4.

[257] Han SB. Investigation of cyclic variations of IMEP under idling operation in spark ignition engines. KSME International Journal 2001;15:81–7. https://doi.org/10.1007/BF03184801.

[258] Szwaja S, Naber JD. Combustion of n-butanol in a spark-ignition IC engine. Fuel 2010;89:1573–82. https://doi.org/10.1016/j.fuel.2009.08.043.

[259] Bade Shrestha SO, Karim GA. Considering the Effects of Cyclic Variations when Modeling the Performance of a Spark Ignition Engine, 2001, p. 2001-01–3600. https://doi.org/10.4271/2001-01-3600.

[260] Mittal G, Raju MP, Sung C-J. Computational fluid dynamics modeling of hydrogen ignition in a rapid compression machine. Combustion and Flame 2008;155:417–28. https://doi.org/10.1016/j.combustflame.2008.06.006.

[261] Li Y, Zhou C-W, Somers KP, Zhang K, Curran HJ. The oxidation of 2-butene: A high pressure ignition delay, kinetic modeling study and reactivity comparison with isobutene and 1-butene. Proceedings of the Combustion Institute 2017;36:403–11. https://doi.org/10.1016/j.proci.2016.05.052.

[262] Bugler J, Marks B, Mathieu O, Archuleta R, Camou A, Grégoire C, et al. An ignition delay time and chemical kinetic modeling study of the pentane isomers. Combustion and Flame 2016;163:138–56. https://doi.org/10.1016/j.combustflame.2015.09.014.

[263] Zhang K, Banyon C, Burke U, Kukkadapu G, Wagnon SW, Mehl M, et al. An experimental and kinetic modeling study of the oxidation of hexane isomers: Developing consistent reaction rate rules for alkanes. Combustion and Flame 2019;206:123–37. https://doi.org/10.1016/j.combustflame.2019.04.011.

[264] Zhang Y, Somers KP, Mehl M, Pitz WJ, Cracknell RF, Curran HJ. Probing the antagonistic effect of toluene as a component in surrogate fuel models at low temperatures and high pressures. A case study of toluene/dimethyl ether mixtures. Proceedings of the Combustion Institute 2017;36:413–21. https://doi.org/10.1016/j.proci.2016.06.190.

[265] Al Rashidi MJ, Thion S, Togbé C, Dayma G, Mehl M, Dagaut P, et al. Elucidating reactivity regimes in cyclopentane oxidation: Jet stirred reactor experiments, computational chemistry, and kinetic modeling. Proceedings of the Combustion Institute 2017;36:469–77. https://doi.org/10.1016/j.proci.2016.05.036.

[266] Al Rashidi MJ, Mármol JC, Banyon C, Sajid MB, Mehl M, Pitz WJ, et al. Cyclopentane combustion. Part II. Ignition delay measurements and mechanism validation. Combustion and Flame 2017;183:372–85. https://doi.org/10.1016/j.combustflame.2017.05.017.

[267] Al Rashidi MJ, Mehl M, Pitz WJ, Mohamed S, Sarathy SM. Cyclopentane combustion chemistry. Part I: Mechanism development and computational kinetics. Combustion and Flame 2017;183:358–71. https://doi.org/10.1016/j.combustflame.2017.05.018.

[268] Wagnon SW, Thion S, Nilsson EJK, Mehl M, Serinyel Z, Zhang K, et al. Experimental and modeling studies of a biofuel surrogate compound: laminar burning velocities and jet-stirred reactor measurements of anisole. Combustion and Flame 2018;189:325–36. https://doi.org/10.1016/j.combustflame.2017.10.020.

[269] Kukkadapu G, Kang D, Wagnon SW, Zhang K, Mehl M, Monge-Palacios M, et al. Kinetic modeling study of surrogate components for gasoline, jet and diesel fuels: C7-C11 methylated aromatics. Proceedings of the Combustion Institute 2019;37:521–9. https://doi.org/10.1016/j.proci.2018.08.016.

[270] Zhang Y, El-Merhubi H, Lefort B, Le Moyne L, Curran HJ, Kéromnès A. Probing the low-temperature chemistry of ethanol via the addition of dimethyl ether. Combustion and Flame 2018;190:74–86. https://doi.org/10.1016/j.combustflame.2017.11.011.

[271] Mehl M, Wagnon S, Tsang K, Kukkadapu G, Pitz WJ, Westbrook CK, et al. A comprehensive detailed kinetic mechanism for the simulation of transportation fuels 2017.

[272] Pelucchi M, Cai L, Pejpichestakul W, Tripathi R, Wagnon SW, Zhang K, et al. Computational Chemistry Consortium: Surrogate Fuel Mechanism Development, Pollutants Submechanisms and Components Library, Naples: 2019. https://doi.org/10.4271/2019-24-0020.

[273] Ritter ER, Bozzelli JW. THERM: Thermodynamic property estimation for gas phase radicals and molecules. International Journal of Chemical Kinetics 1991;23:767–78. https://doi.org/10.1002/kin.550230903.

[274] Agbro EB. Experimental and Chemical Kinetic Modelling Study on the Combustion of Alternative Fuels in Fundamental Systems and Practical Engines. PhD. University of Leeds, 2017.

[275] Seta T, Nakajima M, Miyoshi A. High-Temperature Reactions of OH Radicals with Benzene and Toluene. J Phys Chem A 2006;110:5081–90. https://doi.org/10.1021/jp0575456.

[276] Reaction Design. Reaction Workbench 15112. San Diego: 2012.

[277] Pepiot-Desjardins P, Pitsch H. An efficient error-propagation-based reduction method for large chemical kinetic mechanisms. Combustion and Flame 2008;154:67–81. https://doi.org/10.1016/j.combustflame.2007.10.020.

[278] Mittal G, Chaos M, Sung C-J, Dryer FL. Dimethyl ether autoignition in a rapid compression machine: Experiments and chemical kinetic modeling. Fuel Processing Technology 2008;89:1244–54. https://doi.org/10.1016/j.fuproc.2008.05.021.

[279] Minetti R, Ribaucour M, Carlier M, Fittschen C, Sochet LR. Experimental and modeling study of oxidation and autoignition of butane at high pressure. Combustion and Flame 1994;96:201–11. https://doi.org/10.1016/0010-2180(94)90009-4.

[280] Saylam A, Ribaucour M, Pitz WJ, Minetti R. Reduction of large detailed chemical kinetic mechanisms for autoignition using joint analyses of reaction rates and sensitivities. International Journal of Chemical Kinetics 2007;39:181–96. https://doi.org/10.1002/kin.20232.

[281] Li S, Petzold L. Software and algorithms for sensitivity analysis of large-scale differential algebraic systems. Journal of Computational and Applied Mathematics 2000;125:131–45. https://doi.org/10.1016/S0377-0427(00)00464-7.

[282] Saltelli A, Chan K, Scott EM. Sensitivity Analysis: Gauging the Worth of Scientific Models. Wiley; 2000.

[283] Ruscic B. Uncertainty quantification in thermochemistry, benchmarking electronic structure computations, and Active Thermochemical Tables. International Journal of Quantum Chemistry 2014;114:1097–101. https://doi.org/10.1002/qua.24605.

[284] Fridlyand A, Goldsborough SS, Al Rashidi M, Sarathy SM, Mehl M, Pitz WJ. Low temperature autoignition of 5-membered ring naphthenes: Effects of substitution. Combustion and Flame 2019;200:387–404. https://doi.org/10.1016/j.combustflame.2018.10.028.

[285] Rockstroh T, Fridlyand A, Ciatti S, Cannella W, Goldsborough SS. Autoignition behavior of a full boiling-range gasoline: Observations in RCM and GCI engine environments. Combustion and Flame 2019;209:239–55. https://doi.org/10.1016/j.combustflame.2019.07.013.

[286] Saytzev SG, Soloukhin RI. Study of combustion of an adiabatically-heated gas mixture. Symposium (International) on Combustion 1961;8:344–7. https://doi.org/10.1016/S0082-0784(06)80522-9.

[287] Ciezki HK, Adomeit G. Shock-tube investigation of self-ignition of n-heptane-air mixtures under engine relevant conditions. Combustion and Flame 1993;93:421–33. https://doi.org/10.1016/0010-2180(93)90142-P.

[288] Gallagher SM, Curran HJ, Metcalfe WK, Healy D, Simmie JM, Bourque G. A rapid compression machine study of the oxidation of propane in the negative temperature coefficient regime. Combustion and Flame 2008;153:316–33. https://doi.org/10.1016/j.combustflame.2007.09.004.

[289] Uygun Y, Ishihara S, Olivier H. A high pressure ignition delay time study of 2-methylfuran and tetrahydrofuran in shock tubes. Combustion and Flame 2014;161:2519–30. https://doi.org/10.1016/j.combustflame.2014.04.004.

[290] Griffiths JF, Whitaker BJ. Thermokinetic interactions leading to knock during homogeneous charge compression ignition. Combustion and Flame 2002;131:386–99. https://doi.org/10.1016/S0010-2180(02)00417-0.

[291] Lee C, Vranckx S, Heufer KA, Khomik SV, Uygun Y, Olivier H, et al. On the Chemical Kinetics of Ethanol Oxidation: Shock Tube, Rapid Compression Machine and Detailed Modeling Study. Zeitschrift Für Physikalische Chemie 2012;226:1–28. https://doi.org/10.1524/zpch.2012.0185.

[292] Mittal G, Burke SM, Davies VA, Parajuli B, Metcalfe WK, Curran HJ. Autoignition of ethanol in a rapid compression machine. Combustion and Flame 2014;161:1164–71. https://doi.org/10.1016/j.combustflame.2013.11.005.

[293] Elsworth JE, Haskell WW, Read IA. Non-uniform ignition processes in rapid-compression machines. Combustion and Flame 1969;13:437–8. https://doi.org/10.1016/0010-2180(69)90115-1.

[294] Davidson DF, Gauthier BM, Hanson RK. Shock tube ignition measurements of iso-octane/air and toluene/air at high pressures. Proceedings of the Combustion Institute 2005;30:1175–82. https://doi.org/10.1016/j.proci.2004.08.004.

[295] Leschevich VV, Martynenko VV, Penyazkov OG, Sevrouk KL, Shabunya SI. Auto-ignitions of a methane/air mixture at high and intermediate temperatures. Shock Waves 2016;26:657–72. https://doi.org/10.1007/s00193-016-0665-9.

[296] Mittal G, Chomier M. Interpretation of experimental data from rapid compression machines without creviced pistons. Combustion and Flame 2014;161:75–83. https://doi.org/10.1016/j.combustflame.2013.08.020.

[297] Varga T, Turányi T, Czinki E, Furtenbacher T, Császár A. ReSpecTh: a joint reaction kinetics, spectroscopy, and thermodynamics information system. Proceedings of the European Combustion Meeting – 2015, Budapest, Hungary: 2015.

[298] Santner J, Goldsborough SS. Hot-spot induced mild ignition: Numerical simulation and scaling analysis. Combustion and Flame 2019;209:41–62. https://doi.org/10.1016/j.combustflame.2019.07.017.

[299] Mével R, Boettcher PA, Shepherd JE. Absorption cross section at 3.39μm of alkanes, aromatics and substituted hydrocarbons. Chemical Physics Letters 2012;531:22–7. https://doi.org/10.1016/j.cplett.2012.01.069.

[300] Darcy D, Nakamura H, Tobin CJ, Mehl M, Metcalfe WK, Pitz WJ, et al. A high-pressure rapid compression machine study of n-propylbenzene ignition. Combustion and Flame 2014;161:65–74. https://doi.org/10.1016/j.combustflame.2013.08.001.

[301] Kumar K, Mittal G, Sung C-J. Autoignition of n-decane under elevated pressure and low-to-intermediate temperature conditions. Combustion and Flame 2009;156:1278–88. https://doi.org/10.1016/j.combustflame.2009.01.009.

[302] Kumar K, Sung C-J. An experimental study of the autoignition characteristics of conventional jet fuel/oxidizer mixtures: Jet-A and JP-8. Combustion and Flame 2010;157:676–85. https://doi.org/10.1016/j.combustflame.2010.01.001.

[303] Kumar K, Sung C-J. A comparative experimental study of the autoignition characteristics of alternative and conventional jet fuel/oxidizer mixtures. Fuel 2010;89:2853–63. https://doi.org/10.1016/j.fuel.2010.05.021.

[304] Kumar K, Sung C-J. Autoignition of methanol: Experiments and computations. International Journal of Chemical Kinetics 2011;43:175–84. https://doi.org/10.1002/kin.20546.

[305] Das AK, Sung C-J, Zhang Y, Mittal G. Ignition delay study of moist hydrogen/oxidizer mixtures using a rapid compression machine. International Journal of Hydrogen Energy 2012;37:6901–11. https://doi.org/10.1016/j.ijhydene.2012.01.111.

[306] Kukkadapu G, Kumar K, Sung C-J, Mehl M, Pitz WJ. Experimental and surrogate modeling study of gasoline ignition in a rapid compression machine. Combustion and Flame 2012;159:3066–78. https://doi.org/10.1016/j.combustflame.2012.05.008.

[307] Nyong O, Woolley R, Blakey S, Alborzi E. Optimal piston crevice study in a rapid compression machine. IOP Conf Ser: Mater Sci Eng 2017;243:012018. https://doi.org/10.1088/1757-899X/243/1/012018.

[308] Baulch DL. Chapter 3 Kinetics databases. In: Pilling MJ, editor. Comprehensive Chemical Kinetics, vol. 35, Elsevier; 1997, p. 235–92. https://doi.org/10.1016/S0069-8040(97)80018-0.

[309] Chung J, Lee S, An H, Song S, Chun KM. Rapid-compression machine studies on two-stage ignition characteristics of hydrocarbon autoignition and an investigation of new gasoline surrogates. Energy 2015;93:1505–14. https://doi.org/10.1016/j.energy.2015.09.077.

[310] Gauthier BM, Davidson DF, Hanson RK. Shock tube determination of ignition delay times in full-blend and surrogate fuel mixtures. Combustion and Flame 2004;139:300–11. https://doi.org/10.1016/j.combustflame.2004.08.015.

[311] Lee C, Ahmed A, Nasir EF, Badra J, Kalghatgi G, Sarathy SM, et al. Autoignition characteristics of oxygenated gasolines. Combustion and Flame 2017;186:114–28. https://doi.org/10.1016/j.combustflame.2017.07.034.

[312] Javed T, Lee C, AlAbbad M, Djebbi K, Beshir M, Badra J, et al. Ignition studies of n-heptane/iso-octane/toluene blends. Combustion and Flame 2016;171:223–33. https://doi.org/10.1016/j.combustflame.2016.06.008.

[313] Andrae JCG. Comprehensive chemical kinetic modeling of toluene reference fuels oxidation. Fuel 2013;107:740–8. https://doi.org/10.1016/j.fuel.2013.01.070.

[314] Materego MC. Auto-ignition characterisation of synthetic fuels via Rapid Compression Machine. phd. University of Leeds, 2015.

[315] Vuilleumier D, Kozarac D, Mehl M, Saxena S, Pitz WJ, Dibble RW, et al. Intermediate temperature heat release in an HCCI engine fueled by ethanol/n-heptane mixtures: An experimental and modeling study. Combustion and Flame 2014;161:680–95. https://doi.org/10.1016/j.combustflame.2013.10.008.

[316] Shibata G, Urushihara T. Realization of Dual Phase High Temperature Heat Release Combustion of Base Gasoline Blends from Oil Refineries and a Study of HCCI Combustion Processes. SAE International Journal of Engines 2009;2:145–63.

[317] AlRamadan AS, Galassi RM, Ciottoli PP, Valorani M, Sarathy SM. Multi-stage heat release in lean combustion: Insights from coupled tangential stretching rate (TSR) and computational singular perturbation (CSP) analysis. Combustion and Flame 2020;219:242–57. https://doi.org/10.1016/j.combustflame.2020.05.026.

[318] Hwang W, Dec J, Sjöberg M. Spectroscopic and chemical-kinetic analysis of the phases of HCCI autoignition and combustion for single- and two-stage ignition fuels. Combustion and Flame 2008;154:387–409. https://doi.org/10.1016/j.combustflame.2008.03.019.

[319] Yamamoto A, Oshibe H, Nakamura H, Tezuka T, Hasegawa S, Maruta K. Stabilized three-stage oxidation of gaseous n-heptane/air mixture in a micro flow reactor with a controlled temperature profile. Proceedings of the Combustion Institute 2011;33:3259–66. https://doi.org/10.1016/j.proci.2010.05.004.

[320] Szybist JP, Splitter DA. Pressure and temperature effects on fuels with varying octane sensitivity at high load in SI engines. Combustion and Flame 2017;177:49–66. https://doi.org/10.1016/j.combustflame.2016.12.002.

[321] Dec JE. A Computational Study of the Effects of Low Fuel Loading and EGR on Heat Release Rates and Combustion Limits in HCCI Engines, 2002, p. 2002-01–1309. https://doi.org/10.4271/2002-01-1309.

[322] Sjöberg M, Dec JE. Combined Effects of Fuel-Type and Engine Speed on Intake Temperature Requirements and Completeness of Bulk-Gas Reactions for HCCI Combustion, 2003, p. 2003-01–3173. https://doi.org/10.4271/2003-01-3173.

[323] Babayev R, Houidi MB, Shankar VB, Aljohani B, Johansson B. Injection Strategies for Isobaric Combustion, 2019, p. 2019-01–2267. https://doi.org/10.4271/2019-01-2267.

[324] Machrafi H, Cavadias S. Three-stage autoignition of gasoline in an HCCI engine: An experimental and chemical kinetic modeling investigation. Combustion and Flame 2008;155:557–70. https://doi.org/10.1016/j.combustflame.2008.04.022.

[325] Gorbatenko I. Auto-ignition and heat release of alternative engine fuels. PhD Thesis. University of Leeds, 2019.

[326] Westbrook CK, Pitz WJ, Boercker JE, Curran HJ, Griffiths JF, Mohamed C, et al. Detailed chemical kinetic reaction mechanisms for autoignition of isomers of heptane under rapid compression. Proceedings of the Combustion Institute 2002;29:1311–8. https://doi.org/10.1016/S1540-7489(02)80161-4.

[327] Griffiths JF, Hughes KJ, Porter R. The role and rate of hydrogen peroxide decomposition during hydrocarbon two-stage autoignition. Proceedings of the Combustion Institute 2005;30:1083–91. https://doi.org/10.1016/j.proci.2004.08.179.

[328] Vuilleumier D, Selim H, Dibble R, Sarathy M. Exploration of Heat Release in a Homogeneous Charge Compression Ignition Engine with Primary Reference Fuels, 2013, p. 2013-01–2622. https://doi.org/10.4271/2013-01-2622.

[329] Hébrard É, Tomlin AS, Bounaceur R, Battin-Leclerc F. Determining predictive uncertainties and global sensitivities for large parameter systems: A case study for n -butane oxidation. Proceedings of the Combustion Institute 2015;35:607–16. https://doi.org/10.1016/j.proci.2014.06.027.

[330] Ellis C, Scott MS, Walker RW. Addition of toluene and ethylbenzene to mixtures of H2 and O2 at 772 K: Part 2: formation of products and determination of kinetic data for H+ additive and for other elementary reactions involved. Combustion and Flame 2003;132:291–304. https://doi.org/10.1016/S0010-2180(02)00439-X.

[331] Pelucchi M, Cavallotti C, Faravelli T, Klippenstein SJ. H-Abstraction reactions by OH, HO2, O, O2 and benzyl radical addition to O2 and their implications for kinetic modelling of toluene oxidation. Phys Chem Chem Phys 2018;20:10607–27. https://doi.org/10.1039/C7CP07779C.

[332] da Silva G, Bozzelli JW. Kinetic modeling of the benzyl+HO2 reaction. Proceedings of the Combustion Institute 2009;32:287–94. https://doi.org/10.1016/j.proci.2008.05.040.

[333] Cao J-R, Back MH. The heat of formation of the ethyl radical. International Journal of Chemical Kinetics 1984;16:961–6. https://doi.org/10.1002/kin.550160803.

[334] Goldsmith CF, Magoon GR, Green WH. Database of Small Molecule Thermochemistry for Combustion. J Phys Chem A 2012;116:9033–57. https://doi.org/10.1021/jp303819e.

[335] Olm C, Varga T, Valkó É, Hartl S, Hasse C, Turányi T. Development of an Ethanol Combustion Mechanism Based on a Hierarchical Optimization Approach. International Journal of Chemical Kinetics 2016;48:423–41. https://doi.org/10.1002/kin.20998.

[336] Varga T, Olm C, Nagy T, Zsély IG, Valkó É, Pálvölgyi R, et al. Development of a Joint Hydrogen and Syngas Combustion Mechanism Based on an Optimization Approach. International Journal of Chemical Kinetics 2016;48:407–22. https://doi.org/10.1002/kin.21006.

[337] Benson SW, Buss JH. Additivity Rules for the Estimation of Molecular Properties. Thermodynamic Properties. The Journal of Chemical Physics 1958;29:546–72. https://doi.org/10.1063/1.1744539.

[338] Benson SW. Thermochemical Kinetics: Methods for the Estimation of Thermochemical Data and Rate Parameters. Wiley; 1976.

[339] Cohen N, Benson SW. The Thermochemistry of Alkanes and Cycloalkanes. The Thermochemistry of Alkanes and Cycloalkanes, John Wiley & Sons, Ltd; 1992, p. 215–87. https://doi.org/10.1002/0470034378.ch6.

[340] Sabbe MK, Saeys M, Reyniers M-F, Marin GB, Van Speybroeck V, Waroquier M. Group Additive Values for the Gas Phase Standard Enthalpy of Formation of Hydrocarbons and Hydrocarbon Radicals. J Phys Chem A 2005;109:7466–80. https://doi.org/10.1021/jp050484r.

[341] Flitcroft T, Skinner HA, Whiting MC. Heats of hydrogenation. Part 1.—Dodeca-3:9 and -5:7 diynes. Trans Faraday Soc 1957;53:784–90. https://doi.org/10.1039/TF9575300784.

[342] Skinner HA, Snelson A. Heats of hydrogenation. Part 3. Trans Faraday Soc 1959;55:404–7. https://doi.org/10.1039/TF9595500404.

[343] Bretschneider E, Rogers DW. A new microcalorimeter: Heats of hydrogenation of four monoolefins. Microchim Acta 1970;58:482–90. https://doi.org/10.1007/BF01224151.

[344] Rogers DW, Skanupong S. Heats of hydrogenation of sixteen terminal monoolefins. Alternating effect. J Phys Chem 1974;78:2569–72. https://doi.org/10.1021/j100618a008.

[345] Rogers DW, Papadimetriou PM, Siddiqui NA. An improved hydrogen microcalorimeter for use with large molecules. Mikrochim Acta 1975;64:389–400. https://doi.org/10.1007/BF01219204.

[346] Rogers DW, Dagdagan OA, Allinger NL. Heats of hydrogenation and formation of linear alkynes and a molecular mechanics interpretation. J Am Chem Soc 1979;101:671–6. https://doi.org/10.1021/ja00497a031.

[347] Wiberg KB, Wasserman DJ. Enthalpies of hydration of alkenes. 1. The n-hexenes. J Am Chem Soc 1981;103:6563–6. https://doi.org/10.1021/ja00412a005.

[348] Molnar A, Rachford R, Smith GV, Liu R. Heats of hydrogenation by a simple and rapid flow calorimetric method. Applied Catalysis 1984;9:219–23. https://doi.org/10.1016/0166-9834(84)80066-4.

[349] Steele WV, Chirico RD. Thermodynamic Properties of Alkenes (Mono-Olefins Larger than C4). Journal of Physical and Chemical Reference Data 1993;22:377–430. https://doi.org/10.1063/1.555937.

[350] Mehl M, Vanhove G, Pitz WJ, Ranzi E. Oxidation and combustion of the n-hexene isomers: A wide range kinetic modeling study. Combustion and Flame 2008;155:756–72. https://doi.org/10.1016/j.combustflame.2008.07.004.

[351] Meng X, Rodriguez A, Herbinet O, Wang T, Battin-Leclerc F. Revisiting 1-hexene low-temperature oxidation. Combustion and Flame 2017;181:283–99. https://doi.org/10.1016/j.combustflame.2017.03.031.

[352] Hippler H, Reihs C, Troe J. Shock tube UV absorption study of the oxidation of benzyl radicals. Symposium (International) on Combustion 1991;23:37–43. https://doi.org/10.1016/S0082-0784(06)80239-0.

[353] Papina TS, Pimenova SM, Luk'yanova VA, Kolesov VP. Standard enthalpies of formation of benzyl alcohol and α,α,α-trichlorotoluene. Russian Journal of Physical Chemistry (English Translation) 1995;69:1951–3.

[354] Burke SM, Simmie JM, Curran HJ. Critical Evaluation of Thermochemical Properties of C1–C4 Species: Updated Group-Contributions to Estimate Thermochemical Properties. Journal of Physical and Chemical Reference Data 2015;44:013101. https://doi.org/10.1063/1.4902535.

[355] vom Lehn F, Cai L, Pitsch H. Investigating the impacts of thermochemical group additivity values on kinetic model predictions through sensitivity and uncertainty analyses. Combustion and Flame 2020;213:394–408. https://doi.org/10.1016/j.combustflame.2019.12.011.

[356] Tajti A, Szalay PG, Császár AG, Kállay M, Gauss J, Valeev EF, et al. HEAT: High accuracy extrapolated *ab initio* thermochemistry. The Journal of Chemical Physics 2004;121:11599–613. https://doi.org/10.1063/1.1811608.

[357] Merchant SS, Goldsmith CF, Vandeputte AG, Burke MP, Klippenstein SJ, Green WH. Understanding low-temperature first-stage ignition delay: Propane. Combustion and Flame 2015;162:3658–73. https://doi.org/10.1016/j.combustflame.2015.07.005.

[358] Curran HJ. Rate constant estimation for C1 to C4 alkyl and alkoxyl radical decomposition. International Journal of Chemical Kinetics 2006;38:250–75. https://doi.org/10.1002/kin.20153.

[359] Marinov NM. A detailed chemical kinetic model for high temperature ethanol oxidation. International Journal of Chemical Kinetics 1999;31:183–220. https://doi.org/10.1002/(SICI)1097-4601(1999)31:3<183::AID-KIN3>3.0.CO;2-X.

[360] Sivaramakrishnan R, Su M-C, Michael JV, Klippenstein SJ, Harding LB, Ruscic B. Rate Constants for the Thermal Decomposition of Ethanol and Its Bimolecular Reactions with OH and D: Reflected Shock Tube and Theoretical Studies. J Phys Chem A 2010;114:9425–39. https://doi.org/10.1021/jp104759d.

[361] Vélez E, Quijano J, Gaviria J, Roux MV, Jiménez P, Temprado M, et al. Calorimetric and Computational Study of 3-Buten-1-ol and 3-Butyn-1-ol. Estimation of the Enthalpies of Formation of 1-Alkenols and 1-Alkynols. J Phys Chem A 2005;109:7832–8. https://doi.org/10.1021/jp051161y.

[362] Kondo S, Takahashi A, Tokuhashi K. Theoretical calculation of heat of formation and heat of combustion for several flammable gases. Journal of Hazardous Materials 2002;94:37–45. https://doi.org/10.1016/S0304-3894(02)00011-0.

[363] Yu L, Mao Y, Li A, Wang S, Qiu Y, Qian Y, et al. Experimental and modeling validation of a large diesel surrogate: Autoignition in heated rapid compression machine and oxidation in flow reactor. Combustion and Flame 2019;202:195–207. https://doi.org/10.1016/j.combustflame.2019.01.012.

[364] Yu L, Wang S, Wang W, Qiu Y, Qian Y, Mao Y, et al. Exploration of chemical composition effects on the autoignition of two commercial diesels: Rapid compression machine experiments and model simulation. Combustion and Flame 2019;204:204–19. https://doi.org/10.1016/j.combustflame.2019.03.007.

[365] da Silva G, Bozzelli JW. Variational Analysis of the Phenyl + O2 and Phenoxy + O Reactions. J Phys Chem A 2008;112:3566–75. https://doi.org/10.1021/jp7118845.

[366] Zhang F, Nicolle A, Xing L, Klippenstein SJ. Recombination of aromatic radicals with molecular oxygen. Proceedings of the Combustion Institute 2017;36:169–77. https://doi.org/10.1016/j.proci.2016.06.021.

[367] Emdee JL, Brezinsky K, Glassman I. A kinetic model for the oxidation of toluene near 1200 K. J Phys Chem 1992;96:2151–61. https://doi.org/10.1021/j100184a025.

[368] Tsang W. Heats of Formation of Organic Free Radicals by Kinetic Methods. In: Martinho Simões JA, Greenberg A, Liebman JF, editors. Energetics of Organic Free Radicals, Dordrecht: Springer Netherlands; 1996, p. 22–58. https://doi.org/10.1007/978-94-009-0099-8_2.

[369] Janoschek R, Rossi MJ. Thermochemical properties of free radicals from G3MP2B3 calculations. International Journal of Chemical Kinetics 2002;34:550–60. https://doi.org/10.1002/kin.10082.

[370] Metcalfe WK, Burke SM, Ahmed SS, Curran HJ. A Hierarchical and Comparative Kinetic Modeling Study of C1 − C2 Hydrocarbon and Oxygenated Fuels. International Journal of Chemical Kinetics 2013;45:638–75. https://doi.org/10.1002/kin.20802.

[371] Ghosh MK, Howard MS, Dooley S. Accurate and standard thermochemistry for oxygenated hydrocarbons: A case study of ethyl levulinate. Proceedings of the Combustion Institute 2019;37:337–46. https://doi.org/10.1016/j.proci.2018.07.028.

[372] Paraskevas PD, Sabbe MK, Reyniers M-F, Papayannakos N, Marin GB. Group Additive Values for the Gas-Phase Standard Enthalpy of Formation, Entropy and Heat Capacity of Oxygenates. Chemistry – A European Journal 2013;19:16431–52. https://doi.org/10.1002/chem.201301381.

[373] Ince A, Carstensen H-H, Reyniers M-F, Marin GB. First-principles based group additivity values for thermochemical properties of substituted aromatic compounds. AIChE Journal 2015;61:3858–70. https://doi.org/10.1002/aic.15008.

[374] Li Y, Curran HJ. Extensive Theoretical Study of the Thermochemical Properties of Unsaturated Hydrocarbons and Allylic and Super-Allylic Radicals: The Development and Optimization of Group Additivity Values. J Phys Chem A 2018;122:4736–49. https://doi.org/10.1021/acs.jpca.8b02912.

[375] Kalghatgi GT. Developments in internal combustion engines and implications for combustion science and future transport fuels. Proceedings of the Combustion Institute 2015;35:101–15. https://doi.org/10.1016/j.proci.2014.10.002.

[376] Irimescu A. Performance and fuel conversion efficiency of a spark ignition engine fueled with iso-butanol. Applied Energy 2012;96:477–83. https://doi.org/10.1016/j.apenergy.2012.03.012.

[377] Elfasakhany A. Experimental investigation on SI engine using gasoline and a hybrid iso-butanol/gasoline fuel. Energy Conversion and Management 2015;95:398–405. https://doi.org/10.1016/j.enconman.2015.02.022.

[378] Li Y, Ning Z, Yan J, Lee TH, Lee CF. Experimental investigation on combustion and unregulated emission characteristics of butanol-isomer/gasoline blends. J Cent South Univ 2019;26:2244–58. https://doi.org/10.1007/s11771-019-4170-z.

[379] Anselmi P, Matrat M, Starck L, Duffour F. Combustion characteristics of oxygenated fuels Ethanol-and Butanol-gasoline fuel blends, and their impact on performance, emissions and Soot Index, 2019, p. 2019-01–2307. https://doi.org/10.4271/2019-01-2307.

[380] Kang D, Fridlyand A, Goldsborough SS, Wagnon SW, Mehl M, Pitz WJ, et al. Auto-ignition study of FACE gasoline and its surrogates at advanced IC engine conditions. Proceedings of the Combustion Institute 2019;37:4699–707. https://doi.org/10.1016/j.proci.2018.08.053.

[381] Pera C, Knop V. Methodology to define gasoline surrogates dedicated to auto-ignition in engines. Fuel 2012;96:59–69. https://doi.org/10.1016/j.fuel.2012.01.008.

[382] Al-Mughanam TAU. Fundamental characterisation of the flame propagation of synthetic fuels. Ph.D. University of Leeds, 2013.

[383] Davis SG, Law CK. Determination of and Fuel Structure Effects on Laminar Flame Speeds of C1 to C8 Hydrocarbons. Combustion Science and Technology 1998;140:427–49. https://doi.org/10.1080/00102209808915781.

[384] Farrell JT, Johnston RJ, Androulakis IP. Molecular Structure Effects On Laminar Burning Velocities At Elevated Temperature And Pressure. SAE Transactions 2004;113:1404–25.

[385] Farrell JT, Weissman W, Johnston RJ, Nishimura J, Ueda T, Iwashita Y. Fuel Effects on SIDI Efficiency and Emissions, 2003, p. 2003-01–3186. https://doi.org/10.4271/2003-01-3186.

[386] Abdi Aghdam E, Burluka AA, Hattrell T, Liu K, Sheppard CGW, Neumeister J, et al. Study of Cyclic Variation in an SI Engine Using Quasi-Dimensional Combustion Model, 2007, p. 2007-01–0939. https://doi.org/10.4271/2007-01-0939.

[387] Roberts PJ. Fuel and residual effects in spark ignition and homogeneous charge compression ignition engines. Ph.D. University of Leeds, 2010.

[388] Ozdor N, Dulger M, Sher E. Cyclic Variability in Spark Ignition Engines A Literature Survey, 1994, p. 940987. https://doi.org/10.4271/940987.

[389] Morgan N, Smallbone A, Bhave A, Kraft M, Cracknell R, Kalghatgi G. Mapping surrogate gasoline compositions into RON/MON space. Combustion and Flame 2010;157:1122–31. https://doi.org/10.1016/j.combustflame.2010.02.003.

[390] Kalghatgi G, Babiker H, Badra J. A Simple Method to Predict Knock Using Toluene, N-Heptane and Iso-Octane Blends (TPRF) as Gasoline Surrogates. SAE Int J Engines 2015;8:505–19. https://doi.org/10.4271/2015-01-0757.

[391] Agafonov GL, Naydenova I, Vlasov PA, Warnatz J. Detailed kinetic modeling of soot formation in shock tube pyrolysis and oxidation of toluene and n-heptane. Proceedings of the Combustion Institute 2007;31:575–83. https://doi.org/10.1016/j.proci.2006.07.191.

[392] Richter H, Howard JB. Formation of polycyclic aromatic hydrocarbons and their growth to soot—a review of chemical reaction pathways. Progress in Energy and Combustion Science 2000;26:565–608. https://doi.org/10.1016/S0360-1285(00)00009-5.

[393] Frenklach M. Reaction mechanism of soot formation in flames. Phys Chem Chem Phys 2002;4:2028–37. https://doi.org/10.1039/B110045A.

[394] Knyazkov DA, Slavinskaya NA, Dmitriev AM, Shmakov AG, Korobeinichev OP, Riedel U. Structure of an n-heptane/toluene flame: Molecular beam mass spectrometry and computer simulation investigations. Combust Explos Shock Waves 2016;52:142–54. https://doi.org/10.1134/S0010508216020039.

[395] Agbro E, Tomlin AS, Zhang W, Burluka A, Mauss F, Pasternak M, et al. Chemical Kinetic Modeling Study on the Influence of *n* -Butanol Blending on the Combustion, Autoignition, and Knock Properties of Gasoline and Its Surrogate in a Spark-Ignition Engine. Energy Fuels 2018;32:10065–77. https://doi.org/10.1021/acs.energyfuels.8b00962.

[396] Khan AF, Roberts PJ, Burluka AA. Modelling of Self-Ignition in Spark-Ignition Engine Using Reduced Chemical Kinetics for Gasoline Surrogates. Fluids 2019;4:157. https://doi.org/10.3390/fluids4030157.

[397] Ahmed A, Goteng G, Shankar VSB, Al-Qurashi K, Roberts WL, Sarathy SM. A computational methodology for formulating gasoline surrogate fuels with accurate physical and chemical kinetic properties. Fuel 2015;143:290–300. https://doi.org/10.1016/j.fuel.2014.11.022.

[398] Martyr A, Plint MA. Engine Testing: Theory and Practice. Butterworth-Heinemann; 2007.

[399] Duan X, Liu J, Yao J, Chen Z, Wu C, Chen C, et al. Performance, combustion and knock assessment of a high compression ratio and lean-burn heavy-duty spark-ignition engine

fuelled with n-butane and liquefied methane gas blend. Energy 2018;158:256–68. https://doi.org/10.1016/j.energy.2018.03.014.

[400] Khan AF, Burluka A, Neumeister J, OudeNijeweme D, Freeland P, Mitcalf J. Combustion and Autoignition Modelling in a Turbocharged SI Engine. SAE Int J Engines 2016;9:2079–90. https://doi.org/10.4271/2016-01-2234.

[401] Sileghem L, Alekseev VA, Vancoillie J, Van Geem KM, Nilsson EJK, Verhelst S, et al. Laminar burning velocity of gasoline and the gasoline surrogate components iso-octane, n-heptane and toluene. Fuel 2013;112:355–65. https://doi.org/10.1016/j.fuel.2013.05.049.

[402] Wu F, Law CK. An experimental and mechanistic study on the laminar flame speed, Markstein length and flame chemistry of the butanol isomers. Combustion and Flame 2013;160:2744–56. https://doi.org/10.1016/j.combustflame.2013.06.015.

[403] Vuilleumier D, Kim N, Sjöberg M, Yokoo N, Tomoda T, Nakata K. Effects of EGR Constituents and Fuel Composition on DISI Engine Knock: An Experimental and Modeling Study. SAE Technical Paper, 2017.

[404] Kim N, Vuilleumier D, Sjöberg M, Yokoo N, Tomoda T, Nakata K. Using Chemical Kinetics to Understand Effects of Fuel Type and Compression Ratio on Knock-Mitigation Effectiveness of Various EGR Constituents, 2019, p. 2019-01–1140. https://doi.org/10.4271/2019-01-1140.

[405] DelVescovo DA, Splitter DA, Szybist JP, Jatana GS. Modeling pre-spark heat release and low temperature chemistry of iso-octane in a boosted spark-ignition engine. Combustion and Flame 2020;212:39–52. https://doi.org/10.1016/j.combustflame.2019.10.009.

[406] Bata RM, Elrod AC, Lewandowskia TP. Butanol as a Blending Agent with Gasoline for I. C. Engines, 1989, p. 890434. https://doi.org/10.4271/890434.

[407] Popuri SSS, Bata RM. A Performance Study of Iso-Butanol-, Methanol-, and Ethanol-Gasoline Blends Using a Single Cylinder Engine, 1993, p. 9329-53. https://doi.org/10.4271/932953.

[408] Westbrook CK, Pitz WJ. Detailed Kinetic Modeling of Autoignition Chemistry, SAE Transactions, 1987;96:559-74. https://doi.org/10.4271/872107.

[409] Isomäki R, Pitkäaho S, Niemistö J, Keiski RL. Biobutanol Production Technologies. In: Abraham MA, editor. Encyclopedia of Sustainable Technologies, Oxford: Elsevier; 2017, p. 285–91. https://doi.org/10.1016/B978-0-12-409548-9.10112-5.

[410] Yusoff MNAM, Zulkifli NWM, Masjuki HH, Harith MH, Syahir AZ, Kalam MA, et al. Performance and emission characteristics of a spark ignition engine fuelled with butanol isomer-gasoline blends. Transportation Research Part D: Transport and Environment 2017;57:23–38. https://doi.org/10.1016/j.trd.2017.09.004.

[411] Wess J, Brinek M, Boles E. Improving isobutanol production with the yeast Saccharomyces cerevisiae by successively blocking competing metabolic pathways as well as ethanol and glycerol formation. Biotechnology for Biofuels 2019;12:173. https://doi.org/10.1186/s13068-019-1486-8.

[412] Sherkhanov S, Korman TP, Chan S, Faham S, Liu H, Sawaya MR, et al. Isobutanol production freed from biological limits using synthetic biochemistry. Nature Communications 2020;11:4292. https://doi.org/10.1038/s41467-020-18124-1.

[413] Ibrahim MF, Kim SW, Abd-Aziz S. Advanced bioprocessing strategies for biobutanol production from biomass. Renewable and Sustainable Energy Reviews 2018;91:1192–204. https://doi.org/10.1016/j.rser.2018.04.060.

[414] Zaharin MSM, Abdullah NR, Masjuki HH, Ali OM, Najafi G, Yusaf T. Evaluation on physicochemical properties of iso-butanol additives in ethanol-gasoline blend on performance and emission characteristics of a spark-ignition engine. Applied Thermal Engineering 2018;144:960–71. https://doi.org/10.1016/j.applthermaleng.2018.08.057.

[415] Elfasakhany A. Investigations on performance and pollutant emissions of spark-ignition engines fueled with n-butanol–, isobutanol–, ethanol–, methanol–, and acetone–gasoline blends: A comparative study. Renewable and Sustainable Energy Reviews 2017;71:404–13. https://doi.org/10.1016/j.rser.2016.12.070.

[416] Vlachos TG, Bonnel P, Perujo A, Weiss M, Mendoza Villafuerte P, Riccobono F. In-Use Emissions Testing with Portable Emissions Measurement Systems (PEMS) in the Current and Future European Vehicle Emissions Legislation: Overview, Underlying Principles and Expected Benefits. SAE Int J Commer Veh 2014;7:199–215. https://doi.org/10.4271/2014-01-1549.

[417] Johnson MV, Goldsborough SS, Serinyel Z, O'Toole P, Larkin E, O'Malley G, et al. A Shock Tube Study of n- and iso-Propanol Ignition. Energy Fuels 2009;23:5886–98. https://doi.org/10.1021/ef900726j.

[418] Moc J, Black G, Simmie JM, Curran HJ, Maroulis G, Simos TE. The Unimolecular Decomposition and H Abstraction Reactions by HO and HO2 from n-Butanol. AIP Conference Proceedings 2009;1148:161–4. https://doi.org/10.1063/1.3225261.